



8th IEEE Conference
Wrocław University of Technology
Brandenburg Technical University
Technical University of Ostrava
Technical University of Košice
University Carlos III of Madrid
May 10-13 2009



Politechnika Wroclawska



Universidad
Carlos III de Madrid

International Conference on Environment and Electrical Engineering 2009



8 IEEE International Conference on Environment and Electrical Engineering

Karpacz, Poland

10-13. May 2009

Editors: H. Schwarz Z. Leonowicz

co-sponsored by IEEE Poland

FOR PUBLIC RELEASE

PUBLIC RELEASE
PREPRINT



8th IEEE Conference
Wrocław University of Technology
Brandenburg Technical University
Technical University of Ostrava
Technical University of Košice
University Carlos III of Madrid
May 10-13 2009



Politechnika Wroclawska



Universidad
Carlos III de Madrid

International Conference on Environment and Electrical Engineering 2009

8th IEEE International Conference on Environment and Electrical Engineering

Karpacz, Poland

10-13. May 2009

Editors: H. Schwarz Z. Leonowicz

co-sponsored by IEEE Poland

ISBN 978-3-940471-10-9

Program Committee

Chairman Harald Schwarz Brandenburg Technical University (Germany)

- * Sahin Albayrak Technische Universität Berlin (Germany)
- * Carlos Álvarez Ortega Carlos III University of Madrid (Spain)
- * Hortensia Amaris Duarte Carlos III University of Madrid (Spain)
- * Chiara Boccaletti University of Rome “La Sapienza” (Italy)
- * Holger Borowiak Siemens AG (Germany)
- * Antonio Bracale Università degli Studi di Napoli Federico II (Italy)
- * Guido Carpinelli Università degli Studi di Napoli Federico II (Italy)
- * Manuel Pérez-Donsión Vigo University (Spain)
- * Iftikhar A. Durranius German Arab Technology Group Jeddah (Saudi Arabia)
- * Radomir Gono Technical University of Ostrava (Czech Republic)
- * Dariusz Grabowski Silesian University of Technology (Poland)
- * Jan Izykowski Wroclaw University of Technology (Poland)
- * Przemyslaw Janik Wroclaw University of Technology (Poland)
- * Jin Jiang University of Western Ontario (Canada)
- * Juha Karvanen National Public Health Institute (Finland)
- * Antoni Klajn Wroclaw University of Technology (Poland)
- * Wlodzimierz Koczara Warsaw University of Technology (Poland)
- * Fabio Leccese Università degli Studi Roma Tre (Italy)
- * Dirk Lehmann Brandenburg Technical University (Germany)
- * Zbigniew Leonowicz Wroclaw University of Technology (Poland)
- * Veleslav Mach Technical University of Ostrava (Czech Republic)
- * Dusmanta Kumar Mohanta Birla Institute of Technology (India)
- * Eduardo I. Ortiz-Rivera University of Puerto Rico-Mayaguez
- * Waldemar Rebizant Wroclaw University of Technology (Poland)
- * M. Jaya Bharata Reddy Birla Institute of Technology (India)
- * Stanislav Rusek Technical University of Ostrava (Czech Republic)
- * Tomasz M. Rutkowski Lab. for Advanced Brain Signal Processing, RIKEN (Japan)
- * Paco Ruz Universidad Politécnica de Cartagena (Spain)
- * Tarlochan S. Sidhu University of Western Ontario (Canada)
- * Tomasz Sikorski IASE & Wroclaw University of Technology (Poland)
- * Krzysztof Siwek Warsaw University of Technology (Poland)
- * Toshihisa Tanaka Tokyo University of Agriculture and Technology (Japan)
- * Pierluigi Tenca Ansaldo Sistemi Industriali S.p.A. (Italy)
- * Jan Wilbert European Aeronautic Defence and Space Company EADS N.V
- * Ying Xin Innopower Superconductor Cable (China)
- * Liu Zhaoxu Electric Power Research Institute - EPRI (China)

Honorary Committee

Honorary Chairman Tadeusz Lobos Wroclaw University of Technology (Poland)

- * Janusz Fleszynski Wroclaw University of Technology (Poland)
- * Matthias Müller-Mienack Vattenfall Europe Transmission GmbH (Germany)
- * Stanislaw Osowski Executive Committee IEEE Poland Section
- * Marian Sobierajski Wroclaw University of Technology (Poland)
- * Zbigniew Sroka Wroclaw University of Technology (Poland)

**The Eighth IEEE International Conference on Environment and Electrical
Engineering, Karpacz, 10-13 May 2009**

IEEE 2009

Welcome from the Conference Chair

In the time of increased awareness about the environment problems by the public opinion and intensive international effort to reduce emissions of greenhouse gases, as well increase of the generation of electrical energy to facilitate industrial growth, the conference offers broad contribution towards achieving the goals of diversification and sustainable development.

The scope of the Conference is to promote a Forum, where people involved with electrical power systems may exchange their experiences and present solutions found for actual and future problems. The conference offers prominent academics and industrial practitioners from all over the world the forum for discussion about the future of electrical energy and environmental issues and presents a base for identifying directions for continuation of research.

This year, the organizers from Wroclaw University of Technology and Brandenburg Technical University received strong support from our new partners: Technical University of Ostrava (Czech Republic), Technical University of Kosice (Slovakia) and Carlos III University of Madrid (Spain). We gratefully acknowledge the support from sponsors.

The renewed interest in electrical engineering and energy topics in general contributes to the revival of the industry and encourages us to announce the next IEEE 2010 Conference which will be held in May 2010 in Prague (Czech Republic).

Harald Schwarz

BTU Cottbus (Germany)

Sponsors of IEEEIC 2009



ZPUE S.A.
ul. Jędrzejowska 79c
29-100 Włoszczowa, Poland
www.zpue.pl



W. Investment Group



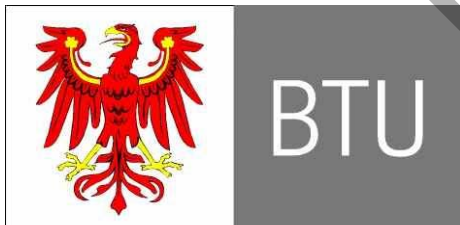
Institute of Power Systems Automation, Ltd.
ul. Wystawowa 1
51-618 Wrocław, Poland, www.iase.wroc.pl

•
•
•
•
Visegrad Fund

International Visegrad Fund
www.visegradfund.org



Urząd Marszałkowski Województwa Dolnośląskiego
www.umwd.dolnyslask.pl



Brandenburgische Technische Universität Cottbus



[Wrocław University of Technology](http://www.wroclawuniversityoftechnology.pl)

EEEIC 2009

Regular Papers

<u>Disturbances correlated to compensation of reactive power in a system with wind generation – estimation of transient components' parameters</u> Przemyslaw Janik, Zbigniew Leonowicz, Jacek Rezmer, Piotr Ruczewski, Zbigniew Waclawek, Hortensia Amaris, and Carlos Alvarez	1
<u>Electrical Energy Measurements for Rome LV Customers by Distributed Web-Server Instruments</u> Fabio Leccese (invited paper)	8
<u>Optimal Capacitor Placement on Interconnected Distribution Systems in Presence of Nonlinear Loads Using Genetic Algorithms</u> Ahmad Galal Sayed	13
<u>Computer Relaying Software Reliability Evaluation Using Event Tree</u> Aditya Anil, Dusmanta Kumar Mohanta, Diptendu Sinha Roy, and Ajit Kumar Panda	19
<u>Relationship between Production Capacity of Wind Power Stations and Needs of Ancillary Services</u> Vaclav Cerny, Andrea Fialova, Lucie Houdova, Petr Janecek, and Eduard Janecek	23
<u>Extracting Electricity from Groundwater Flow - A New Environment Friendly Source of Energy Case Study: Iran</u> Majid Labbaf Khaneiki and Ali Asghar Semsar Yazdi	27
<u>Fault Liability and Maintenance Cost Modeling of a Steam Turbine</u> Lenka Houdova, Libor Jelinek, and Eduard Janecek	32
<u>Voltage Stability Analysis of Grid Connected Wind Generators</u> Nguyen Tung Linh	36
<u>Organic solar cells based on ZnO nanowires layer</u> Jiri Podzemsky and Wolfgang Schade	41
<u>Wind Turbine Cylinders with Spiral Fins</u> Radomir Gono, Stanislav Rusek, and Miroslav Hrabecik	45
<u>Reliability Standards for Large Interconnections</u> Petr Horacek and Petr Havel	49
<u>Shields of Electromagnetic Wave Based on Amorphous and Nanocrystalline Soft Magnetic Materials</u> Mariusz Ozimek, Dominika Gaworska-Koniarek, and Wieslaw Wilczynski	54
<u>Impedance-Source Inverter-Based High-Power DC/DC Converter for Fuel Cell Applications</u> Mikhail Egorov, Dmitri Vinnikov, Ryszard Strzelecki, and Marek Adamowicz	57
<u>Voltage division over the interrupter units of a high voltage circuit breaker without grading capacitors</u> Henryk Stuermer	61
<u>Adjustable Speed Generation System For Wind Turbine Power Quality Improvement</u> Wlodzimierz Koczara, Grzegorz Iwanski, and Zdzislaw Chlodnicki	65
<u>Current progress in ambient energy harvesting using piezoelectric materials and electroactive polymers</u> Pawel Zylka	69
<u>Thin Film Adhesion Measuring of Conductive Silicon Rubber Depending on Power and Coating Time in Magnetic Sputtering Method</u> Artur Napierala and Jan Ziaja	73
<u>Electrical behaviour of current conducting silicon rubber</u> Artur Napierala	77
<u>On Hilbert Transform and its application to assessment of electrical signal waveform distortion</u> Tomasz Sikorski and Piotr Ruczewski	79
<u>Voltage Dependence of Hologram Generation Dynamics in Nematic Liquid Crystal Hybrid Panels</u> Agata Anczykowska, Stanislaw Bartkiewicz, Lech Sznitko, and Jaroslaw Mysliwiec	83

<u>Relevance of a Safety Factor for Wind Power Trading in Comparison with the Utilization of a Storage</u> Steve Völler and J.F. Verstege	87
<u>The Probabilistic Integration of Demand-Side Load and Generation in a Representative Irish Distribution Network</u> Keith Sunderland and Michael Conlon	91
<u>Planning of Ancillary Services Securing Power System Operation</u> Ondrej Novak, Tomas Strnad, Petr Horacek, and Josef Fantik	95
<u>Biofuels- the power from plants</u> Grzegorz Pawel Maliga and Amar Mohan Patil	99
<u>Guideline for the Investigation of PEM Fuel Cell Systems in Automotive Applications</u> Maik Heuer, Mathias Kaebisch, Guenter Heideck, and Zbigniew Styczynski	103
<u>Wind Turbine Driven Doubly-Fed Induction Generator With Grid Disconnection</u> Chitti Babu B, Mohanty K B, and Poongothai C	107
<u>Possibilities of Utilization of Energy Briquettes</u> Gabriel Borowski	110
<u>Optimum location and sizing of passive filters in distribution networks using genetic algorithm</u> Mahdi Ghiasi Varzeghan, Vahid Rashtchi, and Sied Hadi Hoseini	114
<u>Balancing Voltage Source Direct Torque Control of Induction Motor with Three level Inverter</u> Aberrahmane Berkani and Hacene Rezine	118
<u>Remote Irrigation controller under photovoltaic energy</u> Mohamed Lassaad Benzaoui	124
<u>Implementation of Inter-area Angle Stability Prediction in Wide Area Control</u> Ahmed A. Daoud	127
<u>Some aspects of technical, economical and wind simplified analysis for 18 MW wind farm in Poland</u> Waldemar Dolega	133
<u>The aspects of combustion and co-combustion biomass</u> Grzegorz Pawel Maliga and Amar Mohan Patil	137
<u>Control and Stability Analysis of Doubly Fed Induction during Voltage Sags</u> Kairous Djilali Djilali, B. Belmadani, and M. Benghanem	141
<u>Application and Comparison of LQR and Robust Sliding Mode Controllers to Improve Power System Stability</u> Sahar Saffar Shamsirgar, Mohammad Golkhah, Hojat Rahmati, and Mohammad Ali Nekoui	145
<u>A Survey of Solar Energy Power Systems</u> Adekunle Babatope Ajayi	151
<u>Reducing the Short Circuit Levels in Kuwait Transmission Network. (A Case Study)</u> Mahmoud Gilany and Wael Al-Hasawi	155
<u>Impact of Inverter-fed Multi-Motor Drives on the Quality of Electric Power in the Mains</u> Maciej Stanislaw Pawlowski	160
<u>Modeling analysis and solution of Power Quality Problems</u> Mahesh Singh, Vaibhav Tivari, and Rajkumar Jhapte	164
<u>Power System Real Time Simulation Testing Using IEC 61850</u> Yogesh Devidas Sonawane, Pankaj M. Patil, Naresh D. Sonawane, and Sayali Y. Sonawane	170
<u>Economical Benefits by Contribution of Large Wind Farms to Voltage Control</u> Ahmad-Rami Al-Awaad	175

<u>Optical properties of thin films of polyazomethine with triphenylamine unit in the main chain prepared by spin-coating method</u>	179
Marcin Palewicz, A. Iwan, J. Doskocz, W. Strek, and D. Sek	
<u>A new approach to a solar cell problem</u>	183
Bronislaw Swistacz	
<u>Proposed Techniques for Identifying Faulty Sections in Closed-Loop Distribution Networks</u>	185
Wael Al-Hasawi and Mahmoud Gilany	
<u>Charcoals Used as Electrode Material in Supercapacitors</u>	190
B. Szubzda and R. Kulinski	
<u>Wavelets for detection of voltage dips and micro interruptions</u>	193
Zbigniew Leonowicz	
<u>Two Modified Methods for Harmonic and Flicker Measurement based on RWPC considering spectral leakage and edge effects</u>	196
Marjan Saadati and Seyed Saeidollah Mortazavi	
Student Papers	
<u>Combustion Characteristics of Palm Wastes in Fluidized Bed Combustor</u>	200
Rosyida Permatasari, Kang Kin Hui, and Mohammad Nazri Mohd. Ja'afar	
<u>Dynamic Brake Regulator and Protection System in Locomotive</u>	204
Farzad Takbiri and Siamak Farshad	
<u>Lightning Phenomenon - Introduction and Basic Information to Understand the Power of Nature</u>	208
Luke Staszewski	
<u>Signal Processing Techniques used in Power Quality Monitoring</u>	212
Umar Naseem Khan	
<u>Optimization of the costs of road lighting systems.</u>	216
Andrzej Maćków	
<u>Contemporary high voltage gapless surge arresters</u>	218
Rafal Kurnatowski	
<u>Evaluation of Chaotic Ferroresonance in Power Transformers Including Nonlinear Core Losses</u>	220
Ataollah Abbasi, Mehrdad Rostami, Hamid Radmanesh, and Hamid Reza Abbasi	
<u>Primary Energy Market and Electric Market interaction</u>	226
Nuno Soares Domingues	
<u>Measurements of electromagnetic compatibility using GTEM chambers</u>	230
Marcin Dębowski	
<u>Distributed Generation and Power Quality</u>	232
Umar Naseem Khan	
<u>Using Ultracapacitors for Saving Energy in Regenerative Braking in Hybrid Vehicles</u>	236
Amar Mohan Patil and Gregor Pawel Maliga	
<u>Solar energy in Spain</u>	240
Dariusz Szymanski	
<u>Single Phase STATCOM-Its Control Algorithm</u>	243
Linju Jose	
<u>Transients phenomena in capacitive voltage transformers- distance protection point of view.</u>	247
Rafal Kurnatowski	
<u>Power quality in automatic restoration systems using stand alone generators</u>	249
Piotr Danielski and Marcin Dębowski	

<u>Ocean Power: tidal and wave energy</u> Dennis Grzelak, Nico Brose, and Lennardt Schünemann	253
<u>Overvoltage Protection Devices</u> Cezary Pawel Szafron	257
<u>High-voltage direct current technology</u> Tomasz Drobik	260
<u>Transient response of doubly fed induction generator under voltage sag using an accurate model</u> Alireza Abbaszadeh, Saeed Lesan, and Vahid Morteza pour	263
<u>Reverse electrodialysis for power generation</u> Sameer Deshmukh	268
<u>Microbial Fuel Cells to produce electricity</u> Sameer Deshmukh and Yogesh Khambha	272
<u>Cable Shielding to Minimize Electromagnetic Interference</u> Anke Fröbel	280
<u>Fault Location System for Transmission Lines in One-terminal By using Impedance-Traveling Wave Assembled Algorithm</u> Sachin Ramrao Yerekar	283
<u>Market behaviour to promote renewable energy</u> Nuno Soares Domingues	287
<u>The future goes offshore...</u> Robert Hoyer, Henry Römer, and Jonathan Saudhof	293
<u>Strong Electromagnetic Impulse Generation</u> Daniel Pyda	296
<u>Detection of Fault Position with Respect to the Compensating Bank in Series Compensated Line by Measurement of Phase Shift for Distance Relay Input Currents</u> Piotr Mazniewski and Jan Izykowski	300
<u>Lightning Protection of Aircraft</u> Lukasz Mackowiak	304
<u>Elimination of Chaotic Ferroresonance in Power Transformers Including Nonlinear Core Losses Applying of Neutral Resistance</u> Ataollah Abbasi, Mehrdad Rostami, Hamid Radmanesh, and Hamid Reza Abbasi	308
<u>Geothermal energy as a renewable energy source</u> Stefanie Kitscha, Jürgen Schmecke bier, and Marcel Steckel	314
<u>Slot harmonics in stator current as symptoms of reparation of induction motors</u> Jan Stanislaw Pytlarz and Paweł Ewert	318
<u>Model of a Wind Turbine with PMSG and Wind Park Configuration</u> Michal Piotr Jankow	321
<u>Load Modeling For Power System Analysis</u> Jakub Kepka	325
<u>Loads and Synchronous Generator Modeling</u> Robert Pliszczak	329
<u>Renewable energy from the oceans – Wave power, tidal power and ocean streams</u> Lars Bork, Bastian Garnitz, Thomas Krisch, and Carsten Schwartze	333
<u>Carbon Capture and Storage – Part of the solution to the climate change problem?</u> Robin Kuscheck, Sören Schlüter, and Martin Noack	337
<u>FFT algorithm optimization using Stream SIMD Extension instruction set</u> Pawel Dawidowski	

<u>Abuse of transmission congestion existing naturally or created by bidding strategies in order to exert market power</u> Abouzar Estebarsari, Seyyed Mohammad Sadeghzadeh, and Mehrdad Rostami	339
<u>"Banning of Incandescent Bulbs" and Its Influence to Electromagnetic Compatibility</u> Yan Lu	341
<u>Reactive power in one-phase circuits with periodical voltages – reactive power compensation</u> Sebastian Slabosz	346
<u>Grid integration of renewable energy sources</u> P. Kammer and Andreas Kober	349
<u>Solar potential of the Sahara Desert with an introduction to solar updraft power plants</u> Stefanie Fiedermann, Jadranka Halilovic, and Torsten Bogacz	353
<u>Power Quality in distribution power networks with photovoltaic energy sources</u> Ricardo Albarracin Sanchez and Hortensia Amaris	357
	360

PUBLIC RELEASE
PREPRINT

Disturbances correlated to compensation of reactive power in system with wind generation – estimation of transient components' parameters

P. Janik, Z. Leonowicz, J. Rezmer, P. Ruczewski, Z. Waclawek, H. Amaris*, C. Ortega*

Wroclaw University of Technology, Wybrzeże Wyspiańskiego 27, 50-370 Wrocław (Poland)

Electrical Engineering Dep., Universidad Carlos III de Madrid, Av. de la Universidad 30, 28911 Leganés Madrid (Spain)

Abstract—precise computation of current components is a key prerequisite for reliable assessment of power quality. Especially in networks with wind generation we may observe increased number of possible disturbing phenomena. This paper presents an approach to accurate computation of currents components with two similar parametric methods based on singular value decomposition (SVD) and Prony model. Those methods seem to be applicable for the detection of non integer multiples of the main frequency in decaying signals. Results of both methods have been compared and evaluated. with respect to traditional Fourier approach.

Index Terms—power quality, transients, SVD, Prony method.

I. INTRODUCTION

The widespread implementation of wind energy conversion systems is a reality. Wind is seen as a clean and renewable energy source, so the development of wind generation technologies is welcomed and supported by ecologists and governments. In the next years we will have even more generator units connected to the grid [1].

Wind turbines, despite of their advanced control systems and power electronic converters, influence in many different aspects the electrical system they are connected to [2, 3]. So far, the electrical distribution networks were designed and operated under the assumption of centralized generation and an energy flow from the substation to the consumer. It is no more the case [3, 4]. The connection of wind generators could lead to many disturbances, such as: voltage fluctuations, flickers, harmonics, instability, blind power regulation problems, and transients [10]. Power quality issues connected with wind generation are not only important because of technical aspects, they are also crucial on the free energy market.

There are at least three main wind generators structures, which can be easily pointed out [4]. The simplest and previously popular is the squirrel-cage induction generator connected directly to the grid. Usually, that type of turbines has a fixed pitch of turbine blades. Second is the doubly-fed induction generator. The stator winding of this generator is coupled with the

system grid, and the rotor winding is connected to a voltage-source converter. The converter adjusts the frequency of the rotor feeding current in order to enable variable speed operation. The wind generator operates in wide spectrum of wind speeds and has lower impact on the grid, but the investment costs are higher. The third structure of wind generation unit has a synchronous machine. The rotating shaft and generator are coupled directly without gear box. That generators type requires a back-to-back converter for the grid connection, but it can be operated in wide wind change range. Additionally, voltage, active and reactive power can be controlled, as in double feed induction generator.

Many of the wind energy converters installed today still have a squirrel-cage induction machine connected directly to the grid [6, 7]. This type of the generator cannot perform voltage control and it absorbs reactive power from the grid. Phase compensating capacitors are usually directly connected. That type of wind turbine is cheap and robust and therefore popular, but from the system analysis point of view it has some drawbacks [4].

An important disadvantage is that during the switching of the phase compensating capacitors, transients occur [7], which can be disturbing for sensitive equipment, protection relays and insulation. Also the impact on power quality indices can not be neglected [5, 10].

Transient overvoltages can theoretically reach peak values up to 2.0 pu. High current transients can reach values up to ten times the nominal capacitor current with a duration of several milliseconds [8].

The purpose of this paper is the assessment of transients in electrical system for wind turbines equipped with an asynchronous generator. A wind energy converter connected to a distribution system was modeled in Matlab SimPowerSystemsTolbox [9].

The Prony model and SVD method were considered as appropriate tools for the parameters estimation of transients. The analysis was carried out for different operation conditions of the wind energy converter.

II. COMPUTATIONAL METHOD FOR SPECTRUM ESTIMATION BASED ON SINGULAR VALUE DECOMPOSITION (SVD)

The proposed method, based on Singular Value Decomposition (SVD) [14, 15, 16], is a technique for modeling sampled data as a linear combination of exponentials.

Accordingly, the signal $x(t)$ can be described mathematically as a sum of N exponential components:

$$x(t) = A_1 e^{s_1 t} + A_2 e^{s_2 t} + \dots + A_N e^{s_N t} \quad (1)$$

where: A - signal amplitude, $s = \alpha + j\omega$ - complex frequency.

For practical reasons we consider only digital signals, sampled with the interval T

$$t = [nT] \quad (2)$$

The signal samples are given by

$$x_n = A_1 (e^{s_1 T})^n + A_2 (e^{s_2 T})^n + \dots + A_N (e^{s_N T})^n = A_1 z_1^n + A_2 z_2^n + \dots + A_N z_N^n \quad (3)$$

The practical realization of the proposed method imposes designing of a digital filter with finite impulse response (FIR). This filter (Fig. 1) should block all signal components. The filter transmittance in general form is given by

$$H(z) = 1 + h_1 z^{-1} + h_2 z^{-2} + \dots + h_N z^{-N} \quad (4)$$

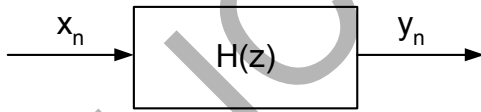


Fig. 1. Basic digital filter scheme as a practical realization of proposed analysis method

The filter response is given by

$$Y(z) = H(z) \cdot X(z) \quad (5)$$

The blocking property of the considered filter results in

$$y_N = x_N + h_1 x_{N-1} + h_2 x_{N-2} + \dots + h_N x_0 = 0$$

$$y_n = 0 \text{ for } n \geq N \quad (6)$$

Equation (6) can also be written in a practice relevant matrix form

$$\begin{bmatrix} x_1 \\ x_2 \\ \vdots \\ x_{N-1} \\ x_N \end{bmatrix} = \begin{bmatrix} 0 & 1 & 0 & \dots & 0 \\ 0 & 0 & 1 & \dots & 0 \\ \dots & \dots & \dots & \dots & \dots \\ 0 & 0 & 0 & \dots & 1 \\ -h_N & -h_{N-1} & -h_{N-2} & \dots & -h_1 \end{bmatrix} \begin{bmatrix} x_0 \\ x_1 \\ \vdots \\ x_{N-2} \\ x_{N-1} \end{bmatrix} \quad (7)$$

or

$$\mathbf{x}_1 = \mathbf{S} \mathbf{x}_0 \quad (8)$$

Generally, the realization of proposed method implies using M -column matrices instead of one column vectors of input signal samples x_n .

$$\mathbf{X}_1^{(M)} = \mathbf{S} \mathbf{X}_0^{(M)} \quad (9)$$

The construction of the $\mathbf{X}_1^{(M)}$ matrix is given in (10).

The $\mathbf{X}_0^{(M)}$ matrix is constructed in a similar manner.

$$\mathbf{X}_1^{(M)} = \begin{bmatrix} x_1 & x_2 & x_3 & \dots & x_{M-1} & x_M \\ x_2 & x_3 & x_4 & \dots & x_M & x_{M+1} \\ x_3 & x_4 & x_5 & \dots & x_{M+1} & x_{M+2} \\ \dots & \dots & \dots & \dots & \dots & \dots \\ x_{N-1} & x_N & x_{N+1} & \dots & x_{N+M-3} & x_{N+M-2} \\ x_N & x_{N+1} & x_{N+2} & \dots & x_{N+M-2} & x_{N+M-1} \end{bmatrix} \quad (10)$$

Similarly, equation (3) can also be given in a modified matrix form

$$\mathbf{x}_1 = \mathbf{W}_0 \mathbf{Z} \mathbf{A} \quad (11)$$

where

$$\mathbf{W}_0 = \begin{bmatrix} 1 & 1 & 1 & \dots & 1 & 1 \\ z_1 & z_1 & z_1 & \dots & z_1 & z_1 \\ z_1^2 & z_2^2 & z_3^2 & \dots & z_{N-1}^2 & z_N^2 \\ \dots & \dots & \dots & \dots & \dots & \dots \\ z_1^{N-2} & z_2^{N-2} & z_3^{N-2} & \dots & z_{N-1}^{N-2} & z_N^{N-2} \\ z_1^{N-1} & z_2^{N-1} & z_3^{N-1} & \dots & z_{N-1}^{N-1} & z_N^{N-1} \end{bmatrix} \quad (12)$$

$$\mathbf{Z} = \begin{bmatrix} z_1 & 0 & 0 & \dots & 0 & 0 \\ 0 & z_2 & 0 & \dots & 0 & 0 \\ 0 & 0 & z_3 & \dots & 0 & 0 \\ \dots & \dots & \dots & \dots & \dots & \dots \\ 0 & 0 & 0 & \dots & z_{N-1} & 0 \\ 0 & 0 & 0 & \dots & 0 & z_N \end{bmatrix} \quad (13)$$

$$\mathbf{A} = [A_1 \ A_2 \ \dots \ A_{N-1} \ A_N]^T \quad (14)$$

Considering (8) and (11) the following equation can be formulated

$$\mathbf{W}_0 \mathbf{Z} \mathbf{A} = \mathbf{S} \mathbf{W}_0 \mathbf{A} \quad (15)$$

finally

$$\mathbf{S} = \mathbf{W}_0 \mathbf{Z} \mathbf{W}_0^{-1} \quad (16)$$

The latest equations shows, that $z_1, z_2, z_3, \dots, z_N$ are the eigenvalues of the matrix \mathbf{S} .

Regarding (9) the matrix \mathbf{S} may be calculated

$$\mathbf{S} = \mathbf{X}_1^{(M)} \mathbf{X}_0^{(M)T} (\mathbf{X}_0^{(M)} \mathbf{X}_0^{(M)T})^{-1} \quad (17)$$

Knowing the $z_1, z_2, z_3, \dots, z_N$ values the complex frequencies (3) $s_1, s_2, s_3, \dots, s_N$ may be easily calculated. Similarly the values of amplitudes $A_1, A_2, A_3, \dots, A_N$ may be derived from (11).

III. PRONY MODEL APPLIED FOR COMPUTATION OF SPECTRAL COMPONENTS IN SIGNALS

The Prony method is a technique for modeling sampled data as a linear combination of exponential functions [8]. Although it is not a spectral estimation technique, the Prony method has a close relationship to the least squares linear prediction algorithms used for AR and ARMA parameter estimation. Prony method seeks to fit a deterministic exponential model to the data in contrast to AR and ARMA methods that seek to fit a random model to the second-order data statistics. Assuming N complex data samples, the investigated function can be approximated by p exponential functions:

$$y[n] = \sum_{k=1}^p A_k e^{(\alpha_k + j\omega_k)(n-1)T_p + j\psi_k} \quad (18)$$

where

$n = 1, 2, \dots, N$, T_p - sampling period, A_k - amplitude,

α_k - damping factor, ω_k - angular velocity, ψ_k - initial phase.

The discrete-time function may be concisely expressed in the form

$$y[n] = \sum_{k=1}^p h_k z_k^{n-1} \quad (19)$$

where

$$h_k = A_k e^{j\psi_k}, \quad z_k = e^{(\alpha_k + j\omega_k)T_p}$$

The estimation problem is based on the minimization of the squared error over the N data values

$$\delta = \sum_{n=1}^N |\varepsilon[n]|^2 \quad (20)$$

where

$$\varepsilon[n] = x[n] - y[n] = x[n] - \sum_{k=1}^p h_k z_k^{n-1} \quad (21)$$

This turns out to be a difficult nonlinear problem. It can be solved using the Prony method, that utilizes linear equation solutions.

If as many data samples are used as there are exponential parameters, then an exact exponential fit to the data can be made.

Consider the p -exponent discrete-time function:

$$x[n] = \sum_{k=1}^p h_k z_k^{n-1} \quad (22)$$

The p equations of (5) may be expressed in matrix from as:

$$\begin{bmatrix} z_1^0 & z_2^0 & \dots & z_p^0 \\ z_1^1 & z_2^1 & \dots & z_p^1 \\ \vdots & \vdots & & \vdots \\ z_1^{p-1} & z_2^{p-1} & \dots & z_p^{p-1} \end{bmatrix} \begin{bmatrix} h_1 \\ h_2 \\ \vdots \\ h_p \end{bmatrix} = \begin{bmatrix} x[1] \\ x[2] \\ \vdots \\ x[p] \end{bmatrix} \quad (23)$$

The matrix equation represents a set of linear equations that can be solved for the unknown vector of amplitudes.

Prony proposed to define the polynomial that has the exponents as its roots:

$$F(z) = \prod_{k=1}^p (z - z_k) = (z - z_1)(z - z_2) \dots (z - z_p) \quad (24)$$

The polynomial may be represented as the sum:

$$F(z) = \sum_{m=0}^p a[m] z^{p-m} = a[0]z^p + a[1]z^{p-1} + \dots + a[p-1]z + a[p] \quad (25)$$

Shifting the index on (5) from n to $n-m$ and multiplying by the parameter $a[m]$ yield:

$$a[m]x[n-m] = a[m] \sum_{k=1}^p h_k z_k^{n-m-1} \quad (26)$$

Equation (9) can be modified into:

$$\sum_{m=0}^p a[m]x[n-m] = \sum_{k=1}^p h_k z_k^{n-p} \left\{ \sum_{m=0}^p a[m] z_k^{p-m-1} \right\} \quad (27)$$

The right-hand summation in (10) may be recognized as a polynomial defined by (8), evaluated at each of its roots yielding the zero result:

$$\sum_{m=0}^p a[m]x[n-m] = 0 \quad (28)$$

The equation can be solved for the polynomial coefficients. In the second step the roots of the polynomial defined by (8) can be calculated. The damping factors and sinusoidal frequencies may be determined from the roots z_k .

For practical situations, the number of data points N usually exceeds the minimum number needed to fit a model of exponentials, i.e. $N > 2p$. In the over determined data case, the linear equation (11) should be modified to:

$$\sum_{m=0}^p a[m]x[n-m] = e[n] \quad (29)$$

The estimation problem is based on the minimization of the total squared error:

$$E = \sum_{n=p+1}^r |e[n]|^2 \quad (30)$$

IV. SIMULATION OF SYSTEM WITH INDUCTION GENERATOR AND CAPACITORS

The wind generator with compensating capacitors is shown in Fig.2. The simulation was done in Matlab using the SimPowerSystem Toolbox [9].

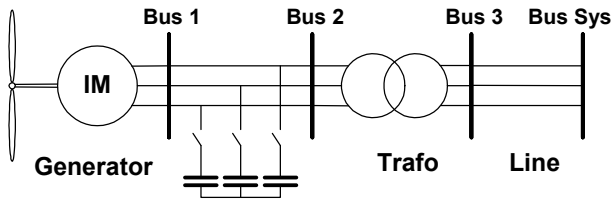


Fig. 2. Induction generator with compensating capacitors.

A wind turbine generates power and accordingly a mechanical torque on the rotating shaft, while the electrical machine produce an opposing electromagnetic torque [4]. In steady state operation, the mechanical torque is converted to real electrical power and delivered to the grid. The power generated by the wind turbine is [4, 6]

$$P = \frac{1}{2} \rho A C_p V^3 \quad (31)$$

and the torque can be found as

$$T = \frac{P}{\omega_s} \quad (32)$$

where ρ - density of air, A - swept area of the blade, C_p - performance coefficient, V - wind speed, T mechanical torque, P - output power of the turbine, ω_s rotor speed of the turbine. At the constant wind speed, the C_p coefficient depends on the rotor speed ω_s and pitch angle and is often presented in a table form [10]. The turbine characteristic used in simulation is shown in Fig. 3.

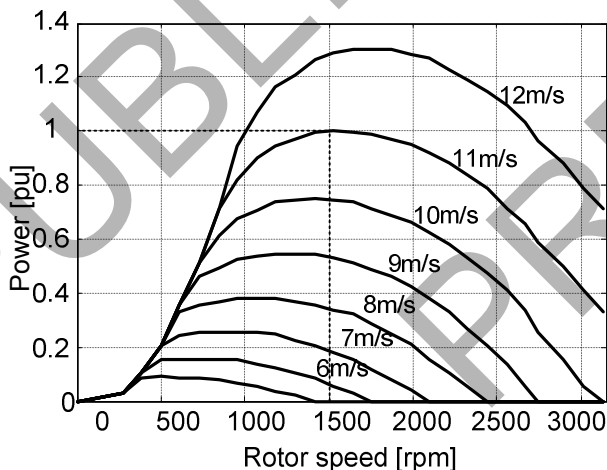


Fig. 3. Induction generator output power vs. angular velocity

The pitch control dynamic can be neglected in power system transient analysis [6]. The simulated generator is a 150 kW, 400 V, 1487 rpm, induction machine. It is connected to the grid through a Dyg 25/0.4 kV distribution transformer which nominal power was varied between 0.5 and 2 MW during the research process and other parameters were set with accordance to [11]. A typical 5 km overhead line [11] connected the generator to a system. The system was represented by equivalent

source with short circuit capacity of 100 MVA and X/R ratio of 7. The induction generator reactive power demand varies with the produced real power [10]. During the research different compensation levels were simulated. Simulation results correlate with measured values [7].

V. RESULTS OF SIGNAL ANALYSIS

The capacitors indicated in Fig. 2 were build as a bank of separately closed units, what is close to practice [7]. In this practical case two-stage phase-compensating capacitors were connected at the wind turbines. One small ($C1=0.5$ mF), for low rotor speed and both ($C1+C2=1.7$ mF), when the wind turbines operated at higher rotor speed.

Transients occurring during switching of the capacitor bank are shown in Fig. 4. Clearly visible are two stages of switching.

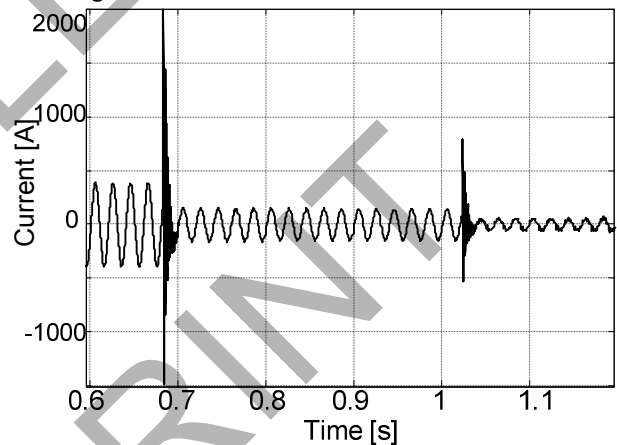


Fig. 4. Currents during two steps of capacitor closing – one phase.

A. Disturbances due to first capacitor switching

The analysis of transients after the first capacitor are analyzed in this chapter. More detailed waveform of the current is shown in Fig. 5.

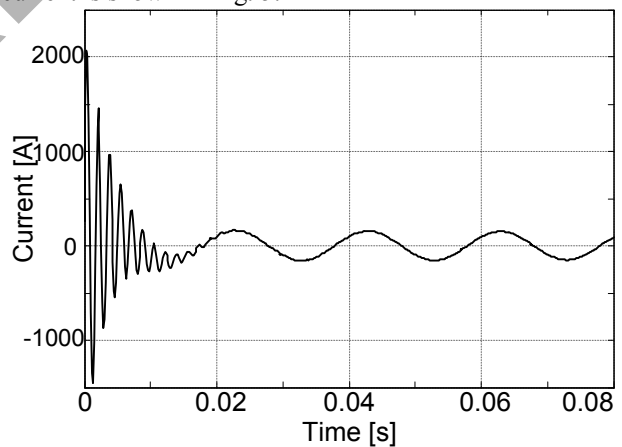


Fig. 5. Transient current during the first step of capacitor closing.

Fourier analysis indicated two spectral components (Fig. 6). However, the computation of amplitude of a decaying component is not accurate using Fourier.

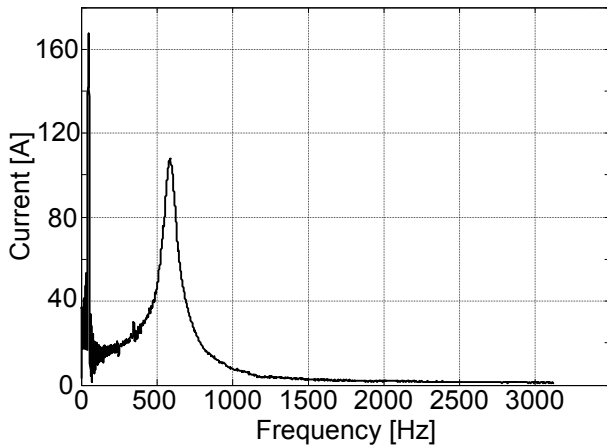


Fig. 6. Fourier transform of the current during first capacitor closing

Therefore Prony and SVD approach were used to compute detailed signal parameters.

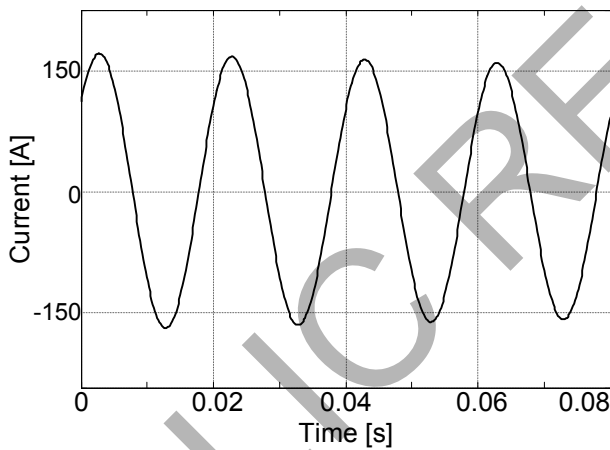


Fig. 7. First component in the current, reconstructed with Prony method

Fig. 7 and 8 depict the main 50 Hz current component and the switching transient reconstructed with parameters given by Prony model.

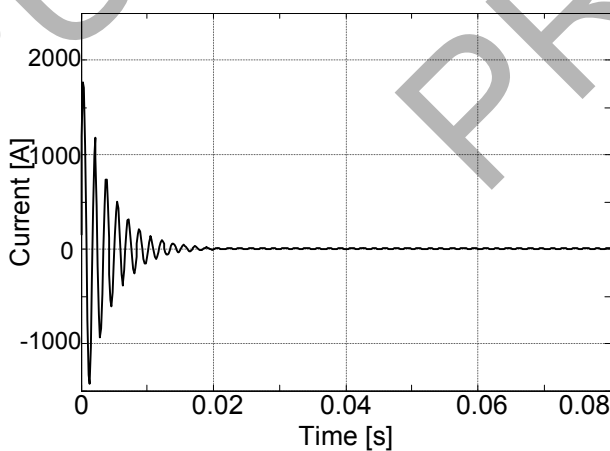


Fig. 8. Second component in the current, reconstructed with Prony method.

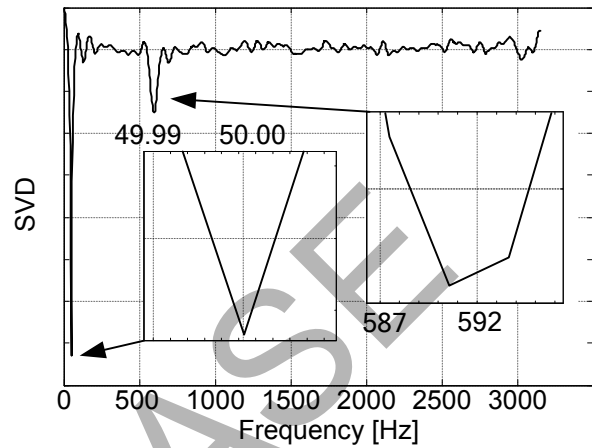


Fig. 9. Two spectral components computed with SVD method

Similar results have been achieved with SVD. Frequencies indicated by Prony are shown in Fig. 9.

Detailed information of the first and second signal component obtained with Prony and SVD model are given in Table I. The information includes the values of amplitude – A , decaying time constant – τ , frequency – f , and initial phase – ψ .

TABLE I
CURRENT COMPONENTS AFTER FIRST CAPACITOR SWITCHING

Signal com. [No.]	I [A]	τ [s]	f [Hz]	ψ [rd]
Prony				
1.	162,9	--	49,86	0,87
2.	2225	0,004	592,2	1,5
SVD				
1.	164,7	--	49,43	0,90
2.	2128,9	0,004	588,2	1,52

B. Disturbances due to second capacitor switching

Similar procedure was applied for the transient current after closing of the second capacitor (Fig. 10).

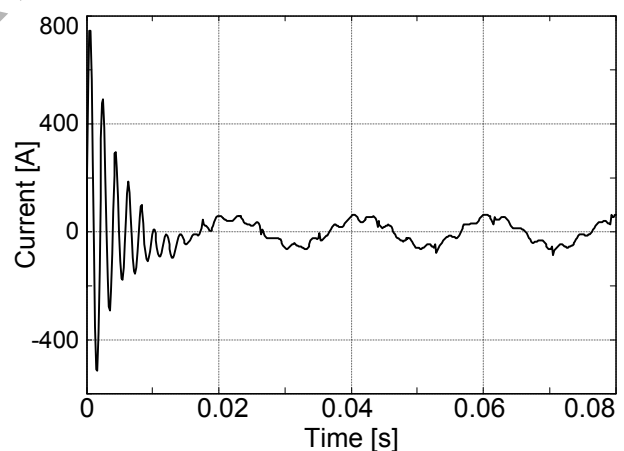


Fig. 10. Current after second capacitor closing

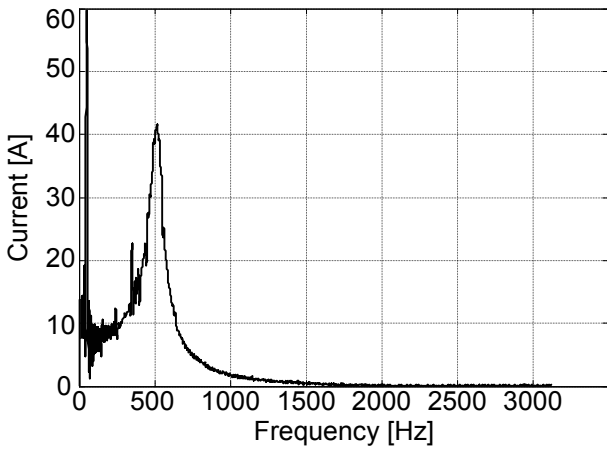


Fig. 11. Fourier transform of the current during second capacitor closing

Fourier transform (Fig. 11) of the current in Fig 10 indicates three components.

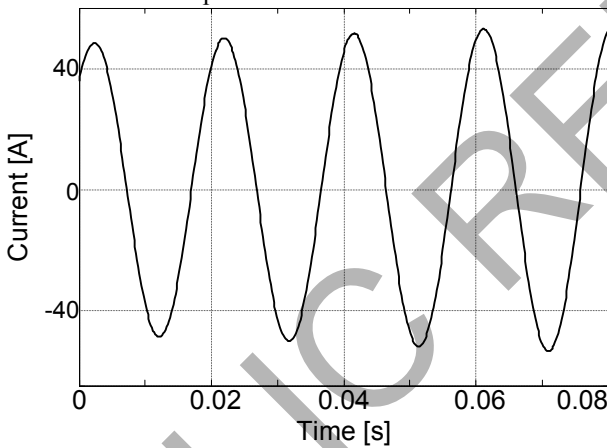


Fig. 12. First component in the current, reconstructed with Prony method

Fig. 13, 13 and 14 depicts the three components given by the Prony model.

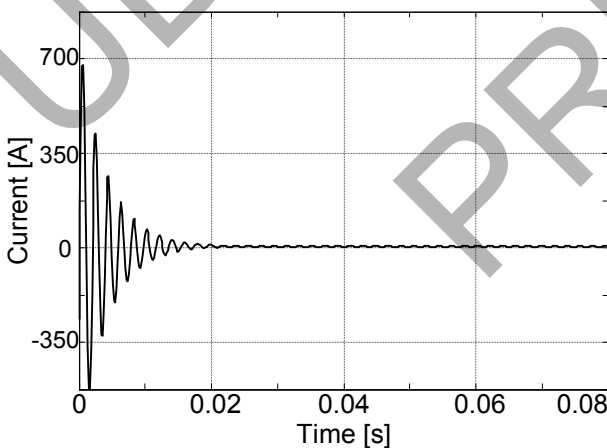


Fig. 13. Second component in the current, reconstructed with Prony method.

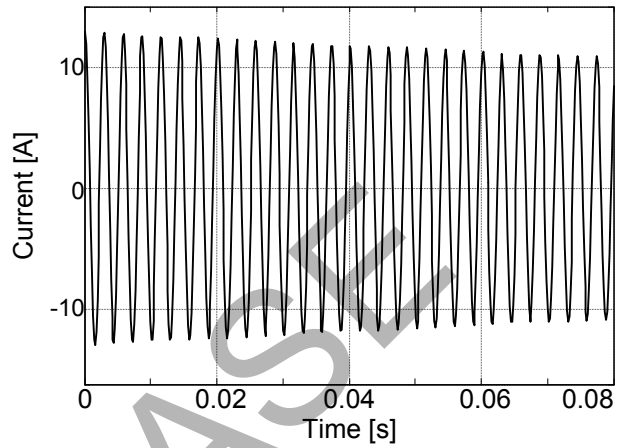


Fig. 14. Second component in the current, reconstructed with Prony method.

Similar results were obtained with SVD method (Fig. 15).

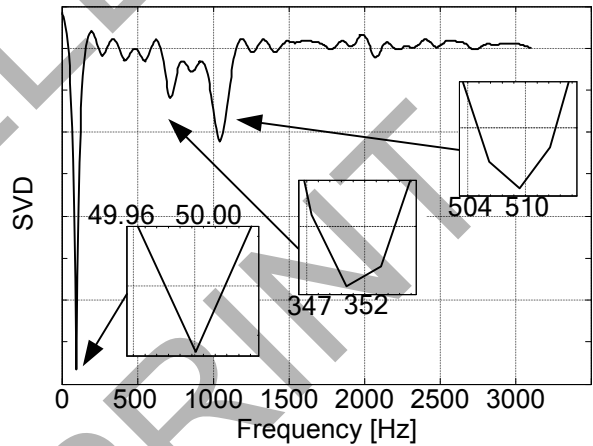


Fig. 15. Three spectral components computed with SVD method

Detailed information of the three components obtained with SVD and Prony method is given in Table II. The information includes the values of amplitude – A , decaying time constant – τ , frequency – f , and initial phase – ψ .

Signal com. [No.]	I [A]	τ [s]	f [Hz]	ψ [rd]
Prony				
1.	51.21	--	50.97	0.75
2.	13.84	0.44	349.2	0.30
3.	831.0	0.004	519.2	1.91
SVD				
1.	48.85	--	50.45	0.76
2.	12.08	0.47	352,11	0.32
3.	736,8	0.004	512.27	2.01

VI. CONCLUSIONS

The research results show, that the Prony model and SVD method are useful for transient estimation in systems with wind generators and compensating capacitors. Those methods enabled accurate estimation of amplitude, time constant, phase and frequency of transients' components of simulated signals. The current waveform and its parameters depend on the capacitor to be switched. Those dependences could be observed during simulation.

Application of both Prony Model and SVD method required a signal model. Fourier transform, as non parametric method, did not require a signal model or even the number of components, but could not compute signal parameters besides frequency. Two signal components were predefined, so the rest was considered noise.

The order of the signal model could be easily extended to detect additional components. Both methods delivered similar results, however, application of Prony model seems more suitable for estimation of signal parameters.

REFERENCES

- [1] Hammons T.: *Status of Integrating renewable electricity production in Europe into the grids*. Proceedings of Universities Power Engineering Conference, Cork (Ireland), 2005, p.73
- [2] Hanzelka Z., Mroz M., Pawelek R., Pitek K.: *Quality Parameters of 15kV supply voltage after connection of wind farms-case study*. Proceedings of Conference on Harmonics and Quality of Power, Cascais (Portugal), September 2006, on CD, paper ID 124
- [3] Quinonez-Varela G., Cruden A., Grant A. D., Castaneda A.: *Electrical Integration Assessment of Wind Turbines into Industrial Power System: The Case of a Mining Unit*. Proceedings IEEE Power Tech Conference, Porto (Portugal), September 2001, paper ID DRS3-292
- [4] Chompoo-inwai Ch., Wei-Jen L., Fuangfoo P., Williams M., Liao J. R.: *System Impact Study for the Interconnection of Wind Generation and Utility System*. IEEE Trnas. on Industry Applications, vol. 41, January 2005, pp 163-168
- [5] IEC 61400-21 *Wind turbine generator systems. Part 21: Measurement and assessment of power quality characteristics of grid connected wind turbines*.
- [6] Tabesh A., Iravani R.: *Transient Behavior of Fixed-Speed Grid-Connected Wind Farm*. Transactions of International Conference on Power Systems Transients, Montreal (Canada), June 2005, Paper No. IPST05-068
- [7] Thiringer T.: *Power Quality Measurements Performed on a Low-Voltage Grid Equipped with Two Wind Turbines*. IEEE Trans. on Energy Conversion, vol. 11, September 1996, pp. 601-606
- [8] Lobos T., Rezmer J., Kolin H.-J.: *Analysis of Power System Transients using Wavelets and Prony Method*. Proceedings IEEE Power Tech Conference, Porto (Portugal), September 2001, paper ID EMT-103
- [9] The Mathworks: *SimPowerSystems User's Guide*. The Math Works Inc., 2006
- [10] Lubosny Z.: *Wind Turbine Operation in Electric Power Systems*. Springer Verlag, Berlin Heidelberg (Germany), 2003
- [11] SIEMENS: *Electrical Engineering Handbook*, 1987
- [12] Bhatti A. M.: *Practical Optimization Methods*. Springer Verlag, New York (USA), 2000, pp. 288-302
- [13] Larsson A. Thiringer T.: *Measurement on and Modelling of Capacitor-Connecting Transients on a Low-voltage Grid Equipped with Two Wind Turbines*. Proceedings IPST Conference, Lisbon (Portugal), 1995
- [14] T Lobos, T. Kozina, H.-J. Koglin: "Power system harmonics estimation using linear least squares method and SVD", in IEE Proc., Generation Transmission and Distribution, vol. 148, No. 6, 2001, p. 567-572,
- [15] T. Will: "Introduction to the Singular Value Decomposition" Available: <http://www.uwlax.edu/faculty/will/svd/index.html>
- [16] L. Hexi, W. Guorong, Shi Y.; Z. Weimin, "The Automatic Recognition of Welding Targets Based on Normalized SVD of Image Matrix" in Proc. International Conference on Mechatronics and Automation, ICMA 2007 ,August 2007, pp. 3100 - 3104

Electrical Energy Measurements for Rome LV Customers by Distributed Web-Server Instruments

Fabio Leccese

Electronic Engineering Department, University of Roma "Roma Tre"
Via della Vasca Navele n.84, 00146, Roma, Italy, tel. +390657337085, fax +390657337101

leccese@uniroma3.it

Abstract-Power Quality (PQ) measurements for low voltage (LV) customers, domestic and business, have been carried out in order to detect the behaviour of the electric net over time and the quality of the electric energy being bought. In order to measure PQ parameters, we realized an instrument based on web server personal computers, which are common in office or in domestic environment. This allows us to conjugate the high PC calculus capability with the possibility to send data via internet to a central server; moreover, the use of the existing hardware infrastructure makes the instruments extremely cheap.

I. INTRODUCTION

With the constant rise of raw materials' prices and the consequent increase of the power supply purchase costs, the necessity to evaluate the quality of this good is becoming more and more important[1,2,3]. In fact, the low prices of the power supply have, in the recent past, discouraged PQ analyses leaving them only to professionals and experts that normally work in the research environment. In the electrical market, only big companies have specialists, the energy managers, able to buy the energy needed for the proper functioning of business [4] with the idea to try to make the costs, related to consumptions, matched with the quality of the energy purchased. Anyway the absence of continuative measurements carried out on the electrical net makes impossible to evaluate the quality of electrical energy, forcing the companies to adopt alternative solutions to compensate the possible lack of quality. It is the case of big companies like Telecom Italia that, in order to assure the continuity of the service, adopts complex and redundant electric plants, but also of LV customers that, for example, use UPS connected to their PCs. This is reflected into additional costs which are almost exclusively covered by the customers[5].

LV customers are particularly affected by this problem: both because their little commercial dimensions lower their capability to bargain over the price of power supply and, above all because they cannot fully realize their needs and expectations towards this good. This incapacity is strictly due to the "lack of knowledge" of the electrical energy since we do not have biological sensors and so we have big difficulties to estimate it [6].

To compensate this situation the first thing to do is constantly measuring the electrical net evaluating the PQ parameters. Currently this is difficult to obtain because of the high costs of high accuracy PQ analyzers [7].

In this article we propose the results of a first measurements campaign in the Rome area realized by means of instruments distributed over the territory, inserted in LV plant, with the aim to analyze the PQ parameters of power supply for LV customers. After a discussion regarding the design choices for the instrument, we will show the first monitoring results.

II. THE LOCAL INSTRUMENT

The instruments are conceived to be cheap with the idea to be easily placed in the final customers' site in order to realize a net more and more widespread. The peculiarity of this instrument is the exploitation of an already existent web architecture for other aims. In fact, inside offices, shops or houses, LV customers do own servers, which are always active and constantly connected to the internet. We thought of using the high calculus capability of these PCs, often not adequately exploited, to locally elaborate the electrical energy samples coming from an analogical interface connected to the PC audio card that acts as an A/D card. After the data acquisition and elaboration, the results are sent to a central server placed at the University of Roma Tre. Using existing PCs, it is obvious that the costs are reduced, as compared to the analogical interface and to the set up procedure.

Currently, the local instrument is composed of three principal parts:

- a PC, which the customers already own and often used for other aims; for example as web server or net data storage system, always switched on and always connected to the internet with an ADSL line;
- an analogical interface with sensors for current i and voltage connected to the stereo "line in" of the PC audio card;
- the software capable of analyzing PQ parameters.

A. The PC and the Audio Card Calibration

It is not important the model of the PC, the only significant element is that it must have an audio card. Therefore, it is necessary, to characterize some important parameters as R_{in} and the maximum input voltage and calibrate it, to verify its transfer function and, in case it is necessary, equalize it by software.

A preventive calibration of the instrumentation, necessary to characterize the audio card, it is also necessary. We used a Yokogawa FG120[8] function generator calibrated, both in

amplitude and in frequency, in a specialized Anritsu laboratory certified by the Italian Calibration System. For the first we connected the function generator to a digital multimeter Fluke 8840A[9] with true RMS option and to a Lecroy Waverunner LT342[10] oscilloscope to verify if the Yokogawa fixed V_{pp} sinusoidal waves output would be constant in the time. By this test we verified that the function generator gives voltage linear values. For the frequency calibration we used an Anritsu MS2691A[11] spectrum analyzer. Thanks the “flatness function”, it is possible to record and to show a frequency array spaced of 50 Hz starting from 50 Hz up to 1500 Hz and pre fixed on the function generator.

Figures 1a and 1b show the calibration bench and the linear response of the Yokogawa on the oscilloscope monitor.

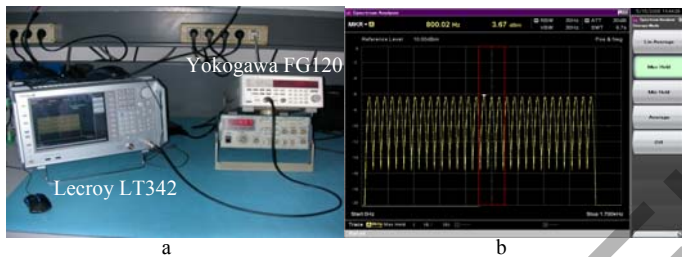


Figure 1. Calibration instrumentations bench (a) and the response of the Yokogawa FG120 function generator (b).

The function generator low secondary harmonics emissions are reported in table 1 for a fundamental of 50 Hz:

TABLE I
SECONDARY HARMONICS EMISSION FOR YOKOGAWA FG120

Frequency	50 Hz fundamental	100 Hz	500 Hz	1 kHz	1.5 kHz
Amplitude	0 dB reference amplitude	-73 dB	-80 dB	-82 dB	-85 dB

After the function generator calibration we determined the audio card characteristics that are summarized in table 2 for the first PC.

TABLE II
AUDIO CARD CHARACTERISTICS

No distortion input dynamic	Nominal input voltage	Input Resistance	Low cut off frequency	Crosstalk
$V_{max} = 2.8 V_{pp}$ [@ 1 kHz]	$V_n = 2 V_{pp}$	$R_{in} = 10 k\Omega$	17 Hz	none

The first step has been to determine the input impedance of the line-in building a measurement circuit by the following electric scheme (Fig. 2).

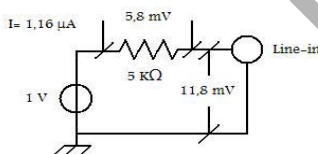


Figure 2. Measurement circuit to determine the audio card input impedance.

Applying a voltage reference of 1 V coming from the function generator and using a measurement resistance of 5 kΩ ($\pm 0.1\%$), we measured a voltage of 5.80 mV on the digital multimeter. Using this it is possible to determine the current that flows on the resistor equal to 1.16 mA and so the R_{in} equal

to: $R_{in} = 11.8 \text{ mV} / 1.16 \mu A = 10.17 \text{ k}\Omega$.

The procedure has been executed for both channels leaving without load the channel not analyzed.

After that, to determine possible crosstalk phenomena between the two input channels, we used a 1 kΩ resistor on the channel previously left idle, observing if on the other channel was induced interference. Repeated this procedure for both channels we analyzed the data by an FFT don't checking interference.

Then we verified the input stage dynamic characterizing the maximum input voltage to avoid saturation phenomena. We fixed the Yokogawa sinusoidal output voltage to a frequency of 1 kHz and a incremental amplitude started from 0.2 V_{pp} up to the saturation limit characterized at 2.8 V_{pp} . After this limit the card saturates and distortion phenomena start to appear.

Another test allows us to determine the audio card low cut off frequency: fixing the Yokogawa output voltage to a value of 2 V_{pp} we varied the frequency decreasing it starting from a value of 1024 Hz up to 2 Hz. Fig. 3 shows that the low cut off frequency is equal to 17 Hz (-3 dB) while to 50 Hz we have -1 dB. Fig. 3 shows the audio card low frequency response.

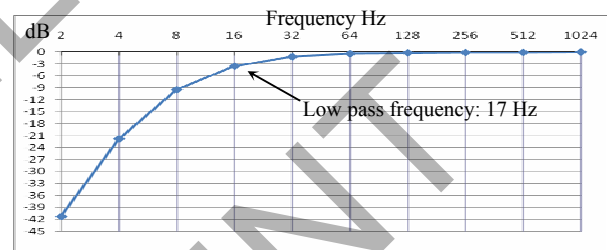


Figure 3. Audio card frequency characteristic.

The latter test allows verifying the real sampling frequency used by the audio card (nominally 8 ksamples/s). We used the Yokogawa FG120 function generator to record in one second a sinusoidal signal of 50 Hz, counting how many samples were contained in ten periods. This procedure permits to determine the exact sampling time to be correctly taken in account in DFT.

B. The Analog Interface

We used, as voltage sensor, a transformer LEM LV 25-P[12] while, as current sensor, a current transformer LA 55-P[13] both suited for electronic measurements of DC and AC voltages.

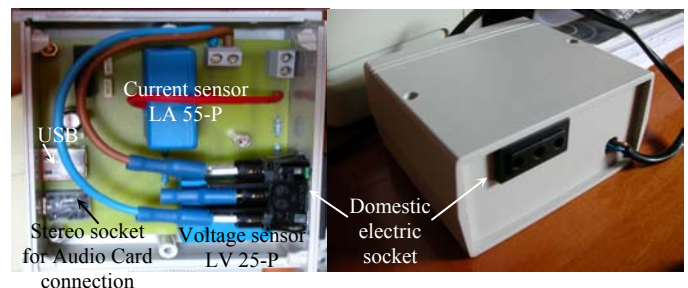


Figure 4. Analogical interface circuit.

The first shows a bandwidth of 0 ÷ 40 kHz while the second 0 ÷ 200 kHz. They are active sensors and need a supply of ± 5

V, carried out by a DC/DC integrated converter fed through the USB port of the PC. Every sensor is connected to a channel of the stereo socket of audio card by a stereo jack. In Fig. 4 is shown the analog interface inserted in a proper box.

C. The Software

Exploiting the Windows DLL[15], in particular the “winmm.dll”, it is possible to manage the audio card to acquire data from the line-in. The software, developed in Visual Basic 6.0[16], allows us to choose the sampling frequency, to acquire data for a prefixed time window and to elaborate the data by a DFT algorithm. To not overload the server and so to better manage the acquisition with the server activities of the PCs, we decided to acquire 1 buffer every ten seconds. Each buffer is composed by 8,192 samples obtained at a sampled frequency of 8 kHz, frequency standard previewed by the acquire card, for a total acquisition time equal to 1.024 s. After the acquisition the software elaborates the data and the next acquisition starts for 10 s after the previous. With this temporization the principal activities of the server is not limited.

The software gives us the frequency of the fundamental and of the harmonics with a resolution of 0.1 Hz and with an accuracy, joined to the previous audio card sample rate calibration, equal to ± 20 ppm. It gives the true RMS value of Voltage and Current with accuracies of $\pm 0.2\%$ and $\pm 0.5\%$ respectively joined with the multimeter used during the calibration. Moreover it gives the percentage of harmonics up to 24th respected the fundamental (THD) both for current and voltage, Apparent, Active, Reactive and Deforming Power.

If the software doesn't identify an exceeding of norm limits[14] for also only one of the analyzed parameters, the samples are immediately deleted and the software records the values of the parameters in a file with date and time.

Otherwise, if the norm limits are exceeded, the software saves also a second file with the series of the samples acquired. In this way, it is possible to verify the samples to establish what problem has been occurred during the acquisition.

During the program debugging, it has been useful to have a visualization section of the program to check the exactness of the data elaboration and to facilitate the visualization of the harmonics level. Fig. 5 shows the visualization section of the program. This section is deactivated in the normal acquisition process.

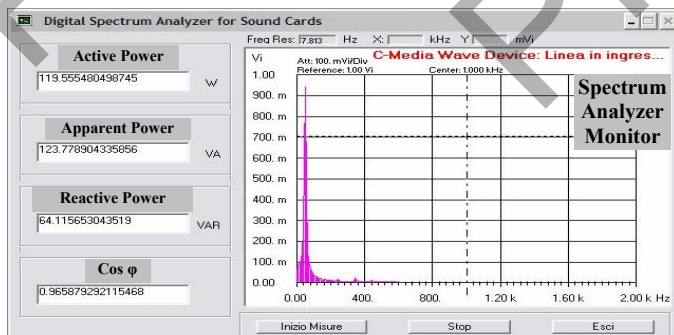


Figure 5. Graphic section of the software.

III. EARLY RESULTS

At the moment, two instruments are active, placed in two different parts of Roma: at Roma Tre University and in an house in Torvaianica in the south part of the city (respectively star and square on the map of Fig. 6) where the PCs are normally used also as server. In the first case the load is the PC itself, in the second case, the analogic interface is connected to a multiple socket connected to an A++ efficiency energy class refrigerant and an electric oven. There are no differences in the electrical energy supply, in fact both the buildings are simply connected to the main without specific dedicated lines. We acquired data for 10 days and the results of our analysis are following synthesized. In the first case the RMS average voltage is 217 V with a standard deviation of 1.095 V and it never exceed the limit. Being the PC a no linear load it hasn't significant to talk about power, instead it is very interesting to see the current input due to its PWM supplier. The next graph shows the voltage and current trend for this load and it has been almost always the same in these ten days.



Figure 6. Position of instruments in Rome territory.

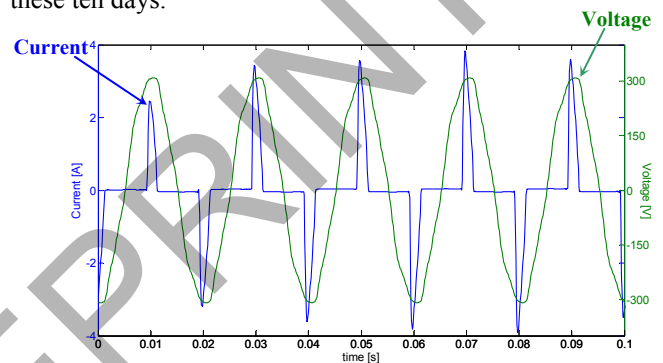


Figure 7. Voltage and Current trend for a PC load.

How it can be seen, the voltage waveform is not a perfect sine wave, but it is significantly distorted. This is clearly due to the kind of loads inside the University that are mainly no linear as computers and instrumentations.

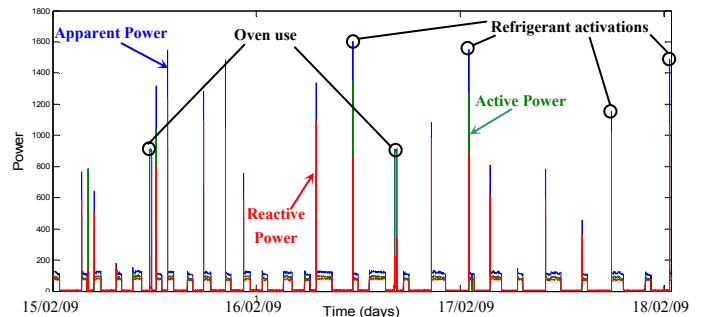


Figure 8. Active, Reactive and Apparent trend for three days (15-18/02/2009) of the second site.

For the second site the RMS average value is 238 V with a standard deviation of 2.2 V and it exceeds the limit of 2.2%. In this case the type of load makes extremely interesting the power analyses. Fig. 8 shows the Active, Reactive and Apparent Power of data acquired by the instrument during three normal working days (15-18/02/2009).

It is possible to know the asynchronous activations and the deactivations of the refrigerant and sometimes the activations and the deactivations of the oven. In case of activation of the only refrigerant the power factor has an average value of 0.78. At the start of the activation, the apparent power reaches a peak of 1.6 kVA. The contribution of the electric oven is almost exclusively active power with a value of about 800 W and, consequently, the power factor is practically equal to 1.

In both cases the frequency and the THD are below the norm limits.

Table 3 shows, respectively for the two sites, how many times, expresses in percentage respect the total number of acquisitions, the nth harmonic exceeds the norm's limit, the average value respect the fundamental and the correspondent standard deviation. As it is possible to see in the first case, the level of the second harmonic often exceeds the limit. In the second site, cause the high level of the fundamental, the harmonics exceeds the limits few times than the first site.

TABLE III
HARMONIC DISTORTION TREND FOR UNIVERSITY (A) AND TORVAIANICA (B) SITES

Harmonics Order	Out of Limits %		Average % compared the fundamental value		Standard Deviation (V)	
	(A)	(B)	(A)	(B)	(A)	(B)
2 nd	12.288	0.992	1.358	0.6993	0.601	0.363
3 rd	0.004	0	1.584	0.4595	0.258	0.243
4 th	0.004	0.036	0.222	0.2903	0.136	0.158
5 th	0	0	1.104	1.5573	0.239	0.392
6 th	0.013	0.4755	0.134	0.1618	0.072	0.103
7 th	0.004	0	1.309	0.3813	0.220	0.178
8 th	0.004	0.0011	0.111	0.1176	0.060	0.078
9 th	0.477	0	0.946	0.2388	0.191	0.111
10 th	0.004	0	0.109	0.0990	0.055	0.061
11 th	0	0	0.945	0.1366	0.191	0.073
12 th	0.009	0	0.085	0.0856	0.042	0.0449
13 th	0	0	0.795	0.1093	0.207	0.060
14 th	0.004	0	0.065	0.0757	0.036	0.042
15 th	0.319	0.0119	0.290	0.1611	0.095	0.088
16 th	0.004	0	0.075	0.0668	0.040	0.039
17 th	0.004	0	0.229	0.0926	0.085	0.050
18 th	0.004	0	0.059	0.0572	0.028	0.03
19 th	0	0	0.138	0.0712	0.060	0.039
20 th	0.004	0	0.048	0.0499	0.025	0.030
21 st	0.004	0	0.539	0.0687	0.028	0.036
22 nd	0.004	0	0.049	0.0444	0.032	0.030
23 rd	0	0	0.049	0.0575	0.025	0.032
24 th	0.004	0	0.046	0.0408	0.022	0.026

How it could be expected, due to the non linear loads present, the THD of the University site is higher than the second site. The 2nd harmonic overshoots more often than the others because the instrument site is close to a mechanic laboratory running an old 1,5 kVA power drill that uses a direct current brake for its AC motor. This brake uses a half-wave rectifier that produces this type of distortion.

IV. CONCLUSIONS

Both cause the increase of energy costs and a more high sensibility towards energy problems, mainly linked with the possible saving in case of anticipate breaking of electrical devices, the needs to control and verify the quality of electrical energy is more and more pressing.

In this article we presented a new instrument based on an analogical self made interface connected between the mono phase LV main and the PC audio card.

The instrument exploits the big calculus capacity of PC so allowing an easy elaboration of the samples and an easy memorization of the power quality normed parameters analyzed. Exploiting an elaborative structure already existent and bought for other applications, the instrument is extremely cheap and so buyable also by LV, domestic or business, customers. The low costs will make easy a rapid distribution on territory of these instruments particularly recommended for those little shops or offices that have a server PC continuously active but not fully used. The instrument calibration process has been also described.

Two instruments have been constructed and, at the moment, they constantly acquire information about the net.

The early results show that a non linear load placed near the first site produces an increase of the 2nd on the electrical LV net, whose effects should be better analyzed and understood, verifying them on all the other devices connected to the same net. Moreover the voltage amplitude and current behaviors over time justify our interests in a better knowledge of the electric net by means of continuous measurements with the aim to correlate possible electrical machine malfunctionings with disturbances coming from the electrical net.

The next steps will be an improvement of the software that has to include an automatic calibration section for the PC audio card to avoid a tiring calibration job, and to increase the acquisition points on territory to know as better as possible the PQ parameters trend.

REFERENCES

- [1] R.C. Dugan, M. F. McGranaghan, S. Santoso, H. W. Beaty, *Electrical Power Systems Quality, Second Edition*, McGraw-Hill, 2004, vol. I, ISBN: 0-0713-8622-X.
- [2] J. Arrillaga, N.R. Watson, S. Chen, *Power System Quality Assessment*, John Wiley & Sons, 2000, ISBN 0 471 98865 0.
- [3] E.F. Fuchs, M.A.S. Masoum, *Power Quality in Power Systems and Electrical Machines*, ISBN 978-0-12-369536-9.
- [4] M. Caciotta, F. Leccese, T. Trifirò, "From Power Quality To Perceived Power Quality," *The IASTED International Conference on Energy and*

Power Systems EPS 2006, 29-31 March 2006, Chiang Mai, Thailand, pp. 94-102, ISBN CD: 0-88986-586-8.

- [5] F. Leccese, "Rome, a first example of Perceived Power Quality of electrical energy: the telecommunication point of view", *International Telecommunications Energy Conference INTELEC 2007*, September 30 – October 4 2007, Rome, Italy, pp. 369-372, ISBN: 978-1-4244-1628-8, IEEE Catalog Number: CFP07INTC, Library of Congress: 88-656128.
- [6] F. Leccese, "A first analysis of Perceived Power Quality for domestic customers," *12th IMEKO TC1 & TC7 Joint Symposium on Man Science & Measurement*, September, 3 – 5, 2008, Annecy, France, ISBN: 2-9516453-8-4.
- [7] Internet information about PQ Analyzers of several producers.
- [8] Yokogawa FG120 User Manual.
- [9] Fluke 8840A Digital Multimeter User Manual.
- [10] Lecroy Waverunner LT342 User Manual.
- [11] Anritsu MS2691A Spectrum Analyzer User Manual.
- [12] LEM LV 25-P Datasheet.
- [13] LEM LA 55-P Datasheet.
- [14] CEI EN 50160 "Voltage Characteristics of Electricity supplied by public distribution systems."
- [15] MSDN: Microsoft Developer Network.
- [16] Visual Basic 6.0 Manual.

Optimal Capacitor Placement on Interconnected Distribution Systems in Presence of Nonlinear Loads Using Genetic Algorithms

Ahmad Galal Sayed (1), Hosam K.M. Youssef (2), Member, IEEE

¹Engineering Consultants Group, Cairo, Egypt

²Electric power and machine Dept., Faculty of Engineering, Cairo University, Egypt

Abstract- Due to simplicity of analysis of radial distribution systems, all previous work studied the effect of nonlinear loads on the optimal solution of the Capacitor Placement Problem (CPP) on only radial distribution systems. The study of the optimal capacitor placement on interconnected distribution systems in presence of nonlinear loads using Genetic Algorithms (GA) is presented in this paper. Results (power losses, operating conditions and annual benefits) are compared with that obtained from radial and loop distribution systems. Computational results obtained showed that the harmonic component affects the optimal capacitor placement in all system configurations. When all loads were assumed to be linear, interconnected and Loop system configurations offer lowest power losses and best operating conditions rather than the radial system configuration while radial system configuration offer best annual benefits due to capacitor placement. In distorted networks, interconnected systems configuration offer lower power losses, best operating conditions and best annual benefits due to capacitor placement.

I. INTRODUCTION

Electric power is supplied to final users by means of Medium Voltage (MV) or Low Voltage (LV) distribution systems, their structures and schemes can differ significantly according to loads location. Overhead lines with short interconnection capabilities are mostly employed in rural areas, whilst cables with a great number of lateral connections for alternative supplies are widespread used in urban areas.

Most power distribution systems are designed to be radial, to have only one path between each customer and the substation. The power flows exclusively away from the substation and out to the customer along a single path, which, if interrupted, results in complete loss of power to the customer. Its predominance is due to two overwhelming advantages: it is much less costly than the other two alternatives (loop and interconnected systems) and it is much simpler in planning, design, and operation.

An alternative to purely radial feeder design is a loop system, which has two paths between the power sources (substations, service transformers) and each customer. Equipment is sized and each loop is designed so that service can be maintained regardless of where an open point might be on the loop. Because of this requirement, whether operated

radially (with one open point in each loop) or with closed loops, the basic equipment capacity requirements of the loop feeder design do not change. In terms of complexity, a loop feeder system is only slightly more complicated than a radial system. Power usually flows out from both sides toward the middle, and in all cases can take only one of two routes. Voltage drop, sizing, and protection engineering are only slightly more complicated than for radial systems.

Interconnected distribution systems are the most complicated and costly but most reliable method of distributing electric power. An interconnected distribution system involves multiple paths between all points in the network. Interconnected systems provide continuity of service (reliability) far beyond that of radial and loop designs: if a failure occurs in one line, power instantly and automatically re-routes itself through other pathways.

Interconnected distribution systems are more expensive than radial distribution systems, but not greatly so in dense urban applications, where the load density is very high, where the distribution must be placed underground, and where repairs and maintenance are difficult because of traffic and congestion, interconnected systems may cost little more than loop systems. Interconnected systems require little more conductor capacity than a loop system. The loop configuration required "double capacity" everywhere to provide increased reliability. Interconnected systems is generally no worse and often needs considerably less capacity and cost, if it is built to a clever design and its required capacity margins are minimized.

The solution procedures of the Capacitor Placement Problem (CPP) start with performing a load flow analysis to analyze the steady-state performance of the power system prior to capacitor placement and after capacitor placement and to study the effects of changes in capacitor sizes and locations.

The biggest advantages of the radial system configuration, in addition to its lower cost, are the simplicity of analysis and predictability of performance. Because there is only one path between each customer and the substation, the direction of power flow is absolutely certain. Equally important, the load on any element of the system can be determined in the most straightforward manner by simply adding up all the customer loads "downstream" from that piece of equipment. Because

load and power flow direction are easy to establish in radial distribution system, voltage profiles can be determined with a good degree of accuracy without resorting to exotic calculation methods; equipment capacity requirements can be ascertained exactly; capacitors can be sized, located, and set using relatively simple procedures (simple compared to those required for similar applications to non-radial (loop and interconnected) system designs, in which the power flow direction is not a given).

The interconnected distribution systems are much more complicated than other forms of distribution, and thus much more difficult to analyze and operate. There is no "downstream" side to each unit of equipment. This complicates load estimation, power flow analysis, and protection planning.

Due to simplicity of analysis of radial distribution systems, all previous work studied the effect of nonlinear loads on optimal solution of CPP on only radial distribution systems. The study of the optimal placement and sizing of fixed capacitor banks placed on distorted interconnected distribution systems using Genetic Algorithms (GA) is presented in this paper. Results (power losses, operating conditions and annual benefits) are compared with that obtained from radial and loop distribution systems. The radial, loop and interconnected distribution systems models are obtained by suitably simplification of a typical Italian grid. Commercial package ETAP PowerStation 4.0 program is used for harmonic load flow analysis, the proposed solution methodology is implemented in Microsoft Visual Basic 6 programming language.

II. PROBLEM FORMULATION

A. Assumptions

The optimal capacitor placement problem has many variables including the capacitor size, location, capacitor cost, voltage and harmonic constraints on the system. There are switchable capacitors and fixed type capacitors in practice. However, considering all variables in a nonlinear fashion will make the placement problem very complicated. In order to simplify the analysis, only fixed type capacitors are considered with the following assumptions:

- 1) *The system is balanced.*
- 2) *All the loads are constant*

B. Capacitor size and cost

Only the smallest standard size of capacitors and multiples of this standard size are allowed to be placed at the buses to have more realistic optimal solution. The capacitor sizes are treated as discrete variable and the cost of the capacitor is not linearity proportional to the capacitor size, this makes the formulated problem a combinatorial one.

C. Objective Function

The objective of the capacitor placement problem is to reduce the total energy losses of the system while striving to minimize the cost of capacitors installed in the system. The objective function consists of two terms. The first is the cost of

the capacitor placement and the second is the cost of the total energy losses.

The cost associated with capacitor placement is composed of a fixed installation cost, a purchase cost and operational cost (maintenance and depreciation). The cost function described in this way is a step-like function rather than a continuously differentiable function since capacitors in practice are grouped in banks of standard discrete capacities with cost not linear proportional to the capacitor bank size.

It should be pointed that since the objective function is non-differentiable, all nonlinear optimization techniques become awkward to apply.

The second term in the objective function represents the total cost of energy losses. This term is obtained by summing up the annual real power losses for the system.

D. Operational Constraints

Voltages along the feeder are required to remain within upper and lower limits after the addition of capacitors on the feeder. Voltage constraints can be taken into account by specifying the upper and lower bounds of the magnitude of the voltages. The distortion of voltage is considering by specifying for maximum total harmonic distortion (THD) of voltages and the maximum number of banks to be installed in one location is taken into account.

E. Mathematical Representation

The capacitor placement problem is expressed mathematically as shown below:

$$\text{Min } F = K_p P_{\text{loss}} + \sum_{j=1}^J K_j^c Q_j^c \quad (1)$$

Subject to:

$$V_{\min} \leq |V_j| \leq V_{\max} \quad (2)$$

$$THD_j \leq THD_{\max} \quad (3)$$

$$Q_j^c \leq Q_{\max}^c \quad (4)$$

Where

$$Q_{\max}^c = LQ_0^c \quad (5)$$

- F The total annual cost function.
- K_p Annual cost per unit of power losses.
- P_{loss} The total power losses.
(Result from ETAP PowerStation Harmonic Load Flow Program).
- J Number of buses.
- K_j^c The capacitor annual cost/kvar.
- Q_j^c The shunt capacitor size placed at bus j.
- V_j The rms voltage at bus j.
(Result from ETAP PowerStation Harmonic Load

	Flow Program).
V_{\min}	Minimum permissible rms voltage.
V_{\max}	Maximum permissible rms voltage.
THD_j	The total harmonic distortion at bus j. (Result from ETAP PowerStation Harmonic Load Flow Program).
THD_{\max}	Maximum permissible total harmonic distortion.
Q_{\max}^c	Maximum permissible capacitor size.
L	An integer.
Q_0^c	Smallest capacitor size.

Bounds for (2), (3) are specified by the IEEE-519 standard [1].

III. GENETIC ALGORITHM

A. Solution Algorithm

Combinatorial optimization problems can be solved either by exact or by approximate methods. In exact methods, all the feasible solutions are evaluated and the best one is selected as the optimal solution. However, exact methods are impractical when a real-life problem is to be evaluated. In this paper, GA will be used for the solution of CPP.

B. Genetic Algorithm Framework

There are four components in the design of a GA-based solution methodology. These include the initialization of the algorithm, fitness evaluation, selection and genetic operators.

Algorithm initialization is the process of randomly generating a set of initial feasible solutions forming the so-called "initial population". The number of these solutions is referred to as the "population size". Each iteration in a genetic algorithm, known as a "generation", results in a new set of feasible solutions.

Genetic algorithm needs some fitness measure to determine the relative 'goodness' of a particular solution. This can be obtained either by direct evaluation of the objective function or by some other indirect means. Fitness evaluation is the criterion guiding the search process of a genetic algorithm.

In genetic algorithms, parents are selected to produce offspring. Selection process can be carried out in different ways as discussed before in chapter three.

Genetic operators are the probabilistic transition rules employed by a genetic algorithm. A new and improved population is generated from an old one by applying genetic operators. Operators used by genetic algorithms include crossover and mutation.

Crossover is the process of choosing a random position in the solution and swapping the characters around this position

with another similarly partitioned solution. The random position is referred to as "the crossover point". In other words, crossover defines the outcome as gene exchange. Crossover operator proved very powerful in genetic algorithms. Mutation is the process of random modification of a particular value of a solution with a small probability. Mutation is applied to alter some genes in the solutions. When a gene exchange resulting from application of a crossover operator is not meeting appropriate restriction, mutation might be very helpful in providing a proper gene exchange amendment. Mutation is generally seen as a background operator that provides a small amount of random search. It increases the population diversity. It also helps expand the search space by reintroducing information lost due to premature convergence. Therefore, it drives the search into unexplored regions.

In addition to the above components, the stopping criterion of the algorithm is of great significance. It determines when the algorithm shall be stopped or terminated and thus, considering the best solution obtained so far as the optimal solution.

C. Design of a successful GA-based solution methodology

In designing a GA-based solution methodology, several decisions concerning the algorithm parameters shall be properly made in order to obtain high-quality solutions. Premature convergence to local optimum may result if the algorithm parameters are not selected in an appropriate manner.

Population size and the way the initial population is selected will have a significant impact on the results. Initial population could be seeded with heuristically chosen solutions or at random. In either case, the initial population should contain a wide variety of structures. The population size and the initial population are selected such that the solution domain associated with the population is sufficiently covered. The population size depends on the criteria for selecting the initial solutions. A constant size population of solutions shall be judged by the algorithm designer. If the population size is too small, the solution domain will not be adequately searched and, thus, resulting in poor performance. Premature convergence to local solutions can be prevented by using a large population size. However, this may slow down the convergence rate.

The performance of a genetic algorithm is highly sensitive to the fitness values. The fitness value may be selected as the objective function to be optimized. Some researchers, however, believe that the objective function value is a naive fitness measure. Therefore, using the objective function value associated with each solution as a fitness measure is rarely a good idea to some researchers. When applying a crossover operator, the resulting offspring can be either feasible or infeasible. There are two ways to deal with infeasible solutions. One way is to design heuristic operators transforming infeasible solutions to feasible ones. The second is by penalizing this infeasibility in the objective function. In the latter case, selection of proper penalty factors is another decision to be made by the algorithm designer.

Crossover rate and mutation rate play a very important role in the performance of genetic algorithm. A higher crossover rate introduces new solutions more quickly into the population. If the crossover rate is too high, high-performance solutions are eliminated faster than selection can produce improvements. A low crossover rate may cause stagnation due to the lower exploration rate. Mutation rate shall not be too high in order not to prevent crossover from doing its work properly. Some researchers reported that a variable mutation rate rather than a fixed one is more beneficial to be utilized. In the initial stage of the GA, it is recommended to start with a high crossover rate and a low mutation rate since the crossover is mainly responsible for the search at this stage. As the algorithm progresses, the crossover operator becomes less productive and therefore, the mutation rate shall be increased.

Simple GA involving just mutation and crossover has proved to be quite powerful enough. Some designers proposed to add an inversion operator where a section of a solution is 'cut out' and then re-inserted reversely. However, it has not been found significantly useful. It may be used instead of mutation operator to explore new regions of the searching domain.

As pointed out earlier, newly generated solutions replace existing solutions in subsequent generations of GA. Two replacement approaches are available to the algorithm designer to select among which. These are the incremental or 'steady-state' approach and the generational approach. In incremental or steady state replacement, once a new feasible solution has been generated, it will replace an above-average fitness value member chosen randomly. Members that fitness values are better than the calculated average are transferred to the next generation with no change. In generational replacement a new population of children is generated to replace the whole parent population. The steady-state replacement approach has the following advantages.

1. If steady-state replacement approach is not employed, there will be no guarantee that the best solution in the current population will survive into the next generation. With this approach, best solutions are always kept in the population and the newly generated solution is immediately available for selection and reproduction.
2. It is more efficient when compared to the generational approach. Faster convergence is usually expected with this approach.
3. It prevents the occurrence of duplicates. Duplication is unhelpful since it wastes resources on evaluating, the same fitness function and it distorts the selection process by giving extra chances to the duplicate solutions to reproduce.

Researchers, however, reported some success with the generational replacement approach. The genetic algorithm can be designed to stop if a pre-specified number of iterations are completed or if no improvement is encountered in the optimal solution during a given number of consecutive iterations. The stopping criterion shall be properly tuned with the other parameters like the population size, crossover rate and

mutation rate in order to obtain a high quality solution.

D. Application of GA to the CPP in distorted distribution systems

Because of its simplicity, generality and ability to cope with practical constraints, a genetic algorithm has been designed to solve the general CPP in a distribution system. The following remarks shed some light on the design aspects of the algorithm as applied to the CPP:

- The population size is a fixed value and the same is determined empirically by trial and error process.
- The objective function itself is used to provide fitness values of the newly generated solutions. Once a new solution is generated, its associated feasibility is checked. If the solution is infeasible, the penalty factor is applied.
- Selection, crossover and mutation are applied as genetic operators in the algorithm design. No additional operators such as the inversion operator are considered in the design process.
- The algorithm is designed based on a fixed, rather than a variable, mutation rate throughout the search.
- Steady-state replacement approach is selected in the design of the algorithm.
- The algorithm is designed to stop after predetermined number of generation.

Based on the above remarks, a GA-based solution methodology applied to the CPP has been implemented. The algorithm implementation can be summarized as follows:

In this paper the representation by means of strings of integers was chosen. Each gene(i) (represent buses) of the chromosome (its length is equal to the total number of the system buses (m)) can store a 0, which indicates absence of capacitors on the corresponding bus or an integer different from 0 that indicates the number of added capacitor sizes that is added in the bus(i). Therefore a chromosome can be represented as Figure (1)

Bus number	1	2	3	m-2	m-1	m
gene	0	3	4	2	1	3

Figure 1: A genetic algorithm chromosome of the capacitor placement problem

The algorithm procedure can be summarized as follow:

1. Input GA parameters, i.e. population size, crossover rate, mutation rate, selection type, crossover type, mutation type and termination mode.
2. Generate a set of initial solutions, forming the initial population, randomly.
3. Run ETAP Power Station 4.0 program to calculate system power losses, bus voltages and total harmonic distortion at each bus.
4. Calculate the associated fitness value (objective function) of each solution.
5. Check the constraints and applying the penalty factor (by adding 1E10 to the fitness value) if the constraints is not satisfied.
6. Create a new population by performing selection,

crossover and mutation on the individuals.

- Discard the old population and iterate using the new population if the stopping criterion is not satisfied.

IV. NUMERICAL RESULTS

A. Test System data

The distribution network models are obtained by suitably simplification of a typical Italian grid [2]. Single line diagram of the network is shown in Fig. (2) and the system data as follows:

Two 132 kV HV networks with the same short circuit power MVAsc of 6000 MVA;

Two HV/MV substations, comprising each a 132 kV HV busbar, a 132/20 kV 40 MVA transformer and a 20 kV MV busbar;

A feeder, subdivided in three line sections (L01, L12 and L23) of 3 km each with % positive sequence impedance (100 MVA base) $R=5.17$, $X=4.23$, $Z=6.68$

A series of further passive overhead feeders;

Link lines between various feeder (Lm1 and Lm2);

Configuration switches (S1, S2, S3, S4, S5 and S6).

Table (1) show the system load data

The proposed GA was applied to the test system-2 for three different network configurations:

- Radial configuration (S1 open, S2 open, S3 open, S4 open, S5 open and S6 open);
- Loop configuration (S1 open, S2 open, S3 close, S4 close, S5 close and S6 close);
- Interconnected configuration (S1 close, S2 close, S3 open, S4 open, S5 open and S6 open).

Table (1): Test system load data

Bus No.	Load (80% motor, 20% static)	
	MW	MVAR
1	5.25	5.356
2	5.25	5.356
3	5.25	5.356
4	4.5	2.18
5	4.5	2.18
6	4.5	2.18
7	4.5	2.18
8	4.5	2.18
9	4.5	2.18
10	4.5	2.18
11	4.5	2.18
12	4.5	2.18

Commercially-available capacitor sizes with real costs/kvar were used in the analysis. It was decided that the largest capacitor size Q_{cmax} should not exceed the total reactive load, i.e., 35688 kvar. The yearly costs of capacitor sizes as described in [3]

Optimum shunt capacitor sizes have been evaluated for the following cases:

- Case (1): All loads are assumed to be linear
- Case (2): Each 40 MVA transformer has harmonic current

source –typical IEEE- XFMR Magnet.

K_p was selected to be 168 \$/kW, and the voltage limits on the rms voltages were selected as $V_{min}=0.95$ pu, and $V_{max}=1.05$ for case (1) and $V_{min}=0.93$ pu, and $V_{max}=1.05$ for case (2). The maximum THD was selected as $THD_{max} = 5$

B. Test System results

Table (2) Comparison of results between radial, loop and interconnected distribution systems for case (1)

Variable	Before OCP			Case (1)		
	Radial	Loop	Interconnected	Radial	Loop	Interconnected
Q_{C1} (kvar)	---	---	---	4050	3600	3900
Q_{C2} (kvar)	---	---	---	3900	4050	4050
Q_{C3} (kvar)	---	---	---	4050	3900	3600
Q_{C4} (kvar)	---	---	---	1500	1800	3600
Q_{C5} (kvar)	---	---	---	3300	2400	3300
Q_{C6} (kvar)	---	---	---	1650	2700	2100
Q_{C7} (kvar)	---	---	---	3450	3300	3450
Q_{C8} (kvar)	---	---	---	750	3300	2400
Q_{C9} (kvar)	---	---	---	3450	3450	2400
Q_{C10} (kvar)	---	---	---	1800	2400	1200
Q_{C11} (kvar)	---	---	---	2250	2550	2100
Q_{C12} (kvar)	---	---	---	2700	1650	2250
Total capacitor (kvar)	---	---	---	32850	35100	34350
Min. voltage(pu)	0.91	0.91484	0.92671	0.96535	0.97364	0.97521
Max. voltage(pu)	0.95516	0.95516	0.94462	0.98778	0.98860	0.98554
Power losses (kW)	1244.1	1211.1	1206.5	812.8	795.7	796.8
Cap. cost (\$/year)	---	---	---	6142.8	6301.65	6156.9
Total cost (\$/year)	209008	203464	202692	142685	139904	139952
Benefits (\$/year)	---	---	---	66323	63560	62739

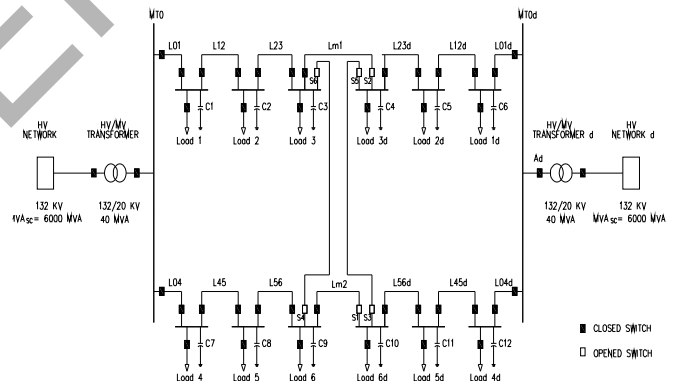


Figure 2: Test system - Simplified Typical Italian Grid

Table (3) Comparison of results between radial, loop and interconnected distribution systems for case (2)

Variable	Before OCP			Case (2)		
	Radial	Loop	Interconnected	Radial	Loop	Interconnected
QC1 (kvar)	---	---	---	2700	900	3600
QC2 (kvar)	---	---	---	3000	3150	3450
QC3 (kvar)	---	---	---	2550	3450	3150
QC4 (kvar)	---	---	---	1350	2100	2700
QC5 (kvar)	---	---	---	2100	1650	1800
QC6 (kvar)	---	---	---	2100	2850	750
QC7 (kvar)	---	---	---	300	2400	1650
QC8 (kvar)	---	---	---	2850	2100	1800
QC9 (kvar)	---	---	---	2550	2550	1650
QC10 (kvar)	---	---	---	3450	2400	3000
QC11 (kvar)	---	---	---	900	1350	3600
QC12 (kvar)	---	---	---	3000	2400	300
Total capacitor (kvar)	---	---	---	26850	27300	27450
Min. voltage(pu)	0.9099	0.9148	0.92669	0.948	0.9544	0.9649
Max. voltage(pu)	0.9551	0.9551	0.94461	0.98657	0.9866	0.9772
Max. THD (%)	2.68	2.68	2.65	4.95	4.99	4.96
Power losses (kW)	1244.2	1211.1	1206.5	873.7	844.928	828.92
Cap. cost (\$/year)	---	---	---	5007	4992	5135
Total cost (\$/year)	20903	20347	202707	151788	146940	144413
Benefits (\$/year)	1	4	---	57242.9	56534	58293

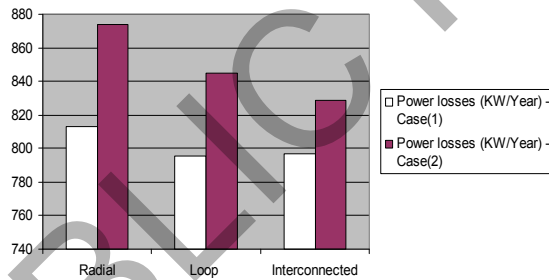


Figure 3: Power losses (Kw/year) for case (1) & (2)

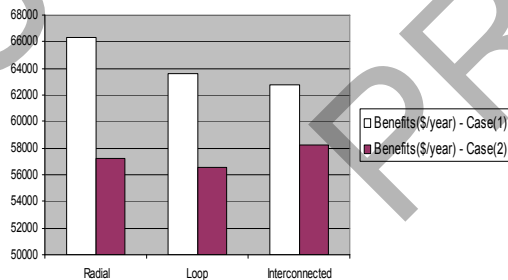


Figure 4: Benefits (\$/year) for case (1) & (2)

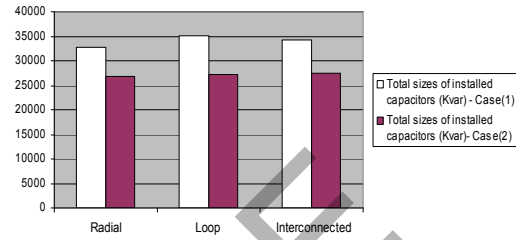


Figure 5: Total sizes of installed capacitors (Kvar) for case (1) & (2)

V. CONCLUSION

The study of the optimal capacitor placement on interconnected distribution systems in the presence of nonlinear loads using Genetic Algorithms (GA) is presented in this paper. Results (power losses, operating conditions and annual benefits) are compared with that obtained from radial and loop networks. The radial, loop and interconnected distribution systems models are obtained by suitably simplification of a typical Italian grid. Computational results obtained showed that the harmonic component affects the optimal capacitor placement in all system configurations. When all loads were assumed to be linear, interconnected and Loop system configurations offer lowest power losses and best operating conditions rather than the radial system configuration while radial system configuration offer best annual benefits due to capacitor placement. In distorted networks, interconnected systems configuration offer lower power losses, best operating conditions and best annual benefits due to capacitor placement.

REFERENCES

- [1] IEEE Recommended Practices and Requirements for Harmonic Control in Electrical Power Systems, IEEE Std. 519-1992, 1993.
- [2] M.Brenna, R.Faranda and E.Trioni, "Non-conventional Distribution Network Schemes Analysis with Distributed Generation", TEQREP, Bucharest, 2004
- [3] Y. Baghzouz, S. Ertem, "Shunt Capacitor Sizing for Radial Distribution Feeders with Distorted Substation Voltages", IEEE Trans. on Power Delivery, Vol. 5, No. 2, April 1990, pp. 650-657.

Ahmad Galal Sayed received the B.Sc. degree in electrical power and machines from the Faculty of Engineering at Alexandria University, Egypt, in 2003. He is currently working toward the M.Sc. degree in the department of electrical power and machines, Faculty of Engineering, Cairo University. His research interest includes computer aided analysis of power systems, and power system harmonics.

Computer Relaying Software Reliability Evaluation Using Event Tree

Aditya Anil[#], D.K Mohanta[#], D.S Roy^{*1}, A.K Panda^{*2}

[#]Department of Electrical and Electronics Engineering
Birla Institute of Technology (Deemed University)
Mesra, Ranchi-835215, India

^{*1}Department of Computer Science and Engineering

^{*2}Department of Electronics and Communication Engineering
National Institute of Science and Technology,
Berhampur - 761008, India

Abstract- Software reliability evaluation has emerged as an area of importance in recent times with the proliferation of software based systems. But highly dependable software systems used for safety critical application, such as computer relays for power system transmission line protection produce little failure data. Hence a statistical method known as statistics of extreme is used for reliability evaluation. This paper deals with calculation of exceedance probability of computer relay and using this data an event tree of computer relay has been drawn.

I. INTRODUCTION

The reliability evaluation of software based systems has become a major concern. Hardware reliability can be resolved much consistently compared to software reliability, which is a rather less explored field until recent times [1]. The reliability assessment of software requires the previous history of failure data based on which a statistical estimation is put forward. Nevertheless for novel and highly dependable software systems, such failure data is scarcely available and thus formulation of statistical estimation of reliability index from such meager available data does not seem viable [2].

Statistics of the extremes is a special branch of statistics which deals with scenarios involving extreme events and can model distribution of rare events, those for which very few or no available data is present to work with as in the case of computer relay's software evaluation where the failure data is very less.

For determining the design, procedural weakness & various hazardous consequences due to faults (initiating accidental event) event tree is developed for computer relay's software. An event tree is an inductive procedure that shows all the possible outcomes, resulting from an accidental or initiating event, taking into account whether all the safety barrier are functioning or not.

In this paper, the software reliability evaluation of a computer relay is investigated, whose algorithm is based on the use of wavelet-fuzzy combined approach for detection, classification and location of faults on a transmission line. With the extensive use of fast and accurate digital signal processing techniques such as the wavelet transform, detection and

classification of different faults have been done very easily [3]–[4].

II. SOFTWARE RELIABILITY EVALUATION

Computers have pervaded to all aspects of modern society. Practically speaking, the existence of software based systems in our lives is omnipresent and the size and complexity of computer-intensive systems are growing day-by-day. Thus the reliability evaluation of software based systems has become a major concern. Especially for safety critical system like computer relay, reliability evaluation is extremely necessary. But as the number of fault found in the different modules of software is very rare, hence for reliability evaluation statistics of extreme is used.

In this paper, the software reliability evaluation of a computer relay has been obtained, the computer relay has three modules and Monte Carlo simulation was employed for incorporating the stochastic nature of fault occurrence in the system. Using this data, the failure probability and the corresponding Cdf for each of the three module of computer relay were calculated. By using the principles of statistics of extreme failure probability and exceedance probability were found out.

A. Statistics of Extreme

Software reliability modeling is a long-established approach, wherein a system's past failure data is analyzed for prediction of future behavior [5]. But software systems that are supposed to be built for highly dependable applications is difficult to analyze using conventional software reliability growth models owing to reasons such as the novelty of the software to be developed, sparingly few available failure data.

Statistics of extremes offers a modeling scheme that is independent of the test sampling order, the amount of available data and furthermore it does not require a priori knowledge about the underlying distribution of any parameter. a distribution F converges to some asymptotic form in its extreme tails [5]. Condition that a distribution F converges to an asymptotic form in its maximum tail if

$$\lim_{n \rightarrow \infty} F_X^n(a_n + b_n x) = H(x) \quad (1)$$

For applying statistics of extremes, the first step is to plot the empirical cumulative distribution function (Cdf) of available failure data in a Gumbel type probability paper [6] to find out its domain of attraction. Reference [7] shows that for most distributions the domain to attraction belongs to any one of the three Gumbel type asymptotic families, namely the Gumbel Type I, Gumbel Type II or Gumbel Type III [6]. The next step is to determine the software reliability estimate for highly dependable system employing a graphical based analysis using the form of empirical Cdf plot.

For obtaining the reliability indices needed for software evaluation, failure probability and exceedance probability is needed. These indices are calculated using the following equations [8]:

$$F_S(s) = \exp(-\exp(-s)) \quad (2)$$

$$\text{Where } s = -k \ln \left(\frac{x - \varepsilon}{w - \varepsilon} \right) = -\ln[-\ln[F_S(s)]] \quad (3)$$

$$K = \frac{-s}{\ln(x - \varepsilon) - (\omega - \varepsilon)} \quad (4)$$

$$F_S(s) = F_{X1}(X1 \leq x) = 1 - \exp\left[-\left(\frac{x - \varepsilon}{\omega - \varepsilon}\right)^k\right] \quad (5)$$

$$P_{X1}(X1 \geq x) = [1 - F_{X1}(X1 \leq x)] \quad (6)$$

Where ω is the characteristic smallest variable of initial variate x , ε is the lower bound which is assumed to be 1 in this case and k is the inverse measure of dispersion of initial variate x . $F_{X1}(X1 \leq x)$ is the probability that the number of failure is less than x (failure probability). Whereas $P_{X1}(X1 \geq x)$ gives the exceedance probability of the software.

III. CASE STUDY AND RESULT

Fault data is obtained from the Monte Carlo simulation result, from this fault data corresponding Cdf has been calculated for each of the three modules of the computer relay. Here detail calculations of detection module have been shown.

From the Cdf plot shown in "Fig.(1)" characteristic smallest value ω has been calculated which comes out to be 38 for detection module. Therefore $(x - \varepsilon)$ is 37. The value of S can be extrapolated using "Fig. (1)". The probability of having less than $(x - \varepsilon) = 24$ software failure is approximately = 0.80. i.e., $F_S(s) = 0.80$ as shown in table 1. Calculating S for $(x - \varepsilon) = 24$ gives $S = 1.5$. K is calculated using eqn. (4), which comes out to be 3.47. Therefore the failure probability expression for detection module is given as

$$F_{X1}(X1 \leq x) = 1 - \exp\left[-\left(\frac{x - \varepsilon}{37}\right)^{3.47}\right] \text{ from this expression by}$$

putting different values of x ; failure probability for different potential software failure for detection module can be obtained and using eqn. (6) exceedance probability is calculated for different number of software failures and tabulated in table 2.

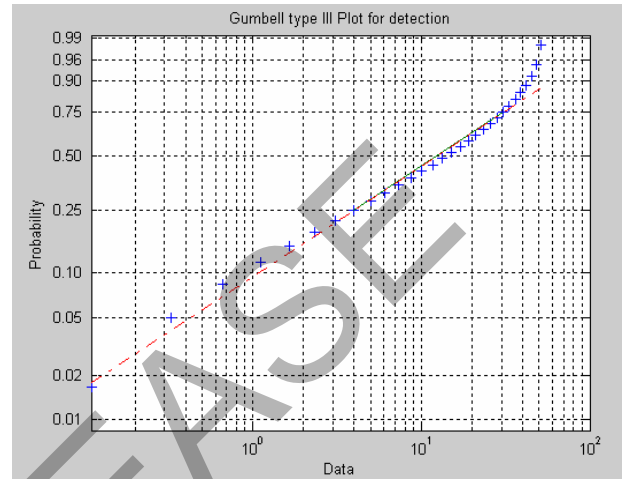


Figure 1. Gumbell Type III (Empirical Cdf) plot for Detection Module

TABLE 1 Cdf data of Detection Module

Fault type	Fault #	Probability	CDF
AG (LI)	1	.033	.0011
AG (MI)	2	.066	.003
AG (HI)	3	0.1	.0066
BG (LI)	4	0.133	.0111
BG (MI)	5	0.166	.0166
BG (HI)	6	0.2	.0233
CG (LI)	7	.233	.0310
CG (MI)	8	.266	.0399
CG (HI)	9	.300	.0499
ABG (LI)	10	.333	.0610
ABG (MI)	11	.366	.0732
ABG (HI)	12	.40	.0865
BCG (LI)	13	.433	.1010
BCG (MI)	14	.466	.1165
BCG (HI)	15	.500	.1332
CAG (LI)	16	.533	.1509
CAG (MI)	17	.566	.1698
CAG (HI)	18	.600	.1898
AB (LI)	19	.633	.2109
AB (MI)	20	.666	.2331
AB (HI)	21	0.7	.2564
BC (LI)	22	0.733	.2809
BC (MI)	23	0.766	.3064
BC (HI)	24	0.80	.3331
CA (LI)	25	0.833	.3608
CA (MI)	26	0.866	.3897
CA (HI)	27	0.90	.4197
ABC (LI)	28	0.933	.4508
ABC (MI)	29	0.966	.4830
ABC (HI)	30	1	.5163

Table 2.Exceedance Probability of Detection Module

Exceedance Probability	Z : No. of Potential lifetime software failure				
	2	5	9	12	15
$P_x (X \geq x)$	0.99999	0.9996	0.9951	0.9853	0.9663

For fault classification modules, from the Cdf plot in “fig. 2”, the smallest characteristic value, ω comes out to be 31 & $(x - \varepsilon) = 30$. As in the previous calculation for detection module, from the Cdf data, and the Cdf plot shown in “Fig. 2” a value of S is extrapolated. The probability of having less than $(x - \varepsilon) = 32$ software failure is approximately 0.3299. Calculating S for $(x - \varepsilon) = 32$ gives $S = -0.1034$. Thereafter from eqn. (4), K is found out to be 1.603. Thus, the analytical expression for the failure probability for classification module

$$F_{x1} (X1 \leq x) = 1 - \exp \left[- \left(\frac{x - \varepsilon}{30} \right)^{1.603} \right]$$

Using the eqn.(6) exceedance probability values are tabulated in table 3.

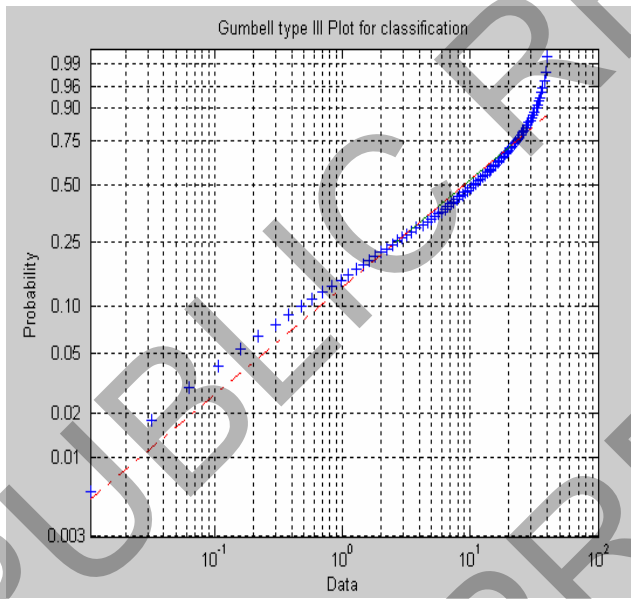


Figure 2. Gumbell Type III (Empirical Cdf) plot for classification Module

Table 3.Exceedance Probability of classification Module

Exceedance Probability	Z : No. of Potential lifetime software failure				
	2	8	14	27	36
$P_x (X \geq x)$	0.9957	0.9158	0.7808	0.4550	0.2743

In “Fig. 3” the Cdf plot for fault location module is shown. The extrapolated value of S is 0.66 and k comes out to be 1.741. Therefore the final expression obtained for failure probability for fault location modules comes out to be

$$F_{x1} (X1 \leq x) = 1 - \exp \left[- \left(\frac{x - \varepsilon}{33} \right)^{1.74} \right]$$

Using eqn. (6) the exceedance probability for fault location is tabulated in table 4.

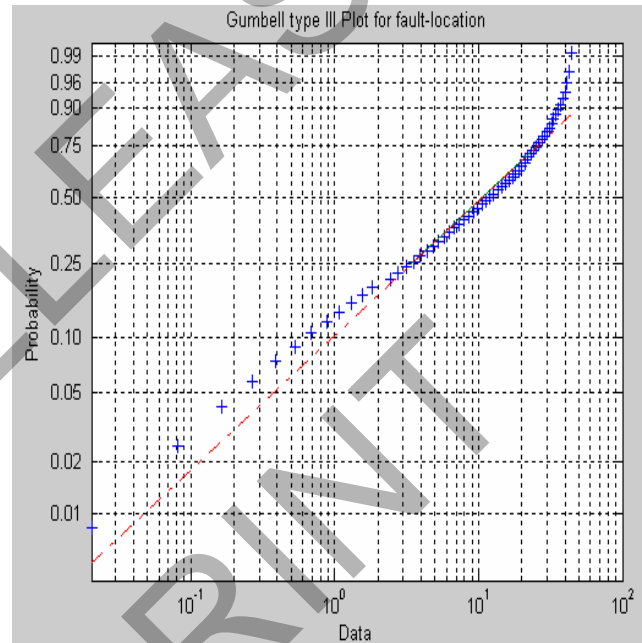


Figure 3. Gumbell Type III (Empirical Cdf) plot for fault location Module

Table 4.Exceedance Probability of fault location Module

Exceedance Probability	Z : No. of Potential lifetime software failure				
	2	8	15	23	31
$P_x (X \geq x)$	0.9977	0.9349	0.7986	0.6103	0.4286

For software reliability evaluation of computer relay’s software, event tree is used, as shown in “fig (4)”. Event tree gives us the insight knowledge of the consequences, due to initiating fault [9]. These consequences will depend upon the functioning of the safety barriers. Here in this case for a computer relaying, its three modules namely detection, classification and fault location are the safety barriers.

Therefore, if all the three safety barriers are working, then the system will be considered as a Risk free or healthy system. The main job of a relay is to detect the faults. Hence if the first

safety barrier, which is detection module of a computer relay, fails then the consequence will be termed as Risky, even if the other two modules are operational. And if first safety barrier is working and other two or one of the two is non-functional then the system is in marginal state.

From the event tree, the probability that the accidental event (fault) will lead to unwanted consequences if the safety-barriers are non functional is computed. Also probability of 'Risk free state' of computer relay is calculated. These values are tabulated in table 5.

For getting these probability values the exceedance probability for two numbers of failures has been taken for each of the three modules from table 2, 3 & 4 respectively. Therefore when all the modules are in 'Up state' the reliability comes out to be 0.9935 and the relay is said to be in Risk Free state & when all are in 'down state' reliability is 9.89×10^{-11} .

Table 5 State Probability of Event Tree

State	Fault Detection	Fault Classification	Fault location	Probability
1	Down	Down	Down	9.89×10^{-11}
2	Down	Down	Up	4.29×10^{-8}
3	Down	Up	Down	2.29×10^{-8}
4	Down	Up	Up	9.93×10^{-6}
5	Up	Down	Down	9.88×10^{-6}
6	Up	Down	Up	4.29×10^{-3}
7	Up	Up	Down	2.29×10^{-3}
8	Up	Up	Up	0.9935

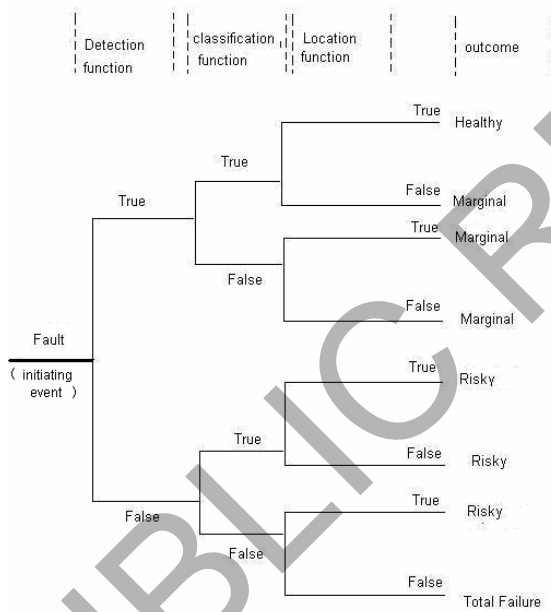


Figure 4 Event Tree of Computer Relay

IV. CONCLUSION

The reliability evaluation for computer relaying demonstrates the efficacy of the proposed approach for assessing the risk associated with such software which rarely fails, but whose failures lead to catastrophic consequences such as blackouts. By using event tree, various state probabilities are evaluated for system planning. Also the least risk state probability serves as an indicator regarding the system reliability involving safety critical applications such as computer relay.

REFERENCES

- [1] D. S. Roy, D. K. Mohanta, A. K. Panda, "Software reliability allocation of digital relay for transmission line protection using a combined system hierarchy and fault tree approach", *IET Software*, October, 2008, vol. 2, no. 5, pp. 437 – 445.
- [2] E. J. Gumbel, "Statistics of extremes", Columbia Press, New York, 1958
- [3] M. Jayabharata Reddy., D.K. Mohanta.: "A wavelet-neuro-fuzzy combined approach for digital relaying of transmission line faults", *Int. J. Electrical. Power Component. System*, 2007, 35, (12), pp. 1385–1407
- [4] M. Jayabharata Reddy. D.K. Mohanta., "Performance evaluation of adaptive network based fuzzy inference system approach for location of faults on transmission lines using Monte Carlo simulation", *IEEE Trans. Fuzzy System.*, 2008, 16, (4)
- [5] Michael R. Lyu (Ed.), Handbook of Software Reliability Engineering, McGraw-Hill, 1995."
- [6] E. Castillo, E. Alvarez, A. Cobo, T. Herrero, "An Expert System for the Analysis of Extreme Value Problems", 1993; University of Cantabria, Spain
- [7] E. Castillo, Extreme Value Theory in Engineering, 1988; Academic Press
- [8] L.M. Kaufman, J.B. Dugan, B.W. Johnson, "Using statistics of the extremes for software reliability analysis of safety critical systems", *Proc. Ninth Int'l Symposium on Software Reliability Engineering*, 1998 Nov, pp 355 - 363.
- [9] Marvin Rausand, System Reliability Theory, second edition, 2004, Wiley & sons.

Relationship between Production Capacity of Wind Power Stations and Needs of Ancillary Services

Vaclav Cerny, Andrea Fialova, Lucie Houdova, Petr Janecek and Eduard Janecek
Department of Cybernetics, Faculty of Applied Sciences, University of West Bohemia
Univerzitni 8, 306 14 Plzen, Czech Republic

Abstract—Number of wind power stations has been increasing in the world for last years. Of course, this causes that electrical power amount produced by this kind of power station and subsequently delivered to electricity transmission systems has also been growing. On one hand, this brings positive effects with respect to living environment because production of coal, gas or nuclear power stations can temporarily be reduced while wind blows. On the other hand, this sets enhanced demands on needs of ancillary services. This paper deals with these connections and demonstrates obvious consequences that arise from them.

I. INTRODUCTION

Wind energy produced by wind power stations is one of renewable resources that has become very popular and used world wide in recent years. It brings many benefits to mankind particularly with respect to living environment. For instance, production of other types of power stations such as coal, gas or nuclear is supposed to be reduced due to wind blowing because, as a result, wind power stations produce extra electrical power that is delivered to electricity transmission systems. This implies that living environment is less polluted because production of 'messy' power stations is restrained.

Nevertheless, the problem is that time periods within which wind is going to blow together with volume of blowing is hardly ever reliably predictable to the future. This causes that production of wind power stations cannot be scheduled in advance. Therefore, the production is not usually taken into account while electricity transmission system operation planning performed by TSOs (Transmission System Operators) is under construction. On the contrary, extra electrical power produced by wind power stations and delivered to electricity transmission systems (while wind blows, of course) is classified as a failure that exhibits by way of temporary power surplus in the systems. Consequently, such a failure is assumed to be decayed by employment of appropriate types of ancillary services performed by TSOs as well. It is obvious that this matter of fact puts increased requirements towards needs of particular types of ancillary services.

Seeing that wind blowing 'strategy' can be considered as a random variable, the approach presented in the paper and dealing with relationship between production capacity of wind power stations and needs of ancillary services is based on probability theory and mathematical statistics [1], [2]. Fundamentals of the approach focused on stochastic modelling [3], [4] of electricity transmission system operation from both technical and economical points of view have already been

established in other papers [5], [6], [7], [8]. Therefore, only main ideas of the approach will be introduced at the beginning of the paper. Subsequently, it will be presented that extra electrical power delivered to electricity transmission systems by production of wind power stations under the circumstance that wind blows causes growth of power reserves of certain types of ancillary services. In other words, TSOs are forced to assure larger amount of certain types of ancillary services when electricity transmission system operation planning is under construction. It is obvious that this implies financial cost increase with respect to operation of the system.

II. MAIN IDEAS OF THE APPROACH

At the beginning, relevant monitored data and measured signals have been recognized from the system operation reliability point of view. Since the reliability of the system operation is particularly linked with power balance control, those data and signals have included a power balance deviation in the closed loop mode $dP_{ct}(t)$, power control injections $R(t)$ supplied to the system by activations/deactivations of ancillary services, starts and ends of forced power unit outages and time durations related to the outages (times between failures and of repairs). The deviation $dP_{ct}(t)$ is then decomposed.

A. Decomposition of $dP_{ct}(t)$

It holds that:

$$dP_{ot}(t) = dP_{ct}(t) + R(t), \quad (1)$$

$dP_{ot}(t)$ is a power balance deviation in the open loop mode. The deviation represents behavior of the system without any control actions and it is easily obtained from (1). The deviation can be expressed as follows:

$$dP_{ot}(t) = dP_o(t) + T(t), \quad (2)$$

$dP_o(t)$ is a power balance deviation in the open loop mode of undisturbed system operation (without any forced power unit outages) and $T(t)$ constitutes the outages. The deviation is obtained by excluding sectors where the outages occur from $dP_{ot}(t)$. Those sectors are identified in virtue of the information about the starts and ends of the outages. The components $dP_o(t)$ and $T(t)$ are modelled.

B. Probabilistic model of $dP_o(t)$

Whereas $dP_o(t)$ is a random variable, it is modelled by a proper distribution from a probabilistic viewpoint. It has been proved by fit tests that the most proper distribution for modelling $dP_o(t)$ is the Gaussian distribution:

$$f_G(dP_o) = \frac{1}{\sqrt{2\pi}\sigma_{dP_o}(t)} e^{-\frac{[dP_o - \mu_{dP_o}(t)]^2}{2\sigma_{dP_o}^2(t)}}, \quad (3)$$

$f_G(dP_o)$ is a probability density function. The parameters of the distribution (mean $\mu_{dP_o}(t)$ and standard deviation $\sigma_{dP_o}(t)$) are computed from the real signal $dP_o(t)$.

C. Probabilistic model of $T(t)$

The forced power unit outages $T(t)$ are modelled by the Markov process with two states (see Fig. 1) [9], [10].

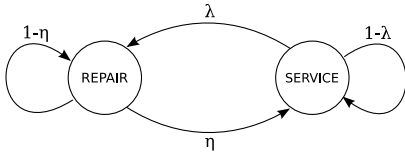


Fig. 1. State diagram of Markov process

The transient rates are given by the relations:

$$\lambda = \frac{1}{MTTF}, \quad \eta = \frac{1}{MTR}, \quad (4)$$

$MTTF$, MTR are mean times between failures and of repairs. The mean times are obtained through statistical processing of given times between failures and of repairs for particular units. The model is described by the equations:

$$\frac{d}{dt} \begin{bmatrix} p_s(t) \\ p_r(t) \end{bmatrix} = \begin{bmatrix} -\lambda & \eta \\ \lambda & -\eta \end{bmatrix} \begin{bmatrix} p_s(t) \\ p_r(t) \end{bmatrix}, \quad p_s(t) + p_r(t) = 1, \quad (5)$$

$p_s(t)$ is a service probability and $p_r(t)$ a repair probability.

The forced outages are mostly caused by mechanical failures (e.g. seizure, leakage, fatigue, etc.). Therefore, dependencies among co-temporary outages are not considered in the model. Partial outages are not taken into account either because they are not very frequent, their durations are usually short and amplitudes small. This means that they do not have any substantial effect on the reliability of the system. Modelled power units inhere in the bottom of the well - known bathtub curve with respect to their life cycles. This means that the failure and repair rates are about constant. Thus, the Markov process is precise enough for the modelling.

D. Probabilistic model of $dP_{ot}(t)$ and $R(t)$ determination

Consequently, the probabilistic models of $dP_o(t)$ and $T(t)$ are aggregated into a model of the power balance deviation in the open loop mode $dP_{ot}(t)$ that is described by the Gaussian sum [11], [12] with the probability density function:

$$f_{G_s}(dP_{ot}) = \sum_i \frac{P_i(t)}{\sqrt{2\pi}\sigma_{dP_o}(t)} e^{-\frac{[dP_{ot} - \mu_{dP_o}(t) - T_i]^2}{2\sigma_{dP_o}^2(t)}}, \quad (6)$$

where $P_i(t)$ are probabilities of the outages and all their possible combinations and T_i are appropriate amplitudes. The sum is used for determination of the overall positive and negative volumes of ancillary services $R^+(t)$, $R^-(t)$ under a required reliability level of the system operation. The level is given as a percentage share of $dP_{ot}(t)$ amplitudes larger than $\pm 100MW$ along all of its possibly existing amplitudes (the share is called as **Value at Risk** - VaR):

$$R^+(t) = F_{G_s}\left(1 - \frac{VaR}{2}\right), \quad R^-(t) = F_{G_s}\left(\frac{VaR}{2}\right). \quad (7)$$

Since an analytical formula of a cumulative distribution function of the Gaussian sum F_{G_s} is not known, $R^+(t)$ and $R^-(t)$ have to be computed by a numerical algorithm.

E. Decomposition of $R(t)$ and economical optimization

The overall volumes are then divided into power reserves of particular ancillary services on behalf of statistical and dynamical characteristics of specific components involved in $dP_{ot}(t)$ that should be decayed by corresponding types of the services (a random component \Rightarrow secondary frequency and power control, a direct - energetic component \Rightarrow tertiary control, a forced outage \Rightarrow quick - start, a long - time power imbalance \Rightarrow non - spinning stand - by reserve, emergency assistance, control energy purchase, etc.).

Finally, the power reserves are economically optimized. The reserves are re - disposed by the optimization in such a way that the required reliability level (VaR) is kept and costs to their purchase are minimized at the same time.

F. Monte-Carlo simulation

In order to make sure that the whole optimization procedure of the system operation planning is well done, a Monte - Carlo simulator is employed to verify that the power reserves of particular ancillary services are large enough for guaranteeing the required reliability level of the system operation. The simulator models and simulates electricity transmission system operation in the closed loop mode. This means that it involves models that constitute the open loop (model of undisturbed system operation, model of forced power unit outages) as well as models that constitute the feedback (models of the ancillary services mentioned above). The simulator works then under saturation limits of the services that are given by their corresponding limited power reserves.

Remark: The approach/method presented in the paper has been developed for the TSO of the Czech Republic - CEPS a.s. since 2005 in terms of the Center for Applied Cybernetics. It is routinely used by the Czech TSO for electricity transmission system operation planning. Therefore, all results, which will be presented here, have been obtained through analyses and simulations of the Czech electricity transmission system operation. Nevertheless, the approach/method is general enough in order that it is applicable to any other areas. As a consequence, appropriate results and conclusions obtained can also be considered as sufficiently prevailing despite the approach/method being developed for the concrete area and its TSO.

III. WIND SPEED AND POWER

A. Wind speed variability

Electrical power produced by wind power stations is dependent on time - position wind speed variability. Position wind speed variability is given by landscape articulation. Whereas, time wind speed variability is assessed by changes of weather conditions. Moreover, wind speed variability is also influenced by various random fluctuations that represent chaotic wind behavior. Therefore, it is quite useful to describe wind speed by its statistical characteristics – mean and standard deviation. Values of these characteristics depend on a position of being situated. In other words, they depend on longitude, latitude and altitude values, respectively. Values of the characteristics for the area of the Czech Republic are illustrated on Fig. 2, 3.

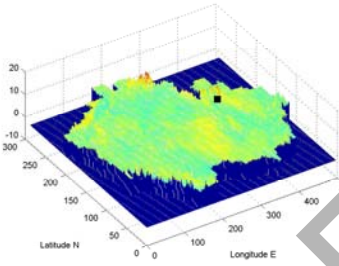


Fig. 2. Mean of wind speed

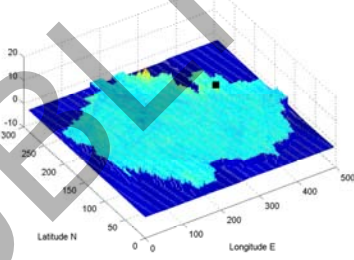


Fig. 3. Standard deviation of wind speed

B. Wind power variability

As a matter of course, wind power produced by a wind power station and speed of wind, which blows around the station, are closely associated with each other. The formula that connects wind power produced by a wind power station and wind speed around the station is the following:

$$P(t) = \frac{1}{2} \eta \rho u^3(t) \quad (8)$$

where $P(t)$ is wind power produced by a wind power station, η is an efficiency coefficient of a wind power station, ρ is air density and $u(t)$ is wind speed. The coefficient η and the density ρ are assumed to be constant. On the other hand, the

power $P(t)$ and the speed $u(t)$ are supposed to be time - varying. This means that they can vary within a specified time horizon of production. Subsequently, the formula (8) can be used for determination of mean and standard deviation of wind power produced by a wind power station whose position is given by specification of its longitude, latitude and altitude:

$$P_m = \frac{1}{2} \eta \rho u^3, \quad u^3 = (\alpha u_m + \beta u_{std})^3 \quad (9)$$

where P_m is mean of wind power produced by a wind power station within a specified time horizon of production, u_m is mean of wind speed within the horizon and u_{std} is its standard deviation within the horizon. The coefficients α, β are known.

$$P_{std} = \frac{\bar{u}^3}{PD}, \quad \bar{u}^3 = \frac{u_{std} u^3}{0.35 u_m} \quad (10)$$

where P_{std} is standard deviation of wind power and the coefficient PD is also known. The coefficients α, β and PD and the constant 0.35 have been identified from data.

Consider a wind power station whose location is marked on Fig. 2, 3. Curves of mean and standard deviation of wind speed and corresponding mean and standard deviation of wind power produced by the station are shown in Fig. 4, 5, 6, 7.

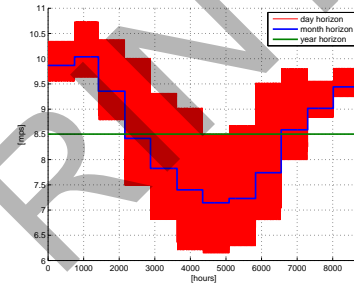


Fig. 4. Mean of wind speed

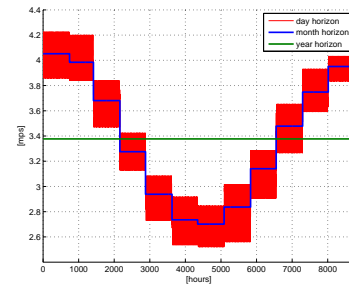


Fig. 5. Standard deviation of wind speed

Remark: Values of means and standard deviations of wind speed and wind power are periodic with a time period that is equal to 1 day (24 hours) in terms of the day horizon. The reason is that the values are about consistent for the same hours through particular days of a month.

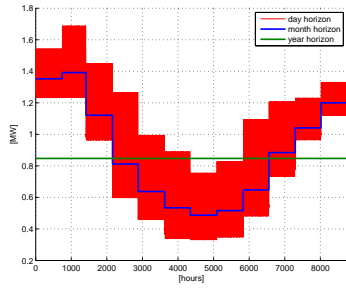


Fig. 6. Mean of wind power

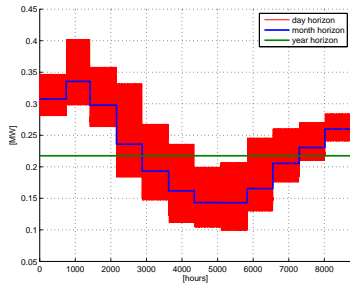


Fig. 7. Standard deviation of wind power

IV. NEEDS OF ANCILLARY SERVICES

As a matter of fact, extra electrical power produced by wind power stations and delivered into electricity transmission systems while wind blows influences overall volumes of ancillary services $R^+(t)$ and $R^-(t)$ defined by (7). The volumes appear larger in comparison with that case when the power is not considered in terms of standard computations. The reason is that means and standard deviations of the power, which becomes a part of the power balance deviation in the open loop mode $dP_{ot}(t)$, are included in means and standard deviations of this quantity whose mathematical model is given by the Gaussian mixture (6). Consequently, power reserves of certain kinds of ancillary services also get larger. This fact is illustrated with the help of values in the following tables:

- 1) take a wind power station with installed power 1 GW:

SC	TC^+	TC^-
+11%	-54%	+190%

- 2) take a wind power station with installed power 2 GW:

SC	TC^+	TC^-
+42%	-74%	+479%

It is clear from the values mentioned in the tables that wind power stations with their extra power production cause increased demands (in comparison with standard electricity transmission system operation without any wind power station built) on needs of secondary control - SC (a spinning ancillary service working in an automatic mode that responds to a given setpoint up to 10 minutes), increased demands on needs of negative tertiary control - TC^- (a spinning or non-spinning ancillary service working in a dispatcher mode that responds to

a given setpoint up to 30 minutes) and decreased demands on needs of positive tertiary control. The demands are especially laid on the negative tertiary control. The reason is that actual power production of base - load power units has to be restricted due to random extra power production of wind power stations so that power balance equilibrium within electricity transmission system operation under 50Hz frequency is guaranteed. Unfortunately, these restriction procedures result in life cycle reduction of power units whose actual power production is restrained in such a way.

V. CONCLUSION

The paper presents relationship between production capacity of wind power stations and needs of ancillary services. It is demonstrated here that extra power production of wind power stations puts increased demands on power reserves of certain types of ancillary services. Consequently, this implies that financial costs of electricity transmission system operation with wind power stations involved are higher in comparison with the operation without any wind power station plugged in. Furthermore, stability of the system with wind power stations gets worse because their power production level is hardly ever predictable and this induces that electricity transmission system operation gets more control - intensive.

ACKNOWLEDGMENT

The work was supported by the Ministry of Education of the Czech Republic under the project No. 1M0567.

REFERENCES

- [1] T.W. Anderson, *The Statistical Analysis of Time Series*, John Wiley & Sons, New York, 1971.
- [2] A. Papoulis and S.U. Pillai, *Probability, Random Variables and Stochastic Processes*, McGraw-Hill, New York, 2002.
- [3] G.R. Chen and S.H. Hsu, *Linear Stochastic Control Systems*, CRC Press, London, 1995.
- [4] L. Arnold, *Random Dynamical Systems*, Springer-Verlag, Berlin, 1998.
- [5] E. Janecek, V. Cerny, A. Fialova, and J. Fantik, *A New Approach to Modelling of Electricity Transmission System Operation*, Proceedings of the IEEE PES Power Systems Conference & Exposition, Atlanta, Georgia, USA, October 29 – November 1, 2006, 1429 – 1434.
- [6] P. Havel, P. Horacek, and J. Fantik, *Optimal Planning Strategy of Ancillary Services Ensuring Secure Operation of Power System*, Proceedings of the IEEE International Conference Powertech, Lausanne, Switzerland, July 1 – 5, 2007.
- [7] V. Cerny, P. Janecek, A. Fialova, and J. Fantik, *Monte-Carlo Simulation of Electricity Transmission System Operation*, Proceedings of the 17th IFAC World Congress, Seoul, South Korea, July 6 – 11, 2008, 4588 – 4593.
- [8] P. Havel, P. Horacek, V. Cerny, and J. Fantik, *Optimal Planning of Ancillary Services for Reliable Power Balance Control*, IEEE Transactions on Power Systems, Vol. 23, No. 3, August 2008, 1375 – 1382.
- [9] K. Maslo and S. Vnoucek, *Modelling of Steam Unit Outages*, Proceedings of the 6th International Conference on Probabilistic Methods Applied to Power Systems, Madeira Island, Portugal, September 25 – 28, 2000.
- [10] R. Billinton and Y. Li, *Incorporating Multi-state Unit Models in Composite System Adequacy Assessment*, Proceedings of the 8th International Conference on Probabilistic Methods Applied to Power Systems, Iowa State University, Ames, USA, September 12 – 16, 2004.
- [11] H.W. Sorenson and D.L. Alspach, *Recursive Bayesian Estimation Using Gaussian Sums*, Automatica, Vol. 7, No. 4, 1971, 465 – 479.
- [12] D.L. Alspach and H.W. Sorenson, *Nonlinear Bayesian Estimation Using Gaussian Sum Approximations*, IEEE Transactions on Automatic Control, Vol. 17, No. 4, 1972, 439 – 448.

Extracting Electricity from Groundwater Flow; A New Environment Friendly Source of Energy Case Study: Iran

By: Majid Labbaf Khaneiki, Ali Asghar Semsar Yazdi
International Center on Qanats and Historic Hydraulic Structures
Under the auspices of UNESCO
Mojtame Edarat, Daneshjoo Blvd.
Yazd, Iran

Abstract- In Iran, extracting energy from groundwater flow was an ancient technical tradition which unfortunately has been abolished in the wake of the advent of modern means of power generating. The subterranean irrigational canals called Qanat in Persia made it possible to build many watermills rotating with the force of groundwater. Qanat is a gently sloping subterranean canal, which tap a water-bearing zone at a higher elevation than cultivated lands. At present there exist some 32000 active qanats running all over Iran, discharging about 9 billion cubic meters groundwater a year. The head of water in a qanat canal with a discharge of 80 liters per second is such that the flow can spin a millstone weighing over 800 kilos, in a traditional way in which the friction is so high. In this paper we depict the possibility of replacing the abandoned traditional watermills with the modern optimized turbines to generate electricity in an environment friendly way. The qanat holding countries like Iran, Oman, Afghanistan, China and Iraq can consider the qanat system a new source of energy, which not only can supply water to the rural communities but also can provide them with cheap, renewable and clean electricity. In closing, we describe some considerable initiatives taken in Iran to make use of the groundwater flow in the qanat canals to generate electricity.

I. WHAT IS QANAT?

Qanat is a gently sloping tunnel which drains the groundwater from aquifer and leads it to the surface by using gravity flow conditions. In fact Qanat benefits from the differences between earth surface elevations to convey water from upstream aquifer to the earth surface down slope. To function this way, Qanat enjoys a number of vertical shafts, a subterranean canal and an appearance. In other words, A qanat is a combination of some shaft wells and a horizontal tunnel with a gentle slope (less than surface gradient) being able to collect the seepage of groundwater and drain it out to the down slop lands.

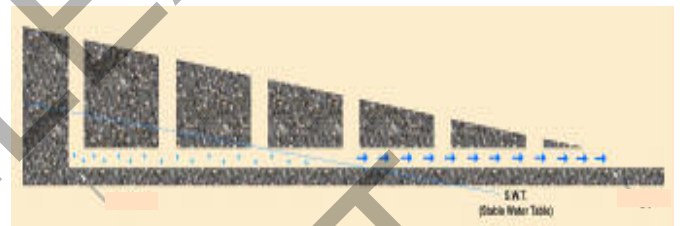


Figure 1. Longitudinal section of qanat

Therefore, qanat can be considered a groundwater drainage system that conveys the build up of groundwater to be used for drinking or irrigation. As shown in the picture below, a qanat is made up by two main sections; water production section and water transport section. That part of the qanat gallery which runs through water bearing zone is called water production section whose function is to collect the seepage. This water is transferred to the earth surface through water transport section which runs through dry zone.

II. QANAT BUILDING AND QANAT DIAGRAM

As it has mentioned, qanat is an underground gallery that conveys water from an aquifer or a water source to lower-elevation irrigated fields. In practice, a qanat consists of a series of vertical shafts in sloping ground, interconnected at the bottom by a tunnel with a gradient gentler than that of the ground. The first shaft is usually sunk into an alluvial fan to a level below the groundwater table. Shafts are sunk at intervals of 20 to 200 meters in a line between the groundwater recharge zone and the irrigated land. From the air, a qanat system looks like a line of anthills leading from the foothills across the desert to the greenery of an irrigated settlement.

The different parts of a typical Qanat are shown in the figure below, described as follows:

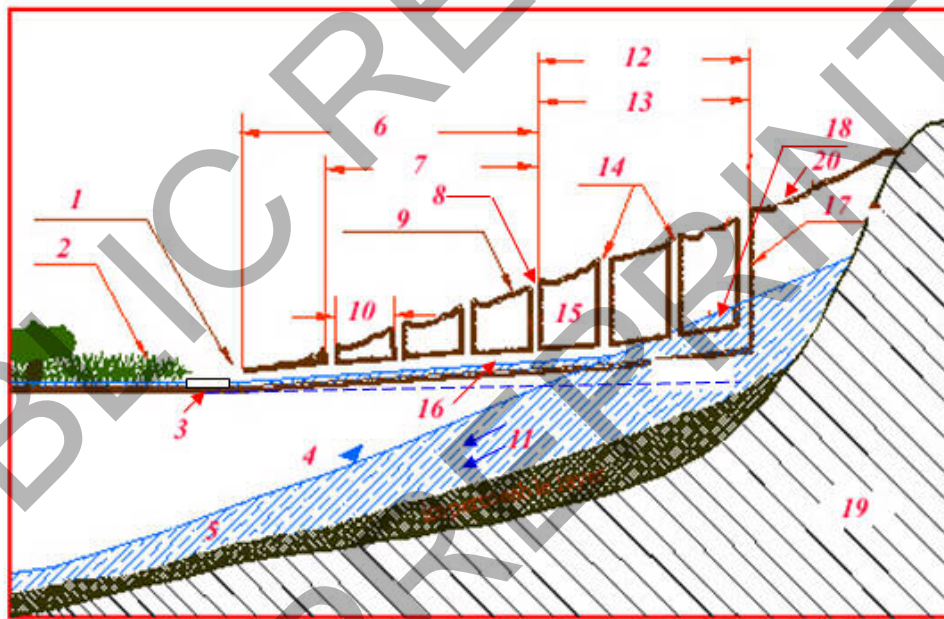
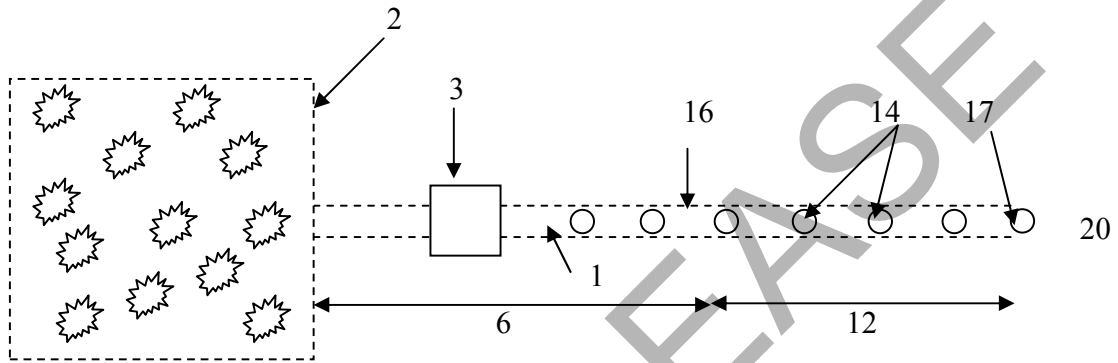


Figure 2. Qanat Diagram

IV. WATERMILL

- | | |
|----------------------------|---------------------------------|
| 1- Qanat exit point | 11- Ground water flow direction |
| 2- Irrigated land (farm) | 12- Water production section |
| 3- Pool | 13- Yielding wells |
| 4- Water table | 14- Vertical shafts (wells) |
| 5- Aquifer | 15- Permeable layer |
| 6- Water transport section | 16- Qanat gallery |
| 7- Dry wells | 17- Mother well |
| 8- Transition zone | 18- Dynamic water table |
| 9- Ground surface | 19- Rock bed |
| 10- Well distance | 20- Infiltration zone |

III. QANAT GALLERY

The Qanat gallery or tunnel is called in Persian "*Rahrow*" or "*Kooreh*", which is an almost horizontal tunnel dug to get access to groundwater reserve, and to transfer this water to the earth surface. The dimensions of the tunnel are taken to be such that the workers can easily go through and work in it. This tunnel is between 1.0 and 1.5 meters high, and its width is less than half the height. The tunnel and surface gradient is crucial in extracting energy from the water flowing down. If the earth surface and tunnel slope would be such that the tunnel and the earth surface intersect at a relatively short distance, the watermill can be constructed.



Figure 3. Qanat Gallery

Qanat related structures are ranked among the most interesting architectural structures, and most of them are relics of the past and considered historical heritage now. The most important qanat related structure built in Iran is watermill which is a structure constructed in order to grind grain. Its main parts are drop tower or water house, two millstones, rotor blades of watermill and an axis which connects rotor blades and upper millstone vertically.

The operation of watermill is based on the potential energy of water due to the depth of drop tower. The deeper drop tower, the more water's energy was generated. Sometimes the depth of a drop tower reaches to 10 meters in order to increase the water pressure.

When qanat's water reaches to the water house, it pours down the well and hit the blades. The water pressure which changes to velocity, make the blades rotate, imparting energy to the rotor and to the upper millstone. The lower millstone is motionless. Therefore the friction between the upper and lower millstones turns the wheat into flour. Sometimes, several watermills might be operated by the water of only one qanat.

According to the way in which watermill draws on the energy of water, the watermills can be classified into two groups as: a) potential watermill b) kinetic watermill

The two types of watermill are based on the difference between the heights of water input and output. In kinetic watermills the axis is horizontal, drawing on the water flow directly, whereas in potential watermills a difference between the heights of water inflow and outflow should be built artificially, such that the required energy to run the watermill would be generated. This type of watermill with vertical axis is the same as built in the qanat gallery.



Figure 4. Watermill

As mentioned a qanat is a subterranean canal to convey groundwater on to the earth surface, and this canal is intended to surface just near the cultivated area or village where the water is to be used. But in many cases the water table is such that the exit point of qanat does not show up just where the workers want, but some distance upslope from the village. Thus the workers have to channel this water again by digging a well and an almost horizontal tunnel from the exit point to wherever they need water. When the water is transferred through such an underground canal, the water less evaporates and it is less likely to take water illegally on its way to the village.

When the water is to be re-channeled, first a shaft well is sunk, from the bottom of which a tunnel is dug up, stretching out to the earth surface near the village. This shaft well can be drop tower for a watermill underground where the build up of water in the well can provide adequate water pressure to rotate the millstone. At the bottom of the well, a small hole is made such that water can spout out of it and hit the rotor blades of the watermill. Thus the rotor blades would turn and the movement would be imparted to the upper millstone by a shaft which passes through a hole in the lower millstone and then turns the upper one horizontally. There is a gap through which wheat can be put between the two millstones whose friction turns the wheat into flour. The distance between the two millstones is adjustable by a handle so that the wheat can be grinded soft or hard. The vertical axis that imparts the spin of rotor to the upper millstone is braced such that its bottom turns on a piece of iron stone which is fixed in a hole in a tree trunk. The bottom of the axis is so sharpened and covered in a metal cap that the friction between the axis and the iron stone at its base would be minimized.

Nowadays this technology has been abolished, because wheat is subsidized and purchased by the government, and is grinded in big factories. So the villagers no longer need the underground watermills to grind wheat. Nevertheless the idea of this paper – generating electricity – was inspired by the abandoned watermills, and we place turbine on the way of groundwater though this time its product is electricity not flour.

V. QANAT TURBINE

According to the classification of the hydropower projects, generating electricity of qanat is among the group of "Pico-Hydro" which includes the projects generating between several hundreds watts and 5 kilowatts to supply electricity to the regions out of the range of power network for domestic and limited uses. We conducted a study in the province of Yazd in Iran on the potential that the qanats have to generate electricity. In this area some 3200 qanats are running, most of which enjoy a head less than 8 meters, so it seems that the

suitable turbines for these qanats are Francis, Kaplan and the propeller turbines. Taking into account the diagram 1 that depicts the suitable turbines in relation to the qanats head and discharge, the turbines of Kaplan and Banki Michell have the most efficiency, because most of the qanats in this province enjoy a head less than 8 meters and a discharge below 1 cubic meter per second. This diagram also helps find out the limits of the electricity less than 10 megawatts. In terms of a low discharge (below 150 liters per second) which is applicable to the province of Yazd, the optimum type of turbine can be determined by the two following diagrams. In case we take the minimum electricity to be some 400 watts just to provide power needed for light and ventilation in the qanat itself, the qanats with low discharge require a head of 10 meters, which can not be found in Yazd. But in terms of the qanats with relatively high discharge and low head, the turbines of Powerpal and Nautilus seem suitable.

In closing we can conclude that: 1) the maximum electricity extracted from such turbines is 1 kilowatt, but considering the length of qanats which is tens of kilometers it is quite possible to install a series of turbines along the tunnel to get more electricity. 2) those qanats whose discharge is below 45 liters per second do not meet the requirements of this project, because this project is in line with the product of net head multiplied by discharge, so in case of lower discharge we need higher head which can not be higher than 8 meters considering the structural condition of the qanats in Yazd.

Due to these requirements, out of 3200 qanats in the province of Yazd, 100 qanats whose discharge is over 45 liters per second providing appropriate head have been singled out. Each of these 100 qanats can house one or several turbines, such that the total electricity generated by them would amount to thousands of kilowatts.

VI. CONCLUSION

Qanat which is an environment friendly technique and does not bring about any environmental backlashes is able to merge with another green technology; hydro turbine which generates electricity in harmony with nature to satisfy the small local demands. This initiative has two advantages: 1) it gives a new function to the ancient qanats and increases their chance to survive. 2) it can improve the economical conditions of the locals by giving rise to a new income source, taking into account that the Iranian government has a policy to purchase electricity from whoever can generate it through an environment friendly method like wind or water turbines.

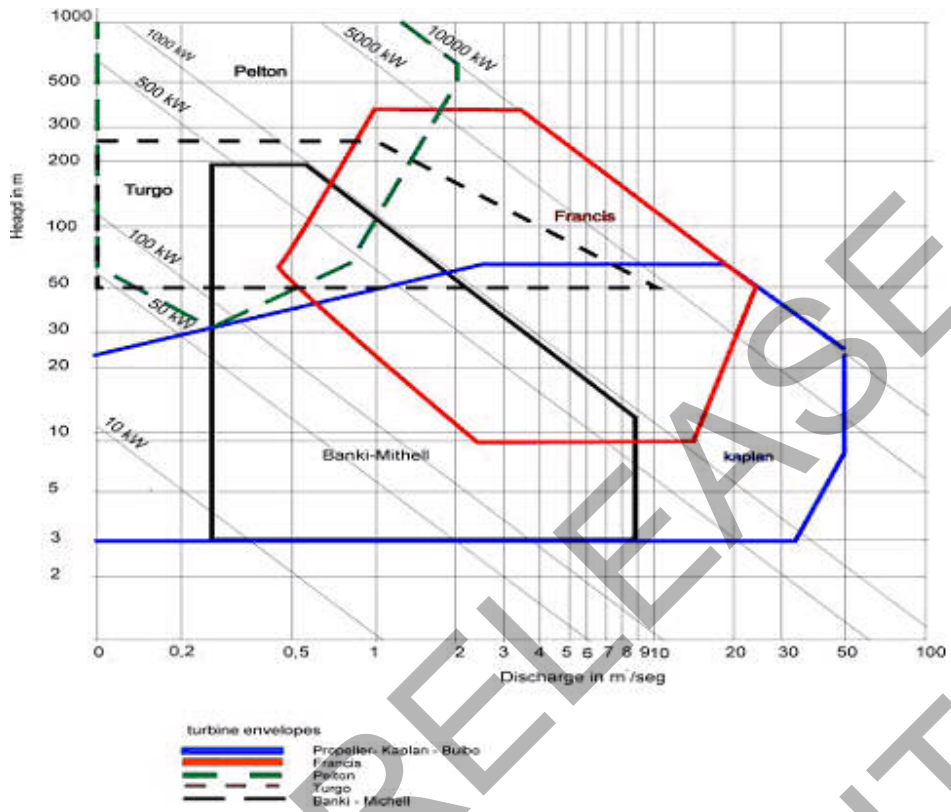


Diagram 1. turbines suitable for different ranges of head and discharge

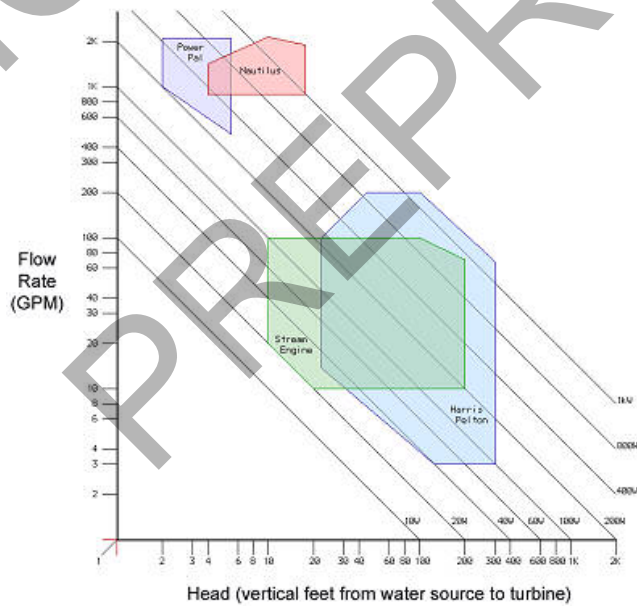


Diagram 2. Effective operating parameters for various water turbines, showing relation of head and flow to expected power out put of each

Fault Liability and Maintenance Cost Modeling of a Steam Turbine

Houdova Lenka, Jelinek Libor, Janecek Eduard
Department of Cybernetics, University of West Bohemia
Univerzitni 8, 306 14, Plzen
Pilsen, Czech Republic

Abstract - This paper focuses on modeling of power stations technological equipment reliability. There is described a method of failure model creation, based on failure and repairs data of a particular components, and cost model creation, based on costs specification. At first there is mentioned the data processing procedure, problems of appropriate stochastic parameters inference and total characterization of failure model connected with small number of data and their dependence on operational conditions in concrete. This model should be able to predict the future conditions and to estimate important evaluation indicators. For that reason it is necessary to introduce the software, which is used for simulation, visualization and optimization future development of evaluation indicators possibilities. This work is a part of the joint project of the UWB and Škoda Power company called "Operational availability and maintenance cost optimization with the computer support".

I. INTRODUCTION

One of the basic tasks of management in operational reliability control area is planning and making the strategic decisions. It is important especially in energetic, where an effect of maintenance prove at fault liability and expensiveness of potential consequences. Planned and preventive maintenance activities are instruments for technological equipment lifetime raising and for contractual power supply provision. These activities have decisive effect to total operational cost too. In order to be optimal this service task, it is necessary to make an extended analysis, failure causes and effects calculations with respect to task effect and production progress strategy.

The aim of this paper is to bring out the problem of processing the information from steam turbine operation to proper form for effective maintenance planning especially based on cost evaluation of outage risk and maintenance.

The principle is the creation of the probability model of operational condition from historical data. This model should be able to predict the future conditions and to estimate important evaluation indicators. With the aid of input conditions and simulation parameters changes it is possible to make sensitivity analysis of indicators in reliability interval, iterative optimizations and finding of the best strategic solution according to given criteria e.g.

II. DATA PROCESSING

A. Data processing basic themes

Model design stem from demand after the components fault

liability character of steam turbine realization in accordance to component failure and repairs data, obtained from Škoda Power (producer). The main aim is time development monitoring of technological unit fault liability. According the analysis there was find out, that the fundamental problem is finding so-called 'hidden failure model' of components without planned maintenance execution (left scheme) based on failure data of components at real operation without applying the planned maintenance (right scheme), see fig. 1.

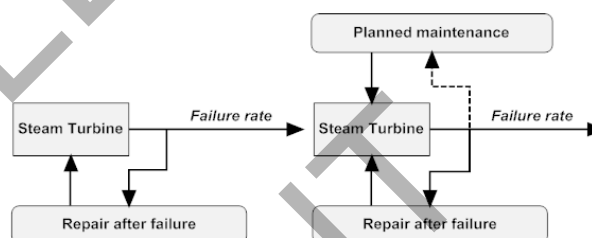


Figure 1. Scheme of failure model with and without planned maintenance

Reduction of planned maintenance effect is possible to solve with expert based adjustment of failure data set or model parameters. To components, which was called for repair at planned maintenance, is attached a failure. Further way is to take a presumption, that failure rate will be rise after the time of planned maintenance interval. The modified model has more pessimistic character then the original, but it is more realistic.

Other problem is definitely small number of failure data of selected component with the low or zero observed fault liability and high technical lifetime. In the case, it is not possible to approximate more complicated stochastic functions by ordinary way. Therefore complex data processing must be used with respect to knowledge based presumptions.

These presumptions are:

- time progression of components failure rate matches to bathtub curve,
- mean failure rate can be determined from designed technical lifetime.

According to the assumptions is possible to set a shape of the estimation parametric function curve or to extend a statistical failure data.

B. Statistical analysis

For stochastic probability distribution of failure origination special parameters must be defined. These can be taken from producer of components or from some reliable database (only

if there was guaranteed an identical form of definition, comparable construction and components properties). However, mostly this information is not available. Then it is necessary to use a standard statistical solution ([1],[2],[3]). According to the historical data about time duration between failures and repair duration it is possible to estimate needful parameters by data analysis. For statistical parameters estimation it is necessary to have a sufficient number of correct values obtained by many realizations. It follows, that the sparse data is necessary to put together for resultant estimation credibility. For compounding of components is used a bunching algorithm repeatedly, orientated firstly to similarity of particular components failure frequency histogram and then to mean time of repair. McQueen bunching algorithm (so-called k-means) is used for implementation. After data compounding it is already possible to estimate standardized group parameters of failure characteristics, which can be later linear recalculate for particular component parameters (with using predefined particular mean time between failure).

For fault liability of mechanical parts definition it is most often applied Tri-weibull stochastic function [2]:

$$I(x) = \frac{b_1 x^{b_1-1}}{h_1^{b_1}} + \frac{b_2 x^{b_2-1}}{h_2^{b_2}} + \frac{b_3 x^{b_3-1}}{h_3^{b_3}} \quad (1)$$

It takes into account time progression of failure rate because of aging very well (otherwise bathtub curve). Module Weibull analysis of Availability Workbench (AWB) software by company Isograph is used to bathtub curve forming. Needful parameters β' a η' characterizing the interlay curve are obtained by cumulative probability graph after particular data groups import.

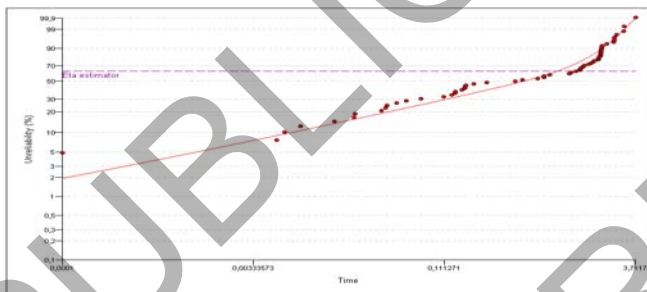


Figure 2. Example of Cumulative probability graph

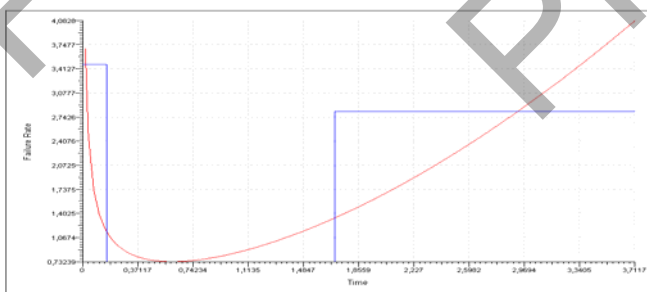


Figure 3. Example of Failure rate graph

On the figures 2 and 3 is displayed a standardized progression of given group failure rate. The results of automatic parameters estimation for particular groups need not to be always satisfactory, that is why it is necessary to adjust them by hand for proper form of failure rate curve (according to expert estimations). After standardized parameters recalculation into particular components parameters is obtained sufficient information for components failure rate progression modeling. For recalculation there is used the time transformation. The basic criteria for this transformation is the curve shape conservation and its proportional expansion to real values of mean time between failures computed from data. The time transformation is applied to Tri-weibull distribution parameters of each component:

$$\begin{aligned} b &= b' \\ h &= h' \cdot MTTF' \end{aligned} \quad (2)$$

where β' and η' are original parameters of standardized distribution for component groups and $MTTF'$ is mean time to failure of particular component.

III. AVAILABILITY AND COST MODEL

A.. Model creation

One of the basic efficiency indicators of steam turbine energy operation is availability, from which is possible to calculate specific technical fault liability. Time progress can be obtained by simulation according to real operation behavior. For implementation of availability model there is used module AvSim of software Availability Workbench.

This module offers the tools for definition and editing of stochastic models string data structure in a several most widespread formalisms and hierarchical structured levels of components characterization to the component cause of failure level.

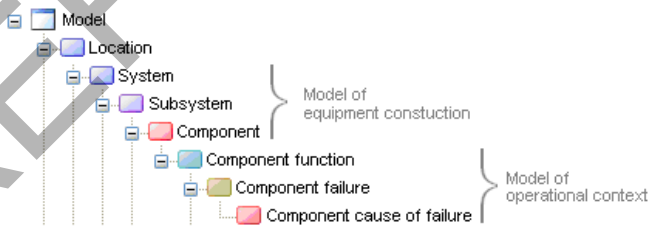


Figure 4. Hierarchical structured levels of components

In model structure point of view, there is used serial sequence principle of selected critical components reliability blocks (the particular components operational probability multiply themselves). Decisive aspect is certainly failure cause and effect ([4]).

To model there can be assigned a various additional information and operational conditions including of costs specification, which are fundamental for cost model. This model is created in other module of AWB called RCMCost.

Simulation is proceeded by Monte-Carlo ([5]) method. There are discerned between the operational and failure condition. Availability is determine as relative ratio of operation duration and total time in view. A number of realizations of random processes are generated and resultant condition is computed as the mean.

B. Planned maintenance effects on fault liability modeling

For every component there exists parameters set, which represents failure origin probability distribution in Tri-weibull function form. Appropriate failure rate function representation is the best way how to characterize the risk progress of failure origin in time on similar conditions and presumptions, under them was the function derived from real failure data.

Due to the information of the major part of the components technical lifetime the parameter estimation is achieved, which eliminates planned maintenance effect from data (at least in part). This effect can be modeled independently (in the various times).

Effect of planned maintenance to the failure rate development is so-called age reduction from probability aspect, which developed a reduction of effective lifetime of every component and whole modeled equipment.

The failure rate progress is changed by the planned maintenance implementation to the model in accordance to the original data. The simulation results should agree with the real data.

Figure 5 shows the example of common component failure rate progress in calendar time – without planned maintenance, when failure rate curve follows up the bathtub curve and with planned maintenance, which is made every 5 years.

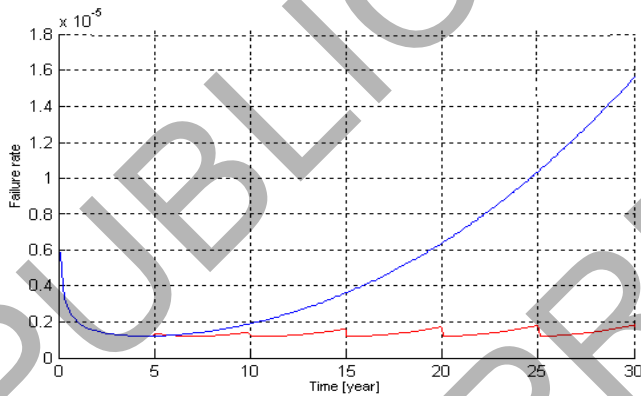


Figure 5. Example of common component failure rate

C. Model verification

Because of small number of data reliable the stochastic distribution parameters estimations aren't fully. That's why it is not possible to consider the result of first simulations to be the final result. It is important to set up the common model so that the simulations results could be comparable with real condition of concrete equipment.

Due to presumptions and hypothesis it is necessary to specify the model according to some stable characteristic

of fault liability, which can be analyzed from data. Mean of year's availability relating to whole monitored operational term is chosen as the verification characteristic. By the ratio of real availability (calculated from data) and simulation availability (estimated by model on the same conditions) the fault coefficient is determined. This fault coefficient is used for proportional optimization of the correction coefficient in accordance to statistical relevancy of number of data.

D. Model correction

The aim of correction is the linear reduction of the failure rate function value. Coefficient of correction depends on number of data for each component and it can be computed in accordance to formula:

$$K = \frac{Q + N}{1 + N}, \quad (3)$$

where Q is optimization parameter, which is changed by ΔQ in every iteration, and N is real failure number of data, from which is estimated given parameter set. This computation is based on presumption, that unavailability increase because of added components failures is necessary for unavailability reduction compensation, especially for components from small number of data.

Model parameters correction is based on transformation of stochastic distribution coefficients. In the case of exponential distribution the simplest way is multiplying by one parameter K – mean time to failure with correction:

$$I^*(x) = \frac{I(x)}{K} = \frac{1}{K \cdot MTTF}, \quad (4)$$

In the case of Tri-weibull distribution the situation is more complicated. It is necessary to multiply every term denominator, then total failure rate become reduced independently from time and curve form is saved. It is appropriate to make correction just for η coefficients in denominator. Calculation is made in accordance to formula:

$$I^*(x) = \frac{b_1 x^{b_1-1}}{(K^{b_1} \cdot h_1^{b_1})^{b_1}} + \frac{b_2 x^{b_2-1}}{(K^{b_2} \cdot h_2^{b_2})^{b_2}} + \frac{b_3 x^{b_3-1}}{(K^{b_3} \cdot h_3^{b_3})^{b_3}}, \quad (5)$$

Result of iterative optimization is parameters of particular components failure model set correction.

IV. AVAILABILITY AND COST SIMULATION, OPTIMIZATION

For getting the close results after model correction and verification it is necessary to correct and completely characterize the availability and cost model from all perspectives (labour, spares, equipment, failure effects, prices etc.). Used software AWB has strictly defined needed resources and functionalities. The scheme of resources and functionalities can be seen on the figure 6.

Simulations made by AWB are focused on fault liability indicator development location. There are randomly generated failure events in defined time horizon and number of realizations according to the required parameters.

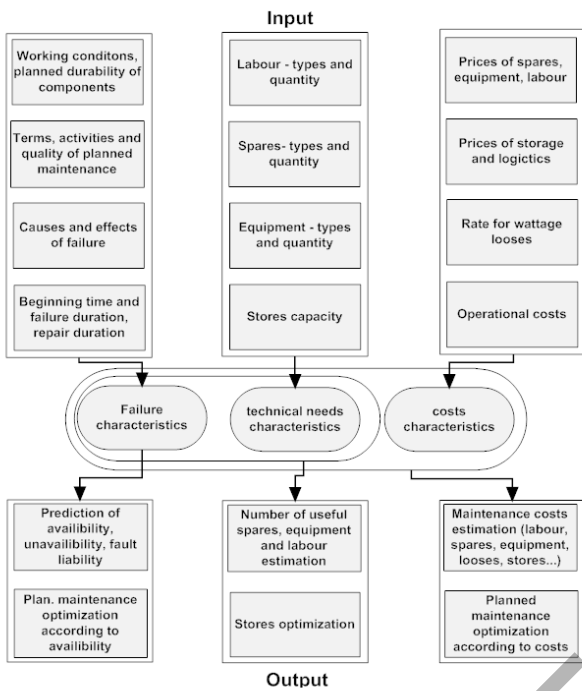


Figure 6. Scheme of needful resources and functionalities of AWB

The simulation results are mean values of availability in every particular period (1 year e.g.) in simulation horizon. According to project assignment the attention is concentrated on simulation of the history and prediction of availability and specific technical fault liability. Many parameters are set up or adjusted according to the expert estimations. On the figure 7 there is shown running of the specific technical fault liability in history.

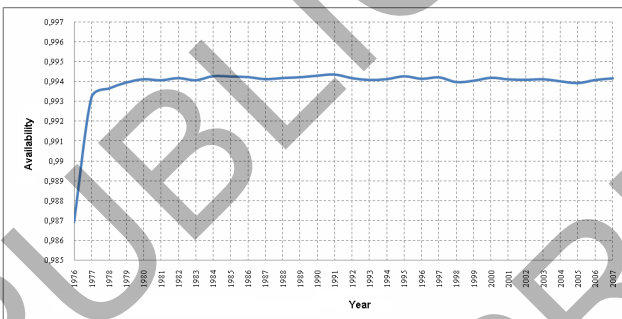


Figure 7. Common steam turbine availability simulation (history)

Cost simulations and planned maintenance interval optimizations are made in RCMCost. Parameters of failure origin probability distribution for cost model are imported from AvSim module and additionally there are rated by cost every maintenance units and failure effects. Software enables the optimal interval calculation from the cost and from the availability perspective.

Simulations are aimed at general and ordinary maintenance interval cost optimization. Optimal interval is a compromise between maintenance costs and costs to repair after failure (see fig. 8).

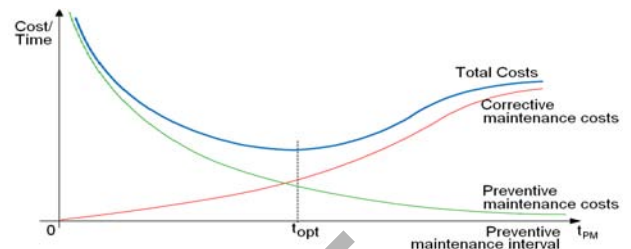


Figure 8. Principal of cost optimization

It is very important to execute the sensitivity analysis, which can show the potential range of resultant characteristics for selected availability parameters estimation interval. Sensitivity analysis can be taken for relative change of mean time to failure of particular components, mean time of repair or for age reduction factor (it characterizes the quality of repair) changes – see fig.9.

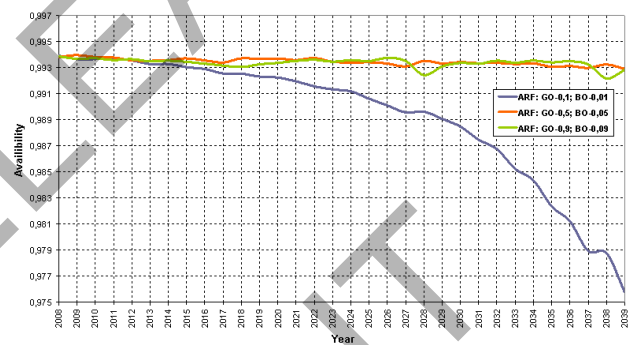


Figure 9. Sensitivity analysis of age reduction factor (ARF)

V. CONCLUSION

Fault liability modeling and simulations of condensing steam turbine described above is focused on availability and cost prediction (with the option to change the operational condition, particular terms and planned maintenance range). As the results it can be computed for example expected operational availability values, which could be used for power supply provision guarantee or as recommendation for planned maintenance optimal time and range. These resultant technical-economic indicators are useful for turbine producers, which must guarantee the failure-free operation and service, and for users (energy companies), which can predict their own management conditions and the expansion planning.

REFERENCES

- [1] J. Novotny, *The Steam Turbine 200 MW Reliability*, Diploma work: ZCU Plzen, 2008, in Czech only
- [2] A. Papoulis, *Probability, Random Variables, and Stochastic Processes*, 4th ed., Boston, 2002
- [3] V. Kuchar, *Methodology of Reliability Data in UE CEZ a.s. Evidence*, I&C Energo Brno: Brno, 2006, in Czech only
- [4] Isograph, "AWB 2007 user guide," Isograph Limited, 2007
- [5] M.A. Tanner, *Tools for Statistical Inference*, 3rd ed., Springer Verlag: New York, 1996

VOLTAGE STABILITY ANALYSIS OF GRIDS CONNECTED WIND GENERATORS

¹Nguyen Tung Linh²; Trinh Trong Chuong;
¹Electric Power University ²Ha Noi University of Industry

Abstract

Wind generators can have a significant impact on the power flow, voltage profile and the power quality for customers and electricity suppliers. This requires a suitable tool to analyze the influence of wind generators on the distribution system. This paper presents a method to find the steady-state voltage stability region for each bus of a distribution power system, considering the presence of wind power generation. The maximum permissible load of each bus is calculated, so that it can operate with the voltage within the limits allowed by the power system utilities.

Keywords: Wind generator, Voltage stability

1. Introduction.

Recently wind power generation has been experiencing a rapid development in a global scale. The size of wind turbines and wind farms are increasing quickly; a large amount of wind power is integrated into the power system. As the wind power penetration into the grid increases quickly, the influence of wind turbines on the power quality and voltage stability is becoming more and more important. It is well known that a huge penetration of wind energy in a power system may cause important problems due to the random nature of the wind and the characteristics of the wind generators. In large wind farms connected to the transmission network (110 kV – 220 kV) the main technical constraint to take into account is the power system transient stability that could be lost when, for example, a voltage dip causes the switch off of a large number of wind generators.

In the case of smaller installations connected to weak electric grids such as medium voltage distribution networks, power quality problems may become a serious concern because of the proximity of the generators to the loads. The existence of voltage dips is one of the main disturbances related to power quality in distribution networks. In developed countries, it is known that from 75% up to 95% of the industrial sector claims to the electric distribution companies are related to problems originated by this disturbance type. These problems arise from the fact that many electrical loads are not designed to maintain their normal use behaviour during a voltage dip. The aim of this paper is to conduct a voltage stability analysis using an iterative power system simulation package, to evaluate the impact of strategically placed wind generators on distribution systems with respect to the critical voltage variations and collapse margins. This paper concludes with the discussion of wind generators excellent options for voltage stability.

2. Induction machines.

Induction machines are used extensively in the power system as induction motors but are not widely used as generators. Despite their simplicity in construction, they are not preferred as much as synchronous generators. This is mainly due to the defined relationship between the export of P and absorption of Q. However, induction generators have the benefits of providing large damping torque in the prime mover, which makes it suitable for the application in fixed speed wind turbines. The fixed speed wind turbine uses a squirrel cage induction generator that is coupled to the power system through a connecting transformer as shown in Figure 1. Due to different operating speeds of the wind turbine rotor and generator, a gearbox is used to match these speeds. The generator slip slightly varies with the amount of generated power and is therefore not entirely constant.

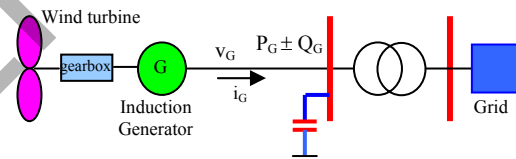


Figure 1: Modelling wind turbine connected grid

However, because these speed variations are in the order of 1 per cent this wind turbine is normally referred to as constant speed. Nowadays, this type of wind turbine is nearly always combined with stall control of the aerodynamic power, although pitch-controlled constant speed wind turbine types have been built in the past. Induction machines consume reactive power and consequently, it is present practice to provide power factor correction capacitors at each wind turbine. These are typically rated at around 30 per cent of the wind farm capacity. As the stator voltage of most wind turbine electrical generators is 690V, the connecting transformer of the wind turbine is essential for connection to the distribution network and should be considered when

modeling the electrical interaction with the power system [3].

3. Impacts of WGs.

Connecting a generation scheme to a distribution network will affect the operation and performance of the network depending on the scheme and rating of the generator itself. The impacts are as follows:

- Power Flows
- Voltage stability
- Fault Analysis
- Impact of WTs on the Networks

3.1 Voltage Stability

A system experiences a state of voltage instability when there is a progressive or uncontrollable drop in voltage magnitude after a disturbance, increase in load demand or change in operating condition. The main factor, which causes these unacceptable voltage profiles, is the inability of the distribution system to meet the demand for reactive power. Under normal operating conditions, the bus voltage magnitude (V) increases as Q injected at the same bus is increased. However, when V of any one of the system's buses decreases with the increase in Q for that same bus, the system is said to be unstable. Although the voltage instability is a localised problem, its impact on the system can be wide spread as it depends on the relationship between transmitted P , injected Q and receiving end V . These relationships play an important role in the stability analysis and can be displayed graphically [1].

PV Curves

When considering voltage stability, the relationship between transmitted P and receiving end V is of interest. The voltage stability analysis process involves the transfer of P from one region of a system to another, and monitoring the effects to the system voltages. This type of analysis is commonly referred to as a PV study.

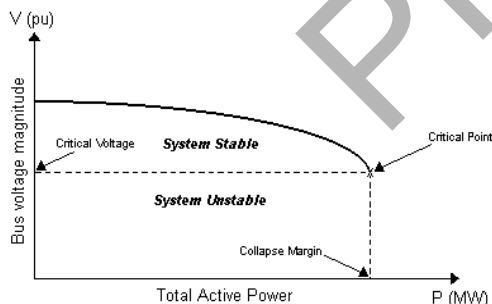


Figure 2: Characteristic P-V

The Figure 2 shows a typical PV curve. It represents the variation in voltage at a particular bus as a function of the total active power supplied to loads or sinking areas. It can be seen that at the “knee” of the PV curve, the

voltage drops rapidly when there is an increase in the load demand. Load flow solutions do not converge beyond this point, which indicates that the system has become unstable. This point is called the Critical point. Hence, the curve can be used to determine the system's critical operating voltage and collapse margin. Generally, operating points above the critical point signifies a stable system. If the operating points are below the critical point, the system is diagnosed to be in an unstable condition [5].

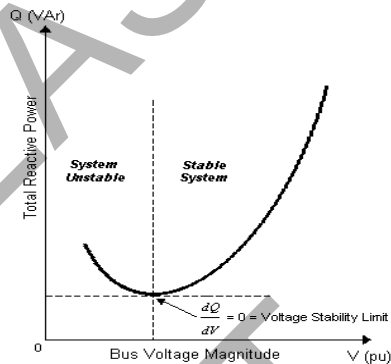


Figure 3: Charactic Q-V

QV Curves

Voltage stability depends on how the variations in Q and P affect the voltages at the load buses. The influence of reactive power characteristics of devices at the receiving end is more apparent in a QV relationship. It shows the sensitivity and variation of bus voltages with respect to reactive power injections or absorptions. Figure 3 shows a typical QV curve, which is usually generated by a series of load-flow solutions. Figure 3 shows a voltage stability limit at the point where the derivative dQ/dV is zero. This point also defines the minimum reactive power requirement for a stable operation. An increase in Q will result an increase in voltage during normal operating conditions. Hence, if the operating point is on the right side of the curve, the system is said to be stable. Conversely, operating points in the left side of the graph are deemed to be unstable [4, 5].

PQ curves.

The maximum permissible loading of a system, within the voltage stability limit, is usually determined from the well known $P-V$ curve or $Q-V$ curve. The $P-V$ curve is plotted for a constant power factor and the $Q-V$ curve is plotted for a constant power. A series of computer simulations is required to generate a family of these curves [6]. There are other methods to find the voltage stability limit of a system, such as multiple load flow solutions, singularity criterion of the Jacobian matrix [7]. It is an established fact that the voltage collapse occurs when the system load increases beyond a certain limit. If the limiting values of P and Q are known, the voltage stability margin for a given operating point can

directly be determined. This requires the plotting of voltage stability boundary of the system in $P-Q$ plane, however, using the limiting values of P and Q . To the best knowledge of the author, no such work has been reported so far that can determine the voltage stability margin using the $P-Q$ curve.

In this letter, the limiting or critical values of P and Q at the voltage collapse point are first determined and then used to plot the voltage stability boundary in $P-Q$ plane. Unlike the conventional $P-V$ or $Q-V$ curves, no fixed value of power or power factor is used in generating the stability boundary [8]. Using the above curve, the voltage stability margin in terms of P , Q , or S (for a given power factor) can easily be determined when the initial operating point is known. Consider the equivalent π model of a distribution line connected between bus i and bus j as shown in Fig.4.

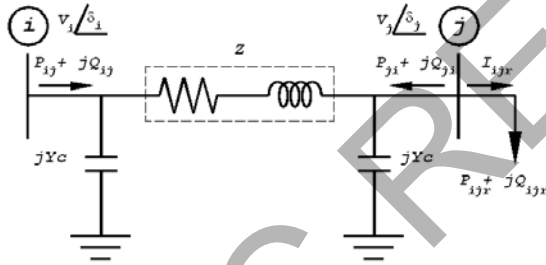


Fig.4: The π model distribution line connected between bus i and bus j

We can formulate the relationship between injected current and voltage at any buses based on generalized ABCD parameters as follows:

$$V_i \angle \delta_i = AV_i \angle \delta_i + BI_j \quad (1)$$

where $A = 1 + ZYc$ and $B = Z$. The complex form of A and B can be expressed as shown in (2).

$$A = a_1 + ja_2 \text{ and } B = b_1 + jb_2 \quad (2)$$

The receiving end current, I_{jr} , can be expressed:

$$I_{jr} = (P_{jr} - jQ_{jr}) / V_j \angle -\delta_j \quad (3)$$

Substitute A and B from (2) and I_{jr} from (3) into (1) resulting in (4).

$$V_i \angle \delta_i = (a_1 + ja_2)V_j \angle \delta_j + \frac{(b_1 + jb_2)(P_{jr} - jQ_{jr})}{V_j \angle -\delta_j} \quad (4)$$

or:

$$c_1 V_j^4 + (c_2 P_{jr} + c_3 Q_{jr} - V_i^2) V_j^2 + c_4 (P_{jr}^2 + Q_{jr}^2) = 0$$

$$\text{or: } aV_j^4 + bV_j^2 + c = 0 \quad (5)$$

where:

$$a = c_1 = a_1^2 + a_2^2; b = c_2 P_{jr} + c_3 Q_{jr} - V_i^2; c = c_4 (P_{jr}^2 + Q_{jr}^2)$$

$$c_1 = a_1^2 + a_2^2; c_2 = 2(a_1 b_1 + a_2 b_2); c_3 = 2(a_1 b_2 + a_2 b_1)$$

$$c_4 = b_1^2 + b_2^2$$

The solution of (5) is the square of the receiving end voltage. Thus the receiving end voltage can be calculated from (6).

$$V_j = \sqrt{\frac{-b \pm \sqrt{b^2 - 4ac}}{2a}} \quad (6)$$

There are two solutions for (6), the lower solution lies on the lower part of the $P-V$ curve and is unstable [4]. Thus, the available solution is a stable one on the upper half, which can be expressed as in (7).

$$V_j = \sqrt{\frac{-b - \sqrt{b^2 - 4ac}}{2a}} \quad (7)$$

The point where the two trajectories, i.e. stable and unstable lines, are joined is the nose or bifurcation point. In addition, this is the point where the maximum power can be transferred, which is the condition $b^2 - 4ac = 0$. Substitute coefficients of the quadratic equation from (4) into (7) and rearrange, we obtain (8).

$$(c_2^2 - 4c_1 c_4) P_{jr}^2 + (c_3^2 - 4c_1 c_4) Q_{jr}^2 - 2c_2 V_i^2 P_{jr} - 2c_3 V_i^2 Q_{jr} + 2c_2 c_3 P_{jr} Q_{jr} + V_i^4 \quad (8)$$

The relationship between P_{jr} and Q_{jr} of (8) is a locus of the collapsing point on the $P-Q$ plane which separates the operating points into feasible and infeasible regions. The calculation method to obtain the predicted collapsing point can be illustrated in Fig.5.

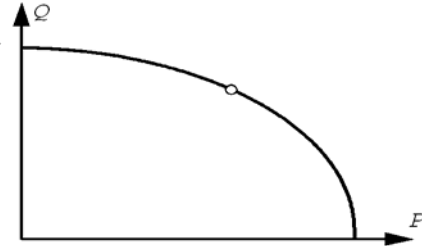


Fig.5: The predicted collapsing point calculation.

3.2 Test Systems.

Fig. 6 shows the simplified diagram of test system. It has 20 buses operating at the voltage of 12.47 kV, 19 circuits/transformers, and the hypothetical wind power is connected at bus 20 at 0.69 kV. The detailed of the system is not showed but it has only one circuit of 138 kV [4]. The power wind farm is a variable speed directdrive synchronous generator connected to the Point of Common Coupling, (PCC) by a full-load converter. It can be represented by a $P-Q$ bus or a $P-V$ bus, since it has the capacity to control the reactive power.

Table 1. LINE PARAMETERS OF DISTRIBUTION SYSTEM IN PER UNIT ON 40 MVA BASE.

Line number	From	To	Resistance	Reactance
1	1	2	0.1196	0.1263
2	2	3	0.125	0.1505
3	2	9	0.0713	0.0185
4	2	10	0.0664	0.0702
5	3	4	0.0936	0.1129
6	3	5	0.6294	0.7586
7	5	6	0.3123	0.3766
8	5	7	0.624	0.4947
9	5	8	0.6559	0.5201
10	10	11	0.0561	0.0592
11	10	16	0.0859	0.0908
12	11	12	0.0471	0.0496
13	11	15	0.037	0.0095
14	12	13	0.08	0.0844
15	12	14	0.0257	0.0067
16	16	17	0.0229	0.0059
17	16	18	0.0286	0.0075
18	19	1	0	0.28
19	20	12	0	0.28

TABLE II: DISTRIBUTION SYSTEM BUS DATA AFTER THE CONVERGENCE OF THE POWER FLOW.

Bus number	P_L MW	Q_L MVAR	P_G MW	Q_G MVAR
1	0.4	0.15	0	0
2	0.4	0.15	0	0
3	0.4	0.15	0	0
4	0.5	0.2	0	0
5	0.5	0.2	0	0
6	0.6	0.25	0	0
7	0.5	0.2	0	0
8	0.5	0.2	0	0
9	0.8	0.3	0	0
10	0.75	0.3	0	0
11	1	0.4	0	0
12	2	0.85	0	0
13	1	0.35	0	0
14	0.75	0.3	0	0
15	0.75	0.3	0	0
16	1.5	0.6	0	0
17	0.5	0.2	0	0
18	0.5	0.2	0	0
19	0	0	6.3	6.8
20	0	0	7.5	0

The loads are distributed considering the thermal limits of the conductors. The line parameters, loads and Generator data are at the Tables I and II. The load is increased with steps of 0.5% in all loads, starting from a normal operating point. The limits of the safe voltage in distribution buses are 0.95 to 1.05 per unit. The system was simulated considering two different scenarios.

• *First:* the wind power generation is connected and operates as a P-Q bus with unit power factor. His particular operating point for actual operation state is $P_G = 7.5$ MW and $Q_G = 0.0$ MVAR . The Wind Power can also be represented by a P-V bus with the reactive power limits, so that when the limits are reached, it becomes a P-Q bus. In modern wind turbine system it is possible to control the power factor, provides in this way, an additional source of reactive to help the power systems to control de voltage.

• *Second:* without Wind Power Generation.

Fig. 7, 8 show the first scenario and the second for the load buses 13 of the system.

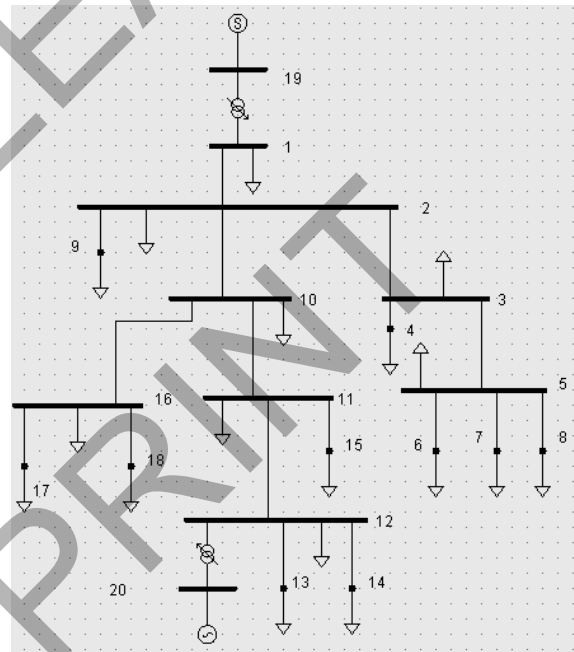


Fig.6: Distribution Power System Test.

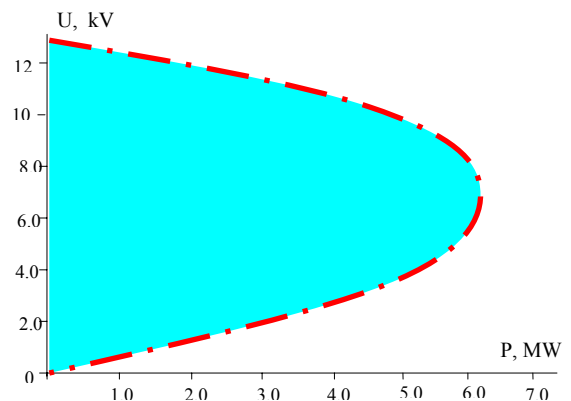


Fig. 7. Loading in bus 13 - Voltage stability region with the contribution of wind power.

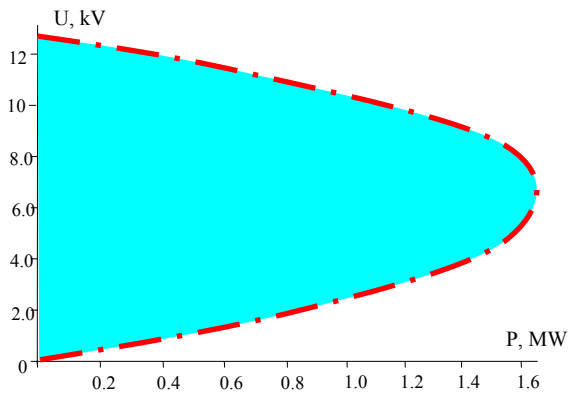


Fig. 8. Loading in bus 13 - Voltage stability region without wind power.

4. CONCLUSION

A very efficient method is presented to determine the maximum permissible load that can be allowed in each bus of a distribution power system. To ensure the reliability of the results, a comparison between the proposed and a previous analytical method is carried out in a simple two bus system connected by a single transmission line. The results are very close and the proposed method was applied on a distribution power system. The presence of wind power is considered in order to analyze the effect of this generation on voltage operation and at the voltage stability limits. The voltage stability limit region and a sub-region in which the voltages at the bus are in acceptable ranges are defined for different power factors. For practical purposes, the PQ curves can be useful to determine the capacity of certain buses of the system to support an increasing in the load demand. Of course, to meet the new demand, the limits of secure voltages must be determined. P-Q curves can help the utilities in the choice the best point to connect the wind farms.

5. References.

- [1]. P.Kundur: *Power: System Stability and Control*, New York: McGraw-Hill, 1994.
- [2]. Ake Anderson; *Power quality of wind turbines*; Thesis Degree of Doctor of Philosophi; Chalmers University of Technology; Goteborg Swedent 2000.
- [3]. Fritz W. Mohn, C. Zambroni de Souza: *Tracing PV and QV Curves with the Help of a CRIC Continuation Method*, IEEE Trans. on Power Systems, Vol. 21, N° 3, pp.1115- 1122, 2006.
- [4]. McGraw-Edison Company, Power System Division: *Distribution-System Protection Manual*.
- [5]. M. Chinchilla, S. Arnalte, J.C. Burgos, and J.L. Rodriguez: *Power limits of grid-connected modern wind energy systems*, *Renewable Energy*, September 2005, pp. 1455-1470.
- [6]. Richard Piwko, Nicholas Miller, Juan Sanchez Gasca, Xiaoming Yuan, Renchang Dai, James Lyons;

Integrating Large Wind Farms into Weak Power Grids with Long Transmission Lines; IEEE/PES Transmission and Distribution Conference & Exhibition, China, 2005.

[7]. L. S. Barros, W. S. Mota, D. F. P. Moura; *Matrix Method to Linearization and State Space Representation of Power Systems Containing Doubly Fed Induction Machines Operating as Wind Generators*; 2006 IEEE PES Transmission and Distribution Conference and Exposition Latin America, Venezuela.

[8] Poul Sørensen, Anca Hansen, Lorand Janosi, John Bech, Birgitte Bak-Jensen; *Simulation of Interaction between Wind Farm and Power System*; Risø National Laboratory, Roskilde December 2001.

Organic solar cells based on ZnO nanowires layer

Jiří Podzemský¹, Wolfgang Schade²

¹Czech Technical University, Faculty of Electrical Engineering
Technická 2

Prague, Czech Republic

²TU Clausthal, Institute of Physics and Physical Technologies
Leibnitzstr. 4

Clausthal-Zellerfeld, Germany

Abstract- In our research we are looking for alternative to solar cells based on silicon. We are using zinc oxide (ZnO) which is N type semiconductor instead of silicon. To reach PN junction P type polymer is used. ZnO is in form of well aligned nanowires. Since the distance between nanowires is smaller than the mean free path of electrons almost all emitted electrons are collected. We use vapor-liquid-solid (VLS) method to create ZnO nanowires. Used substrate was sapphire, silicon and silica glass. Small solar cell was manufactured and its open circuit voltage under light was measured.

I. INTRODUCTION

Scientists all around the world are looking for new energy resources or are improving current techniques of conversion to electric energy. Conversion from sunlight is one of promising method. Except sufficient natural conditions, the growing price of silicon is one of its disadvantages. Conventional solar cell uses tree or comb structure of contacts to collect emitted electrons. These structure must be fine enough comparable with mean free path of electron. If not so, emitted electrons recombine inside the semiconductor material and are not generating desired current. One way how to collect all emitted electrons is to make the structure of contact very fine. In our case one of contacts is semiconductor zinc oxide in form of well aligned nanowires. Herewith collecting electrode is inside the structure of solar cell and makes active part of PN junction. In addition the structure of ZnO nanowires is very fine.

Zinc oxide is transparent N type semiconductor material with wide direct band gap 3.4 eV at room temperature. This direct band gap is profitable for use in solar cell applications. Other properties of ZnO favorable for electronic applications include its stability to high-energy radiation and to wet chemical etching. Radiation resistance makes ZnO a suitable candidate for space applications (it corresponds to fact that solar panels are used as a power source) [4].

II. EXPERIMENTS AND RESULTS

There are many methods how to create well aligned structure of zinc oxide nanowires. We used vapor-liquid-solid method (see fig. 1) [1]. This method is very sensitive to the substrate because the principle of this method is based on epitaxial growth. It is necessary to have substrate with internal structure very similar to structure of zinc oxide, low lattice mismatch is required. Such we used silica glass, sapphire and silicon. The

experiments were done also with ordinary lab glass, but the result was like expected (in means no structure of zinc oxide was created on it). The lattice mismatch also influences a structure of created nanowires layer. Sapphire as a material with internal structure very similar to one of zinc oxide allows the growth of perpendicular zinc oxide wires. On the other hand on substrate made of silicon and silica glass the wires have disordered structure.

In process of manufacturing of zinc oxide nanowires we put onto glass boat our substrate covered with gold film and near to the substrate we put mixture of ZnO powder and graphite powder (see fig. 4). This boat is given into the furnace with defined heating cycle (maximum temperature is $1100 \div 1200$ °C). Argon atmosphere was used. ZnO powder is reduced by graphite to Zn vapor and CO/CO₂. The Zn vapor is transported to substrate and creates alloy with gold. When the alloy (droplet) is saturated, Zn oxidizes with oxygen and nucleates under the Zn-Au alloy droplet. Such ZnO nanowire (with Zn-Au alloy tip) is formed. The position where nanowire will appear is selected by the presence of gold clusters. Such we can create pattern of zinc oxide nanowires. The thickness of gold which we use in our experiments is 2.5 nm. All substrates had dimensions 10x10 mm.

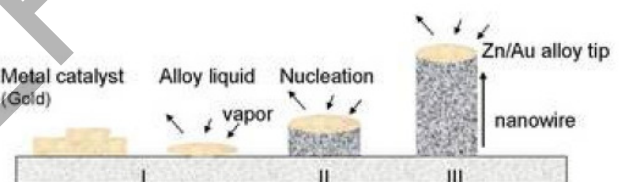


Figure 1. Basic scheme of the VLS process in a tube furnace [2].

When the maximum temperature was kept for the duration of desired time the furnace is turned off and the cooling is provided under the natural cooling. When the temperature inside is near to the room temperature, the boat with our substrate is taken out of the furnace.

The diameter of nanowire grown on silicon and silica glass was similar and was about 100 nm, on sapphire the nanowire was thicker with diameter about 350 nm (see fig. 2). The diameter of nanowire on the substrate depends on the thickness of gold cluster. Thicker gold cluster creates thicker nanowire.

The length of nanowires depends on the time during which the maximum temperature is applied. The type of substrate does not influence the length a lot. The time changed from 35 to 60 minutes and the related length varied from 1 to 15 μm . Also the length of nanowires was not constant on the same substrate. For example on the same substrate a length of nanowires varied from 7 to 13 μm . That is obvious from the position of the substrate on the boat (see fig. 4).

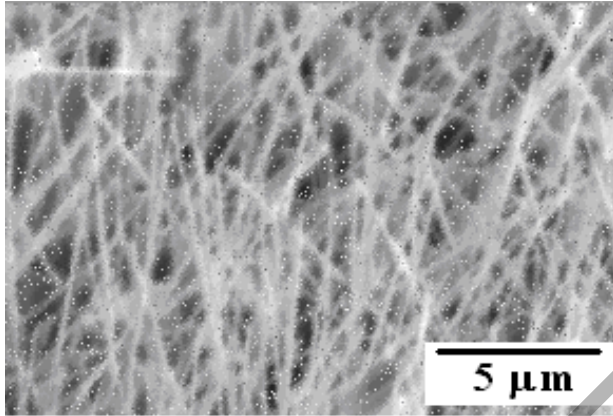


Figure 2. SEM image of structure of ZnO nanowires on silicon substrate.

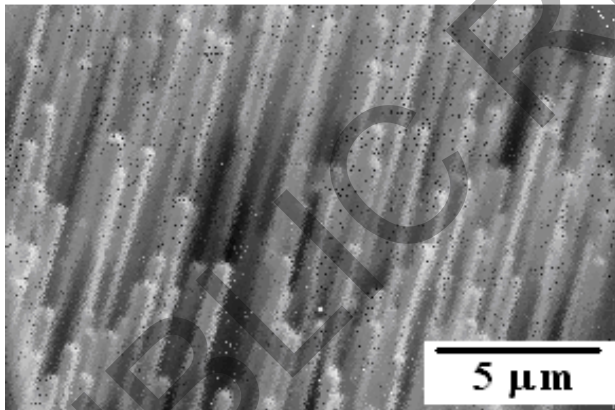


Figure 3. SEM image of structure of ZnO nanowires on sapphire substrate.

The method of VLC growth is very sensitive. The furnace has to have temperature zones to reach temperature gradient to allow vapor of zinc to condensate. The result if layer of ZnO is created or not very depends on the position of our substrate and position of zinc oxide source inside the tube furnace.

Droplet of polymer (P type semiconductor) is applied on the surface of substrate covered with ZnO nanowires and when the polymer is dried polymer and ZnO are contacted with silver varnish. Such created solar cell is on fig. 5.

Used polymer as a P semiconductor was PEDOT (commercial name Clevios P by company H.C. Starck) with chemical name poly(3,4-ethylenedioxythiophene) poly(styrenesulfonate) aqueous dispersion. Different concentrations and thickness of polymer was tested. Polymer

was dilute with distilled water to reach concentration 1:3, 1:5, 1:8 (polymer : distilled water). Concentrated polymer was applied in different thicknesses. Different thickness was prepared such that we put drop of concentrated polymer on the substrate and we regulated the volume of concentrated polymer with syringe. Such we sucked out concentrated polymer but the diameter of created drop was same. That was very easy way how to control the thickness. When dried the area was same but the thickness of polymer differed.



Figure 4. Boat with mixture of zinc oxide and graphite on the sides, substrate is put in the centre of the boat. White part is reacted ZnO. Situation after heating cycle – substrate is covered with ZnO.

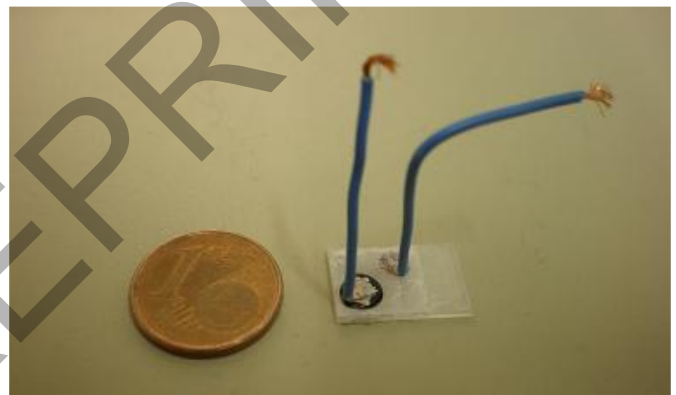


Figure 5. Realization of solar cell.

Open circuit voltage of created solar cell was measured under light intensity 45 000 lx. Spectrum and intensity of light is on the fig. 6 (for comparison sunlight is depicted also). Reached open circuit voltage for each combination of thickness of polymer and concentration of PEDOT polymer is shown in Table I. After measuring open circuit voltage, thickness of polymer and zinc oxide layer was measured with using atomic force microscope. Measured values are in Table II.

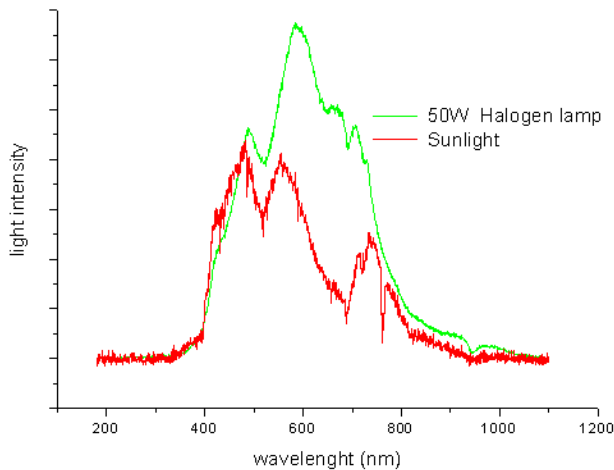


Figure 6. Spectrum and light intensity of halogen lamp and sunlight in the laboratory.

TABLE I
OPEN CIRCUIT VOLTAGE OF SOLAR CELL WITH DIFFERENT THICKNESS OF POLYMER ON SILICON. LIGHT INTENSITY IS 45 000 LX. ALL VALUES ARE IN MILLIVOLTS.

conc.	thickness of polymer		
	high	medium	low
1:3	0.8	0.6	0.1
1:5	0.6	0.2	0.2
1:8	0.2		

TABLE II
THICKNESS OF POLYMER AND ZINC OXIDE LAYER ON SILICON

conc.		thickness of polymer		
		high	medium	low
1:3	ZnO	7.05	9.4	12.75
	poly	2.46	1.51	1.36
1:5	ZnO	9.87	13.61	9.58
	poly	3.5	3.18	1.51
1:8		high		
	ZnO	13.95		
	poly	5.08		

As shown in the table I, the highest open circuit voltage on silicon substrate was reached for polymer PEDOT concentration 1:3 (0.8 mV). That is why we decided to apply this concentration in case of using silica glass as a substrate. In case of silica glass we applied 4 types of thickness of polymer PEDOT in concentration 1:3. Thickness of zinc oxide nanowires layer was constant in all surface of our substrate and was 1.22 μm . Results of measured open circuit voltage are in

Table III. Highest open circuit voltage was 0.9 mV and this was reached for thickness of polymer 2.3 μm (thickness of zinc oxide nanowires was 1.22 μm). Such we got highest open circuit voltage than in case of silicon substrate. We demonstrated that values gained in case of silicon substrate are not influenced by the material of substrate because we got maximum voltage comparable to one on silicon which is N type semiconductor. Silica glass is insulator.

TABLE III
THICKNESS OF POLYMER AND OPEN CIRCUIT VOLTAGE OF SOLAR CELL CREATED ON SILICA GLASS. LIGHT INTENSITY 45 000 LX. THICKNESS OF ZINC OXIDE 1,22 MICRONS.

	thickness of polymer			
	high	medium 1	medium 2	low
polymer (μm)	3.44	2.3	1.83	0.99
OCV (mV)	0.8	0.9	0.6	0.3

PEDOT polymer was also applied on nanowires on sapphire. There was not measured any voltage. The reason is very simple. The nanowires are perpendicular and there are not in electrical contact.

III. CONCLUSION

Organic solar cell based on layer of zinc oxide nanowires was created. N part of junction was zinc oxide, P part polymer PEDOT. Maximum reached open circuit voltage was 0.9 mV. Base material of substrate does not influence gained voltage, serves only as a substrate for creation of zinc oxide nanowires. It is not supposed to manufacture solar panels with method mentioned above (vapor-liquid-solid method) because this method is limited by material of substrate. Materials which serve as a substrate for creation of zinc oxide nanowires are expensive and the process is energy expensive. But with chemical methods we can create zinc oxide nanowires structure with very cheap way (cheap substrate, cheap chemicals, low temperature) [5, 6]. This method could be very promising for the future. Although the voltage for one cell is not very high, we are able to manufacture huge low cost solar panels which could be embodied to roofing or facade rendering of our houses.

ACKNOWLEDGMENT

The authors gratefully thank Farzaneh Fattahi for technical supports.

REFERENCES

- [1] P. Yang, *Controlled Growth of ZnO Nanowires and Their Optical Properties*, in *Advanced Functional Materials*, vol. 12, pp. 323-331, May 2002.
- [2] <http://www.lac.tu-clausthal.de/forschung/projekte/abteilung-2-und-3/zinc-oxide-nanowires-for-photonic-applications/>
- [3] B. Shaijng, C. Chunxiang, W. Qingzhou, and B. Ling, *Growth of ZnO Nanowires in Aqueous Solution by a Dissolution-Growth Mechanism*, in *Journal of Nanomaterials*, vol. 2008, Article ID 610541.
- [4] D. C. Look, *Recent advances in ZnO materials and devices*, in *Material Science and Engineering*, vol. 80, pp. 383-387, March 2001.

- [5] W. Xufeng, B. Hua, L. Chun, L. Gewu, and S. Gaoquan, *Controlled one-step fabrication of highly oriented ZnO nanoneedle/nanorods array at near room temperature*, in The Royal Society of Chemistry, pp. 1655-1657, March 2006.
- [6] Z. Zhongping, Y. Haidong, S. Xiaoqiong, and H. Mingyong, *Near-room-temperature production of Diameter-tunable ZnO nanorod arrays through natural oxidation of zinc metal*, in Chemistry A European Journal, vol. 11, pp. 3149-3154, 2005.

Wind Turbine Cylinders with Spiral Fins

Radomír Goňo, Stanislav Rusek, Miroslav Hrabčík
VŠB-TU Ostrava
17. listopadu 15
Ostrava, Czech Republic

Abstract- Paper describes the world's first wind turbine system that rotates with cylinders which have spiral-shaped fins coiled around instead of common propeller-type blades. When the spiral cylinders catch the wind, rotating force is generated due to the aerodynamic properties caused by Magnus Effect. On the basis of experiments made by MECARO Co.Ltd it is possible to state that this type of power station is better than propeller type - more effective, cheaper the construction cost and stronger in the strong wind.

I. INTRODUCTION

The Magnus effect is the phenomenon whereby a spinning object flying in a fluid creates a whirlpool of fluid around itself, and experiences a force perpendicular to the line of motion and away from the direction of spin. The overall behavior is similar to that around an aerofoil with a circulation which is generated by the mechanical rotation, rather than by aerofoil action [1]. In many ball sports, the Magnus effect is responsible for the curved motion of a spinning ball. The effect also affects spinning missiles, and is used in some flying machines.

German physicist Heinrich Magnus first described the effect in 1853, but according to James Gleick [2], Isaac Newton described it and correctly theorized the cause 180 years earlier, after observing tennis players in his Cambridge College.

A. Principle

When a body (such as a sphere or circular cylinder) is spinning in a fluid, it creates a boundary layer around itself, and the boundary layer induces a more widespread circular motion of the fluid. If the body is moving through the fluid with a velocity V the velocity of the fluid close to the body is a little greater than V on one side, and a little less than V on the other. This is because the induced velocity due to the boundary layer surrounding the spinning body is added to V on one side, and subtracted from V on the other. In accordance with Bernoulli's principle, where the velocity is greater the fluid pressure is less; and where the velocity is less, the fluid pressure is greater. This pressure gradient results in a net force on the body, and subsequent motion in a direction perpendicular to the relative velocity vector (i.e. the velocity of the body relative to the fluid flow).

B. Calculation of lift force

The Kutta–Joukowski theorem relates the lift generated by a right cylinder to the speed of the cylinder through the fluid, the density of the fluid, and the circulation.

Equation (1) demonstrates the manipulation of characteristics needed to determine the lift force generated by inducing a mechanical rotation on a ball.

$$F = \frac{1}{2} \cdot \rho \cdot V^2 \cdot A \cdot l \quad (1)$$

F = lift force

ρ = density of the fluid

V = velocity of the ball

A = cross-sectional area of ball

l = lift coefficient

The lift coefficient l may be determined from graphs of experimental data using Reynolds numbers and spin ratios. The spin ratio of the ball is defined as ((angular velocity * diameter) / (2 * linear velocity)).

For a smooth ball with spin ratio of 0.5 to 4.5, typical lift coefficients range from 0.2 to 0.6.

The lift coefficient can be approximated using the Thin Airfoil Theory or Lifting-line theory.

II. MECARO

MECARO Co. was founded in 1998 as MECARO Akita, and started as the company mainly dealing with designing and manufacturing machinery used in the production line of factories.

Wind changes its course so irregularly in Japan that it is said that Japanese wind “pulsates”. Akita is a windy region with the wind blowing from Sea of Japan, and yet almost all the wind turbines standing here are foreign-made.

With the collaboration of the partnership with the government, industry and academia, and four years of trial and error, they were finally able to transform the Magnus theory into the wind turbine. This was a moment when MECARO Akita came into being as the wind turbine manufacturer.

MECARO Co., in Akita Prefecture (in northern Japan) launched large-scale production and sales of the Vortex-model wind turbine, in April 2007. It is the world's first wind turbine based on the principle of the Magnus effect, enabling the turbine to turn using lift generated by spinning cylinders with spiral fins instead of the usual propeller-like blades.

The wind turbine effort of this company in northern Japan, where fairly stiff winds often blow, began when the Akita

This work was supported by the Czech Science Foundation (No. GA ČR 102/09/1842)

government supplied its founder with information about efforts in Russia [3] (where turbine power generation has been ongoing for years) to use the surface effect for power generation. Mecaro carried out experiments on wind turbine generators and found a way to enhance the Magnus effect on the wind turbine "blade" surface by making "striations" on it.

The effect had been identified several centuries ago in Europe, but Mecaro made an adaptation for wind turbine use wherein "fins" arrayed into a spiral design were added to cylinders that have replaced conventional blades. The five-cylindrical product markedly improves wind power generation efficiency even if rotated at a slow pace and furthermore can withstand gale force weather. Moreover, it is responsive to the wind's fluctuations while also being quieter than other turbines available, since the greater lift provided by the fins allows for lower speed rotation of the propellers.

Theoretical analysis had not been fully developed on the Spiral Magnus turbine, so the Japanese firm then contacted the NASA Ames Research Center in California in order to utilize their giant wind tunnel for testing, which was conducted in January and February of 2007. The results verified the efficacy and safety of the system. More improvement work is being carried out with assistance from Kogakuin University as well as the University of Tokyo. Mecaro has obtained patents in Japan and Korea in relation to the Spiral Magnus turbine, in addition to having other applications pending elsewhere.

According to New Energy and Industrial Technology Development Organization (NEDO) which partially subsidized the Mecaro endeavor, there are more than a thousand wind turbine power generators operating in Japan now, but problems such as noise pollution and the need to comply with new building codes to ensure such facilities can withstand typhoons as well as tremors have cropped up recently.

Considering that other Asian countries prone to typhoons, cyclones and other natural phenomena would still want to make use of wind power, it is foreseen that the Mecaro system will soon gain adherents outside of Japan.

The lift of the Vortes is four times that of conventional propeller-type wind turbines, and the turbine operates at any wind speed. Thanks to the greater lift, its rotational speed can be lowered to around 25 percent of that of propeller-type turbines, resulting in lower noise levels.

Its cylindrical, durable blades and low rotational speed reduces this wind turbine's vulnerability to damage caused by aerial objects. In addition, since the spinning cylinders are controlled depending on wind speed, the Vortes can operate without a brake, and there is no concern about excess rotational speed in the case of strong wind--another safety feature. These technical improvements make it possible to install the Vortes even in or near residential areas, where there would otherwise be noise or safety concerns.

Until now, wind power generation has not been considered a viable investment for electricity generation except for large megawatt-scale turbines. In the case of a 10 kilowatt turbine (equivalent to electrical power consumption of five or six

typical households), however, the Magnus wind turbine has succeeded in reducing the power-generating cost to 45 yen (about U.S. 38 cents) per kilowatt, below the cost of solar power generation.

III. PROPELLER TYPE WIND TURBINE

A common propeller type wind turbine catches wind by the propeller-shaped blades, and rotate the rotor Fig. 1.

Propellers pick up the wind and generate aerodynamic lift Fig. 2 (lifting force / rotating force). Fig. 3 shows influence of Wind Flux Distribution.

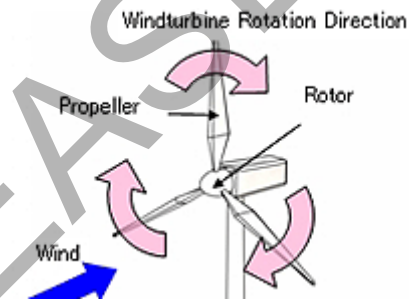


Figure 1. A common propeller type wind turbine.

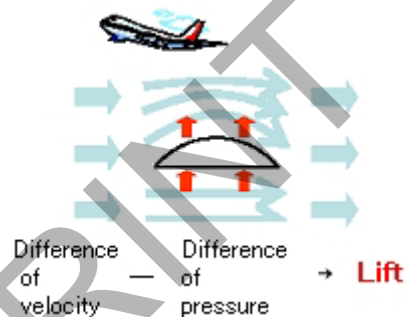


Figure 2. Aerodynamic lift.

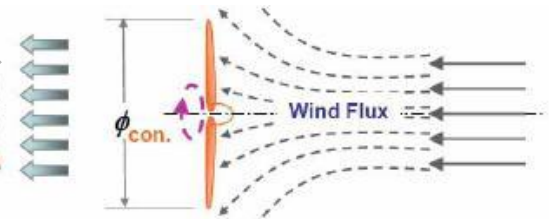


Figure 3. Influence of Wind Flux Distribution.

IV. SPIRAL MAGNUS WIND TURBINE

Spiral Magnus is the world's first wind turbine system that rotates with cylinders which have spiral-shaped fins coiled around instead of common propeller-type blades. When the spiral cylinders catch the wind, rotating force is generated due to the aerodynamic properties caused by Magnus Effect. With this principle applied, Spiral Magnus is a product with high power generation capability and safety.

Each of the five blades (cylinders) of Spiral Magnus Wind Turbine spins driven by the built-in motor and wind blowing through the cylinders rotates the rotor (Fig. 4).

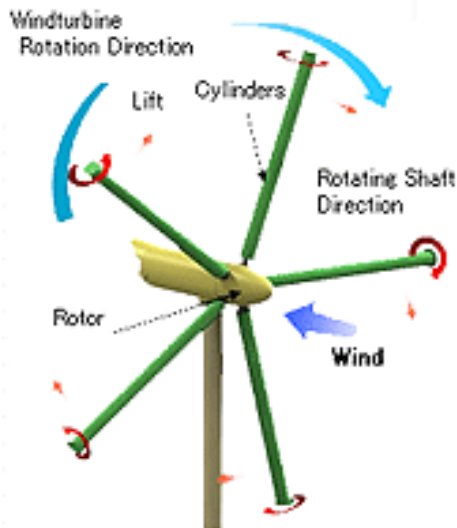


Figure 4. Spiral Magnus Wind Turbine.

This system uses a mechanism to generate more lift (lifting force / rotating force) from the wind power captured by the cylinders by effectively utilizing the aerodynamic properties of Magnus Effect (Fig. 5).

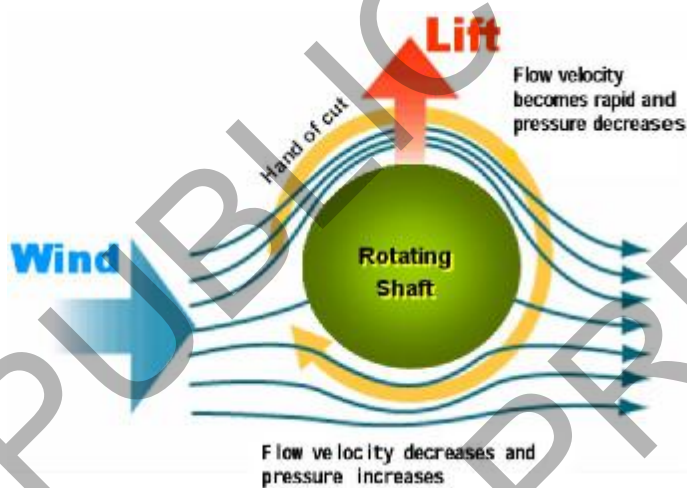


Figure 5. Aerodynamic lift of Magnus Effect.

Each cylinder alone can produce small power, but the five cylinders working together can generate enough power to rotate the wind turbine that has a heavy generator in it. The aerodynamic lift force works in the same way on a propeller-type wind turbine and an airplane although the force is created differently. Fig. 6. shows influence of Wind Flux Distribution.

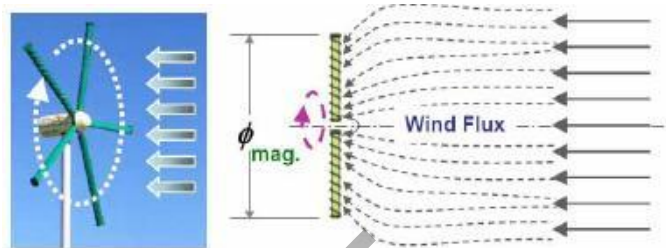


Figure 6. Influence of Wind Flux Distribution.

V. HISTORY

The first application was a power ship. 1852 A German scientist Heinrich Gustav Magnus discovered the phenomenon of the Magnus Effect. 1926 A German-born aviation engineer Anton Flettner built a rotor-ship harnessing the power of Magnus Effect to make the ship move, and made a successful voyage across the Atlantic (Fig. 7).



Figure 7. Anton Flettner's rotor-ship.

1983 The Barrel-blade windmill experiment in U.S. (Fig. 8)

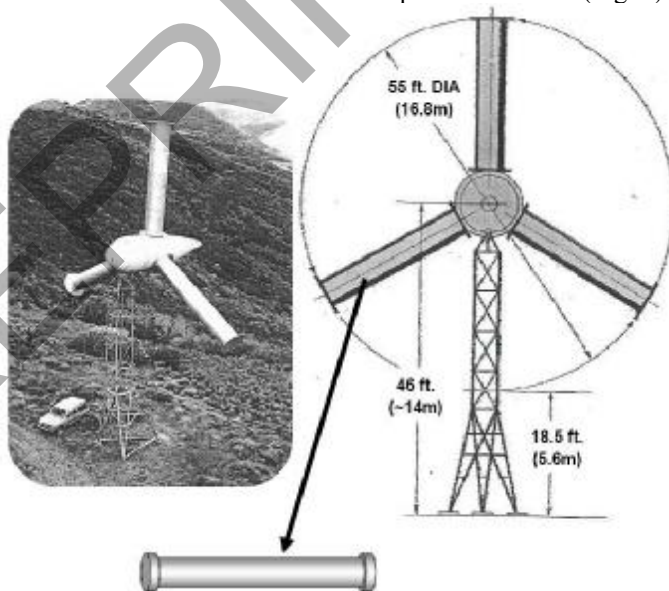


Figure 8. Hanson's Wind Turbine.

Since then, many countries have tried to develop the cylinder-blade windmill, but have not been successful to put into practical use. There was a problem to overcome that the smooth surface of the cylinders required top speed spinning of

the cylinders, which consumed more power than the wind turbine could generate.

MECARO tried to solve this problem by coiling the spiral fins around the cylinders, and tested at Akita Prefectural University (Fig. 9).

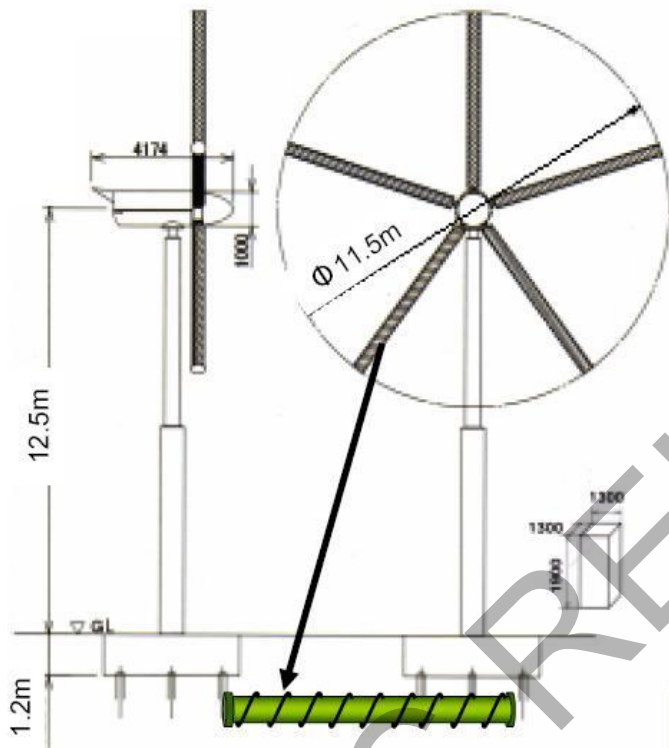


Figure 9. Spiral Magnus.

Result was that lifting forces gained from the spiral cylinders were several times larger than those from non-spiral cylinders (Fig. 10).

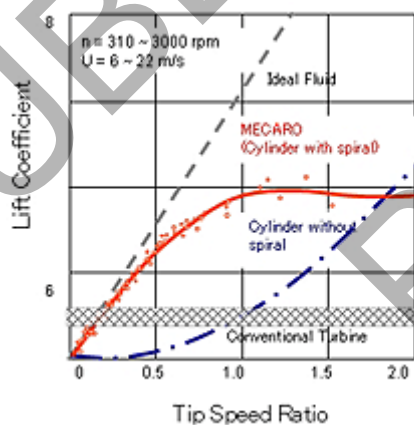


Figure 10. Data per one cylinder.

That is because the spiral fins capture more of wind stream, and effectively harness the wind as the lifting force. Based on this finding, there were good possibilities that they might be

able to develop an efficient wind turbine that is safe and stable with low rotational speed, and yet capable of generating high power. From this point, we set out our long, process of trial and error and evolution.

VI. APPLICATION

Spiral Magnus is less intimidating because rotational speed is about a one-sixth of common propeller types. Noise level is so low that you can hardly hear it through the breeze of natural wind. There is less chance of bird strike because of the slow rotational speed.

The rotating cylinders (blades) have excellent power generating stability since they are automatically optimized to various wind velocities for efficient wind capturing. The generating capacity is determined reflecting Japan characteristic wind pattern of fluctuating air stream and wind velocities, based on actual field data accumulated through proof tests at Ogata Village, Akita.

There are two possibilities of connection to system:

- 1) On-grid System (Interconnection Type) - system interconnects Commercial Power Supply, working as Sub Power Supply for Factory or Building
- 2) Off-grid System (Stand Alone Type) - system is working as Stand-alone Type Power Supply, or Emergency Power Supply.

VII. CONCLUSION

The experiment plant of 11.5 m in diameter was constructed in the Akita Prefecture Ogata village Japan for the proof of the power generation efficiency of a new Magnus Windmill.

There is a big feature that a new Magnus Windmill is better than past propeller type wind power generation the power generation efficiency and cheaper the construction cost. A wind turbine with Magnus effect can be used in a wide range of wind velocities including storm winds.

Application of the Magnus Effect is a relatively new area which still leaves plenty of room for analysis to be made. In parallel with commercializing product, MECARO will continue to work on the analysis through the joint research with Tokyo University and Kogakuin University in their pursuit of product innovation. How can be further improved efficiency? What shape shall be ultimately perfect? These are the questions we are seeking answer for.

REFERENCES

- [1] Clancy, L.J., *Aerodynamics*, Pitman Publishing Limited, London 1975, ISBN 0 273 01120 0.
- [2] Gleick, James. 2004. Isaac Newton. London: Harper Fourth Estate.
- [3] Patent of Russia RU 2189494 C2, 2002.
- [5] Shuchi, S., Ito, J., Murakami, N., Kikuchi, H., Kami-yama, S. A study on Magnus effect for a rotational cylinder with an additional structure. Proceedings of International Conference of Akita Prefectural University 2004, Akita, Japan (in Japan).
- [6] C. A. Pomeroy, "Revolutionary Spiral Fin Turbine," in *The Japan Journal*, August 2008 Vol. 5 No. 4.
- [7] MECARO Co.Ltd., company web site and documents.

Reliability Standards for Large Interconnections

Petr Horáček, Petr Havel

Czech Technical University in Prague, Faculty of Electrical Engineering
Technická 2, 166 27 Prague 6, Czech Republic
{horacek,havel}@fel.cvut.cz

Abstract—Every interconnection must be operated so that the system frequency is maintained at given setpoint and all control areas of the interconnection meet their active power exchange obligations. Compliance with reliability standards is required. The paper discusses performance indices and standards definitions used in North America and Europe (synchronous interconnection of 24 European countries joining UCTE - Union for the Co-ordination of Transmission of Electricity) with the aim of choosing the most appropriate set. A particular example of indices and standards applied for the Czech control area of the UCTE interconnection including their use in Ancillary Services planning is provided.*

I. INTRODUCTION

Generation and load in an electric grid must be balanced to assure stable grid operation. New power market conditions resulting from the process of liberalization and privatization dramatically changed the responsibilities of power generation companies, transmission owners, dealers and other market players. The process of transfer of ownership and operation of all high-voltage transmission lines to a regional power pooling and transmission entity with no interest in generation has been completed in North America and Europe where linkages between distribution, transmission, and generation occur across markets – regulated and unregulated – rather than through internal organization. The ultimate instance assuring stable frequency and defined power flows in the grid are balancing authorities responsible for individual control areas. Operation of control areas should be orchestrated so the cooperation, in terms of exchange of balancing power, is mutually balanced, otherwise penalties apply.

The state of the power system is described by the frequency error of the interconnection Δf and an area control error ACE_{area} . Additionally the area net interchange error ΔP_{area} might be also considered. The system frequency error is calculated as

$$\Delta f = f_{actual} - f_{desired} \quad (1)$$

and each control area calculates the Area Control Error (ACE) as an inadvertent interchange less frequency bias

$$ACE_{area} = (Interchange_{actual} - Interchange_{scheduled}) + K_{area} \Delta f = \Delta P_{area} + K_{area} \Delta f \quad (2)$$

* This work was supported by the Ministry of Education of the Czech Republic under the project 1M0567 and by the Czech TSO under the project “Reliability and economy of system services”.

where K_{area} in MW/Hz is an amount of power that would be theoretically released through automatic primary control in generators when the system frequency drops 1Hz from the scheduled value. K_{area} is the frequency bias setting for the area. $Interchange_{actual}$ is the sum of active power measured on all tie-lines and $Interchange_{scheduled}$ is the desired, scheduled value. Interchange is positive when the area is exporting, area generation exceeds area load. Note that the standard formula for calculating ACE [1] uses frequency bias coefficient B_{area} in MW/0.1Hz (a negative number, not necessarily constant) rather than K-factor with the obvious relation

$$K_{area} = -10B_{area} \quad (3)$$

The load at each time instant is a random variable and this randomness penetrates to the variables measured and monitored, such as interconnection frequency and the active power flows on the tie lines.

These variables are assumed to be random processes described by the mean value and variance. The correlation between frequency error and ACE of the area is chosen as a metric of each area’s control performance. We need to impose an upper bound on that correlation whereas we need not care about the negative correlation since it indicates a favorable performance of the particular area.

The generic performance criterion considered says that the expected correlation between interconnection frequency error and the area’s ACE should be bounded by the allowed frequency discursion and the required frequency bias of the area:

$$E\{\Delta f_1 \cdot ACE_{1area}\} \leq std(\Delta f_1) \cdot (K_{area} \cdot std(\Delta f_1)) = (std(\Delta f_1))^2 \cdot (-10B_{area}) \quad (4)$$

where index 1 means a clock-minute (1 minute) average of the respective variable. The operator $E\{\cdot\}$ is an expected value and $std(\cdot)$ stands for standard deviation of the argument. The principle forms the basis of currently applied standards in North America’s interconnections and is followed by European’s UCTE interconnection in an indirect way as well.

Similarities and differences between performance standards used in the above mentioned interconnections and a particular example of standards adopted by the Czech Transmission System Operator are going to be discussed in the following chapters.

II. PERFORMANCE STANDARDS

A. Performance Standards in North America

Today, North American Electric Reliability Corporation (NERC) defines three Control Performance Standards (CPS) for the assessment of control areas generation control performance: CPS1, CPS2 and DCS [1]. All control areas in North America implemented CPS by 1998.

The motivation to develop the theories that led to the development of CPS1 and CPS2 came from the need to find criteria whose fulfillment would equitably divide responsibility between control areas for satisfying the condition

$$\text{RMS}\{\Delta f_T\} = \varepsilon_T, \quad (5)$$

where Δf_T is average frequency error over T minutes, ε_T is the target to be chosen by the interconnection and RMS stays for root mean square error.

CPS1 requires each Balancing Authority to operate such that, on a rolling 12-month basis, the scaled average of clock-minute averages of the ACE of the area multiplied by the corresponding clock-minute averages of the interconnection's frequency error is less than a specific limit. CPS1 is a statistical measure of ACE variability. CPS1 measures ACE in combination with the interconnection's frequency error. The CPS1 requires that the average of the clock-minute averages of a control area's ACE over a given period divided by its K-factor times the corresponding clock-minute averages of the frequency error shall be less than a given constant

$$\text{AVG}_{\text{Period}} \left[\frac{\text{ACE}_{\text{Area}}}{K_{\text{Area}}} \Delta f_1 \right] \leq \varepsilon_1^2. \quad (6)$$

The constant ε_1 in Hz is derived from the targeted frequency bound (the targeted RMS value of one-minute average frequency error based on frequency performance over a given year).

CPS1 measures control performance by comparing how well a control area's ACE performs in conjunction with the frequency error of the entire interconnection. Criterion (7) can be viewed as a correlation between ACE and Δf . Positive correlation means undesired performance (the area control error contributes to the frequency deviation from the desired value) and is therefore limited by the upper bound ε_1^2 . Negative correlation occurs when ACE helps to compensate the total ACE of the interconnection and is helping to offset the system frequency deviation.

CPS2 is a statistical measure of ACE magnitude designed to bound ACE ten-minute averages and provides an oversight function to limit excessive unscheduled power flows that could result from large ACE:

$$\text{AVG}_{10_\text{minute}} (\text{ACE}_{\text{Area}}) \leq 1.65 \varepsilon_{10} \sqrt{K_{\text{Area}} K_{\text{interconnection}}}, \quad (7)$$

$$= L_{10}$$

where $K_{\text{interconnection}}$ is the sum of K-factors in the entire interconnection and ε_{10} is the targeted RMS of ten-minute average frequency error. Each Balancing Authority shall operate such that its average ACE for at least 90% of clock ten-minute periods (6 non-overlapping periods per hour) during a

calendar month is within a specific limit, referred to as L_{10} , which is a statistically derived ten-minute average ACE limit. Analysis and further discussion on CPS1 and CPS2 can be found in [5, 6, 7].

The purpose of the Disturbance Control Standard (DCS) is to ensure the Balancing Authority is able to utilize its contingency reserve to balance resources and demand and return interconnection frequency within defined limits following a reportable disturbance. The application of DCS is limited to the loss of supply and does not apply to the loss of load. A disturbance is defined as any event that is $\geq 80\%$ of the magnitude of the control area's most severe single contingency. A control area is responsible for recovering from a disturbance within 10 minutes by recovering the amount of the disturbance or returning ACE to zero. A disturbance is not reportable if it is greater than the control area's most severe contingency.

Control area must comply with the DCS 100% of the time. Extra reserves must be carried for the quarter following the quarter in which the non-compliance occurs.

Each control area can meet the CPS standards by any means they wish. Some balancing authorities developed AGC logic that allows meeting CPS and DCS standards automatically.

A control area not meeting the CPS is not allowed to sell control services to other parties external to its metered boundaries. This impacts those purchasing control services from this control area. This is a significant penalty given new operating environments.

B. Performance Standards in Europe

Speaking about Europe we focus on the largest European interconnection, the UCTE. According to the UCTE Operation Handbook (OH) [2] the individual ACE_{Area} needs to be controlled to zero on a continuous basis in each control area. In addition, frequency deviation should decay to the given setpoint in less than 15 minutes and any power outage should be compensated accordingly. Both large and/or long lasting ACE deviations should be avoided as much as possible. No additional explicit requirement on ACE behavior is explicitly defined. This is because UCTE requires each Balancing Authority to apply well defined characteristics of the primary frequency control loops distributed throughout each area and an area secondary load-frequency controller characteristics are prescribed as well so the method used by generators and TSOs is not arbitrary. The only parameter that can influence meeting the general OH requirements would be the amount of regulation reserve available for primary and secondary control and also the level of tertiary reserves available to restore the capacity of the secondary load-frequency control so it does not operate close to the saturation level set by the reserved capacity. In addition, as the tertiary control doesn't run in automatic mode, the use of tertiary reserve depends on the dispatch rules of the TSO's operator.

The general quality requests are sometimes specified in more rigorous way by individual balancing authorities for their internal use. An example specification is described in the next section. The mean and the standard deviation of ACE is used

sometimes for comparing operations of control areas of a single interconnection [3].

C. Performance Indices Adopted by Czech TSO

Performance indices introduced and used by the Czech TSO were designed at the time when Czech Republic was part of the CENTREL control block of the UCTE (CZ,HU,PL,SK). Internally, there were strict requirements every TSO had to follow. In addition to the UCTE's OH, $|ACE_1|$ should be kept below 100MW and $|ACE_{60}|$ below 20MW. These requirements formed the basis for introducing indices for the CZ TSO.

The important principle, which is by the way adopted in setting limit values for CPS1 and CPS2 criteria, is that the grid performance should not deteriorate in time. Calculating individual performance indices on historical data and periods where the grid operation was generally considered to be satisfactory, gives the indices setting which we wouldn't like to exceed in the future. CPS1 and CPS2 set the limit values in relation to the area's K-factor, which distributes the responsibility of balancing authorities throughout the interconnection on fair and well defined basis.

Seven indices describing reliability are defined in [8] and shown in Table I. Indices $rACE_1$ and $rACE_{60}$ are statistical measures of ACE having relation to NERC's CPS2. $rACE_{1t}$ is linked to UCTE requirement on frequency recovery in less than 15 minutes after a forced generation unit outage and thus it is related to NERC's DCS index.

While NERC's CPS2 limit L_{10} gets adapted and may change from year to year and stationary 90% compliance is required over years, CEPS' limits L_1 and L_{60} are constant and compliance required is not stationary and gets adapted according to area's recent performance

TABLE I – CZ Performance Indices

$rACE_1$	%	Probability that the absolute average value of one-minute (clock minute) averages of ACE exceeds $L_1 = 100$ MW over given period.
$rACE_{60}$	%	Probability that the absolute average value of one-hour averages of ACE exceeds $L_{60} = 20$ MW over given period.
$rACE_{1t}$	%	Probability of arriving Events ^{*)} over given period.
μ_{ACE_1}	MW	Average value of one-minute averages of ACE over given period.
σ_{ACE_1}	MW	Standard deviation of one minute averages of ACE over given period.
$\sigma_{ACE_{60}}$	MW	Standard deviation of one hour averages of ACE over given period.
E_{Event}	MWh	Summed energy (absolute value) of all Events recorded over given period.

^{*)} The Event shown in Figure 1 is defined as ACE_1 exceeding L_1 for at least 10 consecutive minutes. Errors exceeding L_1 lasting for less than 10 minutes are not counted. Event energy is calculated from ACE_1 time series.

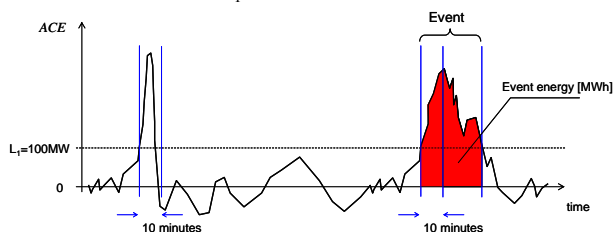


Figure 1. Event identification.

The limit values for CEPS' performance standards (Table II) are determined statistically from historical records of ACE.

TABLE II – Settings from recent ACE evaluation approved by the TSO

Performance index	Limit value
$rACE_1$	3.8 %
$rACE_{60}$	2.2 %
$rACE_{1t}$	0.053%

Let's define CZ performance standards in the way reminding NERC's CPS and DCS standards.

CPS_{CZ1} is designed to bound ACE one-minute averages and provides an oversight function to limit excessive unscheduled power flows that could result from large ACE:

$$AVG_{1_minute}(ACE_{area}) \leq L_1 = 100MW \quad (8)$$

Czech TSO shall operate such that its average ACE for at least $(100-rACE_1)\%$ of clock one-minute periods (60 non-overlapping periods per hour) during a calendar year is within a specific limit, referred to as L_1 .

CPS_{CZ2} is bounds sixty-minute averages of ACE and provides an oversight function to limit excessive unscheduled power flows that could result from large and/or longer lasting ACE:

$$AVG_{60_minute}(ACE_{area}) \leq L_{60} = 20MW \quad (9)$$

Czech TSO shall operate such that its average ACE for at least $(100-rACE_{60})\%$ of clock one-minute periods (60 non-overlapping periods per hour) during a calendar year is within a specific limit, referred to as L_{60} .

DCS_{CZ} ensures that the TSO is able to utilize its contingency reserve to balance resources and demand and return ACE within defined limits following a reportable disturbance that is any disturbance resulting in ACE exceeding L_1 limit both for loss of generation as well as loss of load. A control area is responsible for recovering from a disturbance within 15 minutes in at least $(100-rACE_{1t})\%$ of fifteen-minute periods (4 non-overlapping periods per hour) during a calendar year by returning ACE below L_1 .

While control area must comply with NERC's DCS 100% of the time, the compliance with DCS_{CZ} is weaker. On the other hand larger number of reportable disturbances are taken into account because the L_1 limit is set much lower.

III. USE OF PERFORMANCE INDICES AND STANDARDS

In order to determine power reserves in the form of AS, which would technically suffice for proper power balance control with acceptable reliability, it is necessary to refer to reliability standards. The principle of using performance indices $rACE_1$ and $rACE_{60}$ for determining total reserves needed to guarantee that the control area will perform according to the standards is shown in Figure 2 illustrating how total minimal volumes of power reserves $RZ_{2min}^+ \geq 0$ and

$RZ_{\Sigma\min}^- \geq 0$ are determined from the cumulative distribution function of ACE_{OV} , estimated ACE of the uncontrolled area. According to the reliability standards, the absolute value of ACE is allowed to exceed the threshold 100 MW in $rACE_1$ % of cases during the defined period. If this splits symmetrically to positive and negative values, ACE_{OV} higher than 100MW should be compensated by the control reserves except for $(100-rACE_1/2)\%$ of cases. Hence, we need at least $RZ_{\Sigma\min}^+ \geq 0$ and $RZ_{\Sigma\min}^- \geq 0$ reserves to meet the standards of reliability, the level of which is derived from the control area satisfactory performance in the past provided by Table II. Reserves decrease number of occasions when ACE violates the threshold illustrated in Figure 2 by changing the shape of the probability distribution function of ACE of the uncontrolled area (curve 1) to the one of controlled area (curve 2). Legend attached to point 3 shows how to read the information described by the probability distribution function associated with ACE.

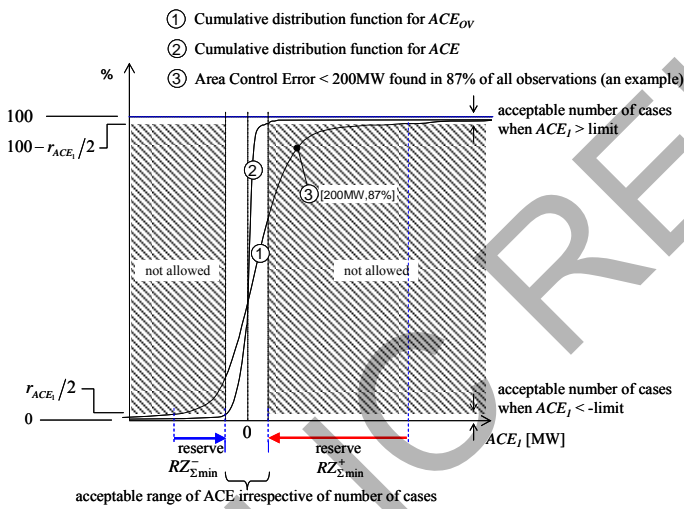


Figure 2. Cumulative distribution function of the open-loop ACE and its use.

The secondary reserve $RZSR_{\min}$ should compensate for the fast variations of the open-loop ACE and the tertiary reserves $RZTR_{\min}^+$, $RZTR_{\min}^-$ compensate for the slow ACE variations. The minimal needs of these services are determined similarly to the total needs but with utilizing cumulative distribution functions of ACE_{OV_slow} and ACE_{OV_fast} .

The values of the minimal AS requirements are in the form of time series, which reflects the fact that the behavior of ACE also varies; typically, it is more uncertain in “transitions periods” with changeable weather and temperature, such as in spring or fall.

More information on the use of reliability standards in power reserve planning can be found in [4].

IV. CONCLUSION

NERC’s CPS1 offers a system wide approach which favors behavior leading to better overall system performance while allowing more freedom to individual areas concerning the way how the area’s balancing authority manages its ACE. Keeping

ACE as close to zero as possible at all times, as implicitly demanded by the UCTE Operation Handbook, is more restrictive as it does not count for solidarity exceeding the level provided by primary frequency control.

The question what performance standards are better suited for practical needs, those used in North American or European interconnection, is difficult to answer as technical and market conditions differ. There is, however, no much difference in the performance of the interconnection when looking at the RMS value of one-minute average frequency error based on frequency performance over a given year for instance, $\varepsilon_{UCTE_2007} = 21\text{mHz}$, $\varepsilon_{10UCTE_2007} = 17\text{mHz}$, $\varepsilon_{Eastern_1998} = 18\text{mHz}$. The Czech performance indices were not originally linked to NERC’s CPS1, CPS2 and DCS standards, however a link between them exists. Thorough investigation is carried out to find limitations of both sets and decide what indices are more relevant to practical needs of the ISO/TSO not only for performance monitoring but also for Ancillary Services planning.

Note that Czech Area compliance with CPS1 for the year 2007 was over 100% having

$$\text{AVG}_{12_month} \left[\frac{ACE_{1CZ} \Delta f_{UCTE}}{K_{CZ}} \right] = 0.00042\text{Hz}^2 < \varepsilon_{UCTE}^2 = 0.00044\text{Hz}^2 \quad (10)$$

and the minimum compliance with CPS2, where

$$L_{10CZ} = 1.65\varepsilon_{10UCTE} \sqrt{K_{CZ} K_{UCTE}} = 101 \text{ MW} , \quad (11)$$

was 98.2%, which is much better than the required 90% in DCS. Using (11) for calculating L_{1CZ} and L_{60CZ} provides the following result

$$L_{1CZ} = 122.4 \text{ MW}, L_{60CZ} = 61.4 \text{ MW} . \quad (12)$$

This result indicates that CENTREL’s limits $L_1=100\text{MW}$ and $L_{60}=20\text{MW}$ for CZ were rather strict. On the other hand compliance with limits (12) would be required in DCS monthly while compliance with CENTREL limits was required on yearly basis only.

The paper opens the discussion on selection and use of performance standards in large interconnections.

REFERENCES

- [1] *Reliability Standards for the Bulk Electric Systems of North America*, North American Electric Reliability Corporation, Princeton, NJ (2008)
- [2] *UCTE Operation Handbook*, v2.2/20.07.04, Union for the Co-ordination of Transmission of Electricity, Brussels (2004)
- [3] P. Havel, P. Horáček, J. Fantík, and E. Janeček, “Criteria for evaluation of power balance control performance in UCTE transmission grid”, *Proc. 17th IFAC World Congr.*, Seoul, 2008
- [4] P. Havel, P. Horáček, V. Černý, and J. Fantík, “Optimal Planning of Ancillary Services for Reliable Power Balance Control”, *IEEE Trans. Power Systems*, Vol. 23, No. 3, pp. 1375-1382, August 2008
- [5] N. Jaleeli, and L.S. VanSlyck, “NERC’s new control performance standards”, *IEEE Trans. Power Systems*, Vol. 14, No. 3, pp. 1092-1099, August 1999
- [6] M. Yao, R.R. Shoults, and R. Kelm, “AGC Logic Based on NERC’s New Control Performance Standard and Disturbance Control Standard”, *IEEE Trans. Power Systems*, Vol. 15, No. 2, pp. 852-857, May 2000
- [7] G. Gross, and J.W. Lee, “Analysis of Load Frequency Control Performance Assessment Criteria”, *IEEE Trans. Power Systems*, Vol. 16, No. 3, pp. 520-525, August 2001

PUBLIC RELEASE
PREPRINT

Shields of Electromagnetic Wave Based on Amorphous and Nanocrystalline Soft Magnetic Materials

Mariusz Ozimek^{1,2)}, Dominika Gaworska-Koniarek¹⁾, Wiesław Wilczyński¹⁾

¹⁾Electrotechnical Institute Wrocław Division of Electrotechnology and Materials Science (IEL/OW),
55/61 M. Skłodowskiej-Curie Street

²⁾Wrocław University of Technology, Faculty of Electrical Engineering,
8 Janiszewskiego Street
Wrocław, Poland

Abstract- The paper presents results of measurement of electromagnetic wave shielding effectiveness by shields based on $\text{Fe}_{73.5}\text{Cu}_1\text{Nb}_3\text{Si}_{13.5}\text{B}_9$ soft magnetic material in nanocrystalline and amorphous form. Manufactured shields were characterised by good elastic properties. The research was carried out in frequency band of 300 MHz – 1 GHz. The highest shielding effectiveness was obtained for sample made of amorphous tape - at frequency of 700 MHz it equals 42 dB.

I. INTRODUCTION

Present economic development causes considerable electromagnetic (EM) radiation emission growth. The source of this emission are not only TV/radio stations, radar systems but also different kinds of technical devices [1, 2]. Intensive growth of demand for electric energy, its transmission and development of electronic, telecommunication and information technology result in significant increase of electromagnetic distortion in human environment. In their everyday life people incessantly meet with a lot of devices such as microwave ovens, screens, inductive heaters, alarms, mobile phones etc. which emit electromagnetic radiation. The cables supplying electric energy for receivers as well as wires used for information transfer are also sources of EM radiation.

To minimize the effect of electromagnetic radiation on living organisms usually various types of shields are used. An electromagnetic radiation shield limits the flow of electromagnetic field between two locations (one with EM field and the other without it), by separating them with a barrier made of material with specified electric and magnetic properties. Typically it is applied to enclosures, separating electrical devices from the 'outside world', and to cables, separating wires from the environment the cable runs through. The application of shields with proper electric conductivity σ , permittivity ϵ , magnetic permeability μ and appropriate thickness ensures harmonic coexistence of electromagnetic environment with systems and devices which are the part of this environment [3, 4, 5].

In Electrical Institute Division in Wrocław research work is carried out concerning new composite materials designed for EM shields. The investigation, among others, is focused on developing of magnetic filler for warp in form of

nanocrystalline and amorphous materials. High-tech nano- and micro- fillers added to polymer warp due to their shielding, elasticity and easy forming properties can be applied for cables and wires shielding or as kits protected from EM radiation.

materials

In the experiment the amorphous soft magnetic tape of $\text{Fe}_{73.5}\text{Cu}_1\text{Nb}_3\text{Si}_{13.5}\text{B}_9$ was used for preparation of electromagnetic radiation shields. A part of this tape underwent thermal treatment at temperature of 510 °C in argon atmosphere to obtain magnetic nanocrystallites of $\alpha\text{-Fe}(\text{Si})$ embedded in amorphous matrix. Magnetic properties and shielding effectiveness were examined for both amorphous and nanocrystalline tapes. Magnetic measurements at frequency of 50 Hz were performed by means of computerized measuring system MAG-RJJ-3.0.

Figures 1 – 2 present the hysteresis loops and total specific loss of examined materials.

Test results indicate that nanocrystalline tape is characterized by lower coercivity ($H_c < 1$ A/m) and total specific loss than its amorphous precursor. Crystallization process resulted also in a growth of magnetic permeability and saturation induction of material. Saturation induction of amorphous tape amounts of 0.6 T whereas this value for nanocrystalline tape amounts to about 1.2 T. Initial permeability of examined tape after thermal treatment increased by about 5 times and reached $\mu \approx 100\,000$.

II. EXPERIMENT

The EM shields based on amorphous material were prepared in form of a tape with thickness of 20 μm and width of 10 mm glued onto thin sheet of paper. The tape strips were arranged in such way to eliminate the gaps between the adjacent strips.

Nanocrystalline tape due to its high brittleness can not be applied in form of tape strips. Therefore it was pulverized. The particle size after milling was lower than 80 μm . For reference purpose the amorphous tape was also milled. Final powders dispersed in resin was spread onto textile material and paper sheet. Its mass density on surface amounted to 12 mg/cm^2 . The sample with addition of carbon fibers dispersed in the same type of resin as in case of basing powder was also

manufactured. The shields obtained in such way were characterized by good elastic properties.

layer of copper foil (0.1 mm and 0.2 mm). The research was carried out in frequency band of 300 MHz – 1 GHz.

III. RESULTS

Shielding effectiveness of manufactured shields are presented in Figs. 3 – 6. The influence of form of applied soft magnetic material (tape or powder) on shielding effectiveness is noticeable.

When it comes to shield made of amorphous tape glued onto sheet of paper the electromagnetic wave shielding changed in range of 9 dB - 42 dB. The highest one (>40 dB) was noted at frequency 710 MHz - 740 MHz. Further increase of frequency resulted in decrease of shielding to 25 dB. In the range of 800 MHz – 1000 MHz shielding effectiveness did not significantly change and amounted about 25 – 30 dB. It should be noticed that samples' thickness was 0,1 mm. Addition of thin copper foil did not have a significant effect on shielding effectiveness results. It indicates that thickness of copper foil is not sufficient to shield an electromagnetic wave effectively.

Pulverization of amorphous material caused deterioration of its shielding properties. In this case the shielding effectiveness is almost constant and does not exceed 10 dB. At frequency of 800 MHz and higher it even dropped below 5 dB. Similar results were also obtained for milled nanocrystalline tape. The addition of carbon fibers to nanocrystalline powder brought about negligible changes in shielding effectiveness.

Shielding effectiveness of specimens made on the basis of milled nanocrystalline and amorphous soft magnetic materials is comparable despite the high difference in magnetic permeability value of blank materials. It might suggest that the size of particles was not properly matched to frequency band. Apart from that, the weaker shielding properties of these samples result from the worse magnetic properties of pulverized materials. Internal stress induced during milling process significantly influenced the magnetic permeability reduction. Additionally non uniform covering of surface by soft magnetic powder also affects samples shielding effectiveness.

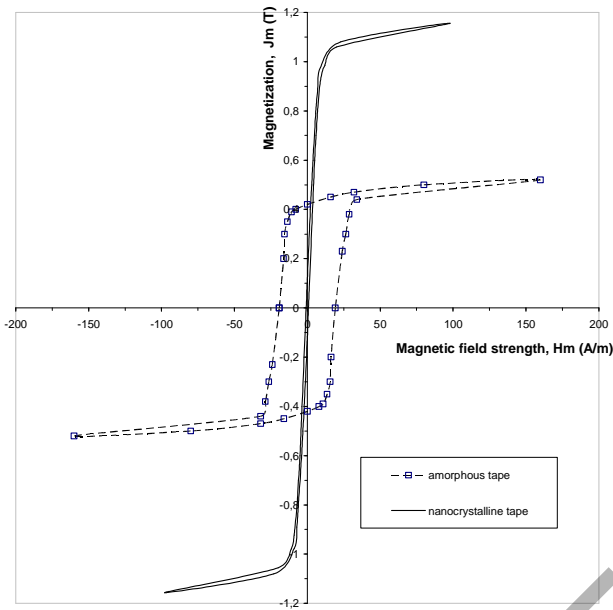


Fig. 1. Hysteresis loop of $Fe_{73.5}Cu_1Nb_3Si_{13.5}B_9$ alloy in amorphous and nanocrystalline form

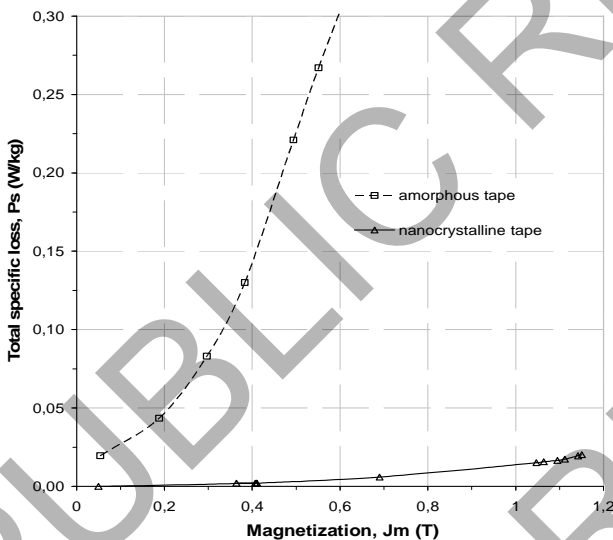


Fig. 2. Total specific loss of $Fe_{73.5}Cu_1Nb_3Si_{13.5}B_9$ alloy in amorphous and nanocrystalline form ($f = 50$ Hz)

Shielding effectiveness of examined materials was measured according to MIL-STD 285 American standard [6]. Transmitting and receiving antenna were situated at a distance of 3 m from each other in shielded room. Receiving antenna with wooden support was placed in brass housing which was padded inside of ferrite layer. A sample was fixed in opening cut in one of housing side. At first a background measurement (without the sample) was made. In next step, the examined samples were placed in housing and their shielding effectiveness was tested. For shields based on amorphous tape the tests were conducted for samples with and without thin

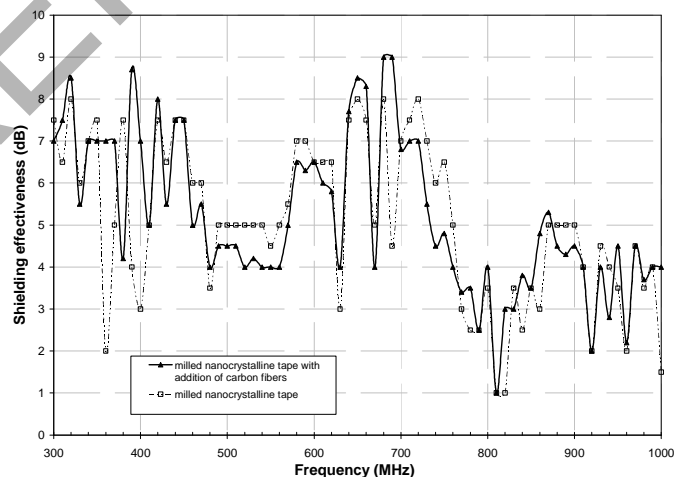


Fig. 3. Shielding effectiveness of nanocrystalline milled material

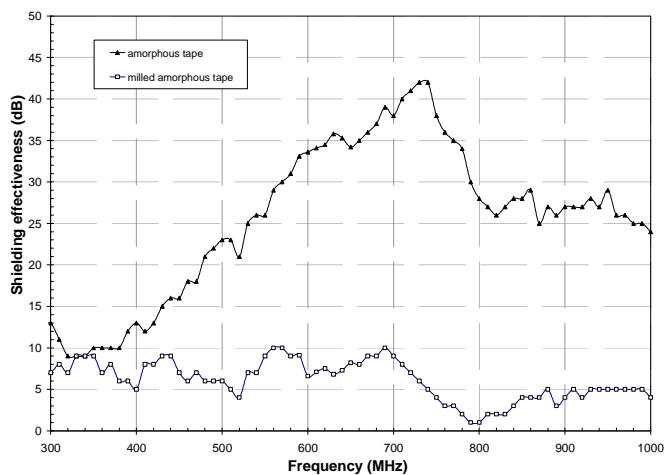


Fig. 4. Shielding effectiveness of amorphous material in tape and powder form

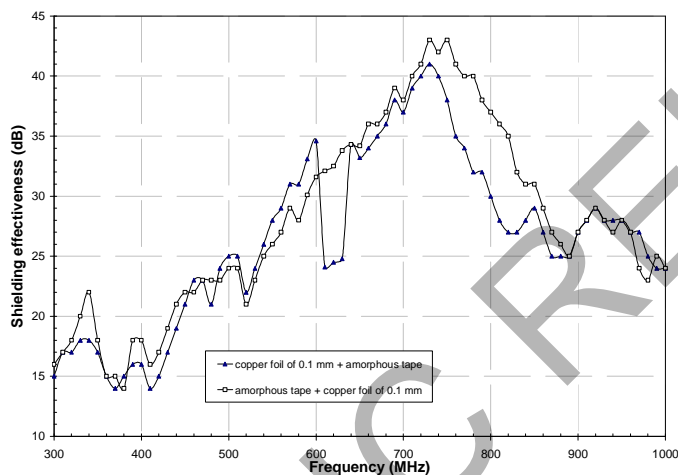


Fig. 5. Shielding effectiveness of amorphous tape with copper foil with thickness 0.1 mm

IV. SUMMARY

The paper presents results of measurement of electromagnetic wave shielding effectiveness by shields based on nanocrystalline and amorphous soft magnetic materials. The research was pilot study with the object of examination of prospects and usefulness of mentioned above materials as the fillers of composite electromagnetic wave shields. That is why the research was concentrated only on "pure" soft magnetic materials (or with small addition of carbon fibers) without composite substrates.

Shielding effectiveness of samples made of soft magnetic amorphous tape is high what indicates that material in such form is proper for usage on EM shields

The obtained results of shielding effectiveness in case of specimens based on pulverized materials are not satisfactory. These kind of shields require amelioration of preparation technology and further tests.

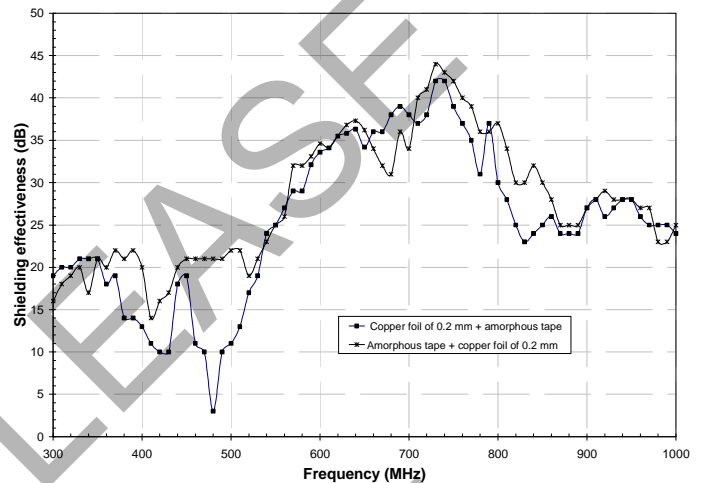


Fig. 6. Shielding effectiveness of amorphous tape with copper foil with thickness 0.2 mm

REFERENCES

- [1] Sokalski L., „Pola elektromagnetyczne i ich niejonizujące oddziaływanie na organizmy żywe”, *Przegląd Elektrotechniczny*, No 4, pp. 100-103, 1999.
- [2] Wac-Włodarczyk A., Mazurek P.A., „Analiza zaburzeń elektromagnetycznych emitowanych w lokalnej sieci przez komputery PC”, *Przegląd Elektrotechniczny*, No 12, pp. 890 – 893, 2003.
- [3] Sarto M. S., et al., “Nanolayered Lightweight Flexible Shields with Multidirectional Optical Transparency”, *IEEE Transactions on Electromagnetic Compatibility*, vol. 47, No. 3, pp. 602-611, 2005.
- [4] Lutsev L.V., et al, Dielectric and magnetic losses of microwave electromagnetic radiation in granular structures with ferromagnetic nanoparticles. *Journa of Physics: Condensed Matter*. No 15, pp. 3665-3681, 2003.
- [5] Lundgren U., et al., Shielding Effectiveness Data on Commercial Thermoplastic Materials, *IEEE Transactions on Electromagnetic Compatibility*, vol. 4, pp. 766-773, 2006.
- [6] MIL-STD 285, *Method of Attenuation Measurement for Enclosures, Electromagnetic Shielding, for Electronic Test Purposes*, U.S. Government Printing Office, Washington: 1956.

Impedance-Source Inverter-Based High-Power DC/DC Converter for Fuel Cell Applications

Mikhail Egorov⁽¹⁾, Dmitri Vinnikov⁽¹⁾, Ryszard Strzelecki⁽²⁾, Marek Adamowicz⁽³⁾

⁽¹⁾Tallinn University of Technology, Department of Electrical Drives and Power Electronics
Ehitajate tee 5, 19086 Tallinn, Estonia

⁽²⁾Electrotechnical Institute, Pożaryskiego 28, 04-703 Warsaw, Poland

⁽³⁾Gdynia Maritime University, Department of Electrical Engineering
Morska 81-87, 81-345 Gdynia, Poland

Abstract- This paper presents the possibility of implementation of fuel cells with low output voltage range for supplying the high-voltage loads. For matching the different voltage levels and for the providing of galvanic insulation the isolated DC/DC interface converter is required. For increasing of power density, efficiency and flexibility the interface DC/DC converter with three-phase intermediate AC-link is proposed. The one of features of the proposed topology is the impedance source inverter utilized in the input stage of the converter. The paper is devoted to study of theoretical background of the topology proposed, which is verified by the simulations.

I. INTRODUCTION

Fuel cells (FC) have achieved global attention as alternative power sources due to the environmental concerns. In this paper the possibility of FC interconnection with the high-voltage load is studied. Generally, the FCs are used as power sources with the output voltage variation between 40 V and 80 V. For supplying the high-voltage, high-power loads it is necessary to boost the relatively low output voltage of the FC to certain operating voltage level (for example, 600 V DC), required by the end user. Moreover, for the safety reasons the isolation transformer should be used for decoupling the low-voltage input and the high-voltage output sides of the converter. Thus, the step-up isolated DC/DC converter topology should be used in presented application. Practically, it can be realized by several approaches [1]:

- conventional PWM inverter with the step-up transformer and rectifier,
- combination of boost converter with conventional PWM inverter and step-up transformer with rectifier,
- impedance-source inverter with isolation transformer and rectifier.

The most technically feasible solution is the implementation of impedance-source inverter (ISI) widely known as Z-source inverter. The ISI (Fig. 1) employs impedance network coupled with the main inverter circuit and has unique properties of voltage step-up and DC/AC conversion [1], [2].

For improving the power density, efficiency and flexibility of the system the intermediate AC-link of the proposed converter is realized with the three-phase architecture (Fig. 1). Compared to recently popular single-phase intermediate AC-link (full-bridge single-phase isolated DC/DC converter) the resulting advantages of the three-phase approach are obvious:

1. lower RMS current through the inverter and rectifier switches (higher power transfer through the switch with the same level of switch current and voltage stresses);
2. reduced isolated transformer's volume (and weight) due to reduced overall yoke volume and reduced voltage and magnetic stresses;
3. three-phase transformers and inductors are generally smaller and lighter than their counterpart single phase ones, for the same processed power. As a result, the energy losses in three-phase transformers and inductors will diminish.
4. reduced size of the output filter due to a dramatic increase (by a factor of three) of ripple frequency of the dominant harmonic;

The ISI implemented at the converter input side has the unique feature that it can boost the output voltage of the fuel cell by introducing a shoot through operation mode, which is forbidden in traditional voltage source inverters. Thus, the varying output voltage of the fuel cell is first preregulated to a certain value (for example, 600 V) by adjusting the shoot through duty ratio. Afterwards, the isolation transformers are being supplied with the voltage with constant amplitude value and certain duty cycle. With such feature the proposed three-phase isolated DC/DC topology with ISI could provide cheaper, reliable and efficient approach for fuel cell powered systems.

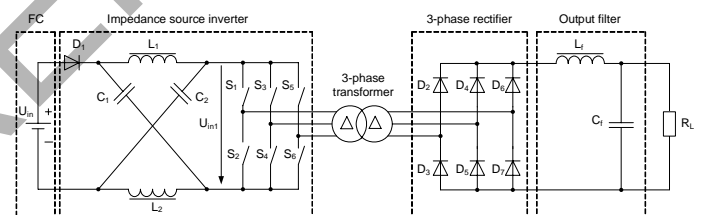


Figure 1. Proposed topology of the step-up isolated DC/DC converter for fuel cell applications.

The given paper provides the design guidelines of the proposed topology. The operation of interface converter will be studied in two boundary operating points - at the minimum and maximum output voltages of the fuel cell. The rated power of the interface converter is 10 kW and the desired output voltage is 600 V DC. The general specifications of the interface converter are submitted in Table I.

TABLE I.
GENERAL SPECIFICATIONS OF THE INTERFACE CONVERTER

Input voltage range, U_{in}	40...80 V DC
Converter output power, P	10 kW
Desired DC-link voltage, U_{in1}	400 V
Output voltage, U_{Load}	600 V DC
Load current, I_{Load}	16.7 A
Switching frequency, f_{sw}	10 kHz
Type of switching devices	IGBT
Peak-to-peak current ripple through Z-source inductors	60%
Desired voltage ripple on the Z-source capacitors	3%

II. DESIGN RECOMMENDATIONS FOR THE ISI

As was reported in previous section, the ISI implemented in proposed topology has unique features compared with the traditional voltage source inverter. It is a two port network that consists of split inductors L_1 and L_2 and capacitors C_1 and C_2 connected in X shape (Fig. 1). This impedance network is basically operating in two states: first is shoot-through when one or more inverter legs are short circuited. Second state is the non shoot-through state, when inverter is in active state as a traditional voltage source inverter. Between the inverter bridge terminals appears sum of the capacitor and inductor voltage, referred to DC link voltage in voltage source inverter [1], [2], [4], [5]. Switching between shoot-through states and non shoot-through states allows boost voltage of capacitors U_c and voltage of the inverter bridge over input voltage U_{in} .

During the design of ISI the most challenging is the estimation of values of the reactive components of the impedance network [6]. The component values should be evaluated for the minimum input voltage of the converter, where the boost factor and the current stresses of the components become maximal. Calculation of the average current of an inductor

$$I_L = \frac{P}{U_{in}}. \quad (1)$$

The maximum current through the inductor occurs when the maximum shoot-through happens, which causes maximum ripple current. In our design, 60% peak-to-peak current ripple through the Z-source inductor during maximum power operation was chosen. Therefore, the allowed ripple current is ΔI_L , and the maximum current through the inductor is I_{Lmax} :

$$I_{Lmax} = I_L + I_L \cdot 30\%. \quad (2)$$

$$I_{Lmin} = I_L - I_L \cdot 30\%. \quad (3)$$

$$\Delta I_L = I_{Lmax} - I_{Lmin}. \quad (4)$$

The boost factor of the input voltage is:

$$B = \frac{1}{1 - 2D_z} = \frac{U_{in1}}{U_{in}}, \quad (5)$$

where D_0 is the shoot-through duty cycle:

$$D_z = \frac{B - 1}{2B}. \quad (6)$$

The capacitor voltage during that condition is

$$U_c = \frac{U_{in} + U_{in1}}{2}. \quad (7)$$

Calculation of required inductance of Z-source inductors:

$$L = \frac{T_z \cdot U_c}{\Delta I_L}. \quad (8)$$

where T_0 - is the shoot-through period per switching cycle:

$$T_z = D_z \cdot T. \quad (9)$$

Calculation of required capacitance of Z-source capacitors:

$$C = \frac{I_L \cdot T_z}{U_c \cdot 3\%}. \quad (10)$$

Table II shows the initial and calculated values of all the parameters of the impedance system.

TABLE II.
INITIAL AND CALCULATED VALUES OF THE IMPEDANCE SYSTEM

Parameters	Fuel cell voltage	
	40 V	80 V
Boost factor B	10	5
Shoot-through duty cycle D_z	0.45	0.4
Z-source inductance $L_1 = L_2, \mu H$	66	
Z-source capacitance $C_1 = C_2, \mu F$	1705	
Average current of Z-source inductor I_L, A	250	125
Maximum current of Z-source inductor I_{Lmax}, A	325	162.5
Minimum current of Z-source inductor I_{Lmin}, A	175	87.5
Ripple current of Z-source $\Delta I_L, A$	150	75
Z-source capacitor voltage U_c, V	220	240

III. MODELING OF TRANSIENT PROCESSES OF THE Z-SOURCE INVERTER

To control the ISI all the traditional PWM schemes can be used. In discussed application to generate a desired output voltage a modified PWM with shoot-through states is used to boost the voltage. This control principle of the method is shown in Fig. 2 (T_0 - cycle, T - cycle of triangular carrier, T_z - time of shoot-through state, $U_{AB,BC,CA}$ - line voltages, SA, SB, SC - signal generators).

The traditional PWM switching sequence based on the triangular carrier method is shown in Fig. 2. To control the shoot-through states, the two straight lines are introduced. When the triangular waveform is greater than the upper envelope or lower than the bottom envelope, the inverter switches turn into the shoot-through state. The duty cycle of the shoot-through state is varying between two predefined values and is inversely proportional to the fuel cell voltage.

In this circuit topology the parameters of reactive elements, like L and C are used as obtained from calculations. The inductors L_1 and L_2 and capacitors C_1 and C_2 have the same inductance and capacitance values, respectively, thus the impedance network becomes symmetrical [4], [7].

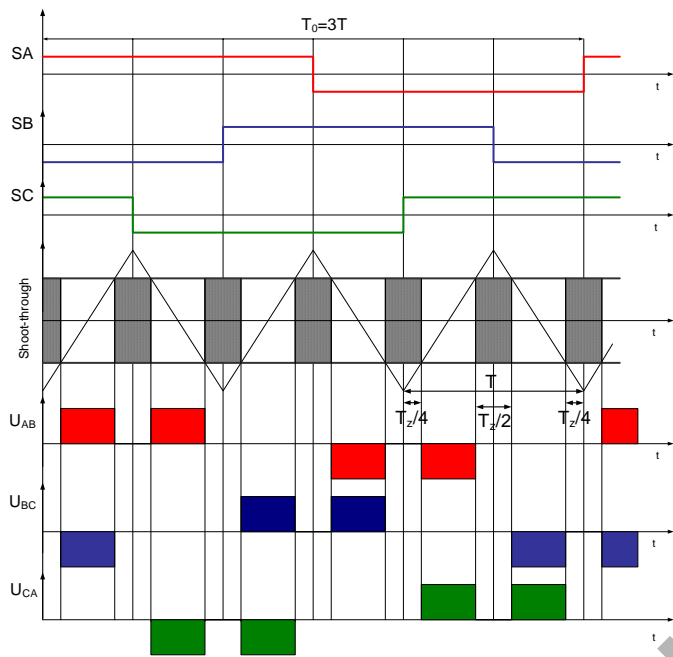


Figure 2. Control principle of the Z-source inverter.

Simulations were carried out by help of simulation package *PSIM*. The simulation circuit is presented in Fig. 3.

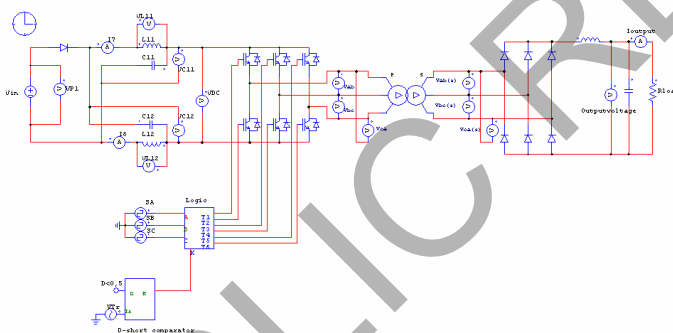


Figure 3. Simulation model (*PSIM*) of the proposed converter.

The simulations of the proposed converter were performed for two operating points – with the fuel cell voltages of 40 V and 80 V, and for the rated output power (10 kW). The isolation transformer assumed for the simulations was the “delta-delta” connected three-phase single core isolation transformer with the turns ratio of 1:2.5. The simulation results are presented in Figs. 4 - 13.

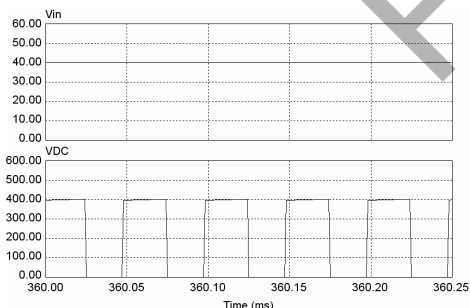


Figure 4. Voltage of fuel cell and DC-link voltage at the maximum boost factor.

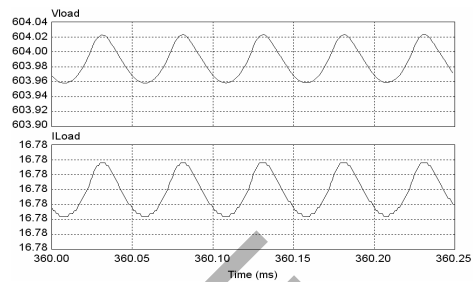


Figure 5. Output voltage and current ripples.

1. Modeling with the fuel cell voltage $U_{in} = 40$ V.

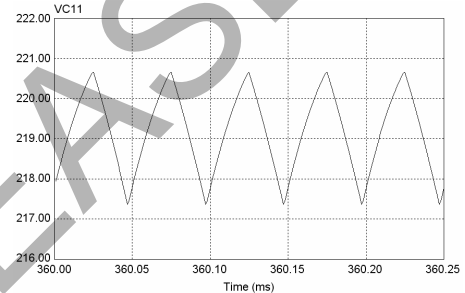


Figure 6. Voltage of the Z-source capacitor.

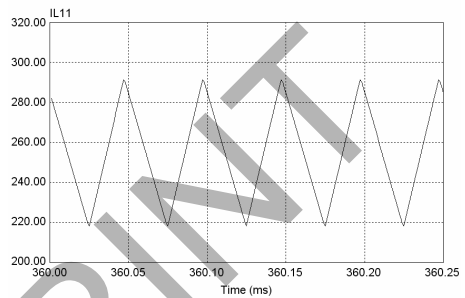


Figure 7. Current of the Z-source inductor.

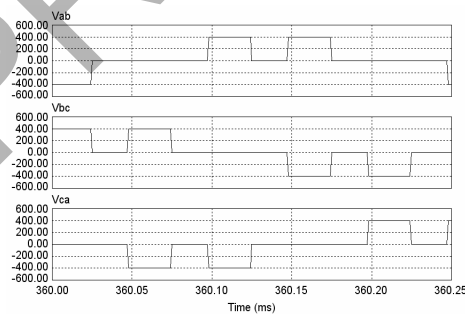


Figure 8. Voltage of the primary winding of the isolation transformer.

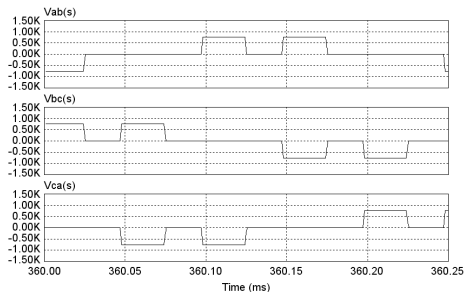


Figure 9. Voltage of the secondary winding of the isolation transformer.

2. Modeling with the fuel cell voltage $U_{in} = 80$ V.

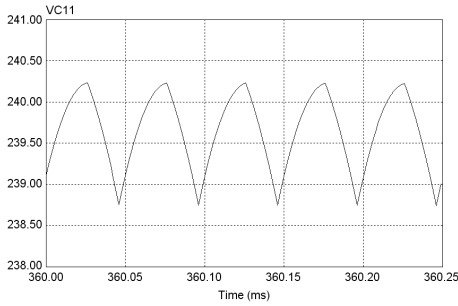


Figure 10. Voltage of the Z-source capacitor.

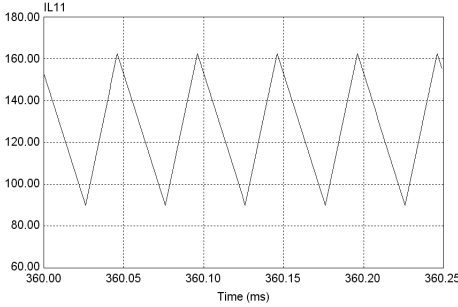


Figure 11. Current of the Z-source inductor.

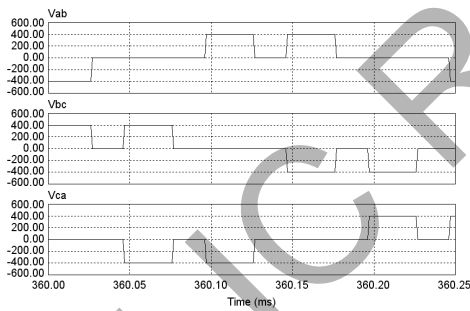


Figure 12. Voltage of the primary winding of the isolation transformer.

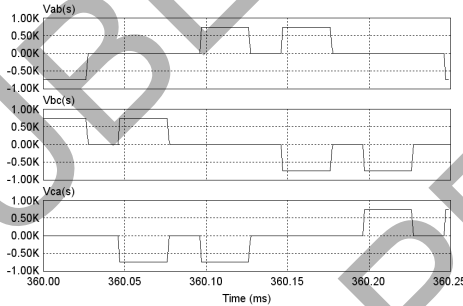


Figure 13. Voltage of the secondary winding of the isolation transformer.

IV. ANALYSIS OF SIMULATION RESULTS

The simulations performed show that the proposed ISI is capable of boosting the varying voltage of the fuel cell to the desired level ($U_{in1} = 400$ V). After the preregulation for achieving the required output voltage on the load terminals ($U_{Load} = 600$ V) the further increasing of voltage was realized by the three-phase step-up transformer.

The calculated voltage ripple on the Z-source capacitors is 3% at 40 V and 3% at 80 V (see Table II). The simulated values of voltage ripple on the Z-source capacitors at input voltages of 40 V and 80 V were 1.36% and 0.83%, respectively, which is much better result than the result obtained by the calculations. The calculated current ripple through the Z-source inductor is 60% at 40 V and 60% at 80 V. The values of ripple current received from the simulations were 28% and 57% at input voltages of 40 V and 80 V, respectively. The output voltage of the DC/DC converter remains constant (600 V DC) in all boundary operating points. The output voltage and current ripple were below 1%, which is very good result for such a powerful system.

V. CONCLUSIONS

The paper presented a new step-up isolated DC/DC converter for the fuel cell applications. By help of theoretical analysis and simulations it was stated and verified that the implementation of the Z-source inverter in the primary side of the isolated DC/DC converter could provide an effective boost of the input voltage only by the introduction of the shoot-through switching state. The desired DC-link voltage is preregulated by the variation of the shoot-through duty cycle, which is inversely proportional to the operating voltage of the fuel cell.

The simulations showed that the proposed converter is operating as predicted, without intolerable voltage and current ripples on its input and output sides. The future work is aimed to development, assembling and testing of the scaled prototype (3 kW) of the proposed converter.

ACKNOWLEDGMENT

Authors thank Estonian Science Foundation (Grant ETF8020 "Research of Advanced Control and Diagnostics Systems for the High-Power IGBT Converters" and Grant ETF7572 "High Power DC Voltage Converters with High Frequency Transformer Link") for their financial support.

REFERENCES

- [1] R. Strzelecki, and G. Benysek, *Power Electronics in Smart Electrical Energy Networks*, © 2008 Springer-Verlag London Limited.
- [2] Fang Zheng Peng, "Z-source inverter," *IEEE Transactions on Industry Applications*, Volume 39, Issue 2, Mar/Apr 2003 Page(s): 504 – 510.
- [3] Vinnikov, D.; Isolated DC/DC Converter Topology with a Three-phase Intermediate AC-Link. 2006 International Baltic Electronics Conference, 2-4 Oct. 2006, pp.1 – 4.
- [4] Fang Zheng Peng and Yi Huang "Z-source inverter for power conditioning and utility interface of renewable energy sources".
- [5] J. Rabkowski, "The bidirectional Z-source inverter as an energy storage/grid interface". International conference "Eurocon 2007", Warsaw, September 9-12, pp. 1629 - 1635.
- [6] Mitch Olszewski "Z-Source Inverter for Fuel Cell Vehicles", Michigan State University, Department of Electrical and computer Engineering, Oak Ridge National Laboratory, August 31, 2005.
- [7] F. Peng, M. Shen, and Z. Qian, "Maximum boost control of the Z-source inverter," Annual IEEE Power Electronics Specialists Conference, pp. 255-260, 2004, Aachen, Germany.

Voltage division over the interrupter units of a high voltage circuit breaker without grading capacitors

Henryk Stürmer
LS EVH, BTU Cottbus
Cottbus, Germany

Abstract-In this paper the voltage division over the interrupter units of a high voltage circuit breaker without grading capacitors is investigated. A method of measuring capacitances and earth capacitances is presented. High voltage tests were made.

I. INTRODUCTION

In a modern high-voltage circuit breaker in lower voltage levels (up to 300kV) one interrupter unit is used per phase. In higher levels two, three or four switching lines in serial circuit are used.

Both in off-position and disconnection of the load or short circuit current the interrupter units are stressed by different voltages. In order to be able to stress a specified number of interrupter units by high voltage, the voltage is equally divided by grading capacitors to all interrupter units. The grading capacitors are connected in parallel to the interrupter units. For example for a quad breaking circuit breaker a voltage division of 25/25/25/25% is aspired and for a twice breaking circuit breaker a division of 50/50% is aspired. Using available grading capacitors the voltage division is 53/47% and 27/26/24/23%.

Because the grading capacitors are an important expense factor for high-voltage circuit breakers for several years it's tried to apply multiple breaking circuit breakers without grading capacitors. The voltage division is the most important factor. The result from the calculation of a twice breaking circuit breaker is 80/20%, for a quad breaking circuit breaker without grading capacitors it is 80/10/5/5%. In both cases one interrupter unit has 80% of the voltage; the other units have only a small voltage.

If you make a dielectric or switching capacity testing you can see, the circuit breaker is able to keep a higher voltage like the calculation showed.

The following facts could be the reasons:

- The calculation is too inexact.
- Only the capacities are considered; there could be More effects.

It's difficult to measure the voltage division between the interrupting units by common measurement equipment because the measurement equipment has a noticeable influence to the voltage division.

The equivalent circuit used consists of capacities. The capacities are to determine.

The following problems are to research:

- Development of a qualified measuring method: Measurement of circuit breaker-capacities by

Measurement of capacitive current and with bridge, Measurement of earth capacities by measurement of Capacitive current, voltage measurement

- Simulation of circuit breaker and measurements: Field and transient simulations
- Several High Voltage Tests: ac-tests and impulse tests
- Analysis of the effects, which determine the voltage Division and which determine the several forms of the Voltage stress
- Analysis of the equivalent circuit
- Comparison of the findings and the test readings and Declare, why the circuit breaker operates better than in The calculation
- Test problems: capacities between test object and Measuring equipment/environment

II. MEASUREMENT OF CAPACITANCES BY CURRENT MEASUREMENT

Measurement of the capacitance of a reference capacitor

To determine the capacitance of a capacitor the capacitive current was measured at two fixed voltages.

A shielded cable was used from the capacitor to the ampere meter.

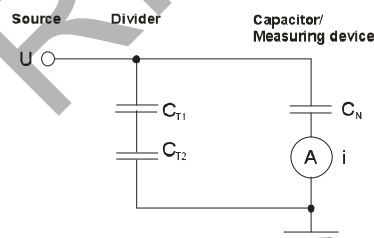


Figure 1: Current measurement at a reference capacitor

The test circuit consists of the source, the divider, the capacitor and the measuring device. The source is a high voltage transformer and the divider is a capacitive divider. The test object is a reference capacitor. To measure the current an ampere meter was used. The measurement was made at two different voltages. The ohmic resistance and the inductivity are nearly zero. So the resistance is nearly the reactance of the circuit. The capacitance can be calculated

$$X \approx \frac{u}{i} \quad (1); \quad C \approx \frac{1}{2\pi f \cdot X} \quad (2)$$

U [kV]	i [μA]	X [MΩ]	measured Capacitance C [pF]	Capacitance of the reference capacitor [pF]
10,08	328	30,7	103,58	103,63
50,05	1634	30,6	103,92	103,63

The capacitance calculated from the measured current is exact. The error is small.

Measurement of the earth capacitance

To measure the full earth capacitance, the ampere meter was installed on the upper side of the capacitor (on the top). The ampere meter and the influence to the earth capacitance have to be small. The ampere meter was located near the capacitor to minimize the error of the connection from ampere meter to the capacitor. A short connection had to be used.

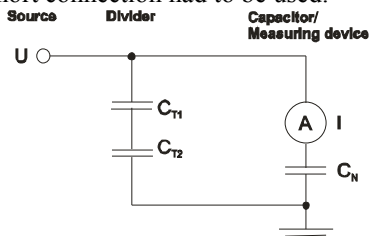


Figure 2: Measurement of the full earth capacitance

The capacitance was $\approx 190\text{pF}$. A field simulation of the full earth capacitance follows to a later time.

In the following picture is the first measurement to see. The ampere meter is on the side of the capacitor, better would be on top. More tests and simulations will follow to compare several measure points.



Figure 3: Measurement of the full earth capacitance of the reference capacitor

III. MEASUREMENT OF THE CAPACITANCES OF THE CIRCUIT BREAKER

The capacities of the twice breaking circuit breaker were measured by bridge and current measurement. In the following is an overview of the tests in the high voltage hall. The measurements were made on three test places, where the circuit breaker stood.

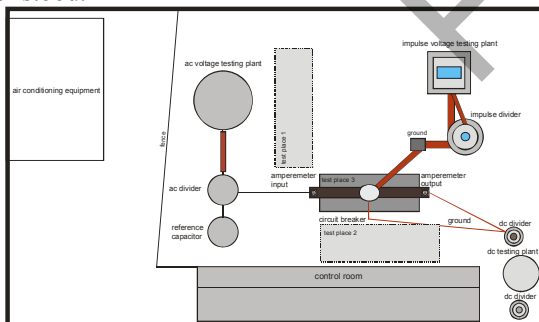


Figure 4: test overview

Measurement of the current

To determine the capacities of the circuit breaker there were made several measurements of input and output current. Two measuring devices were mounted on the left and the right side of the circuit breaker. The devices were located on a metallic surface, so the change of capacities is very small.

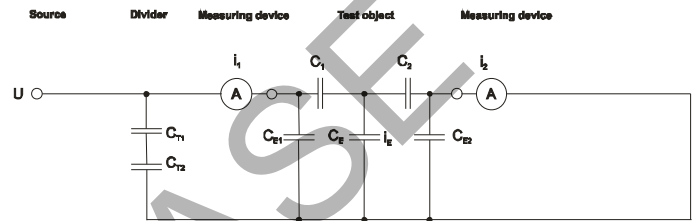


Figure 5: Current measurement



Figure 6: Voltmeter for current measurement

The capacities of the circuit breaker are:

- Capacities of the interrupter units C_1, C_2
- Left and right earth capacity C_{E1}, C_{E2}
- Middle earth capacity C_E

To calculate the searched capacities three equations are needed.

Many different tests were made:

- *the output of the circuit breaker opened:*
 - Interrupter unit 1 and 2 opened
 - Interrupter unit 1 and 2 closed
 - Interrupter unit 1 closed, interrupter unit 2 opened
 - Interrupter unit 1 opened, interrupter unit 2 closed
- *the output of the circuit breaker grounded:*
 - Interrupter unit 1 and 2 opened
 - Interrupter unit 1 closed, interrupter unit 2 opened
 - Interrupter unit 1 opened, interrupter unit 2 closed

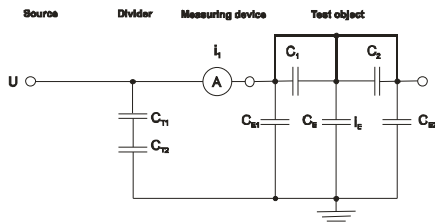
The measurements were made up to 50kV, for example in one configuration the input current was $540\mu\text{A}$ at a voltage of 50kV.

The results of the measurement showed conflicts between different measurements. It is better to calculate the capacities only with measurement values from input ampere meter.

If the capacity of the interrupter units is known, for instance from measurement by bridge or current measurement, there are only two measurements needed for tests:

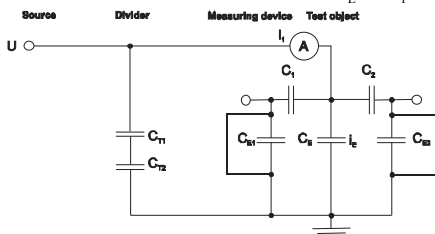
The input and output cables were long and some meters parallel to earth. So the operation of the circuit breaker was imitated and the influence to the capacities was low.

1) Measurement of earth capacities: $C = C_E + C_{E1} + C_{E2}$ (3)

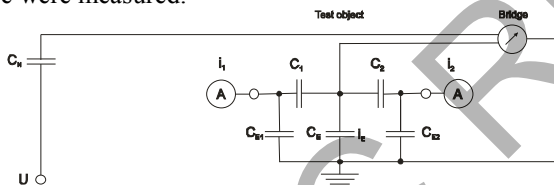


2) Measurement of interrupter units and middle earth capacities:

$C = C_E + C_1 + C_2$ (4)



With the bridge the capacities between the test object and the source were measured.



Picture 7: Example of measurement of capacitance between test object and source

Some pF were measured and the output current measurement was wrong because of the leakage capacitance between circuit breaker and the transformer with the divider.

The second error was the earth capacity.

The measurements were made on three different places for the test object. If the circuit breaker was near the source the error of the capacity of the interrupter units was greater. If the circuit breaker was far away from the source the measured capacity of the interrupter units was decreased, but because of the borders in the high voltage hall the earth capacities were increased. The circuit breaker was here near the side of the high voltage hall and the control room.

For the first measurements the results show good values. For a better accuracy the measurements will be repeated in free a field.

Measurement by bridge

The capacity of the interrupter units were measured by a bridge. The measurements were made up to 50kV.

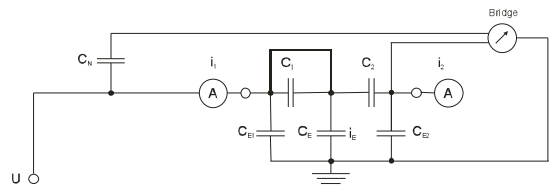


Figure 8: An example of measuring by bridge

The biggest capacity was measured on test place 1, the capacity between source and circuit breaker was the highest and an error was made.

The source cable was assembled in different places and the difference between measured capacitances was over 10%.

On test place 2 and 3 the capacity was over 10% smaller than on test place 1.

Voltage measurement

The voltage over the interrupter units were measured directly. The voltage was 20kV. Two voltmeters were used. Because the input resistance is too low, series capacitances were used.

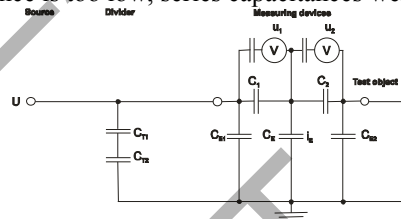


Figure 9: Voltage measurement

The measuring devices were installed. The first interrupter unit was shorted and a high voltage was applied. The divider ratio of measuring device 2 was calculated. The procedure was made for measuring device 1 with shorted unit 2. When the ratios were known, the voltages over the units were measured.

Errors are here the leakage capacitance of cables and the voltmeters with divider capacitances.

Problems of the current and bridge measurements

The measured capacities are very small. It's difficult to measure these capacities. The cable and the environment have an influence to the measurement.

These errors have also an influence to high voltage tests on a circuit breaker.

An example:

An interrupter unit has the capacitance of 15pF and the middle earth capacity is 40pF. If the circuit breaker is near the transformer, there are leakage capacities in parallel from the transformer and divider to the circuit breaker.

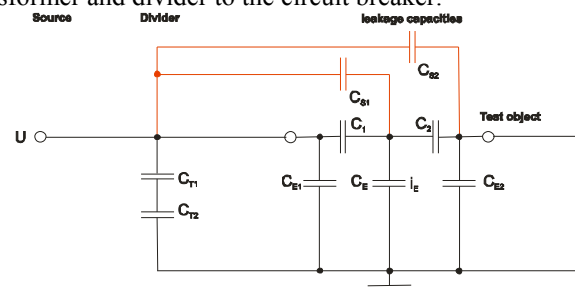


Figure 10: Leakage capacities of a twice breaking circuit breaker near the source

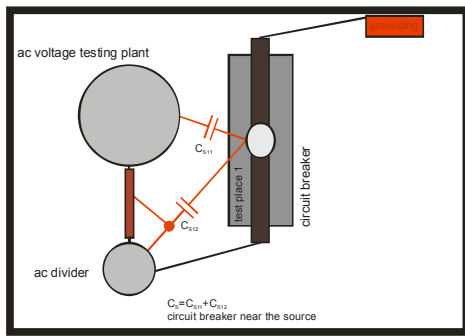


Figure 11: Leakage capacities of a twice breaking circuit breaker near the source

The parallel leakage capacitance $C_{S1} = C_{S11} + C_{S12}$ increases the capacitance of interrupter unit 1. The voltage ratio is changed.

An example, where $C_{S1} = 3\text{pF}$ is.

C is calculated from capacities C_2, C_E and C_1, C_{S1} .

$$C = \frac{1}{\frac{1}{C_1 + C_{S1}} + \frac{1}{C_E + C_2}} \quad (5); \quad \frac{U_1}{U} \approx \frac{C}{C_1 + C_{S1}} \cdot 100\% \quad (6)$$

C_1 [pF]	C_{S1} [pF]	C_E [pF]	C [pF]	$U1$ [%]	$\frac{U_1}{U_2}$
15	0	40	11,8	78,6	78,6% / 21,4%
15	3	40	13,6	75,3	75,3% / 24,7%

If the circuit breaker is some meters away from the transformer and the divider, the leakage capacitance decreases.

IV. HIGH VOLTAGE TESTS

The following high voltage tests were made:

- AC tests with breakdown and withstand alternating Voltage
- Impulse tests: positive and negative lightning impulse Voltage and switching surge tests

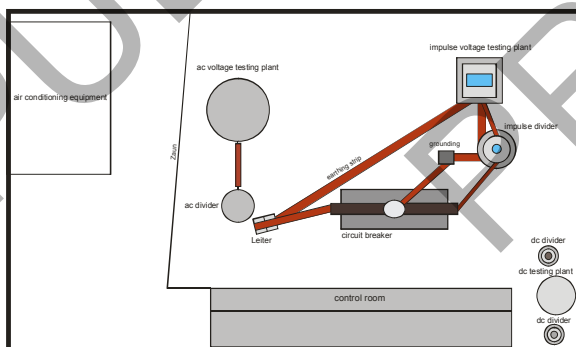


Figure 12: test overview: impulse tests

The ac tests were made up to 700kV and the impulse tests up to 1150kV.

The ac and impulse tests were made with one interrupter unit and the complete circuit breaker. The 50%-break down voltages, several statistical parameters and the Weibull distribution were calculated. The 0,1%- and 99,9%-break down voltages were calculated from the Weibull distribution.

The voltage distribution over the circuit breaker was calculated from the ratios of break down voltage of one interrupter unit over the complete circuit breaker.

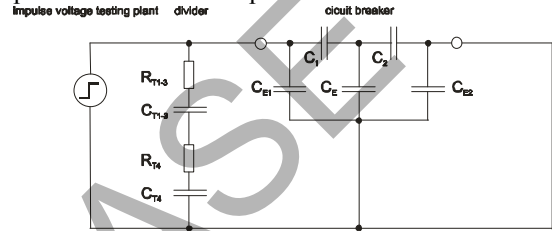


Figure 13: impulse tests

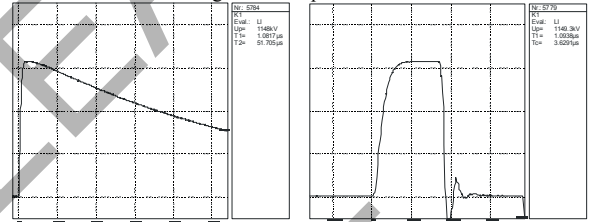


Figure 14: examples of impulse tests: lightning impulse and chopped lightning impulse

V. FORECAST

The following points are planned for the future.

- Measurements in free field
- Field simulation of the reference capacitor
- Field simulation of the circuit breaker in the high Voltage hall
- Transient simulation of the circuit breaker in a network
- Measurement and simulation of a circuit breaker model
- Analysis of the equivalent circuit
- Analysis of the results and the effects of the circuit Breaker

VI. BIOGRAPHY



Henryk Stürmer was born in Cottbus, Germany. He studied at BTU Cottbus electrical engineering. He worked several years in energy distribution in the industry and in industrial projects at the BTU Cottbus.

Adjustable Speed Generation System For Wind Turbine Power Quality Improvement

Włodzimierz Koczara koczara@isep.pw.edu.pl

Grzegorz Iwanski iwanskig@isep.pw.edu.pl

Warsaw University of Technology, Poland

Zdzisław Chłodnicki zdzislaw.chlodnicki@cummins.com

Warsaw University of Technology, Poland &
Cummins Generator Technologies, Stamford, UK

Abstract- The paper presents an emerging technology of electricity generation based on decoupled theory. The decoupled generation system operates in wide speed range and control strategy is oriented to select regions of high efficiency of the driving engine. This system is used to operate parallel to renewable energy source that is unstable and not reliable. In case of high power available from the renewable the decoupled adjustable speed generation reduces its speed what results in low fuel consumption. However when the renewable source power is decreasing the adjustable speed generation system increases its speed following points of high efficiency of the driving Diesel engine. The paper presents topologies of the combined systems including variable speed wind powered generation system and adjustable speed generation system driven by Diesel engine. Moreover ability of the adjustable speed to provide power is discussed.

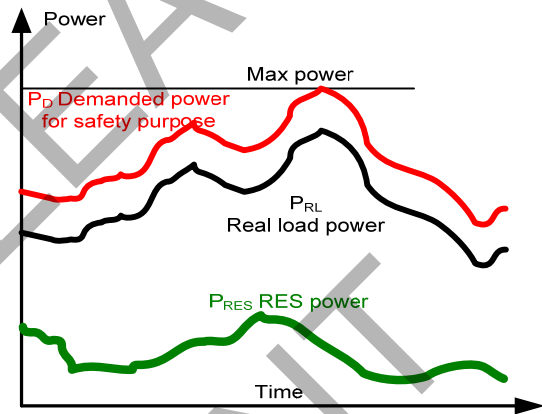


Fig. 1. An example of electricity power demand and renewable available power

I. INTRODUCTION

The lack of energy, unstable prices of energy, increasing prices of fossil fuels and environment protection result in increase of interest of renewable energy sources. An alternative to fossil fuel based electricity generation are usually wind and solar power. However both wind and solar power depend on weather conditions. Fig. 1 shows an example of typical variation of power as a function of time. There is a load power P_{RL} , renewable source available power P_{RES} , and P_D power demanded to keep stability of the system. The renewable power P_{RES} varies and frequently, in time of high power demand, this power is not available. Therefore the renewable source is mainly source of the energy that reduces general consumption of fossil fuels but not the sources of high quality power. So to provide high quality power, including renewable sources, it is needed to provide an additional generating system that is fully controllable. This additional generation system will compensate renewable power fluctuation and will deliver demanded power P_D at any time. Moreover it is advantageous to use controllable energy storage that acts as instant source of power P_{St} . Fig. 2 shows topology

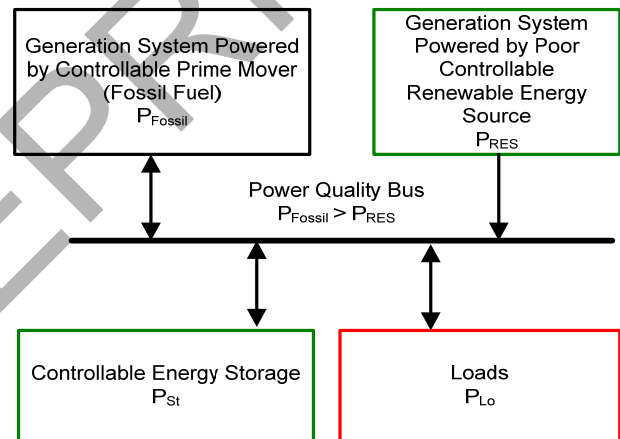


Fig.2. Topology of compensated generation system including renewable and fossil fuel powered electricity sources.

of the generation system that is able to fulfill drawing maximal energy from renewable source (power P_{RES}). Hence the fossil fuel based source power P_{Fossil} produces high quality power and usually is much higher than RES power P_{RES} .

The modern variable speed generation systems based on double fed induction generator (DFIG) are connected to AC bus as is shown in Fig. 3. A synchronous generator SG operates with fixed speed according grid frequency.

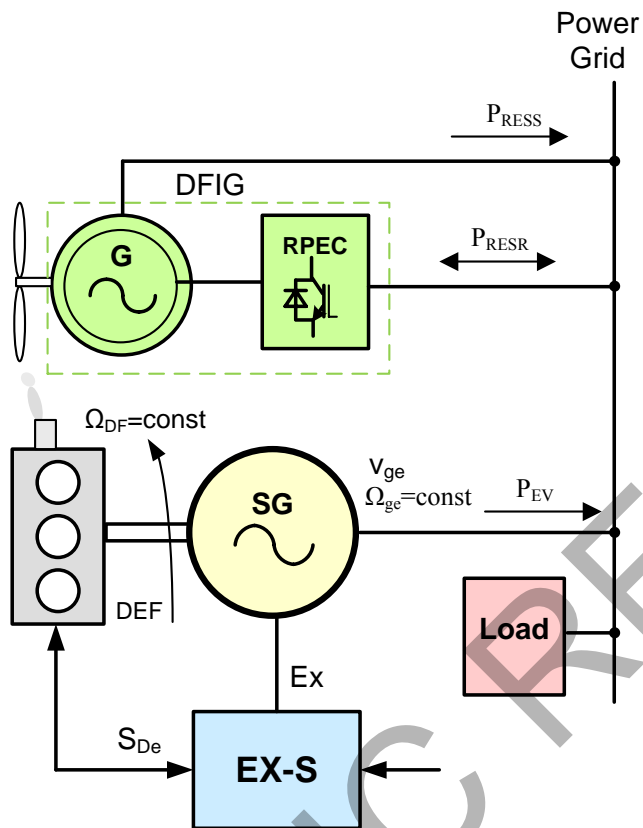


Fig. 3. Typical connection wind turbine DFIG to AC power grid.

The conventional generation system is driven, for instance, by an internal combustion engine [15]. Such system efficiency or specific fuel consumption (g/kWh) depends on load. So, in case of low power demand i.e. in case high power delivered by RES, the specific fuel consumption of the engine is high. Therefore energy saving, responding RES operation, is accorded by significant losses produced by the engine. It is then question how economical is the RES operation?

The fossil fuels are strategy issue of supply countries and fossil fuels prices are not stable and producing great perturbation in world economy. Fig. 4 shows prices of oil during last 60 years. We remember that in Summer 2008 barrel of oil price was much higher than \$100. Therefore parallel to great efforts, promoting renewable energy, the same efforts have to be done in the field of reduction of primary energy consumption by improvement of efficiency engines fed by fossil fuels.

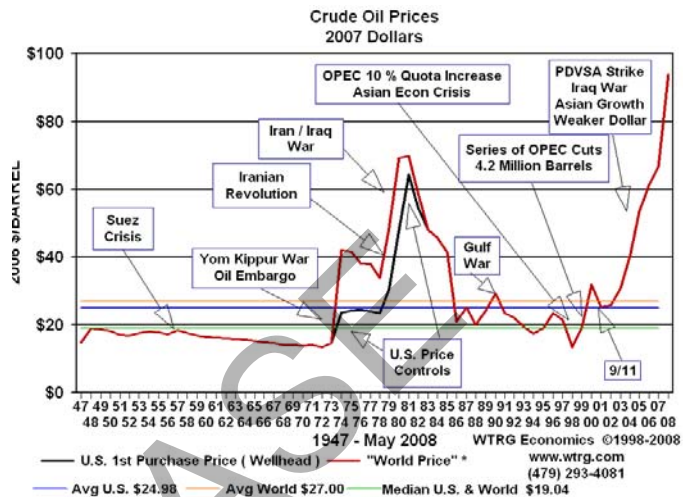


Fig. 4. History of oil prices.

II. ADJUSTABLE SPEED GENERATION SYSTEM APPLICATION

The adjustable speed generation system [1, 2, 5, 14, 16] produces AC voltage that frequency is independent to speed. Such a system (Fig. 5), described as ASGS, is used to

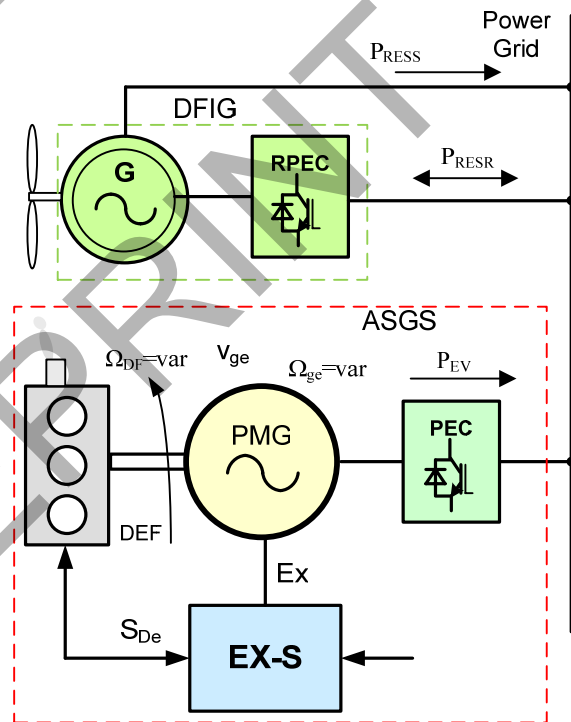


Fig. 5. Decoupled adjustable speed generation system ASGS as efficient generation system connected parallel to wind driven DFIG.

compensate the renewable DFIG power fluctuation. The adjustable speed generation system operates in regions of low fuel consumption. Fig. 6 shows maximal power of the Diesel engine P_{dmax} as function of speed. The adjustable speed

generation system uses engine power along line $A_1-A_2-A_3$ i.e. in the region of low specific fuel consumption g (g/kWh).

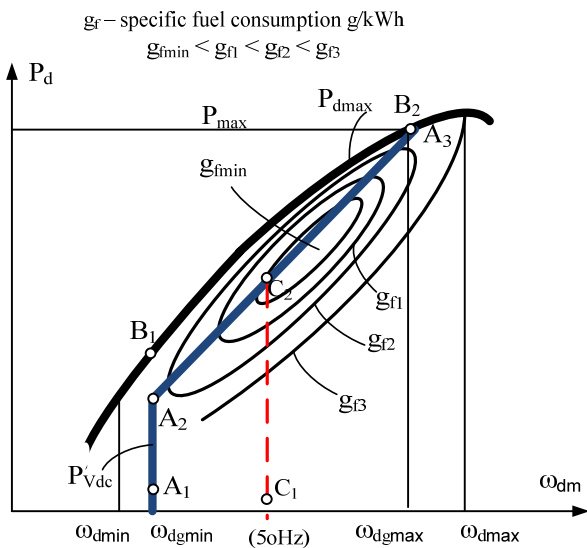


Fig. 6. Power and specific fuel consumption of the Diesel engine operating with fixed and variable speed.

Comparing to conventional fixed speed operation (line C_1-C_2) we do notice that most of fixed speed operation is along high specific fuel consumption.

The adjusted load torque, produced by the generator, is close to maximum torque. So when series of step load appear then speed is adjusted and output voltage (Fig. 7) is maintained

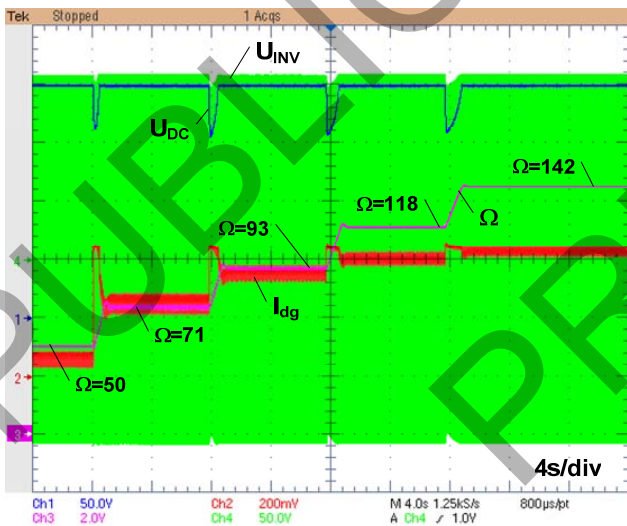


Fig. 7. Response of the adjustable speed generation system on set of step loads.

(voltage U_{AB-INV}). However when at low speed step of high power is applied than output voltage is dropping significantly (Fig. 8)

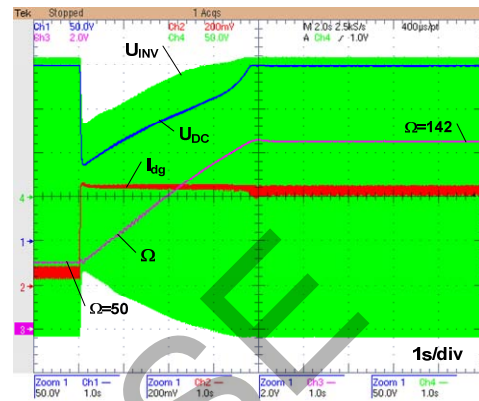


Fig. 8. Response of the speed Ω and output voltage U_{INV} of the adjustable speed generation system on the high step load on the low speed.

To avoid this low quality voltage effect it is used an additional energy storage system shown in Fig. 9.

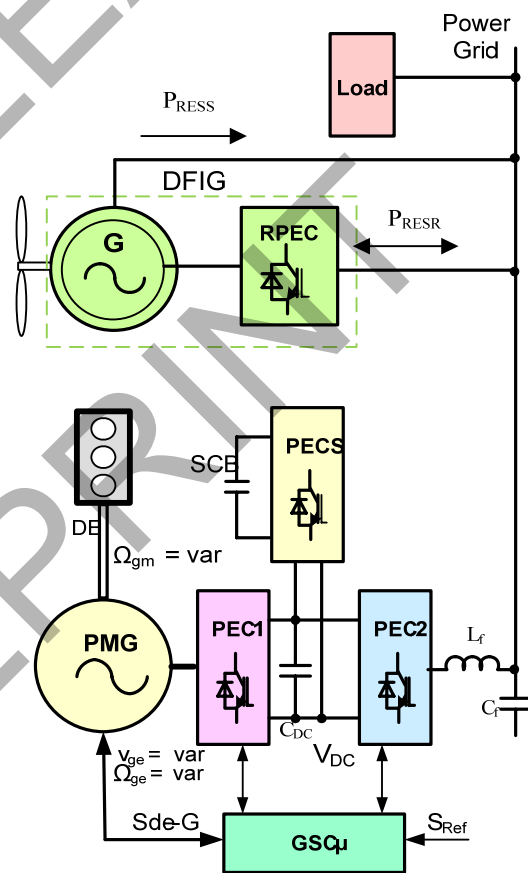


Fig. 9. Topology of the connection of decoupled generation system and variable speed wind powered DFIG.

The energy storage SCE, based on supercapacitor, supplies the load during short time needed to the engine acceleration. An effect of the energy storage application is shown in Fig. 10. The step of load as in case shown in Fig. 10 is not producing

significant voltage changes because the supercapacitor supplies converter DC link voltage U_{DC} by the current I_{sc} .

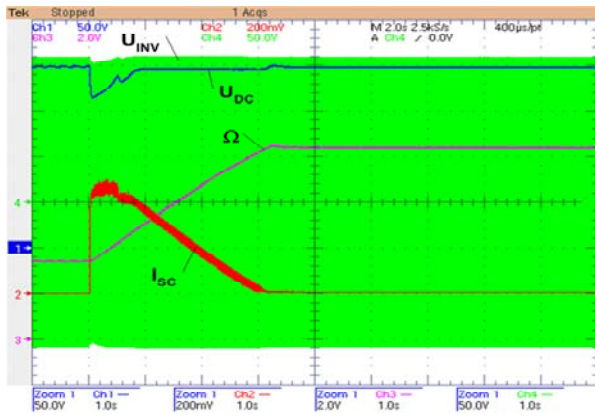


Figure 10. Response of speed Ω , the supercapacitor current I_{sc} and the output AC voltage U_{INV} on high step load at low speed

III. SUMMARY

The adjustable speed generation performances confirm its ability to produce power in region of high efficiency. The system adjusts its power by speed. The maximum power rate is limited by need of speed acceleration. When an addition energy storage is applied then system is able to provide high quality power at any step load. This ability indicates that the adjustable speed may be selected as future system for improvement systems including RES especially wind turbine driven generators.

REFERENCES

[1] Z.Chlodnicki, W.Koczara, N.Al-Khayat: Laboratory Simulation of the Variable Speed Generation System. EPE Journal Vol. 17 nr 4 Janvier 2008.

[2] R. Srzelecki, G. Benysek: Power Electronics in Smart Electrical Energy Networks, Springer London, 2008.

[3] Bolognani S., Venturo A., Zigliotto M.: Novel Control Technique for High-Performance Diesel-Driven Generator-Sets. Conference Proceedings on Power Electronics and Variable Speed Drives, 18-19 September 2000. Conference Publication No. 475 © IEE 2000, pp. 18-523.

[4] W. Koczara, M. Moskwa, N. L. Brown: Autonomous Adjustable Speed Decoupled Generation Systems and their Parallel Operation. Proceedings of 39 Power Electronics Specialists Conference PESC, 15-19 June 2008, Rhodes, Greece.

[5] W. Koczara, Z. Chlodnicki, E.Ernest, N. L. Brown: Hybrid Generation System. Proceedings of 3rd International Conference on Ecological Vehicles and Renewable Energies, Monte Carlo March 27-30, 2008. Monaco.

[6] R. H. Staunton, B. Ozpineci, T. J. Theiss, and L. M. Tolbert, Review of the State-of-the-Art in Power Electronics Suitable for 10-kW Military Power Systems, ORNL/TM-2003/209, October 2003.

[7] A. Krasnodebski: Asynchronous Thyristor By-pass Increasing Short Circuit Capability of Variable Speed Generating Set. PhD thesis. Warsaw University of Technology, Warsaw, Poland 2007.

[8] L. Grzesiak, W. Koczara, M. Da Ponte, "Novel Hybrid Load-Adaptive Variable-Speed Generating System", Proceedings of IEEE Industrial Electronics Conference Vol.1, p.271-276, Pretoria, 1998.

[9] N. Al-Khayat, R. Seliga, W. Koczara, B. Kaminski, A. Krasnodebski, "DSP Control of Variable Speed Integrated Generator", IEEE-ISIE 2002, International Seminar on Industrial Electronic L'Aquila, Italy, July 2002.

[10] W. Koczara, L. Grzesiak, M. Da Ponte, "Application of a Permanent Magnet Machine in the Novel Hygen Adjustable Speed Load Adaptive Electricity Generating System", IEEE-IEMD Seattle 10-12 May 1999.

[11] G. Iwanski and W. Koczara, "Control system of the variable speed autonomous doubly fed induction generator" Proceedings of International Power Electronics and Motion Control Conference – EPE-PEMC'04, Riga, Latvia

[12] G. Iwanski and W. Koczara, "Sensorless Direct Voltage Control Method for Stand-Alone Slip-Ring Induction Generator" Proceedings of 11th European Conference on Power Electronics and Applications – EPE'05, Dresden, Germany.

[13] Koczara, E. Ernest, N. Al-Khayat: „VSIG - Variable Speed Integrated Generation System For Distributed Generation“, Proceedings of the Fifth IASTED International Conference on Power and Energy Systems, June 15-17 2005, Benalmadena, Spain, 335-340 str., ISBN: 0-88986-465-9, ISSN: 1482-7891.

[14] Hygen – variable speed generating system for quality electric power supply. Technical overview. Volt-Ampere, Pretoria, South Africa.

[15] J. Klimstra: Reliable power from renewables with assistance from reciprocating engines. Managing with wind Wartisla 2007.

[16] Variable Speed Integrated Generator (VSIG) – product profile. NEWAGE (in present time Cummins Generator Technologies) Stamford UK.

Current progress in ambient energy harvesting using piezoelectric materials and electroactive polymers

Pawel Zylka

Wroclaw University of Technology, Institute of Electrical Engineering Fundamentals
Wybrzeze Wyspianskiego 27, Wroclaw, Poland

Abstract- A review on current progress in energy harnessing micro-generators using active materials (ceramic and polymeric piezoelectric materials as well as electroactive polymers) is presented. A problem of effective electrostatic energy extraction from those capacitive-in-nature energy supplies is illustrated experimentally. It is shown that using Macro Fiber Composite (MFC) piezoelectric transducers working in resonant mode and matching the load to the MFC impedance it is possible to attain 10 % generation efficiency.

I. INTRODUCTION

Energy harvesting, scavenging, and harnessing – these are all almost analogous terms related to research and engineering activities aimed at extracting energy in electric form from various ambient energy reservoirs, which generally cannot be scaled up for full-size, power-plant energy generation schemes. There are many ambient energy pools that could be exploited by autonomous, low-power fuel-less generators: waste heat, electromagnetic hum, vibrations, localized air movement or human-generated power. In addition, traditional “renewable energy resources” like water flow, tidal and wind energy or sun radiation can also be exploited at the miniature scale by energy micro-harvesters. All environments are now being populated by miniaturized, micro-power electronic devices working in wireless sensor networks or just as mobile gadgets. A dream to power all those devices without batteries making them perpetual or at least to supplement mobile supply scheme is the driving force of the research oriented on ambient energy harnessing. Serious interest in those problems, partially motivated by climate change and global warming, is also reflected by several R&D organizations (e.g. DARPA, CEALITEN) and companies aiming at harnessing energy from ambient vibrations, leg and arm motion, shoe impacts, and blood pressure for self-powered systems.

II. KINETIC ENERGY HARVESTING

Different techniques are being proposed for powering up remote, unattended, implantable or wearable sensors, short-distance wireless communication stations, RFID tags or personal health monitors. Generating electricity from ambient vibrations or kinetic motion is one of those approaches applicable as a renewable substitute for batteries in micro-power electronic products making timed use of accumulated energy. Kinetic energy in the form of motion or vibrations is generally the most versatile and ever-present [1]. Operating principles of motion-driven ambient energy microscavengers relay on utilization of inertial forces acting on a proof mass

fitted with a damper which simultaneously serves as an electromechanical transducer converting kinetic into electrical energy. Vibration stimuli are extensively present but vary widely in amplitude and frequency thus micro-generators are designed as resonant systems matched to vibration spectrum of the source. Non-resonant or dynamically tunable devices are also being designed, as broadband operation is required for maximizing output power when the source has a complex or time-variable vibration spectrum [2].

A. Electrostatic generators

Although miniature human-powered electromagnetic dynamos has been used for a long time to supply flashlights and portable radios yet the electrostatic: capacitive, piezoelectric and electroactive polymer (EAP) generators possess a serious advantage over other competing electromagnetic generation schemes: electricity is generated “intrinsically” thus virtually all moving parts are eliminated so the mechanical complexity of the generator is seriously reduced which makes it lightweight, reliable and wear-proof.

In electrostatic generators, external mechanical force is engaged to do work against the attraction of charged electrodes of a variable capacitor. Two modes of such operation are applicable: switched and continuous. In the switched regime the capacitive transducer and the supplementary circuitry is reconfigured by a set of contactors at different stages of the generation cycle. Such electrostatic transducers require a pre-charging voltage source in order to operate. As the device capacitance is reduced against electrostatic attractive forces it produces current flow into the pre-charging source.

Most of the miniaturized electrostatic energy scavengers are being build as integrated micromachined chips using MEMS fabrication processes. Micromechanical vibration energy scavengers use pre-charged capacitors with capacitance-modulating variable air gap formed between comb electrodes [3]. In order to avoid pre-charging circuitry electret layer may be deposited on capacitor electrode - Arakawa *et al.* has designed a microseismic electrostatic generator using spin-coat-deposited polymeric electret capable of delivering 6 μ W of energy for 1 mm amplitude 10 Hz oscillation [4].

Recent years have brought in new concepts emerging on the rims of high voltage engineering and materials science. These are related to electroactive polymers (EAP) also described as artificial muscles. The last name comes from their ability to directly convert electrical energy into mechanical work and

motion (linear or bending) without any moving parts found in classical electrical drives. Electronic EAPs are one of the main sub-class in broad family of EAP material systems. These are dielectric polymeric materials that change shape or dimensions due to shift or limited migration of electrons in response to electric field stimuli. Dielectric EAP actuators (DEA) display also inverse effect – when working in so-called generator mode they generate electricity from mechanical deformation. In this mode DEA can be perceived as a variable capacitance device. The electrical capacitance is initially charged when the DEA transducer is in the stretched, high capacitance, state. When it is then mechanically contracted it goes back to its low capacitance state and the elastic stresses in the DEA material film works against the compressive Maxwell stress (electric field pressure resulting from opposite charges attraction), thus increasing electrical energy in form of voltage raise. Therefore, energy harvesting from ambient “reciprocating” power sources is also possible by means of dielectric EAP materials.

A recent theoretical analysis indicates that typical human-motion-generated displacements available for inertial microgenerators (approx. 5 mm motion at 1 Hz) can provide energy density of up to $4 \mu\text{W}/\text{cm}^3$ and up to $800 \mu\text{W}/\text{cm}^3$ can be extracted from high-pitched machine-induced stimuli (approx. 2 nm motion at 2.5 kHz) [5]. As typical human applies over 100 % of his own weight across the shoes at every heel strike therefore, cushioned shoe soles can be significantly compressed even during normal walk. Assuming an average person weighting 75 kg, 5 mm sole compression, regular walking speed of 2 steps/s this indicates that roughly about 7 W of power could be available just from heel strikes. Company SRI Intl. has designed and tested a multilayer EAP shoe generator, schematically illustrated in fig. 1. When the device is compressed, the coupling liquid or gel medium contained in the bellows forces out and stretches a thin, elastic layer of electroded EAP through circular openings in the upper perforated plate sealing the bellows. In normal walking conditions such boot energy scavenger was delivering energy output of 0.8 J per every step with just 3 mm heel compression and provided 0.8 W of power [6]. The company Artificial Muscle Inc. has also presented plans to build switched EAP-based power supply units operating on wind or tidal energy. Flapping (flag- or string-like) power generators made of cyclic-distorted DEA fibers are proposed to populate windy locations and floats secured to the sea bottom on stretchable elastic strings made up of dielectric EAP fibers provide extensional motion by riding on tidal or wind- generated waves [7].

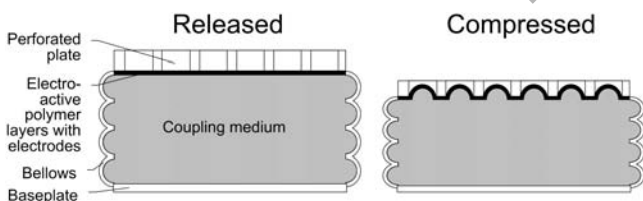


Figure 1. Schematic view of electroactive polymer heel energy harvester module developed by SRI Intl. (sketch based on [8]).

SRI Intl. has already started tests of a prototype buoy-mounted, ocean wave-powered DEA generator. The “Hyper Drive” generator utilizes sleeve-like EAP polymer transducers generating an average output power of more than 5 W under typical ocean wave conditions, which is enough to power up a buoy-mounted radio [9].

B. Piezoelectric continuous mode generators

Although theoretical modeling shows that EAP-based switched energy scavengers using highly compliant electroactive polymers and running at high voltages can provide energy density up to 1,5 J/g and much better performance figures than piezoelectric generators, the latter (despite their intrinsic material properties limiting efficiency due to low electromechanical conversion efficiency and high brittleness and thus low tolerance for high and abrupt mechanical stress) are extensively utilized in construction of continuous mode electrostatic generators. The advantage lays in no requirement for circuitry reconfiguration and no pre-charging source. In this case mechanical work is partially stored in the energy of the electric field associated with the induced polarization of the piezomaterial. Neutralization current flows if an external load is shorting the electrodes deposited on the piezoelement. Effective piezoelectric energy harvesting requires piezoelectric materials with elevated electromechanical coupling coefficients, thus ceramic (PZT) materials dominate those designs.

The company Adaptiv Energy is promoting its kinetic energy harvesting solutions based on Ruggedized Laminate Piezo (RLP) composite combined with efficient, very-low-loss MOSFET power extraction electronics. The RLP technology allows to compress piezoceramic material in order to increase the voltage per strained unit area. The RLP is a stainless steel flat spring double-side laminated with a piezoelectric ceramics and copper electroding layers. Appropriate thermal cycling during bonding process introduces initial compressive prestressing into the piezoelectric material, giving greater density and flexibility and thus provides added output voltage. RLP transducer uses calibrated mass to match the exploitable vibration spectrum [10]. Ocean Power Technologies company exploits strips of piezoelectric foil to harness the power of flowing water, in the form of 18-inch-long “eels” that flap in turbulent water flow like a weeds in the wind [11]. Energy scavenging by piezoelectric generators has also been recently perceived by automotive industry, especially car automation designers and manufacturers. Kim *et al.* discuss the use of a piezoelectric cymbal transducers to generate electricity to supply car remote onboard sensors from the vibration of a car engine [12]. Dynamic strain coupled from the rolling tire of a car has also been recently patented as a power source for a wireless tire condition monitoring system [13].

Energy scavengers operating in continuous mode may also be used to extract energy from human motion. A heel strike may be used to flatten a piezoelectric (PZT) unimorph bender and toe-off action may bend a multilayer polymeric piezoelectric bimorph stave made of PVDF (polyvinylidene

fluoride) foil. Such combined system was shown to produce 1.3 to 8.3 mW during a standard walk depending on the location of transducer (toe/heel) and available displacement range [14]. The East Japan Railway Company has been testing an experimental system that produces electricity as people pass through subway ticket gates. The gates are fitted with floor-embedded energy-scavenging mats with series of piezo-element diaphragms that generate electricity as commuters walk over and compress the mat. 90 m² energy-scavenging floor was producing on average 0.14 kWh of energy a day with peak performance of 0.21 kWh on busy weekends [15].

C. Electric energy extraction from electrostatic scavengers

Another challenging issue is an effective extraction of electrical energy from capacitive-in-nature, high internal resistance piezoelectric and EAP elements. Electrostatic harvester cannot be simply load by ohmic resistor as it results in poor overall efficiency of the generator. Energy generated by piezoelectric and most EAP scavengers is available in form of high voltage peaks which are hazardous for low-voltage electronics if no appropriate conditioning circuitry is used. To demonstrate those problems an experiment, described in the following paragraph, was run using a simple model of the piezoelectric energy scavenger build of Macro Fiber Composite (MFC) transducers. MFC is a novel complex multilayer composite material consisting of PZT piezoceramic fibers laminated with epoxy resin and sheets of mechanically tough polyimide foil fitted with interdigitated electrodes.

III. EXPERIMENTAL

A piezoelectric energy scavenger model was build of two M-8557-P1 type MFC transducers (Smart Materials GmbH, Germany) fixed to a phosphor bronze flat beam (1 mm thick) using DP460 epoxy adhesive and connected in parallel to increase magnitude of the generated current. The assembly was permanently fixed at one end, its free tip was deflected by 3 mm and allowed to freely vibrate at its own resonant frequency until completely damped. The voltage produced over a variable low-inductance load resistor was recorded by means of a digital oscilloscope fitted with 1:10 10 M Ω passive probe. An exemplary voltage train recorded for 100 k Ω load resistance is illustrated in fig. 2. The maximal voltage amplitude registered in this case was exciding 150 V and even higher voltages were recorded for high resistive loads (252 V for 10 M Ω). The signal frequency spectrum contains a strong component related to the fundamental mode of the beam mechanical free vibration (approx. 54,5 Hz) as well as a number of higher harmonics, related to other modes of oscillations. The recorded voltage trains were then processed to calculate the mean total energy dissipated at the resistive load - the results obtained for different loads are illustrated in fig. 3.

IV. DISCUSSION

There is an optimal load which results in the maximal energy output of the MFC energy harvester. The harvester model is producing oscillatory voltage response, therefore the optimal load is equivalent to the impedance of MFC transducers which

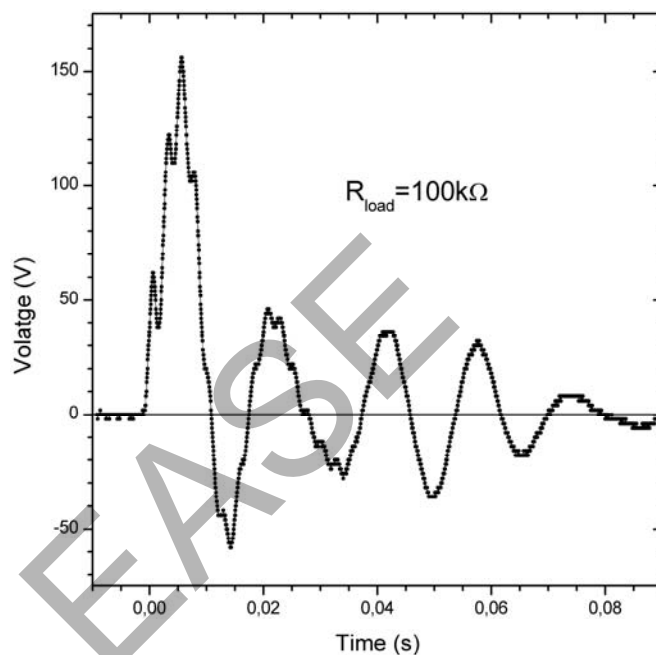


Figure 2. Exemplary voltage train generated over 100 k Ω resistive load by MFC energy scavenger model working in resonance mode.

form capacitive-in-nature alternating voltage source. Taking into account the mechanical resonant frequency of the model (54,5 Hz) and MFC stack capacitance (21.9 nF, measured for 50 Hz excitation) one obtains impedance of approx. 133 k Ω . The calculated value is somewhat higher than the optimal load determined experimentally (approx. 100 k Ω) and the discrepancy may be attributed to higher frequency components present in the real voltage response spectrum and to non-flat frequency-capacitance MFC characteristics. The obtained results are consistent with findings of Swallow *et al.* for resonant harvesters build using piezoelectric fiber composites (PFC) and polymeric piezoelectrics (PVDF) [16].

The mechanical energy stored in the harvester model beam displaced by 3 mm equals to 12.9 mJ (the elastic modulus of the model composite beam has been determined as 2.88 kN/m). Therefore, even for the optimal electric load, only slightly over 10 % of the stored mechanical energy may be extracted from oscillating MFC electromechanical transducer model. The reason for that is a fact that only a portion of the total mechanical energy “pumped” into the beam (when it is bent) is stored in the electric field associated with the piezoelectric effect due to low electromechanical coupling factor of the material. Also, some energy fraction is dissipated as the Joule heat over the MFC internal resistance.

The above simple experiment shows, that it is not only necessary to transform open-circuit high voltages generated by piezoelectric transducers into low voltages accepted by interdigitated circuits. Advanced power converters for use with piezoelectric and EAP generators are essential in order to maximize the power harvested as the circuitry needs to present an optimal load resistance to the piezoelectric/EAP generating

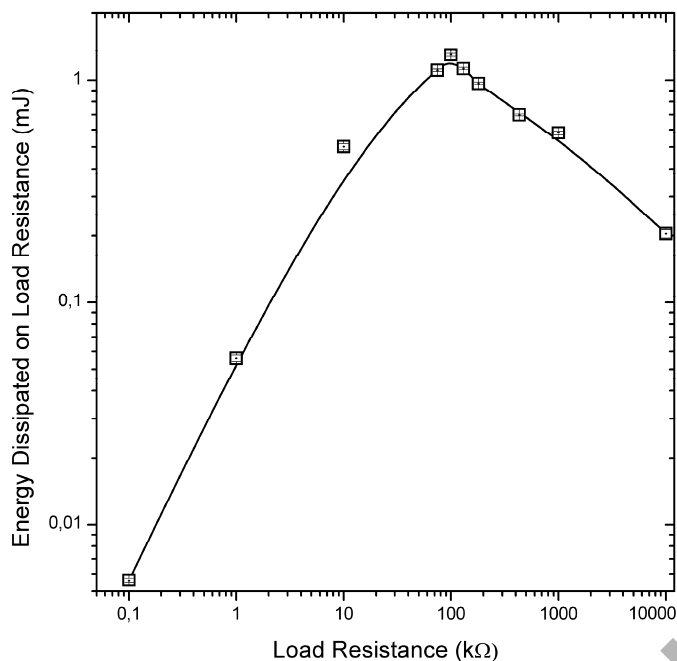


Figure 3. Energy dissipated at the resistive load by MFC energy scavenger model working in resonance mode.

element. Most of the recent work on power electronics intended for kinetic harvesters has been done for piezoelectric transducers: adaptive control voltage converters, synchronous half-wave voltage doublers and synchronous rectifiers [17] as well as new energy storage like supercapacitors or solid state thin-film batteries has been proposed and tested. Ren *et al.* have also shown that combining active energy harvesting control system (i.e. varying elastic properties of the transducer between the opposite generation phases by imposing an external electric field to zero a strain change in the active material or by imposing other electric boundary conditions to modify the energy harvesting cycle) together with high electromechanical yield electrostrictive polymer can provide harvested electric energy density of approx. 40 mJ/cm^3 at 10 % efficiency [18]. Similar approach is also required in case of EAP harvesters as they are capacitive voltage sources too.

V. CLOSING REMARKS

MP3 player powered by build-in yoyo energy harvester has been recently nominated as the best human powered device design during Core77 Design Challenge 2008 – it will provide round-the-clock listening to music everywhere without a risk of running out of batteries. And this I just one example of numerous new gadgets which are just about to come. There is no doubt that ambient energy harnessing using motion- or vibration-driven low-power generators is a topic of substantial and increasing research and engineering attention. Although there are many different techniques available to harvest raw energy from ambient “energy pools”, it seems to be justified to state that devices using electroactive polymers and piezo-

materials are now the most promising as they allow to put away most of movable and wearable parts and require very moderated maintenance efforts. It is expected that the time in which this technology will be demonstrated for military applications (so-called smart soldier concept) extends from 2-5 years and 3-7 years is needed in case of domestic appliances (e.g. mentioned MP3 players) [19].

ACKNOWLEDGMENT

The research work presented herein was financially supported within the framework of 2007–2009 science funding program as individual research project no. NN510 2117 33.

REFERENCES

- [1] P. D. Mitcheson *et al.*, “Energy Harvesting From Human and Machine Motion for Wireless Electronic Devices,” *Proc. IEEE*, vol. 96, No. 9, pp. 1457–1486, Sept. 2008.
- [2] S. Roundy and Y. Zhang, “Toward Self-tuning Adaptive Vibration-based Micro-generators,” *Proc. SPIE*, vol. 5649, pp. 373–384, Feb. 2005.
- [3] S. Meninger, J. O. Mur-Miranda, R. Amirtharajah, A. P. Chandrakasan, and J. H. Lang, “Vibration-to-electric energy conversion,” *IEEE Trans. Very Large Scale (VLSI) Syst.*, vol. 9, pp. 64–76, Feb. 2001.
- [4] Y. Arakawa, Y. Suzuki, and N. Kasagi, “Microseismic power generator Using Electret Polymer Film,” *Proc. 4th Intl. Workshop on Micro and NanoTechnology for Power Generation and Energy Conversion Applications*, November 2004, Kyoto, Japan, pp. 187–190.
- [5] P.D. Mitcheson *et al.*, “Architectures for Vibration-Driven Micropower Generators,” *J. Microelectromech. Sys.*, vol. 13, no. 3, pp. 429–440, 2004.
- [6] R.D. Kornbluh *et al.*, “Electroelastomers: Applications of Dielectric Elastomer Transducers for Actuation, Generation, and Smart Structures,” *Proc. SPIE*, vol. 4698, pp. 254–270, 2002.
- [7] <http://artificialmuscle.com>, link valid on 2009.02.13.
- [8] H. Prahlad, R. Kornbluh, R. Pelrine, S. Stanford, J. Eckerle, and S. Oh, “Polymer Power: Dielectric Elastomers and Their Applications in Distributed Actuation and Power Generation,” *Proc. ISSS 2005 Intl. Conf. on Smart Materials Structures and Systems*, July 28–30, 2005, Bangalore, India, pp. SA100-SA107.
- [9] <http://www.sri.com/news/releases/080307.html>, link valid on 2007.09.04.
- [10] P. Buckley, “Energy Harvesting Feeds Ultra-low-power Device Growth,” *EE Times Deutschland* (electronic version available on-line at <http://ectimes.eu/germany>, January 2009).
- [11] G. Taylor and S. Kammann, “Experimental and Theoretical Behavior of Piezoelectric-Electrostrictive ‘Eel’ Structures,” in *DARPA Energy Harvesting Program Rev.*, ed. R. Nowak, 2000; (www.darpa.mil/dso/).
- [12] H. Kim, S. Priya and K.Uchino, “Modeling of Piezoelectric Energy Harvesting Using Cymbal Transducers,” *Jpn. J. Appl. Phys.*, vol. 45, pp. 5836–5840, 2006.
- [13] “Vehicular Mounted Piezoelectric Generator,” US patent 4,504,761, Patent and Trademark Office, 1985.
- [14] N.S. Shenck and J.A. Paradiso, “Energy Scavenging with Shoe-Mounted Piezoelectrics,” *IEEE Micro*, vol. 21, no. 3, pp. 30–42, 2001.
- [15] Y. Takefuji, “Known and Unknown Phenomena of Nonlinear Behaviors in the Power Harvesting Mat and the Transverse Wave Speaker,” *Proc. NOLTA 2008 Intl. Symposium on Nonlinear Theory and its Applications* Budapest, Hungary, Sept. 7–10, pp. 239–244, 2008.
- [16] L. M. Swallow, J. K. Luo, E. Siores, I. Patel, and D. Dodds, “A Piezoelectric Fibre Composite Based Energy Harvesting Device for Potential Wearable Applications,” *Smart Mater. Struct.*, vol. 17, pp. 1–7, 2008.
- [17] E. Lefeuvre, D. Audigier, and D. Guyomar, “Buck-boost Converter for Sensorless Power Optimization of Piezoelectric Energy Harvester,” *IEEE Trans. Power Electron.*, vol. 22, pp. 2018–2025, Sep. 2007.
- [18] K. Ren, Y. Liu, H. F. Hofmann, and Q. Zhang, “An Active Energy Harvesting Scheme with an Electroactive Polymer,” *Appl. Phys. Lett.*, vol. 91, pp. 132910.1–132910.3, 2007.
- [19] M. Cain, “Characterization of MEMS Energy Harvesting Devices,” *NPL Environmental Measures*, iss. 3, p. 7, Summer 2007.

Thin Film Adhesion Measuring of Conductive Silicon Rubber Depending on Power and Coating Time in Magnetic Sputtering Method

A.Napierala
Brandenburg Technical University Cottbus
Germany
J.Ziaja

Institute of Electrical Engineering Fundamentals of Wrocław University of Technology
50-370 Wrocław, Poland

Abstract- Coating silicon rubber with another material is not facile task due to the fact, that this substance exhibits very poor adhesiveness coming from the low surface tension. Adhesion properties can be improved by means of addition filler and plasma treatment. The analyzed sample is a conductive silicon rubber, which was coated using magnetic sputtering method. This method bases on plasma activity in strong magnetic fields. The adhesion in modified material was evaluated on the basis of cross-cut test by different coating time and target power.

I. INTRODUCTION

Silicon rubbers have outstanding properties like excellent elasticity, temperature-resistant, hydrophobia which are in great important in high insulation voltage technique. But silicon rubber can also presents very seriously hurdle in another possible electrical application due to low surface tension, which aggravates coating silicon rubber with metal. In order to increase adhesiveness incorporation of carbon black and filler can be applied [1]. This sample consists of silicon rubber and carbon black, which after mixing were manufactured using injection moulding processes. This material unfortunately is not appropriate for much utilization e.g. electrodes, high voltage plugs because of insufficient electrical contact. In order to overcome this problem reliable coating film is necessary, which due to above mentioned reason can be achieve only by means advances coating engineering. Thin film technology, which was used, is called magnetic sputtering. This method is in generally physical vapour deposition process. In magnetic sputtering magnetic field is superposed on the cathode and glow discharge, which is parallel to the cathode surface. The electrons in the glow discharge show cycloidal motion, and the centre of the orbit drifts in the direction of $E \times B$ with the drift velocity of E/B , where E and B denote the electric field in the discharge and the superposed transverse magnetic field, respectively [2]. The construction of magnetron(magnetic) sputtering system is shown in Fig.1.

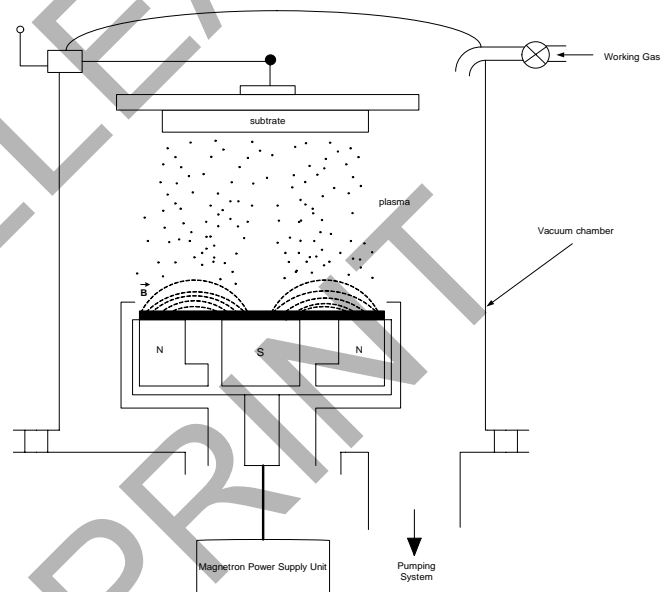


Figure1. Magnetron sputtering system

Magnetic Sputtering Method differs from other sputtering techniques in that the majority of the plasma is confined to region near the target surface by using strong magnetic fields to bend the trajectories of the secondary electrons. Advantages, which conclude: increased deposition rates, reduced substrate heating during deposition, reduced working gas pressure requirements had to taken into consideration by choosing this surface coatings method [3]. Concerning this method there are many parameters, which have an effect on final coating [4,5]. The aim of this research was to draw a conclusion about dependency between target power, coating time and adhesiveness. In terms of power at first we have to distinguish between target power and circling power, whose are connected with very important element concerning magnetron sputtering method - power supply unit. In our experiment magnetron was

cannot withstand specific for scratch test condition, if the substrate is not hard enough.

Figure 4 and 5 show the failure of this method- impossibility of determination critical load for delaminating.

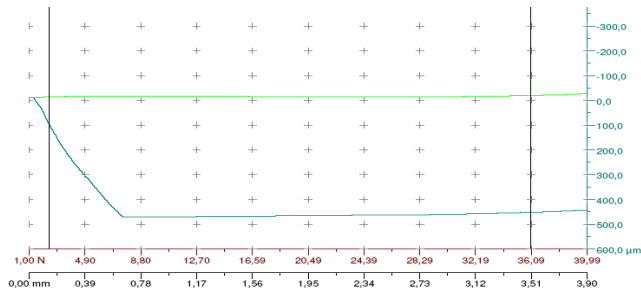


Figure4. Scratch test faulty results

- Penetration depth
- Residual depth

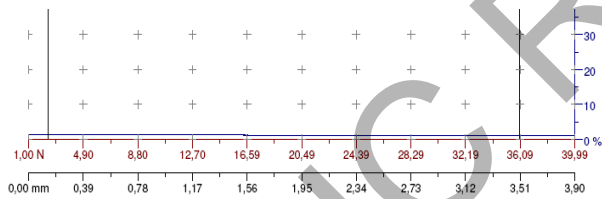


Figure5. Scratch test faulty results in terms of acoustic emission

- Acoustic emission

B. Cross-cut test

The second adhesion test namely cross-cut test was carried out according to the norm DIN EN ISO 2409. The test consists in making a series of parallel cuts through the film in one direction and a second series at right angles to the first. I make six cuts 2 mm apart in each direction, forming 25 squares (Fig.6 and 7). Cutting distance was chosen adequate to above mentioned norm for soft material with layer thickness till 60 μm.

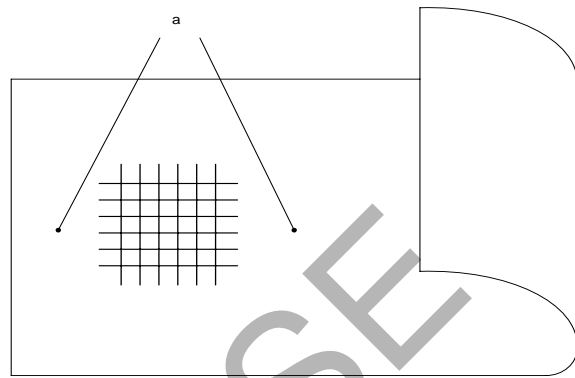


Figure6. Location adhesive tape for cross-cut surface [5]

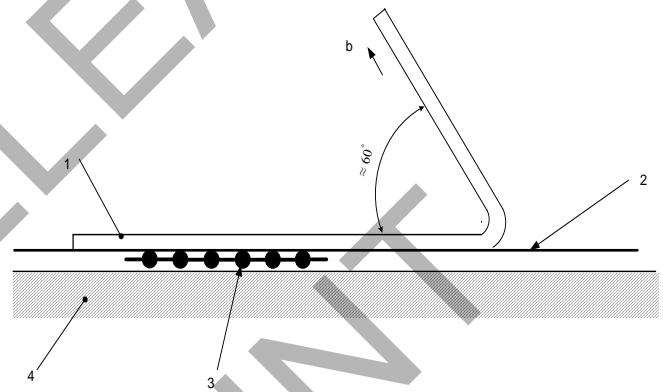


Figure7. Location of cross-cut surface straight before peel off [5]

- Legend
- 1 adhesive tape
 - 2 coating
 - 3 cuts
 - 4 substrate

- a smoothed
- b peel off direction

III.RESULTS AND DISCUSSION

As mentioned above scratch test method turned out an inappropriate method for such kind of coated material. The result of the second method has been juxtaposed in Table 2.

TABLE 2
ADHESION EVALUATION

Lp.	coating material	target power	time	pressure	adhesion evaluation according to DIN EN ISO 2409
		kW	min	Tr	-
1	titanium	2,2	5	$9,8 * 10^{-3}$	0
2	titanium	3,1	5	$9,8 * 10^{-3}$	0
3	titanium	4,3	6	$9,8 * 10^{-3}$	0
4	titanium	5,7	6	$9,8 * 10^{-3}$	0
5	aluminium	2,0	2	$9,8 * 10^{-3}$	0
6	aluminium	2,0	2	$9,8 * 10^{-3}$	0
7	aluminium	2,0	5	$9,8 * 10^{-3}$	0
8	aluminium	2,0	10	$9,8 * 10^{-3}$	0
9	aluminium	3,1	5	$9,8 * 10^{-3}$	0

The evaluation oscillates between 0 till 5, where 5 is the indicator for the poorest adhesion.

The results pointed clearly out that coating shows excellent adhesion regardless of target power and coating time and metal coatings. Figure 6 shows the sample after test with any indication of peeling off.

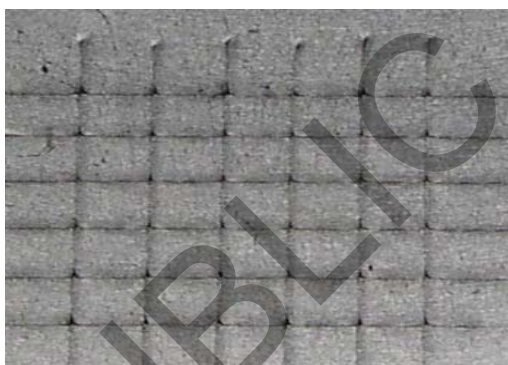


Figure8. View of the sample after cross-cut test

Unfortunately it is very difficult to evaluation adhesion by means another method due to properties of aluminium. It is very difficult to solder aluminium, what impede other adhesive test methods.

The adhesion of a film to the substrate is strongly dependent on the chemical nature, cleanliness, and microscopic topography

substrate surface. The adhesion is better for high values of kinetic energy of incident species, absorption energy of the deposit, and initial nucleation density. Effective power P_E is proportional to coating velocity [6], which indicates that with power increase will also coating thickness rise. In our experiment the maximal value of target power was limited to 5,7 kW due to considerably sample temperature increase, which in turn could cause undesirable side effects. The explanation for outstanding adhesion is twofold. First reason is that general magnetron sputtering technique guarantee for very good adhesion. The second one is due to the fact that our parameters were determinated maybe in too narrow range, which demand further research.

IV. CONCLUSION

Film adhesion measuring of conductive silicon rubber doesn't indicate any significant difference in terms of target power and coating time. Magnetron sputtering coating technique turned out very good tool in terms of reliable adhesion. Our experiments show that in spite of poor adhesion properties of silicon rubber achievement of good coatings are possible. Unfortunately other properties of this material namely low harness make some testing method unfeasible.

REFERENCES

- [1] E-S. Kim , H-S. Kim, S-H. Jung, J-S. Yoon, "Adhesion Properties and Thermal Degradation of Silicone Rubber" *Journal of Applied Polymer Science* vol.103, 2782-2787, 2007
- [2] K.Wasa, M. Kitabatake, H. Adachi "Thin Film Materials Technology", Springer-Verlag, 2004
- [3] D.S. Rickerbery, A. Matthews "Advanced Surface Coating: a Handbook of Surface Engineering", Blackie & Son Ltd, 1991
- [4] P. Richard, J. Thomas , D. Landolt, G. Gremand, "Combination of scratch-test and acoustic microscopy imaging for the study of coating adhesion" , *Surface and Coating Technology* vol.91, 83-90, 1996.
- [5] Paints and varnishes –Cross-cut test (ISO 2409:2007); German version EN ISO 2409:2007
- [6] W.M. Posadowski, "Nowoczesne techniki rozpylania magnetonowego," *Electronika*, 4/2006.

Electrical behaviour of current conducting silicon rubber

A.Napierala
Brandenburg Technical University Cottbus
Germany

Abstract- Conductive plastic gain more and more interest in electrical industry due to few advantages in comparison to metal like light weight and rustles properties and to some extent lower material price. The idea of using such materials is not new. These kinds of materials have been applied for many years in fields like electromagnetic shielding or voltage grading, where there strongly entrench his position. Recently new possible applications are being taking into consideration, which have in common that conductive plastic should conducting significant among of current. This paper inspects a mechanism of current conducting be means of percolation theory and resulting with that consequence.

I. INTRODUCTION

In order to achieve a very low resistance in plastic material, which are at normal state insulator it is necessary to add conductive fillers, which enhance electrical conductivity. The most commonly filler used for this purpose is carbon black. The reason for that are first and foremost the low price, rust-proof and opportunity to adjust the carbon black conductivity depending on combustion process [1]. A mixture of plastic and high conductive carbon black presents a new material, which exhibits various value of resistance according to percentage of conductive filler. The typical characteristic of conductive plastic is showed in figure 1. The dependency between resistance and carbon black concentration shows highly unlined characteristic, which could be elucidated by different physical processes namely mechanical tunnelling and percolation.

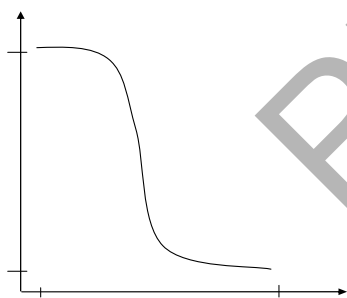


Figure1. Volume resistivity versus the carbon black content

II. ELECTRON TRANSPORT IN CONDUCTOR-FILLED PLASTIC SYSTEMS

A. Quantum Mechanical Tunnelling

If carbon black loading has a very small fraction then the electron transport is being conducted by means of so called tunnelling. For the conductive element, the conductance is merely its ohmic value. But for the insulating silicon rubber, matters are more complicated. Two conductive particles whose separation is large compared to atomic dimension see each other through a resistance controlled by the bulk resistivity of the silicon rubber itself. However, when the distance is small ($\leq 100 \text{ \AA}$), electrons may tunnel quantum mechanically between conductive fillers, leading to a lower resistance than would be expected from the insulator alone. A comprehensive examination of normal quantum tunnelling can be found in Sheng. The basic concept in the Sheng proposal is that there exists across any tunnel junction a voltage that is sum of two pieces. One part is simply due to the externally applied source; the other part is contributes by quantum thermal fluctuations with the junction barrier [2].

B. Percolation theory

For a small volume fraction of the conducting filler particles, the resistivity of composite is close to that of silicon rubber matrix (but not equal to due to above mentioned tunnelling process). As the volume fraction of the conducting filler particles increase, the particles come into contact with one another to form the conduction paths through the composite. As a result, the resistivity drops by many orders of magnitude at a critical threshold. One a saturation region of conducting filler particles is reached; there are a large number of conduction paths, resulting in a low resistivity [3]. This critical threshold where the resistivity so rapidly drops is called percolation threshold. The value of percolation threshold is no constant but depends of many factors and from one sample to another fluctuates. The factors, which contribute to this, are: size, aspect ratio, structure, allocation, roughness of carbon particles and kind of silicon rubber. Taking into consideration all this factors and precisely prediction of percolation threshold is a very difficult task. Generally it can be deduced that a high aspect ratio and high conductive chemical structure of fillers contribute to advantage of forming the conducting network, so that percolation threshold is lower.

III. RESULT OF CURRENT STRESS

A. PTC Effect

The most significant result of current conducting through conductive silicon rubber was increase of resistance with temperature rise (see Fig. 2). Because black carbon has negative temperature coefficient of resistance, that means the resistance decreases with temperature increase, this effect must have an explanation in another material properties. A straightforward explanation is to ascribe the observed experimental facts to self-heating of sample. The thermal expansion coefficient of silicone rubber is 2.0-2,5 as big as other organic rubber ;meanwhile, the thermal conduction coefficient of silicon rubber is also very high, so, serious self heating results in increasing temperature of the sample [4]. The thermal expansion coefficient resulting in volume expansion causes breakdown of conductive pathways what contribute to resistance increase.

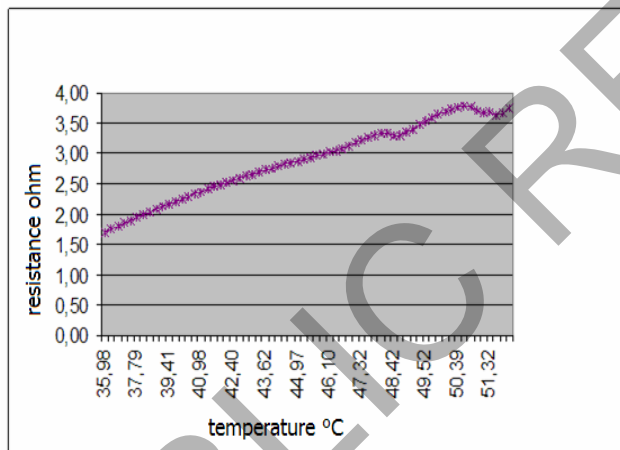


Figure2. Resistance of conductive silicon rubber as a function of temperature

This effect can be reduced at higher carbon black loading if the contact pressure will be applied. At higher carbon black loading, the conductive networks increase and the average interparticle gap becomes smaller. Therefore, the contact pressure of particle becomes higher and the network breakdown process becomes less efficient. As a result, the rate of increase in resistivity is reduced [5].

B. Switching Effect

During high power switching material absorb high energy, which leads to partial material ablation. After the high energy impulse is terminate the material is capable of switching again. This is in contrast to the switching under low current density and voltage condition where there are no outward indications of this switching event.

IV. CONCLUSION

Conductive carbon black composites have been researched in many respects including electrical conduction properties and dielectric behaviour. Because carbon black–silicon rubber obey different conduction mechanisms it is very important to know accurate and relevant characteristics. Because this material exhibit positive temperature coefficient the most feasible application can be associated with current limiter device.

REFERENCES

- [1] H.J.Mair, S.Roth, "Elektrisch leitende Kunststoffe," Carl Hanser Verlag München, Wien, 1989
- [2] R.D.Sherman, L.M.Middelma, S.M.Jacobs, "Electron Transport Processes in Conductor- Filled Polymers , " *Polymer Engineering and Science*, vol.23, No.1, January 1983
- [3] Y.Ishigure, S.Iijima, H.Ito, T.Ota, H.Unuma, , "Electrical and elastic properties of conductor-polymer composites," *Journal of Material Science*,34:2979-2985,1999
- [4] J.Zhang,S.Feng,X.Wang, "Resistivity and Thermal Reproducibility of Carbon Black and Metallic Power Filled Silicone Rubber Heaters," u *Journal of Applied Polymer Science* ,vol.94,587-592,2004.
- [5] E.S Park,L.W.Jang J-S.Yoon, "Resistivity and Thermal Reproducibility of Carbon Black and Metallic Power Filled Silicone Rubber Heaters", *Journal of Applied Polymer Science*,vol.95,1122-1128,2005.

On Hilbert Transform and its application to assessment of electrical signal waveform distortion

Tomasz Sikorski*

Institute of Power Systems Automation Ltd., Wystawowa 1, 51-618 Wrocław, Poland

Piotr Ruczewski

Wrocław University of Technology, Wybrzeże Wyspiańskiego 27, 50-370 Wrocław, Poland

Abstract - In order to achieve full description of the distorted signals applied method of analysis should take into consideration two kind of desirable parameters: those which characterizes time behavior of the waveform, and those which gives information about frequency components. This paper follows by the idea of Hilbert Transform (HT) which allows to construct analytic signal and introduce the term of instantaneous amplitude (IA), instantaneous phase (IP) and instantaneous frequency (IF). Unfortunately, application of HT, especially in point of instantaneous frequency, gives meaningful results for restrictive class of signals. The accurate representation is achieved for monocomponents signals. Practical application of HT can be preprocessed by selected signal decomposition method. This paper provides some analytic derivation of HT and its digital application for not decomposed and decomposed signals.

I. INTRODUCTION

Dynamic complex phenomena require extended performance of applied signal processing methods. One-dimensional Fourier spectrum analysis, however very useful and fast digital applicable, can be insufficient, providing only general information about extracted signal components, with loss of its time-varying nature. The frequency analysis can provide the frequency details, but unfortunately, we don't know when the frequency changes occurred. In case of dynamic phenomena the assumption of the stationarity can not be fulfilled. Signal processing has provided the solution for given problem using two techniques: joint time-frequency analysis (JTFA) or decomposition of the signal and calculation of instantaneous amplitude and instantaneous frequency for particular signal components. This paper is concentrated on mechanism and meaning of Hilbert transform (HT) for calculation of instantaneous magnitude and instantaneous frequency.

Hilbert transform allows constructing orthogonal signal to the given one. Having the pair of signal and its orthogonal form we can define complex analytic signal with real part as given signal and imaginary part as the orthogonal effect of Hilbert transformation. Obtained analytic signal is complex function of time. For every time instant we can recalculate amplitude as well as phase of the local, in point of time, complex value. It leads to new characteristics, which represents changes of amplitude and changes of phase in time. Derivative of phase in time is defined as instantaneous frequency [1],[2],[3],[4].

Successful application of Hilbert transform is possible only for narrow range of signals. The meaningful results are achieved in case of monocomponents signals. Thus, in practical cases, the HT is applied not strictly for investigated signal, usually containing many components, but for single selected component, obtained using some signal decomposition method. There are several signal decomposition methods including orthogonal polynomial expansion, Fourier expansion or wavelet expansion. Last work of Huang brought new idea of signal expansion into the set of so called intrinsic mode function (IMF), which represents the oscillatory mode embedded in the signal. The algorithm, which serves the idea of representation of the signal by the set of IMF oscillatory modes, is called empirical mode decomposition (EMD) and was derived by Huang et al. Obtained elements of expansion can be putted through an examination by Hilbert transform in order to track instantaneous amplitude and instantaneous frequency of particular components of the expansion. Described approach is known as Hilbert Huang Transform (HHT) [5],[6],[7]. Some selected application of Hilbert spectrum has found its place also in electrical engineering [8],[9],[10],[11].

The aim of presented studies is to describe Hilbert transform technique and to test its usefulness for fundamental benchmark cases of monocomponent and pseudomonocomponent signals. In order to investigate the methods several experiments were performed supported by analytic derivation and digital simulation. One of the contributions of this paper is the exploration of Hilbert transform in comparison with its continuous and digital realization. The intention of presented results is to familiarize with Hilbert engine as crucial element in process of calculation of instantaneous amplitude, phase and frequency.

II. HILBERT TRANSFORM AND INSTANTANEOUS PARAMETERS

The Hilbert transform of given real signal $x(t)$ allows to obtain its orthogonal form $y(t)$ as follows [1],[2],[3],[4]:

$$\begin{aligned} y(t) &= H\{x(t)\} = \frac{1}{\pi} \int_{-\infty}^{+\infty} \frac{x(\tau)}{t-\tau} d\tau \\ x(t) &= H^{-1}\{y(t)\} = -\frac{1}{\pi} \int_{-\infty}^{+\infty} \frac{y(\tau)}{t-\tau} d\tau \end{aligned} \quad (1)$$

* This work is supported by Ministry of Science and Higher Education, Poland, in 2007-2010 as scientific project.

Above definition can be presented in convolution form:

$$\begin{aligned} y(t) &= \frac{1}{\pi t} * x(t) \\ x(t) &= \left(-\frac{1}{\pi t}\right) * y(t) \end{aligned} \quad (2)$$

Having a pair of orthogonal components we can defined complex analytic signal $z(t)$ as:

$$\begin{aligned} z(t) &= x(t) + jy(t) = |z(t)| \cdot e^{j\psi(t)} \\ |z(t)| &= \sqrt{(x(t))^2 + (y(t))^2}; \psi(t) = \arg(z(t)) \end{aligned} \quad (3)$$

Here reveals definition of instantaneous amplitude (IA) recognized as:

$$IA(t) = |z(t)| = \sqrt{(x(t))^2 + (y(t))^2} \quad (4)$$

Simultaneously, we can distinguish instantaneous phase (IP) as phase of analytic signal or as imaginary part of natural logarithm of complex analytic function:

$$\begin{aligned} IP(t) &= \psi(t) = \arg(z(t)) \text{ or } IP(t) = \text{Im}\{\ln z(t)\} \\ \ln(z(t)) &= \ln(|z(t)e^{j\psi(t)}|) = \ln(|z(t)|) + j\psi(t) \end{aligned} \quad (5)$$

Finally, instantaneous angular frequency can be defined as derivative of instantaneous phase in time.

$$\begin{aligned} \omega(t) &= \frac{d\psi(t)}{dt} \\ \text{or } \omega(t) &= \text{Im}\left\{\left(\ln(z(t))\right)'\right\} = \text{Im}\left\{\frac{z'(t)}{z(t)}\right\} \\ \omega(t) &= \frac{x(t)y'(t) - y(t)x'(t)}{x^2(t) + y^2(t)} \end{aligned} \quad (6)$$

Additional scaling by factor $1/2\pi$ leads to instantaneous frequency (IF):

$$IF(t) = f(t) = \frac{1}{2\pi} \omega(t) = \frac{1}{2\pi} \frac{d\psi(t)}{dt} \quad (7)$$

Application of Hilbert transform in definition form (1) is difficult. Effective way utilizes its convolution form (2) and some relations between Fourier transform and the convolution. Required in this approach is the Fourier transform of investigated signal $x(t)$. Having:

$$\begin{aligned} F\{x(t)\} &= X(j\omega) \\ F\left\{\frac{1}{\pi t}\right\} &= -j \text{sgn } \omega = \begin{cases} -j, & \text{for } \omega > 0 \\ 0, & \text{for } \omega = 0 \\ j, & \text{for } \omega < 0 \end{cases} \end{aligned} \quad (8)$$

we can recalculate Fourier transform of orthogonal component $y(t)$ as:

$$\begin{aligned} F\{y(t)\} &= Y(j\omega) = F\left\{\frac{1}{\pi t}\right\} \cdot F\{x(t)\} \\ Y(j\omega) &= -j \text{sgn } \omega \cdot X(j\omega) \end{aligned} \quad (9)$$

Hilbert transform of given signal can be now uncovered as inverse Fourier transform:

$$y(t) = F^{-1}\{Y(j\omega)\} \quad (10)$$

Construction of complex analytic signal $z(t)$ according to (3) is the initial point for further calculation of instantaneous amplitude and frequency. Selected analytic derivation and computer application of instantaneous amplitude and instantaneous frequency calculation was performed.

A. Monocomponent sinusoidal case

The area of interests includes sinusoidal signals, mainly studied in electrical engineering fundamentals. Thus, firstly we have considered monocomponent sinusoidal signal $x(t) = A \sin(\omega_0 t + \psi_1)$, supported by analytic derivation presented in Table I. Fig 1 presents the numerical results when the investigated signal is 50Hz sinusoidal function with amplitude equals one and phase initial equals 0. Referring to the comments in Table I limitation of phase from $-\pi$ to π makes instantaneous phase a linear periodical function instead of linear continuous function. Further numerical calculation of instantaneous frequency according to (7) brings local delta Dirac components. Its localization depends on the placement of ‘‘artificial’’ phase jump from $-\pi$ to π , which can be associated with phase initial of investigated sine signal. Mentioned influence depicts Fig. 2.

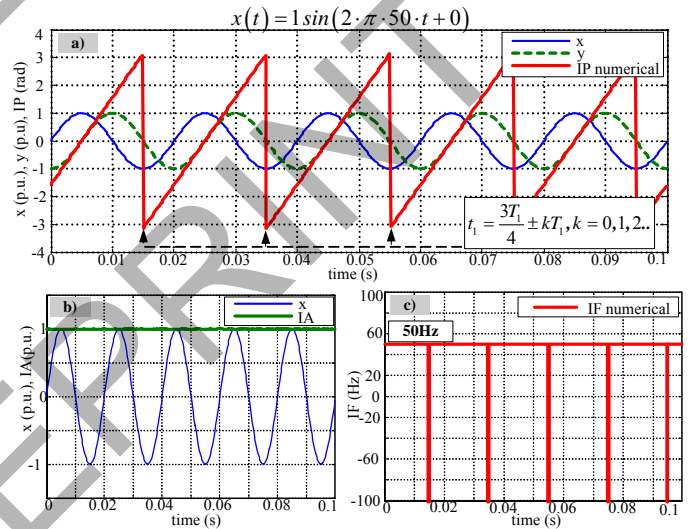


Fig. 1. Example of numerical calculation of Hilbert transform: (a) investigated signal $x(t)$ and its orthogonal form $y(t)$ with instantaneous phase $IP(t)$; (b) signal and instantaneous amplitude $IA(t)$; (c) instantaneous frequency $IF(t)$

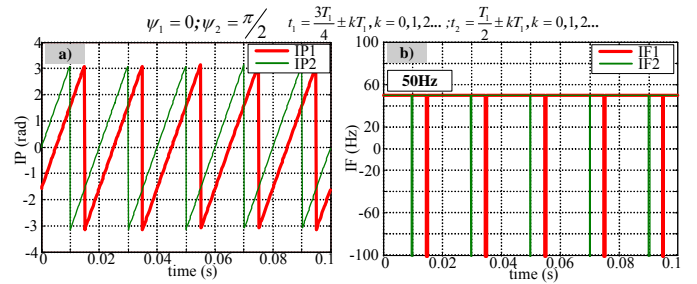


Fig. 2. Influence of phase initial of sinusoidal component on numerical application of Hilbert transform: (a) instantaneous phase $IP(t)$; (c) instantaneous frequency $IF(t)$

TABLE I

ANALYTIC DERIVATION OF INSTANTANEOUS AMPLITUDE AND FREQUENCY OF: $x(t) = A_1 \sin(\omega_1 t + \psi_1)$ Step 1: Derivation of Hilbert transform of orthogonal component $y(t)$ using Fourier form of given signal $x(t)$ and formulas (9) and (10):

$$x(t) = A_1 \sin(\omega_1 t + \psi_1) \xrightarrow{\text{Fourier}} X(j\omega) = jA_1\pi \left[e^{-j\psi_1} \delta(\omega + \omega_1) - e^{j\psi_1} \delta(\omega - \omega_1) \right]$$

$$Y(j\omega) = -j \operatorname{sgn} \omega \cdot X(j\omega) = -j \operatorname{sgn} \omega \cdot jA_1\pi \left[e^{-j\psi_1} \delta(\omega + \omega_1) - e^{j\psi_1} \delta(\omega - \omega_1) \right] = \operatorname{sgn} \omega A_1\pi \left[e^{-j\psi_1} \delta(\omega + \omega_1) - e^{j\psi_1} \delta(\omega - \omega_1) \right]$$

$$= -A_1\pi \left[e^{-j\psi_1} \delta(\omega + \omega_1) + e^{j\psi_1} \delta(\omega - \omega_1) \right] \xrightarrow{\text{Inverse Fourier}} y(t) = F^{-1} \{ Y(j\omega) \} = -A_1 \cos(\omega_1 t + \psi_1)$$

Step 2: Definition of instantaneous amplitude and phase referring to analytic signal $z(t)$:

$$IA(t) = |z(t)| = \sqrt{(A_1 \sin(\omega_1 t + \psi_1))^2 + (-A_1 \cos(\omega_1 t + \psi_1))^2} = A_1$$

Comments: Instantaneous amplitude of monocomponent signal confirms constant character of its amplitude.

$$IP(t) = \psi(t) = \arg(z(t)) = \operatorname{arctg} \left(\frac{-A_1 \cos(\omega_1 t + \psi_1)}{A_1 \sin(\omega_1 t + \psi_1)} \right) = \operatorname{arctg}(-\operatorname{ctg}(\omega_1 t + \psi_1)) = \operatorname{arctg} \left(\operatorname{tg} \left(\omega_1 t + \psi_1 - \frac{\pi}{2} \right) \right) = \omega_1 t + \psi_1 - \frac{\pi}{2}$$

Comments: Instantaneous phase is a linear function of time with coefficient equals ω_1 . In practical or digital realization the angle is limited to $\langle -\pi, \pi \rangle$.Introducing mentioned limitation given linear function becomes periodical linear function with period $T_1 = \frac{2\pi}{\omega_1}$. We can distinguish the time constant when the function of instantaneous phase obtains the border value π and then jumps to $-\pi$:

$$\omega_1 t + \psi_1 - \frac{\pi}{2} = \frac{2\pi}{T_1} t_1 + \psi_1 - \frac{\pi}{2} = \pi \rightarrow t_1 = \left(\pi + \frac{\pi}{2} - \psi_1 \right) \frac{T_1}{2\pi} = \left(\frac{3\pi}{2} - \psi_1 \right) \frac{T_1}{2\pi} \pm kT_1, k = 0, 1, 2, \dots$$

Step 3: Calculation of instantaneous angular frequency:

Method 1 using derivative and real and imaginary part of analytic signal:

$$\omega(t) = \frac{d\psi(t)}{dt} = \frac{x(t)y'(t) - y(t)x'(t)}{x^2(t) + y^2(t)} = \frac{A_1 \sin(\omega_1 t + \psi_1) A_1 \sin(\omega_1 t + \psi_1) \omega_1 + A_1 \cos(\omega_1 t + \psi_1) \omega_1 A_1 \cos(\omega_1 t + \psi_1)}{A_1^2 \sin^2(\omega_1 t + \psi_1) + A_1^2 \cos^2(\omega_1 t + \psi_1)} = \frac{A_1^2 \omega_1}{A_1^2} = \omega_1$$

Method 2 using combined derivative and trigonometry approach:

$$\operatorname{tg} \psi(t) = \frac{y(t)}{x(t)} = \frac{-\cos(\omega_1 t + \psi_1)}{\sin(\omega_1 t + \psi_1)} = -\operatorname{ctg}(\omega_1 t + \psi_1) \xrightarrow{d/dt} \frac{1}{\cos^2 \psi(t)} \psi'(t) = - \left(\frac{-1}{\sin^2(\omega_1 t + \psi_1)} \right) \omega_1 \rightarrow \psi'(t) = \frac{\cos^2 \psi(t)}{\sin^2(\omega_1 t + \psi_1)} \omega_1$$

$$\cos^2 \psi(t) = \frac{1}{1 + \operatorname{tg}^2 \psi(t)} = \frac{1}{1 + \operatorname{ctg}^2(\omega_1 t + \psi_1)}; \sin^2(\omega_1 t + \psi_1) = \frac{1}{1 + \operatorname{ctg}^2(\omega_1 t + \psi_1)} \rightarrow \psi'(t) = \frac{\cos^2 \psi(t)}{\sin^2(\omega_1 t + \psi_1)} \omega_1 = \omega_1$$

Method 3 using direct derivative of phase function:

$$\omega(t) = \frac{d\psi(t)}{dt} = \frac{d}{dt} \left(\omega_1 t + \psi_1 - \frac{\pi}{2} \right) = \omega_1$$

Comments: Obtained derivation underline constant character of angular frequency of investigated monocomponent signal. However, taking into consideration mentioned practical representation of instantaneous phase function as periodical form limited in range $\langle -\pi, \pi \rangle$ with "artificial" phase jump from π to $-\pi$ in time instant equals t_1 , we have to consider not only constant function ω_1 but also delta Dirac function in t_1 .

TABLE II

ANALYTIC DERIVATION OF INSTANTANEOUS AMPLITUDE AND FREQUENCY OF: $x(t) = A_1 \sin(\omega_1 t + \psi_1) + A_2 \sin(\omega_2 t + \psi_2)$

Referring to above steps for monocomponent the instantaneous amplitude, phase and frequency of dual sine signal can be presented as:

$$z(t) = x(t) + jy(t) = A_1 \sin(\omega_1 t + \psi_1) + A_2 \sin(\omega_2 t + \psi_2) - j \left[A_1 \cos(\omega_1 t + \psi_1) + A_2 \cos(\omega_2 t + \psi_2) \right]$$

$$\rightarrow IA(t) = |z(t)| = \sqrt{A_1^2 + A_2^2 + 2A_1A_2 \cos((\omega_2 - \omega_1)t + (\psi_2 - \psi_1))}$$

$$\rightarrow IP(t) = \operatorname{arctg} \left(\frac{y(t)}{x(t)} \right) = \operatorname{arctg} \left(\frac{-A_1 \cos(\omega_1 t + \psi_1) + A_2 \cos(\omega_2 t + \psi_2)}{A_1 \sin(\omega_1 t + \psi_1) + A_2 \sin(\omega_2 t + \psi_2)} \right)$$

$$\rightarrow IF(t) = \frac{1}{2\pi} \frac{A_1^2 \omega_1 + A_2^2 \omega_2 + (A_1 A_2)(\omega_2 + \omega_1) \cos((\omega_2 - \omega_1)t + (\psi_2 - \psi_1))}{A_1^2 + A_2^2 + 2A_1A_2 \cos((\omega_2 - \omega_1)t + (\psi_2 - \psi_1))}$$

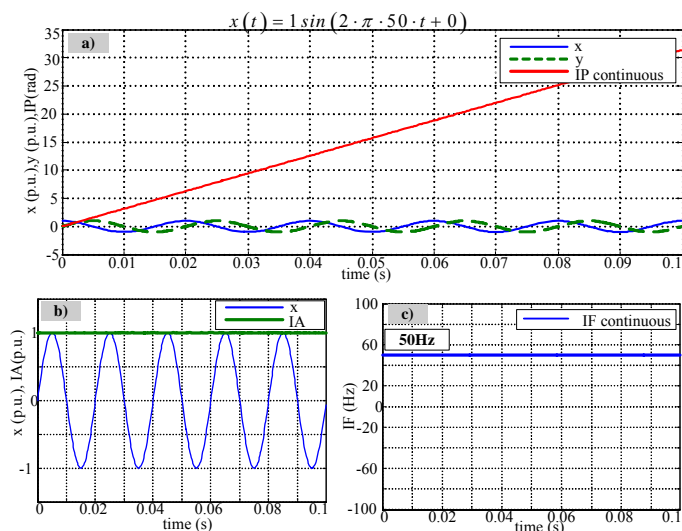


Fig. 3. Example of continuous calculation of Hilbert transform of monocomponent signal: (a) investigated signal $x(t)$ and its orthogonal form $y(t)$ with instantaneous phase $IP(t)$; (b) signal and instantaneous amplitude $IA(t)$; (c) instantaneous frequency $IF(t)$

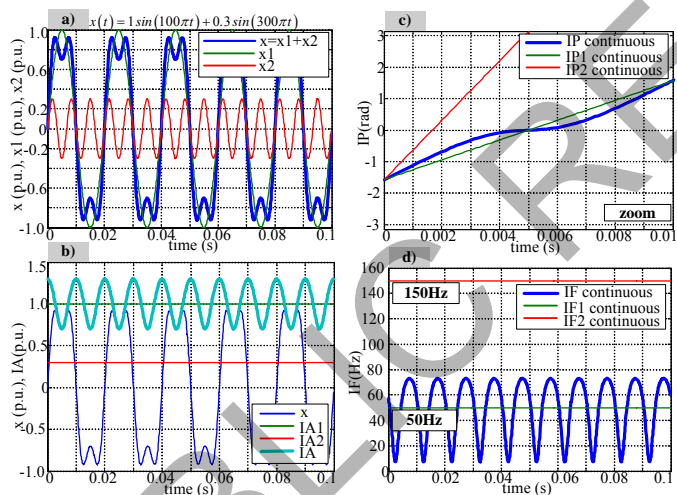


Fig. 4. Example of continuous calculation of Hilbert transform of dual component signal: (a) investigated signal $x(t)$ and its components $x_1(t)$ and $x_2(t)$; (b) instantaneous amplitude $IA(t)$; (c) instantaneous phase $IP(t)$; (d) instantaneous frequency $IF(t)$

True instantaneous amplitude, phase and frequency normally is not weighted by numerical limitation and can be rather interpreted as continuous functions. In comparison to Fig 1 we have constructed Fig. 3, presenting Hilbert transform and further calculation of instantaneous characteristics of signal parameters after correction of the phase function in continues mode, without the limitation $\langle -\pi, \pi \rangle$. Presenting trend represents intuitive expectation for constant amplitude and frequency of investigated monocomponent sine signal.

B. Dualcomponent sinusoidal case

In order to further exploration of Hilbert idea we have also reintroduce previous derivation into sum of sinus signals $x(t) = A_1 \sin(\omega_1 t + \psi_1) + A_2 \sin(\omega_2 t + \psi_2)$. Obtained formulas

describing instantaneous amplitude, phase, and frequency are grouped in Table II. Mentioned instantaneous characteristic of signal parameters is also shown in Fig. 4, including comparison with instantaneous characteristics of particular signal components. We can distinguish general comment that direct application of Hilbert transform, and its further utilization to instantaneous parameters calculation, is not sufficient for distorted signal. The initial decomposition process is required preceded the Hilbert calculation. Having particular components of the signal we can perform Hilbert tool and obtain complex information about its time-varying aspects.

III. CONCLUSION

Hilbert transform is a one of the tool for creation of analytic signal which can be treated as initial form of the signal for calculation of instantaneous characteristic of the signal as instantaneous amplitude, phase or frequency. Presented in the paper numerical application confirms some limitation and restriction of direct application of the Hilbert method. The solution is supporting the Hilbert calculation by previous decomposition of the signal. Application of Hilbert tool, and calculation of instantaneous parameters for every decomposed components can bring complex information about time-varying nature of investigated distortion.

REFERENCES

- [1] Bedrosian E., "The Analytic Signal Representation of Modulated waveform", Proceedings of the IEEE, 1962, pp. 2071-2076.
- [2] Bedrosian E., "A product theorem for Hilbert transforms", Proceedings of the IEEE, 1963, pp. 868-869.
- [3] Alavi-Sereshtki M.M., Prabhakar J.C., "A tabulation of Hilbert Transforms for Electrical Engineering", IEEE Trans. Communications, vol. Com-20, no. 6, 1972, pp.1194-1198.
- [4] Boashash B., "Estimating and Interpreting the Instantaneous frequency of Signal - Part 1: Fundamentals and Part 2: Algorithms and Applications", Proceedings of the IEEE, vol. 80, no. 4, 1992, pp. 520-568.
- [5] Huang N. E. et al., "The empirical mode decomposition and the Hilbert spectrum for nonlinear and non-stationary time series analysis", Proceedings of The Royal Society 454, 1998, pp. 903-995.
- [6] Huang N. E., Shen S. S., *Hilbert-Huang transform and its applications*, World Scientific Publishing, 2005.
- [7] Rilling G., Flandrin P., "One of two frequencies? The Empirical Mode Decomposition Answers", IEEE Trans. on Sig. Procc., vol. 56, no.1, 2008, pp.85-95.
- [8] Andrade M.A., Messina A.R., Rivera C. A., Olugin D., "Identification of Instantaneous Attributes of Torsional Shaft Singals using Hilbert Transform", IEEE Trans. on. Pow. Systems, vol. 19, no.3, 2004, pp.1422-1429.
- [9] Marei M.I, Abdel-Galil T.K., El-Saadany F.El., Salama M.M.A., "Hilbert Transform Based Control Algotihm of the DG Interface for Voltage Flicker Mitigation", IEEE Trans. on. Pow. Deliv., vol. 20, no.2, 2005, pp.1129-1133.
- [10] Senroy N., Suryanarayanan S., Riberio P.F., "An improved Hilbert-Huang Transform for Analysis of Time-Varying in Power Quality", IEEE Trans. on. Pow. Deliv., vol. 22, no.4, 2007, pp.1843-1850.
- [11] Sikorski T., Ziaja E., "Advanced signal representation methods for analysis of transient states in embedded generation systems", Systems - Journal of Transdisciplinary Systems Science, vol. 13, 2008, pp. 66-72.

Voltage Dependence of Hologram Generation Dynamics in Nematic Liquid Crystal Hybrid Panels

Agata Anczykowska, Stanislaw Bartkiewicz, Lech Sznitko, Jaroslaw Mysliwiec
Institute of Physical and Theoretical Chemistry
Wroclaw University of Technology
Wybrzeze Wyspianskiego 27
50-370 Wroclaw, Poland

Abstract - In this paper we present results of the study of dynamics of diffraction efficiency in hybrid liquid crystal panels (HLCP) dependent on applied voltage. In the experiment we used laser to write a hologram by modifying the alignment of liquid crystal molecules. Simultaneously we used a second laser to read the recorded gratings. We proposed the model explaining the dynamics of the gratings formation which is composed of three different following processes related to the charge carriers generation and their mobility in the photo conducting polymer.

I. INTRODUCTION

Nowadays photonic devices with a potential use for information storage and processing are the subject of increasing interest and development. The photo induced refractive index changes in nematic liquid crystals are very popular among different physical processes enabling the creation of real time holograms. When properly used in optical systems they allow for pattern recognition, moving object extraction, optical filtering, and realization of associative memories. Implementation of such tasks requires sensitive, fast and reversible recording media. The process of hologram formation and erasure generally relies on optical build-up of transient diffraction gratings in a material. [1-2] These gratings understood as a spatial modulation of index of refraction or absorption arise as a result of various non-linear optical processes which are not well described yet. Many parameters require optimization, and with some improvements the hybrid liquid crystal panels (HLCP) could become a very efficient storage medium for large amounts of data in small areas.

The purpose of the research reported in this contribution was to investigate the dynamics of diffraction efficiency in HLCP dependent on applied voltage.

II. EXPERIMENT

A. Sample

The investigated liquid crystal panel was made by sandwiching nematic liquid crystal between two ITO (Indium Tin Oxide) glass plates onto which thin layers of photo-conducting polymer were spin-coated. Scheme of the sandwich-type HLCP is shown in Fig.1.

For sample preparation we used poly(N-vinylcarbazole) sensitized on visible light spectra by doping the trinitrofluorenone molecules (PVK + TNF).

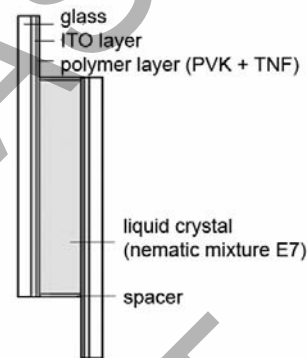


Figure 1. Hybrid nematic liquid crystal panel (HLCP)

The thickness of this layer was about 100 nm. The multicomponent nematic liquid crystal mixture E7 (Merck, Darmstadt, Germany) was used as the “optically active” medium.

The distance between ITO plates was set by 10 μm spacers. Surfaces of the photo-conducting thin layers were uniaxially brushed to preliminary direct the molecules of the liquid crystal without the influence of an applied voltage.

B. Experimental set-up

All measurements were done in a typical degenerated two wave mixing experiment set-up which is schematically shown in Fig. 2 [3].

Nd:YAG laser “L1”, which operates on wavelength $\lambda = 532$ nm was used to write a hologram by modifying the alignment of liquid crystal molecules. The writing laser beam was firstly partially attenuated by the grey filter “F” and then was divided into two beams “Iw(1)” and “Iw(2)” by the beam splitter “BS”. The intensities of these beams were not equal so the gradient filter “GF” was used to compensate for the difference.

The mirror “M” was used to direct beam “Iw(2)” onto sample “HLCP” to allow interference with beam “Iw(1)” within the sample volume. Interfering beams caused modulation of the refractive index Δn .

A second laser He-Ne “L2”, which operates on wavelength $\lambda = 632.8$ nm was used to read the stored image.

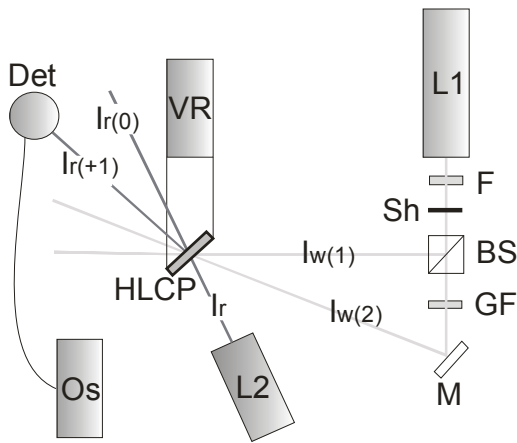


Figure 2. Experimental set-up for degenerated two wave mixing measurements. L1 – Nd:YAG laser, L2 – He-Ne laser, F – grey filter, GF – gradient filter, Sh – shutter, BS – beam splitter, M – mirror, S – sample, VR – voltage regulator, Det – detector, Os – oscilloscope.

Power of the first order diffraction beam “Ir(+1)” was measured by silicon detector “Det” coupled with digital oscilloscope “Os”.

Power Supply “VR” of DC voltage connected to the sample was regulated within the range of 0-50V. Diffraction efficiency was measured in dependency of applied to the HLCP voltage. All the following parameters were fixed. The reading angle (angle between normal to the sample surface and reading beam) was set to $\beta = 12^\circ$, the writing angle (the angle between writing beams Iw(1) and Iw(2)) was set to $2\theta = 4^\circ$ and the tilt angle (the angle between bisector of writing beams and normal to the sample surface) was $\alpha = 0^\circ$. The power of writing beams were Iw(1) = Iw(2) = 19mW and the power of reading beam was Ir = 15mW.

III. THEORY

Experimentally diffraction efficiency η is calculated from the measured intensity of light in a certain diffraction order. This figure is determined as the ratio of intensity of diffracted light in a first diffraction order Ir(+1) to the intensity of incident light Ir.

$$\eta = \frac{Ir(+1)}{Ir} \quad (1)$$

Theoretically diffraction efficiency η (for thin diffraction gratings) is determined by using the Raman-Nath approximation. This approximation can be used to link diffraction efficiency with the alteration of the composite refractive index by Δn^* Bessel functions J_1 [4,5]

$$\eta = |J_1(\phi)|^2 \quad (2)$$

$$\phi = \frac{2\pi\Delta n^* d}{\lambda} \quad (3)$$

$$\Delta n^* = \Delta n + i \frac{\Delta\kappa\lambda}{4\pi} \quad (4)$$

where d – the thickness of the liquid crystal panel
 λ – wavelength of the writing laser
 $\Delta\kappa$ – modulation of absorption coefficient
 Δn – modulation of refractive index

If absorption of the refractive material is insignificantly small, the Bessel function parameter for thin diffraction gratings can be written in the form of

$$\phi = \frac{2\pi\Delta n d}{\lambda} \quad (5)$$

For the writing laser wavelength of light of $\lambda = 632.8$ nm and the thickness of the liquid crystal panel, $d = 10\mu\text{m}$ parameter value $2\pi d/\lambda = 99.1$.

The sinusoidal light modulation caused by interfering light in the volume of sample generates charge carriers in PVK:TNF layers. Number of generated carriers is proportional to the intensity of incident light, so generation is strongest in the places where constructive interference occurs and none where destructive interference occurs.

When the sample is illuminated, DC voltage is applied and when it's value is over Freedericksz potential, the generation of the charges and their drift into the photo-conducting layers provides changes to the local electric field, which results in liquid crystal molecules reorientation and then spatial refractive index modulation in the sample.

The charge generation and transport in HLCP can be divided into three different following processes ($\Delta n_1, \Delta n_2, \Delta n_3$). These three processes are characterized by the following parameters:

- amplitudes determining the quantitative contribution of each of the processes. (n_{1M}, n_{2M}, n_{3M})
- stable in time angles between different diffraction gratings ($\phi_{1/2}, \phi_{1/3}, \phi_{2/3}$) determining their relative position
- time constants (τ_1, τ_2, τ_3) determining the rate of exponential growth of gratings writing
- time constants of erasing functions ($\tau_{1e}, \tau_{2e}, \tau_{3e}$)

Basing on the preceding assumptions we developed the following mathematical model for description of modulation of the refractive index during diffraction gratings writing process which is based on gratings coupling [6].

$$\Delta n = [\Delta n_1^2 + \Delta n_2^2 + \Delta n_3^2 + 2 \cdot \Delta n_1 \cdot \Delta n_2 \cdot \cos(\phi_{1/2}) + 2 \cdot \Delta n_1 \cdot \Delta n_3 \cdot \cos(\phi_{1/3}) + 2 \cdot \Delta n_2 \cdot \Delta n_3 \cdot \cos(\phi_{2/3})]^{1/2} \quad (6)$$

$$\Delta n_i = n_{iM} (1 - e^{-t/\tau_i}) \cdot e^{-t/\tau_{ie}}, \quad i = 1, 2, 3 \quad (7)$$

IV. RESULTS AND DISCUSSION

Temporal evolution of diffraction efficiency was measured for different values of applied to the HLCP voltage. The experimental data indicate that diffraction efficiency generally increases with increasing voltage. This is due to the fact that the number of generated charge carriers responsible for the efficiency of the process of hologram writing depends on applied to the HLCP voltage. Temporal evolution of diffraction efficiency for different values of applied to the HLCP voltage is shown in Fig. 3.

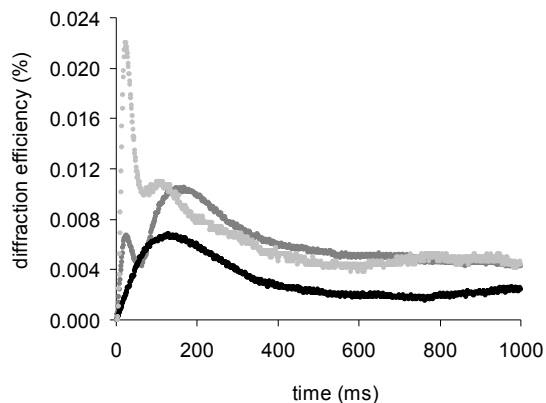


Figure 3. Temporal evolution of diffraction efficiency for different values of applied to the HLCP voltage.
Black curve – 32V, dark grey curve – 40V, light grey curve – 50V.

Diffraction efficiency depends on the modulation of the effective refractive index, which described by formula (6) consists of three different following processes (Δn_1 , Δn_2 , Δn_3). For the processes of diffraction gratings formation most of the parameters characterizing those three processes change when applied to the HLCP voltage changes as shown in Table 1.

The first process which occurs in first few milliseconds after irradiation of the sample can be explained as generation of electrons and holes in the bright regions of both PVK:TNF layers, diffusion of holes into the dark regions of polymer layers on anode side (redistribution of holes near the border between PVK:TNF layer and liquid crystal at anode side). Time constant of the first diffraction grating ($\tau_1 = 20\text{ms}$) remains constant, so it can be concluded that it is independent of voltage applied to the HLCP. Amplitude of this process (n_{1M}) increases with increasing voltage and time constant of the erasing function (τ_{1e}) decreases.

The next process occurs within several tens of milliseconds and is connected with the depletion of faster holes at cathode side and charge transfer in external electric field. Time constant of this process (τ_2) changes linearly with changing inverse voltage and time constant of the erasing function (τ_{2e}) has infinite value so it can be assumed that it has no effect on the process of writing of the second grating.

The last process takes a few hundred milliseconds. Charge is transferred from side holes located on anode to the molecules of liquid crystal which results in the flow of the cations through the sample volume and their arrival to PVK:TNF layer at the cathode side. This process leads to neutralization of electrons present in the cathode. Time constant of this process (τ_3) also changes linearly with changing inverse voltage and time constant of the erasing function (τ_{3e}) has infinite value similarly to the second process so it can be assumed that it has no effect on the process of writing of the third grating.

TABLE I
THE SET OF APPROXIMATION PARAMETERS FOR THE SERIES OF EXPERIMENTAL CURVES OF WRITING DYNAMICS OF THE HOLOGRAM CALCULATED USING THE EQUATION (6)

U [V]	τ_1 [ms]	τ_2 [ms]	τ_3 [ms]	n_{1M} [10^{-5}]	n_{2M} [10^{-5}]	n_{3M} [10^{-5}]
32	20.0	56.0	580.0	0.0	26.0	37.0
36	20.0	47.0	554.0	70.8	104.9	98.7
40	20.0	39.5	534.0	97.2	125.9	113.0
44	20.0	33.5	517.0	154.6	182.9	170.7
48	20.0	28.0	504.0	237.1	259.5	264.4
50	20.0	25.5	498.0	294.8	306.7	288.0

U [V]	τ_{1e} [ms]	τ_{2e} [ms]	τ_{3e} [ms]	$\phi_{1/2}$ [rad]	$\phi_{1/3}$ [rad]	$\phi_{2/3}$ [rad]
32	1300	∞	∞	2.81	0.00	2.81
36	1050	∞	∞	3.01	-0.01	3.02
40	858	∞	∞	3.00	-0.05	3.05
44	700	∞	∞	3.04	-0.06	3.10
48	580	∞	∞	3.05	-0.08	3.13
50	520	∞	∞	3.06	-0.09	3.15

Approximated curves very accurately coincide with the experimental data obtained for various experimental conditions. In Fig.4. experimental data of dynamics of diffraction efficiency and estimated values for the process of hologram writing for applied to the HLCP voltage $U = 40\text{V}$ are shown.

After shutter release a rapid increase in the diffraction efficiency was observed. After 25 ms it reached the local maximum value of 0.0067%, then started to decrease and reached a minimum value of 0.0043% in the 55 ms of experiment, then rise again to the maximum value of 0.0104% in the 165 ms of experiment and decreased slowly to the value of 0.0044% and stabilized after 1000 ms from the start of the experiment.

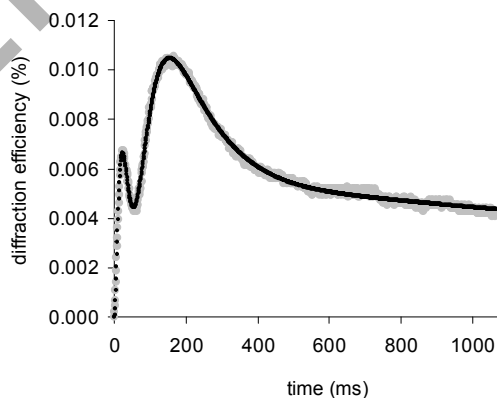


Figure 4. Typical time dependency of diffraction efficiency for HLCP. Gray points – experimental data, black points – estimated values (parameters of estimation can be found in Table 1.)

V. CONCLUSION

In conclusion, we have demonstrated the results of the comparison between experimental and estimated data.

The presented mathematical model which takes into account the existence of charge carriers (holes and electrons) and their mobility in the photoconducting polymer fairly well describes the three-step process occurring inside the HLCP during the hologram writing.

The calculated parameters characterizing proposed mathematical model show that the dynamics of the hologram writing is linked to the generation and transport of charge carriers (diffusion and drift) in the external electric field.

ACKNOWLEDGMENT

The authors wish to thank the Wrocław University of Technology for financial support.

REFERENCES

- [1] I.C. Khoo, "Liquid Crystals Physical Properties and Nonlinear Optical Phenomena", *J.Wiley, New York*, 1995.
- [2] S. Bartkiewicz, A. Miniewicz, A. Januszko, J. Parka., "Dye-Doped Liquid Crystal Composite for Real Time Holography", *Pure and Applied Optics*, Vol. 5, p. 799, 1996.
- [3] J. Mysliwiec, D. Jarzab, K. Janus, S.Bartkiewicz, "Study of Self-Diffraction Process in Photoconducting Polymer-Nematic Liquid Crystal Hybrid Structure" *Applied Physics Letters*, Vol. 90, p. 121120, 2007.
- [4] H.J Eichler, P. Gunter, D.W. Pohl, "Laser Induced Dynamic Gratings" *Springer - Verlag, Berlin*, 1986.
- [5] A. Sobolewska, S. Bartkiewicz, "Three Gratings Coupling During the Holographic Grating Recording Process in Azobenzene-functionized Polymer", *Applied Physics Letters*, Vol 92, p. 253305, 2008.
- [6] N. Reinke, A.Draude, T. Fuhrmann, H. Franke, R.A Lessard, "Electric Field Assisted Holographic Recording of Surface Relief Gratings in an Azo-glass", *Applied Physics B*, Vol. 78, pp.205-209, 2004.

Relevance of a Safety Factor for Wind Power Trading in Comparison with the Utilization of a Storage

S. Völler, J.F. Verstege

Institute for Power System Engineering, University of Wuppertal
Rainer-Gruenter-Straße 21
42119 Wuppertal, Germany

Abstract- In Germany renewable energy sources are paid by law with a constant amount for the supplied energy. Thus, the operators of such plants have no intention to take part at the energy market yet, but there exists possibilities to earn a better payment, so already some facilities act in the market and in the future this participation will be more and also necessary.

This work analyses the opportunities for the participation at an energy exchange and at the control power market. To interact with the market, wind farms have to supply a constant power for a specified time. Due to the fluctuations of wind energy it is not possible to guarantee a constant power based on wind forecasts. Thus, the wind farm cannot sell their maximal estimated energy but only a reduced value. The aim of the work is to figure out this specific "safety factor". Later on, the results are compared both technically and economically with the use of a storage unit, where the full amount of energy can be traded.

I. INTRODUCTION

Renewable energy is a constant growing part of the worldwide energy supply. In Germany the most important source is wind energy. In comparison to conventional power plants the most renewables have the main disadvantage of delivering fluctuating energy why they cannot be used to guarantee a steady supply.

In spite of this disadvantage, the renewable energy is extra supported because it is a sustainable and environment friendly energy form and an important alternative for future supply. In Germany this official support is regulated by law by the government through the Renewable Energy Sources Act (EEG) [1]. The owners of renewable production facilities get a priority feed-in into the grid, where the grid operator must take-over the energy and pay a fix refund for the generated energy. This payment is often higher than the average production cost in conventional power plants but sometimes lower than achievable prices at energy markets.

II. SAFETY FACTOR

To take part at an energy market the production facility has to provide a constant power for a specified time (e.g. 15 minutes or 1 hour). This is the so called "scheduled energy". Fluctuating energy sources like wind energy have not the ability to supply this scheduled energy because the forecast of the next day wind speed is not so accurate. The prediction of the produced energy is possible, but during the day the wind power may be not in the time when it is awaited. Due to wind

delay the expected power may shift by one hour. Because of this forecast uncertainty, the wind farm owner cannot trade the whole produced wind energy. He has to insert a safety factor, by which the maximal possible wind power is reduced. By reducing the power, the wind farm owner is able to supply a (lower) scheduled power, but will not violate his supply contract in the case, that the wind power is another than predicted.

An example is shown in Fig. 1. Concerning to the wind forecast (blue line) the wind farm owner sells the wind energy in 1-hour-contracts (orange + grey bars) to a customer. The height of power he uses is always the maximal possible power for this one hour, what is also the minimal wind power in this time. At the day of delivery the supplied wind power has another curve (red line), so a part of the sold energy can not be supplied and the before sold scheduled energy have to be reduced (grey bars). Thus, the wind farm owner has to pay a penalty because he cannot fulfill his contract.

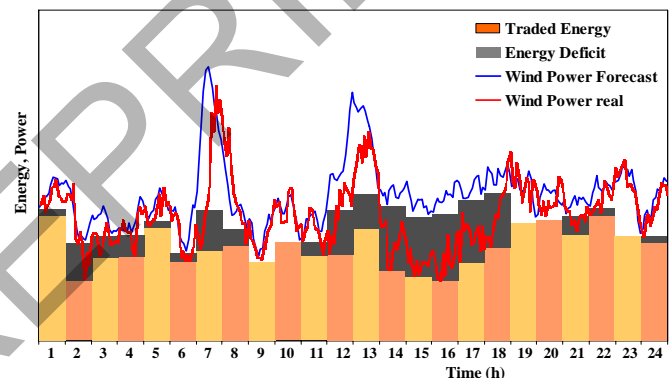


Figure 1. Example of energy deficit by trading the maximum power depending on the forecast compared to the real wind power

By this situation, the wind farm owner has to decide, whether it is cheaper for him to pay the penalty and sell the maximal possible scheduled energy or he reduces the scheduled energy by a safety factor (e.g. he sells only 80 % of the maximum). Doing the last option, he loses income because he cannot sell this energy to a better price, but on the other side he has not to pay penalties. This may work with an energy exchange, but at the control power market the supplier is pledged by contracts to be able to supply the scheduled power at 100 % of the time he offers.

III. SIMULATION SYSTEM

The basic simulation system consists of a wind farm with 250 MW and a storage system. These components were modeled in a simulation environment, which was designed for optimal operation planning of energy supply systems using a mixed integer linear programming (MILP) [2]. The required technical parameters of the wind energy farm and the storage system are implemented into the model, whereby it is secured that the facilities will run within their specifications. In this work the program uses the optimization to make decisions where the generated wind energy will be sold. For this purpose different payment sources exist, which each represents another customer (e.g. an energy exchange). For each scenario and their combination the optimization tries to find the best result by maximize the amount of coverage for the wind farm operator. Equation (1) shows the objective function.

$$OF = \sum_{i=1}^I \sum_{t=1}^T (R_{i,t} - C_{i,t}) \cdot x_{i,t} \longrightarrow \text{MAX} \quad (1)$$

R	revenues
C	costs
x	optimization variable
i, I	index of number of elements
t, T	index of time intervals

The simulation expects a "day-ahead" sale of energy with forecasts for wind & prices and makes a daily optimization with 96 time intervals of 15 minutes each for one complete year. The system uses also data from the next two days as input. Thus, the usage of the storage unit can be more optimized for a longer time period. In the case the prices are higher the next day, the optimization system maybe decides to store only energy to the storage at present day and sell it completely at the next day. As input for the components historical time-variant curves were used for price trends and wind speed. So it is guaranteed that the wind speed in the summer is corresponding to the energy market price in the summer.

IV. BASIC SIMULATION DATA

For the simulations, scenarios were devised in order to reproduce the energy market situation in Germany [3]. The main focus in this work was on the energy and control power market, but the model also included possibilities to participate at other markets, e.g. congestion management [4].

A. Energy Market

After the liberalization of the electrical grid the different European energy markets arose. This scenario is based on data from the European Energy Exchange (EEX). At the EEX suppliers and customers can trade at different markets, whereas in this work is considered only the spot market. There is the possibility to offer hour-bids (in this work called "Peak") with

a minimum of 0.1 MW for 1 hour. The bidding is for the next day and following the daily load, the price between noon and afternoon is much higher than during night, so there can be a worthwhile energy shifting.

B. Control Power

To ensure a secure operation of the electrical grid, it is necessary to use control power for the regulation of energy and frequency fluctuations. There exist two types of control power: first is positive control power which demands extra energy feed into the grid (e.g. increased supply from power plants) and the second is negative control power which reduces the energy feed into the grid or increases the load (e.g. with pumped hydro storages). The different types of control power (primary, secondary, tertiary control power) are realized today mainly with large conventional power plants.

These simulations contain only tertiary control power (TC). After 15 minutes the TC has to be activated and takes place up to 1 hour. Suppliers have to deliver at least ± 15 MW and the bidding is for the next day. The transmission system operator purchases this power at a control power market, where accredited power plants are able to offer their power. Wind energy farms may also take part, because wind turbines are able to supply control power [5]. There exist already renewable energy sources which deliver control power. Besides hydropower, small and midsized power plants (wind, photovoltaics, combined heat and power) working together in generation pools to satisfy with the requirements.

The power plants get a fix amount of money only for providing the power ready (demand charge). The price depends on the demand at the power market; typically the negative control power is expensive during the night and cheap at the day, while it is reverse at the positive control power. The special interest at negative control power for wind farms is the possibility to sell the reserved energy also at a source without a contract, e.g. the EEG. As long as the negative control power is not required, the wind turbine can run on full power and sell the energy. Only at the time of demand, the turbine must throttle the output and loss the extra income.

C. Energy Storage

Energy storages are suited for making the energy supply independent of time. They can accept and deliver energy from the grid if there is a surplus or a shortage. Storages are not only used for this technical issue but also for economical purposes. During the night energy is charged into the storage and during the high demand at the daytime it is feed back into the grid, e.g. with pumped hydro storages. Thus, the expensive peak load energy can be avoided partly.

For the simulations the storage is used both for technical and economic issues. It charges the wind energy when the price at the energy market is low and discharges when the price is high. The storage also assures a secure supply of the scheduled energy. According to the wind farm, a storage was chosen with a power of 100 MW and 800 MWh (redox flow battery).

D. Further Specifications

The running costs (operating and maintenance) of the storages were integrated into the optimization while fixed costs for the storage or other expenses (e.g. fees for participation at energy market) are not part of the optimization. They will be offset later with the simulation outputs to get the overall result. It is also assumed that the wind energy farm already exists, so its costs are not part of this work.

V. RESULTS

The safety factor was varied between 0 to 20 % according to the maximal possible power, as described in chapter II. With these different values, the various scenarios were simulated for one the same year to compare the results, according to violation of the scheduled energy and also to the income of the wind farm owner.

In Fig. 2, an example day of the day-ahead simulation is displayed. The wind power (*Wind*) will be sold between 7.00 and 21.00 to the energy exchange, supplying always a constant power block for one hour (*Peak1*, *Peak2*). In the morning, a four hour block of negative tertiary control power (*nTCI*) will be delivered, which will be provided by throttling the wind farm (*TnTC*). The rest of the energy will be sold via the EEG (*EEG*) with a payment of 80 €/MWh. It is obvious, that the optimization will sell as much energy as possible to the highest price, so the maximal power is always the maximal wind power, concerning to the wind forecast.

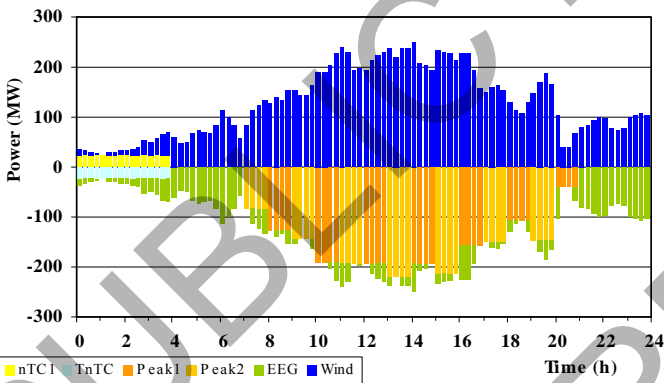


Figure 2. Optimized day-ahead sale of the wind energy without a safety factor

On the day of delivery, the wind speed differs from the predicted wind the day before, so the produced wind power does not fit the scheduled energy what was sold the simulation before to the day-ahead markets. In Fig. 3, the sold scheduled energy to the energy exchange (*PeakS*) and to the control power (*nTCp*) cannot be delivered (*PeakSh*, *nTCpH*). Therefore the missing energy has to be taken from other sources (*EnTCB*). In these cases, the wind farm owner has to pay a higher price to purchase this (balancing) energy (*BEPeak*) or has to pay penalties to the customer, because he could not fulfill the contract. The rest of the energy is sold via the EEG

like before, because the energy is feed directly into the grid without any contract like it is produced.

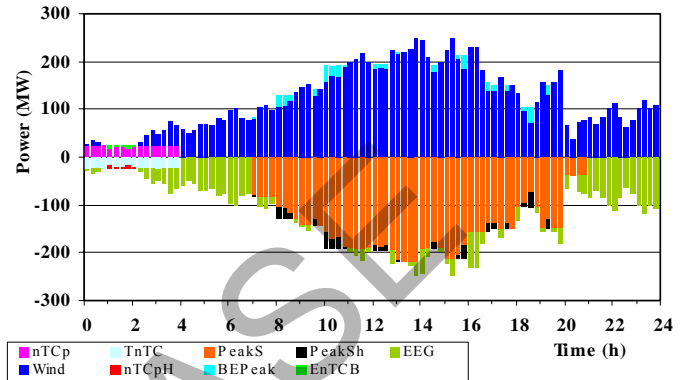


Figure 3. At day of delivery differences occur between supply and sale

If there will be a safety factor, then the amount of maximal possible power will be reduced. In Fig. 4 this value is reduced by 15 %, which can be seen in the purple (*PeakSF*) and dark green color (*nTCSF*). This energy can be sold also to the EEG the next day or it will be later throttled if necessary. With this "buffer" the wind farm owner can compensate differences between the wind forecast from the day-ahead optimization and the real wind. So on the day of delivery the missing energy (Fig. 5) is reduced, compared to Fig. 3.

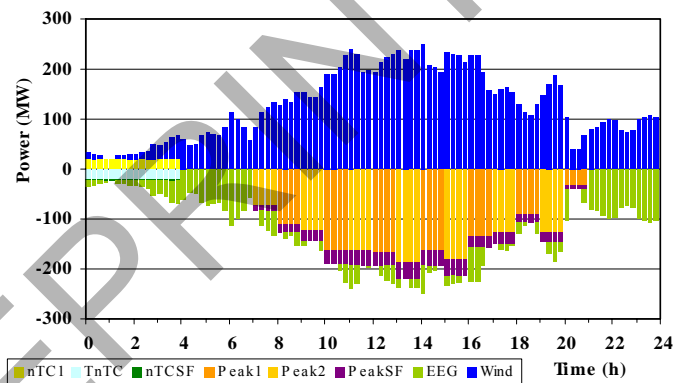


Figure 4. Optimized day-ahead sale of the wind energy with a safety factor of 15 %

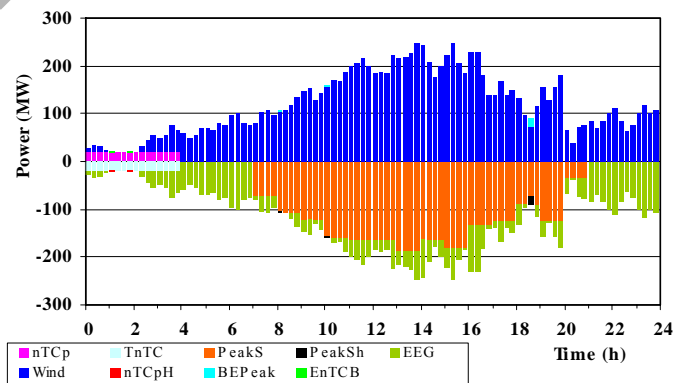


Figure 5. Supply with reduced violations due to the safety factor

In the case a storage is combined with the wind farm, a safety factor is not necessary because the storage will balance the difference between forecast and real wind. Furthermore the storage can increase the income of the owner because now it is possible to speculate on the market as described before. The same day as before is showed in Fig. 6. With the storage the optimization decide to buy energy in the morning (EP) and charge the storage (Sc). The storage is then discharged to maximize the energy which is delivered to the energy exchange (Sd) and it also supports the control power, which is increased in the morning and evening by the storage ($ScnTC$).

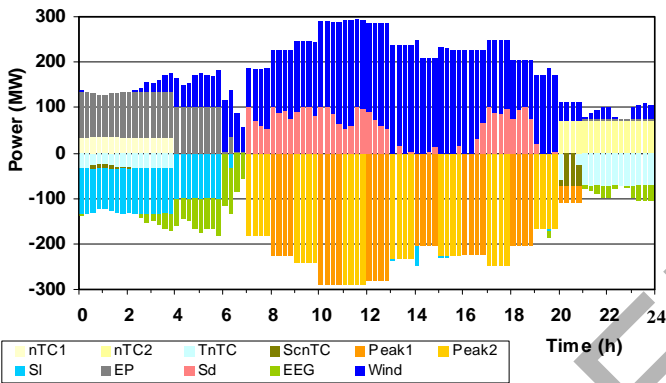


Figure 6. Day-ahead optimization including the storage

At the day of delivery (Fig. 7) the storage is able to manage the different wind speeds and no violation of the control power occurs, only balancing energy for energy exchange is needed.

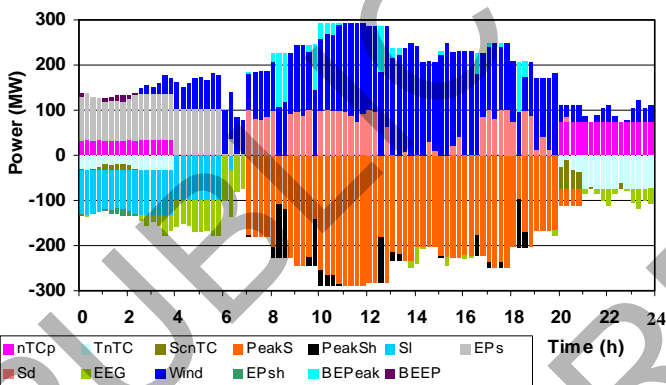


Figure 7. With a storage no violations occur and the income is increased

These simulations were made for each day of a chosen year for the different scenarios. At the end, the income/expenses of the wind farm owner including penalties and the annual storage capital costs (10 m€) have to be compared to give an answer to the question, which safety factor (SF) is necessary and whether the implementation of a storage is worthwhile. The results are shown in Table I. The first column shows the number of violations of the provided control power, because if there are violations, the wind farm is banished from further participations at this market. The next column is the results of the optimization for one year; the part of the penalty fees and

balancing energy of the result and the last column shows the total income including storage costs if included.

TABLE I
OVERVIEW OF THE RESULTS FROM THE DIFFERENT SCENARIOS OF ONE YEAR

Scenario	Violations TC	Results in Euro		
		Optimization	Part of Penalty	End Result
SF = 0 %	74x	24 772 532	4 904 755	24 772 532
SF = 5 %	27x	28 178 166	1 222 412	28 178 166
SF = 10 %	9x	28 644 179	480 272	28 644 179
SF = 15 %	4x	28 582 357	254 864	28 582 357
SF = 20 %	1x	28 458 636	109 144	28 458 636
Storage & SF = 0 %	0	37 330 143	3 359 631	27 330 143

VI. CONCLUSION

This work showed, that it is essential to use a safety factor in the case, that the wind farm operator wants to participate at an energy market without a storage. Under some circumstances it is possible to allow violations of the scheduled energy, e.g. at the energy exchange. Nevertheless, the suppliers have to deliver the sold energy and so they have to buy it somewhere else (for higher prices) or have to pay penalties. At the control power market a non-compliance is not accepted, so in the case the wind farm is not able to supply the sold energy, it is locked out from further trade and cannot take part anymore at this market. Therefore it is necessary to include a safety factor (e.g. 20 %) to be on a safe side. However, including this factor will decrease the income of the wind farm because of selling less energy to the high price payment. An energy storage can handle this problem and is also able to increase the income by a better trading of the energy at the market. Thus, a storage has both technical and economical benefits for the system [6].

REFERENCES

- [1] "Act Revising the Legislation on Renewable Energy Sources in the Electricity Sector and Amending Related Provisions (Renewable Energy Sources Act)", Federal Ministry for the Environment, Nature Conservation and Nuclear Safety, in: *Federal Law Gazette 2008 I No. 49*, Bonn, 31 October 2008
- [2] P. Hackländer, J.F. Verstege, "Accelerated MILP-Strategies for the Optimal Operation Planning of Energy Supply Systems", in *Operations Research Proceedings 2002*, Springer-Verlag, Berlin, Heidelberg (2003) pp. 259-264
- [3] S. Völler, J.F. Verstege, "Investigation of new Payment Models for Wind Farms in Combination with Energy Storages", in *Proceedings of International Youth Conference on Energetics*, Budapest, Hungary, 2007
- [4] A.F. Kaptue Kanga, S. Völler, J.F. Verstege, "Congestion Management with Energy Storages", accepted paper for CIGRÉ/IEEE PES Symposia *Integration of wide-scale Renewable Resources into the Power Delivery System*, Calgary, Canada, 2009
- [5] A.-R. Al-Awaad, S. Völler, J.F. Verstege, "Contribution of Wind Power Plants to Frequency Control", accepted paper for *4th International Exergy, Energy and Environmental Symposium (IEEES-4)*, Sharjah, United Arab Emirates, 2009
- [6] S. Völler, A.-R. Al-Awaad, J.F. Verstege, "Benefits of Energy Storages for Wind Power Trading", *IEEE International Conference on Sustainable Energy Technologies (ICSET)*, Singapore, Republic of Singapore, 2008

The Probabilistic Integration of Demand-Side Load and Generation in a Representative Irish Distribution Network

Keith Sunderland¹
Dublin Institute of Technology, Ireland
keith.sunderland@dit.ie

Michael F. Conlon¹
Dublin Institute of Technology, Ireland
michael.conlon@dit.ie

Abstract-This paper introduces a methodology for investigating the behaviour of a distribution network incorporating both load variations and variable micro-wind generation output. The probabilistic methodology is applied to a representative model of the Irish Distribution Network. Application of a selection of commercially available micro-wind turbines to the model is investigated for a range of load and generation scenarios based on a standard load profile and varying mean wind speed. Analysis of the results of the analysis forms the basis for defining the limitations of the methodology but also presents the opportunities for future work.

I. INTRODUCTION

This paper advances the work in [1], where a model was developed to analyse the impact on a distribution network, in the terms of voltage rise of increasing penetration of micro generation and more specifically, micro-wind generation. Indeed, [1] was itself based on the systems described in [2] and [3]. In a report commissioned by *Sustainable Energy Ireland* (SEI) investigating the costs and benefits of embedded generation in Ireland [3], analysis for the context of micro-generation stated that voltage rise problems would not be encountered for the worst case scenario (each consumer having 1.1kV of generation whilst at minimum load of 0.16kVA).

This model is compiled employing MATLAB[®] to implement a *Distflow* routine as outlined in [4]. The Distflow approach derives the bus voltage of a weakly meshed network by iteratively evaluating the Load Flow solution of the modeled network under varying load/generation scenarios.

The Representative Irish Network which is considered in this analysis is shown in Figure 1. The system comprised of:

- One 500MVA Source
- Two 10 MVA Transformers (YY0, 38/10.5kV), auto-tapping to -20/+10% in steps of 1.67% and an AVC scheme with bandwidth of 2.5%
- Five, 10kV Distribution feeders with one modeled in detail
 - This feeder is 3km long with 1.5km being 185mm² 10kV PICAS and the remaining 1.5km being of 95 mm², 10kV PICAS
- The detailed feeder contains ten 10/0.433kV Substations (fixed tap transformer), each substation having four LV feeders.
- One of the LV Feeders is modeled in detail

- This feeder is 300m long with 150m being 185mm² 415V CNE and the remaining 150 being of 95mm², CNE.

The model developed in [1] was compiled for a range of scenarios:

- Maximum Demand on each substation (of each 10kV feeder), 0% Generation
- Minimum Demand on each substation (of each 10kV feeder), 0% Generation
- Minimum Demand on each substation (of each 10kV feeder), 100% Generation

Each substation, serves 312 customers (over three phases) and each customer is modeled as having an *After Diversity Maximum Demand* (ADMD) of 1.28kVA and the potential of affording a micro-generation technology with capacity of 1.1kVA. Each substation was modeled with a load factor of 50%.

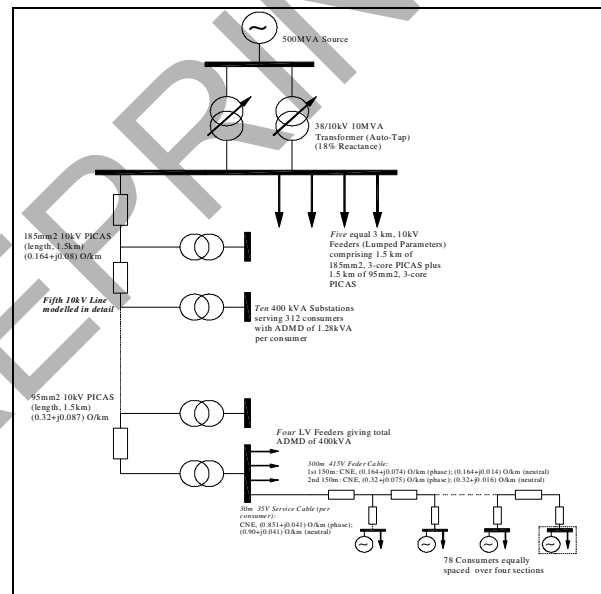


Figure 1: 38/10/0.4 kV Distribution Network Model

These scenarios represent the extremes of possibility. This paper further develops this model by integrating variable load and generation. This is implemented by using a probabilistic approach to the modeling of the wind speed of the micro-wind turbines. This variable micro-wind generation is combined with load profile data as provided in [6] which

represents standard domestic load profiles developed for the Irish Electricity Market. These were utilized to determine the variation in voltage profile for the LV network as a result of both load and micro-wind generation. Similar work has been undertaken for a *Small Scale Energy Zone* (representing a total of 96 LV consumers) in [5] where a dynamic model which integrated variable wind speed in terms of a minimum load of 0.16kVA and a percentage of customers having a 1.1kW generator connected, produced results suggesting that voltage tolerance is breached at 114% penetration level.

The approach taken here is to apply a single (but variable) wind speed to all connected generation. This is considered acceptable as it is assumed that there would be little variation of wind in the area (excluding the effects of obstruction or shading) encompassed by the representative Distribution Network. Independently varying 'bulk' connected load of the connected consumers at the sectionalized connections of the LV feeder was also considered acceptable as a compromise to individual manipulation of each consumer's load.

Analysis of voltage profile over the course of representative days in different seasons was implemented for a sample of commercially available micro-wind generator units relative to the load profile.

Distflow is employed as the optimal methodology to derive the load flow results for the network as standard load flow approaches (Newton Raphson, Gauss Seidel etc.), have difficulties in converging due to the high X/R ratios characteristic of distribution networks.

II. THE METHODOLOGY

Figure 2 illustrates a flow chart describing the methodology utilized in deriving the bus voltages for the network model

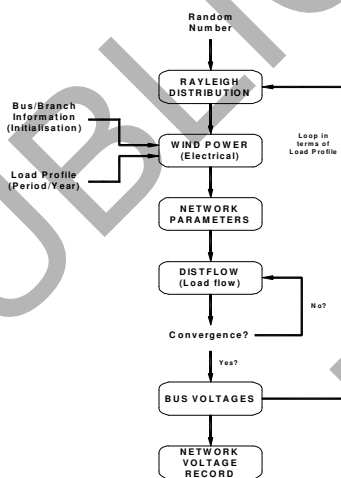


Figure 2: Flow Chart illustrating the methodology in deriving a load flow solution for variable load/gen

The approach is summarized as follows:

- A random number is generated in MATLAB and through (1) a Rayleigh probability distribution is created to represent a varying wind speed.

$$V(i) = V_{Mean} \times \sqrt{\frac{-4}{\pi} \times \log(1 - F)} \quad (1)$$

where:

$V(i)$ is speed derived for each iteration of the program and N is the total number of time periods considered. The analysis is carried out with a 15 minute interval to align with the load model data. F is a uniformly distributed random number. The other assumptions made in relation to the analysis are as follows:

- Uniform penetration of a chosen wind turbine across the network
 - Generation is 'lumped' to the respective buses, but contrary to [1], this lumped generation is variable with respect to the applied simulated wind speed.
- The chosen wind turbine is modeled in terms of
 - Cut-in/out speeds
 - Rated Power (at rated wind speed)
 - Actual power output is based on the derived Rayleigh distribution in conjunction with the specific mean speed
- The load data acquired was for a representative year based on 15 minute intervals [6].
 - Figure (2) illustrates the load variation over the year.
- Automatic tapping of the 10 MVA Transformers is not implemented.

Figure 2 shows the load variation over the course of one year, with a peak demand of 1.73kW and an annual consumption of 6000kWh.

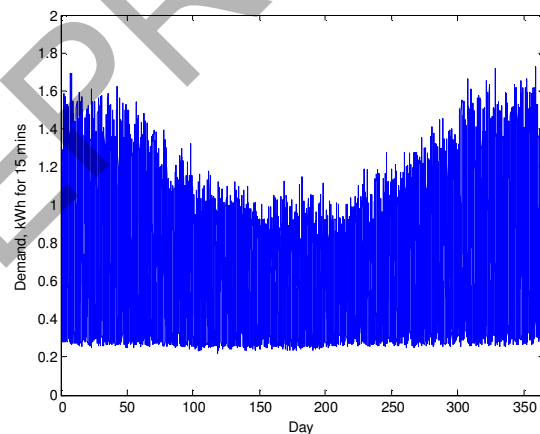


Figure 3: Load Profile Representation of Irish Domestic Dwelling

III. ANALYSIS

Three different types of commercially available wind turbines (Table 1) were modeled for the following scenarios:

- Load/Gen at unity power factor (p.f.)
- Load @ 0.95 p.f.; Gen @ unity
- Load @ unity; Gen @ 0.95 p.f.

- Load/Gen @ 0.95 p.f.
- Two periods over the representative year were considered in detail:
 - The 5th of January and 5th of July, with mean wind speeds of 5.49m.s⁻¹ and 3.65m.s⁻¹ respectively [7]
 - The analysis is performed in terms of the bus at the end of one of the LV feeders

TABLE I
SAMPLE OF COMMERCIALY AVAILABLE WIND TURBINES

Model	Reference	Cut-in Speed	Cut-out Speed	Rated Speed	Rated Power
Whisper 200	Gen 2	3.58 ms ⁻¹	>50 ms ⁻¹	14 ms ⁻¹	1.5 kW
Proven 2.5	Gen 3	2.5 ms ⁻¹	>50 ms ⁻¹	12 ms ⁻¹	2.5 kW
Swift	Gen 4	3.58 ms ⁻¹	>50 ms ⁻¹	14 ms ⁻¹	1.5 kW

IV. SIMULATION RESULTS

The simulations performed, as summarised in Table 2, were in the context of voltage profile across the entire network, but for simplicity, the voltage at the remotest bus on an arbitrary LV branch (400V) was recorded. The voltage magnitude for this bus is measured against the tolerance of +10/-6% of nominal voltage for the Distribution Network. The 5th of January and 5th of July were specifically chosen on the basis that there would be considerable differences to load and generation profiles due to both the associated mean wind speed as well as load profile.

TABLE 2
VARIABLE LOAD AND GENERATION SIMULATION SUMMARY

	5 th January & 5 th July	
	Load	Generation
100% Generation Connection	Unity	Unity
0.95	0.95	Unity
0.95	Unity	0.95
50% Generation Connection	Unity	Unity
0.95	0.95	Unity
0.95	Unity	0.95

The results of the simulations are illustrated in the following graphs. Figure 4 illustrates the relationship between the simulated wind speed and the generation of 5th January with 100% generation at unity pf. The typical daily load demand as obtained from [6] is also shown. The different levels of output from the modeled generators are clearly discernable with the Proven 2.5 having the biggest contribution. As the rated outputs of the Whisper and Swift Models are closely aligned 1kW and 1.5kW respectively, the generated outputs from both models are very similar at given the wind speed profile. Fig. 5 shows the voltage over the course of the day which tracks the simulated wind speed.

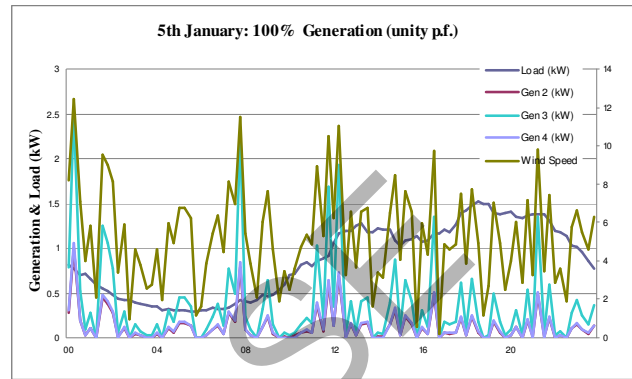


Figure 4: The relationship between generation and wind speed reflected in terms of the Demand profile

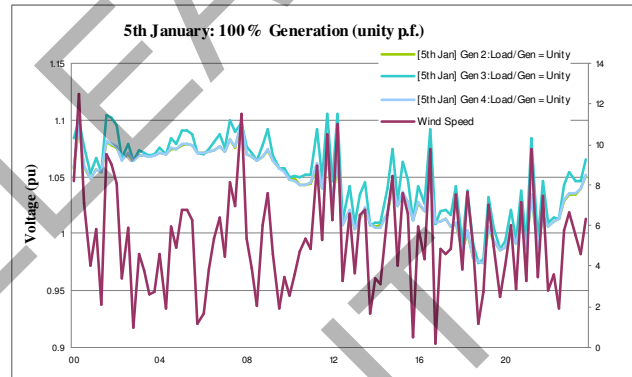


Figure 5: Voltage variation with respect to wind speed for the 5th January

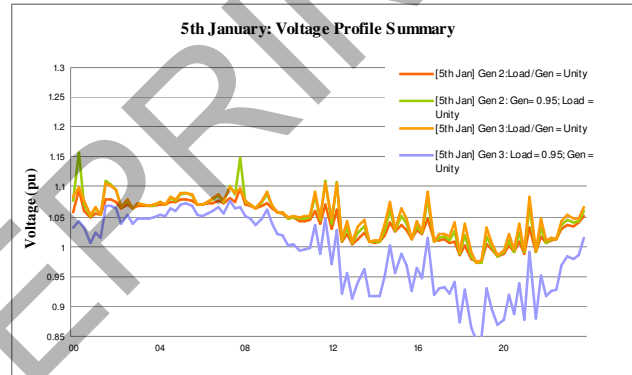


Figure 6: Voltage Profile for all cases during the 5th January

Fig. 6 illustrates the voltage profile for the 5th of January. The same analysis was performed for the 5th of July producing similar results albeit with a lower voltage magnitude due to the lower generation for the date. There are increased levels of generation on the 5th of January due to the increased mean wind speed being employed and as a result, there is a higher voltage level experienced by the bus under scrutiny for the demand applied.

Figures 7 and 8 depict the voltage spread for the varying load/demand ratios for the respective dates under scrutiny. The minimal impact afforded by the generation due to the lower mean wind speed is particularly evident in Figure 8.

Also, the lower consumer demand is also evident in that the breaches of the lower voltage threshold are less frequent and their level diminished.

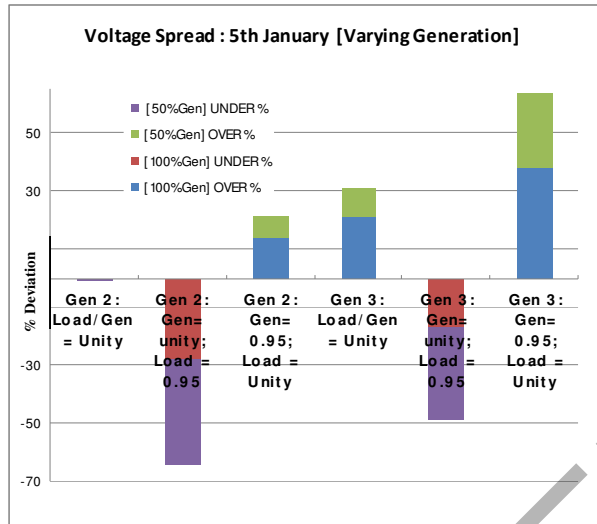


Figure 7: Voltage Spread for all contexts during the 5th January

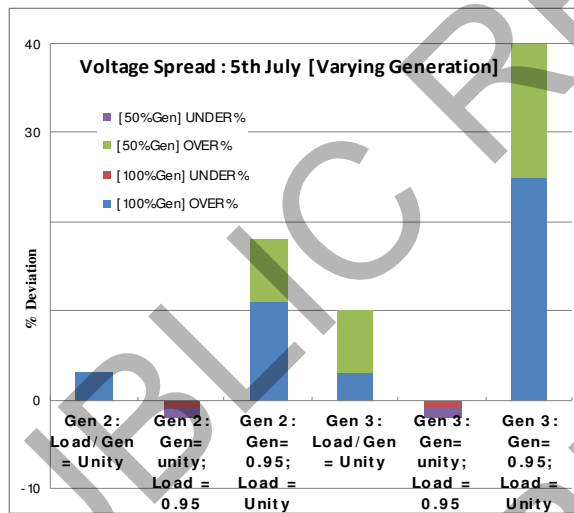


Figure 8: Voltage Proliferation for all contexts during the 5th July

Figure 9 shows the impact on the voltage level with respect to the range of generators. This is placed against the background depicting a probability density function describing the wind speed for the year with mean 6ms^{-1} . Clearly, the Proven 2.5 with its greater output contributes most frequently to breaching the upper voltage limit of 1.1pu. The graph also illustrates that for each of the wind turbines, the most frequent voltage is 1.08pu, which could be considered excessive and this is irrespective of the wind turbine chosen. The mean wind speed of 6ms^{-1} was chosen as a more realistic year-round average.

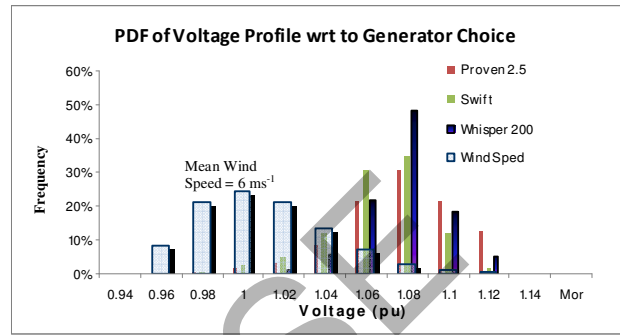


Figure 9: PDF of Voltage Proliferation in terms of the different Generators

CONCLUSION

The work presented introduces a methodology that can investigate distribution network behavior when incorporating both load and generation variation. A sample of commercially available micro-wind turbines were utilized in a representative distribution network model with their outputs based on their characteristics and wind speed derived from a specified probability distribution. This model was subjected to mixed generation and loading conditions and demand was based on a standard load profile for domestic consumers. Voltage variation was monitored. Voltage is dependent on both load as well as generation, with voltage rise resulting from reverse power flows from the connected generation.

Generation based on wind will result in fluctuations matching the turbulent nature of the wind speed. The model had no voltage control on the variable tap distribution transformers and the simulations illustrated this by virtue of both the frequency of voltage tolerance breach and the spread of voltage for the different load/gen scenarios.

Indeed, voltage control by virtue of transformer tapping presents a considerable challenge for demand side management due to the stochastic and variable nature of wind.

REFERENCES

- [1] Sunderland K., Conlon M.F. "The Role of Microgeneration in Irelands Energy Future", Universities Power Engineering Conference, 2008, UPEC 2008
- [2] Ingram. S., P.S.a.J.K., Impact of Small Scale Embedded Generation on the Operating Parameters of Distribution Networks, Department of Trade and Industry. June 2003.
- [3] SEI, *Cost and Benefits of Embedded Generation in Ireland*, Report by PB Power, 2004
- [4] S. Ghosh, D.D., Method for load-flow solution of radial distribution networks
- [5] Cipcigan L.M, Taylor P.C and Trichakis P. "The Impact of Small Scale Wind Generators on LV Distribution System Voltage"
- [6] http://www.rmdservice.com/guidance/standard_load_profiles.htm
- [7] MET Eireann, 30 Year Climatic Averages, <http://www.met.ie/climate/dublinairport.asp>

Planning of Ancillary Services Securing Power System

Ondřej Novák¹⁾, Tomáš Strnad¹⁾, Petr Horáček¹⁾, Josef Fantík²⁾
 {novako5, strnat2, horacek}@fel.cvut.cz, fantik@ceps.cz
¹⁾Czech Technical University in Prague, Faculty of Electrical Engineering
²⁾ČEPS, a.s., Czech Transmission System Operator

Abstract- Procuring sufficient amount of operational reserves used by the Transmission System Operator (TSO) for keeping a balance between generation and load in real-time is a complex task. Extensive balancing power reserves enable keeping the Area Control Error (ACE) close to zero most of the time but the cost of enabling these reserves might be very high. The paper proposes a method of planning sufficient amount of operational reserves or rather Ancillary Services on economical basis. The goal of the presented algorithm is to find AS combination that minimize the cost of AS reservation and at the same time secures transmission system operations. Monte-Carlo simulation scheme of the area operation provides sufficient insight to ACE behavior under different operational reserves. Branch and Bound search scheme is applied to arrive at the best compromise between power security and cost of AS procurement. Short term, one month planning horizon is considered.*

I. INTRODUCTION

Prior to the restructuring and liberalization of the European electricity industry responsibility for security of supply was generally the role of vertically integrated companies with an obligation to supply. Unbundling of the activities has resulted in the establishment of Transmission System Operators (TSO) and changes in roles and responsibilities.

TSO companies from 34 European countries created a new association, the European Network of Transmission System Operators for Electricity (ENTSO-E) in December 2008. The ENTSO-E structure includes three committees for pan-European activities on System Development, System Operation and Market Frameworks being also the main responsibilities of a TSO. TSO is the ultimate instance in the chain of electricity market players participating to active power balancing. Electrical energy market players are economically responsible for meeting their planned individual balances in each settlement time frame. While market players are commercially responsible for their actions in all timescales, after gate closure the TSOs are physically responsible for securing power system operation and maintaining balance between supply and demand by having access to sufficient operational reserves (Fig.1).

Balancing power is a tool used by TSOs to maintain the instantaneous physical balance. Balancing power is a

* This work was supported by the Ministry of Education of the Czech Republic under the project 1M0567 and by the Czech TSO under the project "Reliability and economy of system services"

commodity which is made available on the market in the form of Ancillary Services (AS). One of the tasks of the TSO is to plan and purchase enough AS and activate them timely to meet the grid performance standards and minimize the cost of the AS purchase taking into consideration all physical and market constraints. A TSO might define and use different AS depending on the control area/country specificity of generation sets, however, there are some generic categories present in every control area: Continuous Regulation, Energy Imbalance Management, Replacement Reserves, Voltage Control and Black Start. The paper deals with procurement of all AS categories except voltage control and black start as these do not contribute to power balancing directly.

Performance standards are specified and set for a control area of the UCTE following general requests for all interconnected areas defined in the UCTE's Operation Handbook [1]. An important aspect, which influences the choice and volume of AS, is the cost of the purchase which should be kept low. Simulated operation of the control area under the TSO's Automatic Generation Control and Energy Management System dispatching balancing power in real time, as shown in Fig.1, will be used for generating time series of

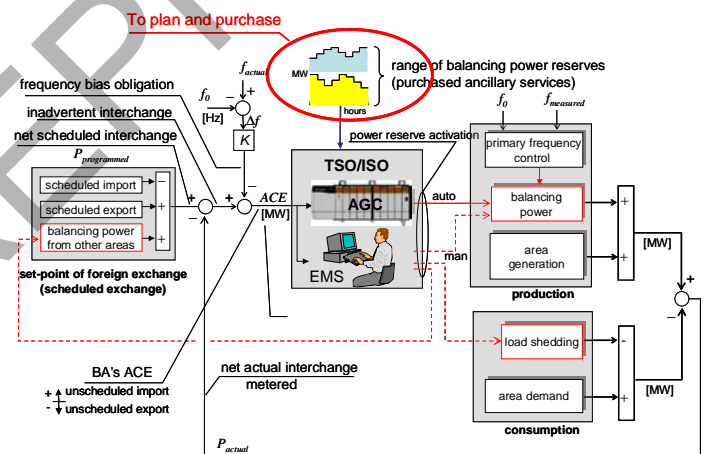


Figure 1 Power balancing in the area as a feedback control system Area Control Error (ACE) for one year area's operation.

Every TSO might adopt different AS planning procedures depending on interconnection and control area specificity. What make the problem more difficult are recent changes in market structures so there is a lack of long term experience in effective AS planning. The principles presented in the paper

might serve as a basis for a general platform adopting various criteria and constraints despite the fact that the approach was developed for one control area of the UCTE interconnection.

In chapter II problem definition is introduced. Chapter III describes proposed solution. In chapter IV achieved results are shown. Final chapter deals with conclusions and outlook for future work.

II. PROBLEM STATEMENT

Goal of presented work is to find AS combination with the least reservation cost that secures reliable transmission system operation. From optimization point of view the problem can be stated as a reservation cost minimization constrained by reliability standards that have to be met.

Reliability standards of the AS combination are evaluated by means of Monte Carlo simulation which incorporates transmission system statistical model parameterized by values obtained from processing of real operational data of the Czech transmission system and dynamic model of the AS activation. The list of AS considered is given in Tab. I as defined by the Grid Code of the Czech TSO [5]. Details of how the Simulator is designed and used in the Monte-Carlo scheme to calculate time series of ACE can be found in [4].

A. Ancillary services definition

In the planning algorithm five types of AS are considered: $RZSR$, $RZTR^+$, $RZTR^-$, $RZQS$ and $RZDZ$. Note that the method allows working with any other AS. AS definition changes from time to time and the algorithm will not be practical is restricted to particular AS only.

TABLE I
ANCILLARY SERVICES

Ancillary Service	Description	Guaranteed	Response time
RZPR (spinning)	primary control	Yes	~ 30 sec.
RZQS (non-spinning)	quick-start reserve (pumped-storage)	Yes	max. 10 min.
RZSR (spinning)	secondary control	Yes	max. 10 min.
RZN30+ (non-spinning)	stand-by reserve load change emergency assistance from abroad	Yes	max. 30 min.
		Yes	
		No	
RZTR+ (spinning)	tertiary control	Yes	max. 30 min.
RZN30- (non-spinning)	load change emergency assistance from abroad	Yes No	
RZTR- (spinning)	tertiary control	Yes	more than 30 min.
RZDZ (non-spinning)	stand-by reserve	Yes	
EregZ (non-spinning)	balancing energy	No	

B. Reliability standards

Result of Monte-Carlo simulation and control performance of used AS combination is expressed by area control error which is given:

$$ACE = \Delta P + K\Delta f, \quad (1)$$

where ΔP is an inadvertent interchange (measured difference between actual and scheduled interchange with neighboring areas), Δf is a frequency error (difference between measured frequency f_{actual} and the frequency set-point f_0) and K is a frequency bias of the control area. Formula (1) matches Fig.1 except for sign (polarity) of ACE. Fig.1 respects the way how ΔP is calculated by Czech TSO. By statistical processing of ACE reliability indices are obtained. Definitions and descriptions of reliability indices used by Czech TSO are shown in Tab. II.

TABLE II
RELIABILITY INDICES

Index name	Index unit	Description
$rACE_1$	%	Probability that the absolute average value of one-minute (clock minute) averages of ACE exceeds 100 MW over given period.
$rACE_{60}$	%	Probability that the absolute average value of one-hour averages of ACE exceeds 20 MW over given period.
$nACE_{1t}$	%	Number of events when ACE remains higher/lower +/- 100MW for time longer than 15 minutes in given period.
E^2_{100}	MWh ²	Sum of squared energy of events when ACE remains higher/lower than +/- 100MW for longer than 10 minutes in given period.
μ_{ACE_1}	MW	Average value of one-minute averages of ACE over given period.
σ_{ACE_1}	MW	Standard deviation of one minute averages of ACE over given period.
$\sigma_{ACE_{60}}$	MW	Standard deviation of one hour averages of ACE over given period.
E_{100}	MWh	Sum of absolute values of energy of events when ACE remain higher/lower than +/- 100MW for time longer than 10 minutes in given period.

C. Reservation cost evaluation

AS reservations cost evaluation is modeled by elasticity curves which respect relation between price and AS bids so that mean unit price for reservation is increasing with increasing amount of AS. Total reservation cost is given by

$$TC = \sum_{\forall RZxx} C_{RZxx} (RZxx) \cdot RZxx, \quad (2)$$

where $RZxx$ stands for ancillary services $RZSR$, $RZTR^+$, $RZTR^-$, $RZQS$ and $RZDZ$ respectively and $CRZxx$ denotes unit mean reservation cost of $RZxx$ given by its elasticity curve.

D. Reliability indices computation

Reliability indices for selected AS combination are generated by means of Monte-Carlo simulation [4]. Two hundreds of simulation runs were simulated for each AS combination to arrive at statistically better conditioned results. The core of the proposed method is the way how AS combination is selected.

III. BRANCH AND BOUND ALGORITHM DESCRIPTION

In this chapter a branch and bound algorithm used in the procedure of generating and selecting prospective combination of ACE is described. Principal scheme of the proposed algorithm is shown in (Fig. 2).

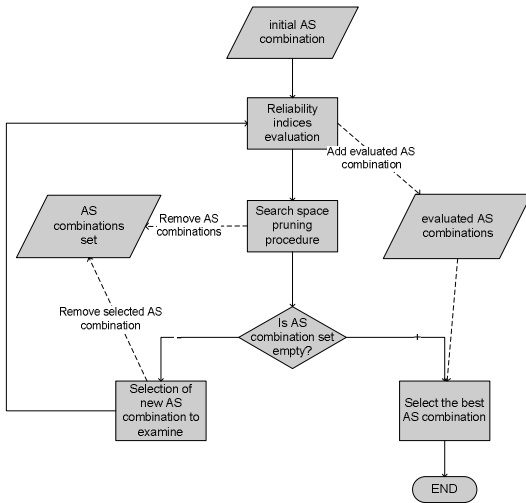


Figure 2 Principal scheme of the algorithm

Before starting the search algorithm several initialisation steps have to be completed. The search space of all AS combinations to examine is defined first. As only discrete values of reservation are expected, all AS reservations are separated into distinct values. Other constraints on reservation may be applied, e.g. minimum recommended volume of secondary regulation specified in [1] or maximum volume of AS certifications in regulation area. Step size and limits used in our studies are show in Tab. III.

TABLE III
Reliability indices

Ancillary service	Lower bound [MW]	Upper bound [MW]	Step size [MW]
RZSR	200	700	50
RZTR ⁺	0	700	50
RZTR	0	400	50
RZQS	300	1000	100
RZDZ	0	200	50

The next step is to specify reference value of reliability indices as a minimum requirement we would like to achieve. Reliability indices can be given directly or by means of reference AS combination. In that case reliability indices are determined by Monte-Carlo simulation with the reference AS combination.

Final step of initialization is to choose initial AS combination. If the reference combination is used then it is also taken as initial AS combination otherwise random selection applies.

A. Reliability indices evaluation

Next step after initialisation is generating ACE in Monte-Carlo simulation scheme of the control area operation and

getting the expected values of reliability indices from statistical processing of ACE time series.

B. Search space pruning procedure

Search space pruning depends on whether or not reliability standards are satisfied. In the first case we obtain upper cost estimation of optimal solution and hence every AS combination with reservation cost equivalent or greater than current upper bound can be removed from search space.

In latter case pruning algorithm is based on presumption of lower amount AS reservation, that is needed to assure reliable control area operation. that if the actual AS combination does not satisfy reliability standards, it is natural to expect that any combination with less reserves will not satisfy reliability standarts either, and can be deleted from the search space. To show that previous idea is correct the concept of monotonicity needs to be introduced. A reliability index is monotone in some AS if lower amount of the AS reservation implies higher value of the index and consequently less reliable control area operation. If monotonicity holds for all reliability indices the pruning method described above can be used. Due to the complexity of the modeled control area and the indices definition, the relation between the amount of AS and the value of indices is difficult to express analytically. Therefore simulation approach was employed to find index-service combinations where monotonicity does not hold:

$rACE_1$ index does not preserve monotonicity in RZTR⁺ and RZTR, (3)

$rACE_{60}$ index does not preserve monotonicity in RZSR, (4)

E^2_{100} and E_{100} do not preserve monotonicity in any AS, (5)

for the rest of reliability indices monotonicity holds. (6)

Therefore any AS combination for which monotonicity holds, and volume of AS is lower then the actual AS combination, can be remove from the search space.

C. Selection of new AS combination to examine

The cheapest AS combination found so far is returned as a solution when the search space is empty the search algorithm stops, otherwise we are looking for the new AS combination which will be examined in the next iteration. As in the previous step of algorithm, the AS selection depends on whether or not reliability standards are satisfied. First of all the next AS combination with lower amount of reserves in less utilized service is selected. If such combination does not exist in search space, AS combination with lower amount of the most expensive service is selected. If such combination does not exist the next AS combination is selected randomly. In the case when the reliability indices are not satisfied AS combination with higher amount of the most utilized service is selected. If such combination does not exist the next AS combination to examine is selected randomly.

By selecting the next AS combination the algorithm continues in next iteration as described in the paragraph A.

IV. SIMULATIONS RESULTS

In this chapter simulation results are presented. The algorithm was used in month-ahead AS planning. AS combination from year-ahead plan was taken as a reference. Reference reliability indices were computed by means of Monte-Carlo simulation of the control area with two hundreds of monthly runs using reference AS combination.

The algorithm performance is shown in two case studies.

A. Case study #1

The control area simulator is fed with three average monthly time series of ACE_0 , where ACE_0 is the expected area control error as would be without TSO's regulation reserve activations. Selected ACE_0 are average in sense of indices values calculated from ACE after TSO's regulation using the reference AC combination. Test inputs were chosen from 200 randomly generated ACE_0 that respect statistical behavior of the Czech control area.

B. Case study #2

Seven monthly ACE_0 time series equidistantly chosen from the same 200 time series as in the case #1, ordered by reliability indices computed with reference AS combination, were used.

Resulting reserves and the relative cost of their procurement in relation to the reference is shown in Tab. IV and Tab. V respectively. Reliability indices of the solutions are given in Tab. VI and Fig. 3.

TABLE IV
FOUND AS COMBINATIONS

	Ancillary services combination				
	RZSR [MW]	RZTR+ [MW]	RZTR- [MW]	RZSQ [MW]	RZDZ [MW]
Reference	290	260	100	570	160
Case #1	340	200	100	600	0
Case #2	280	100	150	700	100

TABLE V
RELATIVE COST OF THE FOUND AS COMBINATIONS

	Reference	Case #1	Case #2
Relative cost of reservation [%]	100,00	99,59	97,75

V. CONCLUSION

Developed algorithm was tested on month-ahead ancillary services planning problem. Ability of presented method was proven by two case studies show the ability of the algorithm of finding better solution than was the reference. However, not all indices were satisfied as can be seen (Fig. 3) that is because of

difference in accuracy between indices evaluation during planning procedure and in evaluation of the found solution by means of two hundreds of Monte-Carlo simulation runs. Minimalisation of this difference is main goal of the future development of the method.

TABLE VI
RELIABILITY INDICES OF THE FOUND AS COMBINATIONS

		Reference	Case #1	Case #2
Reliability indices	$rACE_1$	2,65	2,61	2,68
	$rACE_{60}$	2,86	2,49	2,80
	$nACE_{1t}$	0,07	0,05	0,06
	E_{100}^2	523 265	1 225 797	1 619 786
	μ_{ACE_1}	-0,63	0,15	0,42
	σ_{ACE_1}	45,39	46,17	46,88
	$\sigma_{ACE_{60}}$	11,69	13,04	14,12
E_{100}	25 715	25 766	25 930	

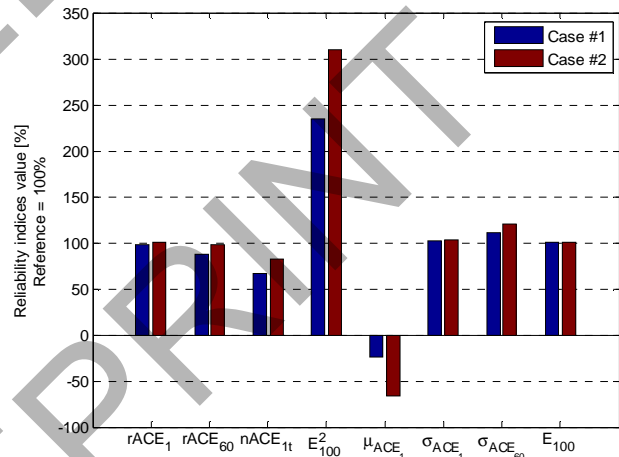


Figure 3 Relative values of reliability indices

REFERENCES

- [1] UCTE Operation Handbook, v2.2/20.07.04, Union for the Co-ordination of Transmission of Electricity, Brussels (2004)
- [2] Reliability Standards for the Bulk Electric Systems of North America, North American Electric Reliability Corporation, Princeton, NJ (2008)
- [3] P. Havel, P. Horáček, V. Černý, J. Fantík: Optimal Planning of Ancillary Services for Reliable Power Balance Control, *IEEE Trans. on Power Systems*, Vol. 23, No. 3, 1375-1382 (2008)
- [4] V. Černý, P. Janeček, A. Fialová, J. Fantík: Monte-Carlo simulation of electricity transmission system operation, in *Proc. 17th IFAC World Congress*, Seoul, Korea, 2008.
- [5] Rules for the Transmission System Operation Extract from the Grid Code, Revision 09, ČEPS a.s., (January 2009), [online], http://www.ceps.cz/doc/kodex/part_I_II_III_an_rev09.pdf

Biofuels- the power from plants

Grzegorz Maliga ^a, Amar Patil ^b

^a Phd's student of Department of Mechanical and Power Engineering, Wrocław University of Technology
grzegorz.maliga@pwr.wroc.pl

^b MSc's student of Department of Computer Science, Wrocław University of Technology
amar.ec006@yahoo.co.in

Abstract

In this paper I try to review five fundamental groups of biofuels which are used as a power source for mechanical engines. However engines could be use as a propulsion in cars or other machines and as a current source when engines cooperate with generators.

The basics biofuels which belong to the fundamental group are: rapeoil, biodiesel, biomethanol, methan from biogas and synthetic biofuel. I present calorific value of these kind of biofuels and compare to earthfuels.

In Europe the leader of production biofuels is Germany. On the basis of this country I present how the biofuel industry developed in the last ten years and what kind of benefits is possible to gain. I describe also political and law conditions which influence by using biofuels.

Finally, I pay attention to the most important result of using biofuels which is influence to environment, because producing and burning biofuels take a part in the same carbon dioxide cycle.

Keywords: biofuels, biodiesel, biomethanol, rapeoil, fuels from biomass

1. INTRODUCTION

At present we have an awareness that the sources of fossil energy are becoming lower. In order to stop the disadvantageous phenomenon of decreasing raw fuels and changing climate, we need to start using gradually a new sources of renewable energy. Renewable energy was common used till the 18th century from that supplies as wind and wood. After the industrialisation changes and improves people started used fossil sources of energy. In the 19th century the renewable sources of energy were completely replaced by coal, oil and earth gas. These changes were as a consequence of huge industrial growing which required a more efficient and high calorific value sources of energy than wood or wind energy. Today result is that 90% of energy which we use becomes from fossil resources. Using and burning coal, oil and earth gas influences very inconvenient on climate and environment because producing energy from raw fossil fuels releases great size of carbon dioxide into atmosphere in short time, which results in greenhouse effect. On possible solution to decrease greenhouse effect is becoming greater of using fuels, which producing and burning

take part in the same dioxide cycle. These kind of fuels are producing from plants and generally are divided in two groups such as: biomass and biofuels. Biomass characterises as raw kind of fuels for example wood, straw or pellets, which are generally burned in furnace in order to produce heat.

Whereas biofuels describe as kind of fuels which are producing from raw biomass such as corn or plants wastes in enrichment process. To biofuels group belong: rapeoil, biodiesel, biomethanol, biomethanol and synthetic biofuel. The biggest advantage of biofuels, compare to biomass, is high level of calorific value sometimes similar to fossil fuels. Current life standarts require from people high mobility, which influences on using some kinds means of transport such as cars, trucks or others. The common feature of propulsion machines is converting one form energy (for example chemical) to mechanical, which occur in internal combustion engines. In order to access satisfactory efficient and working opportunities, are used fuels which have calorific value on level about 40 MJ/kg such as diesel, petrol or liquid petrol gas. These kind of fuels can be replaced only by biofuels, because the calorific value level is comparable and they can be adapt by modern engines developments.

Biofuels are also easy to storage and management, which means that new technology, high investment and infrastructure are not necessary for using biofuels. For these reason in Germany in 2005 the share of biofuels was around 3.6 % of total fuel consumption. The large part of these biofuels is biodiesel.

In the future for become greater the producing of biofuels, larger areas have to be cultivated than now. Interesting is also aspect how is the impact increasing cultivated areas for energy on restrict food production. Whereas the productivity of agriculture has risen constantly and the trend will maintain in the future. For example in Germany the share of freed land for non food production has increased [1]. In 2005 over one million hectares were cultivated for energy production from rapeseed, rye and wheat. Specialist predicted that till 2030 the area for energy production will approach to four million hectares.

The predictions also shows that in Germany the biofuels share of total fuel supply in 2020 can achieve 25%.

II. BIODIESEL

The most widespread of biofuels is biodiesel, because it is adapted to the diesel engines. For example in Germany biodiesel contributes around 18 million tons per year to the fuel consumption [1]. From 2004 the mineral oil corporation add biodiesel to original diesel by 5 %, which allows to carry out technical requirements for vehicle owners.

TABLE I
BIODIESEL BASIC INFORMATIONS [1]

Raw materials:	Rapeseed or other vegetable oils
Annual yield per hectare	1550 l/ha
Fuel equivalent	1l biodiesel substitutes 0.9 l of diesel
Market price	0.75-0.90 EUR/l
CO ₂ reduction	Approx. 70 %
Technical information	Biodiesel in pure form: manufacturer's approval required; mixtures up to 5 % without refitting the engine

From chemistry point of view biodiesel is a vegetable oil's methyl ester or fatty acid methyl. Biodiesel production behaves by ester interchange of vegetable oil. For this reaction the methanol is required and mixed in a ratio of 1:9. In temperature of 50 to 80°C a catalyst is added in quantity around 0.5 to 1 %. The nature of reaction which occurs, the vegetable oil molecule composed of glycerine and three fatty acid chains is broken down. The fatty acids combine with the methanol to form biodiesel. Glycerine is produced and later used in many fields such as pharmaceutical or food industry.

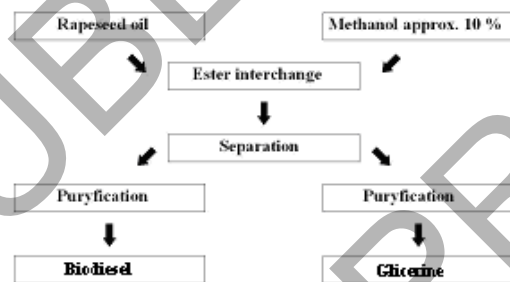


Figure 1. Ester interchange of rapeseed oil to create biodiesel [1]

Using the biodiesel to the engine is depended on viscosity and ignition properties, which are similar to fossil diesel. By adding some components the ability of using in winter is possible without difficult to minus 20°C. Important is also the lubrication effect which is higher than fossil fuels. Consumption of biodiesel is 5 % more than diesel because the yield energy is lower.

The requirements necessary for the fuel quality are defined in the Europe standard DIN EN 14214.

III. BIOETHANOL

Biodiesel and vegetable oil are useful by diesel engines but bioethanol can replace petrol. Bioethanol can be mixed with petrol from mineral oil manufactures in share up to 5 %. For use more share of bioethanol the vehicles should be adapted.

Ethanol is produced by fermenting the sugar included in plants. The sugar starch and cellulose-bearing occur mainly in wheat, rye, maize and sugar beet. In the future by development of well-fitted enzymatic processes also the wood, and straw could be fermented.

TABLE II
BIOETHANOL BASIC INFORMATIONS [1]

Raw materials:	Grain, sugar
Annual yield per hectare	2560 l/ha
Fuel equivalent	1l biodiesel substitutes 0.66 l of petrol
Market price	0.50-0.60 EUR/l
CO ₂ reduction	30- 70 %
Technical information	Can be mixed with fuel by up to 5 %

The raw plants which included sugar are fermented by yeast and enzymes to ethanol. When plants contain the starch, that first the starch is converted into sugar by enzymes. From fermentation process the by-product which occurs in large quantities can be used later as fodder for the biogas plants.

Properties of ethanol improve the quality of petrol, because the alcohol has a higher octane value than petrol. When the octane value is higher, it means the better antiknocking property. But the disadvantage of bioethanol compared to petrol is calorific value, which is one third lower than conventional petrol. After mixing ethanol increases the vapour pressure of fuel.

Since 2005 in Germany many series vehicles are available to run with ethanol proportion up to 85 %, which is called flexible-fuels.

Mixing ethanol with petrol is restricted by petrol fuel standard DIN EN 228 permits mixing of up to 5 % of ethanol with petrol. For example when the 5 % by volume of all petrol fuels were to be replaced by ethanol, this would be around 1.3 million tons per year.

IV BIOMETHANE

Biomethane is called as a biogas, which is for example gained in agricultural facilities, in general by the fermentation of maize silage or manure. To produce biogas can be used many kinds of organic substrate. Farms, which basen on cattle or pigs husbandry, can use animal excrement, as a main material for anaerobic fermentation. On the other hand there are a lot of farms where only plants are used for energy production. In this kind of farms they exploit new renewable materials as crops, grass,

maize, sunflowers and others. To increase biogas production and to utilize non-agricultural but organic wastes some biogas factories use the residues from food industry such as vegetable from wholesales, distiller's wash or grease. The process of residues fermentation provides many benefits, because the dealing cycle of waste food is closed and it is hygienic.

In Germany the substrate, which are used for biogas production are constituted of 48 % animal excrement, 26 % organic waste and 26 % renewable raw materials.

The biogas is end product of fermentation, which is combustible and it is composed as:

- 50-75 % methane
- 25-45 % carbon dioxide
- 2-7 % water
- < 2 % oxygen
- < 2 % nitrogen
- < 1 % ammonia
- < 1 % hydrogen sulphide

The content of energy is dependent on the methane concentration. For example when a substrate as the fats and starch are used, which are easy to break down in fermented mass, the content of methane is greater. Compared to fossil fuels the calorific value of 1 m³ of biogas is substitute for 0.6 l of heating oil.

TABLE III
BIOGAS BASIC INFORMATIONS [1]

Raw materials:	Maize and other energy producing plants
Annual yield per hectare	4950 m ³ or 3560 kg
Fuel equivalent	1 kg of methane substitutes 1.4 l of petrol
Market price	-
CO ₂ reduction	-
Technical information	Biomethane can be used in natural gas vehicles without adjustments

In Germany the producing of biogas is around 23-24 billion m³/year. From agricultural sector provide about 85 % of them. When we compare the amount of biogas to all energy consumption in Germany, it represents only about 3 %.

The biggest disadvantages of gas sources are transport and storage compared to liquid fuels. Methane requires more space for storage and their density of energy is lower. For example in natural gas vehicles, the methane is compressed in peculiar pressure tanks, which are installed and adapted to pressure of 200 bar. The most benefits of using biogas compared to petrol and diesel is very low emission of several toxic substances, mainly nitrogen oxides or reactive hydrocarbons, which can be reduced by up to 80 %. Biogas is able to be used for running the motor vehicles. For example in Germany is about 56 million cars and only 35000 run with natural gas. These cars could use biogas in the future without technical adjustment.

V RAPEOIL

The rapeoil is not only used as raw material for biodiesel production, but can be used originally in specially diesel engines. From wide variety of vegetable oils the rapeoil is most economically cultivated compared to sunflower or soya oil.

Production of rapeoil is divided into two groups: one is industrial and the second is decentralized.

Decentralized yield of rapeoil is conducted on farm by cold pressing, where the rapeseeds are pressed by mechanical force at maximum of 40°C. After pressing suspended solids are captured by filtration or sedimentation from oil. The press cake contains over 10 % of oil, which is used later as a fodder. Industrial production is centralized, where the rapeseeds are pressed at high temperature around 80°C and the oil is extracted from cake with solvent. Later the solvent is separated from the oil by evaporation. Next step is refining process, because the oil still has unpleasant components. The end product is fully refined and has quality as edible oil.

The properties of rapeoil are specific, which makes it different from diesel and using in combustion engines is possible after refitting. First large difference is viscosity, which in low temperatures is up to 10 times higher than diesel. High viscosity leads to technical challenges in winter and cold starting in conventional engines, because the flashpoint is significantly higher than in normal diesel. On the other hand the storage and transport of oil is more safety. Rapeoil is not included in any hazard classes according to the Ordinance for Flammable Liquids.

TABLE IV
RAPEOIL BASIC INFORMATIONS [1]

Raw materials:	Rapeseed oil
Annual yield per hectare	1480 l/ha
Fuel equivalent	1 l of rapeseed oil substitutes 0.96 l of diesel
Market price	0.55-0.75 EUR/l
CO ₂ reduction	>80 %
Technical information	Engine refit necessary

When the raw rapeoil is required to be used as a fuel, the engine should be refitted to adapt to the viscosity and combustion properties of the rapeoil. Same refitting is based on the pre-heating system, where the fuel and injection system are heated before starting engine. Other way is based on 2-tank system, where engine starts with diesel and after required time is changed to rapeoil.

In Germany is about 250 filling stations with rape or vegetable oil. The pure fuel cost is lower than diesel, but the costs for refitting and more frequent oil changes are incurred, from these reasons a driving car with rapeoil fuel becomes economically viable from 100000 kilometers of driving.

VI SYNTHETIC BIOFUELS

The synthetic fuels are new development and still not available on the market. The raw material for this kind of synthetic fuels is biomass. The idea of synthetic biofuels is becoming the biomass to liquid form, which could be adapted to current engine concepts. The most advantage is that very many different materials, such as biological waste, straw or wood, can be used for production the synthetic biofuels.

The process of manufacture the synthetic fuels from biomass is in two stages. In the first stage, which is called gasification, a synthetic gas is produced in a reactor, where the biomass is placed and broken down in the presence of heat, pressure and oxygen. After first stage the synthetic gas compose mainly of hydrogen, carbon monoxide and carbon dioxide. In the second stage componets are synthesised from this, which is able to be processed to synthetic biofuel end product.

The chemical properties of hydrocarbons in synthetic biofuels allow efficient and complete combustion with low exhaust gas emission. The properties can be influenced by changing parameters during synthesis such as the pressure, temerature and catalysts. Modern fuels and engines could be adapted each other and could be able to fulfil the requirements for the less emission and improving energy efficient.

TABLE V
SYNTHETIC BIOFUELS BASIC INFORMATIONS [1]

Raw materials:	Plants and wood
Annual yield per hectare	4030 l/ha
Fuel equivalent	1 l of synthetic fuel substitutes 0.97 l of diesel
Market price	-
CO ₂ reduction	>90 %
Technical information	Can be used in pure form or in mixtures without adjustment of engine

Based on the current knowledge, in the future will be possible to transfer about 50 % of energy contained in vegetable raw materials to synthetic biofuels under optimum conditions. From this reason it can result in large carbon dioxide saving.

VII CONCLUSIONS

In spite of full of promise potencials of biofuels, the combustion engine in combination with fossil diesel and petrol will dominate the transport sector in the future. Propably be not the only strategy to save or replace the fossil fuels. Some of them have immediate effect and other like biodiesel or bioethabol will contribute large amount of fossil fuels. Till 2010 they will share about 5 % of fuels market by mixing with conventional fuels.

From all of biofuels, the synthetic biofuels give the greatest opportunity of potential quantities in the long term, but they will make a contribution after 2010, when them production will be on an industrial scale. Till 2020 their consumption share could increase to 9 %.

The opportunities of biofuels consumption share is depended on tax incentives and promotion of research.

- [1] www.fnr.de
- [2] Harry D. Saunders, Virtual biofuels- A cheaper, better, faster alternative; Energy Policy 36, 1247-1250, 2008.
- [3] C. Bomb, K. McCormick, E. Deurwaarder, T. Kaberger, Biofuels for transport in Europe; Lesson from Germany and the UK, Energy Policy 25, 2256-2267, 2007.
- [4] J. Peters, S. Thielman, Promoting biofuels: Implications for developing countries, Energy Policy 36, 1538-1544, 2008.
- [5] E. Kondili, J. Kaldellis, Biofuel implementation in East Europe: Current status and future prospects, Renewable and Sustainable Energy Reviews, 11, 2137-2151, 2007.

Guideline for the Investigation of PEM Fuel Cell Systems in Automotive Applications

M. Heuer, M. Käbisch, G. Heideck, Z. A. Styczynski
Otto-von-Guericke University Magdeburg
Universitätsplatz 2
Magdeburg, Germany

Abstract-In the context of a research project in the field of energy conversion and drive systems at the Otto-von-Guericke University Magdeburg, four proton exchange membrane (PEM) fuel cell systems of the newest generation have been put into operation. The investigations refer to stationary and mobile applications as well as to lifetime tests of the fuel cell. The plants are presented and scheduled measurements plus the research goals are described. The operational behaviour of the fuel cell and the overall system are evaluated for long-term investigations. A further emphasis is on the behavior of several fuel cells, which are operated with different gas compositions. Because the measurements are still in the early stages, the report mainly describes the project goals and gives an overview of fuel cell technology.

I. INTRODUCTION

Both the conventional and the alternative energy industry are undergoing strong changes due to the intensive price fluctuations of fossil energy sources in the last few years [1]. The future global energy supply can be realized only by an increase in the amount renewable energy, in order to ensure a safe and stable energy supply in public and private life. Apart from the renewable energy from sun, wind, earth energy and biomass, hydrogen is another option, which through industrial or renewable processes makes it possible to convert chemical energy in fuel cells into electricity and use it at any time, independent of the volatile energy supply from alternative energy sources.

The electrical and thermal energy supply from the fuel hydrogen in fuel cells has already been successfully tested at research institutions and in the industry for over 20 years. The market introduction of fuel cell systems to the home energy supply or to the driving power in vehicles is, however, delayed. This delay is due to the current lack of a comprehensive hydrogen infrastructure and also because material problems with the electrolyte and the membrane of the fuel cell have not been solved yet.

In a research project in the field of automotives in a scientific instrumentation proposal of the German Research Foundation, four PEM fuel cell systems with an electrical power between 400W and 5000W are examined under different aspects and future areas of application of PEM fuel cells are tested. The measurements will begin fully in the spring of 2009.

II. INTRODUCING OF FUEL CELL SYSTEMS

The investigations are directed at four PEM fuel cell systems in the electric power range between 400 and 5000W. These are low-temperature fuel cells with a maximum operating temperature of 80°C on the primary water side. The high temperature PEM fuel cells work at temperatures of up to 180°C and have been tested only for a few years in the field of research [2]. The plants in this project, however, are not designed for this type of high temperature PEM fuel cells.

The fuel cell group consists of three systems with an electrical output in the range of 400-500W and one system with an output power of approximately 5kW of electric and 10kW of thermal power. Each plant is different in its procedural process structure and is used for various measurements and investigations. The three small plants are named the "Reformate", "Hydrogen" and "Experimental" plants.

The reformat fuel cell system is operated with hydrogen from an electrolysis plant and carbon dioxide from pressure cylinders. The fuel composition is derived from the actual reforming of natural gas or biogas after the reforming stage. The real proportions of hydrogen and carbon dioxide through the reformation were measured by another fuel cell system with an integrated reformer. These measurements are now available for the simulated gas composition of the reformat plant. Depending on the efficiency of the reformer and electric power of the fuel cell, the proportions of hydrogen is at a maximum of 70% and carbon dioxide at 30%. This unit is designed for long-term studies in the stationary operation for the domestic energy supply. Both the fuel cell system as well as the components of the plant will be investigated after several thousand hours of operation. The hydrogen plant was developed with much more variability in its operation mode and operates with pure hydrogen from the electrolysis plant. Different modes of operation can be implemented, which can be used for different applications. For example a recirculation of unused hydrogen, which does not react at the membrane, is integrated by being pumped back to the inlet hydrogen channel of the fuel cell. The practical effect of recirculation on the fuel consumption and material compatibility of the pumps on the humid and heated hydrogen are an essential aspect of the investigations of this facility.



Figure 1. Fuel cell test benches "Reformate", "Hydrogen" and "Experimental" (from right).

Another focus is the behaviour of the bipolar plates under various operating conditions. The bipolar plates form the gas channels through which the fuel and oxygen lead to the membrane, whereby hydrogen is on the anode side and oxygen of the ambient air is on the cathode side. The correct construction of these channels is responsible for low pressure drops and for an effective use of the air compressor. The air compressor has the largest energy consumption of the fuel cell system. The bipolar plates have been especially designed for each fuel cell system by the manufacturers. The test results of this new generation of bipolar plates and the use of a new membrane show development progress in this field. The hydrogen plant is suitable for investigations in the mobile and portable fields in which pure hydrogen and no gas compositions are used. The system will be tested in the range of auxiliary power units (APU) for automobiles and the possibilities will be explored for a reduction of fuel consumption through the use of a fuel cell.

The third plant is used for system optimization. Individual components are tested and developed with the goal of minimizing energy expenditure and simplifying and optimizing the management processes. The development work in this area should be introduced in the other plants, so that the entire system is improved in its efficiency.

The 5kW plant will be supplied with pure hydrogen from a tank reserve on the university campus. The main focus of this plant lies in the mobile application. The various modes of hydrogen management in the system and the ability of the moistening of the reaction gases to the optimal energy conversion at the cell membrane are the subject of investigations.

All four units are connected via a network and can be controlled in the laboratory as well as with remote access.



Figure 2. 5kW fuel cell facility for mobile tests.

III. FUEL CELL RESEARCH FOR STATIONARY APPLICATION

The power supply for households is being decided ever more strongly by decentralized energy installations directly at the site of the end customers. Solar systems, small wind turbines or wood pellet heating systems will find increased use in single and multi-family houses. In this application market, fuel cell systems offers a great potential as combined heat and power plants, to provide both the electrical and thermal energy. The prerequisites include 40,000 operating hours, low downtime, comparable costs in the range of existing home power systems, and the useful hydrogen production from renewable energy sources. However, an introduction to the market of such stationary fuel cell plants in private households is expected yet. At the moment different projects involving fuel cell plants are being used and tested in households by the end customers in their everyday employment [3].

The tests for stationary applications are based on load profile curves of single and multi-family houses. Load profiles are copied during a longer period. Here, the actual performance of the fuel cell is scaled down to the power in the household. From the result of several thousand operation hours, the achievement performance of the fuel cell and life time prognoses should be determined. Figure 3 shows the load profile of a single family house on one summer day at the weekend. From the existing data records, the fuel cell system can now be operated as a house power supply plant.

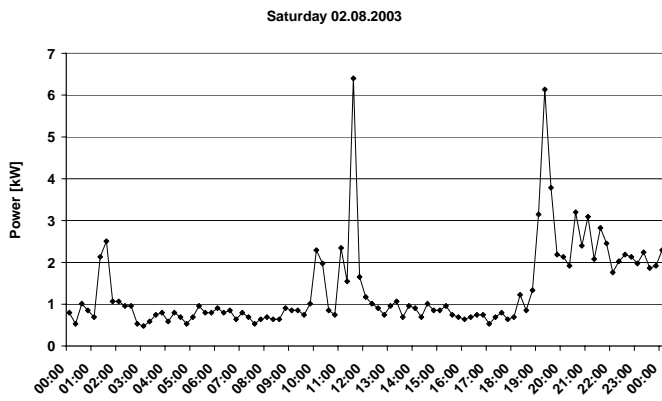


Figure 3. Load profile of a four person household [4].

IV. FUEL CELL RESEARCH FOR MOBILE APPLICATION

The automobile and its different propulsion principles are undergoing great changes. The European Union calls for drastic reductions of emissions in the transport sector through new innovative drive concepts to ensure mobility and to be independent of limited fossil fuels. This can be achieved by more efficient engines, the integration of energy storage such as batteries to minimize the consumption and to reduce local emissions in hybrid vehicles as well as the long-term market conquest by fuel cell and electric vehicles. The battery technology of electric vehicles is not currently in a position to travel distances in excess of 100km, so this energy storage is used especially in urban areas. The fuel cell can travel distances of up to 300km using new storage technologies, like the 700 bar storage of gaseous hydrogen [6]. For example, fuel cell buses have already been driving in the public traffic for several years in Hamburg and Berlin.

Illustration 4 shows the energy expenditure for a distance of 100km for different engines, whose fuel originates from different energy resources. It can be clearly seen that fuel cell vehicles possess less energy expenditure than conventionally moved vehicles only during renewable hydrogen production.

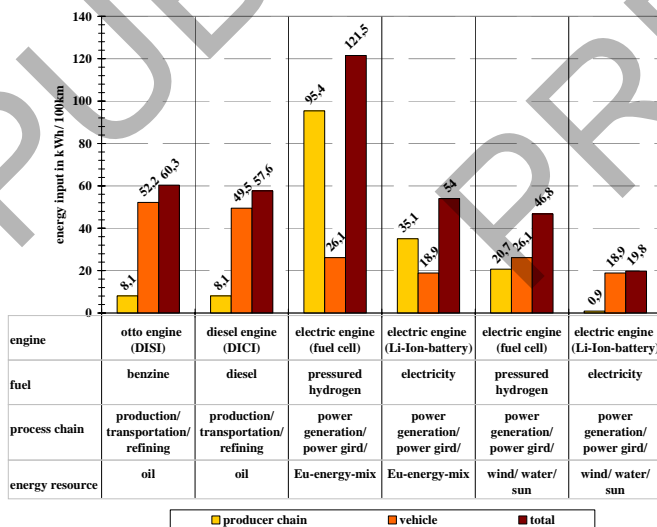


Figure 4. Energy expenditure of different engines and fuels [5].

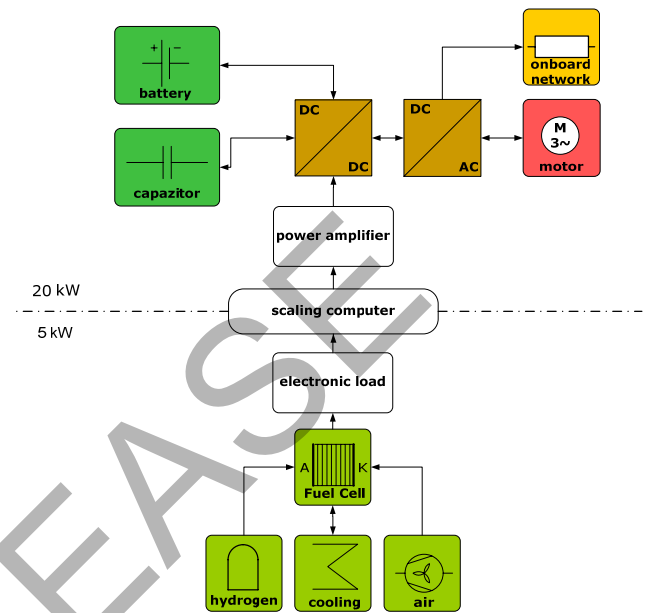


Figure 5. Scheme of the mobile fuel cell system [7].

The reason for this is that at the moment, the production of hydrogen is still energy-intensive. Battery vehicles exhibit in contrast smaller energy expenditure in the European energy mix and especially with regard to the renewable energy supply.

As previously stated, the 5kW system is used in the research project for mobile applications. Figure 5 shows the experimental scheme between the fuel cell and an electric motor. The energy of the fuel cell is delivered to a load and a scaling calculator increases the electric power of 5kW up to 20kW. The use of power electronics, inverters, electrical motor and storage systems such as batteries and super capacitors constitute the entire power train of a vehicle. The whole system is tested by driving cycles and the interaction of the different energy storages is investigated. During rapid load changes, the super-capacitors should guarantee the dynamics of energy supply.

V. LIFETIME PREDICTION OF FUEL CELL AND GREEN FUEL

The lifetime of the fuel cell stack is the main criterion for the market launch of fuel cell systems for various applications. Also after 5,000 or 40,000 operation hours the electrical power output may decrease only insignificantly. The lifetime estimation can be accelerated by lifetime tests. This requires more stringent operating conditions. It should be noted, however, that the meaningfulness of such accelerated tests is limited, because key operating conditions such as downtime and its impact on the fuel cell will be not considered. In contrast, real operating conditions of several plants under realistic dynamic loads are more meaningful. A disadvantage is however the expenditure of time.

A combination of accelerated tests and the influence of key parameters and criteria that can only occur under real conditions will be introduced in the investigations. From these measurements lifetime curves arise for one type of fuel cell,

depending on the design of bipolar plates and type of membrane used and other components. From the comparison of several fuel cells then prognoses for the lifetime and for influence parameters are to be identified.

A further influence parameter on the lifetime is the quality of the fuel and its composition. By using different gas compositions and humidity ratios influencing factors have to be identified and have to be integrated in lifetime forecasts. Above all, the quality of the fuel gas and its monitoring is an important aspect in these studies.

VI. CONCLUSION

This paper gives an overview of the future studies on four new PEM fuel cell systems for mobile and stationary applications. In addition to lifetime predictions and measurements in simulated fuel compositions, system optimization is also in the foreground. The results feed directly into the system optimization of fuel cell systems of project partners.

REFERENCES

- [1] "HZwei," Magazine for hydrogen and fuel cells, Kremmen: October 2008, pp. 3.
- [2] J. Zhang et al. "High temperature PEM fuel cells," Journal of power sources, 2006.
- [3] A. Ballhausen, "Small stationary CHP-systems- overview about the status quo," fuel cell conference, Braunschweig: 2008, pp. 115-124.
- [4] C. Heyde, "Energy management strategies for grid connected photovoltaic plants with battery storages," diploma thesis, Otto-von-Guericke University, Magdeburg: 2006.
- [5] "Well-to-Wheels analysis of future automotive fuels and powertrains in the european context," study of CONCAWE, EUCAR und JRC, 2005.
- [6] "HZwei," Magazine for hydrogen and fuel cells, Kremmen: July 2008, pp. 12-14.
- [7] M. Käbisch, "Test Bench Development for Investigation Fuel Cell Technology in Automotive Application," Proceedings of the ReDiPS Workshop, Athens: September 2007, pp.66-71.

Wind Turbine Driven Doubly-Fed Induction Generator with Grid Disconnection

B.Chitti Babu^{#1}, K.B.Mohanty^{#2} and C.Poongothai^{*3}

[#] Department of Electrical Engineering, National Institute of Technology Rourkela
Rourkela-769008 (India)

¹ bcbabunitrkl@ieee.org

² kbmohanty@nitrkl.ac.in

^{*} Department of Electrical Engineering, Indian Institute of Technology Madras
Chennai-600036 (India)

³ ee08d002@smail.iitm.ac.in

Abstract—This paper describes the transient behaviour of a doubly-fed induction generator (DFIG) driven by wind turbine after its disconnection from the grid. The induction machine runs at a specific speed with the stator disconnected from the grid ($I_s=0$), the rotor is suddenly excited with slip-frequency voltages derived from voltage regulators so as to produce commended open-circuit stator terminal voltage. Behaviour under varying rotor speed typically observed in wind turbines is also reported. A MATLAB computer simulation study was undertaken and results on 1.5 kW wind turbine are presented.

Index Terms- Doubly-Fed Induction Generator (DFIG), Variable-speed wind turbine, Dynamic Modeling, Grid Disconnection, Transient Analysis

I. NOMENCLATURE

V_{qs}, V_{ds} are the three-Phase supply voltages in d-q reference frame, respectively

i_{qs}, i_{ds} are the three-Phase stator currents in d-q reference frame, respectively

$\lambda_{qs}, \lambda_{ds}$ are the three-Phase stator flux linkages in d-q reference frame, respectively

V_{qr}, V_{dr} are the three-Phase rotor voltages in d-q reference frame, respectively

i_{qr}, i_{dr} are the three-Phase rotor currents in d-q reference frame, respectively

$\lambda_{qr}, \lambda_{dr}$ are the three-Phase rotor flux linkages in d-q reference frame, respectively

r_s, r_r are the stator and rotor resistances of machine per phase, respectively

L_{ls}, L_{lr} are the leakage inductances of stator and rotor windings, respectively

ω_e, ω_r are the supply and rotor angular frequency (electrical speed), respectively

T_e is the electromagnetic torque

P_s, Q_s are the stator-side active and reactive powers, respectively

P is the Number of poles

II. INTRODUCTION

For stand alone or autonomous operation, mostly single induction generator or parallel operated induction generators are focused according to available analysed references. These induction generator driven by the individual prime movers employed excitation capacitor bank to build up desired voltage via self-excited phenomena. Hence the value of the excitation capacitor bank and the rotor speed determine the magnitude of the generated voltage and its frequency. Both voltage and frequency need to be controlled to feed the power to the load. But for grid connected operation, there are two types of generators are used. (i.e., single output and double outputs). In order to feed the active power to the grid, the machine should run at a speed greater than the synchronous speed of the revolving magnetic field. (i.e. slip should be negative). The single output generator feeds active power to the grid via only stator side and double output generator feeds electrical power to the grid via both stator as well as rotor side. The latter is also called static Kramer, double-fed or double outputs induction generators. This is only the generator which generates the power more than rated power without overheating. Besides, this kind of power generation usually causes problems in the utility grid system. Because the control on active and reactive power of the machine is complex one. Wind turbines often do not take part in voltage and frequency control and if a disturbance occurs, the wind turbines are disconnected and reconnected when normal operation has been resumed. As the wind power penetration continually increases, power utilities concerns are shifting focus from the power quality issue to the stability problem caused by the wind power connection. In such cases, it becomes important to consider the wind power impact properly in the power system planning and operation. This paper will focus on the grid-connected induction generator feeding power with DOIG during steady state and transient conditions.

This paper describes the transient behaviour of a doubly-fed induction generator (DFIG) driven by wind turbine after its disconnection from the grid. The induction machine runs at a specific speed with the stator disconnected from the grid ($I_s=0$), the rotor is suddenly excited with slip-frequency voltages derived from voltage regulators so as to produce

commended open-circuit stator terminal voltage. Behaviour under varying rotor speed typically observed in wind turbine is also reported. A MATLAB computer simulation study was undertaken and results on 1.5 kW wind turbine are presented.

III. DFIG DYNAMIC MODELLING

A commonly used model for induction generator converting power from the wind to serve the electric grid is shown in Fig.1. The stator of the wound rotor induction machine is connected to the low voltage balanced three-phase grid and the rotor side is fed via the back-to-back IGBT voltage-source inverters with a common DC bus. The network side converter controls the power flow between the DC bus and the AC side and allows the system to be operated in sub-synchronous and super synchronous speed. The proper rotor excitation is provided by the machine side power converter.

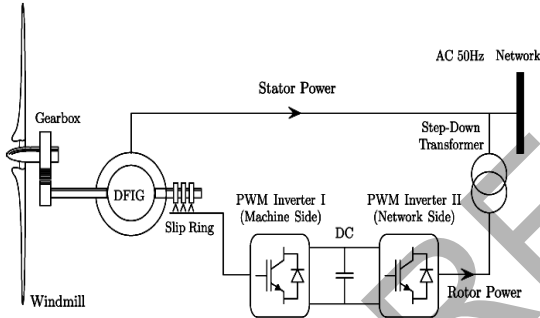


Fig. 1. Model of DFIG Wind Turbine

The general model for wound rotor induction machine is similar to any fixed-speed induction generator as follows.

A. Stator Voltage Equations

$$\begin{aligned} V_{qs} &= p\lambda_{qs} + \omega\lambda_{ds} + r_s i_{qs} \\ V_{ds} &= p\lambda_{ds} - \omega\lambda_{qs} + r_s i_{ds} \end{aligned} \quad (1)$$

B. Rotor Voltage Equations

$$\begin{aligned} V_{qr} &= p\lambda_{qr} + (\omega - \omega_r)\lambda_{dr} + r_r i_{qr} \\ V_{dr} &= p\lambda_{dr} - (\omega - \omega_r)\lambda_{qr} + r_r i_{dr} \end{aligned} \quad (2)$$

C. Power Equations

$$\begin{aligned} P_s &= \frac{3}{2}(V_{ds} i_{ds} + V_{qs} i_{qs}) \\ Q_s &= \frac{3}{2}(V_{qs} i_{ds} - V_{ds} i_{qs}) \end{aligned} \quad (3)$$

D. Torque Equation

$$T_e = -\frac{3}{2} \frac{P}{\omega} (\lambda_{ds} i_{qs} - \lambda_{qs} i_{ds}) \quad (4)$$

E. Stator Flux Linkage Equations

$$\begin{aligned} \lambda_{qs} &= (L_{ls} + L_m) i_{qs} + L_m i_{qr} \\ \lambda_{ds} &= (L_{ls} + L_m) i_{ds} + L_m i_{dr} \end{aligned} \quad (5)$$

F. Rotor Flux Linkage Equations

$$\begin{aligned} \lambda_{qr} &= (L_{lr} + L_m) i_{qr} + L_m i_{qs} \\ \lambda_{dr} &= (L_{lr} + L_m) i_{dr} + L_m i_{ds} \end{aligned} \quad (6)$$

IV. TRANSIENT ANALYSIS DURING GRID DISCONNECTION

Fig (2) shows the three phase stator voltages under normal operating conditions. When the induction machine is running at a particular speed while the stator disconnected from the grid. So the rotor is suddenly got excited due to slip frequency rotor voltages from the voltage regulators in order to produce the commended stator terminal voltage. Since the variation of speed of the rotor, torque could also be varied on the machine. Fig (3) shows the transient response of the stator voltage of induction generator under torque disturbance. It is found that the voltage of the stator becomes slightly small value after disturbance. Fig (4) shows the transient response of the rotor voltage of induction generator under torque disturbance. Fig. (5) shows the transient response of the active power of the induction generator during disconnection. When induction generator is disconnected from the grid, the active powers supplied from induction generator decreases and quickly recover to original value after re-closed to the grid. The changes in a reactive power are also shown in Fig. (6). It is observed that the reactive power absorbed by the induction is also decreases rapidly, but the part of reactive power would be supplied by rotor side converter for compensation during re-closed to the grid. Negative values of active and reactive power indicate the machine working in generating mode.

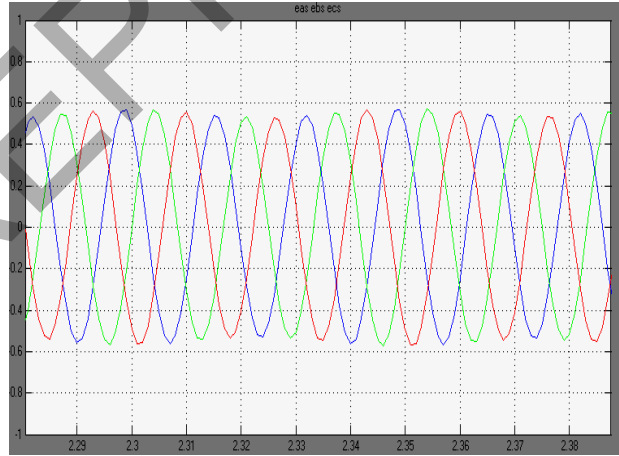


Fig. 2. Response of Three phase Stator voltages of DFIG

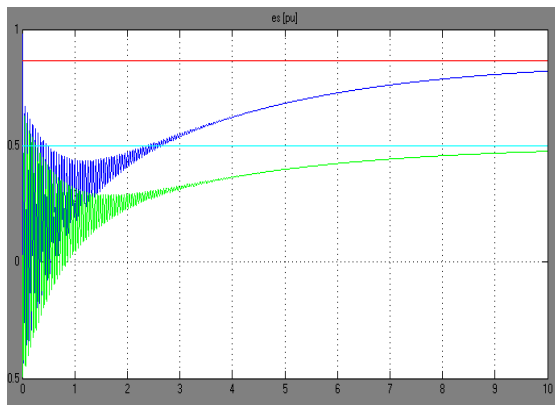


Fig. 3. Transient Response of Stator voltage During Grid Disconnection

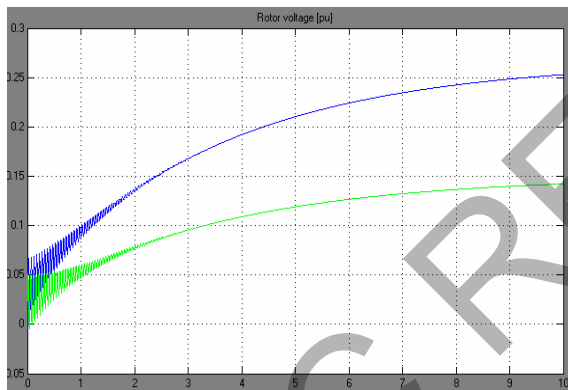


Fig. 4. Transient Response of Rotor voltage During Grid Disconnection

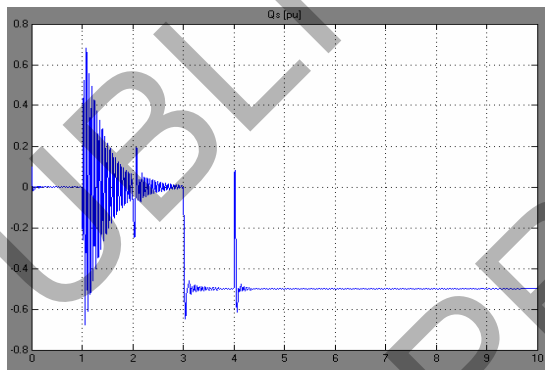


Fig. 5. Transient Response of Active power During Grid Disconnection

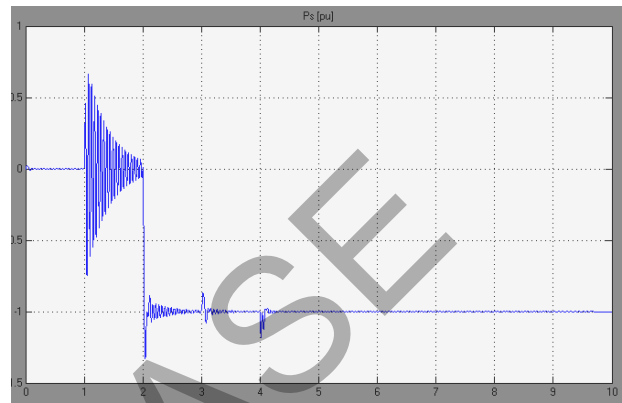


Fig. 6. Transient Response of Reactive power During Grid Disconnection

IV. CONCLUSION

In this paper, dynamic characteristics of double-fed induction generator has been studied during abnormal conditions of the grid. For this, dynamic d-q model was used to derive the dynamic equations of such machine in a synchronous reference frame. The choice of synchronous rotating reference frame makes it particularly favourable for the simulation of double-output configuration in transient conditions. When the stator is disconnected from the grid, the rotor is suddenly got excited due to slip frequency rotor voltages from the voltage regulators in order to produce the commended stator terminal voltage. So active and reactive power of the machine have been decreasing rapidly. For reactive power compensation during these conditions, rotor side converter has to supply necessary reactive power.

REFERENCES

- [1] A.Tapia, G.Ostolaza and J.X. Saenz, "Modeling and control of a wind turbine driven doubly fed induction generator," *IEEE Energy Conversion*, vol. 18, pp. 194-204, June. 2003.
- [2] Yazhou Lei, Alan Mullane, Gordon Lightbody, and Robert Yacamini, "Modeling of the Wind Turbine With a Doubly Fed Induction Generator for Grid Integration Studies," *IEEE Energy Conversion*, vol. 21, pp. 257-264, Mar. 2006.
- [3] C. S. Demoulias and P. S. Dokopoulos, "Transient behaviour and self excitation of wind-driven induction generator after its disconnection from the power grid," *IEEE Energy Conversion*, vol. 5, pp. 272-278, 1990.
- [4] P. S. Nagendra Rao and S. S. Murthy, "Performance analysis of grid connected induction generators driven by hydra/wind turbines including grid abnormalities," in *Proc. 24th Intersociety on Energy Conversion Engineering Conference*, 1989, pp. 2045-2050.
- [5] L. Wang, Ya-Feng Yang and Sung-Chun Kuo, "Analysis of Grid-connected Induction Generators Under Three-phase Balanced Conditions," in *Proceedings of IEEE 2002*, pp. 413-417.
- [6] J.G.Slootweg, H. Polinder, and W.L.Kling. "Dynamic modeling of wind turbine with doubly fed induction generator," in *Proc. IEEE Power Eng. Soc. Summer meeting*, Vancouver, BC, Canada, Jul. 15-19, 2001.
- [7] B.H.Chowdhary, Srinivas Chellapilla, "Doubly-fed induction generator for variable speed wind power generation" *Transactions on Electric Power System Research*, Vol. 76, Jan 2006. pp. 786-800S.N.Bhadra, S.Banerjee, "Wind Electrical Systems", Oxford University Press.

Possibilities of Utilization of Energy Briquettes

Gabriel Borowski
Lublin University of Technology
20-618 Lublin, Nadbystrzycka 38, POLAND
e-mail: g.borowski@pollub.pl

Abstract. The analysis of mineral coal briquettes from charcoal and biomass together with molasses as a binding agent for utilization in industrial energy were presented. The physical-chemical properties of the material investigated, consisting of raw waste material, are described. The process for preparing the material into briquettes comprised of crumbled and mixed constituents, together with the specific reduction of moisture of the mixture, are presented. The effect of the selected parameters of the consolidation process in the pressing stamp on the toughness of briquettes is investigated. Analysis was made of such parameters as: contribution of the biomass in the mixture of charcoal and binder, moisture in the mixture, press pressure on the formation, and seasoning. The results confirm the possibility of utilizing high quality energy briquettes. They possess the high material strength as well as high value combustible fuel, which qualifies them for utilization in industrial energy.

1. INTRODUCTION

Coal-biomass briquettes are an ecological source of energy and even frequently utilized in the production process for heating energy as well as in electric heating, such as in individual households. Briquettes produced at present contain pit coal, brown coal (lignite), coke together with biomass in the form of sawdust, peat, straw or other raw materials. Briquettes thus produced are without any additions or additional binding agents. Frequently used binders are starch, sugar, soda lye, water glass, lime, gypsum, and many others. The addition of these fine-grained binding agents to the composition of the briquettes increases their toughness [1, 2, 3].

For making the briquette charcoal-biomass mixture, stamping presses as well as rollers may be used. Rolled briquettes are definitely more efficient than those that are punched, and ought to have a wider application for production continuity. Stamping presses, however, check the determined properties of briquettes in laboratory conditions and also for the production of the specimens in small series. The mixture for merging on the press has to be appropriately prepared. Each individual ingredient has to be added in determined proportions, binder added, then thoroughly mixed together and the paste dried to a certain moisture [3].

Coal-biomass briquettes intended for burning in furnaces are characterized by a high energy effect. Their material strength has to be adjusted to transport conditions and storage, through which the toughness ought to be kept throughout the seasonal periods. In the case of transportation in sealed containers, the briquettes should be marked for additionally high water resistance.

Briquettes with biomass used as energy fuel comply with the standard regulations for the protection of the environment, especially in area of low emissions of harmful substances into the atmosphere [7]. The mass production of briquettes requires, moreover, preparation of high quality criteria and repeatable quality of this product. Appropriate laboratory experiments were carried out to put this aim into effect. The present work recommends preparation in this way of the mixture and manufacture of coal-biomass briquettes on a laboratory scale.

2. MATERIALS FOR ENERGY BRIQUETTES

The materials investigated were pit coal and sawdust from deciduous trees (oak and beech). The binder added to the mixture was molasses, a by-product obtained during the refining of sugar. The selection of this binder from among many others was motivated by the results of the author's investigations with fine-grained briquette materials which confirmed the effect of molasses on the material strength of briquettes [3]. Also significant is the fact that it did not create any increase in harmful emissions during the burning process of briquettes of molasses in comparison with test controls.

The value of burnt biomass of deciduous wood rose in median to 19,000 kJ/kg. In comparison, the value of burning pit coal rose in median to 28,000 kJ/kg (Table 1). During the burning time the biomass produced a small amount of ash which did not contain harmful substances and may be utilized as mineral fertilizer [6].

The basic chemical ingredients of pit coal and biomass employed for energy are the same. The individual elements in chemical conjunction appear, however, in different proportions. The resulting measurements presented in Table 1 confirm that the biomass contains about four times more oxygen, twice as few charcoal elements, and likewise sulphur and nitrogen. The consequence of these properties is a higher air content and higher reactivity of biomass [8].

From the ecological point of view, the advantageous characteristics of wood biomass are significantly lower, in comparison with coal, sulphur and ash value measurements. The contribution of ash formed in wood burning is on the level of 2% and is significantly lower than for burning coal. The value of the air part, however, is significantly higher in biomass than with coal. The content of the element coal in the biomass is on the level typical for organic combinations [5].

Biomass possess a lower pouring density and therefore a bigger ingredient surface is required in comparison to the coal storage area. The biomass density increases on average

TABLE 1
CHARACTERISTIC OF CHARCOAL AND BIOMASS

Parameter	Pit coal	Biomass of deciduous wood
Density poured (kg/m ³)	880	80
Combustible value (kJ/kg)	28,000	19,000
Moisture value in investigation (%)	7.1	12.0
Value of air part (%)	26.6	66.5
Ash value (%)	12.2	2.0
Sulphur value (%)	0.9	0.1
Oxygen (%)	7.0	30.2
Coal (%)	81.0	42.0
Nitrate (%)	1.1	0.5

80 kg/m³ at the same time as coal increases to ca. 880 kg/m³ (Table 1).

The characteristic biomass attributes in its fresh form is a high value of moisture which increases as high as 50%. It is advantageous to decrease its moisture to a value lower than 15%. A high moisture content in the biomass also has an influence on its cost and profit. A higher weight of biomass relative to the appreciable water content increases the cost of transportation. The utilization of waste wood is therefore profitable through application of drying and integration of raw materials before its transportation to energy works. A very important characteristic mixture of coal-biomass is the complete additiveness of organic substances of both fuel. In this mixture, the coal plays a stabilizing role in the burning process. In comparing energy, 2 tons of biomass are equal to 1 – 1.5 tons of pit coal [4].

The combustible value of coal briquettes with 20% massive participation of wood biomass rises to ca. 24,000 kJ/kg, which is sufficient in order to employ it as a source of warming energy in electric generating plants. Such briquettes, moreover, are an ecological fuel complying with regulations for protecting the environment, relative mainly to the limitation of SO₂ emissions into the atmosphere, thanks to which desulphurisation of fumes is not required [9].

3. TOUGHNESS OF BRIQUETTES

Fine grain coal belongs to the materials that showed weak susceptibility for integration in pressing into briquettes. It is therefore desirable that the activity has the aim of changing the properties of the material. In investigations to date, the integration of fine grain materials has played a significant role factor combining the prepared material [2, 3].

The preparation of material for making into briquettes includes the crumbling and mixing as well as drying to a moisture level below of 12%. An electric mill is used for the crumbling. The relatively significant difference in the physical properties of coal and fibrous materials suit to two types of mill – coal hammer and shears (cutting) for fine graining into biomass. Coal together with sawdust were crumbled to the moment granules of less than 2 mm are obtained for analytical tests. The prepared briquettes were investigated for the balance participation of the biomass decreased in relation to coal to 20% and 25%. In

accomplishing, the briquettes checked also only the coal. The molasses content in the role of binder, defined previous investigations, decreased to ca. 8% [3].

The ingredients were mixed in an electric mixer and then taken for thermal drying to a precise level of moisture. Investigation of the moisture was accomplished with the aid of laboratory moisture tester from the KETT firm, type FD-620. The drying temperature was increased to 100°C. The prepared briquette mixture was placed in the laboratory press. The maximum pressure of each individual press was increased to 35 MPa, whereas the press displacement was 200 mm.

Preparation and accomplishment of special forming unit to briquetting of fine grain waste materials were assembled in the matrix and punch. The matrix enables obtain briquettes of cylindrical shape and a suitable height of briquettes obtained of approximately 2/3 diameter. It is possible to quickly change the matrix and stamp for the purpose of obtaining briquettes of different dimensions and form.

The toughness of the briquettes were defined through resistance to gravity drop, together with the strength of compression. Resistance of the briquettes to gravity drop was evaluated through the percentage of decrease in mass after dropping the briquettes at least three times from a height of 2.0 m on to a steel plate. After each drop, the test piece was put through a sieve with openings smaller than the minimum dimension of the briquette. Briquette resistance to gravity is illustrated in the equation below:

$$K = \frac{B_z}{B} \cdot 100\% \quad (1)$$

where: B – briquette mass before dropping,
B_z – mass remaining in filled sieve.

The gravitational resistance to drop should be attain a value higher than 90%. The value of compression strength destroying the briquette was defined experimentally as follows, that the cylindrical disc was placed between the flat surface of the compress experimental piece until the moment of destruction of its structure. The investigation carried out used an endurance test machine ZWICK Z100. The value of compression strength destroying the briquette should be attain at least 1.5 MPa.

4. ANALYSIS OF RESULT OF RESEARCH

Fresh and seasoned briquettes were tested. Analysis of the following parameters was undertaken: biomass contribution, moisture of the coal-biomass mixture with binder, pressure of stamping press and seasoning. Data from the analysis is presented in Table 2, as well in Figures 1 and 2.

The data presented in Table 2 shows that the majority of examples of gravitational resistance to drop obtained a value higher than 90%. This resistance is insufficient through integration in the material of moisture greater than 10%. It was ascertained that the mixture should contain a 6 – 9% of moisture. High resistance of the briquettes obtained by a

TABLE 2
TOUGHNESS OF SELECTED COAL-BIOMASS BRIQUETTES

Test No.	Moisture (%)	Punch pressure (Mpa)	Biomass participation (%)	Maximum compression strength destroying briquettes (Mpa)		Resistance to gravity drop (%)	
				fresh	seasoned	fresh	seasoned
1	11.5	30.0	20.0	1.08	1.54	80.0	82.0
2	9.6	30.0	20.0	4.81	7.37	89.0	90.5
3	8.0	35.0	20.0	4.42	6.80	97.5	98.2
4	7.9	35.0	25.0	5.30	8.14	95.6	96.3
5	7.5	30.0	25.0	6.03	9.24	94.8	95.6
6	7.4	35.0	25.0	7.45	11.64	97.1	99.0
7	6.6	35.0	0.0	1.19	1.83	82.6	83.5
8	6.3	30.0	20.0	4.84	7.44	93.7	94.0

punch press with pressure of 30 as well as 35 MPa. through which the greatest pressure value applied the biggest degree of crush; therefore, in effect, the material strength was higher. This is significant if the contribution of biomass in the briquettes is increased. For example, a 25% contribution of biomass in the samples produced with a smaller resistance; on the other hand, however, through increasing the strength value of pressure, samples are produced with a high toughness.

It was observed that in gravitational resistance drop tests the greatest resistance was proved in tests falling on to the surface of the circular disc, and the lowest when dropped on to the edge or flat part. This confirms the justification for constructing such a matrix and punch, so that the briquettes had not strong edges and even walls. Round-shaped briquettes can be formed in a roll press.

The data presented shows that briquettes consisting only of coal have a decidedly lower resistance to compression than briquettes with additional biomass. The use of biomass therefore increases the material strength of briquettes. Analysis of the data shows that the maximum strength value of compression is somewhat higher for briquettes with a 20% biomass, and lower for those with 25% biomass through using the same pressure strength in the press. It is justified to use a higher press pressure in the example of compressing material containing a higher biomass content.

Figure 1 presents data showing the seasoned precept of briquettes. Seasoned briquettes are characterised by a higher resistance to pressure than fresh ones. The results of experiments show that in the period of three weeks their resistance to pressure increases; however, seasoning for a longer time is disadvantageous. There is a distinct decrease in resistance to pressure after 50 days of seasoning the briquettes.

Analysis of the running curve in Figure 2 shows three phases in the compression of the briquettes. In the first phase, a small rise in compression strength induces a big relationship between the moving parts of the endurance machine, between

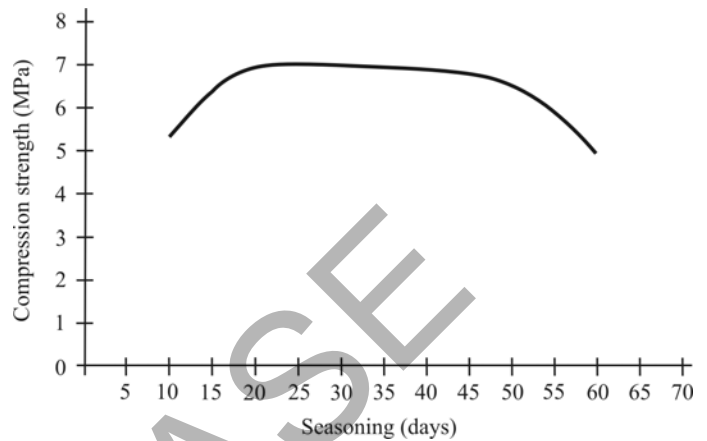


Figure 1. Reliability on compression of briquettes in relation to seasoning

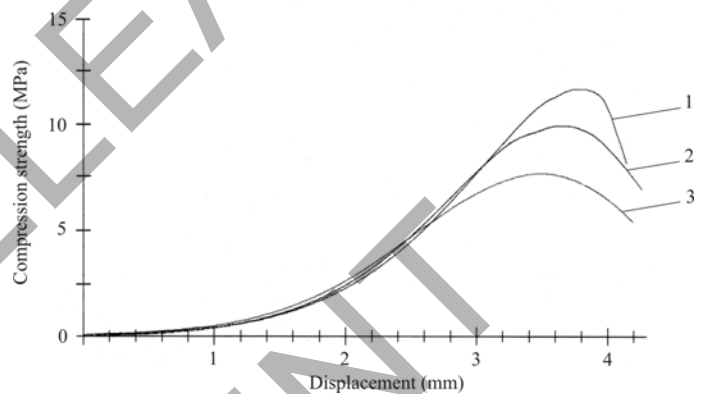


Figure 2. Course of compression strength of selected briquettes : 1 – made with punch pressure of 35 MPa, 2 – made with punch pressure of 30 MPa, 3 – like (2) with lower humidity of the mixture

which there are the test piece. The cause of this is a porosity of the briquettes. In this phase the compression process is introduced; therefore, there is a reciprocal close relationship between the ingredients of the fine grain structure of the briquettes. The next phase of the process is characterized by a stepwise increase in strength up to the maximum value whereby the test piece are destroyed.

5. CONCLUSION

The production of energy briquettes from coal and biomass produced a high toughness. An adhesive like molasses added in to the residual mixture produces increased material strength. Additional increase of mass participation of biomass does not produce a significant decrease in resistance of the briquettes, but lessen the energy effect during their burning in furnaces. The acquisition of a high value of resistance to gravitational drop, together with resistance to the compression, to a large degree depends on the moisture of the mixture, pressing stamp pressures, and likewise the period of briquette seasoning. It was proved that briquettes showed sufficient resistance, even in fresh form; however, it is advantageous to use them during a period of 2–4 weeks.

On the basis of the results of the investigation, the following are proposed:

1. During the process for preparing the mixture for making into briquettes, it is essential to select definite proportions of ingredients. The most advantageous conditions to assure the addition of the molasses in the amount of ca. 8% for the making of briquettes of grained materials, together with the drying of the mixture to a moisture level within the range of 6–9%. Seasoned briquettes influence their toughness.
2. The use of molasses as a binder significantly influences the increase in the material strength. They have sufficient resistance, even through the increase in biomass participation, but in this case it depends on the minimal burning output value of the briquettes in relation to the required energy effect acquired during burning in furnaces.
3. The energy effect during burning of briquettes in industrial furnaces should be obtained.
4. Briquetting of energy raw materials brings advantages for decreasing the consumption of materials, together with a lowering cost of transports and storage.

REFERENCES

- [1] Altun N.E., Hicyilmaz C. and Kk M.V., 2001. Effect of Different Binders on the Combustion Properties of Lignite: Part I. Effect on thermal properties. *Journal of Thermal Analysis and Calorimetry*. Akadmiai Kiad with Springer Science & Business Media B.V., Formerly Kluwer Academic Publishers B.V., Vol. 65, No 3, 787–795.
- [2] Borowski G., 2007. The possibility of utilizing coal briquettes with a biomass. *Environment Protection Engineering*. Wroclaw University of Technology, Vol. 33, No 2, 79–86.
- [3] Borowski G. and Kuczmaszewski J., 2005. Investigation on Briquetting of Metal Wastes From Bearing Industry. *Waste Management & Research*. Sage Publications Ltd. Copenhagen, 5(23), 473–478.
- [4] Gnutek M., Moron W. and Rybak W., 2002. Problems of burning and co-burning of coal and biomass. *Czysta Energia*, 9, 47–54.
- [5] Kubica K., 2003. Burning biomass and its co-burning with coal – technicalities, uses and limits, In: Clean and Green Energy – clean air in the Silesian Voivodship. Katowice, pp. 95–106.
- [6] Niedziolka I. and Zuchniarz A., 2006. Analysis of energy from selected types of biomass of vegetable origin. *Motrol*, 8A, 232–237.
- [7] Purohit P., Tripathi A.K., Kandpal T.C., 2006. Energetics of coal substitution by briquettes of agricultural residues. *Energy*, Elsevier Ltd., 31, 1321–1331.
- [8] Sciazko M. and Zielinski H., 2003. Thermo-chemical processing of coal and biomass. Polish Academy of Sciences, Zabrze-Krakow, pp. 125–132.
- [9] Sciazko M., Zuwała J. and Pronobis M., 2006. Advantages and disadvantages of co-burning biomass in energy furnaces in the light of exploitation experiences during the first year of co-burning biomass on an industrial scale. *Energetyka*, 3, 207–220.

Optimum location and sizing of passive filters in distribution networks using genetic algorithm

M. Ghiasi, V. Rashtchi, H. Hoseini
Engineering student and faculties of Zanjan University
Zanjan, Iran

Abstract-The harmonic distortion of voltage has become an important subject in power quality, especially after use of power electronic equipment and nonlinear loads. Simple method to limitation of harmonic distortion is using of passive filters. The objective of this paper is to determine the location and size of passive filters in distribution networks economically, by using genetic algorithm. With using of genetic algorithm and new coding here some of other methods limits for passive filters locations are removed. The purpose of the genetic algorithm is to minimize the cost of passive filters and, at the same time, to reach the harmonic limitations defined by standard IEEE-519. This algorithm is applied to IEEE 13-bus distribution network and the results are shown, finally

I. INTRODUCTION

With increasing use of power electronic equipment and nonlinear loads, the level of voltage harmonic distortion in distribution networks are significantly increasing. As harmonics propagate through the system, they result in increased losses and possible equipment loss-of-life. Also Overcurrents or overvoltages resulting from resonances can damage equipment. Additionally, harmonics can interfere with control, communication, and protective equipment. With this reasons different research institutes have studied about the proper limitation of harmonic disturbance levels and released different standards.

Among the several methods used to reduce these harmonic disturbances, the more employed are the tuned passive filters due to their simplicity and economical cost.

The important problem of using passive filters are determining location and sizing of them, which is reach standard levels of harmonic distortion with applying minimum cost of passive filters [1, 2].

In reference [3], the objective is to propose a new approach for designing a passive LC filter of the full-bridge rectifier by using genetic algorithms (GAs). The objective of the fitness function in the GA program is to find out the maximum PF of the ac mains with the smallest inductor value.

Reference [4] describes the application of genetic algorithm to calculate the R-L-C parameters of passive harmonic filters that may be installed in the customers' houses. The main goal is to minimize the harmonic impedance in some specific frequencies and to maximize the fundamental frequency impedance in order to minimize losses.

Reference [5] presents a method that applies the Combinatory optimization by microgenetic algorithms for the location and optimum project of passive harmonic filters. The

minimization of total voltage harmonic distortion and active power losses has been used as objective function. In this reference, the problem consists of planning two passive harmonic filters, whose harmonic tuning orders are 4.7 and 6.6, respectively.

Reference [6] describes the application of genetic and a microgenetic algorithm to the problem of locating and sizing passive filters in an electric network affected by harmonic disturbances. In this work, the objective function to be minimized is the value of voltage harmonic distortion. In this reference, the input data are the number of filters and the relevant order of these filters.

In this work by using genetic algorithm and new coding, location and sizing of passive filters is determined so with installing them the standard levels for voltage distortion is achieved with minimum cost of passive filters. By comparing with other methods the number and harmonic order of passive filters is automatically determined in this work.

Standard limitation that is considered here is standard IEEE-519 for harmonic limitation.

In the next part of this paper first modeling of passive filters, based of new coding and finally the result of applying the new method to IEEE- 13-bus distribution network will be illustrated.

II. PASSIVE FILTERS

The most common type of passive filter is the single-tuned "notch" filter. This is the most economical type and is frequently sufficient for the application. The notch filter is series-tuned to present low impedance to a particular harmonic current and is connected in shunt with the power system (usually near the loads that produce harmonics). Thus, harmonic currents are diverted from their normal flow path on the line through the filter.

Shunt passive filters depend on three design parameters: 1- the tuning harmonic order, 2- the quality factor Q, the filter band and the residual harmonic voltage depend on Q, 3- the capacitor rating at the fundamental frequency.

Inductive reactance and resistor values at the fundamental frequency are:

$$X_L = \frac{X_C}{n^2} \quad R = \frac{X_L}{Q}$$

This is important point that the values of capacitor rating at the fundamental frequency and the quality factor are discrete. The typical value of quality factor is between 30 and 60 for

single-tuned “notch” filter. Moreover, the standard IEEE for capacitor rating is available.

Based of new coding, in this work for each candidate buses for installing passive filter, four filter branches are considered, that each of these four filters is used for different harmonic orders. The load buses that produce harmonics are considered as candidate buses. For each of four filters seven bits are considered in chromosome. The first bit shows presence or absence, next three bits show the quality factor and the latest three bits show the capacitor rating. With this coding method the chromosome size is equal to $7 \times 4 \times \text{candidate buses}$.

III. OBJECTIVE FUNCTION

Objective function is the cost of filter branches. This cost contains the cost of capacitors, inductors, and resistors. So:

$$fitfun = cprice + lprice + rprice$$

Where, $cprice$, $lprice$ and $rprice$ respectively are price of capacitors, inductors and resistors. The cost of capacitors at different voltage level in distribution networks is available. The cost of filter inductors does not vary greatly for units of different rating. The cost approximation used in the analysis is of the form:

$$\text{Inductor cost} = UK + UL \text{ (MVAR)}$$

Where UK is a constant cost component and UL is the inductor incremental cost per MVAR rating. These values relate to the single phase and must be converting to the three phase.

The power rating of the resistor necessary for Q-adjustment in each filter branch will affect the cost to some extent. However, the nominal resistance of the unit is difficult to predict in a general analysis, because it depends on the natural Q factor of the inductor. For this reason, and because the cost of an air-cooled resistor is small compared with that of the other components, a constant cost per resistor is allocated in the analysis [1].

For eliminating the individual that don't observe the harmonic limitations, a penalty factor is used.

IV. CONSTRAINS

Based on standard IEEE-519, the value of THD at PCC (Point of Common Coupling) in distribution networks below 69 kV must be lower than 5% and the value of IHD lower than 3%. Also practically, the values of capacitor ratings and quality factors are discrete.

V. GENETIC ALGORITHM

The GA is a search mechanism based on the principle of natural selection and population genetics. At the beginning of GAs, representations for possible solutions, which are often called chromosomes or individuals, must be developed. A chromosome consists of a series of genes which can be represented by binary codes. Different combinations of genes form different chromosomes. Each chromosome is a possible solution of the problem. The set of chromosomes is called the population of the generation. Chromosomes in a generation are forced to evolve toward better ones in the next generation by

three basic GA operators, reproduction, crossover, and mutation, and the problem-specified fitness function.

In reproduction, a number of selected exact copies of chromosomes in the current population become a part of the offspring. In crossover, randomly selected subsections of two individual chromosomes are swapped to produce the offspring. In mutation, randomly selected genes in chromosomes are altered by a probability equal to the specified mutation rate. For a binary coding gene, it means that digit 1 becomes digit 0 and vice versa.

The fitness function, also called the objective function, is an evaluation function that plays the role of the environment to distinguish between good and bad chromosomes. Only a certain number of chromosomes screened and selected by the fitness function can survive and pass their genes to the next generation.

Each chromosome of the current population is evaluated by the fitness function and some good chromosomes are selected. Then a new population will be generated by using the three basic GA operators, i.e., reproduction, crossover, and mutation.

A. Reproduction

The reproduction of new individuals is made as follows:

- Find the total fitness of the population:

$$f_{total} = \sum_{i=1}^n f_i$$

Where:

f_i : Fitness of each individual $i(1,2,\dots,n)$

n : Number of individual in the population

- Calculate the probability of reproduction for each individual $i(1,2,\dots,n)$.

$$p_i = \frac{f_i}{f_{total}}$$

- Round p_i $i(1,2,\dots,n)$ and copy each individual i for p_i times at mating pool

- Enter three random individuals instead of last three individuals of population

B. Crossover

The crossover operator follows:

- Select individuals two by two respectively

- Select a filter branch characters in random

Replace it by relative filter branch of next individual by the probability of crossover (p_c)

C. Mutation

The mutation operator follows:

- Select individuals respectively

Reverse the bits relative to absence or presence of filter branches by the probability of mutation (p_m)

VI. CASE STUDY

This paper uses an IEEE standard distribution network to perform the study. This network consists of 13 buses and is representative of a medium-sized industrial plant. The plant is

fed from a utility supply at 69 KV and the local plant distribution system operates at 13.8 KV [7].

The system is shown in figure 1. More information on this network can be obtained at <http://www.ee.ualberta.ca/pwrsys/harmonics.html>.

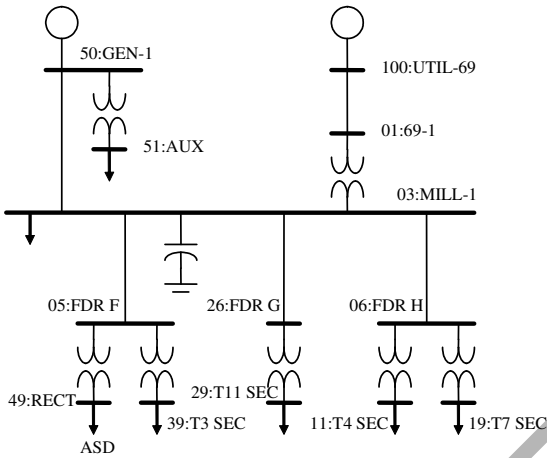


Figure 1: IEEE 13-buses standard network

In this paper in addition to 49:RECT, the 29:T11SEC and 51:AUX is considered also as a nonlinear load.

Standard rating of single-phase capacitors and their costs that released by ABB (according to IEEE and IEC standard), are shown in following table:

Table 1
Standard single-phase capacitor ratings and their costs

XC (KVAR)	PRICE (\$)
50	550
100	625
150	705
200	790
300	950
400	1155
500	1315
600	1455

In this paper the value of UK and UL is considered 500\$ and 90 (\$/MVAR) respectively. p_m , p_c and the size of population are considered 0.15, 0.75 and 10 respectively.

VII. SIMULATION RESULT

Passive filters locate at the primary side of load transformers (PCC's) generally, thus in this problem, the candidate buses for filters are 50:GEN-1, 05:FDR F and 26:FDR G.

The program result is shown in table 2 and Table 3 shows the THD values of buses before and after filtering.

Convergence curves of the algorithm for five individual runs are shown in figure 2.

Table 2
Simulation result

Filter branch	1
Tuning order	7
Location	26:FDR G
XC (KVAR)	150
Q	50
C (μ F)	2.1
L (mH)	68.8
R (Ω)	3.63

Table 3
THD of buses before and after filtering

bus	Initial THD (%)	Final THD (%)
50:GEN-1	10.56	2.48
03:MILL-1	10.93	2.55
51:AUX	9.95	7.72
100:UTIL-69	1.34	0.32
01:69-1	1.36	0.33
05:FDR F	10.93	2.55
49:RECT	11.04	10.23
39:T3 SEC	9.86	2.32
26:FDR G	10.92	2.56
29:T11 SEC	11.12	10.41
06:FDR H	10.93	2.55
11:T4 SEC	10.55	2.47
19:T7 SEC	9.96	2.34

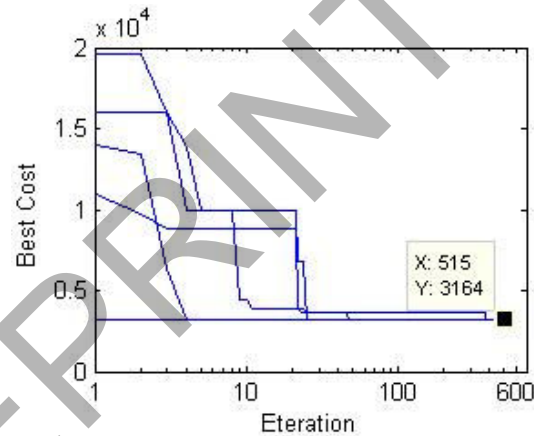


Figure 2: Convergence curves for five algorithm runs

Curve A and B in fig.2 show the changing of transfer impedance between 26:FDR and 29:T11 SEC buses respectively before and after installing passive filter. Because of using of power factor correcting capacitor in network, as shown in fig.3 network has a resonance frequency near the 7th harmonic order. After installing filter this frequency change to two new resonance frequencies far from 7th harmonic order.

In designing passive filters for a network it must be considered that after installing filters new resonance frequency near the nonlinear loads order don't be appeared. However, with using genetic algorithm by consideration a penalty factor in fitness function appearing of this new resonance frequency is prevented.

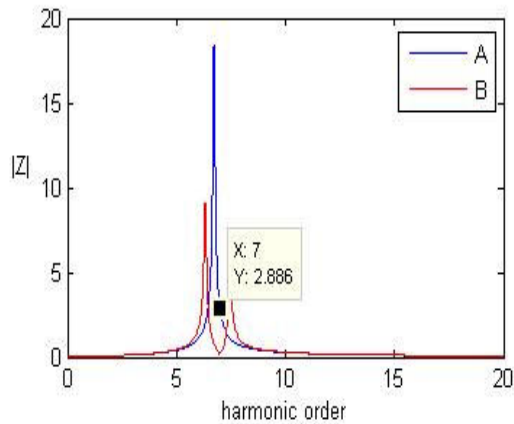


Figure 3: Harmonic impedance before (A) and after (B) filtering

VIII. CUNCLSION

This paper deals with determining the location and size of passive filters by genetic algorithm, economically. The algorithm constrains are the limitation of harmonic distortion

that define by standard IEEE-519. The algorithm determines the number, harmonic order, size and location of passive filters to reach the IEEE standard..

REFERENCES

- [1] J. Arrillaga, N.R. Watson, *Power System Harmonics*, Second Edition, 2003, John Wiley & Sons
- [2] J.S. Subjak and J.S. Mcquilkin, "Harmonics- Causes, Effects, Measurements, and Analysis: An Update", *IEEE Trans. Ind. Applicat.*, Vol.26, pp. 1034-1042, 1990.
- [3] Yaow-ming Chen, "Passive Filter Design Using Genetic Algorithm", *IEEE Transaction On Industrial Electronics*, Vol. 50, No. 1, Feb 2003.
- [4] C.C.M. Moura, M.E.L. Tostes, E.P. Santos, R.C.L. Oliveria, T.M.M. Branco, U.H. Bezerra, "Determination of the R-L-C Parameters of a Passive Harmonic Filter Using Genetic Algorithm", *IEEE Conf. on Harmonics and Quality of Power*, Vol. 2, PP. 495- 500, 2002.
- [5] Franklin M.P. Pamplona, Benemar A. Souza, "Harmonic Passive Filter Planning In Radial Distribution Systems Using Microgenetic Algorithm", *IEEE 11th International Conf. on Harmonics and Quality of Power*, 2004.
- [6] A. Berizzi, C. Bovo, "The Use of Genetic Algorithms for the Localization and the Sizing of Passive Filters", *9th International Conf. on Harmonics and Quality of Power*, Vol. 1, PP. 19-25, 2000.
- [7] Task Force on Harmonics Modeling and Simulation, "Test Systems for Harmonics Modeling and Simulation", *IEEE Trans. On power Delivery*, Vol. 14, No. 2, April 1992.

Balancing Voltage Source Direct Torque Control of Induction Motor with Three level Inverter

Hacene Rezine , Abderrahmane Berkani .

UER Electrotechnique, EMP (Ex-ENITA). BP 17 Bordj-El-Bahri, Algiers, Algeria

Email : Abdouberkani@yahoo.fr

Rezine_hacene_emp@yahoo.fr

Abstract – In this paper we present a new control structure for sensorless induction machine dedicated to electrical drives using a three-level voltage source inverter (VSI). The amplitude and the rotating speed of the flux vector can be controlled freely. Both fast torque response and optimal switching logic can be achieved; the selection is based on the value of the stator flux and the torque.

A novel DTC scheme of induction motors is proposed in order to develop a suitable dynamic. We propose an approach; in which we enhance the response of torque and flux with optimal switching strategies. However, the middle point voltage of the input DC voltages of the three-level NPC voltage source inverter presents serious problems caused by a fluctuation of the DC voltage sources U_{cu} U_{cl} . As consequence to these problems, we obtain an output voltage of the inverter which is asymmetric and with an average value different from zero. In this paper, we will present one solution to minimise this fluctuation. This solution uses a clamping bridge to regulate the input voltages of a threelevel inverter VSI NPC. A scheme of Enhanced direct torque control "EDTC" with complete cascade is simulated for an induction motor. The results obtained indicate superior performance over the FOC one without need to any mechanical sensor.

Key Words - Induction motor, Direct torque control, Voltage source inverter, Flux estimators, Switching strategy optimisation, Neutral-point clamped.

I. INTRODUCTION

The rapid development of the capacity and switching frequency of the power semiconductor devices and the continuous advance of the power electronics technology have made many changes in static power converter systems and industrial motor drive areas. The conventional GTO inverters have limitation of their dc-link voltage. Hence, the series connections of the existing GTO thyristors have been essential in realizing high voltage and large capacity inverter configurations with the dc-link voltage [1]. The vector control of induction motor drive has made it possible to be used in applications requiring fast torque control such as traction [2]. In a perfect field oriented control, the decoupling characteristics of the flux and torque are affected highly by the parameter variation in the machine.

This paper describes a control scheme for direct torque and flux control of induction machines fed by a three-level voltage source inverter using a switching table. In this method, the output voltage is selected and applied sequentially to the machine through a look-up table so that the flux is kept constant and the torque is controlled by the rotating speed of

the stator flux. The direct torque control (DTC) is one of the actively researched control scheme which is based on the decoupled control of flux and torque providing a very quick and robust response with a simple control construction in ac drives [3].

In this paper, the authors propose a new cascade for high voltage and high power applications. This cascade lets to absorb, in network, sinusoidal currents with unity power factor. It constitutes by two-level PWM rectifier, clamping bridge, three-level NPC VSI, induction motor controlled by EDTC strategy.

II. THREE-LEVEL INVERTER TOPOLOGY

Fig. 1 shows the schematic diagram of neutral point clamped (NPC) three-level VSI. Each phase of this inverter consists of two clamping diodes, four GTO thyristors and four freewheeling diodes. Table.I shows the switching states of this inverter. Since three kinds of switching states exist in each phase, a three level inverter has 27 switching states.

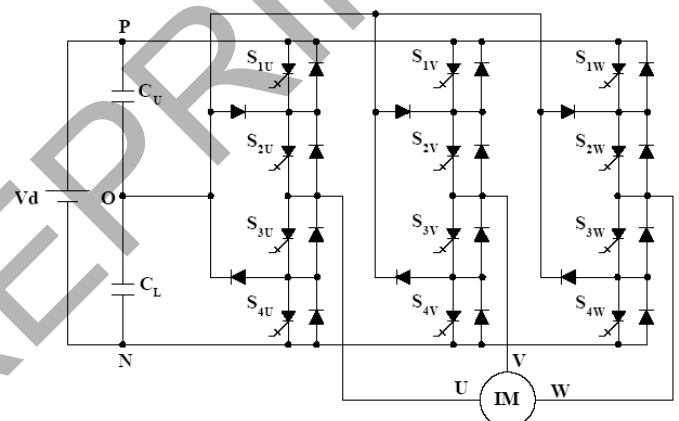


Fig. 1. Schematic diagram of a three-level GTO inverter

Table. I.

Switching states of a three-level inverter

Switching states	S1	S2	S3	S4	SN
P	ON	ON	OFFF	OFFF	Vd
0	OFFF	ON	ON	OFFF	Vd/2
N	OFFF	OFFF	ON	ON	0

A 2-level inverter is only able to produce six non-zero voltage vectors and two zero vectors [2]. The representation of the

space voltage vectors of a three-level inverter for all switching states forming a two-layer hexagon centred at the origin of the (d, q) plane and a zero voltage vector at the origin of the plane, as depicted in fig.2. According to the magnitude of the voltage vectors, we divide them into four groups the zero voltage vectors (V0), the small voltage vectors (V1, V4, V7, V10, V13, V16), the middle voltage vectors (V3, V6, V9, V12, V15, V18), the large voltage vectors (V2, V5, V8, V11, V14, V17)

The zero voltage vector (ZVV) has three switching states, the small voltage vector (SVV) has two and both the middle voltage vector (MVV) and the large voltage vector (LVV) have only one [1].

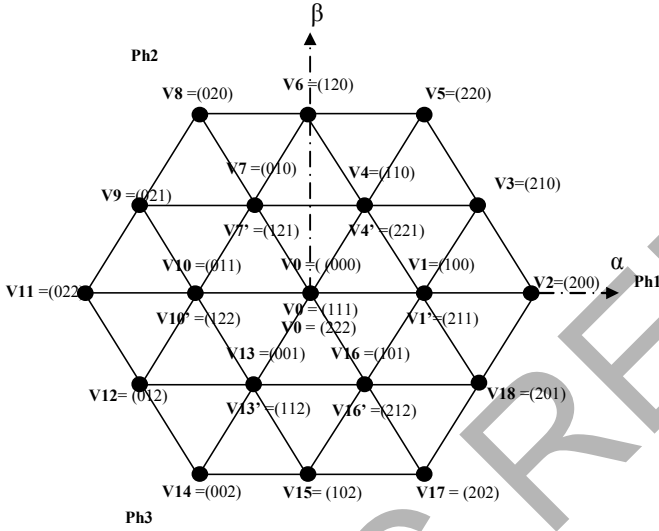


Fig. 2. Space voltage vectors of a three-level inverter

III. INDUCTION MACHINE

Torque control of an induction motor can be achieved on the basis of its model developed in a two axis (d, q) reference frame stationary with the stator winding. In this reference frame and with conventional notations, the electrical mode is described by the following equations:

$$\frac{di_{sd}}{dt} = \frac{1}{\sigma T_r L_s} \varphi_{sd} + \frac{p\Omega}{\sigma L_s} \varphi_{sq} - \frac{1}{\sigma} \left(\frac{1}{T_r} + \frac{1}{T_s} \right) i_{sd} - p\Omega i_{sq} + \frac{1}{\sigma L_s} V_{sd} \quad (1)$$

$$\frac{di_{sq}}{dt} = \frac{1}{\sigma T_r L_s} \varphi_{sq} + \frac{p\Omega}{\sigma L_s} \varphi_{sd} - \frac{1}{\sigma} \left(\frac{1}{T_r} + \frac{1}{T_s} \right) i_{sq} + p\Omega i_{sd} + \frac{1}{\sigma L_s} V_{sq} \quad (2)$$

$$\frac{d\varphi_{sd}}{dt} = V_{sd} - R_s i_{sd} \quad (3)$$

$$\frac{d\varphi_{sq}}{dt} = V_{sq} - R_s i_{sq} \quad (4)$$

The mechanical mode associated to the rotor motion is described by:

$$J \frac{d\Omega}{dt} = \Gamma_{em} - \Gamma_r(\Omega) \quad (5)$$

$\Gamma_r(\Omega)$ and Γ_{em} are respectively the load torque and the electromagnetic torque developed by the machine.

IV. PROPOSED DIRECT TORQUE CONTROL USING A THREE-LEVEL INVERTER

Basically, DTC schemes require the estimation of the stator flux and torque. The stator flux evaluation can be carried out by different techniques depending on whether the rotor angular speed or (position) is measured or not. For sensorless application, the "voltage model" is usually employed [6]. The stator flux can be evaluated by integrating from the stator voltage equation.

$$\varphi_s(t) = \int (V_s - R_s I_s) dt \quad (6)$$

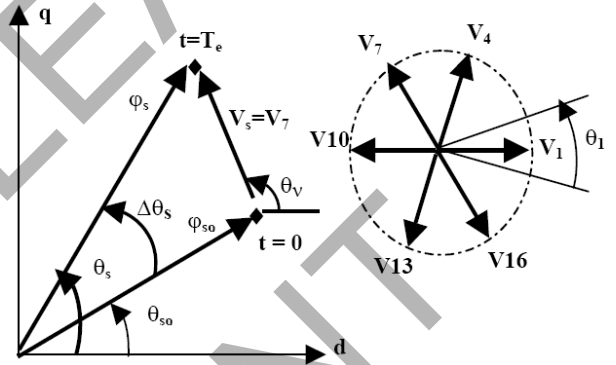


Fig. 3. Flux deviation

This method is very simple requiring the knowledge of the stator resistance only. The effect of an error in R_s is usually neglected at high excitation frequency but becomes more serious as the frequency approaches zero.

The deviation obtained at the end of the switching period T_e can be approximate by the first order Taylor Series as below [6].

$$\Delta\varphi_s \approx V_s \cdot T_e \cdot \cos(\theta_v - \theta_s) \quad (7)$$

$$\Delta\varphi_s \approx T_e \cdot \frac{V_s \cdot \cos(\theta_v - \theta_s)}{\varphi_{so}} \quad (8)$$

Considering the combination of states of switching functions S_u, S_v, S_w . Fig.3 shows the adequate voltage vector selection, we can increase or decrease the stator flux amplitude and phase to obtain the required performance. The electromagnetic torque is estimated from the flux and current information as [2]:

$$\Gamma_{em} = p(i_{sq} \varphi_{sd} - i_{sd} \varphi_{sq})$$

Fig.4. shows a block diagram of the DTC scheme developed by I. Takahashi [2]. The reference values of flux, φ_s^* , and torque Γ_{em}^* , are compared to their actual values and the resultant errors are fed into a multi-level comparator of flux and torque. The stator flux angle θ_s is calculated by:

$$\theta_s = \arctan \frac{\varphi_{sq}}{\varphi_{sd}} \quad (9)$$

and quantified into 6 levels depending on which sector the flux vector falls into. Different switching strategies can be employed to control the torque according to whether the flux has to be reduced or increased.

Each strategy affects the drive behavior in terms of torque and current ripple, switching frequency and two or four quadrant operation capability.

Assuming the voltage drop ($R_s \cdot I_s$) small, the head of the stator flux φ_s moves in the direction of stator voltage V_s at a speed proportional to the magnitude of V_s according to:

$$\Delta\varphi_s = V_s T_e \quad (10)$$

The switching configuration is made step by step, in order to maintain the stator flux and torque within limits of two hysteresis bands. Where T_e is the period in which the voltage vector is applied to stator winding. Selecting step by step the voltage vector appropriately, it is then possible to drive φ_s along a prefixed track curve [6].

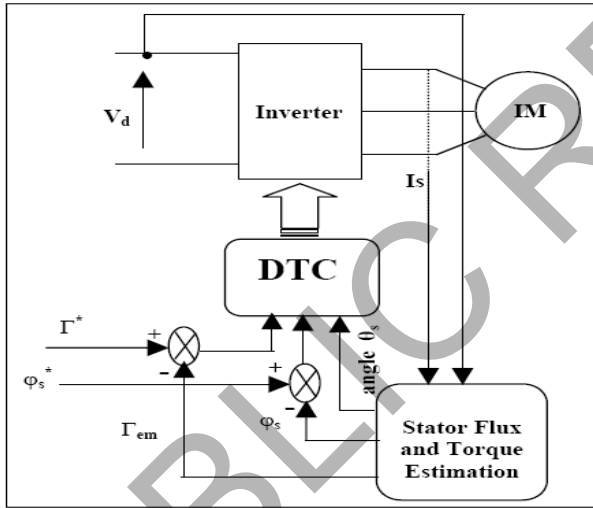


Fig. 4. Block diagram of direct torque control

Assuming the stator flux vector lying in the k -th sector ($k=1,2,\dots,6$) of the (d, q) plane, in the case of three-level inverter, to improve the dynamic performance of DTC at low speed and to allow four-quadrant operation, it is necessary to involve the voltage vectors V_{k-1} and V_{k+1} in torque and flux control.

V. SWITCHING STRATEGY PROPOSED FOR AN ENHANCED DIRECT TORQUE CONTROL

According to this strategy, the stator flux vector is required to rotate in both positive and negative directions. By this, even at very low shaft speed, large negative values of rotor angular frequency can be achieved, which are required when the torque is to be decreased very fast. Furthermore, the selection strategy represented in each table allows good flux control to be obtained even in the low speed range. However, the high dynamic performance, which can be obtained using voltage

vectors having large components tangential to the stator vector locus, implies very high switching frequency.

For flux control, let the variable E_φ ($E_\varphi = \varphi_s^* - \varphi_s$) be located in one of the three regions fixed by the constraints:

$$E_\varphi < E_{\varphi\min}, E_{\varphi\min} \leq E_\varphi \leq E_{\varphi\max}, E_\varphi > E_{\varphi\max} \quad (11)$$

The suitable flux level is then bounded by $E_{\varphi\min}$ and $E_{\varphi\max}$. Flux control is made by a two-level hysteresis comparator.

Three regions for flux location are noted, flux as in fuzzy control schemes, by $E_{\varphi n}$ (negative), $E_{\varphi z}$ (zero) and $E_{\varphi p}$ (positive).

A high level performance torque control is required. To improve the torque control, let the difference ($E_\Gamma = \Gamma_{em}^* - \Gamma_e$) belong to one of the five regions defined by the constraints:

$$E_\Gamma < E_{\Gamma\min2}, E_{\Gamma\min2} \leq E_\Gamma \leq E_{\Gamma\min1}, E_{\Gamma\min1} \leq E_\Gamma \leq E_{\Gamma\max1}, E_{\Gamma\max1} \leq E_\Gamma \leq E_{\Gamma\max2} \text{ and } E_{\Gamma\max2} < E_\Gamma \quad (12)$$

The five regions defined for torque location are also noted, as in fuzzy control schemes by $E_{\Gamma nl}$ (negative large), $E_{\Gamma ns}$ (negative small), $E_{\Gamma z}$ (zero), $E_{\Gamma ps}$ (positive small), $E_{\Gamma pl}$ (positive large). The torque is then controlled by a hysteresis comparator built with two lower bounds and two upper bounds. A switching table is used to select the best output voltage depending on the position of the stator flux and desired action on the torque and stator flux. The flux position in the (d, q) plane is quantified in twelve sectors. Alternative tables exist for specific operation mode. Comparing with switching table for the case of a two-level inverter, it is easily possible to expand the optimal vector selection to include the larger number of voltage vectors produced by three-level inverter [4], [5]. The appropriate vector voltage is selected in the order to reduce the number of commutation and the level of steady state ripple.

The switching strategy in the order of the sector θ_s , is illustrated by each table. The flux and torque control by vector voltage has in nature a discrete behavior. In fact, we can easily verify that the same vector could be adequate for a set of value of θ_s .

θ_1

cflx		2	1	-1	-2
ccpl	ce				
2	1	V5	V4'	V16'	V17
	-1	V5	V4	V16	V17
1	1	V4'	V4'	V16'	V16'
	-1	V4	V4	V16	V16
-1	1	V7'	V7'	V13'	V13'
	-1	V7	V7	V13	V13
-2	1	V8	V7'	V13'	V14
	-1	V8	V7	V13	V14

θ_2

cflx		2	1	-1	-2
ccpl	ce				
2	1	V8	V7'	V1'	V2
	-1	V8	V7	V1	V2
1	1	V7'	V7'	V1'	V1'
	-1	V7	V7	V1	V1
-1	1	V10'	V10'	V16'	V16'
	-1	V10	V10	V16	V16
-2	1	V11	V10'	V16'	V17
	-1	V11	V10	V16	V17

 θ_3

cflx		2	1	-1	-2
ccpl	ce				
2	1	V11	V10'	V4'	V5
	-1	V11	V10	V4	V5
1	1	V10'	V10'	V4'	V4'
	-1	V10	V10	V4	V4
-1	1	V13'	V13'	V1'	V1'
	-1	V13	V13	V1	V1
-2	1	V14	V13'	V1'	V2
	-1	V14	V13	V1	V2

 θ_4

cflx		2	1	-1	-2
ccpl	ce				
2	1	V14	V13'	V7'	V8
	-1	V14	V13	V7	V8
1	1	V13'	V13'	V7'	V7'
	-1	V13	V13	V7	V7
-1	1	V16'	V16'	V4'	V4'
	-1	V16	V16	V4	V4
-2	1	V17	V16'	V4'	V11
	-1	V17	V16	V4	V11

 θ_5

cflx		2	1	-1	-2
ccpl	ce				
2	1	V17	V16'	V10'	V11
	-1	V17	V16	V10	V11
1	1	V16'	V16'	V10'	V10'
	-1	V16	V16	V10	V10
-1	1	V1'	V1'	V7'	V7'
	-1	V1	V1	V7	V7
-2	1	V2	V1'	V7'	V8
	-1	V2	V1	V7	V8

cflx		2	1	-1	-2
ccpl	ce				
2	1	V2	V1'	V13'	V14
	-1	V2	V1	V13	V14
1	1	V1'	V1'	V13'	V13'
	-1	V1	V1	V13	V13
-1	1	V4'	V4'	V10'	V10'
	-1	V4	V4	V10	V10
-2	1	V5	V4'	V10'	V11
	-1	V5	V4	V10	V11

VI. CAPACITOR VOLTAGE BALANCING ALGORITHM

We know that the group small voltage vector "SVV" is divided into two sub-groups of vectors which do not have the same action on the voltage of neutral point voltage of the inverter. On the assumption that $U_0 = U_{Cl}$, use of the vectors of the first sub-group, this vectors obtained with combinations where 1 or 2 states is equal 1, the remaining states being 0, causes to increase the neutral point voltage U_0 of the inverter. On the other hand, the use of the vectors of the other sub-group of the "SVV" group, vectors obtained for combinations where 1 or 2 states is 1, the remaining states being 0, causes to decrease it (opposite effect).

Thus, if one decided to use only the vectors of one of the two sub-groups, in this case the direct control then become equivalent to the direct control of the couple of the induction machine supplied with a 2-levels inverter where DC voltage is equal to the one of the voltages of the condenser. However the input voltage of the 3-levels inverter is maintained constant (13) and is equal:

$$V_d = U_{Cu} + U_{Cl} \quad (13)$$

The use of the vectors of the first sub-group will have for effect to increase the value of the neutral point voltage U_0 . However if we chose $U_0 = U_{Cl}$, the terminal voltage of the condenser Cl will increase and that of the condenser Cu will decrease until being cancelled. It is thus not possible to control the machine by using only the vectors of one sub-group

If we take for example the two vectors $V4$ and $V4'$ which belong each one to one of the two sub-groups of the "SVV" group. They have both the same action on the module of stator flux and the value of the electromagnetic torque. On the other hand, they have contrary actions on the value of the neutral point voltage U_0 . The first will increase it while the second will decrease it. With this property one can control the variations of U_0 by maintaining them in a band of hysteresis centered around the value of reference which is null.

After having measured the voltages of the two condensers, we can calculate the variation (14) which exists between the two and which corresponds to an imbalance of the two condensers:

$$\varepsilon_t = U_{Cl} - U_{Cu} \quad (14)$$

We use hysteresis controller with 2 states to maintain the error in a band of hysteresis of width. $2 \cdot \Delta V_d$

If, $\varepsilon_t < -\Delta V_d$ or if $\varepsilon_t > \Delta V_d$ that means that imbalance between the two condensers becomes unacceptable in a direction or the other. In the first case, it will be necessary to impose a voltage vector which will have as an action to increase the neutral point voltage U_0 of the inverter; the second, one will impose a voltage vector which will have as an action to decrease it.

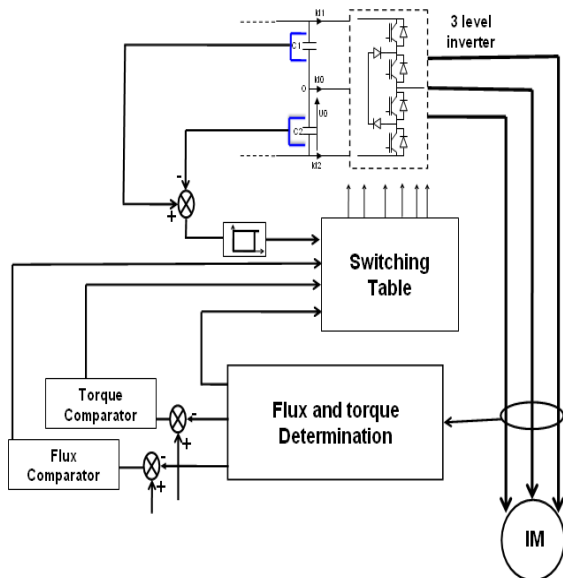


Fig. 5. Voltage unbalancing of the inverter capacitors

VII. THE SIMULATION RESULTS

The goodness of the proposed DTC algorithm has been verified in simulation on a PC. All simulations have been performed in the Matlab/Simulink environment. The used flux and torque constraints are expressed in percent with respect to the flux and torque reference values.

$$E_{\varphi_{\max}} = 3\% , E_{\varphi_{\min}} = -3\% , E_{\Gamma_{\min 1}} = -0.8\% ,$$

$$E_{\Gamma_{\min 2}} = -3\% , E_{\Gamma_{\max 1}} = 0.8\% , E_{\Gamma_{\max 2}} = 3\%$$

The simulation result illustrates both the steady state and the transient performance of the proposed torque control scheme.

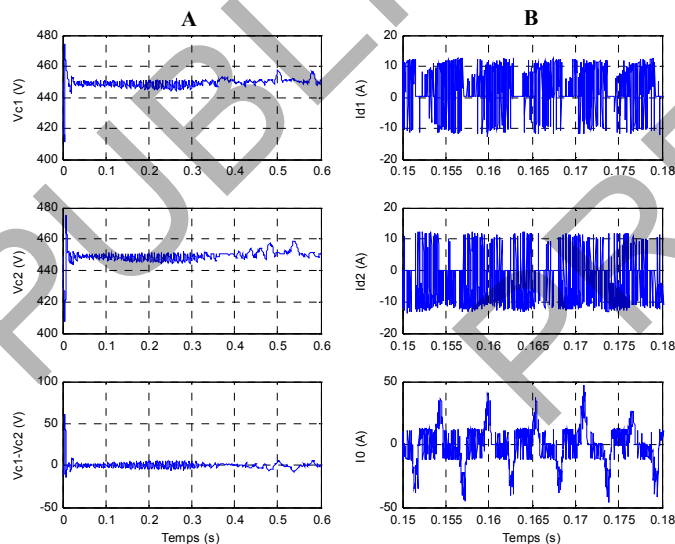


Fig. 6. A) DC input voltage of the inverter Vc1-Vc2 and their difference Vc1-Vc2
B) input currents of the 3-level inverter

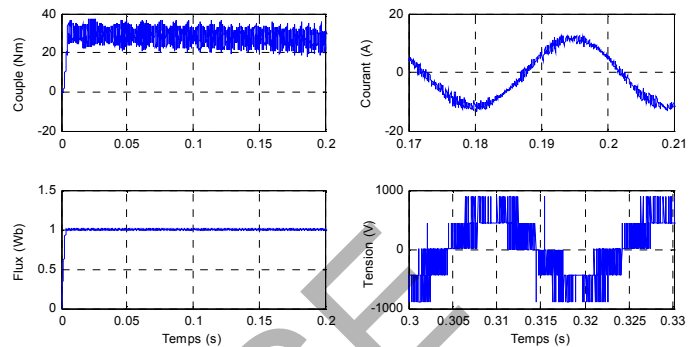


Fig. 7. Performances of the DTC drive associated to its supply at nominal reference of the flux and torque.

from figure (6-A), It can be observed that with the control algorithm the voltages in the capacitors C1 and C2 follow their references and the difference between them is practically low, On the figure (6-B) we can see that the inputs currents in the inverter Id1 et Id2 have the same form but they have are in phase opposition, the mean value of the Id0 current are equal to zero.

From The figure (7), the flux the torque oscillates around their reference values (respectively 1 Wb and 50 N.m), a few torque ripples, and the response time is very short taking into account the time add by the use of the algorithm without any need of more powerful processors. We can see that both of The voltage and current qualities (wave forme, harmonics) are very good which prove also the utility of this simple algorithm.

VIII. CONCLUSION

This paper presents a very simple method of the Direct Torque Control algorithm to be applied to 3-level Diode clamped inverters. The effect of proposed method has been proved by simulations. It is concluded that the proposed control produces better results for transient state operation. And it is suitable for high-power and high-voltage applications. We enhance the DTC approach by introducing two multi-level hysteresis comparators for flux and torque control. We impose the flux angle detection procedure by defining twelve sectors of space and establish a larger table of knowledge rules with optimal switching strategies.

Also, the neutral point voltage can be easily controlled by introducing a clamping bridge to solve the usual problem of unbalanced voltages input in three-level VSI.NPC. From this analysis high dynamic performance, good stability and precision are achieved; the results obtained are full of promise to use this system in high voltage and great power applications as electrical traction.

IX. REFERENCES

- [1] Y.H. Lee, B.S. Suh, and D.S. Hyan, "A novel PWM scheme for a three-level voltage source inverter with GTO thyristors". IEEE Trans. on Ind. Appl, vol. 33 2, March/April 1996, pp. 260-268.
- [2] I. Takahashi and T. Noguchi, "A new quick-response and high-efficiency control strategy of an induction motor". IEEE Trans. on IA, vol. 22, No. 5, Sept/Octo 1986, pp. 820-827

[3] J.C. Trounce, S.D. Round, and R.M. Duke, "Comparison by simulation of three-level induction motor torque control schemes for electrical vehicle applications". Proc. of international power engineering conference, 2007 IEEE .

[4] R. Zaimeddine, and E.M. Berkouk, "A Novel DTC scheme for a three-level voltage source inverter with GTO thyristors". SPEEDAM 2004, Symposium on power electronics, electrical drives, automation & Motion, June, vol. 2, June, 16th-18th 2004, pp. F1A-9-F1A-12.

[5] R. Zaimeddine, and E.M. Berkouk, "A Scheme of EDTC Control using a Three-Level Voltage Source Inverter for an Induction Motor". Proc. of international power engineering conference IEEE 2007

[6] F. Bacha, A. sbai, and R. Dhifai, "Two Approaches For Direct Torque Control of an Induction Motor". CESA Symposium on control, vol. 1, March 1998, pp. 562-568.

REMOTE IRRIGATION CONTROLLER UNDER PHOTOVOLTAIC ENERGY

M. L. BENZAOUÏ*, F. YUCEF ETTOUMI, A. ADANE
University of Science and Technology Houari. BOUMEDIENE (USTHB)
Faculty of Electronic & Computing
BP 32, El-Alia, Bab-Ezzouar 16111, Algiers, Algeria

Fax : 213 21 21 82 14

*Email : benzaoui_m_l@yahoo.com

Abstract- Water is an important thing in the earth, so we must use it economically, especially in the irrigation of fields in the dry areas and in summer days. So that we present in this paper, a conception of a device which permits us to control automatically the uses of water in irrigation. This is by microcontroller. We applied this device in the Sahara of Algeria (oasis).

And to get autonomy of the system, we have preferred to use the Photovoltaic systems as an electrical supply of the installation and a power for water pumping.

The great problem in irrigation is to specify water needs for each plant, which depends of temperature, land humidity, air humidity, wind and the nature of the plant.

In first we have used in the controller device many sensors to get the informations about these parameters which are used as inputs of the test conditions to irrigate.

And next an electronic device based on the microcontroller 16F877 was realised in order to get an automatic control and commands.

Finely we have tested this device to irrigate tomato, between June and July, and results were good.

Key Words: Irrigation, water pumping, Photovoltaic, microcontroller.

I. INTRODUCTION

In rural and remote area, to overcome the lack of water, the photovoltaic (PV) water pumping represents one of the best solutions. This is because solar radiation is generally high in arid zone location where the water is most needed [1].

Also, uses of water are a big problem in these days. The great consumption is in the Industrial uses and the irrigation. So we must find methods to reduce its exploitation.

In general when we irrigate plants we try to see the soil if it's dry, humid and if the climate is hot. We usually irrigate using a great quantity of water and without taking in consideration if the plants needs really water.

In this paper we propose to use a remote device to controller the water pumping and irrigation with photovoltaic supply.

II. IRRIGATION METHODS

There are many methods used in irrigation, as example we can find [1], [2]:

- Irrigation of surface.

- Underground irrigation.
- Irrigation under pivot.
- Irrigation by sprinkling.
- Irrigation drop by drop.

In our work we have chosen the irrigation drop by drop, because it's economic and easy.

For that we need some information of the local climate (microclimate), the plant type and the soil nature [3],[4]. We stocked water in a reservoir by using an electro-valve and pump on the water supply.

An electronic devise based on the microcontroller 16F877 is used with some sensors to survey the water level at the reservoir and activate irrigation (figure1).

And to get autonomy of the system, we used a photovoltaic generator as a power supply.

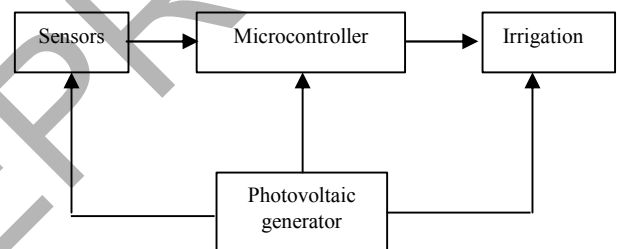


Figure 1: Irrigation System.

III. SENSORS

Information about the microclimate such as the temperature, Soil Humidity, air Humidity are important to get the best way of water uses, also we must know the water level in the reservoir. We have used for this [5]:

A. Temperature

To get the air temperature and the soil one, we have used two CTN resistors as sensors. These measures are compared with a reference temperatures T_{ref} fixed by the user (figure 2). The comparator is a low power dual operational amplifier (LM358). The outputs are connected to the controller

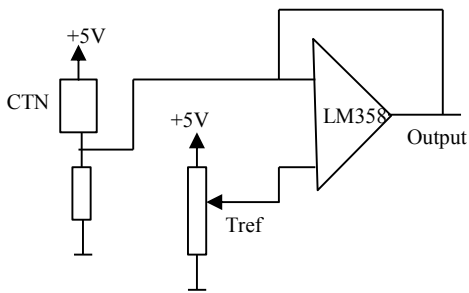


Figure 2: Temperature measurement

B. Humidity

In order to use water when it's necessary (for example the soil is dry), we have to know the humidity of the air and the humidity of the soil, so we have used two sensors (232269190001 of Philips), which are considered as a variable capacitor depended of the humidity.

So we placed these sensors in a Timer (NE555), to generate a cycle of time depended on humidity (figure 3). We use the microcontroller to activate the Timer and calculate the humidity by the measure of $\tau=f(C_H)$.

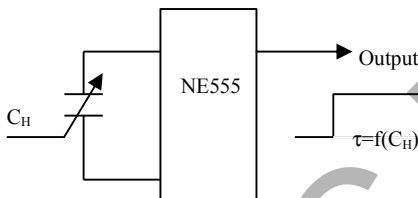


Figure 3: Humidity measurement

C. Water level

When we use the water from the reservoir we can fill or empty it, so we must know the level of the water in the reservoir. For this we have used 4 opto-transistors with 4 LED. In order to measure the 4 water levels.

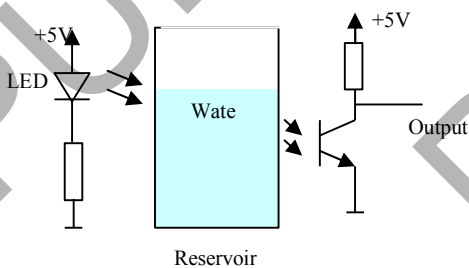


Figure 4: Water level measurement

D. Microcontroller

All these measures are used as inputs of a microcontroller, to get the right time for the irrigation and fill the reservoir. This microcontroller is the PIC 16F877 of MICROCHIP [6]. It has the advantage that it's easy to use and cheaper and sufficient to our application.

IV IRRIGATION

For irrigation we have to use a pump (P1) and a solenoid-valve (EV1) activated by the microcontroller to fill the reservoir. A second one (EV2) used to evacuate water from the reservoir (irrigation) and an other pump (P2) used in irrigation when the reservoir is empty.

We added a state where the reservoir is nearly empty in order to reduce the quantity of water used in irrigation to get more time when the water is enough.

So we have used 4 water levels:

- Full 100%: turn Off EV1 and pump1 and turn On EV2, the irrigation is normal.
- Half empty (50%): turn On P1, EV1 and we have to turn On EV2 in an economical irrigation.
- Nearly empty (20%): turn On P2, EV1 and EV2 used in the necessitate irrigation.
- Empty (0%): turn Off the pump P2 and EV2, turn On EV1 we can not irrigate.

The pumps used are a PP/MH-809-12V (5.5 gal/mn). And the solenoid-valve are EV1L280 [7].

All the irrigation installation is presented in figure 6.

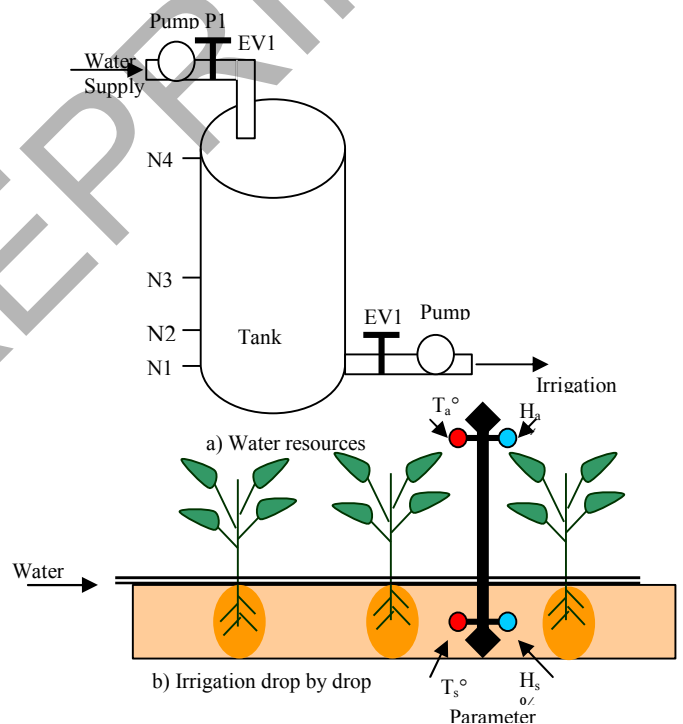


Figure 6: Irrigation system.

V PHOTOVOLTAIC SYSTEM

All the components of our system are chosen to be used under 12V DC, this is in order to use battery and a Photovoltaic (PV) installation.

The photovoltaic generator used is a 12V/50W (PWX500-50 of PHOTOWATT), and the battery is 12V/65AH (VARTA SOLAR) [8].

So the power supply is as in figure 7.

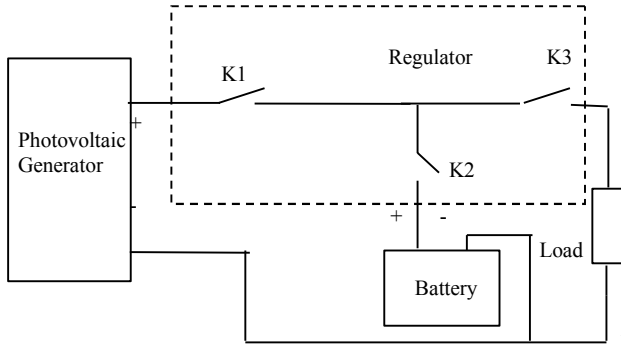


Figure 7: the photovoltaic power supply systeme.

A REGULATOR

In this installation Fig 2, the major problem is in the uses of battery, because it can be damaged easily by the charging current, the cycle of charge's number, and if we charge it up to its limit (charge exceed) or to discharge it under its limit (profound discharge). These thresholds are fixed by the battery characteristics [1]. To resolve these problems, we use a regulator which can be considered as controlled switches K1, K2 and K3 [9]. These have to keep the battery by disconnecting it from the photovoltaic generator if the battery potential is up to its limit, or to disconnect battery from uses if its potential is under its limit [1],[9] and to prolong the battery charge and discharge state and eliminate the quick commutations of switches [9].

Finely we have tested this installation to irrigate tomato, in summer (between June and July), at *Djamaa* a town in the Sahara of Algeria, where there is lack of water, the weather is very hot and dry. We have not used the green houses in order to get the real climate.

The results were good and the plants of tomato has resisted to the climate.

VI CONCLUSION

The aim problem at the Sahara and the Arab countries is water resource, so we have to use it economically especially in the industry and in irrigation. We always, use pump in these regions, which need power supply, so photovoltaic become one of the best solutions to electrify arid areas. We can say that our application is very important to generate it to conserve our reserve of water.

References

- [1] Med. L. BENZAOUI, F. YUCEF ETOUMI and A. ADANE, "Modelling of Photovoltaic Regulator with MPPT". Proceedings of the International Conference on Modeling and Simulation (MS'07 Algeria) July 2 - 4, 2007, Algiers, Algeria
- [2] CEMAGREF, Guide pratique d'irrigation, Dunod 1992
- [3] Zairi A., Mailhol J. C., Nasr Z., Slatni A., & Ruelle P. 1999. Surface irrigation strategies and their impacts on yield and water consumption - The Tunisian case. 50th International Executive Council Meeting, 17th International Congress of ICID. Q 48/1.31, September 11-19, 1999, Granada, Spain. pp. 42-50
- [4] I. Broner, Drip Irrigation for Home Gardens Gardening series no. 4.702.
- [5] G. ASCH Les capteurs d'instrumentation industrielle. Dunod 1989
- [6] C. Travenier Application industrielles des PIC. Edition Dunod 2000
- [7] International Product Catalogue, A Siebe Group Company.
- [8] Natural Resources Canada, Photovoltaic Systems: A Buyer's Guide, catalogue N° : M92-28/2001F ISBN : 0-662-86306-2.
- [9] Med. L. BENZAOUI, F. YUCEF ETOUMI and A. ADANE, "Simulation of water pumping using photovoltaic energy". Proceedings of the International Conference on Electrical Engineering Design and Technologies ICEEDT'08 HAMMAMET, TUNISIA November 8-10, 2008

Implementation of Inter-area Angle Stability Prediction in Wide Area Control

Ahmed A. Daoud

Abstract: This paper proposes a new interarea angle stability prediction algorithm. This proposed algorithm does not require any prior knowledge of system state as it operates directly from measurements drawn from PMUs. The proposed predictor foresees the system stability state for 500 ms in advance. Applying the COI angle concept for the interconnected power systems, inter-area stability can be predicted in a proper time. The proposed method was applied for two standard test systems, two area 4 generator system and IEEE 50 generators test system. The results showed that the prediction accuracy in most cases converges around 1 %. At the worst case the predicted values approaches 7%.

1. INTRODUCTION

Power systems are large interconnected nonlinear systems. They respond to a disturbance over a varying timescale, ranging from milliseconds even to hours. Wide range of contingencies and disturbances occur and abnormal operating conditions may be detected. A different corrective control schemes must be implemented in each type of contingency or disturbance at the right time [1].

Because of deregulation, many power systems around the world are being forced to operate closer to their stability limit because of the operational requirements in an open access environment and the environmental considerations. Power transfers across the interconnected areas of a power system are unpredictable due to market price variations. Inter-connection unforeseen operating conditions and area instability can lead to system blackout [2].

The recent series of blackouts in different countries has further emphasized the need for operators to have better information regarding the actual state of the power system they are operating.

For the last two decades, advances in computer technology and communications provide the operators with the information needed for appropriate control action. At the same time, measurement systems based on phasor measurement units (PMUs) are becoming proven technology and are seen by many utilities as one of the most promising ways of providing phasor information for wide area control [3].

Since many real-time operating decisions, both manual and automatic, are based on software applications using information derived from the phasor measurements through communication, these developments have shown immediate benefits in terms of increased accuracy, stability, and speed of convergence of control action decision making.

Current software and algorithms used in wide-area control are based on phasor measurements of bus voltage and generator reactive power [1]. In some applications, it is effective to use phase angle measurements to detect inter-area angle instability [1].

2. PROBLEM FORMULATION

If a severe disturbance, such as three-phase fault occurs in a tie-line between two areas of an interconnected power system, some of the generators of the power system may accelerate and may lose synchronism. If such a disturbance is not cleared at a proper time, the loss of synchronism may extend to other areas' generators and a blackout may occur [4].

The loss of synchronism after fault clearing is affected by the increase or decrease of the generator relative rotor angle beyond an identifiable threshold.

Phase angle prediction can be used to detect the first swing instability in advance, which gives time to operator to apply the proper preventive control action. Based on phase angle prediction and frequency measurements of critical generators buses from the entire interconnected power system transient stability can be detected and mitigated.

3. PROPOSED ALGORITHM

The phase angle of generator bus and relative phase difference varies through a wide range during system operation. The concept of center of inertia (COI) for the computation of the system phase angle reference is used to determine the interconnection phase angle [3]. This approach is used to quantify the extent of phase angle variations away from the system center.

Since the internal rotor angle cannot directly measured, we approximate the internal angle with the phase angle of generator bus which is normally monitored by PMU [3].

The proposed algorithm is divided into two parts, the first part is calculating the system COI through data collection from PMUs placed on generators bus. The second part, a fast learning algorithm is used to predict

Dr. Ahmed A. Daoud is with the electrical engineering dept., Suez Canal University, Port Fouad, Port Said, Egypt, 42523
E-mail: a.daoud@scuegypt.edu.eg

the fore coming values for COI and consequently determine system stability measure.

3.1 Center of Inertia COI

The COI is calculated in [5] as follows:

$$\delta_{COI} = \frac{\sum_{i=1}^N \bar{\delta}_i H_i}{\sum_{i=1}^N H_i} \quad (1)$$

Where $\bar{\delta}_i$ is the internal generator rotor angle, H_i is the respective generator inertia time constant and N is the total number of generators of the system areas.

As the machine inertia is directly proportional to the real power output, the weight factor of generator inertia time constant can be replaced by generator real power P .

For phase angle measurements in an area i in interconnected power system, we have the approximate center of inertia COI angle reference:

$$\delta_{COI}^i = \frac{\sum_{j=1}^N \delta_j^i P_j^i}{\sum_{j=1}^N P_j^i} \quad (2)$$

Where P_j^i denotes the real power generation schedule at generating plant $j=1, \dots, N$ in area i .

Increasing the number of phase angle measurements, in each area of interconnected power system, accuracy of δ_{COI}^i computation can be increased.

For the entire interconnected power system, the overall center of inertia δ_c can be calculated as follows:

$$\delta_c = \frac{\sum_{i=1}^N \delta_{COI}^i P^i}{\sum_{i=1}^N P^i} \quad (3)$$

3.2 Prediction Algorithm

The proposed prediction algorithm is an adaptation of a proven robotic ball-catching algorithm and has been applied to power system instability prediction as in [4].

The prediction algorithm is divided into two parts described in [6]:

The coarse tuning which is a tracking stage of interconnection center of inertia, δ_c , and

The fine-tuning which is the extended prediction of center of inertia, δ_c .

A. Coarse tuning

The actual calculated center of inertia angular position is represented by δ_c and the predictor is presented by ϕ . The algorithm requires the projection

of angular position δ_c in x-y coordinates and so as to the predictor position.

The x-y components of the predictor will be:

$$\begin{aligned} \phi_{px} &= \cos(\phi_p) \\ \phi_{py} &= \sin(\phi_p) \end{aligned} \quad (4)$$

and the center of inertia angular position will be represented by:

$$\begin{aligned} \delta_{cx} &= \cos(\delta_c) \\ \delta_{cy} &= \sin(\delta_c) \end{aligned} \quad (5)$$

For each sampling instant of PMU the center of inertia angular position x and y components will be updated.

Equations 4, and 5 will be substituted into the coarse tuning objective function:

$$\text{Min}_{T_f, \phi} \left\{ T_f - \alpha(\delta_c \cdot \phi_p) + \beta[(\delta_{cx} - \phi_{px})^2 + (\delta_{cy} - \phi_{py})^2] \right\} \quad (6)$$

where, T_f is a rough estimate of the final prediction time obtained from the equation:

$$\phi_p - \delta_c + T_f(\dot{\phi}_p - \dot{\delta}_c) = 0 \quad (7)$$

$\dot{\delta}_c$, $\dot{\phi}_p$ are the center of inertia and predictor velocities respectively, and are represented by:

$$\begin{aligned} \dot{\delta}_c &= \omega_c = \frac{d\delta_c}{dt}, \\ \dot{\phi}_p &= \nu_p = \frac{d\phi_p}{dt} \end{aligned} \quad (8)$$

and α and β are weighting functions.

The minimization of the objective function is obtained by differentiation of equation (6). The predicted center of inertia angular velocity ν_p in y-direction is driven through the following equation:

$$A_1 \nu_{py}^3 + A_2 \nu_{py}^2 + A_3 \nu_{py} + A_4 = 0 \quad (9)$$

where, A_1, A_2, A_3 , and A_4 are functions of δ_{cx} , δ_{cy} , ω_{cx} , ω_{cy} , α , and β which are known.

The predicted center of inertia angular velocity ν_p in x-direction is driven through manipulating equations (6) and (7)

$$\nu_{px} = \omega_{cx} + \frac{(\phi_{px} - \delta_{cx})}{(\phi_{py} - \delta_{cy})} (\nu_{py} - \omega_{cy}) \quad (10)$$

The optimum predicted center of inertia angular velocity vector can then be obtained, through Solving equation (9) for ν_{py} and equation (10) for ν_{px} .

For each sampling instant the difference between the measured center of inertia δ_c and the predicted center

of inertia φ_p is calculated and compared to a predetermined tolerance TOL . If the difference between the actual and predicted center of inertia is less or equal than pre-specified tolerance [$TOL \geq (\varphi_p - \delta_c)$], the algorithm is switching into the fine-tuning stage of prediction.

B. Fine tuning

The purpose of this stage is fine tune the predicted center of inertia value φ_p after a period of T_f regarding the φ_p trajectory generated from the coarse tuning process. Taylor series expansion has been proven as a good estimator for unknown data. It is used in this stage to fine tune the values obtained from the previous coarse tuning stage.

Angular center of inertia velocity varies continuously and shows a smooth change because of the large inertia of turbine-generator combination of interconnected area power system. In order to fine tune the predicted angular velocity ν_p , and center of inertia angle φ_p , a function extrapolating the three measured points $\omega_c(\zeta_0)$, $\omega_c(\zeta_1)$, and $\omega_c(\zeta_2)$ is defined using Taylor series expansion given by:

$$\nu_p(T_f) = \omega_c(\zeta_2) + \kappa_1(T_f - \zeta_2) + \kappa_2(T_f - \zeta_1)(T_f - \zeta_2) \quad (11)$$

where; ζ_0 , ζ_1 and ζ_2 are the last three time stamps for PMU measurements.

T_f = the prediction period in sec.

$$\kappa_0 = (\omega_c(\zeta_1) - \omega_c(\zeta_0)) / (\zeta_1 - \zeta_0)$$

$$\kappa_1 = (\omega_c(\zeta_2) - \omega_c(\zeta_1)) / (\zeta_2 - \zeta_1)$$

$$\kappa_2 = (\kappa_1 - \kappa_0) / (\zeta_2 - \zeta_0) \quad (12)$$

Integrating equation (11), the function predicting the center of inertia φ_p will be given by:

$$\varphi_p(T_f) = \int_{\zeta_0}^{T_f} \nu_p(t) + \delta_c(\zeta_0) \quad (13)$$

By using the algorithm above, area said to be losing synchronism can be predicted without any prior system configuration and exhausting system calculations. It will be shown by application that the proposed system can predict inter foreseen area instability in a time window permit the application of proper preventive control with acceptable prediction error.

4. APPLICATION TO INTERCONNECTED POWER SYSTEM

4.1 Simple Test System

The applicability of the proposed algorithm to a wide area power system is first studied with a simple system of two areas. The basic topology is depicted in Fig. 1 [5].

The system contains eleven buses and two areas, connected by a weak tie between buses 7 and 9. The left half of the system is identified as area 1 while the right half is identified as area 2.

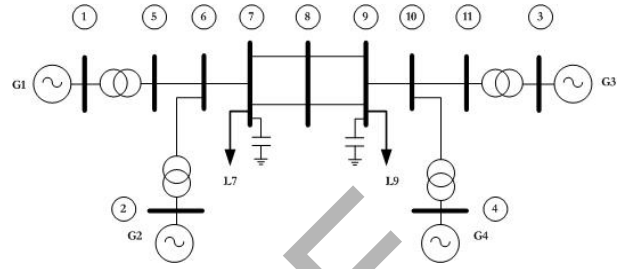


Fig. 1 Single line diagram of simple test system.

4.1.1 Stable conditions

A. Generators COI angles prediction

The system is simulated using Matlab software. The test system contains eleven buses, four generators, four transformers, two shunt capacitors, and two loads. The technical data of the system are obtained from [5].

A three phase fault is initiated at 0.5 s at bus nine of the studied system. The duration of the fault is 0.1 s and is cleared by opening the line 9-8 at 0.6 s. Simulation results showed that the system is stable.

The application of the prediction algorithm showed that the COI generator angles can be predicted for 500 ms with an acceptable accuracy.

Figure 2 shows the actual and predicted COI angles for the four system generators. It is obvious that the predicted values are very close to the actual COI measured values.

The prediction errors between the actual and predicted COI of the four generator buses 1, 2, 3, and 4 are also calculated. Figure 3 shows the prediction error of the four COI and the error is very small compared to the actual value of COI angles.

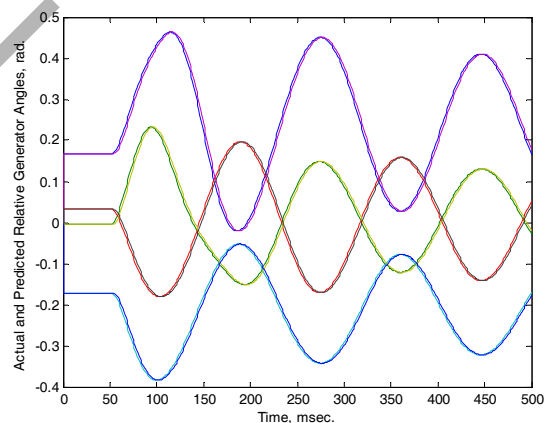


Fig. 2 Actual and predicted COI angles for a prediction time of 500 ms.

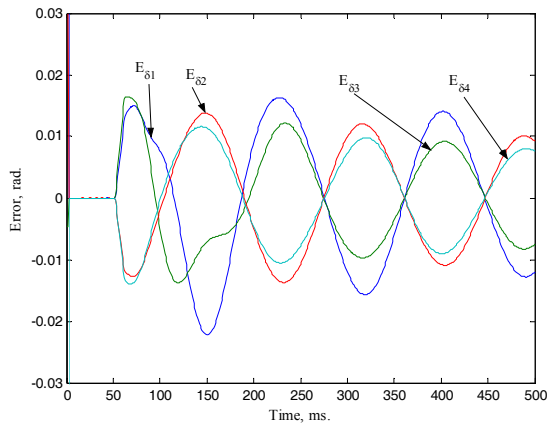


Fig. 3 Prediction error for COI bus angles.

B. Two area systems:

The previously 4 generators test system is divided into two area as given in [5]. Area 1 contains buses 1, 2, 5, 6, and 7, while area A2 contains buses 3, 4, 9, 10, and 11. The two areas are connected through a tie line between bus 7 and 9. The same fault and clearing conditions are applied to the two areas system. The proposed algorithm is applied to the test system to predict the two areas COI angles. Figure 4 shows the simulation result for 500 ms. Results verify that the COI angles of the two areas can be predicted with an acceptable accuracy. From figure 5, the prediction error for the COI angles is around 0.01 radian through most of the prediction period.

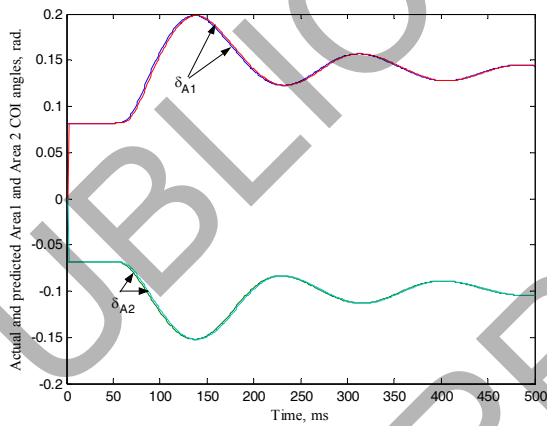


Fig. 4 Actual and predicted COI angles for area 1 and area 2

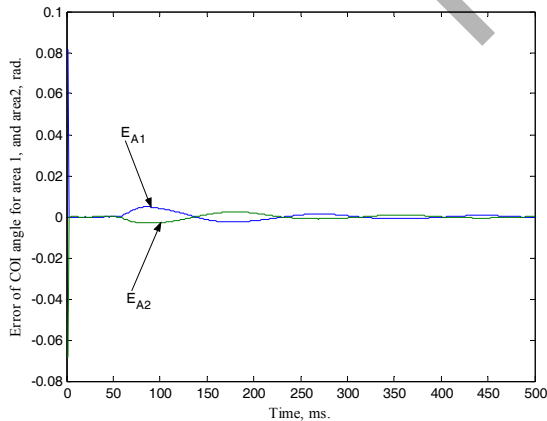


Fig. 5 Error between actual and predicted COI angle for area 1 and area 2

4.1.2 Unstable conditions

When applying a three phase fault at bus 6 at a fault time 0.5 s and clearing the fault 0.11 s later removing line 6-7 at 0.61 s, the system gone unstable. The proposed algorithm is applied to the unstable condition and the prediction results are given in figure 6. Area A1 COI angle decreases in an exponential manner to reach a value of -22.5 radians.

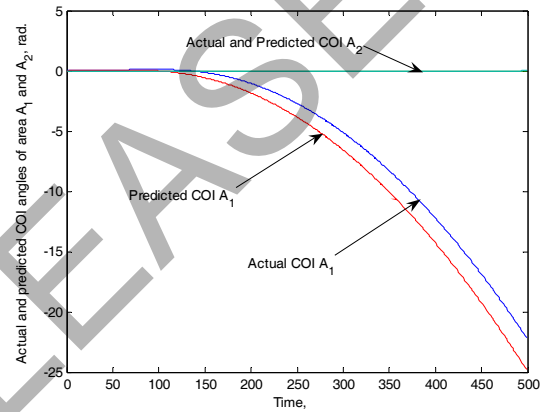


Fig. 6 Actual and Predicted COI angle for two areas network.

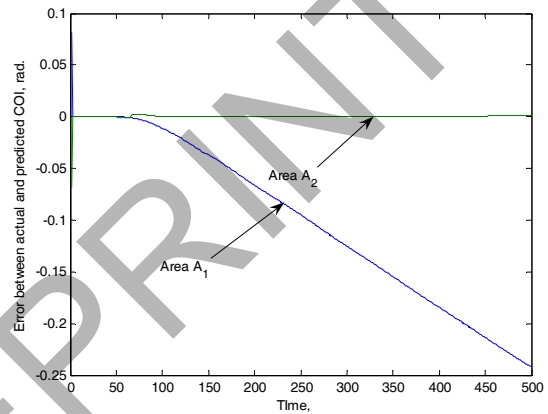


Fig. 7 Error between actual and predicted center of inertia of two areas system

Figure 7 shows the error between actual and predicted COI angles and it was found that the error value increases for unstable area A1 to reach about -0.24 radian.

4.2 IEEE 50 Gen-145 bus Test System

The investigation is, further extended to a larger test system. The IEEE 50 generator test system given by [7] is considered. The system data are given in table 1. Full system details can be found in [7].

Table 1: IEEE 50 Generator Test System Data

No. of Generators	50
No. of Buses	145
No. of Transmission Lines	401
No. of Transformers	52
No. of PV Buses	49
No. of Loads	64
No. of Shunt Reactance	97
System Frequency	50 Hz
Slack Bus	100

To investigate the effectiveness of the proposed algorithm, a three-phase fault was applied at bus 7. Fault was initiated at 0.1 second and cleared at 0.208 second by tripping line 6-7. This fault created an unstable condition for the system as generator at bus 104 (Generator #2) accelerating increasingly as shown in figure 8. In the meanwhile, the other 49 generator maintain equilibrium.

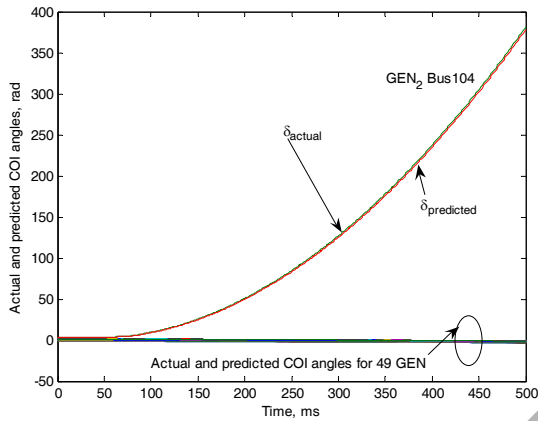


Fig. 8 Actual and predicted generator angle referred to COI at fault conditions

The prediction error is calculated and plotted to show the deviation from the actual COI angle. Figure 9 shows that the prediction error of generator 2 at bus 104 is increasing till a maximum value of 3.25 radians.

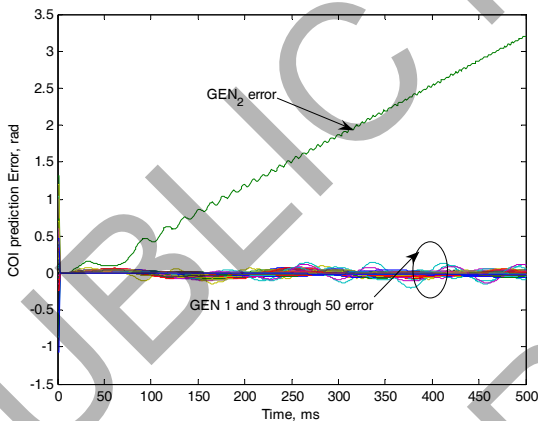


Fig. 9 Prediction error in radians

Separating generators (1, and 3 through 50) prediction error; figure 10 shows that prediction error clustered around zero with maximum value of ± 0.08 radians.

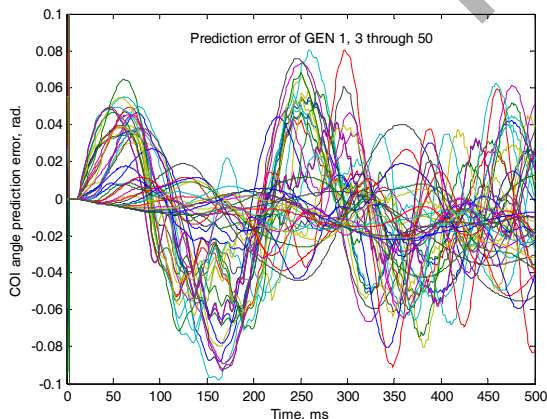


Fig. 10 Prediction error of stable 49 generators

Considering the wide area control and the need to divide the network into interconnected control areas; the system is divided into two areas as shown in table 2[7].

Table 2: IEEE 50 Generator Areas

Area No.	Generator Bus No.
1	115, 116, 130, 131, 132, 134, 135, 136, 137, 139, 140, 141, 142, 143, 144, 145
2	60, 67, 79, 80, 82, 89, 90, 91, 93, 94, 95, 96, 97, 98, 99, 100, 101, 102, 103, 104, 105, 106, 108, 109, 110, 111, 112, 117, 118, 119, 121, 122, 124, 128

Figure 11 shows the COI angle of the two area IEEE-50 generator system. For the fault conditions described above area 2 COI accelerate and the area is going to an unstable zone. Area 1 is stable as the variation of the inter area COI angle is approximately steady.

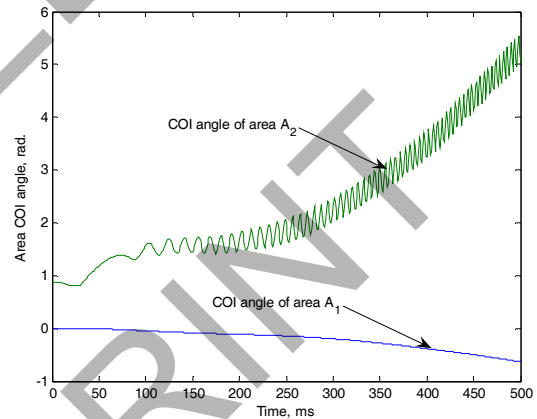


Fig. 11 The distribution of two areas COI angle along simulation time.

Predicting the two areas COI angles, the results shown that a precise approach to the values which have been calculated before.

Figure 12 shows the actual and predicted COI angles of the IEEE-50 generators two control areas. It is clear that the predicted values converged too close to the actual value.

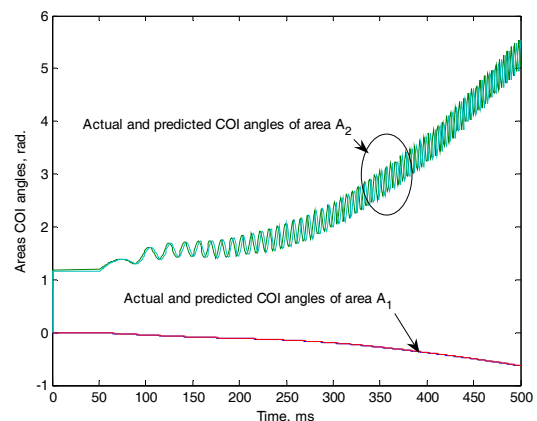


Fig. 12 Actual and predicted COI angles for 500 ms prediction period.

The accuracy of the predicted values is explained calculating the error between the predicted and the

actual COI angles. Figure 13 shows that the prediction error does not exceed 0.3 radians.

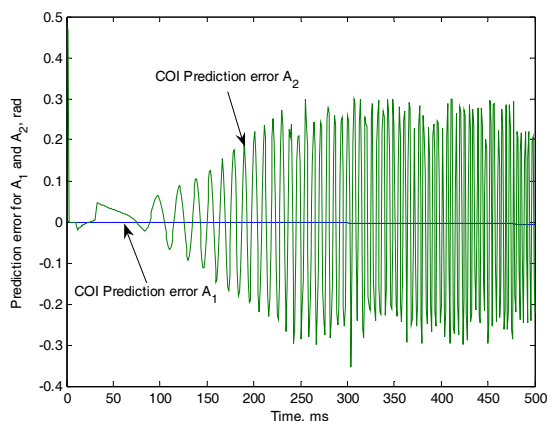


Fig. 13 Prediction error for 500 ms prediction period.

5. CONCLUSIONS

The proposed algorithm is adopted from a proven robot control system and the technology of PMU [2, 3, 6]. The algorithm shows a good accuracy regarding the actual COI angle prediction. No prior knowledge of system state is required. PMU measurements can predict the system stability state for 500 ms in advance. Wide area monitoring and control can be achieved on-line using the proposed algorithm. Severe contingencies can be prevented at the right time as foreseen system state can be predicted in advance. Further investigation on wide area control, such as generator tripping and load shedding, using the proposed method is in progress to proof the applicability of the algorithm.

6. REFERENCES

- [1] D. Hu, and V. Venkatasubramanian, "New wide-area algorithms for detecting angle instability using synchrophasors," in Proc. of the Western Protective Relay Conf., Spokane, WA, USA, 2006, pp 1-37.
- [2] G. Karady, A. Daoud, and M. Mohamed, "On-Line transient stability enhancement using multi-agent technique," in Proc. of IEEE WM02, 2002, pp. 893-899.
- [3] C. Taylor, D. Erickson, K. Martin, R. Wilson, and V. Venkatasubramanian, "WACS-Wide-area stability and voltage control system," in Proc. of the IEEE, Vol. 93, No. 5, May 2005, pp. 892-906
- [4] G. Karady, A. Daoud, M. Mohamed and I. Amin: "Fast learning algorithm for synchronous generator instability prediction," Int'l Journal of Engineering Intelligent Systems, Vol. 12, No. 2, June 2004, pp 67-71.
- [5] P. Kundur, Power System Stability and Control, EPRI, McGraw-Hill, Inc., USA, 1994.
- [6] B. Hove, and J-J Slotine, "Experiments in robotic catching," in Proc. of IEEE Int'l Conf. In Robotics and Automation 1995, Vol. 1, 1995, pp. 380-385
- [7] Washington State University, IEEE test case archive, Available: <http://www.ee.washington.edu/research/pstca/>

Some aspects of technical, economical and wind simplified analysis for 18 MW wind farm in Poland

Waldemar DOLEGA
Institute of Electrical Power Engineering;
The Wrocław University of Technology
Wybrzeże Wyspiańskiego 27
Wrocław, Poland

Abstract- In this paper, simplified analysis of different conditions of wind power expansion in Poland is shown. This analysis is made on basis of simplified computational example for 18 MW wind farm in Poland from the point of view different groups of parameters. Four groups of conditions: wind, geographical, technical and economical are taken into consideration.

I. INTRODUCTION

Renewable energy sources as: wind, hydro, solar, biomass, biogas, geothermal and sea waves are of more and more fundamental importance in electricity production in countries of the European Union. This situation also involves Poland.

From renewable sources, the quickest and the greatest development concerns wind energy. Last years in the world just belongs to wind power energy. Now, there are wind turbines set with a total capacity of over 94000 MW in the world, at the territory of the Europe over 64900 MW [8]. Only in 2008, at the territory of the European Union countries there were in total wind turbines with capacity of 8484 MW set, which means 15% increase of installed capacity in comparison to the previous year [8].

Germany is still leader of the sector in the extent of market size, where the total installed capacity exceeds 23903 MW, the second place in the extent of installed capacity belongs to Spain - over 16754 MW [8]. Moreover, in six countries of the European Union the total installed capacity exceeds 2 GW - in Italy (3736 MW), France (3404 MW), Great Britain (3241 MW), Denmark (3180 MW), Portugal (2882 MW) and Holland (2225 MW) [8].

Wind energy in Poland is still in its early phase in comparison with other countries of the European Union. At country's territory there are 36 wind power plants (only 11 wind farms) with a total capacity of 442 MW [9]. Average capacity of a set turbine amounts to about 1,52 MW. Capacity installed in wind energy -per capita is 0,0037 kW, and per km² of land area 0,45 kW [9]. Wind energy density in Poland is one of the lowest in the Europe. A number of wind farms is very small in composition with fact that there are profitable wind conditions in 30 % area of Poland (Fig.1).

In 2006 total energy production in wind parks in Poland amounted to 388,4 GWh, which means that share of energy production from wind in production of energy in renewable

energy sources in general amounted to 5,8% [4,9]. Share of wind generation in total country energy consumption in 2006 amounted to only 0,16 % [4,9].

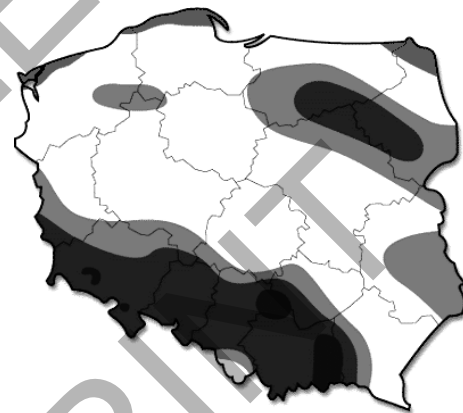


Figure 1. Wind resources in Poland (/colour - localisation/; grey - very profitable /north ends of Poland/; light grey - profitable; medium grey - enough profitable; dark grey - unfavourable /south part of Poland/; black - very unfavourable) [10]

In term 2004-2006, it was a dynamic increase of number and capacity of wind farms (almost 300%). It was installed 183,9 MW in wind farms installed power in this time [9].

A relatively quick development of renewables in Poland (especially wind farms) is connected with special consideration paid to renewables at the national level. It is determined in The Energy Law [1] and Decrees (Ordinances) of Ministers in charge of economic affairs [2,3]. This success was made mainly thanks to support given to renewables.

Support given to renewables in Poland are represented by: green certificate payment (market based), subvention to investment, additional benefits and limited fees for connection renewables to the grid [1-3].

According to The Energy Law and appropriate decrees (e.g. Ordinance of Ministry of Economy from 19.12.2005 about renewable energy purchase obligation [3]) the total balance of electricity in the gross national energy consumption in 2010 must contain 10.4 % share of renewable energy (and respectively: in 2009 - 8.7%). It means that any energy enterprise whose activity consists in electricity generation or trade in electricity, which sells the electricity to the final

customers connected to the grid on the territory of Poland are obliged to purchase electricity from renewables – 8.7% in 2009 and 10.4 % in 2010 [3].

Additionally, polish government plans for 2020 concern installing 13600 MW in wind energy and 20 % share of wind generation in the national energy consumption [4]. It means that in 2009-2020 increase of capacity that is needed amounts to at least 13200 MW, at the same time connecting about 1200 MW a year.

Presently, this subject matter are specially important because of fact, wind energy in Poland is planned to develop very dynamic and in the near period is planed to build many wind farms [9,10].

II. DESCRIPTION OF PROJECT

The main aim of this project was a realisation of computational example of 18 MW wind farm in Poland from point of view different groups of parameters. Four groups of conditions: wind, geographical, technical, and economical were taken into consideration.

First group of conditions were contained wind regime (consistent with mesoscale) as: yearly wind speed, specific yield and Weibull distribution. Yearly wind speed on level: 4, 4.5, 5, 5.5 and 6 m/s, profitable for wind power expansion in Poland, was considered in analysis. This range of values of wind speeds is fitted to conditions which are occurred in Poland (Fig.1.). Wind speed was qualified at a height - 30 m.p.g [10].

Simplification as wind regime for temperature of air - 15°C, pressure of air - 101.3 kPa /specific weight 1.225 kg/m³/. Wind was modelled to use Weibull distribution with shape parameter equal 2. This model was a standard for polish wind conditions [10]. Wind speeds were related to geographical regions in Poland.

Second group of consider conditions were geographical conditions as: localisation of wind farm and surface class. Localisation of wind farm was qualified through connection with yearly wind speed. Surface class (roughness) was considered according to Danish elaboration on level: 0 (surface of water), 1 (open fields with single buildings), 2 (open fields with few buildings /distant about 500 m/) [5,11].

Third group of consider conditions were technical conditions as: unit of wind turbine, producer of wind turbine, rotor area, wind turbine power curve, characterised power of unit of wind turbine. In the frames of investigations some units of leader producers from Denmark are considered [11-13]. These producers are: BONUS, NEG MICON, NORDEX, VESTAS and WIND WORLD. Offer specification of turbine for each producers is taken into considerations [12,13].

For project simulation of wind power plant about 18 MW nominal power were used:

- 30 units about 600 kW nominal power each (Bonus 600/44 Mk IV, NEG Micon 600/43, Nordex N43/600, Vestas V44 600/44 and Wind World 600/42);
- 24 units about 750 kW each (NEG Micon 750/44, Wind World 750/48);
- 18 units about 1 MW each (NEG Micon 1000/60, Bonus 1000/54, Nordex N54/1000);

- 12 units about 1,5 MW each (NEG Micon 1500/72, Nordex S70/1500);
- 9 units about 2 MW nominal power each (Bonus 2000/76, NEG Micon 2000/72, Vestas V66 2000/66).

Fourth group of consider conditions were economical factors as: wind turbine price, installation cost of turbine, total investment cost of turbine, operational & maintenance cost, price per 1 kWh produced electricity, price of green certificate per 1 MWh produced electricity, inflation rate and rate of discount. All incurred costs and economical calculations were realised in EUR currency. Wind turbine prices was taken from offer specification of producers [12,13]. Installation cost of turbine was qualified as 30% wind turbine price [11]. Operational & maintenance cost was considered on level 1.5% wind turbine price yearly [11]. Period of exploitation was qualified as 25 years [5]. Rate of discount was qualified as 8 % [6,10]. Real rate of return was also qualified on level 8%. For simplification, price per kWh produced electricity was taken in calculations as constant in time on level 0.03, 0.04 and 0.05 EUR/kWh. Price of green certificate per 1 MWh produced electricity was qualified as 64.21 EUR/MWh [7]. For economical calculations all prizes, costs and counters (EUR/PLN, USD/PLN, EUR/USD, EUR/DKK) were taken as average level in 2007. Investment was qualified as totally realised from own financial sources. Quantity of subsidies was calculated as the aim to obtain of investment profitability. Economical calculations were realised with reference to hypothetical wind farm about 18 MW nominal power. For simulation, this farm is included from: 30 units about 600 kW nominal power each, 24 units about 750 kW each, 18 units about 1 MW each, 12 units about 1.5 MW each and 9 units about 2 MW nominal power each. All units in the wind farm were produced by the same producer.

III. WIND FARM CALCULATION

In frames this project two main groups of calculations were realised. These calculations were made with using two computer programs elaborated by author.

First group were calculations of year energy output for specified wind turbines, wind speeds, surface classes and Weibull shape parameter. In frames these calculations power input, power output, energy output and capacity factor were calculated.

Technical and economical calculations are related to five analysed configurations of wind farm, 15 basic units, profitable wind conditions (yearly wind speed: 4, 4.5, 5, 5.5 and 6 m/s) and different surface classes suitable for localisation of wind farm (surface class: 0,1 and 2). The main parameters of technical and economical estimate were: yearly total energy output from analysed wind farm, capacity factor of wind farm, total investment costs, total income per year (sale of electricity, sale of green certificates, inclusive), cost of 1 kWh produced electricity from analysed wind farm. Electricity price per kWh on assumed levels are determined as a limit of profitability, according to polish conditions [10].

Process of simulations and analysis was divided into two stages:

- selection of the best solution within given configuration of wind farm,
- selection of the best solution for wind farm.

IV. ANALYSIS OF WIND FARM

Conducted simulations and analysis for individual configurations of wind farm about 18 MW nominal power let to select the best variant for each configuration. Selection was based on three criterions: max. yearly energy output, min. cost of 1kWh produced electricity and max. total income per year from sale of electricity and green certificates. The best solutions for each configurations of wind farm are presented in table 1. The best composition of wind farm was selected of these configuration according to listed earlier criterions.

TABLE 1.
The best solutions inside individual configuration

Composition of wind farm	Producer of turbine	Type of turbine	Nominal power of turbine
30 x 600 kW	Nordex	N43/600	600 kW
24 x 750 kW	NEG Micon	750/48	750 kW
18 x 1MW	NEG Micon	1000/60	1 MW
12 x 1.5MW	Nordex	S70/1500	1.5 MW
9 x 2 MW	Bonus	2000/76	2 MW

Analysis of solutions for optimal localisation of wind farm (surface class – 0) from point of view total energy output for different yearly wind speeds leads to conclusion that the best solution is a wind farm included 18 units NEG Micon 1000/60.

Yearly wind speed has the greatest influence on total energy output of wind farm. A higher yearly wind speed in place of wind farm localisation means larger productivity of wind farm. Even slight deviation from assumed yearly wind speed results in differences in electricity production on level a few dozen or so, and even a few dozen percent. Differences between five considered solutions with reference to total energy output are presented in table 2. Solution with 1 MW units is the best for each analysed yearly wind speed, but in principle solutions with units about largest nominal power are the best.

TABLE 2.

Comparison of total energy output per year (MWh) for analysed 18 MW wind farm for different yearly wind speeds (surface class = 0)

Composition of wind farm	Yearly wind speed, m/s				
	4	4.5	5	5.5	6
30 x 600 kW	11838.9	16803.6	22914.0	29406.3	36280.5
24 x 750 kW	11421.0	16750.9	22842.1	29694.7	36928.1
18 x 1MW	14722.5	20968.3	27660.4	34798.5	42382.8
12 x 1.5MW	12954.4	19026.8	25908.9	33600.6	41292.3
9 x 2 MW	12168.6	17537.1	23621.4	30779.4	37937.3

For example, wind farm included 1 MW units produces 27660 MWh electricity for yearly wind speed on level 5 m/s and it brings in total inclusive income per year on level 2882489 EUR for price for sale of 1 kW produced electricity on level 0.04 EUR (tables 2, 6). The cost of 1 kWh produced electricity from analysed wind farm is equal 0.12 EUR (table 7). This solution is on a limit of profitability, thanks to significant income from sale of green certificates. Solution with 750 kW units is the most disadvantageous. Such farm produces 17 %

less electricity and total inclusive income per year decreases also 17 % i.e. 502113 EUR (tables 2, 6). Producing of 1 kWh electricity costs 0.02 EUR more (table 7).

Significant differences between solutions occur for yearly wind speed on level 6 m/s. The farm included 30 units Nordex N43/600 produces 14 % less electricity than farm included 18 units NEG Micon 1000/60 (table 2). Differences are smaller for other configurations of wind farm.

Similar correlations concern capacity factors for wind farm. Maximum values of capacity factors obtain for yearly wind speed on level 6 m/s. Than wind turbine NEG Micon 1000/60 has capacity factor on level 27 %, however turbines Nordex N43/600 and NEG Micon 750/48 have 23 % (table 3).

TABLE 3.

Comparison of capacity factor (%) for analysed 18 MW wind farm for different yearly wind speeds (surface class = 0)

Composition of wind farm	Producer of turbine	Type of turbine	Yearly wind speed, m/s				
			4	4.5	5	5.5	6
30 x 600 kW	Nordex	N43/600	8	11	15	19	23
24 x 750 kW	NEG Micon	750/48	7	11	14	19	23
18 x 1MW	NEG Micon	1000/60	9	13	18	22	27
12 x 1.5MW	Nordex	S70/1500	8	12	16	21	26
9 x 2 MW	Bonus	2000/76	8	11	15	20	24

Simplified economical analysis leads to conclusion that the wind farm included 18 units NEG Micon 1000/60 has the best economical parameters.

Total inclusive income for wind farm is obtained from sale of electricity and green certificates. It depends mainly on quantity of produced electricity as well as unit price for sale of electricity (1 kWh) and unit price for sale of green certificate (1 MWh). For example, wind farm included 1 MW units brings in total inclusive income per year on level 4416713 EUR for yearly wind speed 6 m/s, however it decreases 65% to level 1534230 EUR for yearly wind speed 4 m/s (table 6).

Influence of unit price for sale of electricity on total income of wind farm for example yearly wind speed 5 m/s is presented in table 4.

TABLE 4.

Comparison of total income per year (EUR) obtained from electricity sale in function of price for 1 kW produced electricity (yearly wind speed = 5 m/s, surface class = 0)

Composition of wind farm	Producer of turbine	Type of turbine	Price for 1kWh, EUR		
			0.03	0.04	0.05
30x600 kW	Nordex	N43/600	687420	916560	1145700
24 x 750 kW	NEG Micon	750/48	685264	913685	1142106
18x1 MW	NEG Micon	1000/60	829811	1106415	1383018
12x1.5 MW	Nordex	S70/1500	777266	1036355	1295444
9 x 2 MW	Bonus	2000/76	708641	944855	1181068

Influence of unit price for sale of green certificate on total income of wind farm for different yearly wind speeds is presented in table 5. For example, wind farm included 1 MW units brings in total income from sale of green certificates per year on level 2721400 EUR for yearly wind speed 6 m/s, however it decreases 65% to level 945332 EUR for yearly wind speed 4 m/s (table 5).

TABLE 5.

Comparison of total income per year (EUR) obtained from sale of green certificates for produced electricity for different yearly wind speeds (surface class = 0)

Composition of wind farm	Yearly wind speed, m/s				
	4	4.5	5	5.5	6
30 x 600kW	760176	1078959	1471308	1888179	2329571
24 x 750kW	733342	1075575	1466691	1906697	2371153
18 x 1MW	945332	1346375	1776074	2234412	2721400
12 x 1.5MW	831802	1221711	1663610	2157495	2651379
9 x 2 MW	781346	1126057	1516730	1976345	2435954

Profitability of wind farm depends strictly on cost of 1 kWh produced electricity. It is connected with yearly wind speed, higher speed means smaller cost (table 6). Cost of 1 kWh produced electricity should be smaller than price per kWh produced electricity. Analysed solutions aren't effective economically even for the highest assumed level of unit price for sale of electricity (0.05 EUR) and yearly wind speed 6 m/s (table7). Effectiveness is obtained thanks to significant income from sale of green certificates.

Wind farm included 1 MW units has the smallest cost of 1 kWh produced electricity. However the largest cost is for wind farm included 750 kW units (table 7).

TABLE 6.

Comparison of total income per year (EUR) obtained from electricity sale and sale of green certificates for different yearly wind speeds (price for sale of 1 kW produced electricity - 0,04 EUR surface class = 0)

Composition of wind farm	Yearly wind speed, m/s				
	4	4.5	5	5.5	6
30 x 600 kW	1233732	1751103	2387868	3064431	3780791
24 x 750 kW	1190184	1745611	2380376	3094487	3848276
18 x 1MW	1534230	2185109	2882489	3626353	4416713
12 x 1.5MW	1349980	1982785	2699965	3501518	4303070
9 x 2 MW	1268089	1827540	2461585	3207519	3953448

TABLE 7.

Comparison of electricity cost per kWh for analysed wind farm for different yearly wind speeds (price for sale of 1 kW produced electricity - 0,04 EUR, surface class = 0)

Composition of wind farm	Producer of turbine	Type of turbine	Yearly wind speed, m/s				
			4	4.5	5	5.5	6
30 x 600 kW	Nordex	N43/600	0.27	0.19	0.14	0.11	0.09
24 x 750 kW	NEG Micon	750/48	0.28	0.19	0.14	0.11	0.09
18 x 1MW	NEG Micon	1000/60	0.22	0.15	0.12	0.09	0.075
12 x 1.5MW	Nordex	S70/1500	0.25	0.17	0.13	0.09	0.08
9 x 2 MW	Bonus	2000/76	0.26	0.18	0.135	0.10	0.08

V. CONCLUSIONS

A quick development of renewables (especially wind farms) in Poland in last years is closely related to good law and economic solutions.

The Energy Law [1] with Ordinances of Ministry of Economy [2,3] are key law acts in Poland for development of renewables.

Support given to renewables in Poland constitutes market based green certificate payment, subvention to investment,

additional benefits and limited fees for connection renewables to the grid.

Green certificate payment (market based) and subvention to investment are key support means given to renewables in Poland.

Green certificate payment is the best solution for development of renewables applied in Poland.

Energy enterprises which generates electricity from renewables in Poland have two sources of income - from sale of physical electricity and - from sale of property rights connecting with certificates of origin (green certificates).

Realised investigations enable to qualify a localisation of wind farm about 18 MW nominal power for different profitable yearly wind speeds, different surface classes and optimum selection of unit for wind farm.

Yearly wind speed has the greatest influence on total energy output of wind farm and electricity cost per kWh produced by it. Growth of yearly wind speed causes considerable growth of total energy output and considerable decrease electricity cost per kWh.

Surface class has considerable influence on total energy output and electricity cost per kWh.

Type of units applied in wind farm has a great influence on total energy output and electricity cost per kWh.

The best solution for analysed 18 MW wind power plant is farm consisted of 18 units NEG Micon 1000/60.

At present market mechanisms wind power farm investments are profitable for good localisations. The main causes of wind farm profitability are market based mechanism of green certificates and subvention to investment from different national and union funds.

REFERENCES

- [1] Act of 10 April.1997 – The Energy Law (Journal of Laws of 2003 No.153, Item 1504, No.203, Item 1966, of 2004 No.29, Item 257, No 34, Item 293, No.91, Item 875, No 96, Item 959, of 2005 No.62, Item 552). /in polish/
 - [2] Ordinance of Ministry of Economy from 4.05.2007 about detailed conditions of power system functions (Journal of Laws of 2007 No.93, Item 623). /in polish/
 - [3] Ordinance of Ministry of Economy from 19.12.2005 about renewable energy purchase obligation (Journal of Laws of 2005 No.261, Item 2187). /in polish/
 - [4] Energy policy of Poland up to 2030 – Project formulated by Ministry of Economy. Warsaw, september 2007. /in polish/
 - [5] T. Burton, D. Sharpe, N. Jenkins, E. Bossanyi: Wind Energy Handbook, John Wiley and Sons Ltd. Chichester, England, 2001.
 - [6] J.F. Manwell, J.G.McGowan, A.L. Rogers: Wind Energy Explained: Theory, Design and Application, John Wiley and Sons Ltd. Chichester, England, 2002.
- www pages
- [7] URE (Energy Regulatory Office) <http://www.ure.gov.pl>
 - [8] EWEA (European Wind Energy Association) <http://www.ewea.org>
 - [9] PWES (Polish Wind Energy Society) <http://www.ptew.pl>
 - [10] Wind Plants – News Bulletin <http://www.elektrownie-wiatrowe.org.pl> /in polish/
 - [11] Know how: Danish Wind Industry Association, www.windpower.org/en/tour.
 - [12] Wind energy: The World of Renewable Energy Industry, www.iwr.de.
 - [13] Wind turbine index: The International Portal for Wind Energy - Branch, www.windfair.net.

The aspects of combustion and co-combustion biomass

Grzegorz Maliga ^a, Amar Patil ^b

^a Phd's student of Department of Mechanical and Power Engineering, Wrocław University of Technology
grzegorz.maliga@pwr.wroc.pl

^b MSc's student of Department of Computer Science, Wrocław University of Technology
amar_ec006@yahoo.co.in

Abstract

Growing world population, increasing energy use, emission carbon dioxide (CO₂) and climate changing are the reasons for searching alternative sources of power. Recently we are vested with numerous alternative sources of energy but biomass is considered as a most powerful and easiest to access.

The biggest problems with burning raw biomass are: first the calorific value of biomass is average half compare to coal, second problem is a big contents of moisture for example in coal 10% of weight is water but biomass include even 35% of water.

For these reasons in huge power plants complete displacing stone fossil and lignite by biomass is not workable. Coal-fired furnaces which are used in power plants are not adapted to burn raw biomass, hence in powerplants co-combustion biomass and coal for power production is most efficiency because this process does not require additional energy. Precious advantage of co-combustion is that technical range of change the fuel feed system is less. Preparing the fuel mixture based on blending biomass with coal on storehaus or in coal mills. The most efficient dose biomass to coal is about 10% weight.

Otherwise in small domestic heat furnace burning a raw biomass with high efficiency is possible for example wood pellets furnaces are popularly used in onefamily houses. These kind of combustion occur, because the furnaces are specific adapted. The calorific value of wood pellets is near 19 MJ/kg which is compare to coal. Wood pellets are assembled for example numerous from energy willow or other kinds of waste wood and preparing the pellets form requires energy addition.

In this paper I demonstrate two ways of burning biomass: combustion and co-combustion. I try to show that selecting the way of burning is depended by size of furnace.

I. INTRODUCTION

Today human life is becoming very mobility and more comfortable, because it is representative aspect of modern civilisation. In different point of view, more comfortable life influences on level of energy consumption. We are aware that increase energy

using is the main reason of growing the greenhouse effect and warming the atmosphere which symptom as the unpredictable changes in climate. In this issue only one effect emission of carbon dioxide and other greenhouse gases by the combustion of fossil is predicted. Currently 90% energy which population use become from fossil supply. It diminishes coal and oil amount. From these reasons we require alternatives to fossil sources of energy, which can be renewable.

In table I are presented the sources of renewable, which were used in Germany in 2007. It shows that biomass is the biggest share of renewable energy and it amounts 48,6%, where 37,9% was used as a source for heating and 10,7% for producing the electricity.

TABLE I
SHARE OF RENEWABLE ENERGY CONSUMPTION IN GERMANY 2007

Nr.	Groups of renewable energy sources	Share %
1.	Biomass (heating)	37.9
2.	Biomass (electricity)	10.7
3.	Biofuels	20.0
4.	Hydropower	9.3
5.	Wind energy	17.8
6.	Solarthermal energy	1.7
7.	Geothermal energy	1.0
8.	Photovoltaic energy	1.7

Potential of using biomass as a source of energy is huge compare to the other kind of renewable fuels. The second important subject of debate is race of energy, which can be produced from biomass. The most share is heating and electricity and these are most useful in today's life. In order to produce heating or electricity from biomass it is necessary to use the burning process, which converts chemical capacity of biomass to thermally kind of energy. Biomass could be burn as a main fuel which is considered as a combustion or the alternative is co-combustion where biomass is only added as a share to fossil fuel for example in 10% amount.

II. BIOMASS

Biomass is regarded as material of organic origin. In this group count not only plants but also animals excrements, plant components, paper, cellulose, organic waste and vegetable oil.

There is a lot of method to use these various organic materials as a source of energy. In some technical solutions raw biomass can be turn into liquid or gaseous form before converting to other kind of energy. Raw organic materials can be burn in furnace to prepare heat. The second way is use the fermentation process by anaerobic digester to yield biogas, which can be latter burn. Third variant is using thermochemical gasification to convert biomass into synthetic gas. But this paper focused only on aspects of combustion and co-combustion.

A. Sources of biomass

Important source of biomass is the forestry. For example in Germany 80% of timber, which is annual growth become felled and used. Felling and preparing timber consequence in a big amount of waste timber, which left in the forest. Timber waste is no useful as a construction timber or for cellulose production, so it is adequate opportunity to use it as a biomass for energy production.

Second source of biomass is agriculture. Currently for production the same amount of food farmers need less and less land. From this reason cultivation of energy crops can increase and in the future it could be great energy potential. Today the residues materials like a straw are used prevalent and are converted for heat in specific furnace. Also the fast growing groups of trees and grass are tested to increase these efficiency, because in the future these could be the main sources of biomass. Production energy crops and plants by farmers becoming greater because using new method of cultivation being economically.

Third source of biomass is food industry. For example in process of preparing fruits or vegetables produce a lot of green waste, which can be used as a biomass. But the biggest disadvantage of using this kind of biomass is large amount of moisture. Before using green waste as a fuel for furnace, it should be dry or mixing with other kind of organic materials, which contain less amount of water.

B. Porcess of growing biomass and carbon dioxide neutral.

The basic of plants growing reason is the photosynthesis occurrence. In this reaction carbon dioxide with water are transformed into oxygen and carbohydrates. The oxygen is released into environment. The main force of photosynthesis is solar energy. The main conclusion could be that for the fact of being the sun is possible to use biomass. The efficiency of producing biomass is depended on naturally differences as the soil and climate opportunities. It is calculated [1] that every year in the World is growing 400 million tones of biomass. This amount of material contains $3000 \cdot 10^{18}$ J of energy. For example human use every year about $400 \cdot 10^{18}$ J, where only $45 \cdot 10^{18}$ J is producing from biomass. These numbers shows that in the future biomass could be use more intensively as a source of energy.

The carbon dioxide aspect in growing plants is important role, because it is fixed by plants, which are called as a carbon dioxide sink. This phenomenon influences on earth's climate balance. Also raw fossil materials are carbon dioxide sink, but fixing existed millions years before. Now the raw fossil contain large amount of carbon and these are easy used as a fuels in combustion process. Combining carbon with oxygen produces carbon dioxide which is main reason of greenhouse effect.

Nature biomass growing and using as a source of energy make that the concentration of carbon dioxide is constant and the cycle is closed, but when the fossil are used carbon dioxide concentration rise.

TABLE II
AMOUNTS OF CO₂ EMISSIONS DEPENDING ON THE ENERGY SOURCE

Energy source	CO ₂ emission (kg/MWh)	Annual CO ₂ emission (kg/a)	CO ₂ savings compared with fuel oil (kg/a)
Fuel oil	342	5472	0
Natural gas	228	3648	1824=33%
Wood pellets	68	1088	4384=80%
Firewood	8.8	141	5331=97%

III CO-COMBUSTION BIOMASS

In huge powerplants, where using power coal as a basic fuel is common, because from the energy point of view, coal characterises two features: effortlessness to purchase and the calorific value is very high level such as $22 \text{ MJ}\cdot\text{kg}^{-1}$. Compare biomass to power coal the calorific value is half lower. Second important issue is fuel feed system, which was designed and adapted only for fossil coal. Replacing whole of fuel feed system requires a huge amount of capital expenditure and it is unfounded from economical point of view. The third issue is problem with adapting the steam boilers to new fuel such as biomass. Majority of steam boilers, which are using in huge power plants are adjusted to coal dust. Coal dust is fed to steam boiler as a powder after milling process. Granularity of the fossil dust is depended on standards of quality and for example in polish power plant industry are using coal dust where R_{90} value is 30% and R_{200} is about 3%. It means that for biomass obtaining similar value of granularity is not possible. Another problem with biomass is level of moisture, which is double compare to coal. Bigger biomass particles and high value of moisture need longer time of burning in boiler combustion chamber compare to coal dust. Different is also the bulk density of biomass because the value is only $0.25\text{-}0.30 \text{ kg}\cdot\text{m}^{-3}$, which is very low compare to coal powder. Another physical properties, temperature of burning and amount of ash reason that the furnaces should be fixed apart to different kind of biomass. During designing process of co-combustion biomass with coal is important to consider the share of added biomass, because it influences directly on parameters of working the steam boiler such as: steam temperature, exhaust temperature, amount and chemical composition of ash or burning waste and slagging the heating surface, which operating conditions is important from heating change point of view. Basing on the results of research [1] co-combustion the biomass, showed that the influence share of biomass does not increase emission of nitrogen oxides (NO_x), sulphur oxides (SO_x) and carbon oxides. For a variety of biomass only adding a rape straw increases contents of sulphur oxides (SO_x) in exhaust gases. Besides adding the biomass to major fuels does not influence on slag and ash properties. Experiments [1] allow for proof that only adding straw changes rheology properties of slag, because especially the corn straw contains high quantity of chlorine. Content chlorine in fuels increases the flow ability of slag which is negative phenomenon, because when the opportunity of slag to flow is higher, its consequences of becoming overgrown the heater surface by slag. When the layer of slag increases on the boiler's surface, it will decrease the heat exchange between exhaust gas and working medium, such as water or steam, because slag

characterises high heat resistance. For example when the heat is exchanging in the way of conduction the efficiency is defined by Fourier's law, which is described by equation (1):

$$Q = \frac{\lambda}{l} \cdot A \cdot \Delta T \quad [1]$$

where Q is the heat flux, W ; λ the thermal conductivity, $W\cdot(\text{m}^2\text{K})^{-1}$; l the thickness of layer heat exchange, m ; A the heat exchange surface, m^2 ; ΔT the temperature difference, K .

Based on the equation (1) it is able to conclude that for the material such as slag, the thermal conductivity is less, so when layer of slag becomes higher, the heat flux decreases.

In huge power plants when the main fuel is coal, the overall efficiency of thermal power plant cycle is about 27-36% and the energy consumption is about 9-13.7 MJ/kWh. When the clear biomass is burning in the same steam boiler the efficiency of thermal cycle becomes lower than before and is about 18-27% and the energy consumption is higher compare to clear fossil and is about 13.7- 21.1 MJ/kWh [2]. The difference between coal and biomass efficiency of thermal cycle is caused by moisture value of biomass [1]. Tests in power plants proved that co-combustion becomes the most efficient way to use biomass by steam boiler. When the share of added biomass is about 7-10% the boiler efficiency is lower only 1% compare to clear coal dust.

In thermal-electric power station of Gorzów the influence of added biomass to steam boiler type OP-140 was researched by [1]. The purpose of investigation was to find the most efficient share value for energetic willow, which is added as a biomass to coal dust. In thermal-electric power plant 30% of energy production is converted into electrical energy form and about 42% converted into thermal form (as hot water and technology steam).

As an alternative fuel added to coal is energetic willow, because the opportunity of access to a huge amount of this kind of biomass is highest compare to other, because the consumption of biomass in power plants achieves high value. The local market is possible to deliver enough amount of willow's timber, this fact becomes willow timber the most attractive as a biomass. Calorific value of energetic willow is comparable to other kind of timber and it is about 10 MJ/kg. Moisture content in raw willow's timber determines about 45%. Based on assumption, the maximum of moisture content should be such as 30%, from this reason before adding, the willow has to be dried. The chemical composition of willow is similar to other timber is presented in table III [1] compare to coal fuel.

Costs of production of raw willow's timber is about 10 \$/t, after milling and drying the total costs become about 20 \$/t, which is still profitable.

TABLE III
CHEMICAL AND THERMAL PROPERTIES OF COAL AND BIOMASS

	Coal dust	Biomass
C	57.39 [%]	35 [%]
H	3.726 [%]	7 [%]
O	6.012 [%]	23.03 [%]
N	0.893 [%]	1.4 [%]
S	0.63 [%]	0.07 [%]
Volatile matter	26 [%]	80 [%]
Calorific value	22,4 [MJ/kg]	13.5 [MJ/kg]

Analysis co-combustion willow's timber in steam boiler OP-140 showed that process of burning two types of fuel together is more beneficial than burning coal and timber apart, because coal stabilizes burning process, which allows to use biomass with variable contents of moisture. Whereas added biomass diminishes emission powders, ashes and gases such as NO_x and SO_x . Timber contains less incombustible parts than coal. The value is about 0.5-3% for timber and almost 12% for coal. When fuel characterises high value of incombustible parts, it causes that exhaust gas contests fixed higher value of powder and ashes. Timber includes only 0.3% of nitrogen, which is two times less compare to coal. Contents of sulphur is near 0.05% where for coal it becomes 0.8%.

In thermal electric power station biomass is added to coal before milling process. The tests [1], which was realized by coal pulverizer type fan MWK-16, showed that the degree of share added biomass till 30% does not influence in negative way on working of coal pulverizer. Blending biomass with coal on coal store before milling decrease the operating costs, because this solution does not need install special kind of feed system for adding the biomass. During milling coals and biomass together taked place not only milling and mixing but also drying the biomass, which is profitable.

During burning process mixed coal with biomass in steam boiler type OP-140 the temperature of exhaust characterizes almost constant value. The analysis of working the combustion chamber showed that adding biomass to coal in value about 10 % does not influence in negative way on work parameters. Process of co-combustion biomass with coal share in range about 7-12% does not change the parameters of steam boiler and the work efficiency is comparable when the same boiler works based only on coal fuel.

IV CONBUSTION BIOMASS IN SMAL-SCALE BOILERS

Biomass contains less energy in proportion to their weight compare to raw fossil materials, from this reason it is better to use them where they occur. Heat and electric energy can be produced in small or medium plants which are decentralized. These kind of boilers are used in blocks, flats, schools, swimming pools or local heating networks. The small heat plants which are supplied by biomass can attain power of between 500 kW to 30 MW. They mostly use woodchips from thinning or wood pellets from industry. These kind of materials are cheap and ensure as a alternative fuel, because many municipalities use woodchips from their own woodland.

For example in rural areas there are more and more used small-scale household biomass boilers supplied with biomass. These kind of burners are generally installed for log and pellets. They get more benefits, because for example pellet boilers run fully automatically.

Log boilers can attain heat capacity from five to several hundred kilowatts. The disadvantage of log burners is that the wood has to be put into furnace still by hand. The combustion is very efficient and cleaner, because a lot of them fixed lambda probe, which control there is enough oxygen for completely burning process and less air pollution such as carbon monoxide.

Pellets are in pressed form object 6 or 8 mm thick and about 10 to 30 mm long. Pellets calorific value is about 18 MJ/kg (2 kg of pellets are equivalent of 1 litre of oil fuel). They are also very easy to transport and take up less space to storage. Pellet boiler are equipped with screw conveyor and fan, which can adjust the level of required heat.

REFERENCES

- [1] D. Futrak, M. Ostap, Współspalanie biomasy w niskoemisyjnym palenisku wirowym na przykładzie prób w EC Gorzów, Conference of Co-Combustion Biomass and Renewable Fuels in Steam Boilers, 12-14 may, 2004.
- [2] Z. Bis, W. Nowak, Autothermal Upgrading of Biomass and Wastes for Co-combustion in Power Systems, Conference of Co-Combustion Biomass and Renewable Fuels in Steam Boilers, 12-14 may, 2004.
- [3] www.nachwachsende-rohstoffe.de
- [4] www.fnr.de
- [5] www.bio-energie.de
- [6] A. Iwanick, Biomass for Steam and Power, Harris Group Inc.
- [6] C. Owczarek, H. J. Krautz, S. Griebel, Cycloid Combustion- a New Concept for Industrial Combustion with Low Calorific Fuels, Chair of power plant technology, Brandenburg Technical University of Cottbus, Germany

Control and Stability Analysis of Doubly Fed Induction during Voltage Sags

*D. Kairous, *B. Belmadani, **M. Benghanem

*Faculty of Science and Sciences Engineering, UHBC, Po Box 151, Chlef 02000, Algeria,

** Electrical engineering Depart. USTO. , Po Box 1505, El Mnaouar, Oran, Algeria

Mail: kdjilali@hotmail.com

Abstract- Large wind turbines are often equipped with Doubly Fed Induction Generator -DFIG-.

Today the penetration level of wind power on the network is high. The power system stability defined as the ability of the system, for given initial operation condition, to regain a normal state of equilibrium after being subjected to a disturbance is the major problem.

In numerous papers the stability problems are pointed out and there are also many papers describing control strategies for wind turbine equipped with DFIG.

In this paper we study dynamic behavior of the DFIG during voltage sag. Also we study the ability of the Control to remind the stability of the system.

I. INTRODUCTION

Wind energy is one of the most important and promising sources of renewable energy due to its clean character and free availability. Many variable speed winds turbines have been used with induction generator, permanent magnet and eventually switched reluctance generators. Nowadays the market is oriented on the design of high power wind generation systems based on multi-pole synchronous machine or doubly fed induction generators (DFIG).

Power system stability has been recognized as an important problem for secure system operation [1]. The pinning of the market of electricity obligates us to make production of the generators near their physical limits, for economic reason. It is thus necessary to evaluate these limits, in particular the risk of instability of network voltage.

Different control strategies for such kind of generator have been proposed for active and reactive power control or voltage and frequency control. Direct field oriented control for active and reactive powers is presented in [2], [3].

In the proposed paper we present the control of the Active and reactive Powers by sliding mode. The system has the ability for simultaneous maximum wind power generation for large speed range of operation and achieves soft and fast synchronization to the grid. Power converters and associated control strategies are simulated using Simulink.

Some simulation results are presented to validate the theoretical analysis and to show the behaviour and performances of the proposed structure for power control.

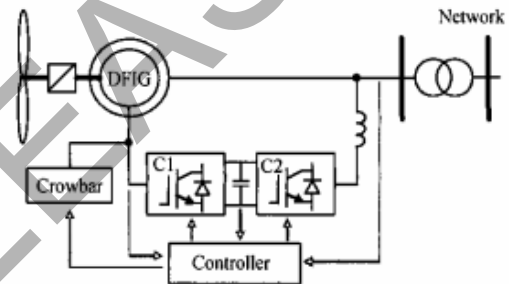


Figure.1. Representation of DFIG-based wind turbine

II. DESCRIPTION OF THE STUDIED SYSTEM

The basic configuration of the whole system is presented in Fig. 1. The rotor of DFIG is connected to the grid through two back to back bridge converters. The grid side converter (GSC) is used to control the DC-link voltage and to keep it constant regardless to the magnitude and direction of the rotor power.

The DFIG is controlled by the rotor side in order to generate the optimal active power depending on the wind speed and turbine characteristics.

III. GRID SIDE CONVERTER CONTROL

The role of the grid side converter is to keep the DC-link voltage constant regardless to the magnitude and direction of the rotor power. A vector control approach is used, allowing independent control of the active and reactive powers flowing between the supply and the GSC.

Fig.2 shows a simplified representation of the grid connected converter. AC-side series inductances accounts for transformer leakage reactance, and series resistances represents inverter and transformer conduction losses

The model of the system is given by the following equation:

$$\frac{d}{dt} \begin{bmatrix} i_a \\ i_b \\ i_c \end{bmatrix} = -\frac{R}{L} \begin{bmatrix} 1 & 0 & 0 \\ 0 & 1 & 0 \\ 0 & 0 & 1 \end{bmatrix} \begin{bmatrix} i_a \\ i_b \\ i_c \end{bmatrix} + \frac{1}{L} \begin{bmatrix} V_a - V_{an} \\ V_b - V_{bn} \\ V_c - V_{cn} \end{bmatrix} \quad (1)$$

With the Park transformation, the equation system of the GSC is given by:

$$\begin{cases} v_{dr} = R i_d + L \frac{d i_d}{dt} - \omega_s L i_q + V_{dn} \\ v_{qr} = R i_q + L \frac{d i_q}{dt} - \omega_s L i_d + V_{qn} \end{cases} \quad (2)$$

The direct axis current is used to regulate the reactive power and the quadratic axis current is used to regulate the DC-link voltage. The reference frame is considered oriented along the stator voltage vector

This method gives possibility to realise independent control of the active and reactive power between the GSC and the supply side.

The voltage components in park frame are given at the output of the PI regulator. The voltage source components and the powers can be written as:

$$\begin{aligned} v_d &= 0, \quad v_q = V \\ P &= v_q i_q \quad \text{and} \quad Q = v_d i_d \end{aligned} \quad (3)$$

By neglecting converter losses, we have:

$$v_{dc} i_{dc} = v_q i_q, \quad C \frac{d v_{dc}}{dt} = i_{dc} - i_m \quad (4)$$

$$v_{dc} C \frac{d v_{dc}}{dt} = P - P_m \quad (5)$$

Based on the above relations, the GSC control diagram can be easily deduced as presented in Fig.2

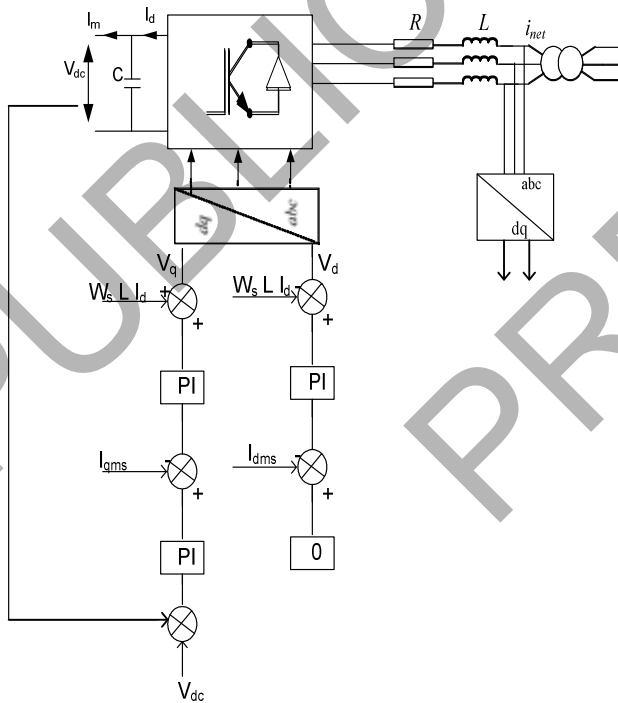


Figure.2. Blocks diagram of the Grid side converter control.

III. SLIDING MODE CONTROL

We will use the sliding Mode Control to control the rotor currents of the DFIG. The goal is to have a more stability in a disturbance cases then the PI regulators. we write the Park model of the DFIG [4] :

$$\begin{cases} V_{dqs} = R_s I_{dqs} + \frac{d\Phi_{dqs}}{dt} - \omega_s \Phi_{qds} \\ V_{dqr} = R_s I_{dqr} + \frac{d\Phi_{dqr}}{dt} - \omega_r \Phi_{dqr} \end{cases} \quad (6)$$

$$\begin{cases} \Phi_{dqs} = L_s I_{dqs} + M I_{dqr} \\ \Phi_{dqr} = L_s I_{dqr} + M I_{dqs} \end{cases} \quad (7)$$

By neglecting the stator resistance of the stator we can write:

$$\begin{cases} V_{ds} = 0 \\ V_{qs} \approx \omega_s \Phi_{ds} \end{cases} \quad (8)$$

$$\begin{cases} \Phi_{dr} = L_r \sigma I_{dr} + \frac{M}{L_s \omega_s} V_{qs} \\ \Phi_{qr} = L_r \sigma I_{qr} + \frac{M}{L_s \omega_s} V_{ds} \end{cases} \quad (9)$$

The general model of the machine is given by:

$$\begin{bmatrix} V_{ds} \\ V_{qs} \\ V_{dr} \\ V_{qr} \end{bmatrix} = \begin{bmatrix} R_s c \Phi_{ds} - R_s c \left(L_r \sigma I_{dr} + \frac{M}{L_s \omega_s} V_{qs} \right) - \omega_s \Phi_{qs} + \frac{d\Phi_{ds}}{dt} \\ R_s c \Phi_{qs} - R_s c \left(L_r \sigma I_{qr} + \frac{M}{L_s \omega_s} V_{ds} \right) + \omega_s \Phi_{ds} + \frac{d\Phi_{qs}}{dt} \\ R_r b \left(L_r \sigma I_{dr} + \frac{M}{L_s \omega_s} V_{qs} \right) - R_r c \Phi_{ds} - \omega_r \left(L_r \sigma I_{dr} + \frac{M}{L_s \omega_s} V_{ds} \right) + L_r \sigma \frac{dI_{dr}}{dt} \\ R_r b \left(L_r \sigma I_{qr} + \frac{M}{L_s \omega_s} V_{ds} \right) - R_r c \Phi_{qs} + \omega_r \left(L_r \sigma I_{dr} + \frac{M}{L_s \omega_s} V_{qs} \right) + L_r \sigma \frac{dI_{qr}}{dt} \end{bmatrix} \quad (10)$$

$$\text{With: } a = \frac{1}{\sigma L_s}, \quad b = \frac{1}{\sigma L_r}, \quad c = \frac{M}{\sigma L_s L_r}$$

The state model is put in the following form:

$$\dot{X} = f(x,t) + g(x,t)U_{dq} \quad (11)$$

With:

$$U_{dq} = [V_{ds} \quad V_{qs} \quad V_{dr} \quad V_{qr}]$$

$$g(x,t) = \begin{bmatrix} 1 & 0 & 0 & 0 \\ 0 & 1 & 0 & 0 \\ 0 & 0 & \frac{1}{\sigma L_r} & 0 \\ 0 & 0 & 0 & \frac{1}{\sigma L_r} \end{bmatrix}$$

$$f(x,t) = \begin{bmatrix} -R_s \sigma \Phi_{ds} + R_s c \left(L_r \sigma I_{dr} + \frac{M}{L_s \omega_s} V_{\varphi_s} \right) + \omega_s \Phi_{\varphi_s} \\ -R_s \sigma \Phi_{\varphi_s} + R_s c \left(L_r \sigma I_{qr} + \frac{M}{L_s \omega_s} V_{\varphi_s} \right) - \omega_s \Phi_{ds} \\ \frac{1}{\sigma L_r} \left(-R_r b \left(L_r \sigma I_{dr} + \frac{M}{L_s \omega_s} V_{\varphi_s} \right) + R_r c \Phi_{ds} + \omega_r \left(L_r \sigma I_{qr} + \frac{M}{L_s \omega_s} V_{\varphi_s} \right) \right) \\ \frac{1}{\sigma L_r} \left(-R_r b \left(L_r \sigma I_{qr} + \frac{M}{L_s \omega_s} V_{\varphi_s} \right) + R_r c \Phi_{\varphi_s} - \omega_r \left(L_r \sigma I_{dr} + \frac{M}{L_s \omega_s} V_{\varphi_s} \right) \right) \end{bmatrix}$$

The slip surfaces in the Park reference are defined to control the rotor currents. They are given by the following equations [5]:

$$\begin{cases} \sigma_d = \lambda(I_{drref} - I_{dr}) \\ \sigma_q = \lambda(I_{qrref} - I_{qr}) \end{cases} \quad (12)$$

Where V_{dr} and V_{qr} are the two control vectors of, they force the trajectory of the system to converge towards surfaces $\sigma_{dq} = 0$.

The vector U_{eqdq} is obtained by imposing $\sigma_{dq} = 0$

$$f(x,t) + g(x,t) V_{dq} = 0 \quad (13)$$

$$U_{\text{eqdq}} = \begin{bmatrix} - \left(-R_r b \left(L_r \sigma I_{dr} + \frac{M}{L_s \omega_s} V_{\varphi_s} \right) + R_r c \Phi_{ds} + \omega_r \left(L_r \sigma I_{qr} + \frac{M}{L_s \omega_s} V_{\varphi_s} \right) \right) \\ - \left(-R_r b \left(L_r \sigma I_{qr} + \frac{M}{L_s \omega_s} V_{\varphi_s} \right) + R_r c \Phi_{\varphi_s} - \omega_r \left(L_r \sigma I_{dr} + \frac{M}{L_s \omega_s} V_{\varphi_s} \right) \right) \end{bmatrix} \quad (14)$$

The Fig. 3 presents the global diagram for the DFIG with sliding mode control.

V. SIMULATION RESULTS

In this section we present the simulation results of the system (Fig.1). The rotor voltage the stator voltage, the speed and the powers are keeping at their nominal values.

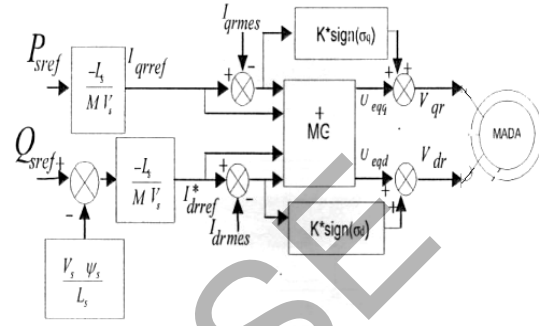


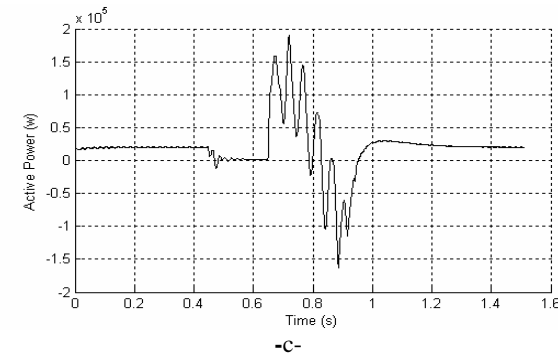
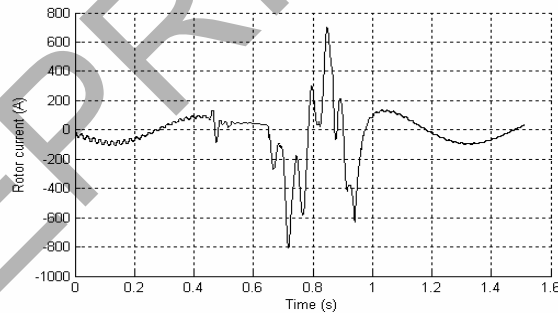
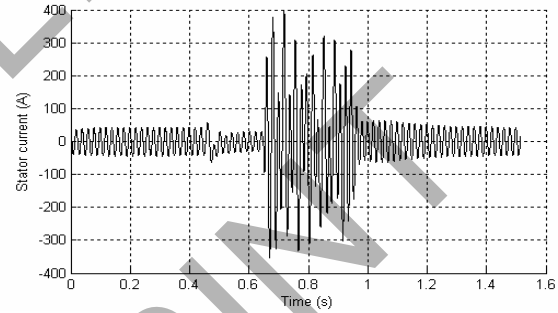
Figure.3. Sliding mode control of the DFIG

powers are keeping at their nominal values.

The DFIG used has a nominal power of 20kw.

We make a voltage sag of 50% during 200 ms (Between $t=0,45s$ and $t=0,65s$).

The results in the Fig.4 (figures of the currents, powers and the torque) prove the validity of proposed model, and the good stability of the system.



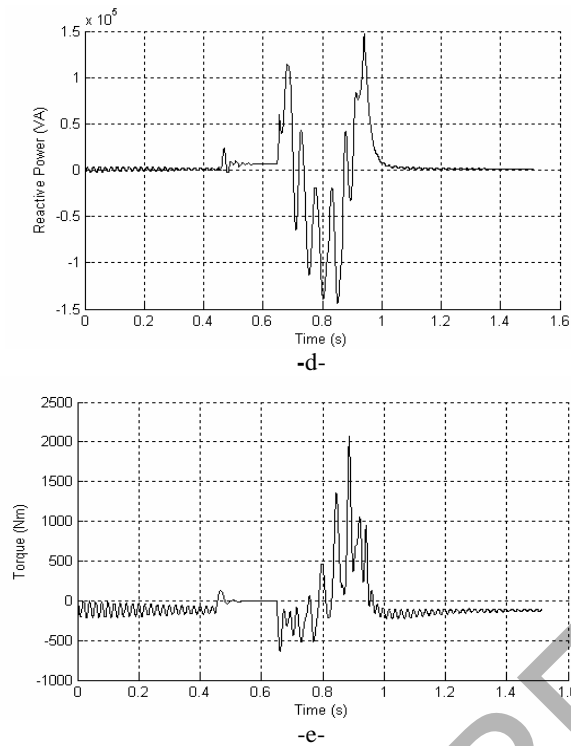


Figure.4. Dynamic behaviour of the DFIG during Voltage sag of 50 %
a- Stator Current, b- Rotor current
c- Active Power. d- Reactive Power. e- Torque

VI. CONCLUSION

In this paper a doubly fed induction generator connected to the grid was presented.

The aim of the paper was to develop the decoupled d-q vector control technique of DFIG supply by a back-to-back PWM converter in the rotor side. The control strategy contains two control levels: DFIG control level (control of active and reactive power using sliding mode approach) and the control of the grid side converter.

The mathematical model of the system (DFIG-Converters-Grid) has been implemented in MATLAB & Simulink.

The main goal of the grid side converter control is to keep the dc-link voltage constant by balancing the real power on the machine side and on the grid side converter, and to compensate reactive power of the DFIG to get the unity power factor.

The control system is applied to the rotating reference frame fixed on the gap flux of the generator. It has been proved that this control system can control the active and reactive power independently and stably.

The simulation results show that we can make decoupling between active and reactive power and in the same time have a good stability in a case of voltage sag.

Also, the DC-link voltage was kept constant to the reference value. The torque has the same dynamic like the active power.

NOMENCLATURE

J, C_{fr} : Inertia and viscous friction

Ω : Mechanical speed

$\Omega_{turbine}$: the turbine angular frequency

V_d, V_q, I_d, I_q : stator and rotor Voltages, currents

$\Phi_{ds}, \Phi_{qs}, \Phi_{dr}, \Phi_{qr}$: Two-phase stator and rotor flux

$i_{ds}, i_{qs}, i_{dr}, i_{qr}$: Two-phase stator and rotor currents

I_{dms}, I_{qms} : Two-phase measured rotor currents

C_r, C_e : Prime mover and electromagnetic torque

R_s, R_r : Per phase stator and rotor resistance

M : Magnetising inductance

L_s, L_r : Total cyclic stator and rotor inductances

ω_s, ω_r : Pulsation

g : Generator slip

i_d, i_q : Two-phase grid side converter currents

v_d, v_q : Two-phase network voltages

v_{dc}, i_{dc} : Dc-bus voltage and current delivered by the grid side converter

P, Q : Active power delivered by the grid side converter and

i_m, P_m : Current and Active power delivered to the rotor side converter

C : Capacitance of the DC-link

R, L : Resistance and Inductance of the grid

P_s, P_r : Stator active power and rotor active power

Q_s, Q_r : Stator reactive power and rotor reactive power

$v_{ds}, v_{qs}, v_{dr}, v_{qr}$: Two-phase stator and rotor

REFERENCES

- [1] P. Kundur, J. Paserba, "Definition and Classification of Power System Stability," *IEEE Transaction on Power Systems*. Vol. 19, N°2, May 2004.
- [2] J R. Pena, R.C. Clark, G.M. Asher, "Doubly Fed Induction Generator using Back-to-Back PWM Converters and its Application to Variable-Speed Wind-Energy generation", *IEE Proc-Elect. Power Appl*, Vol. 143, N°5. 380-387. 1996
- [3] L. Mihet-popa, I. BOLDEA, "Control Strategies for Large Wind Turbine Application", *Journal of Electrical Engineering*, Vol. 7, Edition 3rd, ISSN 1582-4594. 2006.
- [4] P.C. Krause, "Analysis of Electrical Machinery", *McGraw-Hill*, New york, 1994.
- [5] B. Toufik, "Commande à Structure Variable et Etude de l'Integration d'Eolienne à base de Machine asynchrone à Double Alimentation sur le Réseau Electrique", PhD thesis (in French), *University of NANTES*, 2007

Application and Comparison of LQR and Robust Sliding Mode Controllers to Improve Power System Stability

S. Saffar Shamshirgar¹
Sahar_Saffar@yahoo.com

M. Golkhah²
Mohammad.Golkhah@polymtl.ca

H. Rahmati³
h.rahmati1@gmail.com

M. A Nekoui⁴
Manekoui@eetd.kntu.ac.ir

¹M.Sc. student, Islamic Azad University of Sciences and Researches, Tehran, Iran.

²PhD student, Ecole Polytechnique de Montreal, Montreal, Canada.

³M.Sc. student, K. N. Toosi University of Technology, Tehran, Iran

⁴Assistant Professor, Engineering Faculty, Islamic Azad University of Sciences and Researches, Tehran, Iran.

Abstract— Heffron-Philips model has had great popularity to simulate mono or multi machine power systems. Since the stability of this model is related to operating point of synchronous generator(s), many efforts have been made in research papers to design robust and reliable controllers to ensure the stability of the system. A typical mono-machine power system is presented in this paper to make a comparison between behaviors of traditional power system stabilizer and LQR based pss. Characteristics and fundamental concepts of each controller are stated. At the termination of the paper, Sliding Mode method has been engaged so that the power system can be stable in uncertain condition. The results of LQR base and sliding mode based PSSs have been compared under uncertainty.

Keywords— Heffron-Philips model, pss, stability, LQR.

I. INTRODUCTION

Connecting small generation and distribution systems together makes better stability against small disturbances but when a serious problem occurred for one of the connected systems, it also affects the others. These connections have been done between even different countries for economic reasons. Modern power systems have many characteristics such as far distances of consumption from generation declining the power system stability. In order to provide stability for such modern systems, different control systems have been designed and applied in power plants and power transmission lines. Drum level control, Governor, and Automatic Voltage Regulator are such control systems which are applied in power plants. Governor and AVR have bound capability to damp transient state oscillations. Therefore another control system called power system stabilizer, pss, is applied to improve the stability. This additional loop can be applied for both governor and AVR control loops. Applying pss to governor makes many quick variations in the position of mechanical fuel gate making it injured. Hence it is recommended to apply pss to AVR controller [1].

Static Var Compensator, SVC, synchronous condenser, tap changer, and FACTS devices are control systems in power transmission lines.

To simulate and control a generator, it is important to have a model. State space model is a well-known for this aim. The complete model for a synchronous machine has 7 orders. It is efficient to reduce the degree of the system as well as linearization in order to simplify the model. Heffron-Philips

model is such a linear model with 3 orders. This model is considered to apply controllers in this paper.

II. CASE STUDY

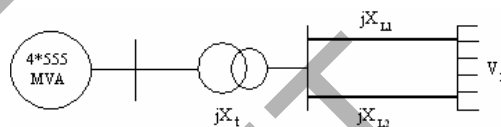


Figure 1. The power system anticipated as case study

Figure (1) indicates a power system as our case study. It includes a power plant comprising four same units. The power plant is connected to a transmission line by a transformer. The line conveys the power to an infinite bus.

Electrical parameters presented on table (1) are pertaining to normal regime operation of the system [1]. The values are in per unit system.

Table 1. Initial values for the power system

Generator constants	$H=3.5$, $D=0.5$, $T'_{do}=8.0$ $X_d=1.81$, $X_q=1.76$, $X'_d=0.3$
Exciter constants	$K_A=10$
Line and transformer constants	$X_{L1}=0.5$, $X_{L2}=0.93$, $X_T=0.15$
Electrical parameters	$P=0.9$, $Q=0.3$, $V_f=1.0 < 36^\circ$ $V_B=0.995 < 0^\circ$

III. HEFFRON-PHILIPS MODEL

Heffron-Philips model for generator is linear model with 3 degrees in state space. Figure (2) shows this model with AVR loop.

The state space matrices corresponding to the presented model in Figure (2) can be formulated as equation (1).

Where $[x_1 \ x_2 \ x_3] = [\omega \ \delta \ e'_q]$ and $[u_1 \ u_2] = [T_M \ u_E]$.

It is easy to calculate all the parameters of equation (1) by using table (1).

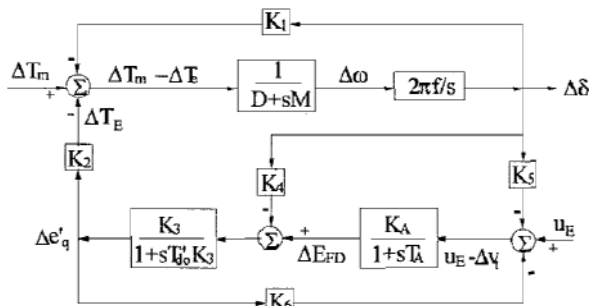


Figure 2. Heffron-Philips model with the AVR controller

$$\begin{bmatrix} \dot{\Delta x}_1 \\ \dot{\Delta x}_2 \\ \dot{\Delta x}_3 \end{bmatrix} = \begin{bmatrix} 0 & \omega_0 & 0 \\ -\frac{k_1}{J} & -\frac{D}{J} & -\frac{k_2}{J} \\ -\frac{k_4}{k_3 T'_{do}} & -\frac{k_5 k_A}{T'_{do}} & -\frac{1}{k_3 T'_{do}} - \frac{k_6 k_A}{T'_{do}} \end{bmatrix} \begin{bmatrix} \Delta x_1 \\ \Delta x_2 \\ \Delta x_3 \end{bmatrix} + \begin{bmatrix} 0 \\ 0 \\ 0 \end{bmatrix} + \frac{1}{J} \begin{bmatrix} 0 \\ 0 \\ 0 \end{bmatrix} \begin{bmatrix} \Delta u_1 \\ \Delta u_2 \end{bmatrix} \quad (1)$$

IV. PSS CONTROL LOOP

Suppose a condition in which the second transmission line is removed under a fault [1]. The aim is to study rotor's speed oscillations and apply a pss to improve the stability resulting in decrement of speed deviations around the steady state value. Steady state values in such a condition can be calculated as equation (2).

$$\begin{aligned} V_{do} &= 0.6836, & V_{qo} &= 0.7298 \\ I_{do} &= 0.8432, & I_{qo} &= 0.4518 \\ \delta_o &= 79.13, & E_{fdo} &= 2.395 \end{aligned} \quad (2)$$

Using these values, coefficients k1 through k6 have below values.

$$\begin{aligned} k_1 &= 0.7643, & k_2 &= 0.8649 \\ k_3 &= 0.323, & k_4 &= 1.4187 \\ k_5 &= -0.12, & k_6 &= 0.3 \end{aligned} \quad (3)$$

Input signal of pss is speed of rotor and the output is a bounded voltage adding to the generator excitation. A block diagram for a regular pss is indicated in figure (3).

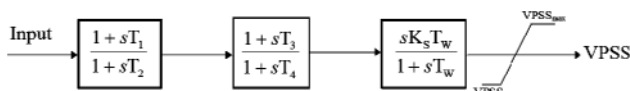


Figure 3. Block diagram of a regular pss

The response of speed deviations of the rotor after removing the second line with and without pss loop is shown in figure (4).

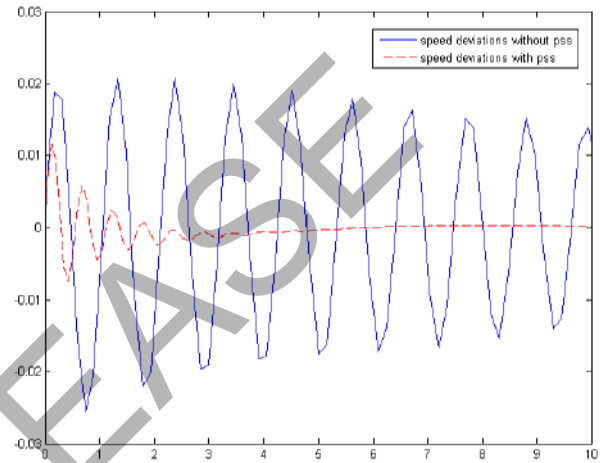


Figure 4. Speed deviations of rotor with and without presence of pss after the fault

Moreover, responses of power angle and deviations of terminal voltage of generator with and without pss can be seen in figure (5) and figure (6) respectively.

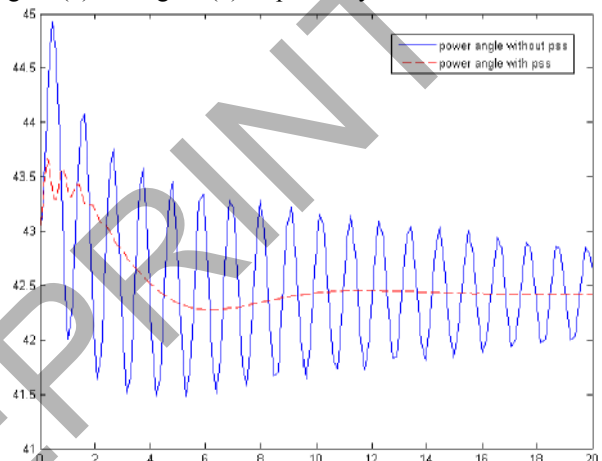


Figure 5. Power angle without and with presence of pss after the fault

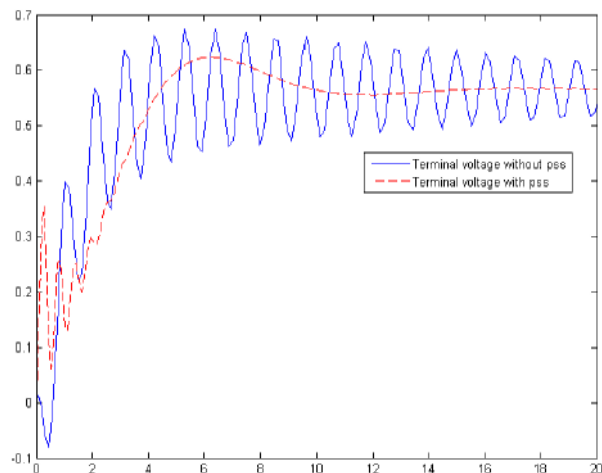


Figure 6. Terminal voltage of the generator with and without presence of pss after the fault

It is proved from figures (4), (5), and (6) that pss has been able to improve stability of the system actually by shifting the eigen values of the matrix A of state space equations to the left areas of s-plane. Since stability concept for a generator and related equipments is angular stability of a power system, you can say that pss extends the angular stability limits of a power system. However, pss can exacerbate instabilities of a power system. It is reasonable because pss is designed to operate around an operating point so it can improve the stability under small disturbances. However, when a large fault occurred, pss can lose synchronism of the generator by providing surplus excitation field. In addition, you may think of tuning a pss to extend more the angular stability but there is indeed a limitation to tune the parameters of pss since its output voltage reaches to saturation levels determined by the actual limitations. If the parameters of pss were selected in a way to have small amplitudes in state variables, the output voltage of pss becomes larger. On the other hand if they were designed in order to have small output voltage of pss, the amplitudes of state variables become larger. Therefore a compromise should be employed.

V. LQR BASED STATE FEEDBACK

Closed loop poles of a linear control system can be emplaced in desired places of s-plane using state feedback and observer control system design. Also its poles can be chosen by choosing appropriate observer gain. Response speed and estimation error dynamics can be defined by choosing closed loop poles. However, optimal selection of closed loop poles is really hard for industrial systems and real processes. Albeit an unstable system can be stabilized by applying states feedbacks, but linear optimal control systems should be engaged for below reasons.

The first reason is that it is hard to find appropriate closed loop poles in which the desired behavior of the system is satisfied. Selecting closed loop pole with great negative real parts makes the dynamic response of the system to be quick while the control effort to be greater than permissible levels. If selection of the closed loop poles makes saturation of control signals, dynamic behavior of the system will not be as same as the desired behavior even it may become unstable.

The second reason is noise which specially occurs in the systems with high gains.

Therefore optimal selection of closed loop poles will lead to a trade-off between speed of dynamic response and control effort.

Suppose the linear system in state space given by equation (4).

$$\begin{aligned} \dot{x}(t) &= Ax(t) + Bu(t) \\ y &= Cx \end{aligned} \quad (4)$$

The purpose is to stabilize the system so that all the state variables become zero by any initial value in maximum speed. There are many criteria to do that. Quadratic integral equation is a well-known such a criterion [2].

$$J = \frac{1}{2} \int_0^{\infty} (\underline{x}^T Q \underline{x} + \underline{u}^T R \underline{u}) dt, \quad (5)$$

Where Q is a non-negative definite matrix which is called weighting matrix. On the other hand, R is a positive definite weighting matrix. Selection of values of these matrixes determines the dynamic speed of the controller as well as amplitudes of state variables and control signals. For example if R is selected small while Q is selected large, more stability will be attained with large control efforts.

Solving an optimal control problem means finding a u(t) by which equation (5) is minimized. Linear Quadratic Regulator, LQR, can solve this problem [2] (see equation (6)).

$$A^T X + XA - XBR^{-1}B^T X + Q = 0 \quad (6)$$

After calculating X from algebraic equation (6), k and u can be calculated from equations (7).

$$\begin{aligned} k &= R^{-1}B^T X \\ u &= -kx \end{aligned} \quad (7)$$

Indeed, LQR is an optimal pole assignment and integral J defines circumstance of assigning closed loop poles as an optimizing criterion.

For our case study R and Q matrixes have been selected as equations (8).

It has been tried to have small control effort and equal importance to the state variables. It is important to note that there will be guaranteed gain and phase margins by LQR. In fact it is not required to verify stability of the system after designing state feedback by LQR because it must be stable.

$$R = \begin{bmatrix} 0.5 & 0 \\ 0 & 0.5 \end{bmatrix}, \quad Q = \begin{bmatrix} 1 & 0 & 0 \\ 0 & 1 & 0 \\ 0 & 0 & 1 \end{bmatrix} \quad (8)$$

VI. OBSERVER DESIGN

If A and C matrixes were observable in equation (4), then the observer can be designed as equation (9) [3].

$$\dot{\hat{x}} = A\hat{x} + Bu + L(C\hat{x} - y) \quad (9)$$

Where \hat{x} denotes estimations of states x. $\bar{x} = \hat{x} - x$ is estimation error and it should reach to zero. \bar{x} can satisfy equation (10).

$$\dot{\hat{x}} = (A + LC)\bar{x} \quad (10)$$

Behavior of estimation error is related on the eigen values of matrix A+LC. For the mentioned case study L has been selected in a way to have -2, -5, and -11 as eigen values of A+LC (equation (11)).

$$L = [1696 \quad -17.2 \quad -2039.9] \quad (11)$$

VII. LQR BASED POWER SYSTEM STABILIZER

The designed observer estimates all the three state variables. Then the estimated states are fed to the inputs by k which is designed using LQR.

Simulation results prove that state variables have significantly smaller amplitudes than those of pss while having small control signals too. Figure (7) indicates the speed deviations while figure (8) and figure (9) indicate the control signals. It can be found from figure (7) that LQR based pss has significant stabilizing characteristics in comparison with the

traditional pss. Also figure (8) and figure (9) prove that control signals are much less in LQR based pss than the traditional one.

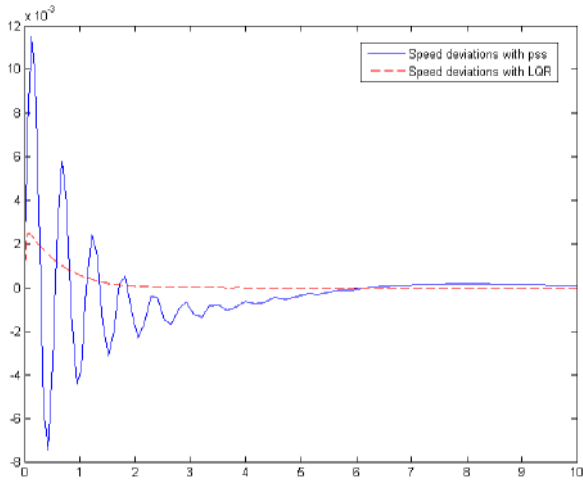


Figure 7. Comparison of speed deviation in LQR based pss and regular pss

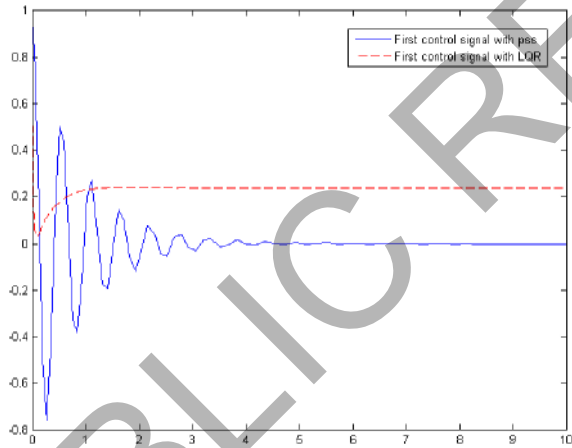


Figure 8. First control signal comparison between the two controllers

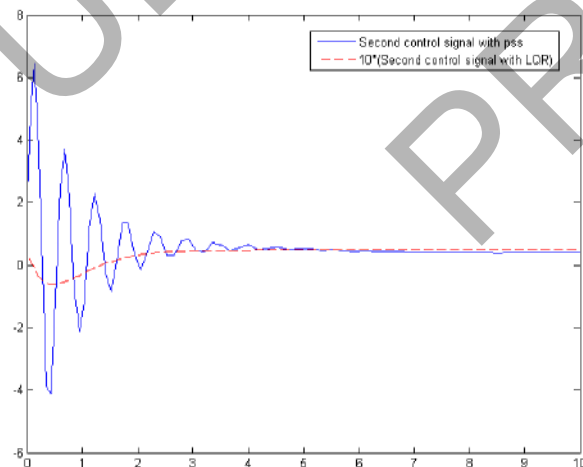


Figure 9. Second control signal comparison between the two controllers

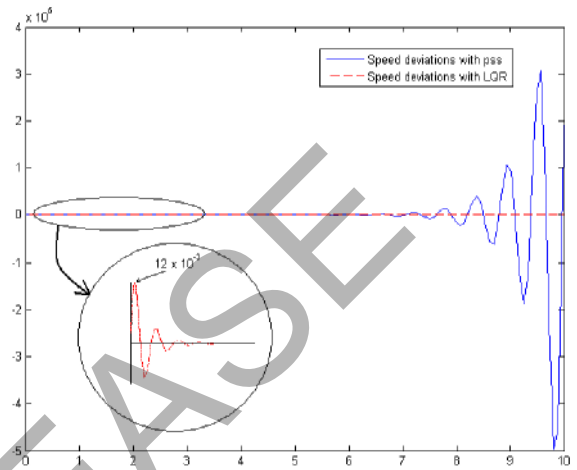


Figure 10. speed deviations of both controller after the heavy fault

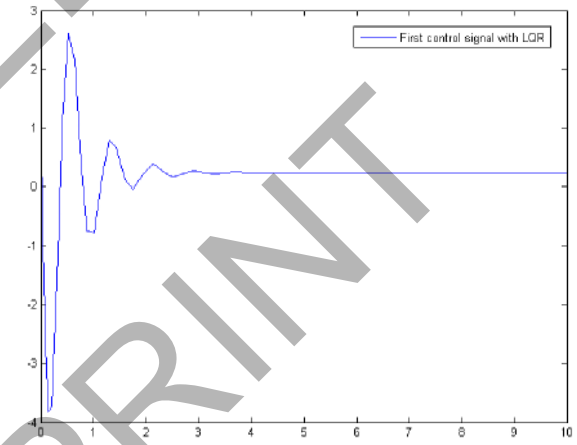


Figure 11. First control signal of the LQR base controller after the heavy fault

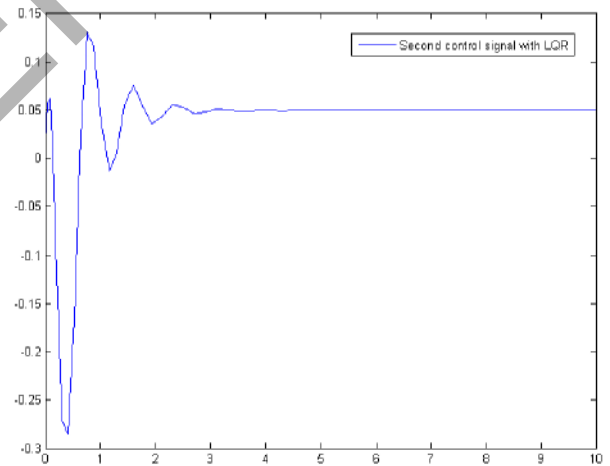


Figure 12. Second control signal of the LQR base controller after the heavy fault

Another simulation has been made to ensure that the LQR based pss has a good reliability. It has been supposed that a three phase short circuit at the received end of the second line has been occurred without removing the line. Figure (10) indicates speed variations of both controllers at the same condition. LQR based controller is still stable while traditional

ps is unable to stabilize the power system. This result proves the extent gain and phase margins of the LQR solution. Figure (11) and figure (12) indicate that the LQR based controller is subjected to have greater control effort to remain stable.

VIII. SLIDING MODE BASED POWER SYSTEM STABILIZER

Reference [4] has proposed sliding mode to design a controller in order to have robust state covariance assignment. This method is briefly illustrated and is employed to have a robust controller for the stability problem of this paper.

The main aim of this controller is to reach the answer paths, trajectories, to a surface. Then the state variables should be tended to asymptotic stability through this surface. To achieve this aim the surface should be made attractive so that it can attract the paths. Hence the controller should be designed to tend the paths to the surface. The controller should have switching ability to keep the path by which the state variables have been reached to the desired surface. Different surfaces and control rules can be determined regarding the system model and control desires. This paper has engaged the proposed method in [4] to determine the plane.

Let plane S to be as (11).

$$S(t) = Cx(t) - \int_0^t (CA + CBG)x(\tau)d\tau \quad (11)$$

Where $S(t) = [S_1(t) \dots S_i(t) \dots S_m(t)]^T \in \mathbb{R}^{m \times 1}$, C and G are constant matrices to be design, C is chosen such that CB is nonsingular, and G is the control feedback gain which should be determined so that the state variables can fit the requirement in the sliding mode [4]. Equation (12) is attained by derivative of (11).

$$\dot{S}(t) = CBu - CBGx \quad (12)$$

Note that $CD=0$. In the sliding mode the states satisfy $\dot{S} = 0$, then we get the equivalent control as follows $u_{eq}(t) = Gx(t)$. Equation (13) can be attained for dynamic sliding mode by replacing this input into system equation.

$$\dot{x} = (A + BG)x \quad (13)$$

If $u(t)$ is anticipated as (14) in which $k > \|\Delta A\|$, α is a positive constant,

$\text{sgn}(S(t)) = [\text{sgn}(S_1(t)) \dots \text{sgn}(S_m(t))]^T$, and $\|x\|$ denotes second norm of x, then the state of the system will converge to the sliding mode surface $s(t)=0$ with probability. We have

chosen $C = \begin{bmatrix} 0 & 0 & 1 \\ 0 & 1 & 0 \end{bmatrix}$, $\alpha = 1$ and $k=1$ so that $CD=0$ and CB is

nonsingular. Eventually G is selected so that the eigen values of $A+BG$ are $\{-3, -6 \pm 5i\}$.

Let compare responses of certain models of LQR and sliding mode. Figure (13) represents the response of LQR based pss and Figure (14) is the response of sliding mode controller. It is proved from these figures that both controllers provide good stability condition for the power system however the amplitude of speed deviations in sliding mode is less than that of LQR controller.

Figures (15), and (16) present the speed deviations in LQR and sliding mode methods respectively under uncertain model. These results prove that the sliding mode controller is robust since even under uncertain model it has been successful to tend the state variables to the surface S. Moreover, Figures (17), and (18) denote the first and second control efforts of both controller.

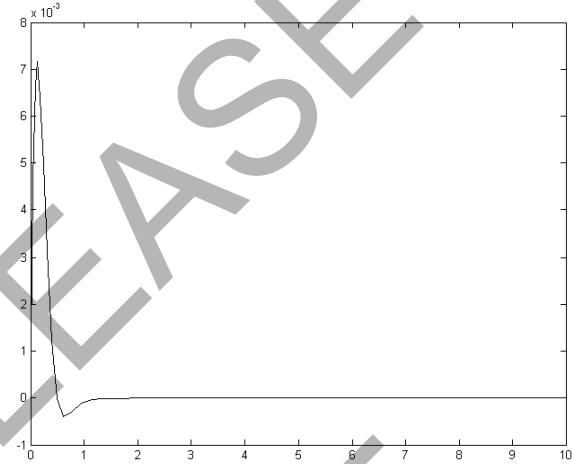


Figure 13. Speed deviations response of LQR based pss in certain model

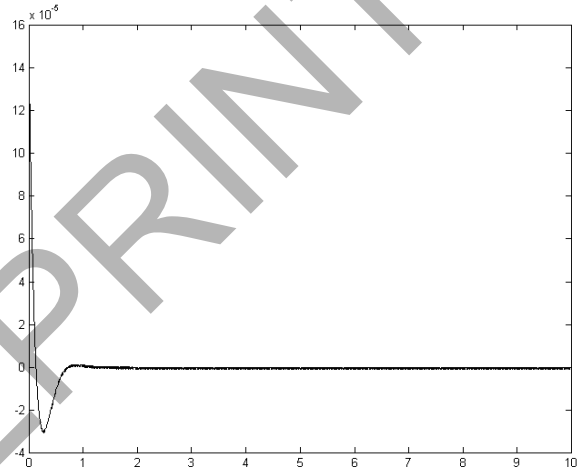


Figure 14. Speed deviations response of sliding mode based pss in certain model

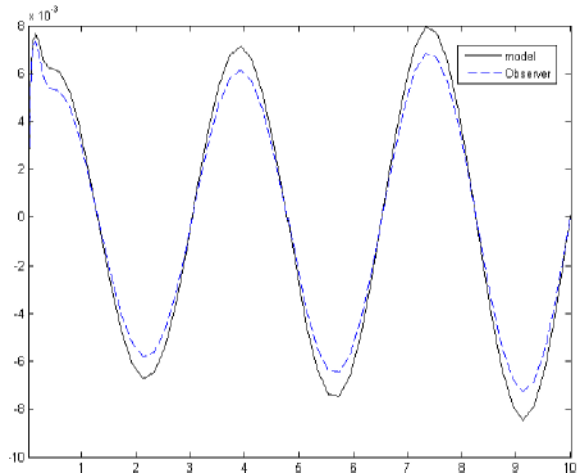


Figure 15. Speed deviations response of LQR based pss in uncertain model

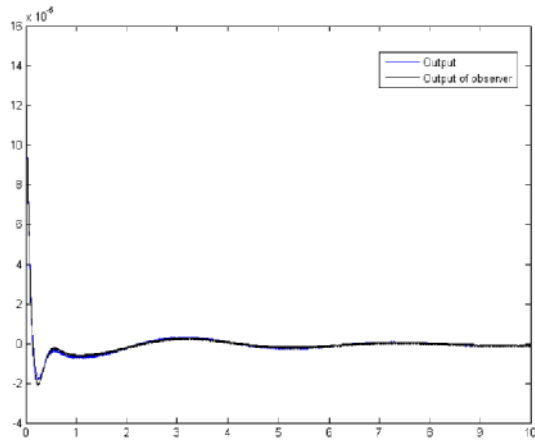


Figure 16. Speed deviations response of sliding mode based pss in uncertain model

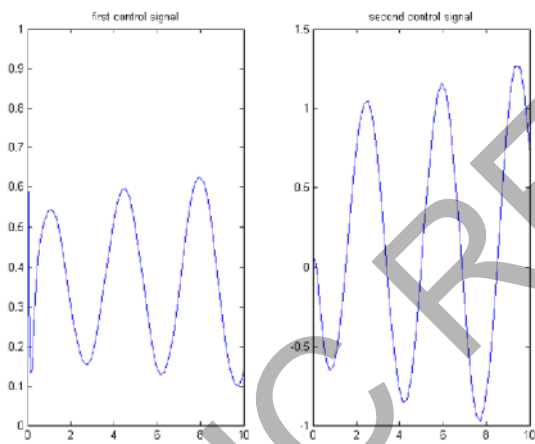


Figure 17. First and second control signals of LQR based pss in uncertain model

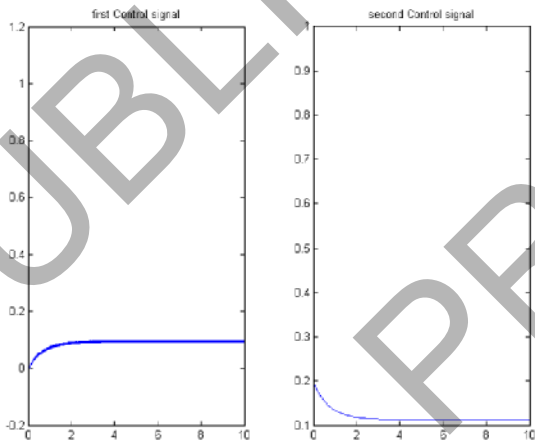


Figure 18. First and second control signals of sliding mode based pss in uncertain model

unstable while the LQR based pss was able to stabilize the power system although the control efforts were increased significantly. This phenomenon can prove the extent gain and phase margins of LQR based state feedback. Therefore a designer can apply LQR to design a power system stabilizer with good gain and phase margins without any worry about control signals since LQR can compromise between values of state variables and control efforts. At the last section, slide mode controller, which supposes to be robust, applied to the power system to pole placement. In certain model the results of both LQR and sliding mode were stable and acceptable taking it into consideration that the state variables have smaller magnitudes in the case of sliding mode controller. Under uncertainty, it was found that LQR controller which is not a robust controller became unstable while sliding mode controller was able to remain stable proving its robustness.

X. REFERENCES

- I. P. Kundur, "Power System Stability and Control", McGraw-Hill, New York, 1994.
- II. William L. Brogan, "Modern control theory", 3rd ed., Englewood Cliffs, N.J., Prentice Hall, 1991.
- III. K. Zhou, J. C. Doyle, and K. Glover, "Robust and Optimal Control. Prentice Hall", New Jersey, 1996.
- IV. Koan-Yuh Chang, Wen-June Wang, "Robust covariance control for perturbed stochastic multivariable system via variable structure control", Elsevier, Systems & Control Letters 37 (1999) 323-328.

IX. CONCLUSION

Fundamental theory of regular pss, LQR based state feedback, observer, LQR based pss, and eventually sliding mode based pss were presented in the paper. Simulation results for a case study including regular pss and LQR based one were presented separately after removing a transmission line from service. LQR based pss yielded better stabilizing parameters while smaller control efforts than the regular pss. Moreover, after applying a heavy fault the regular pss got

A SURVEY OF SOLAR ENERGY POWER SYSTEMS

Adekunle Babatope AJAYI

*Donetsk National Technical University
Bogdana Kmelnitskogo 100
Donetsk 83015, Ukraine*

ABSTRACT

Using the direct space SUN – RAY energy, the proposed solar energy power system is to link up Industrial to Domestic usage (I2D) such that each nation can identify an effective power generation, which brings development to a developing nation and also stability to the develop nation in every facet of her economy. This paper highlights the opportunities for sustaining the developed nations and the developing nations in the implementation of Renewable Energy Sources by taking the Free Gift of Nature (FGN) sun, details some possible architectural configuration and infrastructural requirements. Concerns over global warming are causing shifts in energy policy and energy sourcing around the world. Citizens and governments are carefully weighing their impacts on the environment; many begin to convert to clean renewable energy sources. The European countries are leaders amongst the continents of the world, as well as a nest for the minds of young independent thinkers and countries. Exploration of the renewable energy options will allow any country to understand its potential for reducing its impact on global warming, such that it can weigh the costs of Climate Change with those of upfront economic investment in renewable energy.

Categories and Subject Descriptors

[Energy Applications]: Resource Potential – Investors, Industrial to Domestic (I2D).

General Terms

Management, Documentation, Generation, Transmission

Keywords

Solar Energy, Free Gift of Nature (sun), Power Generation, Transmission, Environmental and Economic Importance of Solar Energy to Industrial and Domestic use.

1. INTRODUCTION

The study of renewable energy sources has been of global concern to the world, and has led many institutions like the European Commission and others to undertake research on sustainable approach to meet the challenges of sustainable energy generation. Renewable energy is a clean energy system

that has no effect during or after generation on the environment and which this has led to continuous improvement on solar energy for a better way of reducing green house effect in the future. This has also helped developed and developing countries to take full advantage of this free gift of nature to promote ecological and social innovation which will ensure more sustainable economy growth, environmental conservation and social stability.

A critical challenge that continues to constrain the advancement of many developing countries is the prevalence of poverty. In spite of an abundance of solar energy most developing nations, lack stable power source, due to low technology advancement, poverty, and poor management of existence facilities.

It is widely accepted that access to electricity is essential to any nation's economy, and is a requirement for modern economic and social development. Electricity opens the door to a host of technologies that promote education, public health, and economic development, such as emissions-free light, refrigeration, and communication devices. Without electricity, communities are unable to participate in the benefits of modern advances and are left isolated and literally in the dark.

The overall objective of the solar energy power system is towards a stable power supply for developing and developed nations of the world. Hence, the sunlight that falls on the surface of a tropical country in one day contains more than twice of the energy the country can consumes in a year.

2. SOLAR RESOURCE

Solar resource is a process through which the sun emits energy at an extremely large and relatively constant rate, 24 hours per day, 365 days per year. Through this process, energy could be converted into usable forms on earth; it would be more than enough to supply the world's total energy demand. However, there are many effects of ionospheric scintillation on the environment that will make the days of the year for solar generation not to be effective: firstly, the earth intercepts only a small fraction of the energy that leaves the sun; secondly, the earth rotates such that a collection device on the earth's surface is exposed to solar energy for only about half of each 24-hour period; and finally, the conditions in the atmosphere, such as clouds and dust, sometimes significantly reduce the amount of solar energy reaching the earth's surface.

In this survey Nigeria will be taken as a case study for reference.

Located on the western part of Africa, Nigeria weather primarily features a tropical climate where the season is very humid and damp. There are two climatic seasons that prevail within Nigeria, namely the wet and the dry seasons. The weather of Nigeria is generally quite hot throughout the year, although there are variations in the climate in certain regions within the country. The southern part of Nigeria is relatively more humid and damp than the northern part of the country. In the southern areas of Nigeria the dry seasons begin from the month of November and lasts till the month of March. The northern regions are much drier in nature in comparison to the southern parts. The dry seasons begin from the month of October and last till the month of April. There are extreme weather conditions in the deserts of Sahara. It is scorching hot in the afternoons and freezing cold during the nighttime.

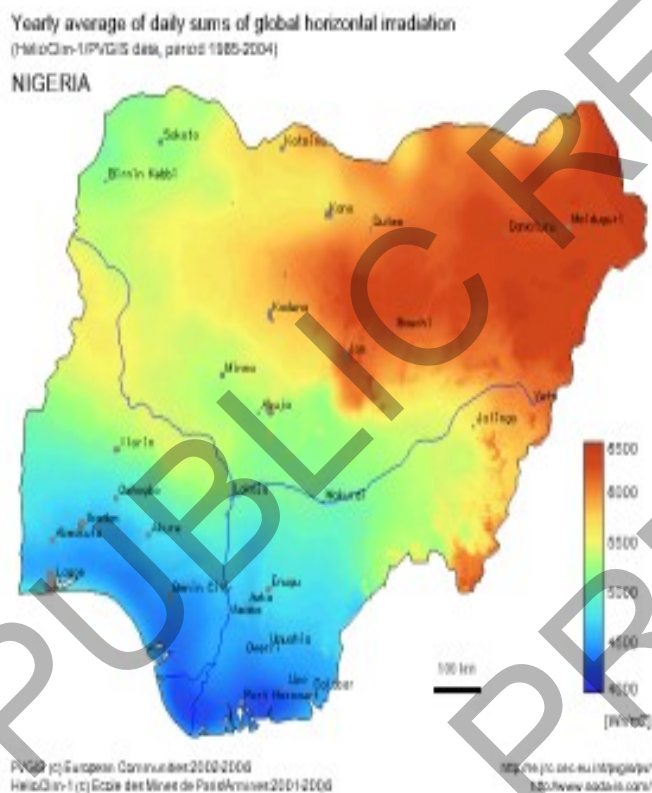


Fig. 1: Map of Nigeria

2.1 Yearly Irradiation in Nigeria

The following map displays the quantity of energy that reached the ground in Nigeria for the whole year. This yearly irradiation is expressed in kWh/m². This map is computed from observations made by meteorological satellites from 1985 to 2004. © European Commission 2002-2006 and HelioClim-1 copyright Mines ParisTech / Armines 2001-2006.

2.2 Climate of Nigeria

Climate is the average weather condition of a place over a given period of years. It is determined primarily by distance from the coast and secondly by elevation (Bradley 1995). The climate of Nigeria is tropical in nature, which is occasionally subjected to variations, depending on the rainfall. During summers, major portion of the country comes under the influence of moisture-laden tropical maritime air. Temperatures are high throughout the year, averaging from 25° to 28°C. In the higher elevations of the Jos Plateau north central area of Nigeria, temperature is at an average of 22°C. Northern Nigeria experiences greater temperature extremes than the south. Rainfall varies widely over short distances from year to year. Nigeria's electrical energy consumption in the year 2001 is 15 × 10⁶ KWh and the tropic of cancer. It's climate varies from tropical to subtropical. There are two major seasons; the dry season lasting from October to March and rainy season lasting from April to October. In the north, it is hot and dry, rainy season extends between April and September. In the south, it is hot and wet season extends between March and December. From December to March, there is a long dry season (Ojo 2000). Therefore, the Temperature range between 32° and 42° humidity is about 95% (Falade 1995).

3. SOLAR POWER

3.1 What is solar power?

Solar power is produced by photovoltaic, or "PV", solar panels and other devices that capture the energy in sunlight and convert it to electricity. This electricity can then be fed directly to a consumer, an electric power grid, or a storage device. Typically, solar panels are installed on the roof of residential or domestic buildings, and use the power generated to meet the owner's energy needs and provide surplus electricity to the grid. Other applications include heating water and providing power in areas where electricity connections are not available, such as on road signs, cellular phone towers, and satellites.

3.2 Environmental and Economical Importance

Solar energy has both the environmental and the economical importance to every nation. Hence, the solar power play a key role in cost effectiveness of any nations economy, create a direct employment of labor force and to foster the development of micro – industries.

The most important factor driving solar energy system generation process is whether the energy it produces is economical. Although there are factors other than economics that enter into a decision of when to use solar energy; i.e. no pollution, no greenhouse gas generation, security of the energy resource etc., design decisions are almost exclusively dominated by the 'level of energy cost'. This similar economic

parameter, gives the expected cost of the energy produced by the solar energy system, averaged over the lifetime of the system. Hence, solar energy power system is a very clean energy that if given financial support by the government and industrialist to reduce the cost of implementing the solar panels for industrial, commercial and residential consumers to afford.

Abundant Supply: Solar power could meet today's total electricity demand by PV systems covering only 0.4% of the nation in a high-sunlight area such as the Southwest — an area about 100 square miles. These panels, in reality, will be installed across the country on roofs and other structures close where it is consumed. Technologies such as PV roof shingles, windows, and flexible fabrics that are easily and cheaply integrated into new and existing buildings are emerging.

Secure and Stable Supply: Because solar power is generated domestically, often at the site where it will be consumed, prices and supplies are immune to blackouts, international uncertainty and do not rely on long-distance supply networks.

Cleaner Air: Solar power does not pollute air or water. It replaces electricity generated from facilities powered by coal, natural gas and other non-renewable fuels, eliminating threats to public health such as carbon monoxide, particulate, and toxic chemical emissions from those facilities. Additionally, when a solar power replaces electricity from a coal-fired power plant it also eliminates a potential source of sulfur emissions - a major component of acid rain.

Reducing Global Warming: Solar power does not produce CO₂ or any other greenhouse gases, thus helping to reduce the risk of climate change.

4. HOW SOLAR ENERGY WORKS

The solar energy technology is the absorption of sun's energy directly converted into electrical. Hence, the solar energy works through the aid of combining solar panel which is also known as photovoltaic cells, solar cells and solar panels. The solar panel is basically used in generating 12Volts DC (Direct Current) and the number of photovoltaic cells used determines the amount of electricity to be generated.

The solar panels absorb sun ray and then convert it to provide DC power to the power center, where a centralized battery bank, or individual home batteries are charged. The energy from the battery bank can then be used directly in DC appliances or can be converted to AC power with an inverter for use in standard AC appliances. The solar panels can only work during daylight hours. The solar production system compliments each other well because it tends to be windy on cloudy, rain days and sunny on calm clear days.

5. GENERATION OF SOLAR POWER

Solar power generation directly converts solar energy into electrical energy through a chemical action taking place in solar cells. These operate based on the photo-voltaic effect, which develops an electromagnetic force (emf) on absorption of ionizing radiation from sun.

Solar energy (Photovoltaics), the direct conversion of sunlight to electricity, is now the fastest growing technology for electricity generation. Present 'first generation' products use the same silicon wafers as in microelectronics. 'Second generation' thin films, now entering the market, have the potential to greatly improve the economics by eliminating material costs. Martin Green, one of the world's foremost photovoltaic researchers, argues in his book that 'second generation' photovoltaics will eventually reach it's own material cost constraints, engendering a 'third generation' of high performance thin films. The book explores, self – consistently, the energy conversion potential of advanced approaches for improving photovoltaic performance and outlines possible implementation paths.



Fig. 2: Solar Power Generation Diagram

6. TRANSMISSION OF SOLAR RAY

When solar ray strikes an object, there are two possible occurrences: the object may reflect the solar energy, or the object may absorb it. Most objects are applicable for this process, to a greater or lesser extent. It is useful knowledge to understand how different materials transmit, reflect, and absorb solar radiation. For instance, in the case of a solar cell, it is important to coat the surface with a material that is a poor reflector—we want as much light as possible to enter the cell. Accordingly, creating comfortable, well-lit homes, schools, and offices requires an understanding of which building materials transmit, reflect, and absorb solar radiation.

REFERENCE



Fig. 3: Solar Panel Diagram

7. CONCLUSION

The survey has gathered resource potential of solar energy and how the solar system development in developed countries and some developing countries (China, South Africa, Gambia, Kenya, Tanzania, Uganda and many more) and its implementation in Nigeria.

The most important factor driving the solar energy system design process is whether the energy it produces is economical. Although there are factors other than economics that enter into a decision of when to use solar energy; i.e. no pollution, no greenhouse gas generation, security of the energy resource etc., design decisions are almost exclusively dominated by the 'level of energy cost'. This similar economic parameter, gives the expected cost of the energy produced by the solar energy system, averaged over the lifetime of the system. Hence, solar energy power system is a very clean energy that should be given support by the government and industrialists to reduce the cost of implementing the solar panels for industrial, commercial and residential consumers to afford.

ACKNOWLEDGMENT

I am grateful to the Electrical Engineering Program Chair of Donetsk National Technical University, Ukraine Prof. Georgy G. ROGOZIN, Adedayo Ademola YUSUFF of Electrical Department, Tshwane University of Technology, Pretoria, South Africa for their encouragement and guidance. I also acknowledge the leadership, support and patience of Michael Adebayo OMIDIORA of Electrical Department, Helsinki University of Technology, Espoo, Finland. <http://www.ngportal.com/momidiora/> and Olaniyan Kayode for his advice and support for making this paper a reality. (ekaynomics@yahoo.com, o.kayode@npc.gov.ng) National Planning Commission, Abuja, NIGERIA

[1] Baranoski, G., Ronke, J., Shirley, P., Trondsen, T., and Bastos, R.

[2] Bradley, D. 1995. Plants point the way to renewable energy. *New Sci.* 121 : 8

[3] Distribution of Solar Energy System :

<http://graphics.stanford.edu/courses/cs348b-competition/cs348b-05/borealis/webpage%20files/writeup.html>

[4] Eskridge, R. E., O. A. Alduchov, I. V. Chernykh, Z. Panmao, A. C. Polansky, and S. R. Doty, A Comprehensive Aerological Research Data Set (CARDS) : Rough and Systematic errors, *Bull. Amer. Meteor. Soc.*, 76, 1759 – 1775, 1995

[5] Eurostat News Releases on the internet
<http://ec.europa.eu/eurostat/>

[6] Falade, T. S. 1995. Solving Housing Problems in Lokoja. B. Sc. Research Report. Department of Architecture, A. B. U. Zaria, Kaduna State, Nigeria.

[7] Florida Solar Energy Center (FSEC) 2006, "Photovoltaics & Distributed Generation, Photovoltaic Fundamentals". Available at <http://www.fsec.ucf.edu/pvt/pvbasics/>

[8] National Renewable Energy Laboratory (NREL), 2006a, "Dynamic Maps, GIS Data, & Analysis Tools, Solar Maps". Available at <http://www.nrel.gov/gis/solar.html#csp>

[9] National Renewable Energy Laboratory (NREL), 2006b, "Photographic Information Exchange" Available at <http://www.nrel.gov/data/pix>

[10] Ojo, O. 2000. Fundamentals of physical and Dynamic Climatology, 1st ed., SEDEC Publ., Lagos, Nigeria

[11] Second EU Sustainable Energy week puts the focus on Energy Supply. January 28 to February 1, 2008
http://ec.europa.eu/news/energy/080128_2_en.html

[12] SoDa :: Services for professionals in Solar Energy and Radiation Maps of Radiation, Irradiance, Irradiation and UV
<http://www.soda-is.com/eng/map/index.html>

[13] Williams, R. H; and Carl, J. W. 1990. Energy from the sun. *Amer. Sci. J.* 43 : 41

Reducing the Short Circuit Levels in Kuwait Transmission Network. (A Case Study)

Mahmoud Gilany
College of Technological Studies,
Kuwait

Wael Al-Hasawi

Abstract: Preliminary studies on Kuwait high voltage transmission system show significant increase in the short circuit level at some of the grid substations and some generating stations. This increase results from the growth in the power transmission systems in size and complexity. New generating stations are expected to be added to the system within the next few years. This paper describes the study analysis performed to evaluate the available and potential solutions to control SC levels in Kuwait power system. It also presents a modified planning of the transmission network in order to fulfill this task.

Keywords: Short circuit current, network splitting, fault current limiter, power transmission planning.

I. Introduction

The topography of the power system network keeps changing as the economy of a nation grows and its power consumption increases. One of the effects due to the growth of energy generation and the expansion of intermeshed transmission networks is the increase in short circuit currents in the power systems. These currents can cause mechanical and thermal stresses and they may damage the equipment. Consequently, the reduction and control of short circuit currents is a must.

The problem in Kuwait started at 2005 when a new emergency generation units were added to the network as a quick measure to avoid load shedding during heavy-load summer season. With the long term plan, new large generating stations are also expected to be installed. As a result, the short circuit level has increased and it is expected to highly increase in the near future.

One solution to reduce the risk of increasing short circuit levels in the power system is to upgrade the protection equipment so that the estimated fault currents are kept within the equipment capacity. This usually involves complete rebuilding of the substation. Nevertheless, this solution does not represent a high cost ratio benefit. It is an expensive solution, especially if primary and secondary breakers with their associated equipment are numerous. In addition to the cost, upgrading of the existing substations can be a

complicated process because of the number of equipment to be substituted, redesigned or tested [1].

Instead of upgrading the network, different techniques aiming at reducing the SC levels were examined, namely:

1. Change the neutral earth policy
2. Un-grounding cable sheath.
3. Changing some lines from AC to DC.
4. Apply current limiters.
5. Dividing the bus bars.
6. Splitting the network

This paper consolidates the experience of the Kuwait power utility with these measures. The study conclusions are presented in the form of power system operation strategy in order to maintain the fault currents within the permissible limits.

II. The Case Study

Kuwait transmission system consists of a 275 kV Grid supplied with three major generating stations with a capacity of approximately 6 GW as shown in Fig. 1. This network is connected to a 132 kV system which includes another 4 GW generating stations. Recently, the power system was connected via 400 kV tie-lines with Saudi Arabia as part of the Gulf network. Figure 1 is a simplified diagram of the 275 Kuwait power transmission systems.

Each bus in the Kuwait network is connected to 3 to 4 275/132 kV transformers. The network connected to the SSUR W 275/132 kV station shown in Fig. 2 is a typical example. Normally, the loops connected to any bus in the 132 kV networks are isolated from the loops connected to the other 132 kV busses. However, there are normally-open connections between these buses.

III. Analysis Study

For the purpose of examining the techniques to control the short circuit, the full Kuwait power network (275 and 132 kV) was implemented using a simulation program ASPEN-Oneliner V9.7 [2], which is a PC-based short circuit and relay coordination program widely used by protection engineers.

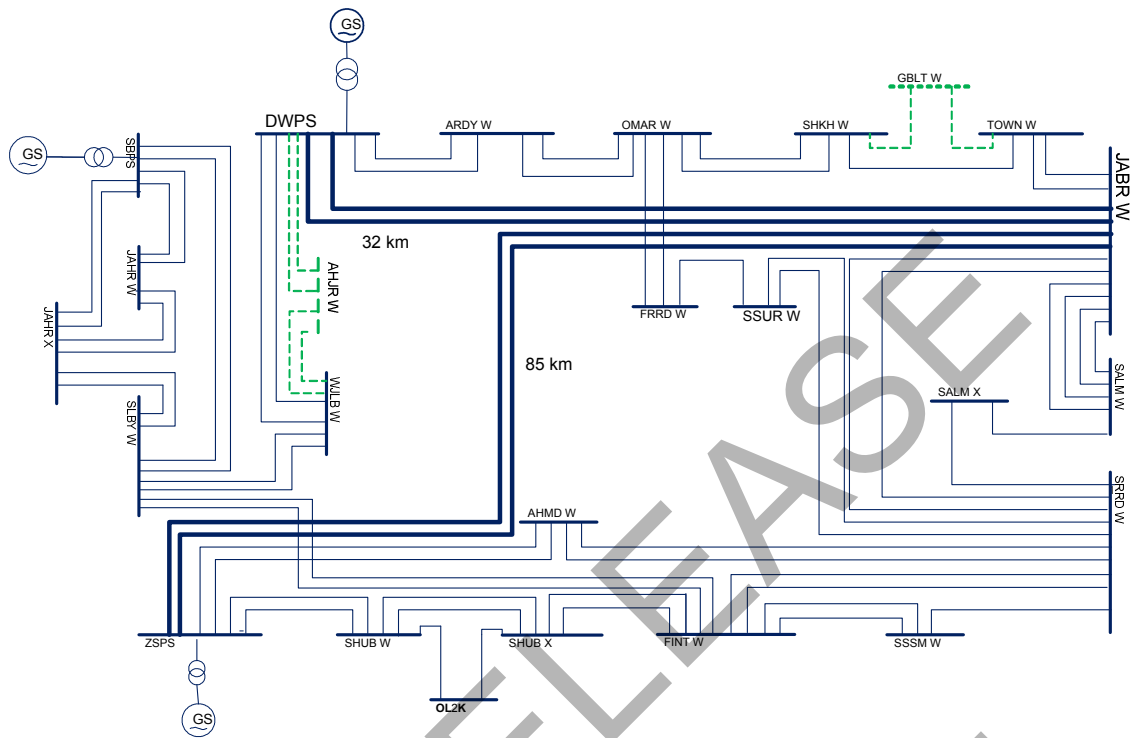


Fig. 1: The under study 275 kV transmission network

The short circuit level is examined at all the 275 and 132 kV stations. The simulation results show that the short circuit currents exceed the permissible levels in some specific points. It reaches 43 kA at some locations in the 132 kV networks where the nominal rupture capacity is 40 kA. The SC level also reaches 67 kA at some generating stations in the 275 kV networks where the rupture capacity is limited to 60 kA. A typical shape of the output results is shown in Fig. 3.

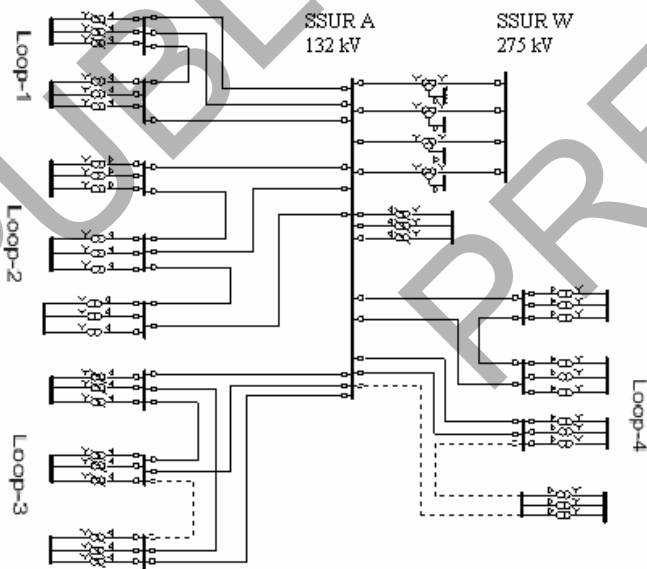


Fig. 2 Typical part of 132 kV network

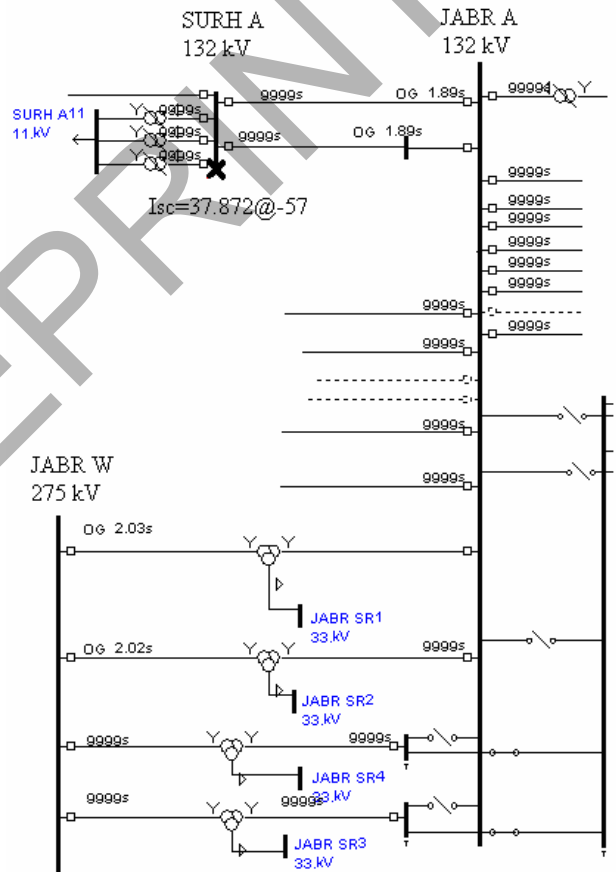


Fig. 3 A SLG fault at SURH A station

This figure shows only a part of the whole network. It represent a SLG fault applied at station SURH A (132 kV). The fault current exceeds 37 kA as shown in the figure.

These results did not take into consideration the expected new generation stations to be installed within the next few years. If the new generation is considered, the situation will be much more critical. Therefore, effective activities have to be planned with aim to reduce the high fault current levels and to avoid critical situations in the future.

In the remaining of this paper, the measures studied to limit fault currents are presented.

A. Changing the Neutral Earth Policy

Within Kuwait power stations, all the transformers (275 kV and 132kV) are solidly earthed. This type of earthing system was chosen to avoid any increase in the neutral voltage during earthing faults. However, the main disadvantage of such a system is the high magnitude of the short circuit currents. It was the right time to test the possibility of changing the earthing policy for some transformers from solidly earthing to earthing through small resistances.

The simulation results show that with 5Ω resistance inserted in the neutral of the local transformers at any substation, the short circuit level dropped by about 10%. It dropped to about 15% with 8Ω resistance. The drawbacks of this technique include the reduction in the sensitivity of the overcurrent relays. Practical considerations prevent the use of higher resistances. The measure has shown to have a limited effect on the SC reduction target.

B. Changing Some Lines from AC to DC

The idea of changing AC lines to DC lines starts as a result of the need to increase the power transfer capability of the existing transmission system without any major new construction. Conversion of an overhead AC lines to DC lines means changes in tower head, insulator assemblies and conductor configuration. There is no need to change the conductors, tower bodies, their foundations and there is no intermediate towers added [3, 4].

One of the main features of DC transmission is the fact that a HVDC connection contributes very little to the short circuit current. In fact, a back-to-back (BTB) dc connection functionally appears to be an open circuit from ac impedance point of view.

It can be seen from the structure of the 132 kV network under study shown in Fig. 2 that it consists of multiple loops connected to every 132kV bus-bar. Most of these feeders are short transmission lines. Consequently, it is neither practical nor economical to convert all the feeders of each loop to DC in order to reduce the SC level at this loop. Instead, the simulations studied the effect of changing some of the "key-

lines" especially those connecting major generation stations in the 275 kV network. For example, changing the two lines between DWPS and JABR W (see Fig. 1) from AC to DC will result in a reduction in the short circuit level at the stations supplied from JABR W power station by about 30%. For example, the SC level at station SURH A in Fig. 3 dropped from 37kA to about 22kA. Similarly, changing the two lines between ZSPS and JABR W station results in a reduction in the SC currents at station SURH A from 37 kA to about 23 kA. However, the high cost of the new equipment required (inverters and converters) and the short distances between most of the stations in Kuwait make this alternative inapplicable.

C. Applying Current Limiters

There is a high interest in fault current limiter as it reduces the expected SC current without affecting the steady state power flow. There are different techniques to reducing the short circuit levels using current limiters. The differences between these techniques include the type and location of different elements (reactor, thyristor controlled series inductor, superconductors, etc.) to limit the current. It also varies according to the network voltage level. The majority of the current limiters are installed in the tie circuits such as the bus tie and utility tie circuits in which the current limiters could perform effectively.

Figure 4 shows a short circuit problem found in the ZSPS station. This generating station consists of 8x300 steam generating units plus 4x80 MW gas turbine units. It has a 275 kV bus-bar with four normally-closed sections. The simulation results show that the SC current reached to a 67.3 kA at the station bus-bar. The rupture capacity is limited to only 63kA.

One of the most common solutions to the high level SC currents is the installation of air-core current limiting inductors (CLI). These CLI are usually installed, although not limited to, in tie buses and in series with the transmission line [5,6]. With a 5Ω reactor added in only one of the three tie-sections of the station, the short circuit level drops to about 52 kA.

The applicability of adding a reactor for such high voltage system is facing many problems [5]. Although these series reactors are the simplest and most economical means of achieving the reduction in the short circuit levels, stresses due to the high rate of rise of transient recovery voltages (TRV) and higher DC offset (X/R ratio) of the short-circuit current will be experienced by the associated circuit breakers. In addition, a high DC offset in the fault current may result in saturation of C.T. cores affecting the performance of the relay protection schemes [7].

The use of superconducting materials in the development of FCL looks promising, although at present costs are still too high. Superconducting materials are used for the reduction of fault currents, due to their unique characteristic of a fast transition from zero resistance at rated current to a finite value with greater current densities. This fast increase in the resistance results in a fast fault current limitation [8].

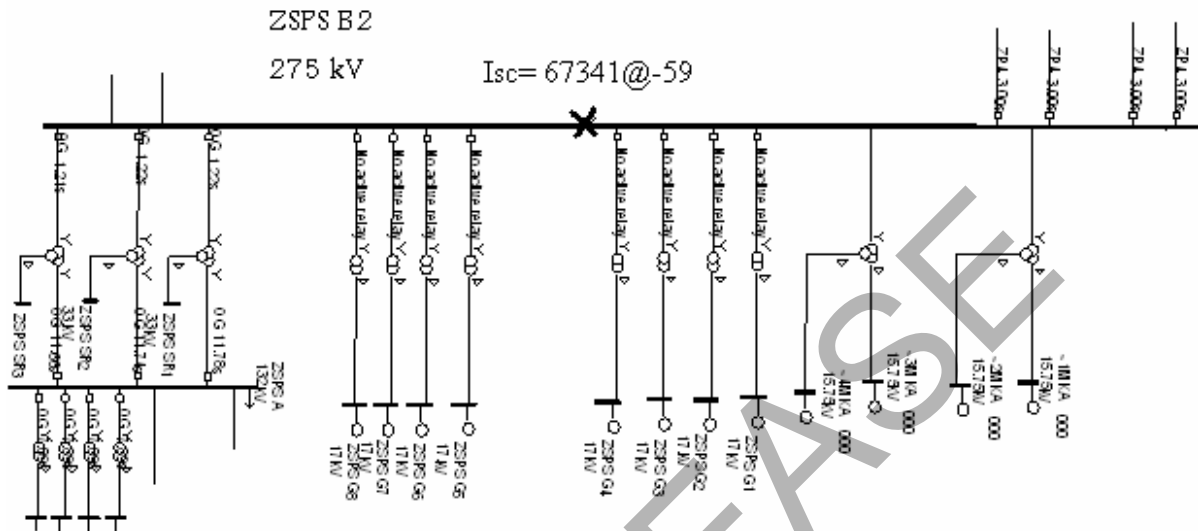


Fig. 4: A short circuit at a generating station

There are some other techniques adopting the concept of the current limiter e.g. series inductor- thyristor-controlled [9], the control regulates the average magnitude of the inductance and hence its current limiting effect. One of the disadvantages of this technique is the harmonic generation and the required use of filters.

D. Dividing the Bus Bar

Increasing the positive, negative, and zero sequence impedances seen by the fault, will result in reducing the short circuit currents. This is achieved in a substation by dividing buses in two or more sections. This solution is quite common and less expensive than upgrading circuit breakers. However, load division requires a careful study since the operating flexibility can be degraded in a significant manner. Also, the reliability can be affected as the number of transformers feeding the load is reduced.

In the system under study, this alternative was examined only at the 132 kV stations to avoid losing the system contingencies if applied on the BBs inside the generating stations. Even with the 132 kV stations, the application is limited to stations which have 4 275/132 kV transformers where the load can be divided equally inside the station. These conditions are not fulfilled in most of the stations.

E. Network Splitting

If the power system enters the emergency mode due to some disturbances, emergency controls will be applied to drive the system back to the alert mode. If the emergency controls fail to bring the system parameters back within their constraints, protective devices will act to prevent the power system components operating under unacceptable conditions

from undergoing damages [10, 11]. This may lead to system islanding, which often produces unstable or generation- load unbalanced islands. One quick solution is to temporarily split the power system

The most difficult part in the study of system splitting problem (SS problem) is to determine the proper splitting points (called splitting strategies) to split the entire interconnected transmission network into islands ensuring generation/load balance and satisfaction of transmission capacity constraints when islanding operation of the system is unavoidable. For a large-scale power system, the SS problem is very complicated in general. Moreover, network splitting presents a temporary (not guaranteed) solution to the developing SC problem.

IV. New Transmission Network Planning

The conclusions from the previous studies show that none of these techniques is perfect in solving the developed problem of increasing short circuit current levels. Taking into consideration that there are at least two new generating stations to be installed within few years, the optimum solution for the Kuwait network in solving the problem of the increasing SC levels is to construct a new higher voltage network (400 kV) and to connect all the new generating stations to this network. At the same time, the existing 275/132 kV network must be split permanently into three networks connected to the new 400 kV as shown in Fig. 5. The SCC, by this way, can be effectively reduced to acceptable levels.

To reach the above stated target, various network topologies are considered. The calculations performed include alternatively applied SCC, load flow and contingency analysis

for the proposed configuration in order to prove the technical requirements.

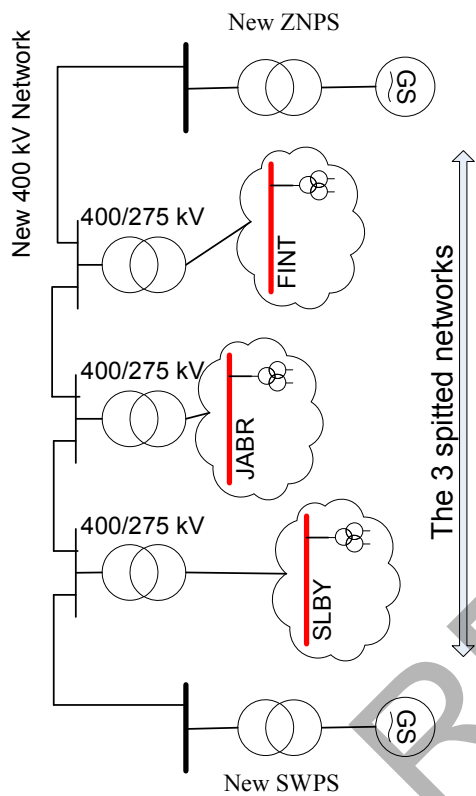


Fig. 5: The proposed power system

V. Conclusions

High level of fault currents is a normal consequence of transmission network expansion that follows the power system development. High fault levels require switchgear and other equipment with high rupture capacities. Reducing the fault level in a power system is cheaper alternative compared to the replacement of the switchgear. This paper presents different measures examined in order to control the high SC current at Kuwait high voltage network. Constructing a 400 kV high voltage network with a permanent Splitting of the existing 275 kV network, prove to be the most suitable solution for the highly increasing SC levels.

Acknowledgments

The financial support from the General Authority for Applied Education and Training in Kuwait (Project No. TS-02-08) is highly appreciated.

References

- [1] J. Panek, H. Elahi, "Substation Voltage Upgrading", IEEE Transactions on Power Delivery, Vol. 4, No. 3, July 1989, pp. 1715- 1724.
- [2] ASPEN-OneLiner Simulation Program.
- [3] H. Rahman and B. H. Khan, "Power Upgrading of Transmission Line by Combining AC-DC Transmission", IEEE Transactions on Power Systems, Vol. 22, No. 1, February 2007, pp. 459- 466.
- [4] Petersson, A., A. Edris, "Dynamic Performance of the Eagle Pass back-to-back HVDC Light Tie", 7th International conf on AC-DC Power Transmission, 2001, pp.220-225.
- [5] Alex Y. Wu, Yuexin Yin, " Fault Current Limiter Applications in Medium and High-Voltage Power Distribution Systems", IEEE Transactions on Industry applications, Vol. 34, No. 1, January/February 1998, pp. 236-242.
- [6] Mehrdad Tarafdar Haghl and Mehdi Abapour, "A New Topology of Fault-current Limiter and its control strategy", SICE-ICASE International Joint Conference, Oct. 18-21, 2006 , Bexco, Busan, Korea, pp. 5530-5534.
- [7] S. K. Lowe, "Circuit Breaker Stresses Associated with H.V. Series Reactors", Electrical Energy Conference, Australian Electrical Research, Canberra 10-12 May 1978, pp. 114-119.
- [8] K. Hongesombut, Y. Mitani, and K. Tsuji, "Optimal Location Assignment and Design of Superconducting Fault Current Limiters Applied to Loop Power Systems", IEEE Transactions on Applied Superconductivity, Vol. 13, No. 2, June, 2003 pp 1828-1831.
- [9] Parihar, P. G.G. Karady, "Characterization of a thyristor controlled reactor", Electric Power Systems Research, No.4, 1997, pp. 141-149.
- [10] Ming Jin, Tarlochan S. Sidhu, and Kai Sun, " A New System Splitting Scheme Based on the Unified Stability Control Framework", IEEE Transactions on Power Systems, Vol. 22, NO. 1, Feb. 2007, pp. 433-441.
- [11] Kai Sun, Da-Zhong Zheng, and Qiang Lu, "Splitting Strategies for Islanding Operation of Large-Scale Power Systems Using OBDD-Based Methods", IEEE Trans. on Power Systems, Vol. 18, No. 2, May 2003, pp. 912-923.

IMPACT OF INVERTER-FED MULTI-MOTOR DRIVES ON THE QUALITY OF ELECTRIC POWER IN THE MAINS.

Maciej Pawłowski

University of Technology Wrocław, Faculty of Electrical Engineering
Plac Piastowski 27, 58560 Jelenia Góra
maciej.pawlowski@pwr.wroc.pl, Tel/fax+(48)757551599

Abstract-The article presents the results of analysis of higher harmonics of current and voltage in networks feeding six-pulse rectifier. Analytical dependences of this phenomena at inductance in a dc circuit is also given. evaluation of this applicability of the analysis for practical purposes, verification measurements is taken. it is done measurements on the reel cutter of a paper-making machine mp-IV in Świecie.

I. INTRODUCTION.

An increased share of power of non-linear receivers on the power network gives rise to significant transfiguration of the feeding power sine waves. The performed analyses [2] [3] clearly indicate that the degree of transfiguration of the feeding power is higher at definite times of day. This refers to user supply networks, on which the number of small recipients, like PC users, significantly increases. Upper harmonics are common in electric networks Their sources are all sorts of non-linear receivers like converter systems, arc furnaces etc. The receivers get a transmuted current and thus become sources of upper harmonic currents [4],[5]. Those currents cause voltage drops at network impedance and distort voltage sinusoid [2],[6],[7]. However, it seems important to suggest a relevant model of power supply network including linear and non-linear receivers and a capacitor set. It is even more vital to discuss the practicality of applying some proposed models. In converter drives, the rectifier load current is an oscillating one since the value of inductance in a DC circuit is limited. The phenomenon has a significant impact on the harmonic spectrum of the input current fed to the rectifier from the mains. Of course, converters are usually equipped with commutation reactors, so the commutation angle γ is not zero. Those factors are especially important with some electric drives, as due to the high circuit dynamics required, the drives have commutation reactors but no smoothing reactors in the load circuits[8],[9].

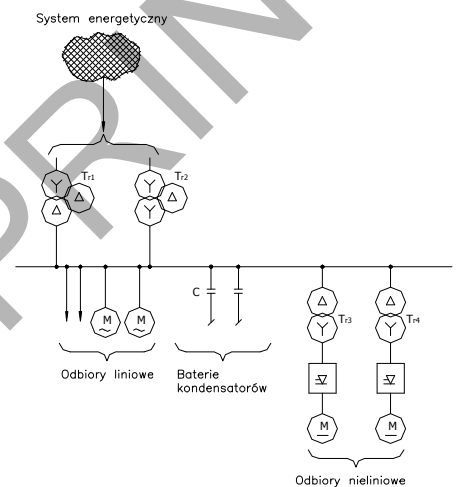
II. SPECIFICATIONS OF SUPPLY SYSTEMS FOR INDUSTRIAL PLANTS

Mixed-type networks are quite frequently used, especially when the internal network has suffered from problems with

compensating for wattless power or with the negative impact of non-linear recipients on power supply network. The impact involves taking transfigured power from the network, which means that the power spectrum will include higher harmonics [10], [2]. So far the analyses of upper harmonics of current have usually neglected the resistance values of all supply system components due to an assumption that their impact on the value of upper harmonics is negligible. The size of distortion of incoming voltage is determined by two major factors, i.e.:

- type of non-linear source of current
- parameters of supply network

Fig. 1 illustrates a standard network supply system.



Tr3, Tr4 - trafo przekształtnikowe

Fig. 1 Standard network supply system

In converter drives, the rectifier load current is an oscillating one since the value of inductance in a DC circuit is limited. The phenomenon has a significant impact on the harmonic spectrum of the input current fed to the rectifier from the mains. Of course, converters are usually equipped with commutation reactors, so the commutation angle γ is not zero. Those factors are especially important with some electric drives, as due to the high circuit dynamics required, the drives

have commutation reactors but no smoothing reactors in the load circuits[8],[9]. Fig.2 shows a schematic diagram of a six-pulse rectifier fed from a transformer of Dy vector group as well as a current waveform $i_w(x)$ in the transformer's secondary at any phase.

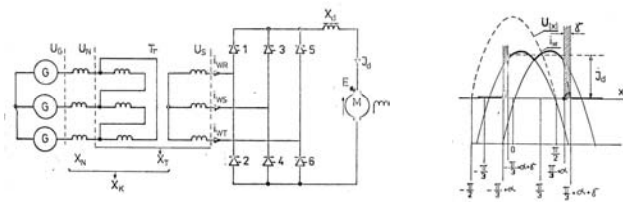


Fig.2. Schematic diagram of a six-pulse rectifier and a waveform of current at any phase, where:

- G – generators
- M – DC induction motor
- 1, 2, 3 to 6 – valves in individual bridge branches.

The oscillation of load current of a rectifier drive depends not only on the load reactance X_d , as it is frequently assumed, but rather on a sum of the load circuit reactance and the commutation reactance $X_d + 2X_K$. If it is assumed that non-linear receivers are 6-pulse SCR transformers (with high shorting power S_Z), then the feeding current will be:

$$i_p(\alpha) = \sqrt{2}I_1 \left(\cos\alpha - \frac{1}{5}\cos5\alpha + \frac{1}{7}\cos7\alpha - \frac{1}{11}\cos11\alpha + \dots \right) \quad (1)$$

where:

$i_p(\alpha)$ is a momentary amperage value at the pri of a transformer, and I_1 is an effective value of the first harmonic.

In the system presented in Fig.1, the passage of non-linear current I_n will cause voltage drops at the resultant impedance of Z_n system. Those voltage drops coincide with the supply voltage sinusoid and cause its distortion. Therefore we can say that

$$|\Delta U_n| = |I_n| \cdot |Z_n| \quad (2)$$

where

$$|Z_n| = \sqrt{R_n^2 + (n \cdot X_{L50})^2} \quad (3)$$

$|\Delta U_n|$ - voltage drop with a harmonic of n -th order at the impedance of Z_n system, $|Z_n|$ - module of system impedance with a harmonic of n -th order, $|I_n|$ - module of power with a harmonic of n -th order, R_n - system resistance with harmonics of n -th order, X_{L50} - system inductive reactance with the basic harmonic of 50Hz, n - harmonic order. The value of resultant impedance of Z_n system will change when upper harmonics filters or a capacitor set is incorporated into the system to

compensate for passive power. Its module will be determined as follows [3]:

$$\frac{1}{Z_{z_1}} = \frac{1}{Z_L} + \frac{1}{Z_S} + \frac{1}{R_o} + \frac{1}{jX_o} + j\frac{1}{X_C} \quad (4)$$

where

$Z_L = R_L + jX_L$ - impedance of supply system,

$Z_S = R_S + jX_S$ - impedance of linear receivers

III. MEASUREMENT-BASED ANALYSIS OF THE HARMONICS PHENOMENON

In the process of evaluating the inter-harmonics amplitude range, the harmonics in the power fed to an MP2 paper-making machine operated in Skolwin were measured and analysed. The machine power supply circuit beyond the marked measurement points is shown in Fig. 3.

The measurement points were established at clamps feeding PANT six-pulse rectifier 500 kW T7.T8 and on the clamps of the secondary winding of Tr7a transformer feeding the group of 1100kW total installed power. Some measurement points were also located in the secondary winding of Tr7 transformer feeding a group of inverters of 1000kW total installed power. Measurements of the harmonics levels for loads and voltages on the primary windings of those transformers.

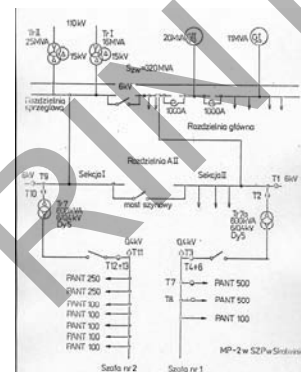


Fig.3. Schematic diagram of the power supply circuit in the A11 switching station feeding the MP2 paper-making machine in Skolwin.

The measurements were performed on a system with an open bus bar and the Tr7a transformer fed from the GII generator at own power plant. Such a measurement setup allows protection of a tested circuit from any impact of the supply system. For comparison purposes, the Tr7 transformer was supplied from the commercial power system.

IV. ANALYSIS OF MEASUREMENT RESULTS.

Measurement results are usually presented in the form of a spectrum of typical – sometimes non-typical – harmonics that are integral multiples of the base frequency [$\omega_1 = 50\text{Hz}$]. This results from the fact that the commonly used measurement instruments use a phaselocked loop and sample the analysed

signal during one or several wave periods. The analysis is done with the Fast Fourier Transform (FFT) or sometimes with the Discrete Fourier Transform (DFT). With inter-harmonics analysis the problem is more complicated since their frequencies are not integral multiples of the base frequency and moreover they often change during the measurements. They manifest themselves as sidebands around the characteristic harmonics. In the beginnings, their appearance would be considered a measurement error and then as a methodological error. Nowadays there is no doubt that those frequencies are actually present in the system [12],[13].

Figure 4 presents current waveform in the T phase of Tr7a transformer feeding the inverter set of MP2 machine drive at the paper mill in Skolwin as well as its spectrum for varied periods of measurement averaging.

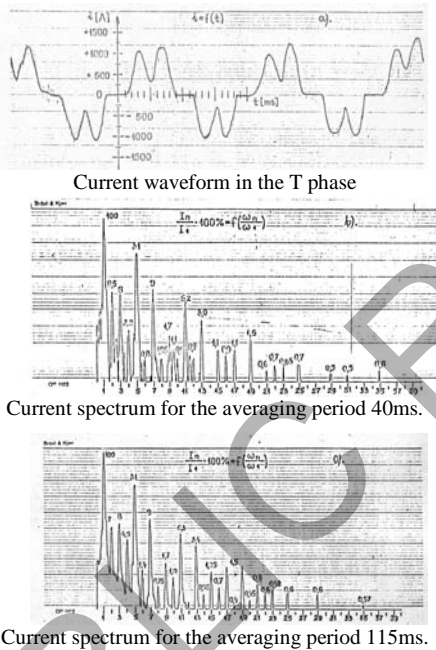


Fig.4. Waveform and amplitude-frequency spectrum of the current feeding the MP2 machine drive Switching station A11, transformer Tr7a, band 2kHz, cabinet no.1

There are well visible sidebands around all the frequencies that are integral multiples of the base frequency. Their amplitudes reach 1.5%. When comparing spectra for various averaging periods, it becomes evident that the spectrum share of those harmonics increases with the length of averaging periods. Another factor affecting the size of inter-harmonics amplitude is the level of distortions in the current fed from the mains.

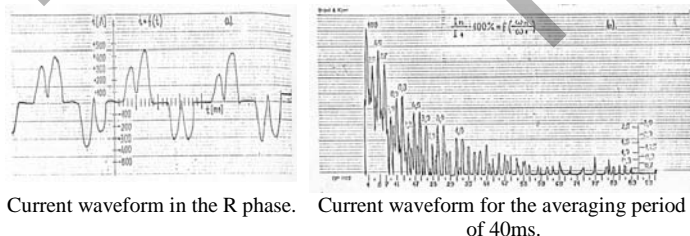


Fig.5. Waveform and amplitude-frequency spectrum of the current feeding drives 1 and 2 of the MP2 press. Switching station A11, transformer Tr7a, band 2kHz, cabinet no1

It is clearly visible in Fig.5 which shows the waveforms for one of the component drives in the same switching station, this time in the R phase, when the amplitude of upper harmonics of current reach 45% of the base.

Similar results were obtained from measurements of other components of a multi-motor drive, as shown in Fig.6. Interesting results were obtained from measurements of the screen drive current, as shown in Fig.6. In this particular case the feeding system apparently works in near-resonance conditions, as proved by the oscillations overlapping with the current waveform. Harmonics amplitudes reach 32% in this case.

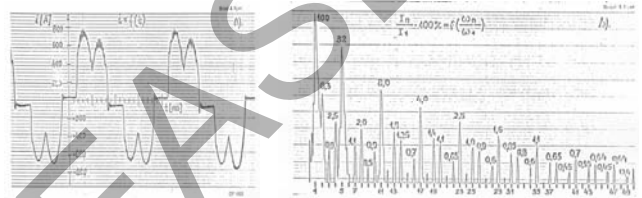


Fig.6. Waveform and amplitude-frequency spectrum of the current feeding the MP2 screen roll drive Switching station A11, transformer Tr7a, band 2kHz, ASEA cabinet

Similar results were obtained from measurements on the primary winding of the feeding transformer. Fig.7 presents the current waveform on the 6kV side of the tested transformer and its spectrum.

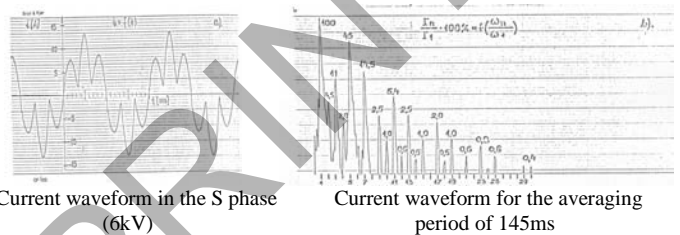


Fig.7. Waveform and amplitude-frequency spectrum of the current feeding the MP2 machine drive Switching station A11, transformer 7a, band 2kHz, cabinet no.1, 6kV level

Conclusions from this measurement are basically identical as those for the secondary winding, even though attenuation by transformer reactance $X_{Tr(k)}$ could be expected. Some attenuation is visible in the voltage harmonics, as shown in Fig.8.

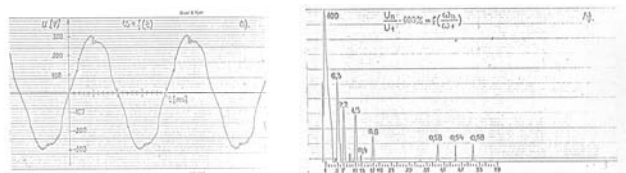


Fig.8. Waveform and amplitude-frequency spectrum of the voltage feeding 0,4 kV the MP2 machine drive Switching station A11, transformer Tr7a, band 2kHz, cabinet no.1

V CONCLUSIONS

1. A significant increase in the number of non-linear receivers results in a significant decrease in electric power quality, especially in multi-motor drive systems.
2. Analytical methods for assessing this phenomena are complicated and their practical application is difficult. Therefore the method of direct measurements is preferable.
3. Multi-motor systems with inverter-fed drives require unconditional application of filters for higher harmonics of the feeding current.

VI DISCUSSION

The article does not include a discussion of the methodology of current harmonics measurements, i.e. the impact of applying various waveform analysers / measurement windows / averaging periods on the measurement results. Differences in measurement results that arise from the above are usually neglected, but they can reach as much as several dozen percent. This problem requires a deep analysis.

REFERENCES

- [1] Arrilaga J., Bradley D., Bodger P.: *Power systems harmonics*. John Wiley 1985
- [2] Pawłowski M., „Analiza oddziaływania tyrystorowych napędów maszyn papierniczych na sieć wewnętrzną papierni”, *Rozprawa doktorska*, Politechnika Wroclawska 1982 r.
- [3] Miedziński B. Okraszewski Z. Szkółka S. Szymański A., „Wyższe harmoniczne jako źródło zagrożeń transformatorów zasilających odbiory wielkiej mocy”, *Mechanizacja i automatyzacja górnictwa* 1999 vol. 11.
- [4] Szachtarin B. Artiuszin C. Gołubiew C. Rukawica K., „Rezonans i chaos w odnoży nieliniowej systemie” *Elektryczność* vol. 2/2000
- [5] Miedziński B. Okraszewski Z. Szkółka S. Szymański A., „Problemy eksploatacyjne związane z wyższymi harmonicznymi prądu i napięcia generowane napędami dużej mocy”, *Węgiel brunatny, wydanie specjalne ISSN*, pp. 1232 – 8782
- [6] Jasiński J. Bartosiewicz M., „Filtr aktywny do kompensacji mocy biernej odkształcenia” *Materiały konferencyjne JEL 2000* r.
- [7] Staszewski K., „Wyższe harmoniczne w sieci kopalnianej 6kV”, *Mechanizacja i automatyzacja górnictwa* vol. 7/367/2001
- [8] Piróg S., „Energoelektronika” *AGH Uczelniane Wydawnictwa Naukowe - Dydaktyczne*. Kraków 1998.
- [9] Moltgen G., „Netzgefuehrte Stromrichter mit Thyristoren”, *Siemens Fachbucher*. Berlin 1974
- [10] Nowak M. Barlik R., „Technika tyrystorowa”, *WNT Warszawa* 1998 r.
- [11] Pawłowski M. Fjałkowski Z., „Rezonans prądów w sieciach przemysłowych 6kV”, *Mechanizacja i automatyzacja górnictwa* 7/367/2001
- [12] Maswood Ali J. ZHU JUN., „Analysis of Harmonic motor controls under nonlinear conditions”, *Electronics Machines and Power system* 28/2000
- [13] Maamar Bettaych, Urasi Qidwai., „A new flux – based harmonic elimination technique”, *Electric Machines and Power System* 27/1999
- [14] Pawłowski M. Szymański A. Fjałkowski Z., „Zjawiska rezonansowe w sieciach przemysłowych” – *Mechanizacja i automatyzacja górnictwa* 2002 vol. 8.
- [15] Żezelenko J.: Wyższe harmoniczne w systemach zasilających odbiorniki Przemysłowe *Energoizdat*. Moskwa 1994

Modeling analysis and solution of Power Quality Problems

Mahesh Singh (Lecturer) SSCET BHILAI INDIA
Vaibhav Tiwari CSIT BHILAI INDIA

Abstract-- A Power quality problem is an occurrence manifested as a nonstandard voltage, current or frequency that results in a failure or a mis-operation of end use equipments. Utility distribution networks, sensitive industrial loads, and critical commercial operations all suffer from various types of outages and service interruptions which can cost significant financial loss per incident based on process down-time, lost production, idle work forces, and other factors. With the restructuring of Power Systems and with shifting trend towards Distributed and Dispersed Generation, the issue of Power Quality is going to take newer dimensions. The aim therefore, in this work, is to identify the prominent concerns in the area and thereby to recommend measures that can enhance the quality of the power, keeping in mind their economic viability and technical repercussions. In this paper electromagnetic transient studies are presented for the following two custom power controllers: the distribution static compensator (D-STATCOM), and the dynamic voltage restorer (DVR). Comprehensive results are presented to assess the performance of each device as a potential custom power solution.

Index Terms-- Power Quality Problems, Power System Restructuring, Voltage Sag, DSTATCOM, DVR, MATLAB.

I. INTRODUCTION

Power quality is certainly a major concern in the present era; it becomes especially important with the introduction of sophisticated devices, whose performance is very sensitive to the quality of power supply. Modern industrial processes are based a large amount of electronic devices such as programmable logic controllers and adjustable speed drives. The electronic devices are very sensitive to disturbances [1] and thus industrial loads become less tolerant to power quality problems such as voltage dips, voltage swells, and harmonics.

Voltage dips are considered one of the most severe disturbances to the industrial equipment. A paper machine can be affected by disturbances of 10% voltage drop lasting for 100ms. A voltage dip of 75% (of the nominal voltage) with duration shorter than 100ms can result in material loss in the range of thousands of US dollars for the

semiconductors industry [2]. Swells and over voltages can cause over heating tripping or even destruction of industrial equipment such as motor drives. Electronic equipments are very sensitive loads against harmonics because their control depends on either the peak value or the zero crossing of the supplied voltage, which are all influenced by the harmonic distortion.

This paper analyzes the key issues in the Power Quality problems, specially keeping in mind the present trend towards more localized generations (also termed as distributed and dispersed generation) and consequent restructuring of power transmission and distribution networks. As one of the prominent power quality problems, the origin, consequences and mitigation techniques of voltage sag problem has been discussed in detail. The study describes the techniques of correcting the supply voltage sag in a distribution system by two power electronics based devices called Dynamic Voltage Restorer (DVR) and Distribution STATCOM (D-STATCOM). A DVR voltage in series with the system voltage and a D-STATCOM injects a current into the system to correct the voltage sag [1]. The steady state performance of both DVR and D-STATCOM is studied for various levels of voltage sag levels.

II. SOURCES AND EFFECTS OF POWER QUALITY PROBLEMS

The distortion in the quality of supply power can be introduced /enhanced at various stages; however, some of the primary sources of distortion [3] can be identified as below:

- A. Power Electronic Devices
- B. IT and Office Equipments
- C. Arcing Devices
- D. Load Switching
- E. Large Motor Starting
- F. Embedded Generation
- G. Electromagnetic Radiations and Cables
- H. Storm and Environment Related Causes etc.

While power disturbances occur on all electrical systems, the sensitivity of today's sophisticated electronic devices makes them more susceptible to the quality of power supply. For some sensitive devices, a momentary disturbance can cause scrambled data, interrupted

communications, a frozen mouse, system crashes and equipment failure etc. A power voltage spike can damage valuable components. Some of the common power quality issues and their prominent impact are summarized in the table below:

Problem	Effects
Voltage sags	Devices/process downtime, effect on product quality, failure/malfunction of customer equipments (such as tripping of large industrial drives) and associated scrap cost, clean up costs, maintenance and repair costs etc.
Transients	Tripping, component failures, flashover of instrument insulation, hardware rebooting, software 'glitches', poor product quality etc.
Harmonics	Excessive losses and heating in motors, capacitors and transformers connected to the system, insulation failure due to overheating and over voltages, loss of conductor life and possible risk of fire due to overheating, malfunctioning of sophisticated electronic equipments, higher dielectric stress and harmonic resonance, saturation in transformer cores, interference with adjacent communication networks, audio (hmn. vide) 'flutter', power supply failure etc.
Flicker	Visual irritation, introduction of many harmonic components in the supply power and their associated effects.

Table1: Various power quality problems and their effects

III. SOLUTIONS TO POWER QUALITY PROBLEMS

There are two approaches to the mitigation of power quality problems. The solution to the power quality can be done from customer side or from utility side [4]. First approach is called load conditioning, which ensures that the equipment is less sensitive to power disturbances, allowing the operation even under significant voltage distortion. The other solution is to install line conditioning systems that suppress or counteracts the power system disturbances. A flexible and versatile solution to voltage quality problems is offered by active power filters. Currently they are based on PWM converters and connect to low and medium voltage distribution system in shunt or in series. Series active power filters must operate in conjunction with shunt passive filters in order to compensate load current harmonics. Shunt active power filters operate as a controllable current source and series active power filters operates as a controllable voltage source. Both schemes are implemented preferable with voltage source PWM inverters [5], with a dc bus having a reactive element such as a capacitor. Active power filters can perform one or more of the functions required to compensate power systems and improving power quality. Their performance also depends on the power rating and the speed of response.

However, with the restructuring of power sector and with shifting trend towards distributed and dispersed generation, the line conditioning systems or utility side solutions will play a major role in improving the inherent supply quality; some of the effective and economic measures can be identified as following:

A. Lightning and Surge Arresters:

Arresters are designed for lightening protection of transformers, but are not sufficiently voltage limiting for protecting sensitive electronic control circuits from voltage surges.

B. Thyristor Based Static Switches:

The static switch is a versatile device for switching a new element into the circuit when the voltage support is

needed. It has a dynamic response time of about one cycle. To correct quickly for voltage spikes, sags or interruptions, the static switch can used to switch one or more of devices such as capacitor, filter, alternate power line, energy storage systems etc. The static switch can be used in the alternate power line applications. This scheme requires two independent power lines from the utility or could be from utility and localized power generation like those in case of distributed generating systems [4]. Such a scheme can protect up to about 85 % of interruptions and voltage sags.

C. Energy Storage Systems:

Storage systems can be used to protect sensitive production equipments from shutdowns caused by voltage sags or momentary interruptions. These are usually DC storage systems such as UPS, batteries, superconducting magnet energy storage (SMES), storage capacitors or even fly wheels driving DC generators [6]. The output of these devices can be supplied to the system through an inverter on a momentary basis by a fast acting electronic switch. Enough energy is fed to the system to compensate for the energy that would be lost by the voltage sag or interruption. In case of utility supply backed by a localized generation this can be even better accomplished.

D. Electronic tap changing transformer:

A voltage-regulating transformer with an electronic load tap changer can be used with a single line from the utility. It can regulate the voltage drops up to 50% and requires a stiff system (short circuit power to load ratio of 10:1 or better). It can have the provision of coarse or smooth steps intended for occasional voltage variations.

E. Harmonic Filters

Filters are used in some instances to effectively reduce or eliminate certain harmonics [7]. If possible, it is always preferable to use a 12-pulse or higher transformer connection, rather than a filter. Tuned harmonic filters should be used with caution and avoided when possible. Usually, multiple filters are needed, each tuned to a separate harmonic. Each filter causes a parallel resonance as well as a series resonance, and each filter slightly changes the resonances of other filters.

F. Constant-Voltage Transformers:

For many power quality studies, it is possible to greatly improve the sag and momentary interruption tolerance of a facility by protecting control circuits. Constant voltage transformer (CVTs) can be used [6] on control circuits to provide constant voltage with three cycle ride through, or relays and ac contactors can be provided with electronic coil hold-in devices to prevent mis-operation from either low or interrupted voltage.

G. Digital-Electronic and Intelligent Controllers for Load-Frequency Control:

Frequency of the supply power is one of the major determinants of power quality, which affects the

equipment performance very drastically. Even the major system components such as Turbine life and interconnected-grid control are directly affected by power frequency. Load frequency controller used specifically for governing power frequency under varying loads must be fast enough to make adjustments against any deviation. In countries like India and other countries of developing world, still use the controllers which are based either on mechanical or electrical devices with inherent dead time and delays and at times also suffer from ageing and associated effects. In future perspective, such controllers can be replaced by their Digital-electronic counterparts.

IV. USE OF CUSTOM POWER DEVICES TO IMPROVE POWER QUALITY

In order to overcome the problems such as the ones mentioned above, the concept of custom power devices is introduced recently; custom power is a strategy, which is designed primarily to meet the requirements of industrial and commercial customer. The concept of custom power is to use power electronic or static controllers in the medium voltage distribution system aiming to supply reliable and high quality power to sensitive users [1]. Power electronic valves are the basis of those custom power devices such as the static transfer switch, active filters and converter-based devices. Converter based power electronics devices can be divided into two groups: shunt-connected and series-connected devices. The shunt connected devices is known as the DSTATCOM and the series device is known as the Static Series Compensator (SSC), commercially known as DVR. It has also been reported in literature that both the SSC and DSTATCOM have been used to mitigate the majority of the power system disturbances such as voltage dips, sags, flicker unbalance and harmonics.

For lower voltage sags, the load voltage magnitude can be corrected by injecting only reactive power into the system. However, for higher voltage sags, injection of active power, in addition to reactive power, is essential to correct the voltage magnitude [8]. Both DVR and D-STATCOM are capable of generating or absorbing reactive power but the active power injection of the device must be provided by an external energy source or energy storage system. The response time of both DVR and D-STATCOM is very short and is limited by the power electronics devices. The expected response time is about 25 ms, and which is much less than some of the traditional methods of voltage correction such as tap-changing transformers.

V. MODELING OF CUSTOM POWER DEVICES AND SIMULATION RESULTS

As mentioned in the previous section that custom power devices could be the effective means to overcome some of the major power quality problems by the way of injecting active and/or reactive power(s) into the system [9]-[11]. This section of the paper deals with the modeling of DSTATCOM and DVR. Consequently some case studies

will be taken up for analysis and performance comparison of these devices. The modeling approach adopted in the paper is graphical in nature, as opposed to mathematical models embedded in code using a high-level computer language. The well-developed graphic facilities available in an industry standard power system package, namely, MATLAB (/Simulink) [12], is used to conduct all aspects of model implementation and to carry out extensive simulation studies.

The control scheme for these devices is shown in Fig.1. The controller input is an error signal obtained from the reference voltage and the value rms of the terminal voltage measured. Such error is processed by a PI controller and the output is the angle δ , which is provided to the PWM signal generator. The PWM generator then generates the pulse signals to the IGBT gates of voltage source converter [10].

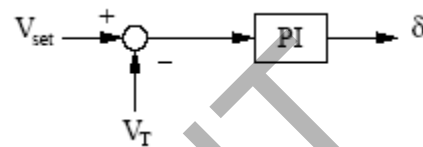


Fig.1. The PI Controller

(A) D-STATCOM

The test system employed to carry out the simulations concerning the DSTATCOM actuation for voltage sag compensation is shown in Fig.2. Such system is composed by a 230 kV, 50 Hz transmission system, represented by a Thevenin equivalent, feeding a distribution network through a 3-winding transformer connected in Y/Y/Y, 230/11/11 kV. To verify the working of a DSTATCOM, a variable load is connected at bus 2. During the simulation, in the period from 500 to 900 ms, the switch S1 is closed. The above test system is simulated under the environment of Matlab-Simulink and power system block set (PSB) the model used for this purpose is shown in the fig.3.

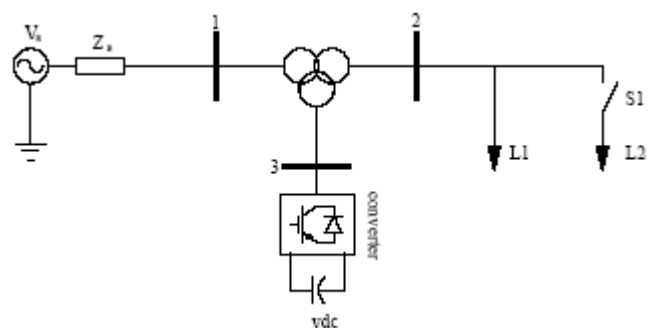


Fig.2. Test system for DSTATCOM

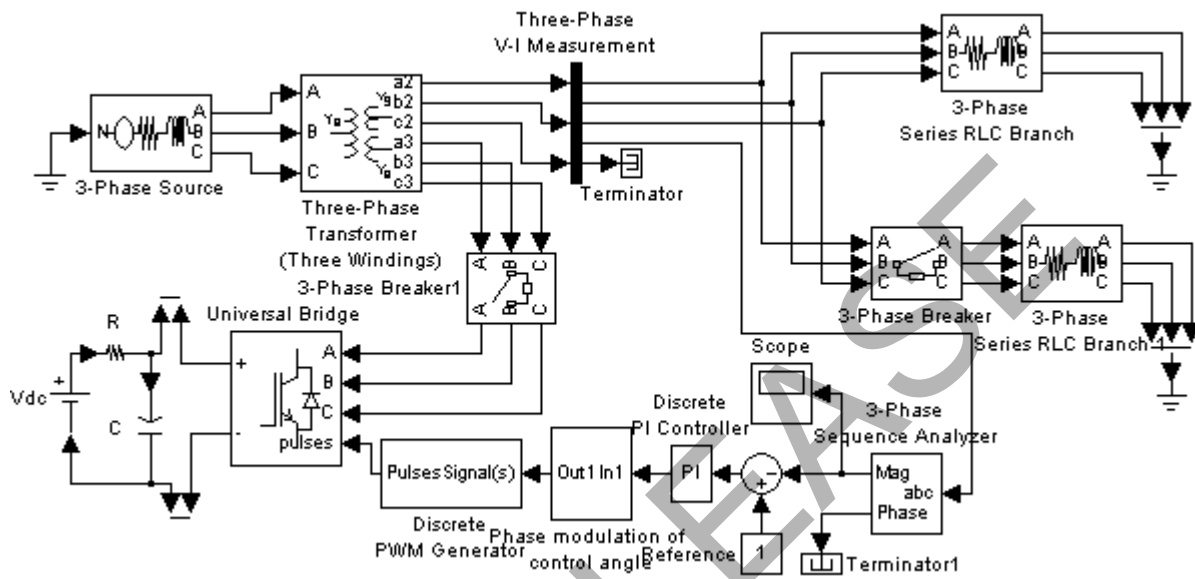


Fig.3. MATLAB Simulation model of DSTATCOM

A set of simulations was carried out for the test system shown in Fig.2. The simulations relate to three main operating conditions.

- 1) In the simulation period 500–900 ms, the load is increased by closing switch S1. In this case, the voltage drops by almost 27% with respect to the reference value.
- 2) At 900 ms, the switch S1 is opened and remains so throughout the rest of the simulation. The load voltage is very close to the reference value, i.e., 1 pu.
- 3) In order to gain insight into the influence that capacitor size has on D-STATCOM performance, simulations were carried out with different size of capacitors. The total simulation period is 1.4 s.

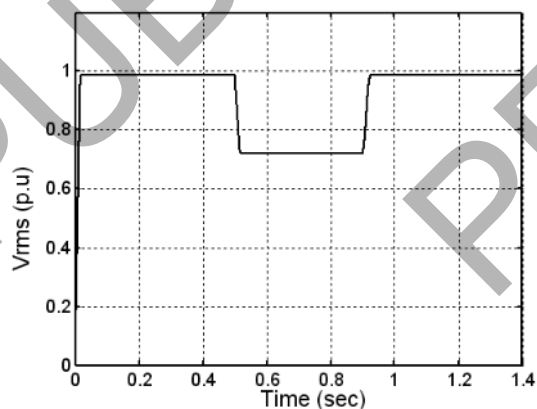


Fig.4. Voltage response of the test system without DSTATCOM

Fig.4. shows the rms voltage at the load point for the case when the system operates with no D-STATCOM. Similarly, a new set of simulations was carried out but now with the D-STATCOM connected to the system. The results are shown in Fig.5(a). Where the very effective voltage regulation provided by the D-STATCOM can be clearly appreciated.

When the Switch S1 closes, the D-STATCOM supplies reactive power to the system. By way of example, Fig.5(a). shows the regulated rms voltage corresponding to a 750 F capacitor, where a rapid regulation response is obtained and transient overshoots are almost nonexistent.

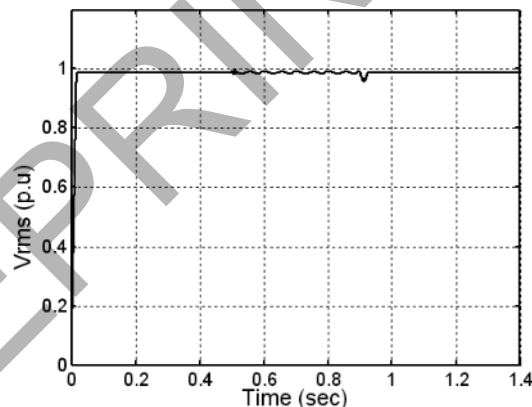


Fig 5(a) Voltage response of the test system 1 with DSTATCOM; With 750µF Capacitor

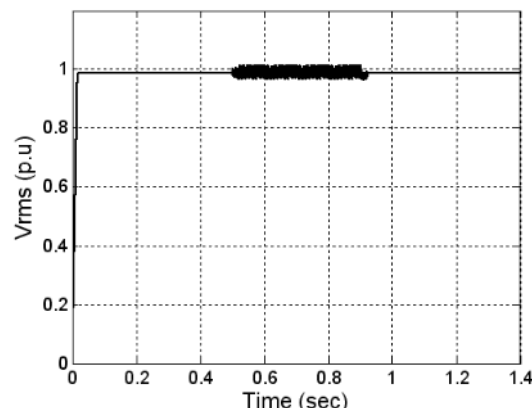


Fig 5(b) Voltage response of the test system 1 with DSTATCOM; With 75µF Capacitor

This contrasts with cases where the capacitor is undersized. For instance, Fig. 5(b) shows the rms voltage for the case when a 75 F capacitor is employed.

(B) DVR

The test system employed to carry out the simulations concerning the DVR actuation is shown in Fig.6. Such network is composed by a 13 kV, 50 Hz generation system, represented by a Thevenin equivalent, feeding two transmission lines through an 3-winding transformer connected in Y / 13/115/115 kV. Such transmission lines feed two distribution networks through two transformers connected in /Y, 115/11 kV. To verify the working of a DVR employed to avoid voltage sags during short-circuit, a fault is applied at point X via a resistance of 0.4 . Such fault is applied from 500 to 900 ms.

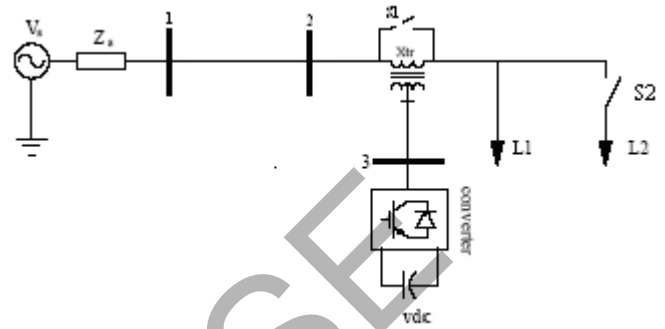


Fig.6. Test system for DVR

The above test system is simulated under the environment of Matlab-Simulink and power system block set (PSB) the model used for this purpose is shown in the fig.7.

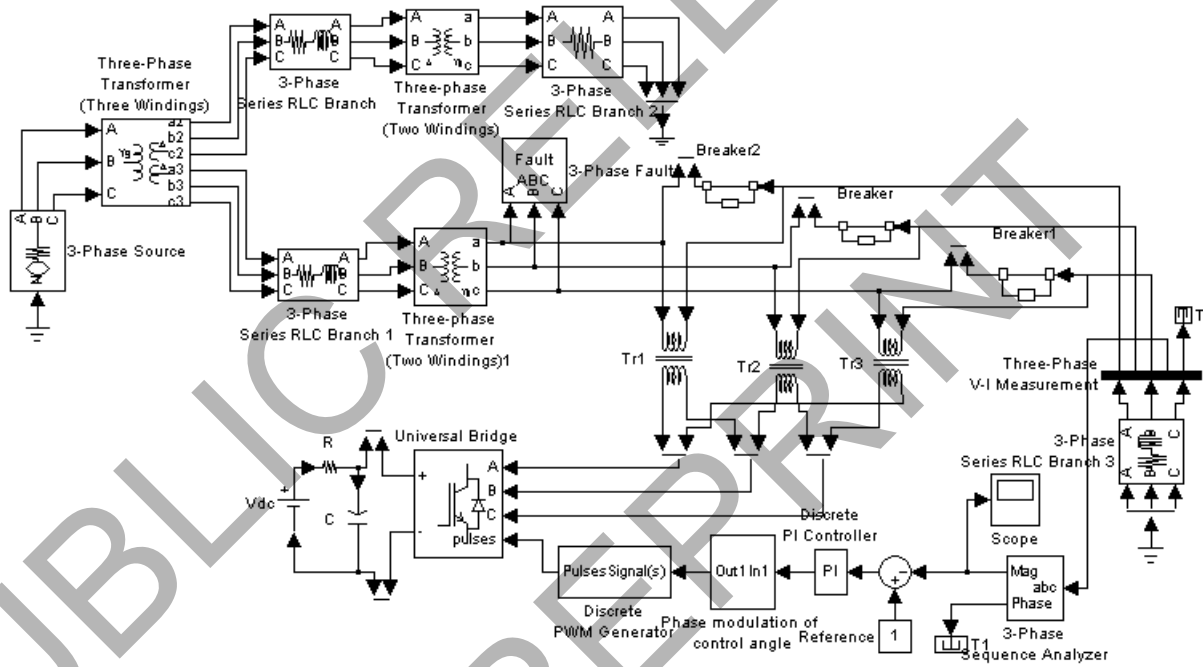


Fig.7 MATLAB Simulation model of DVR

Two simulations studies are carried out as follows:

- 1) The first simulation contains no DVR and a three-phase short-circuit fault is applied at point A, via a fault resistance of 0.4 , during the period 500–900 ms. The voltage sag at the load point is almost 60% with respect to the reference voltage.
 - 2) The second simulation is carried out using the same scenario as above but now with the DVR in operation. The total simulation period is 1.4 s.
- Using the facilities available in MATLAB the DVR is simulated to be in operation only for the duration of the fault, as it is expected to be the case in a practical situation. The results for both simulations are shown in Fig.8 and Fig.9 Voltage response without DVR is shown in Fig.8

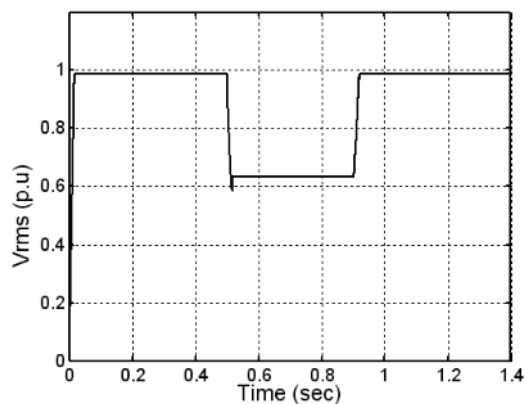


Fig.8 Voltage Response of the test system without DVR.

VII. REFERENCES

When the DVR is in operation the voltage sag is mitigated almost completely, and the rms voltage at the sensitive load point is maintained at 98%, as shown in Fig. 9.

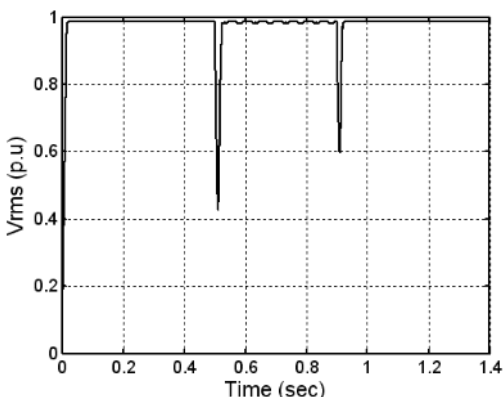


Fig 9 Voltage Response of the test system2 with DVR.

The PWM control scheme controls the magnitude and the phase of the injected voltages, restoring the rms voltage very effectively [13]-[14]. The sag mitigation is performed with a smooth, stable, and rapid DVR response;

VI. CONCLUSIONS

Power quality measures can be applied both at the user end and also at the utility level. The work identifies some important measures that can be applied at the utility level without much system upset (or design changes). This paper has presented models of custom power equipment, namely D-STATCOM, DVR, and applied them to mitigate voltage dip which is very prominent as per utilities are concerned. The highly developed graphic facilities available in MATLAB SIMULINK were used to conduct all aspects of model implementation and to carry out extensive simulation studies on test systems. A new PWM-based control scheme has been implemented to control the electronic valves in the two-level VSC used in the D-STATCOM and DVR. As opposed to fundamental frequency switching schemes already available in the MATLAB SIMULINK. This characteristic makes it ideally suitable for low-voltage custom power applications. It was observed that in case of DSTATCOM capacity for power compensation and voltage regulation depends mainly on the rating of the dc storage device. The simulation results presented shows good accuracy with results reported in index journals.

- [1] H. Hingorani "Introducing custom power" IEEE spectrum, vol.32 no.6 June 1995 p 41-48.
- [2] Ray Arnold "Solutions to Power Quality Problems" power engineering journal 2001 pages: 65-73.
- [3] John Stones and Alan Collinson "Introduction to Power Quality" power engineering journal 2001 pages: 58 -64.
- [4] Gregory F. Reed, Masatoshi Takeda, "Improved power quality solutions using advanced solid-state switching and static compensation technologies," Power Engineering Society 1999 Winter Meeting, IEEE
- [5] G. Venkataramanan and B. Johnson, "A pulse width modulated power line conditioner for sensitive load centers," IEEE Trans. Power Delivery, vol. 12, pp. 844-849, Apr. 1997.
- [6] N.G. Hingorani and L. Gyugyi, "Understanding FACTS: Concepts and Technology of Flexible AC Transmission Systems", 1st edition, The Institute of Electrical and Electronics Engineers, 2000.
- [7] F. Z. Peng, H. Akagi, and A. Nabae, "Compensation characteristics of the combined system of shunt passive and series active filters," IEEE Trans. Ind. Applicat., vol. 29, pp. 144-151, Jan./Feb. 1993.
- [8] M.H.Haque "Compensation of distribution system voltage sag by DVR and DSTATCOM" Power Tech Proceedings, 2001 IEEE Porto , Volume: 1 , 10-13 Sept. 2001 Pages:5 pp. vol.1
- [9] S. S. Choi, B. H. Li, and D. D.Vilathgamuwa, "Dynamic voltage restoration with minimum energy injection," IEEE Trans. Power Syst., vol. 15, pp. 51-57, Feb. 2000
- [10] O. Anaya-Lara, E. Acha, "Modeling and Analysis of Custom Power Systems by PSCAD/EMTDC," IEEE Trans., Power Delivery, PWDR vol-17 (1), pp. 266-272, 2002.
- [11] P.W. Lehn and MR. Iravani, "Experimental Evaluation of STATCOM Closed Loop Dynamics," IEEE Trans. Power Delivery, vol. 13, no.4, October 1998, pp.1378-1384.
- [12] TEQSIM International Inc., "Power System Blockset User'sGuide", 2001.
- [13] M. H. J. Bollen, "Understanding Power Quality Problems—Voltage Sags and Interruptions" Piscataway, New York: IEEE Press, 2000.
- [14] Mohan, T. M. Undeland, and W. P. Robbins, *Power Electronics: Converters, Applications and Design*. New York: Wiley, 1995.

Power System Real Time Simulation Testing Using IEC 61850.

* Yogesh Sonawane Pankaj Patil

yogimba@gmail.com

pankajpatil2k@gmail.com

N.D.Sonawane

starnaresh2k@yehoo.com

Sayali Sonawane

sayali001@gmail.com

* Corresponding Author.

Abstract:—

IEC-61850 becomes more widely accepted in the electrical engineering community, it is important that the testing tools keep pace with this development. IEC 61850 presents new challenges to real time simulation and closed-loop testing of protective relays. Electrical interfaces used for binary signaling and voltage/current amplifiers must be replaced by an Ethernet connection and an IEC 61850 protocol stack. The electrical interfaces of a real time simulator are engineered to provide low latency and deterministic performance appropriate for a real time simulation. Similar attention must be given to IEC 61850 interfaces. Latency must be minimized so that the IEC 61850 interface does not add unacceptable delays to the operation of the simulator. Also, protocol processing must be deterministic to allow real time simulations to be repeatable and dependable. In addition, IEC 61850 specifies new configuration parameters and a new method for configuration called the Substation Configuration Language (SCL). These must be implemented in such a way that they fit within the typical modes of operation of the simulator. The paper presents a successful hardware implementation for IEC 61850 messaging on a real time simulator and discusses the key design criteria. The software required to configure the IEC 61850 will also be addressed along with the advantages in using the IEC 61850 protocol. One of the biggest advantages is brought about by the realization of the IEC 61850-9-2 sampled values, removing the need for amplifiers as the standard interface to protection devices. Sampled values of the voltage and current signals can be sent via Ethernet, making it even more practical to perform testing on a protective relaying scheme rather than just individual devices.

Keywords: *IEC 61850, GOOSE, GSSE, closed-loop testing, real time, power system simulation.*

I. INTRODUCTION

Real time digital simulation using systems such as the RTDS Simulator are often used to perform closed-loop testing of power system protection devices such as relays and protection schemes. IEC 61850 is the international standard for substation automation systems. It defines the communications between devices in the substation and the related system requirements. IEC 61850 supports all substation automation functions and their engineering [1]. As IEC 61850 becomes more widely accepted and implemented by protection device manufacturers and power system utilities, it is important that the testing

tools keep pace allowing these new devices to be tested. Using IEC 61850 for simulation testing also provides a number of benefits and advantages over traditional electrical interfaces such as the simplification of wiring and the potential to reduce the cost of the test setup.

When using IEC 61850, the electrical interfaces used for binary signaling and voltage/current amplifiers are replaced by an Ethernet connection and software implementing IEC 61850. Careful consideration must be given to the integration of IEC 61850 into real time digital simulators to ensure that the integrity of the simulation is not compromised due to nondeterministic or slow performance of the IEC 61850 interface. This paper introduces real time digital simulation testing that includes the use of IEC 61850. A list of advantages for using IEC 61850 in simulation testing is presented along with key design criteria used when incorporating IEC 61850 into a real time digital simulator.

II. SIMULATION TESTING USING REAL TIME DIGITAL SIMULATORS

A. Common Applications

Real time digital simulators are commonly used for closed loop testing of protection and control devices as well as for real time system studies. When conducting closed-loop testing, the simulator acts as the power system and interfaces to the test objects. For closed-loop operation protective relay testing, the simulator must provide real time data (i.e. voltage, current and breaker status) to the relay and sense trip and reclose status from the relay. Since the power system is being simulated, various faults can easily be applied under different network conditions to evaluate the performance of the protection and control. If the protection detects the fault applied, the trip signal will be sensed and the breaker in the simulation opened.

When evaluating the performance of a protective relay or protection system, exhaustive testing is often conducted. This involves applying thousands of faults while varying different system parameters (e.g. fault type, fault location, point-on-wave). Since so many tests are run, it is crucial to keep each test and the time between tests as short as possible. Prior to the advent of IEC 61850, the protection equipment was connected to the simulator using individual wires. The complexity of the wiring is evident even for the

relatively simple double ended line protection test setup shown in Fig. 1. Twelve (12) signals have to be connected from the RTDS.

Simulator to the voltage and current amplifiers. After the signals pass through the amplifiers, twelve (12) more connections have to be made to connect the voltage and current signals to the relays. If the relays are set for single pole trip and reclose, a minimum of twelve (12) contacts must also be connected to the simulator's digital input to control breaker operation. If internal relay elements are to be monitored, even more contacts have to be connected to the simulator. Finally, six (6) breaker status signals must be supplied to the relays at station level voltages (e.g. 125 Vdc) via potential free contacts. All told, there are 30 digital and analogue connections between the relays and the simulator when using traditional methods for the test setup illustrated in Fig. 1. This does not include the 12 signals that must be connected from the simulator to the amplifiers or the monitoring of internal relay elements.

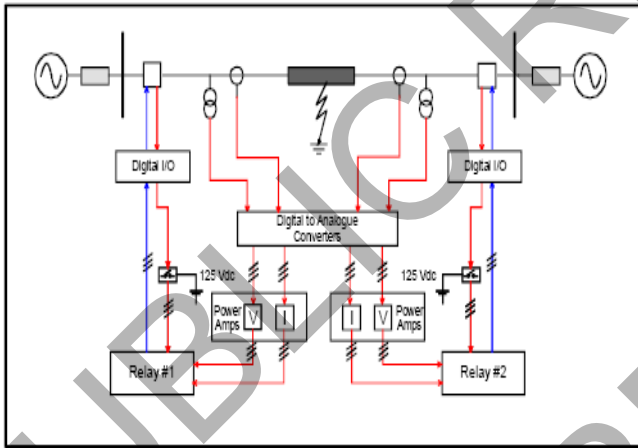


Fig. 1. Test Setup with Standard Electrical Connections

B. Integration Of IEC 61850 In Simulation Testing

IEC 61850 can be used to replace the two types of interfaces between the RTDS Simulator and the devices being tested. IEC 61850 GOOSE/GSSE can replace the hard-wired binary inputs and outputs over what IEC 61850 refers to as a station bus and IEC 61850-9-2 sampled values can replace the hard-wired voltage and current signals from the power amplifiers over what IEC 61850 refers to as a process bus.

IEC 61850 GOOSE/GSSE replaces the hard-wired binary signaling with a message sent over an Ethernet based station bus. All of the hard-wiring needed for status signals can be replaced by a single Ethernet connection between the simulator and the station bus LAN to which the protection devices are connected. The transfer of trip and breaker status through GOOSE/GSSE messages is very fast. Maximum end

to end transfer time is typically specified between 3-10 msec [3].

IEC 61850-9-2 Sampled Values can be used for applying voltage and current signals to devices instead of using analogue current and voltage from amplifiers. Maximum sample to transmission time for an IEC 61850-9-2 sampled value message used for protection is typically specified at less than 3 msec for sample rates faster than 480 samples/cycle [3]. An IEC 61850 device referred to as a Merging Unit (MU) is used to transmit sampled values derived from transducers using IEC 61850-9-2 messages over the process bus. Messages sent by MUs may contain an arbitrary number of current and voltage channels/phases, but initial implementations of 61850-9-2 send messages with instantaneous 3-phase plus neutral voltage and current samples (i.e. 8 signals) [2]. Arbitrary sample rates are permitted by IEC 61850-9-2, but initial implementations of MUs used for protection typically send samples at 80 samples/cycle [3].

With the implementation of IEC 61850 communication for the RTDS Simulator, all signals are passed to and from the protective relays via a separate station bus and process bus both based on Ethernet. The IEC 61850 GOOSE/GSSE facility described in this paper allows up to 32 binary inputs and 32 binary outputs to be provided to as many as 8 different IED's (e.g. relays) from one device. Therefore the trip and reclose signals plus the breaker status signals for the double ended line protection tests can be provided by one Ethernet connection representing a single station bus. An added Ethernet connection is required for a process bus to pass up to 8 sampled value (analogue) signals to each relay. A double ended line protection test setup using IEC 61850 is shown in Fig 2. In the figure, the GTNET-SV is used for the IEC 61850-9-2 interfaces and the GTNET-GSE provides the GOOSE/GSSE interface.

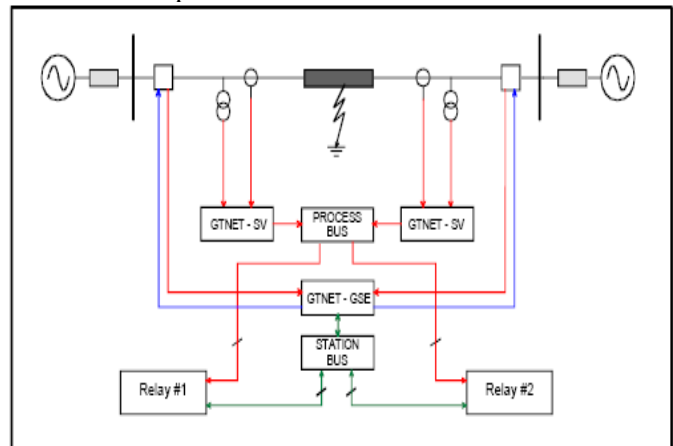


Fig. 2. Test Setup with IEC 61850 Connections

III. ADVANTAGES

There are a number of advantages to using an IEC 61850 interface for simulation testing compared to using traditional electrical interfaces. An obvious advantage is the ability to test IEC 61850 based systems that cannot be tested using traditional electrically interfaced simulators. The use of IEC 61850 in installations is increasing [4], and it is important to be able to test these devices using the IEC 61850 interface. Also, since a goal of IEC 61850 is to provide a comprehensive set of functions [3] to replace proprietary protocols, simulation testing can be performed on products from different vendors using only the IEC 61850 protocol without requiring a combination of industry standard and proprietary protocols. Elimination of the often large and expensive voltage and current amplifiers commonly used in simulation testing reduces the size and cost of the test setup. This in turn makes it more practical to perform testing on larger protective relay schemes rather than on individual devices.

Another major advantage of using IEC 61850 for simulation testing is the reduction in electrical wiring between the simulator and protection devices. Fig. 2 illustrates that when using IEC 61850 for the same test system as shown in Fig. 1, the number of connections between the simulator and the relays is reduced to just 4. In addition, the connections are greatly simplified by using an Ethernet connection rather than individual wires and by eliminating the need for station level breaker status signals.

IV. IMPLEMENTATION OF AN IEC 61850 INTERFACE FOR SIMULATION TESTING

Implementation of an IEC 61850 interface for a power system simulator presents interesting challenges that are generally different than those present when implementing IEC 61850 in typical substation devices such as protection relays and circuit breakers.

A power system simulator must produce reliable, consistent results. The results must be consistent each time the same simulation case is run. There must be low variability in the input and output latency and the latencies must be well understood to allow the analysis of simulation results. The input and output latency must also be minimized to reduce the impact of the interface and allow the widest range of delay adjustment within the simulation, if desired. Although latency must be minimized, it should not be minimized at the expense of variability in latency. Any variation in latency affects the confidence in the timing measurements of DUT operations, which in turn affect the confidence in the simulation as a whole.

The start-up operation of a simulation test case also differs from other substation equipment. Whenever possible, the simulation should require only minimal time to start-up and initialize. This reduces the amount of time to run a single simulation test case and allows multiple simulation runs to be made in the shortest period of time. In addition, the start-up and initialization time should be as consistent as possible. This is because the worst-case initialization delay must be 'out-waited' in order to ensure consistent simulation results. The configuration of the simulator is also different than most other substation equipment. The simulator is frequently reprogrammed to perform different simulations. In addition, the simulator is frequently started, stopped and restarted. In comparison, substation equipment is often set up during commissioning and runs continuously for many months without changes to the configuration other than automatic changes to the settings of the protection functions.

A. Hardware

The IEC 61850 interface for the RTDS Simulator was implemented using a dedicated processing platform. The only responsibility for this processing platform is to handle IEC 61850 communications. Using a dedicated processing platform for IEC 61850 communications allows maximum hardware and software optimization to be performed and allows control over input and output latency – both the amount and the variability from packet to packet. This is because there is no sharing of processing or communications resources between the protocol stack and other unrelated simulation activity as would be the case if the protocol processing was integrated into hardware that was utilized for other simulation functions.

When using a dedicated processing platform, overhead due to communications between the platform and the rest of the simulator must be fast and efficient so that total input and output packet latency is minimal. This can be achieved by utilizing a high performance FPGA for the interface between the protocol hardware and the simulator. Buffering and filtering are easily implemented in an FPGA and provides an efficient interface for the processor and allows more CPU time to be spent processing packets. The accurate time-stamping required for IEC 61850-9-2 is realized by distributing a 1 pulse per second (1 PPS) to the communicating devices. Implementing the 1 PPS input time synchronization functions within an FPGA eliminates processor overhead and dependency on processor interrupt latency. This allows the

processor to spend more time processing packets rather than synchronizing to the 1 PPS input. A key to minimizing the variability in input and output packet latency is to reduce the amount of extraneous, unexpected processing. The LAN can be a source of significant unnecessary processing, but can be minimized in most circumstances. The selection of the Ethernet media access controller (Ethernet MAC) is crucial in minimizing the impact of processing unrelated network activity. The Ethernet MAC must be equipped with the capability to perform packet filtering based on a set of configured addresses. Without hardware-based address filtering, each packet on the network must be read by the CPU to determine if the destination address in the message matches the filter criteria. With hardware address filtering, only packets with selected destination addresses are passed to the processor. Although IEC 61850 does not use Ethernet broadcast packets, such packets can be present on networks and might affect overall network performance. Disabling broadcast traffic during simulation runs can provide further optimization. The combination of hardware address filtering and disabling broadcast traffic reduces the network traffic entering to only those packets that are directly addressed or requested – there is no extra processing even when the network is very active.

B. Software

The RTDS Simulator implements IEC 61850 GOOSE, GSSE and 61850-9-2 Sampled Values under an off-the-shelf real time operating system (RTOS). By utilizing a RTOS with a rich suite of development tools, performance can be easily assessed and optimized. Fig. 3 shows a capture by one of the RTOS tools and shows the processing of a single received GOOSE message. From this capture the approximate processing times, the number of context switches, and all operating system calls such as semaphore and message queue activity can be determined. This type of capture can be used to analyze and optimize the processing of packets.

A third-party IEC 61850 protocol stack was chosen to allow development time to be spent on integration and optimization rather than the implementation of intimate details of the protocol. Full source code was provided with the protocol software so that it was possible to verify the protocol processing was implemented efficiently. The IEC 61850 protocol covers a wide range of functionality from relatively interface related station level reporting of system values and status to the very fast process related station level GOOSE/GSSE messaging and the process

bus transmission of sampled values. Implementing multiple types of messaging at the same time can cause slight unexpected latencies. Since variability of latency must be minimized in a real time simulator,

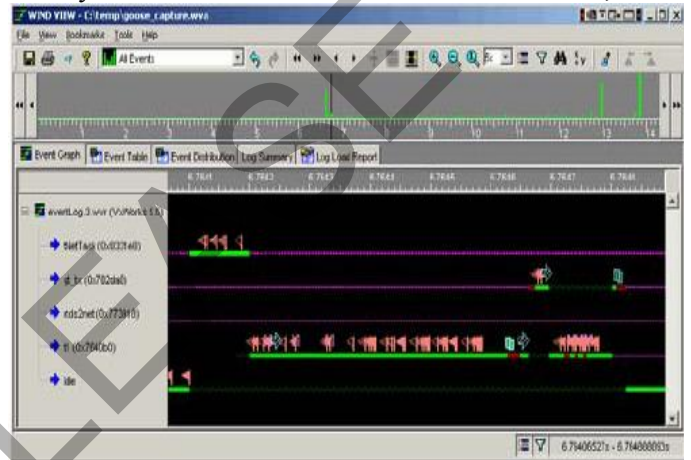


Fig. 3. GOOSE Reception analysis using RTOS Development Tool

each IEC 61850 interface device only runs one type of messaging at a time. For example, a single IEC 61850 interface device can run GOOSE/GSSE or 61850-9-2 sampled values, but not both at the same time. No interface related station level messaging is supported while running GOOSE/GSSE or 61850-9-2 sampled values to avoid any possibility of affecting latency. If required, multiple IEC 61850 interface devices can be simultaneously connected to the simulator to provide the different types of messaging, while still providing excellent protocol performance.

C. Configuration

Digital simulators are commonly programmed for an application every time a simulation case is downloaded. For this reason, all details for the IEC 61850 interface must be determined prior to downloading a test case. When using simulators in batch mode, it must be possible to easily change all simulation parameters from a script file. IEC 61850 configuration of the simulator is easily accomplished using the IEC 61850 SCL features described in IEC 61850-6 [3].

SCL is an extensible markup language (XML) based description language used to describe IEC 61850 IED configurations and communications. A single SCL file can contain a configuration and description of each IED so that the overall simulation configuration can be stored in a single SCL file. An IEC 61850 system engineering software package is used to modify the system configuration and generate an SCL file to be read by the configuration software for each connected IED. The system configuration function can be performed by many different system engineering tools since SCL is not proprietary. The

compiler for the RTDS Simulator reads SCL files to determine the configuration and connections for the IEC 61850 interface. An SCL file can be generated for each test scenario and can be selected through simulator scripts. This allows compatibility between IEC 61850 and the simulator batch mode operation. Some IEC 61850 stacks provide advanced features such as the automatic discovery of multicast destination addresses used by remote IEDs to simplify configuration. These features should be avoided for simulation testing if they affect the deterministic operation of the IEC 61850 interface or if they increase initialization time at the beginning of simulation. Automatic discovery of multicast addresses requires the IEC 61850 interface to process all multicast traffic on the network until a multicast message is received from the designated remote IED. This increase in processing can cause undesirable variations in input and output latency, and must be avoided in a simulation testing environment

V. CONCLUSIONS

An IEC 61850 messaging capability was successfully developed for the RTDS Simulator. The hardware implementation, referred to as the GTNET, is capable of providing both binary input and output as well as sampled value output for voltage and current signals. Great care was given to ensure that the system was deterministic in nature and able to operate error free in conjunction with real time simulations. Both the hardware and software used were optimized to ensure that unacceptable delays were not introduced when starting and stopping simulation cases. A number of advantages were realized through the development of the IEC 61850 messaging capability for the RTDS Simulator. First it created the capability for closedloop testing of newly compliant protection devices. Second it greatly reduced the number of physical connections that had to be made between the simulator and the protection system. For the example illustrated in Fig. 1 and 2, the number of connections was reduced from 30 to just 4. Third, it was no longer necessary to provide breaker status signals using potential free contacts. Finally when using IEC 61850-9-2 sampled values, the need for power amplifiers was eliminated, simplifying the test setup and greatly reducing the cost.

VI. REFERENCES

Websites:

[1] IEC 61850, located <http://www.61850.com>.

Guides:

[2] UCA International Users Group, "Implementation Guideline for Digital Interface to Instrument Transformers Using IEC 61850", R2-1.

Standards:

[3] IEC 61850 Communication networks and systems in substations –All parts, Reference number IEC 61850-SER.

Papers Presented at Conferences:

[4] C. Hoga, G. Wong, "Utilities and Industries of Today: Leading by Following IEC 61850," presented at the 15th Power Systems Computation Conference, Liege, 2005.

[5] Jan.23-24,2009. National conference on "ICEEE09", "Real time simulation & testing by IEC61850"

[6] Jan. 20-22,2007.International conference, "ICAMTM-2006", "Next Generation-Plasma Based Power System"

[7] Jan. 20-22,2007.International conference, "ICAMTM-2006" "SCADA-The Tool Of Development Of Economy"

[8] Dec. 20-23, 2006. IEEE-International Conference, "ADCOM-2006", "Remote Control Of Process Parameters Using Embedded Web Technology "

Bibliography:-

Yogesh D. Sonawane is working with M/S Easun Reyrolle Ltd, Mumbai as Asst. Manager with vast experience in power sector-Energy Management & Automation. Published various papers at National & International conference on Energy Management & Automation.

Pankaj M. Patil is working with M.S.E.T.C.Ltd at Nashik as Engineer-Testing with vast experience in power sector-Testing & commissioning. Published various papers at national & International conference on Energy Management & Automation.

Naresh D. Sonawane is presently working with M/S SHIRO Ltd, Mumbai as Executive-Database Mgmt. with vast experience in development and design software published various papers at national & International conference on Automation & Software support for application.

Sayali Y. Sonawane. Is student and doing Specialization in Software designing and working on various software & Hardware support to applications.

Economical Benefits by Contribution of Large Wind Farms to Voltage Control

A.-R. Al-Awaad, A.F. Kaptue Kanga, J.F. Verstege
Institute for Power Systems, University of Wuppertal,
Rainer-Gruenter-Strasse 21
42119 Wuppertal, Germany

Abstract- Wind energy is the main installed type of renewable energies in Germany. Wind farms owner gets a fix payment for the generated energy. This payment is much higher than the average variable costs of conventional power plants. Wind farms do not participate at voltage control till now. Although, they can supply reactive power into the network. In this study it is assumed, that there is a reactive power market. Large wind farms are connected to high voltage networks. It is shown, that fed reactive power from wind farms can contribute to minimization of the network losses in high and very high voltage networks. This fed reactive power leads to reduction of the complete demanded reactive power to support the voltage control by strong load too. Thereby, a part of costs of transmission system operator will be saved. These saved costs can be a contribution to reduce the fix payment of the generated energy of wind farms.

I. INTRODUCTION

Today, renewable energy plays an important role in energy supply. In some fields the development is still growing, especially at wind energy. It is to be expected, that the installed wind power in Germany until 2020 reaches 60 % of the German total load [1].

In Germany the renewable energy is extra supported by a governmental act (Renewable Energy Sources Act; EEG) [2]. Thus, wind farms owner gets a priority feed-in into the network, where transmission system operator (TSO) must take-over the energy. Based on EEG and before the appearance of wind energy trader, the TSO has to pay a fix payment (EEG payment) to wind farms owner for the generated energy (Fig. 1). This payment is much higher than the average variable costs of conventional power plants.

TSO is responsible for a sure operation of the electrical network. Therefore, he has to support the voltage control [3]. TSO gets a part of the demand reactive power to support the voltage control from the conventional power plants (CPP). In this study it is assumed, that there is a reactive power market. Thus, the TSO has to pay to the CPP owners the price of delivery of reactive energy (Fig. 1).

TSO is responsible for energy transmission between power stations and load. The transmission of the electrical energy causes network losses. TSO gets the demanded active energy to cover the network losses from CPP. TSO has to pay to CPP owners the price of the demand active energy to cover the network losses (Fig. 1).

The TSO forwards the cost based on EEG (EEG payment), cost of delivery of reactive energy to support the voltage control and the cost of cover of network losses to the customers (Fig. 1). These costs are a part of network access price.

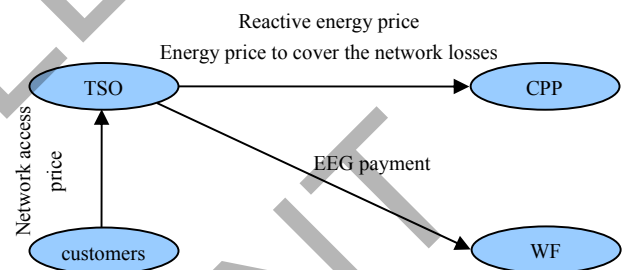


Figure 1. Observed money flow

II. PARTICIPATION OF WIND FARMS AT VOLTAGE CONTROL

Modern wind power plants are implemented either with double fed induction generator or synchronous generator in combination with full-converter. These two types of wind power plants can supply reactive power into the network [4, 5]. New planned large WF are to be connected to the high voltage network [1]. These large WF do not participate at voltage control till now. In this study it is investigated, which economical benefits can be caused to the customers, by reducing the access price, through participation of large WF at voltage control.

III. TEST MODEL

The test model consists of a 380-kV- and two subordinate 110-kV-networks (Fig. 2 - 4). To the first 110-kV-network, 200 MW wind power are connected in four WF. These WF are implemented with double fed induction generators. To the second 110-kV-network, 700 MW wind power are connected in eight WF. These wind farms are implemented with synchronous generators in combination with full-converter. Total strong load of the network is 4.2 GW. Utilization period of WF is 1810 h/year and 6600 h/year of the load.

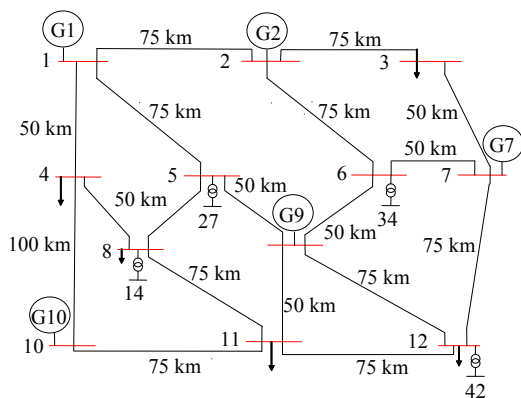


Figure 2. 380-kV-network

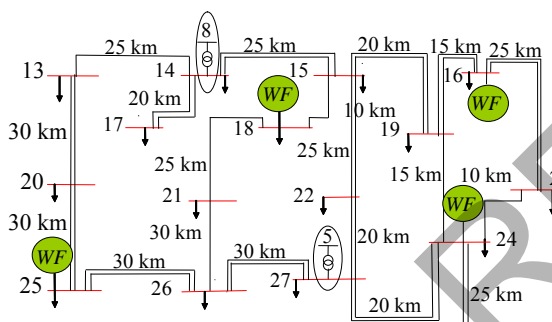


Figure 3. The first 110-kV-network

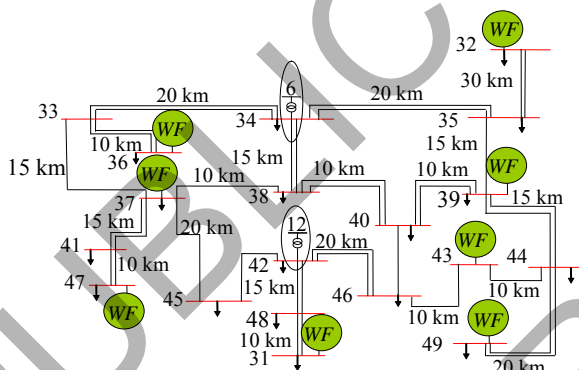


Figure 4. The second 110-kV-network

IV. TEST RESULTS

In this study, the two types of wind power plants (all attached WF) supply reactive power into the network. The network losses and the complete demanded reactive power to support the voltage control are compared with and without reactive power supply of WF. The network is tested for different load and wind velocity cases. In this paper, only two cases are investigated briefly: a week day in winter by weak wind (strong load & weak wind) and a sunday in summer by strong wind (weak load & strong wind). In this work, reactive power supply are adjusted to get minimum network losses.

A. Strong Load & Weak Wind

By strong load, inductive reactive power is required to support the voltage control. In this study, this necessary reactive power is delivered from CPP at 380-kV-network. WF are connected to 110-kV-networks. Thus, a part of the necessary inductive reactive power for the voltage control can be fed from these WF locally. Thereby, overhead lines and transformers can be released from a part of the transmitting inductive reactive power. Thus, the complete fed reactive power of WF and CPP is less than the fed reactive power of CPP alone (Fig. 5). E.g. the fed reactive power can be reduced 8 % approximately at the time between 11:00 and 12:00 o'clock. As a result, with reactive power supply of WF the network losses can be reduced too (Fig. 6). E.g. the network losses can be reduced 6 % at the time between 11:00 and 12:00 o'clock.

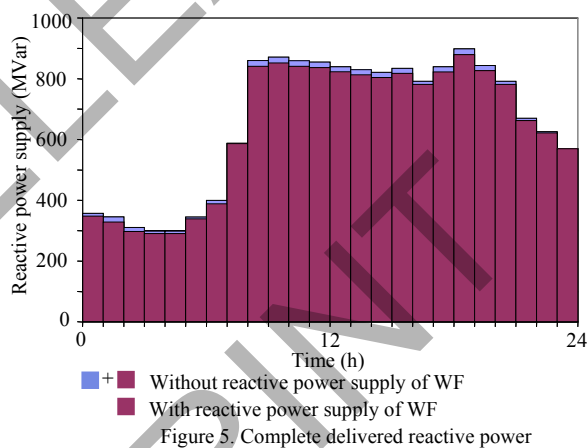


Figure 5. Complete delivered reactive power

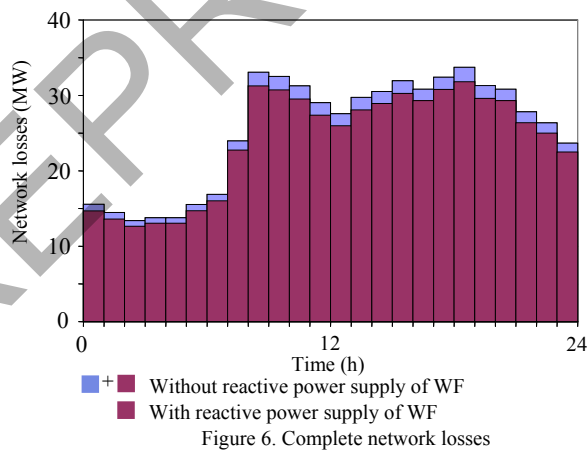


Figure 6. Complete network losses

B. Weak Load & Strong Wind

Early in the morning by weak load and strong wind, the fed active power of WF and CPP into the network is larger than the load. WF have feed in priority. Thus, many CPP have to be disconnected from the network to avoid a power surplus, e.g. from 05:00 to 07:00 o'clock the load is very low. Hence, CPP G10, G2 and G7 have to be disconnected from the network. The CPP, which remain at the network, have to produce the necessary (capacitive) reactive power to support the voltage

control. Thus, a high reactive power flow can be caused and the possibilities to minimize the network losses are limited.

Reactive power supply of WF offers more possibilities to support the voltage control and to minimize the network losses simultaneously. Thus, the complete delivered reactive power of WF and CPP is larger than the complete delivered reactive power of CPP alone in weak load (in the morning and evening, Fig. 7). In this case, WF may supply reactive power, only if the saved costs of network losses are larger than the more costs of delivery of reactive power. Through reactive power supply of WF, the network losses can be reduced, e.g. 5 % approximately at the time from 11:00 to 12:00 o'clock (Fig. 8).

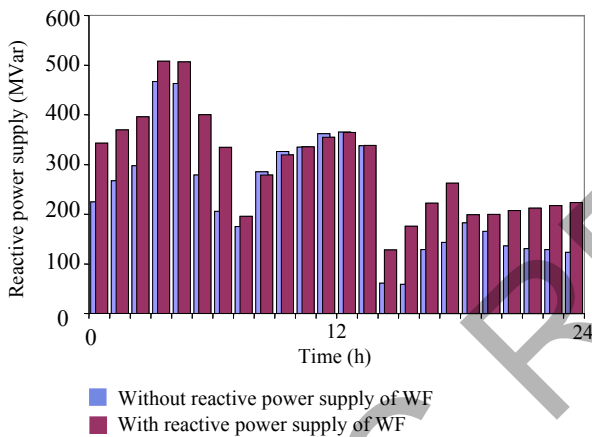


Figure 7. Complete delivered reactive power

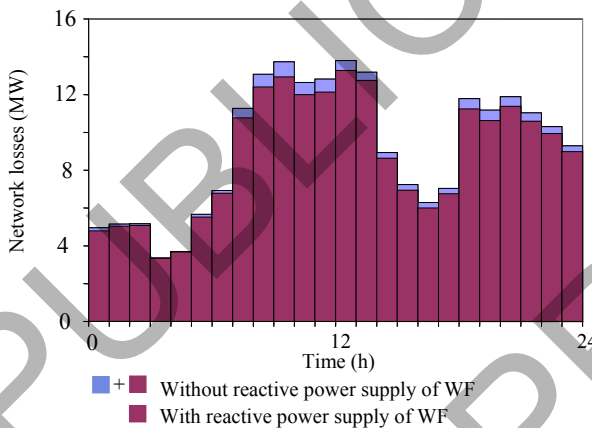


Figure 8. Complete network losses

C. Economical Benefits by Contribution of Wind Farms to Voltage Control for one Year

Tables I and II show the prices of reactive energy delivery to support the voltage control and the prices of active energy delivery to cover the network losses. High tariff (HT) prices by active energy delivery have to be paid from 08:00 to 20:00 o'clock on a week day, else the delivered energy should be paid in low tariff (LT).

Through the contribution of WF at voltage control for one year, the TSO saves a part of costs of covering of network

losses (0.52 m€) and a part of costs of delivery of reactive energy (0.13 m€). WF owner gets more income (1 m€) through delivery of reactive energy, because there is a reactive power market.

TABLE I
PRICES OF REACTIVE ENERGY DELIVERY TO SUPPORT THE VOLTAGE CONTROL

		Price (€/MVarh)
Reactive Energy	Inductive	1
	Capacitive	0.5

TABLE II
PRICE OF ACTIVE ENERGY DELIVERY TO COVER THE NETWORK LOSSES

		Price (€/MWh)	
		HT	LT
Voltage Level	380 kV	50	50
	110 kV	80	60

D. Economical Benefits for Customers

In this study, the EEG payment is 87 €/MWh. In addition to that, it is assumed, that the total income of WF owner and costs of TSO with and without participation of WF at voltage control may not be changed. Therefore, the more income of WF owner and the saved costs of TSO should be transferred to the WF owner as a part of the fix payment (EEG-payment) for the observed year. This leads to reduction of the EEG payment. Thus, the EEG payment can be reduced from 87.00 to 85,98 €/MWh (-1,17 %) in the observed year (Fig. 9).

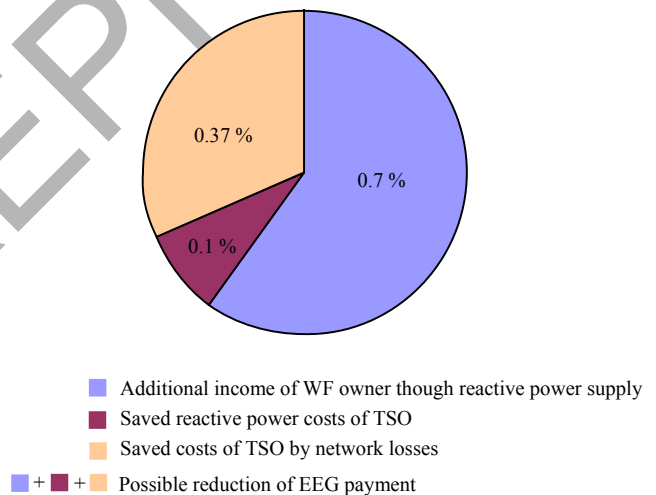


Fig. 9. Possible reduction of EEG payment in the observed year

EEG payment should be paid for 20 years. This payment is not constant for the 20 years, it has a degression. Thus, this payment was 83.76 €/MWh in the year 2007 [2], and the delivered energy of wind farms in Germany reached 39500 GWh in the same year [6]. So based on EEG, customers should

pay for this generated energy 3.3 b€. The reduction of EEG payment with 1.17 % means that, customers should pay 56 m€ less.

V. CONCLUSION

In this study it is assumed, that there is a reactive power market. Wind farms owner gets additional income through participation of wind farms at voltage control. This participation leads to reduction of network losses and the demanded reactive power to support the voltage control by strong load. This means, the transmission system operator saves a part of the demanded costs to cover the network losses and delivery of reactive power to support the voltage control. The additional income of wind farms owner and the saved costs of transmission system operator can be a contribution to reduce the EEG payment, where wind farms owner and transmission system operator should have the same income and costs with and without participation of wind farms at voltage control. Thus, customers pay less for energy of wind farms.

The new research should help to reduce the EEG payment of wind power plants. The new researches show, that wind power plants can support the frequency control too [7]. Contribution

of wind power plants to frequency control leads to reduce the EEG payment too. This reduction is clearly larger than the reduction by participation of wind power plants to the voltage control.

REFERENCES

- [1] "Planning of the Grid Integration of Wind Energy in Germany Onshore and Offshore up to the Year 2020 (dena Grid Study)," German Energy Agency, Berlin, 2005
- [2] "Act on Granting Priority to Renewable Energy Sources (Renewable Energy Sources Act)," Federal Ministry for Environment, Nature Conservation and Nuclear Safety, Federal Law Gazette I, No. 40, Bonn, 2004
- [3] "TransmissionCode 2007 – Network and System Rules of the German Transmission System Operators," Berlin, 2007
- [4] A.-R. Al-Awaad, J. Verstege, "PQ-Curve of Wind Power Plants," European EMTP-ATP Conference, León, Spain, 2007, pp A1
- [5] A.-R. Al-Awaad, J. Verstege, "Contribution of Wind Energy Plants to Voltage Control in High and very High Voltage Networks," First Electrical Engineering Conference, University of Aleppo, Aleppo, Syria, 2007, pp PS04
- [6] "Development of Renewable Energy Sources in Germany in 2007," Federal Ministry for Environment, Nature Conservation and Nuclear Safety, Berlin, 2007
- [7] A.-R. Al-Awaad, S. Völler, J. Verstege, "Contribution of Wind Power Plants to Frequency Control," 4th Energy and Exergy Conference, American University of Sharjah, Sharjah, United Arab Emirates, 2009, in press

Optical properties of thin films of polyazomethine with triphenylamine unit in the main chain prepared by spin-coating method

M. Palewicz^{a,b}, A. Iwan^b, J. Doskocz^c, W. Stręk^c, D. Sek^d

^a Institute of Electrical Engineering Fundamentals, Wrocław University of Technology, Wybrzeże Wyspiańskiego 27
50-370 Wrocław, Poland

^b Electrotechnical Institute Division of Electrotechnology and Materials Science, M. Skłodowskiej-Curie 55/61, 50-369 Wrocław,
Poland

^c Institute of Low Temperature and Structure Research, Polish Academy of Sciences, Okólna 2, 50-422 Wrocław, Poland, P.O.
Box 1410, 50-950 Wrocław 2, Poland

^d Centre of Polymer and Carbon Materials, Polish Academy of Sciences, 34 M. Skłodowska – Curie Street, 41-819 Zabrze,
Poland

Abstract-Thin films of a polyazomethine (PAZ) were prepared from a chloroform solution by spin-coating technique. The solution of the polymer was spread on microscopic cover glass and quartz under nitrogen atmosphere at room temperature and atmospheric pressure. The optical properties of the PAZ were investigated at room temperature under atmospheric pressure. An absorbance, transmittance and reflectance were determined from spectrophotometric measurements. The absorption coefficients and band gap of films material were developed. Surface structure of the PAZ thin layer was checked by AFM measurements. Thickness of the PAZ thin layer on the glass and quartz were determined with ellipsometer at the range from 150 to 220 nm.

I. INTRODUCTION

Investigation of a new kinds of organic materials for photovoltaic devices were begun because of increasing demand of logging energy. Solar panels produced hitherto on industrial scale are based on inorganic crystals like silicon. However, manufacturing of such devices are still expensive and has negative effect on natural environment. For these reasons an organic materials for photovoltaic devices are investigated. Use of the organic materials are supposed to be very promising in photovoltaic devices because of economic reasons and high demand of a products [1]. One of the first solar cells which could be considered as organic origin was characterized by Tang [2]. A thin-film, two-layer organic photovoltaic cell was fabricated from copper phthalocyanine and a perylene tetracarboxylic derivative [2]. However, no product of conducted research has been used in commercial application.

Among them, much attention is paid to triphenylamine (TPA) derivatives because they are promising candidates for photo- and electro- luminescence materials. TPA is a unique molecule possessing useful function such as redox-activity, fluorescence, and transport of positive charge centers via the radical cation species. Being efficient hole conductors TPA are commonly used as photoconductors. Introduction of

azomethine moieties (HC=N) in TPA may lead to new functional materials based on the synergistic effect of both of them. Additionally, polyazomethines are known to display interesting thermal, mechanical, electrical, optical and fiber-forming properties and they are promising materials in optoelectronic and photonic application [3].

PAZ with TPA in the main chain can be used as one of the layers in organic solar cells. The aim of this article is to describe optical properties and texture of thin layer composed from PAZ by spin-coating method.

II. EXPERIMENTAL

PAZ was prepared from dialdehyde and diamine via high temperature solution polycondensation. Properties of the PAZ were confirmed by elemental analysis, FTIR and ¹H, ¹³C NMR spectroscopy and are described in [4]. Structure of the PAZ is shown in Fig. 1. The absorption spectrum of the PAZ in chloroform solution was characterized by one well defined band at 413 nm being responsible for π - π^* transition in the imine group. PAZ emitted blue light in chloroform solution with maximum of emission band at 480 nm under 400 nm excitation wavelength [4].

Solution to spread on substratum was prepared from PAZ and chloroform. Quantity of the used polyazomethine in solid state and chloroform was 36 mg and 2 ml, respectively. Dissolution of the PAZ was executed at room temperature.

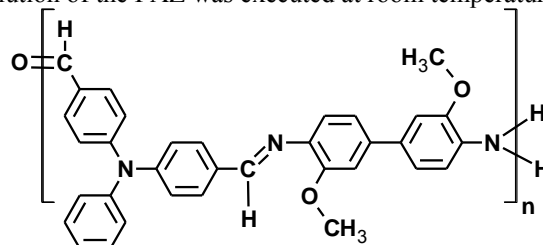


Fig. 1. Chemical structure of the PAZ.

Basis from microscopic cover glass and quartz were situated in ultrasonic washer with deionised water for ten minutes period and then were cleaned in solution of deionised water and 2-propanol (1:1 relation), toluene, lavaged in deionised water and acetone [5].

The thin layers of the PAZ were spread by spin-coating method via drift process on the glass and quartz. To avoid a contamination and defects in thin stratum this process was carried out at room temperature in atmosphere of nitrogen under atmospheric pressure. The values such as rotational speed and time of turn were set on 880 turns per minute by 10 seconds. Two – beam spectrophotometer Cary 5000 was used to measure optical properties of the thin PAZ layer. The absorption (A), transmission (T) and reflectance (R) measurements were performed at room temperature.

Topography of the surface was tested by an atomic force microscope (AFM) in the contact mode. Thickness (d) of the layer was measured using ellipsometer at constant angle.

III. RESULTS AND DISCUSSION

The absorption spectra of the PAZ film on the glass (PAZ/Glass) and on the quartz (PAZ/Quartz) substratum are shown in Fig. 2. Maximum of the absorbance was observed for both samples at 405 nm. Also, on a spectrum related with layer deposited on the glass was noticeable oscillation behavior below 260 nm (See Fig. 2). That phenomenon is related with crystalline structure of basis. Electromagnetic wave in ultraviolet (UV) range was absorbed and converted into phonon oscillation in background of the sample based on the glass, while for light at that length quartz was transparent. To describe dependence of the obtained thin layers form substratum two kinds of them have been used. Besides of the chemical purification quartz was polished. Therefore appropriate prepared basis capacitate to obtained good quality of the thin layer. From the analysis of the absorbance spectrum it was possible to notice the variation of the thickness layer for the glass and quartz, which was confirmed by elipsometric measurements

From transmission (T) and reflectivity (R) measurements an absorption coefficient α is calculated according to the equation (1) given in reference [6,7], where d is film thickness. The typical absorption coefficient plot of the PAZ thin layer on glass and quartz at entire energy scale from 1.2 to 6.0 eV is illustrated in Fig. 3. An increase of the absorption coefficient α was observed on plot from energy value equal to 2.5 eV.

$$\alpha = \frac{1}{d} \ln \left(\frac{(1-R)^2}{T} \right) \quad (1)$$

The absorption edge of the PAZ on the glass and on the quartz was observed between 2.5 and 3.0 eV. For semiconductor materials it is possible to calculate an energy gap (E_G) from relation given by formula (2) [8].

$$\alpha \cdot E = A(E - E_G)^r \quad (2)$$

Where α is absorption coefficient, A is parameter independent of photon energy, E , E_G represent photon and band gap energy, respectively. Index r accepts two values 1/2 or 2 connected with direct and indirect band to band transition. Type of the transition in the investigated material is determined by subscript $r = 2$. Such approach leads to equation (3).

$$(\alpha E)^{1/2} = f(E) \quad (3)$$

Delimitation value of the energy gap (E_G) is determined from linear approximation of equation (3), as is mentioned in [8] for

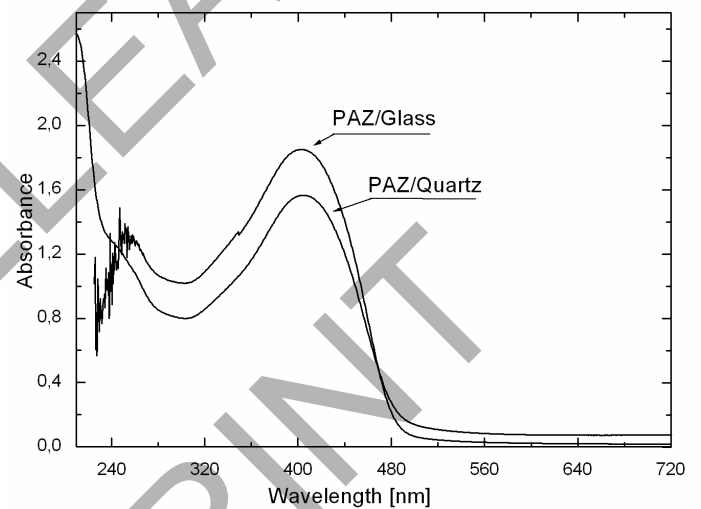


Fig. 2. Absorption spectra of the PAZ film coated on the glass and quartz.

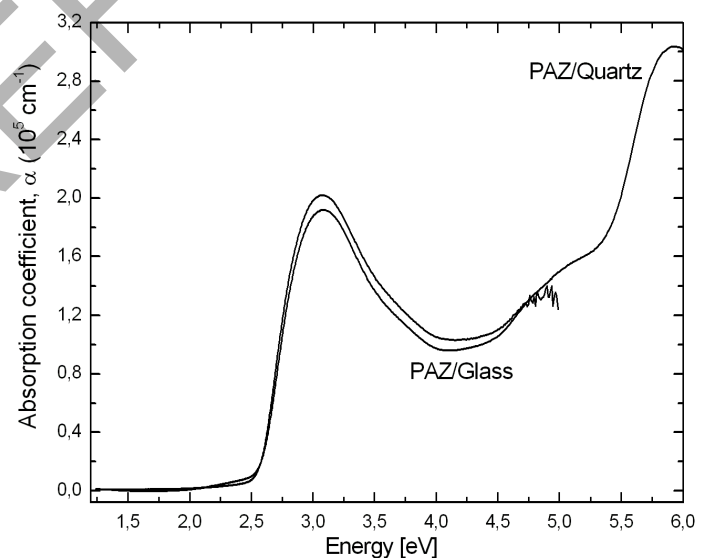


Fig. 3. Absorption coefficient of the PAZ thin layer on the glass and quartz.

amorphous semiconductors. The absorption edge of the PAZ thin layer on the glass and quartz is shown in Fig. 4. Value of the energy gap for samples deposition on the glass and quartz is elevated (2.45 ± 0.02 eV).

Energy gap ($E_G = 2.45$ eV) of the polyazomethine film on the glass and quartz are similar. Insignificant changes into value of E_G related with amount of the solvent in solution were observed. Increasing or decreasing of the band gap about 0.01 eV was caused by different concentration of the chloroform.

Characteristic broad and strongest section at the absorption coefficient allocated at about 3.0 eV (Fig. 3) is due to inter-band transition between delocalized states which are related with interaction of π -orbitals in the polyazomethine [9].

Measurements of the PAZ thickness layer on the glass or quartz substratum were performed with ellipsometer equipment working at constant angle. Real refraction coefficients (n) of the glass, quartz and polyazomethine layer were required to conduct a measurements. Real refraction coefficient $n = 1.42$ of the PAZ was estimated from equation (4) [10], where k , R are imaginary refractive and reflection coefficient, respectively.

$$n = \frac{1 + \sqrt{R}}{1 - \sqrt{R}}, (k = 0) \quad (4)$$

Thickness of the thin PAZ layer on the glass and quartz was changing from 150 to 220 nm (Table I). About 50 nm variation of width between the PAZ spread on the glass and quartz were noticed. Difference in thickness of the PAZ films are related with used basis and technological parameters of the spin-coating method.

Atomic force microscope (AFM) was used to describe surface structure of the PAZ. Images of the PAZ on the glass and quartz are represented in Fig. 5. Relatively homogenous and smooth surface for the PAZ coated on the glass and quartz

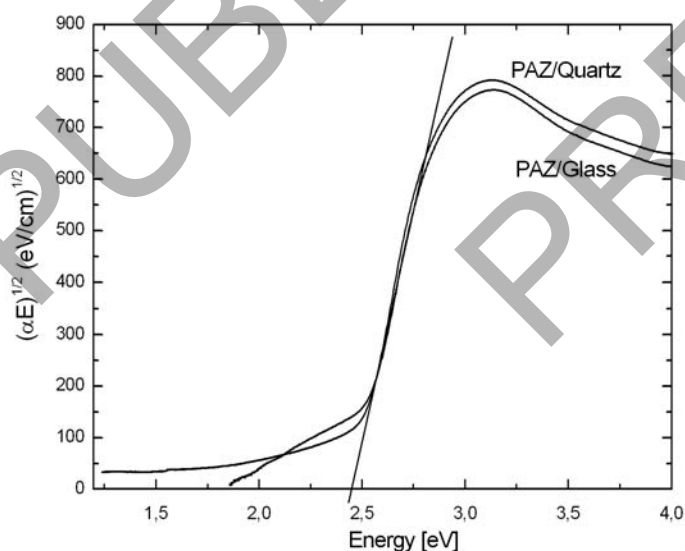


Fig. 4. Absorption edge of the PAZ thin layer on the glass and quartz.

TABLE I
THICKNESS OF THE POLYAZOMETHINE (PAZ) THIN LAYER

Code	Thickness of layer, d [nm]				
PAZ/Glass	200	218	203	208	211
PAZ/Quartz	155	162	155	157	154

films was observed by AFM. Characteristic granulation is typical for the polymers thin layers and also agglomerates are visible in Fig. 5. Scale of the granulated polymers concentration are related with a porosity of the substratum and technological parameters implemented to spin-coater equipment.

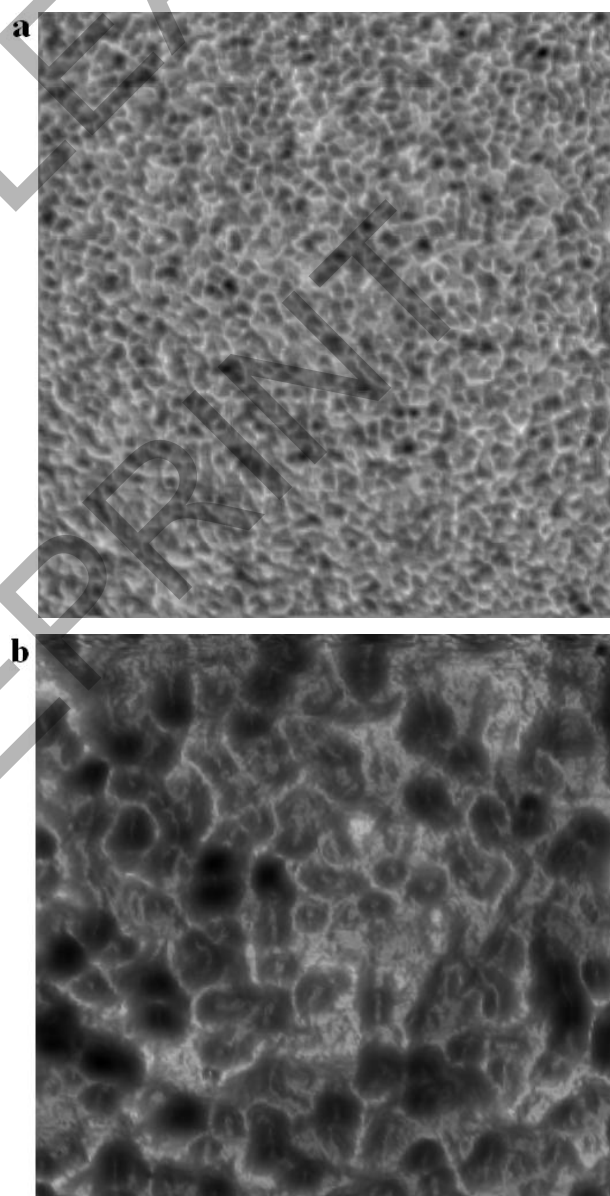


Fig. 5. AFM images ($5 \times 5 \mu\text{m}^2$) of the a) PAZ/Glass and b) PAZ/Quartz.

IV. CONCLUSION

Spin-coating method appeared to be an effective tool to prepare good quality of the polyazomethine (PAZ) thin layer. Optical properties such like the energy gap was obtained in typical way for the amorphous semiconductors. The technological parameters have influence on the energy gap, thickness and surface structure of the investigated polyazomethine. Presented results seem to be helpful to better understanding of the physical properties of that polyazomethine. It can be concluded that the investigated polyazomethine is an amorphous semiconductor with the wide energy gap. Therefore such polyazomethine with the TPA in the main chain could be used to produce photovoltaic devices.

REFERENCES

- [1] Shajing Sun and Niyazi Serdar Sariciftci, "Organic Photovoltaics: Mechanisms, Materials and Devices", Published in 2005 by CRC Press.
- [2] C. W. Tang, "Two-layer organic photovoltaic cell", *App. Phys. Lett.* 48 (1986) 183-185.
- [3] A. Iwan, D. Sek, "Processable polyazomethines and polyketanils: From aerospace to light emitting diodes and other advanced applications", *Progress Polym. Sci.*, 33 (2008) 289-345.
- [4] D. Sek, A. Iwan, B. Jarzabek, B. Kaczmarczyk, J. Kasperczyk, Z. Mazurak, M. Domanski, K. Karon, M. Lapkowski, "Hole transport triphenylamine-azomethine conjugated system: Synthesis and optical, photoluminescence, and electrochemical properties", *Macromolecules*, 41 (2008) 6653 – 6663.
- [5] J. A. Mikroyannidis, I. K. Spiliopoulos, A. P. Kulkarni, S. A. Jenekhe, "Synthesis and optical properties of poly(p-phenylenevinylene)s bearing tetraphenylthiophene or dibenzothiophene moieties along the main chain", *Synth. Met.* 142 (2004) 113–120.
- [6] J. Misiewicz, „Podstawy optyki ciała stałego”, Oficyna Wydawnicza Politechniki Wrocławskiej, Wrocław 1996.
- [7] G.I. Rusu, A. Airinei, M. Rusu, P. Prepelit, L. Marin, V. Cozan, I.I. Rusu, "On the electronic transport mechanism in thin films of some poly(azomethine sulfone)s", *Acta Materialia* 55 (2007) 433–442.
- [8] B. Jarzabek, J. Wieszka, M. Domanski, J. Jurasik, J. Cisowski, „Optical properties of amorphous polyazomethine thin films”, *Journal of Non-Crystalline Solids* 352 (2006) 1660–1662.
- [9] J. Sanetra, "Efekt fotowoltaiczny w organicznych ogniwach słonecznych – wybrane zagadnienia" Monografia, Politechnika Krakowska im. Tadeusza Kościuszki, Kraków 2006.
- [10] B. Jarzabek, J. Wieszka, A. Burinan, G. Poczrowski, „Optical properties of amorphous thin films of the Zn-P system”, *Thin Solid Films* 279 (1996) 204-208.

A new approach to a solar cell problem

Bronislaw Swistacz
Wroclaw University of Technology
Wyb. Wyspianskiego 27
Wroclaw, Poland

Abstract- In this paper a new concept for a space charge transport through a solid placed between the two electrodes is presented. The effect of the light on the electric field distribution and on the shape of current – voltage characteristic is determined. For a space charge distribution some new singular solutions are obtained. In this paper it is found that the system can act as a blocking diode.

Keywords: double injection, space charge, trapping levels.

I. INTRODUCTION

One of the fundamental problems of a macroscopic theory of electric conduction is to find the total concentration of charge carriers in a solid placed between the two electrodes. In this paper, we will assume that the divergence of the electric field distribution will be defined by the total concentration of carriers. Also, we will suppose that the contact processes have an influence on the shape of the electric field distribution, which corresponds to a current – voltage characteristic.

The purpose of this work is to find a shape of a current-voltage characteristic $J(V)$ of the metal – solid – metal system.

2. THE MODEL

In this paper, for an orbital electron in the given atom, we will assume that the total energy (the sum of the positive kinetic energy and the negative potential energy of the electric field of the positive nucleus) is negative and that the zero reference level is at a finite distance from the nucleus. In the case of an isolated atom the total energy of an orbital electron is negative for any distance from the nucleus. When an orbital electron absorbs a portion of the kinetic energy of a photon or a phonon, the total energy of the electron increases. The inverse case is when an orbital electron can lose a portion of the total energy. This is caused by the Coulomb force interaction between the orbital electron and the positive nucleus. Let us take into account the two valence electrons of an isolated atom. When this atom is packed into a solid, these electrons can occupy the higher energy state. Next, when a portion of the kinetic energy is given to the two valence electrons, these electrons can become free. The two empty energy states (which are left by the electrons) represent the two holes. Between the zero and valence levels many energy states (the trapping states) are available for the holes and for the electrons. When an orbital electron absorbs a photon, this electron can pass from the valence level to the zero level via trapping levels. The inverse case is when an orbital electron can pass from the higher trapping level to the lower trapping level and an energy portion is emitted. Analogously, we are known as the allowed transitions for the trapped holes. Such the allowed electron – hole transitions are called carrier generation – recombination

processes. When an external electric field supplies the different kinetic energy to the two adjacent atoms the trapped electron can pass from trap to trap in the given trapping level. When the external electric field is applied the electron can pass from the cathode into a solid. Moreover, this electron can become free. Similarly, the hole injection occurs when the valence electron can pass from the bulk into the anode and the valence state is empty. When the external electric field gives a portion of kinetic energy to the valence electron of an adjacent atom, this electron can pass from the atom to the given atom and can fill the empty state on the valence level. The metal-solid-metal system will be represented by a planar capacitor system (Fig.1). With these above assumptions we can find the electric field distribution $E(x)$ and a current-voltage characteristics $J(V)$, here, J is the current density and V is the applied voltage. In order to find these functions, we have to define the boundary functions describing the mechanisms of carrier injection from the anode and the cathode into the bulk [1-7].

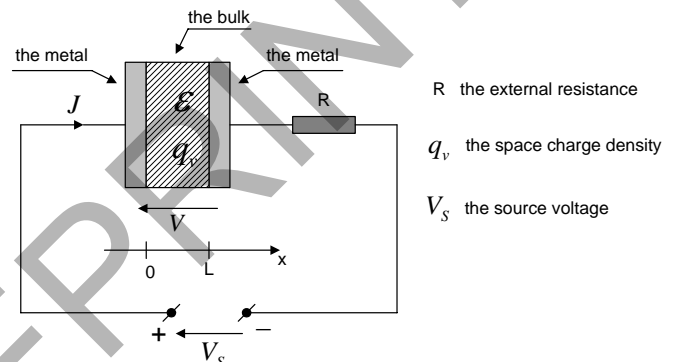


Fig.1 A planar capacitor is connected with an external resistance and a voltage source. Here, (+ -) denote the terminals of a voltage source.

3. DISCUSSION and CONCLUSIONS

When carrier generation processes are dominant, the electric field intensity satisfies a homogenous equation. Upon these conditions there exist two singular particular solutions as well as the general integral. Additionally, when the boundary functions are strongly increasing, we ascertain that there exists a set of values of applied voltage V in which the current density is not defined. This property denotes that the whole system acts as a solar cell. Also, we see that the $J(V)$ curve is strongly increasing and there can be $J(V) \equiv 0$. Therefore, the system acts as a perfect blocking diode and a voltage stabilizer. Also, this mathematical property corresponds to a solar cell.

REFERENCES

- [1] M. A. Lampert and P. Mark : Current injection in solids. Academic Press, New York, 1970.
- [2] K. C. Kao : Double injection in solids with non-ohmic contacts: II. Solids with defects. J. Phys. D.: Appl. Phys., vol. 17, 1984, pp. 1449-1467.
- [3] B. Świstacz : Carrier generation and the switching phenomenon. Further theoretical description. J. Phys.: Condens. Matter, vol. 7, 1995, pp. 10037-1008.
- [4] J. Simon and J.-J. Andre : Molecular Semiconductors. Photoelectrical Properties and Solar Cells. Berlin, Springer, 1985.
- [5] B. Świstacz : Some further description for a current flow through an amorphous solid. A case of an imperfect contact. Electron. Tele. Quart., vol. 53, No. 2, Warsaw, 2007, pp. 143-154.
- [6] B. Świstacz : Bipolar space charge problem for semiconductors and insulators. J. Phys.: Condens. Matter, vol. 7, 1995, pp. 2563-2585.
- [7] B. Świstacz.: A bipolar space charge problem for solids including a secondary electron emission. Electron. Tele. Quart., vol. 53, No 3, Warsaw, 2007, pp. 309-326.

Proposed Techniques for Identifying Faulty Sections in Closed-Loop Distribution Networks

Wael Al-Hasawi

Mahmoud Gilany

College of Technological Studies,
Electrical Technology Dept.,

Kuwait

Abstract— This paper deals with three problems in closed loop distribution systems. The first problem is how to detect and identify the faulty section after a *short-circuit fault* is successfully isolated by the protection system. The second problem is how to identify a section affected with *undetected open-circuit fault*. A novel circuit is suggested in this paper to solve these two problems. The third problem addressed in this paper is the *undetected short-circuit fault* which may lead to a complete shut down of the substation. An effective modification in the trip circuits of the relays protecting the main feeders of the closed loop is suggested to minimize the occurrence of this problem. The validity of the proposed circuits is checked against the specifications of the available equipment used in the network.

Index Terms-- Distribution networks, open-circuit faults, Fault identification, fault detection.

I. INTRODUCTION

Distribution systems being the largest portion of the whole network, diagnosis of faults becomes a challenging task. Faults in distribution systems effect power system reliability, security and quality. Accurate fault location minimizes the time needed to repair damage, restore power and reduce costs. The application of traditional fault location techniques that use fundamental voltages and currents at line terminals for distribution lines with tapped loads is difficult [1].

A fault or a disturbance, which leads to high values of line currents, is generally detected by the protective devices and faulty section is isolated using re-closures and/or circuit breakers. However, the location of the fault and identification of the fault are normally not known.

The system restoration can be expedited very fast if the location of fault is known or can be estimated to some accuracy. Hence, faults in a distribution system have to be detected instantaneously, irrespective of whether they are of permanent or temporary nature, to isolate only faulty section. Identifying the fault section, forming part of fault diagnosis aiming at minimizing the maintenance and repair time.

In the last few decades, considerable amount of work has been done in the area of fault diagnosis particularly to the radial distribution system. The techniques used with systems fed from two ends or ring systems are very limited since the protection of such systems is more complicated [2].

Many standard techniques are based on algorithmic approaches but some literature conferences on Environment and

Artificial Intelligent (AI) such as Artificial Neural Network (ANN). A brief review of some of the fault location techniques can be found in [3]. Most of the ANN based fault location techniques relied on the information about the status of circuit breakers and relays. A brief comparison of various analytical techniques with ANN in transmission system fault location is provided in [4]. Artificial neural networks, when applied directly to fault diagnosis problem utilizing the time variation of fault current as input signal, suffer from the large CPU time required for the training and also dimensionality of the network. Hence, some preprocessing technique is required to reduce input data set.

The Wavelet Transform (WT) theory provides an effective way to examine the features of a signal at different frequency bands. These features may be essential for pattern recognition. Hence, it is well suited for the fault identification and classification in the power systems [5-6].

For open circuit fault detection, there are different techniques. Most of these techniques are designed for overhead distribution networks. One of the algorithms used to detect open conductor is the technique developed by Lee and Bishop from Pennsylvania Power and Light (PP&L) in USA [7]. They developed a prototype Ratio Ground Relay for the detection of broken conductors. This relay depends on the ratio setting between the zero sequence current components and the positive sequence current component.

Another algorithm is developed to identify and locate downed conductor fault case by monitoring the voltage unbalance along the distribution feeder. As the system measures the unbalance voltage at various points so it could give indication of the fault place [8].

Considering the extensive size of the network, these tasks can be effectively achieved through implementing systems utilizing the available high-speed computer and communication technology. The Institute of Electrical and Electronic Engineers (IEEE) has defined Distribution Automation System (DAS) as a system that enables an electric utility to remotely monitor, coordinate and operate distribution components, in a real-time mode from remote locations [9]. The DAS is based on an integrated technology, which involves collecting data and analyzing information to make control decisions, implementing the appropriate control decisions in the field, and also verifying that the desired result is achieved. The software acquires the system data (both static and dynamic) and converts it into an information system. The engineering analysis software provides the control decision utilizing the system information. The decision making feature

of the distribution automation distinguishes it from the normal Supervisory Control and Data Acquisition (SCADA) system [10]. However, such systems may not be accepted because of its high expenses.

This paper takes part of the Kuwait distribution system as a case study. It deals with three types of problems related to closed loop distribution systems.

Two problems are investigated in Section III. The first problem is how to identify successfully the faulty section after a short-circuit fault is successfully detected and isolated by the differential protection system. Under such condition, the affected section is not easily identified. The second problem is related to permanent open-circuit fault which is not detected by any protection system and hence its section is not also identified. A novel circuit is suggested in section III in order to solve these two problems.

The third problem addressed in the paper is related to the permanent short-circuit fault which is not detected by neither the differential relay nor the overcurrent relay, but isolated by the earth fault relay of the high voltage-side. Such a fault results in a complete shut down of the substation. An effective modification in the relays trip circuit is suggested to minimize the occurrence of such a problem and it is covered in section IV of this paper.

The performance of the proposed circuit is compared with the equivalent Distribution Automation System (DAS). The proposed circuit proves a similar performance as DAS with minimum cost.

The problems studied are described by the electrical field engineers and are investigated using ASPEN-OneLiner simulation program, V9.7 [11]. ASPEN OneLiner is a PC-based short circuit and relay coordination program widely used by protection engineers.

II. THE NETWORK UNDER STUDY

A typical 132/11 kV from Kuwait distribution network is shown in Fig. 1. It contains closed loops with different sizes. Every substation (represented with solid circle in the figure) contains three 1000 kVA transformers. The distances between the substations are shown on the drawing. The most right-hand side closed loop is taken as a case study. Differential protection is the applied protective system for every section of the loop. Only the main feeders (F1, F2, and F3) outgoing from the station are protected by additional overcurrent relays.

III. IDENTIFYING A FAULTY SECTION

The objective of this part of the paper is to fast identifying the faulty section – in a similar way like DAS – but with a minimum cost system. The key of the proposed circuits is to get use of the spare wires of the pilot cable - associated with the differential relays - to transmit certain information related to the affected section to a PLC (Programmable Logic Controller) unit in the main 132/11 kV station. Usually, the pilot wire consists of about 16 pair of wires. In many cases, only one or two pairs are used where the others are spare.

The input of the PLC for the studied network consists of eight analog inputs. Information from a limited numbers of the loop's CBs (and associated relays) are required. Only the auxiliary output-contacts of the circuit breakers (and its associated relays) represented with solid rectangular in Fig. 2 are needed in the proposed circuit. The eight input signals are: four "Normally-Close" (NC) output contacts from the CBs represented with solid rectangular plus four auxiliary "Normally-open" (NO) output contacts of its associated relays.

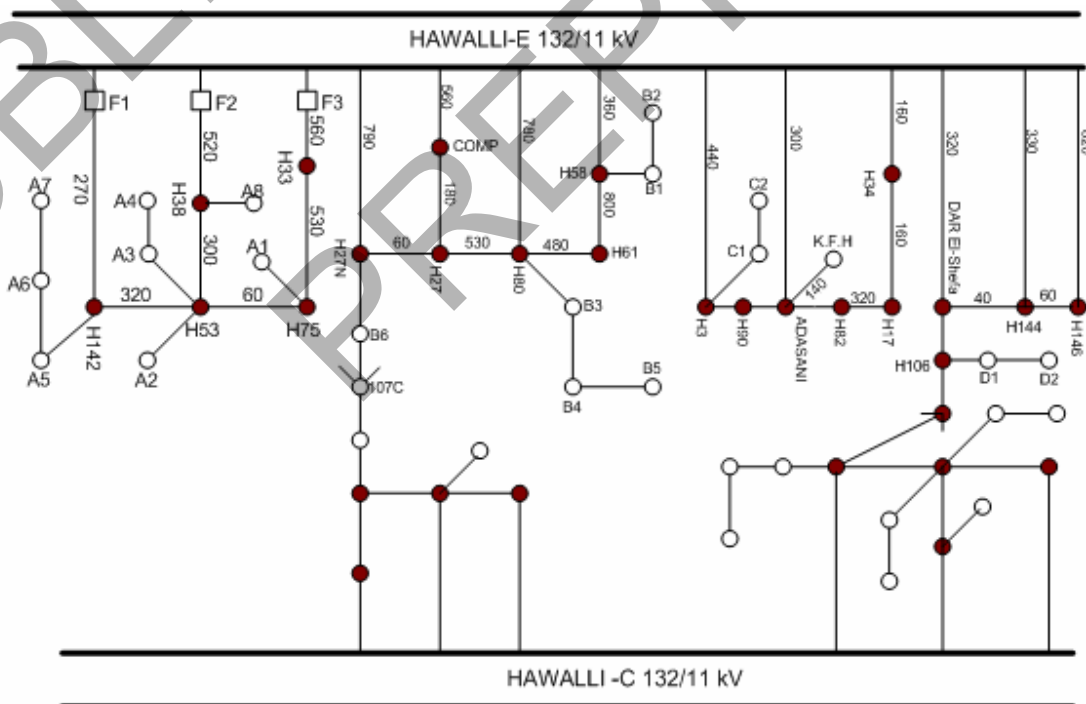


Fig. 1 A typical Distribution Network

The Normally-close auxiliary output contact of any circuit breaker will become "close" only if the circuit breaker's status becomes "open". On the other hand, the auxiliary (NO) output of the relay – which is controlled by the relay algorithm – will become "closed" only if the current through the protected feeder drops to zero *provided that the CB contacts are still closed*.

The last condition is necessary to differentiate between the zero current resulting from a normal feeder opening and the zero current resulting from undetected open circuit fault.

The PLC unit processes the received information and sends SMS message through a modem to a GSM cell phone. The data included in this message informs the maintenance team about the faulty section. The exact fault location within the identified affected section is determined later - off line- using any of the common used cable tracers.

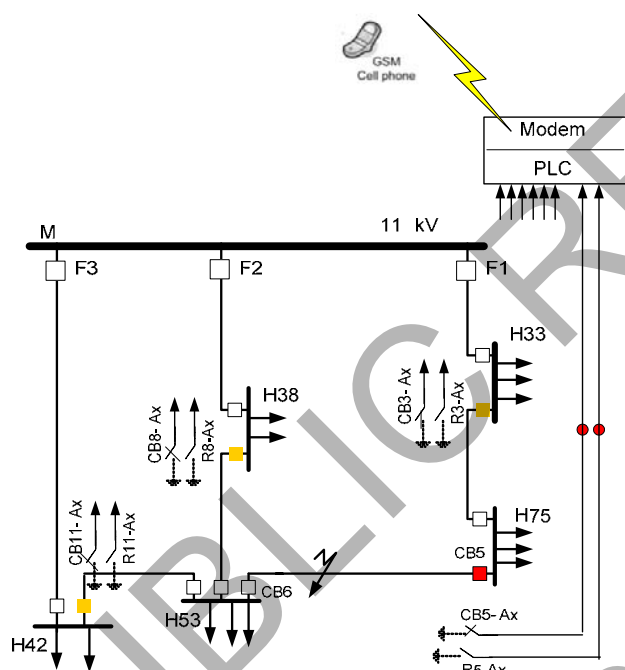


Fig. 2: Identifying an open circuit section from both sides

A. Locating a Detected Short-Circuit Fault

In this case, we assume that there is a short circuit fault which is detected and isolated by the differential protection. The faulty section in this case will be opened from both sides after clearing the fault. For example, for the fault occurred in the section between substations H75 and H53 as shown in Fig. 2, the differential protection system detects this fault and isolates the affected feeder. The two circuit breakers: CB5 and CB6 will then be opened after clearing the fault.

The costumers will not be affected by opening the faulty feeder since the system is originally fed from more than one point. The problem is that the utility maintenance teams will not also feel that there is a fault that has occurred and cleared in that loop or in that section. The only available information which may be useful to attract the attention of the maintenance team to that loop is the disturbance in current distribution in

the three main feeders (F1, F2 and F3) shown in Fig. 2. These currents are monitored by the supreme control center. The maintenance team usually depends on this sole information – current disturbance - to predict the location of affected loop and the opened feeder. In many cases, this variation in the current distribution doesn't give a clear indication about neither the affected loop nor the affected section. The maintenance teams in many cases have to search for it from a substation to another.

In the proposed circuit, the status of the "normally-closed auxiliary contact" of the selected CBs is transmitted to the PLC unit at the substation through the spare wires of the pilot cables. For example, the status of the auxiliary contact of CB5 (see Fig. 2) is transmitted to the main station M using spare wires of two pilot cables: a spare pair from the cable between "H75 and H33" and then the spare cable between "H33 and the main station, M". Only a junction between the two spare wires is required to be added to facilitate this operation.

Once a fault is cleared, the status of the NC auxiliary contact of CB5 will be changed from "open" to "close". Consequently, SMS message will be forwarded to a certain cell phone number stored in the PLC program. The maintenance team is easily informed about the cleared fault and hence the faulty section is identified. Any other detected short circuit fault is identified in a similar way.

An alternative method for identifying the faulty section needs an RTU in each point in the loop plus an efficient communication network between all the load points. Other alternative techniques which depend on calculating the fault distance are not easily implemented with closed loop systems. The main feature of this technique is to instantaneously identify the faulty section – like DAS - but with minimum additional cost added to the existing system (the cost of only one PLC unit per substation). It saves a lot of time and efforts.

B. Locating an Undetected Open-Circuit Fault

Open conductor (downed conductors) from the point of view of distribution utility is a public hazard in the main consideration. It is not a system operation problem since the system could continue without disconnecting such fault [12,13].

The second fault scenario studied in this paper is to have an undetected open circuit fault. This may happen as a result of a cut in the power cable. In this case, the power cable (and may be the pilot cable as well) is opened but the circuit breakers of the faulty section - at both sides - are kept closed.

The only available indication showing that there is a problem is the disturbance in currents distribution in the three main branches of that loop (F1, F2 and F3 in Fig. 2). However, this information is not guaranteed as the variation in the currents may be very small. It is not always easy to identify the affected section based on these current readings. Again, even if we got information about the disturbance in certain loop, this information can't tell us about the faulty section in the affected loop specifically. The maintenance crew has to go through the stations to check the status of the breakers. Inspecting the location of faults is done with manual intervention and are rectified in a time consuming way. For

some faults, it takes a long time and a lot of costs to solve the problem.

With the proposed circuit under such condition, the PLC unit will receive a signal from the NO auxiliary contact of the relay associated with the faulty section once the current in that section drops to zero and provided that the status of the CBs is not changed. The case is then identified as "undetected open-circuit fault".

For example, if undetected open circuit fault is assumed on the section between stations H38 and H53, then the NC auxiliary contact of CB-8 will be kept "open" while the auxiliary NO contact of relay-8 will be changed to "close" status.

IV. AVOIDING UNNECESSARY COMPLETE SHUTDOWN

The third problem addressed in the paper is to have a permanent short circuit fault which is not detected by any of the protection systems in the low-voltage side (neither differential nor overcurrent protection) but it is isolated by the transformer standby-earth fault relay located at the high voltage side. In this case, not only the faulty loop will totally be disconnected but also all the other healthy loops supplied from the same bus bar at the substation (complete shut down).

There several reasons for such a problem. In some cases, there is a poor discrimination between the 132/11 kV transformer primary overcurrent relay and overcurrent relays protecting the outgoing feeders. A typical case is shown in Fig. 3.

The differential protection can't detect such a fault as it occurs directly on the bus-bars of substation H53. The phase overcurrent protection (OP's) for the three main feeders will all trip to isolate the fault.

It can be seen from Fig. 3 that there is a very short time gap between the transformer primary OC relay operation (2.71 sec) and the relay of feeder FD1 (2.69 sec.). There is a degree of uncertainty in knowing which one will trip first. In many cases, both operate at the same time. This coordination problem is one of the reasons that lead to unnecessary complete shutdown of the station.

In some other cases, especially with a single line to ground fault, there is a probability that one of the three overcurrent relays (F1, F2 and F3) may fail to detect the fault.

This case is also expected if the fault occurred while only two of the three 132/11 kV transformers are in service or if the fault occurred through a fault resistance. Under such conditions, the sensitivity of the relay will be reduced. The fault current will find a path to the fault point even after disconnecting the other two relays. If this fault persists for long time, the transformer standby earth fault protection - installed in the transformer neutral connection - will trip the main transformer.

Usually, all the three 132/11 kV transformers are connected in parallel with common standby earth fault relay. It means that the station will be completely shut down under such conditions.

The principle of the proposed solution is based on the fact that if a fault in any section is detected by the corresponding differential relay, then none of the overcurrent relays R1, R2 and R3 (see Fig 4) will operate. On the other hand, closing the contacts of any of the three overcurrent relays R1 or R2 or R3 means that the differential relay for a certain section failed to operate.

The idea of the proposed solution is to accelerate the trip of the other two loop breakers as soon as a fault is detected by any one of the three OC relays. The three CBs will trip simultaneously once any relay contacts is closed as shown in Fig. 4. This will partially prevent the condition of feeding a fault from un-tripped feeder and consequently avoid the complete shutdown.

V. CONCLUSIONS

This paper presents a practical field experience with Kuwait distribution networks. Novel circuits for identifying the faulty section in case of detected short circuit fault and undetected open-circuit fault are presented. Another circuit is presented to avoid the problem of shut down of the whole 132/11 KV station. The proposed-circuits reduced technical and commercial losses, lower electric service restoration time, reduce the equipment damage, and enhanced power quality and reliability. These circuits succeeded to fulfill many tasks of DAS systems with almost neglected cost since it saves the cost of communication network and the cost of the RTUs required at each load point.

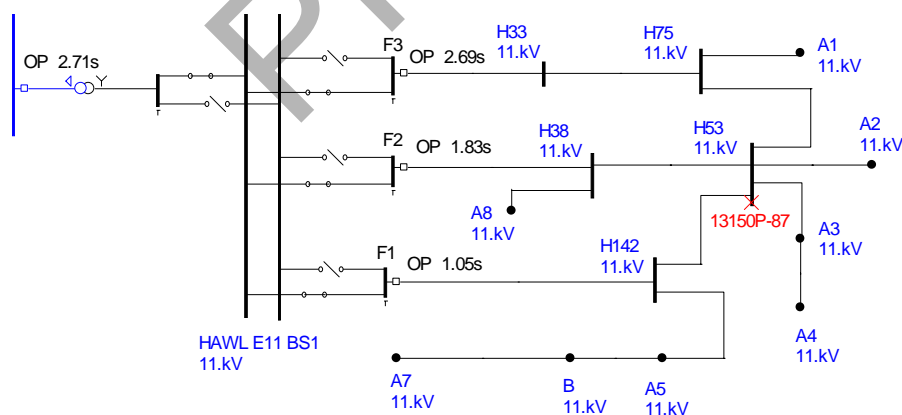


Fig. 3: Three line to ground fault at Bus-bar H53.

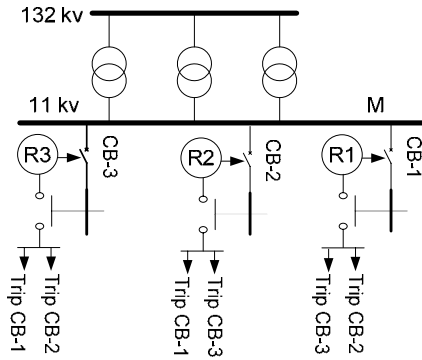


Fig. 4: The modified trip circuit

ACKNOWLEDGMENTS

The financial support from the General Authority for Applied Education and Training in Kuwait (Project No. TS-02-08) is highly appreciated.

REFERENCES

[1] Hassan Nouri, Chun Wang and Terry Davies, "An Accurate Fault Location Technique for Distribution Lines with Tapped Loads", IEEE Porto Power Tech Conference, Porto, Portugal, 10 -13 September, 2001, pp. 488 - 493.

[2] M. da Silva, M. Oleskoviczb, D.V. Coury, "A hybrid fault locator for three-terminal lines based on wavelet transforms", Electric Power Systems Research, Vol. 78, pp. 1980-1988, 2008.

[3] M. M. Saba, R. Das, P. Verho, and D. Novosel, "Review of Fault Location Techniques for Distribution Systems," Power Systems and Communication Infrastructure for the future, Beijing, Sep 2002.

[4] G. K. Purushothama, A. U. Narendranath, D. Thukaram, and K. Parthasarathy, "ANN Applications in Fault Diagnosis," Electric Power System Research, vol. 23, no. 6, pp. 491- 506, Aug. 2001.

[5] U. D. Dwivedi, S. N. Singh and S. C. Srivastava, "Analysis of Transient Disturbances in Distribution Systems: A Hybrid Approach", 2007 IEEE Power Engineering Society General Meeting , Tampa, Florida , USA, 24-28 June 2007.

[6] M. Michalik, M. Lukowicz, W. Rebizant, S.-J. Lee, and S.-H. Kang, "High impedance fault detection in distribution networks with use of wavelet-based algorithm," IEEE Trans. Power Del., vol. 21, no. 4, pp. 1793-1802, Oct. 2006.

[7] R. E. Lee , M. T. Bishop , "Performance Testing of the Ratio Ground Relay on a Four Wire Distribution Feeder", IEEE Trans. On PAS, Vol. PAS-102, No.9, Sept ,1983.

[8] Cesar Senger, "Broken Conductor Protection System Using Carrier Communication", IEEE Transactions on Power Delivery, VOL. 15, NO. 2, April 2000.

[9] R.P. Gupta and R.K. Varma, "Distribution Automation: Present Status". Academic Open Internet Journal, Volume15, 2005.

[10] Musse M. Ahmed, "Electrical Distribution Automation System for Low Voltage (LV) System", First International Power and Energy Conference PECon 2006, November 28-29, 2006, Putrajaya, Malaysia.

[11] ASPEN-OneLiner Simulation Program V9.7, www.aspeninc.com.

[12] IEEE Guide for determining fault location on AC transmission and distribution lines, IEEE Standard C37.114-2004, December 2004.

[13] IEEE Tutorial Course Text, "Detection of Downed Conductors on Utility Distribution Systems", 1989.

Charcoals Used as Electrode Material in Supercapacitors

B. Szubzda, R. Kulinski,
Electrotechnical Institute Division of Electrotechnology
and Materials Science
M. Skłodowskiej-Curie 55/61
Wrocław, Poland

Abstract- In this paper we have been described biomimetical structured charcoals based on acacia, sycamore, coconut and pine, in which capacitance arises in consequence of separation of charges in electrode/electrolyte interface (so-called electrical double layer), due to it's biomimetical structure, are proven to have high porosity and capacitance.

Influence of biomimetical structure on supercapacitive behaviour has been tested by cyclic voltammetry, galvanostatic charge-discharge and self-discharge tests.

I. INTRODUCTION

During whole history of mankind people were trying to draw inspiration from the nature to make their lives better. In the middle of XX century this tendency lead to rise of a new interdisciplinary field of science – biomimetics. So far a large amount of new materials has been discovered e.g.: very light biomorphic cellular ceramics with high thermal and mechanical strength [1], artificial bones made from hydroxyapatite [2], SiOC cellular ceramics used in biomedicine and electronics [3], or lightweight, porous ceramics structures for catalytic use [4, 5].

In recent years investigations on a new type energy storage device, so-called supercapacitor, has been carried out intensively. In supercapacitor high surface area of porous carbon electrode and the phenomenon of electrical double layer at electrode interface is used to obtain high capacitance, power and energy density.

The natural structure of a living tree found to be very porous. This natural porosity is connected with existence of special tissues responsible for a transport of water and soluble mineral nutrients from the roots to the rest of the plant. This natural porosity can be used to obtain an interesting material for supercapacitor electrode.

In this paper different types of pyrolyzed and activated woods was tested as an electrode in supercapacitor.

II. EXPERIMENTAL

A. Preparation of pyrolyzed and activated charcoals

Previously cutted out and prepared raw samples of four types of trees: acacia, sycamore, coconut and pine were carbonized in tubular furnace in controlled atmosphere of Ar gas for 2 hours at 1100 °C. Then samples were activated by treating solid KOH at 700 °C for 90 min. The initial amount of

substrates in weight relation was 1.0 KOH / 0.25 wooden substrate. Charcoals produced that way was then formed in defined shapes and weighted.

B. Electrochemical tests

Previously cutted out and prepared, raw samples of charcoal was tested as supercapacitor electrodes; 1M solution of H₂SO₄, and 6M KOH were used as an electrolyte. All measurements were made in five electrodes system using a device ATLAS 0531 Electrochemical Unit & Impedance Analyser. The reference electrode was saturated calomel electrode.

The range of taken tests:

- Cyclic voltammetry
- Galvanostatic charging and discharging
- Self-discharge tests

III. RESULTS AND DISCUSSION

A. Cyclic voltammetry

Cyclic voltammetry measurements was carried out at a rate of potential increase 1 mV/s to the value of 1.1 V, back to the zero, and then for a negative potential equal -1.1 V and again back to zero.

Analysis of the shape of voltammetric curve (CV) gives an information about electrochemical phenomenon in system, especially about electrodes phenomenon, resistance of system and dynamics of electrical double layer charging and discharging. The width of hysteresis loop corresponds to the ability of electric charge accumulation and is a basis of supercapacitor capacitance calculation. Fig. 1a, 1b, 1c, 1d shows CV for different types of charcoal, before and after activation in 1M H₂SO₄ and 6M KOH.

Activated charcoals are seemed to have wider hysteresis loop, than charcoals before the activation, for both acidic and basic electrolyte. Also the current response are considerably higher than in charcoals before the activation.

B. Galvanostatic charging and discharging

Galvanostatic charging and discharging measurements are very helpful in calculation of supercapacitor capacitance. To charge and discharge the supercapacitor forced, constant

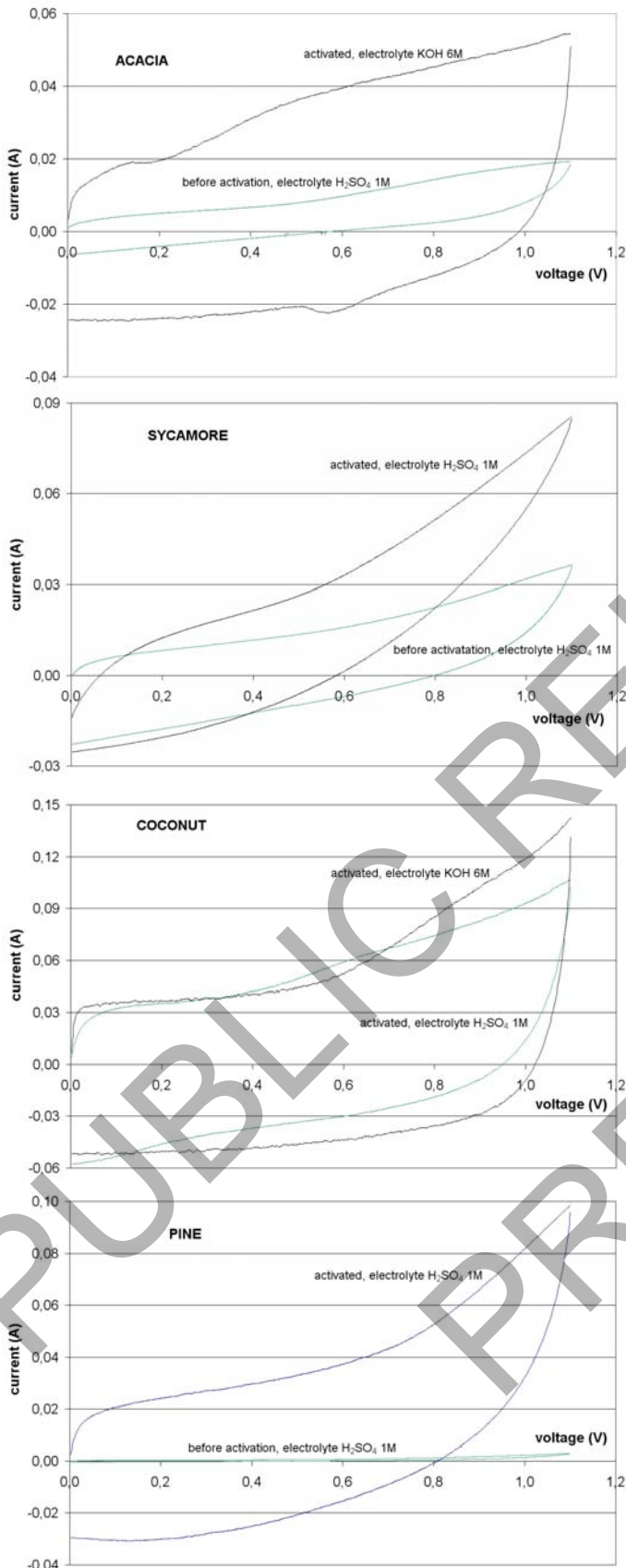


Figure 1. Diagram of cyclic voltmetry for (a) acacia , (b) sycamore, (c) coconut, (d) pine; scan rate 1 mV/s.

current was held and the time when potential between cell electrodes reach previously fixed value was the variable. In this case the current value was set as 1/5 of absolute value of potential, e.g. if potential was set as 600 mV, current was 120 mA. The supercapacitor was charged and then discharged for the following values of cell potential: 100, 200, 300, 400, 500 and 600 mV.

Results of galvanostatic charging and discharging measurements was gathered in Table I. The capacitance of supercapacitor was recalculated with respect to the mass of electrode.

Activation of charcoals are supposed to have a great influence on their capacitive behaviour. In all cases the capacitance is much higher than before the activation, e.g. pine (Fig.1d), where the capacitance is more than hundred times higher. Also it is worth to be noticed that in 6M KOH electrolyte the capacitance is considerably higher than in acidic one (with the exception of activated sycamore).

C. Self-discharge tests

There are many factors that have influence on the behaviour of supercapacitor self-discharge, e.g. ionic mobility, sort and strength of electrolyte, temperature, degree of solvation, factors responsible for matching electrolyte and electrode: wettability, size of electrode pores, and ions of electrolyte.

In measurements supercapacitor was charged to the potential 0,6 V at a rate of potential increase 10 mV/s. This potential was forced for 10 minutes using external power source and then was controlled for the next 11 hours.

The results of measurements was presented in Table II and in Fig. 2.

Leakage current is very important parameter in self-discharge analysis, it determines the amount of energy needed to sustain the electrical double layer. Low leakage current connected with high capacitance, as in activated acacia,

TABLE I
GALVANOSTATIC MEASUREMENTS - CAPACITANCE OF CHARCOALS IN ACIDIC AND BASIC ELECTROLYTE

Sample		Capacitance [F/g]	
		1M H ₂ SO ₄	6M KOH
1	Acacia	27,9	
2	Acacia - <i>activated</i>	79,9	170,6
3	Sycamore	58,8	-
4	Sycamore - <i>activated</i>	141,6	82,6
5	Coconut - <i>activated</i>	220,8	281,5
6	Pine	3,9	-
7	Pine - <i>activated</i>	475,8	-

TABLE II
SELF-DISCHARGE BEHAVIOUR FOR DIFFERENT KINDS OF CHARCOALS, IN ACIDIC AND BASIC ELECTROLYTE

Sample		self-discharge after charging to 600 mV	
		leakage current [mA]	potential after 1 hour [mV]
1	Acacia, H_2SO_4	4,1	155
2	Acacia – activated, H_2SO_4	5,0	135
3	Acacia – activated, KOH	1,6	379
4	Sycamore, H_2SO_4	4,0	437
5	Sycamore – activated, H_2SO_4	9,3	246
6	Sycamore – activated, KOH	3,0	422
7	Coconut – activated, H_2SO_4	10,8	286
8	Coconut – activated, KOH	3,1	529
9	Pine, H_2SO_4	0,2	104
10	Pine – activated, H_2SO_4	10,1	360

sycamore and coconut, is very desirable factor for supercapacitors. It is worth to be noticed that in acidic electrolytes leakage current is over three times larger than in basic ones.

IV. CONCLUSIONS

On the basis of the electrochemical measurements it was concluded that the activation of charcoals is crucial for their capacitance, charge, discharge and self-discharge behaviour.

For all samples supercapacitive properties are seemed to be considerably greater than before the activation. The charcoals obtained in this way appeared to have hydrophilic (activated

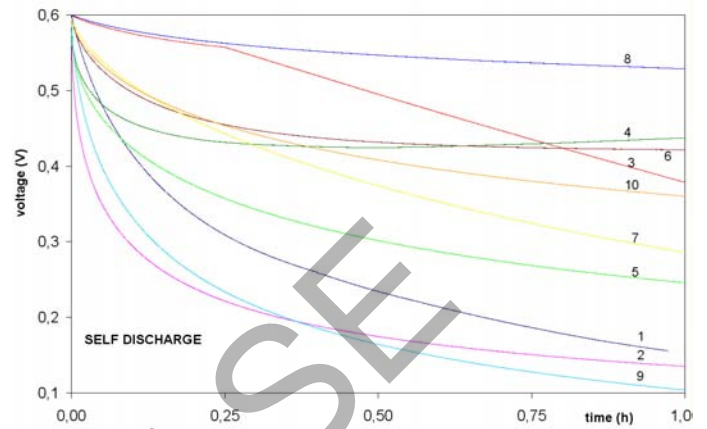


Figure 2. Diagram of self-discharge of supercapacitor after charging to 600 mV (1) acacia, H_2SO_4 , (2) acacia – activated, H_2SO_4 , (3) acacia – activated, KOH, (4) sycamore, H_2SO_4 , (5) sycamore – activated, H_2SO_4 , (6) sycamore – activated, KOH, (7) coconut – activated, H_2SO_4 , (8) coconut – activated, KOH, (9) pine, H_2SO_4 , (10) pine – activated, H_2SO_4 .

coconut and sycamore) or hydrophobic properties (pine and sycamore before the activation).

As a result of voltammetric measurements charcoals in which in range of charging potentials unfavourable electrochemical processes (decomposition of water) does not exist was selected: coconut and pine.

REFERENCES

- [1] H. Sieber, Ch. Hoffmann, A. Kaendl, P. Greil, *Biomorphic Cellular Ceramics*, Advanced Engineering Materials (2000), 2. No. 3, pp. 105 – 109.
- [2] K. Hata, T. Kokubo, *Growth of a Bone-like Apatite Layer on a Substrate by a Biomimetic Process*, J. Am. Ceram. Soc. (1995), 78, 4, pp. 1049-1053.
- [3] P. Colombo, *Novel Processing of Silicon Oxycarbide Ceramic Foams*, Advanced Engineering Materials, (1999) 1, No.3-4, pp. 203-205.
- [4] T. Ota, M. Imaeda, H. Takase, M. Kobayashi, N. Konoshita, T. Hirashita, H. Miyazaki, Y. Hikichi, *Porous Titania Ceramic Prepared by Mimicking Silicified Wood*, J. Am. Cer. Soc. (2000) 83, 6, pp. 1521-1523.
- [5] T. Ota, Y. Hikichi, H. Unuma, M. Takahashi, H. Suzuki, H. Akahane, *Production of Ceramic Woods by Mimicking Fossil Woods*, 9-th Cimatec-World Ceramic Congress, Ceramic Getting into the 2000's – Part C (1999), pp. 531-538.
- [6] B.E. Conway, *Electrochemical Capacitors: Scientific Fundamentals and Technological Applications*, Kluwer Academic/Plenum, 1999.

Wavelets for detection of voltage dips and micro interruptions

Zbigniew Leonowicz
Wroclaw University of Technology
Wyb. Wyspianskiego 27
Wroclaw, Poland

Abstract- In electrical energy power network, disturbances can cause problems in electronic devices therefore their monitoring is fundamental in Power Quality field both to properly dimension protections and to calculate compensations in case of malfunction of the apparatus. In this paper we address the problem of disturbances estimation by using Wavelets signal processing for detection of short, impulse-like voltage dips and micro-interruptions.

Index Terms—Power Quality, Wavelets, voltage dips, micro interruptions..

I. INTRODUCTION

Electric power quality has become an important part of power systems and electric machines, studied from a wide number of points of view. For this purpose there are many of electric parameters that help to describe the phenomena as a whole are reported in standards. In this context, we consider disturbances as the temporary deviation of the steady state waveform caused by faults of brief duration or by sudden changes in the power system [1]. The disturbances considered by the International Electro-technical Commission include voltage dips, brief interruptions, voltage increases, and impulsive and oscillatory transients [2,3, 4].

The first ones are defined by norms as a sudden reduction (between 10% and 90%) of the nominal voltage, at a given point of electrical system, and lasting from half of the fundamental period to several seconds. The dips with durations of less than half a cycle are regarded as transients. The main characteristics of voltage dips are magnitude and duration, which correspond to the remaining bus voltage during the fault and the required time to clear the fault respectively. A voltage dip may be caused by switching operations associated with temporary disconnection of supply, the flow of heavy current associated with the start of large motor loads or the flow of fault currents or short circuits and earth faults. These last ones can be symmetrical (three phase) or non symmetrical (single-phase to ground, double-phase or double-phase-to-ground). The brief interruptions can be considered as voltage sags with 100% of amplitude. The cause may be a blown fuse or breaker opening and the effect can be an expensive shutdown. For instance, supply interruptions lasting up to few seconds may cost a lot in case of interruption of service or stoppage of machines in a production plant. Costs that can quickly grow up with the plant resetting time that can be very long. The main protection of the customer against such events is the installation of uninterruptible power supplies [1].

Brief voltage increases (swells) are brief increases in r.m.s. voltage that sometimes accompany voltage sags. They appear on the unfaulted phases of a three phases of a three-phase circuit that has developed single-phase short circuit. Swells can upset electric controls and electric motor drives, particularly common adjustable-speed drives, which can trip because of their built-in protective circuitry. Swells may also stress delicate computer components and shorten their life. Possible solutions to limit this problem are, as in the case of sags, the use of uninterruptible power supplies and conditioners [5].

Voltage disturbances shorter than sags or swells are classified as transients and are caused by sudden changes in the power system [5]. According to their duration, transient overvoltages can be divided into switching surge (duration in the range of millisecond), and impulse spike (duration in the range of microseconds). Surges are high-energy pulses arising from power system switching disturbances, either directly or as a result of resonating circuits associated with switching devices. Protection against surges and impulses is normally achieved by surge-diverters and arc-gaps at high voltages and avalanche diodes at low voltages.

In this article we focus the attention on disturbances which will gain more importance in the next future because of the increase of electronic apparatus' that can be particularly sensible to this kind of problems if not adequately protected. In fact there are two important aspects that should be taken into account:

In all cases, in power quality is necessary to detect not only the beginning and end of voltage sag but also to determine the sag depth and the associated phase angle jump.

The performance of wavelet signal processing is tested for analysis of short, impulse signals [8].

II. APPLIED WAVELET TRANSFORM ANALYSIS

Wavelet transform is a useful tool in signal analysis. Wavelets provides a fast and effective way of analyzing non-stationary voltage and current waveforms and can be applied for precise computation of the beginning of a disturbing event, as shown in this paper. The ability of wavelets to focus on short time intervals for high-frequency components and long intervals for low-frequency components improves the analysis of signals with localized impulses and oscillations, particularly in the presence of a fundamental and low-order harmonic [6].

The continuous *Wavelet Transform* (WT) of a signal $x(t)$ is

defined as

$$X_{a,b} = \frac{1}{\sqrt{|a|}} \int_{-\infty}^{+\infty} x(t) \psi\left(\frac{t-b}{a}\right) dt \quad (1)$$

where $\psi(t)$ is the mother wavelet, and other wavelets

$$\psi_{a,b}(t) = \left(\frac{1}{\sqrt{|a|}}\right) \psi\left(\frac{t-b}{a}\right) dt \quad (2)$$

are its dilated and translated versions, where a and b are the dilation parameter and translation parameter respectively, $a \in R^+ - \{0\}$, $b \in R$ [7,8].

The discrete WT (DWT), instead of CWT, is used in practice [23]. Calculations are made for chosen subset of scales and positions. This scheme is conducted by using filters and computing the so called *approximations and details*. The *approximations (A)* are the high-scale, low frequency components of the signal. The *details (D)* are the low-scale, high-frequency components. The DWT coefficients are computed using the equation

$$X_{a,b} = X_{j,k} = \sum_{n \in Z} x[n] g_{j,k}[n] \quad (3)$$

where $a = 2^j$, $b = k2^j$, $j \in N$, $k \in Z$.

The wavelet filter g plays the role of ψ [6]. The choice of mother wavelet is different for each problem at hand and can have a significant effect on the results obtained. Orthogonal wavelets ensure that the signal can be reconstructed from its transform coefficients.

As wavelet the *symlets* function was used. The symlets are nearly symmetrical wavelets proposed by Daubechies as modifications to the “db” family - orthogonal wavelets characterized by a maximal number of vanishing moments for some given support (Fig. 1). Dips detection was realized through tracking values of *details (D)* representing higher frequencies in the signal. High value indicated dip. In contrary to other presented method this approach did not use the amplitude parameter of the main component, but was therefore prone to noise and other high frequency disturbances.

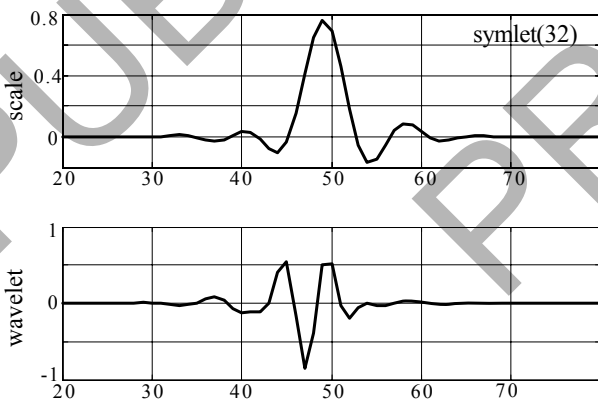


Figure 1. Scale and wavelet symlets function for 32 coefficients

Figure 2 shows the behaviour of the wavelet decomposition of the sinusoidal waveform distorted by one voltage dip. The decomposition was made using the Daubechies 6 wavelet at the

D2 level.

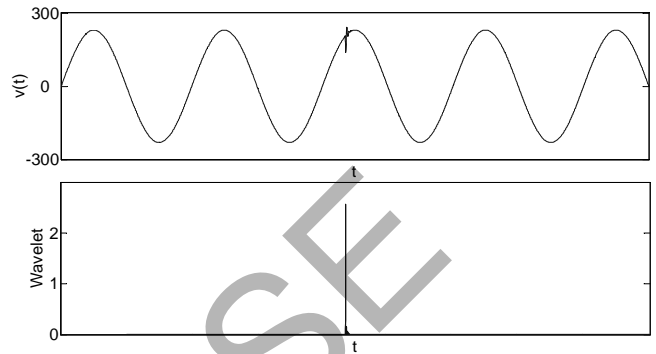


Figure 2. Wavelet decomposition (lower plot) of the sinusoidal waveform (upper plot) distorted by one voltage dip.

III. INVESTIGATIONS, DISCUSSION AND CONCLUSIONS

For experimental testing the performance of the algorithms, we used a synthesized signal realized by MATLAB able to generating voltage dips of different magnitudes.

For evaluating the performance of the method many test signals has been used with different THD and SNR. The THD used are 5.7%, 11.2% and 22.4%. These values were obtained using for each of the first 24 harmonics half of the norm limits, the norm limits, and the double of norm limits [9].

For each of the three THD has been created three signals with a different SNR: 100dB, 80dB and 60dB. The added noise is white Gaussian.

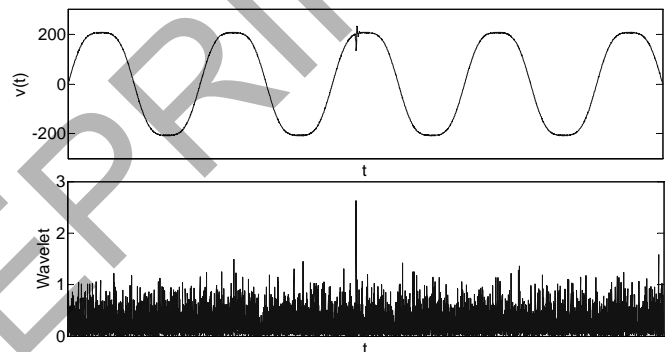


Figure 3. Wavelet decomposition (lower plot) of the sinusoidal waveform with harmonics (upper plot) distorted by one voltage dip.

Higher order frequency components present in the signal deteriorated the detection ability of the method. Two wavelets with significantly different lengths have been used; *Symlet* (length of the filter 32 samples) and *Daub 6* (length of the filter 6 samples).

In the nine test signals 100 dips have been added, one for each period in randomly position. In Tables I and II are reported the percentage of detected dips for 35V and 100V dips of respectively 15% and 43% of nominal voltage.

TABLE I
DETECTION ACCURACY OF 35V DIPS

SNR \ THD	100 dB	80 dB	60 dB
5.7 %	100 %	45 %	12 %
11.2 %	100 %	45 %	17 %
22.4 %	100 %	33 %	14 %

TABLE II
DETECTION ACCURACY OF 100V DIPS

SNR \ THD	100 dB	80 dB	60 dB
5.7 %	100 %	100 %	70 %
11.2 %	100 %	100 %	67 %
22.4 %	100 %	100 %	62 %

The wavelet approach ensures good performance in presence of high THD, but the percentage of detected dips is strongly reduced for high noise level.

REFERENCES

- [1] J. Arrillaga, N.R. Watson, S. Chen, Power System Quality Assessment, John Wiley & Sons, 2000, ISBN 0 471 98865 0.
- [2] IEC 61000-2-1: 1990, Electromagnetic Compatibility (EMC), Part 2: Environment, Section 1: Description of the Environment – for Low-Frequency Conducted Disturbances and Signalling in Public Power Supply Systems.
- [3] IEC 61000-2-2: 1990, Electromagnetic Compatibility (EMC), Part 2: Environment, Section 2: Compatibility Levels for Low-Frequency Conducted Disturbances and Signalling in Public Power Supply Systems.
- [4] IEEE c62.41: 1991, IEEE Recommended Practice on Surge Voltages in Low-Voltage AC Power Circuits.
- [5] UIE-DWG-2-92-D, UIE Guide to Measurements of Voltage Dips and Short Interruptions Occurring in Industrial Installations.
- [6] S. Santoso, E.J. Powers, W.M. Grady, P. Hofmann: “ Power Quality Assesment via Wavelet Transform Analysis,” IEEE Transactions on Power Delivery, 11(2), pp. 924-930.
- [7] M. Misiti, Y. Misity, G. Oppenheim, J-M. Poggi, “Wavelet Toolbox User’s Guide, MathWorks”, 1996.
- [8] H. Amaris, C. Alvarez, M. Alonso, D. Florez, T. Lobos, P. Janik, J. Rezmer, Z. Waclawek: “Application of advanced signal processing methods for accurate detection of voltage dips,” 13th International Conference on Harmonics and Quality of Power. ICHQP 2008, Wollongong, Australia, 28th September-1st October 2008, 6p.
- [9] CEI EN 50160 Power Quality Application Guide: Voltage Characteristic in Public Distribution System.

Two modified method for Harmonic and Flicker measurement based on RWPC considering spectral leakage and edge effects

¹Marjan Saadati , ²Seyed Saeedolah Mortazavi
Shahid Chamran University (SCU)
Golestan Boulevard
Ahvaz, Iran

Abstract- Harmonic is an important issue in electric power systems. A wavelet packet transform (WPT) method is introduced as a powerful tool for detection Harmonics and Flicker. The proposed methods can simultaneously measure the distribution of RMS quantities with respect to individual frequency bands directly from the wavelet transform coefficients. Uniform frequency bands result from the WPT decomposition of power system waveforms can be used for identification of harmonic frequency bands. This paper presents two novel modified methods for harmonic detection and measurement.

However, use of wavelet packet coefficients has some errors such as the edge effects of wavelet filters and spectral leakage. In first method paper proposes to combine two adjacent frequency bands to reduce error caused by spectral leakage. In the recently methods they place frequency of main harmonics on the edge of the bands. It provides huge errors because of non-ideal characteristics of the filters. In second method paper proposes to change the band width of output to 40 Hz. This causes that the main harmonics be in the band no on the edge. This method has got the chance to measure flicker also.

Use of Wavelet Packet Coefficients for harmonic measurement because of Downsampling reduces number of sampling points and energy content of signal making huge error. This paper also offers the use of a compensation method by use of Reconstructed WPC to prevent energy reduction.

In addition, it introduces a modification method to reduce edge effects and spectral leakage. Methods are simulated and experimented. Parameters are compared with true values that it shows satisfactory results.

I. INTRODUCTION

POWER quality is becoming an issue of increasing concern both to utilities and their customers. One of the major power system problems is steady-state waveform distortion due to harmonics; Harmonics be produced by variable speed drives, arc furnaces, personal computers, and other non-linear devices. Since harmonics can severely degrade the performance of power system equipment, it is necessary to always monitor their parameters such as voltage, current, and power.

The traditional discrete Fourier transform (DFT) is proposed

in the and standard as the processing tool for harmonic analysis, using rectangular time windows of ten cycles' width of the fundamental frequency in a 50-Hz system, providing a resolution of 5 Hz. Of course this does not preclude the application of other analysis principles. As is well known, the results obtained using DFT are incorrect in the case of non-stationary signals. A way to overcome this problem is the use of the Short Time Fourier Transform (STFT). The STFT partitions the signal into time segments where the signal is considered stationary, applying the DFT within each segment. Once the size of the time window is selected, the time-frequency resolution obtained is fixed and it is the same for the whole frequency spectrum of the signal. The results obtained show its dependency on the length of the time window selected. An advantage of the STFT method is that it gives information on the magnitude and phase-angle of the fundamental and harmonics [10].

Kalman filters have been used as an alternative method. This method gives information both on the magnitude and phase angle of voltage supply. The detection properties of Kalman filtering and the accuracy in the estimation depend both on the model of the system used and on the magnitude, duration and point-on-wave where the voltage event begins. A possible solution to improve the performance of Kalman filtering is the use of an Extended Kalman filter to better estimate the non-linear process associate with a voltage event.

Wavelet analysis is a powerful signal processing tool specially useful for the analysis of non-stationary signals. The discrete wavelet transform provides a non-uniform division of the time-frequency plane, giving short-time intervals for high-frequency components and long-time intervals for low-frequency components. The use of wavelets for the analysis of harmonics has not been thoroughly investigated until now. Pham and Wong proposed in [2] an approach for identification of harmonics in power systems using a combination of DWT and CWT to quantify harmonic frequency amplitudes and phases. They propose a method to compensate the frequency

¹ Post graduated M.S. degree student in power systems from SCU.

Email address : saadati_s@nisoc.ir

² Dr. S.S. Mortazavi is Assistant Prof. of Elect Engg of Shahid Chamran University.

Email address : mortazavi_s@scu.ac.ir

response of the filters used in the wavelet transform filter banks. Hamid and Kawasaki [6] proposed the use of the wavelet packet transform, with the Vaidyanathan filter, to improve the results obtained using the discrete wavelet transform for root mean square values of voltage and power measurement. Finally Parameswariah and Cox, Eren and Devaney have studied on the selection of mother wavelet [7].

II. HARMONIC DETECTION USING WPT

Use of Wavelet Transform as a powerful signal processing method is receiving increased attention. Initially they use Multi Resolution Analysis (MRA) for voltage event detection. It produces nonuniform frequency band that is unsuitable for harmonic measurements.

To overcome this limitation of the DWT, the wavelet-packet transform (WPT) can be used to obtain a uniform frequency decomposition of the input signal as in the Fourier analysis. In the WPT, both the detail and the approximation coefficients are decomposed to produce new coefficients, this way enabling a uniform frequency decomposition of the input signal to be obtained. By using the WPT and adequately selecting the sampling frequency and the wavelet decomposition tree, the output frequency bands of the multiresolution analysis can be selected to correspond to the frequency bands of the different harmonic components of the input signal. (The mathematical background is found in [1]).

III. HARMONIC DETECTION USING RWPC

However, use of WPC has some errors such as the edge effects of wavelet filters, the content energy reduction of signal during decomposition caused by Downsampling and spectral leakage.

Use of Wavelet Packet Coefficients for harmonic measurement because of Downsampling reduces number of sampling points (by power of 2) and energy content of signal making huge error. This paper proposes using reconstructed wavelet packet coefficient instead of WPC to prevent energy reduction and decrease the error. For saving energy coefficients are reconstructed in each level. Upsampling is used after downsampling. The other half of the story is how those components can be assembled back into the original signal without loss of information. This process is called *reconstruction*, or *synthesis*. The mathematical manipulation that effects synthesis is called the *inverse discrete wavelet transform* (IDWT). Where wavelet analysis involves filtering and downsampling, the wavelet reconstruction process consists of upsampling and filtering. Upsampling is the process of lengthening a signal component by inserting zeros between samples. The filtering part of the reconstruction process also bears some discussion, because it is the choice of filters that is crucial in achieving perfect reconstruction of the original signal. The low- and highpass decomposition filters (L and H), together with their associated reconstruction filters (L' and H'), form a system of what is called *quadrature mirror filters* (QMF). Its theory is presented in [9]. Fig. 4 and 5 show the Reconstruction mechanism and Quadrature Mirror Filters (QMF) respectively [11].

IV. MODIFICATION

A signal can be fully decomposed into levels, given by, where is the total number of data points. Each of these wavelet levels correspond to a frequency band given by $f = 2^v(f_s / N)$ Where f is higher frequency limit of the frequency band represented by the level v ; f_s is sampling frequency; N is the number of data points in the original input signal [7]. The maximum frequency that can be measured is given by the Nyquist theory as $f_{max} = f_s/2$, Where f_s is the sampling frequency.

V. METHOD I

The sampling frequency selected is 1.6 kHz and the sampling window width is 10 cycles of the fundamental frequency (200 ms in a 50-Hz system). The output of the filter bank is divided into thirty two uniform bands of 25-Hz width (coefficients $d1(n)$ to $d32(n)$ in Fig. 6). Decomposition is performed in 5 level and 32 output band. Higher sampling frequencies can be selected to extend the range of harmonic groups computed in the input signals. The extension of the sampling frequency implies the use of a different wavelet decomposition tree to obtain the same output frequency bands. Thus, doubling the sampling frequency is needed.

By set frequency band in 25 Hz band width main harmonics set on the edge of filters. Because of nonideal characteristic of the filters edge effect error occurs and generates spectral leakage. This makes measurement so inaccurate specially in frequencies near $f_{max}/2$. An example of frequency response of LP and HP filters is presented in Fig.7 that shows nonideal characteristics and edge effect. More investigation of spectral leakage caused by edge effect is there in [3-5]. Paper has focus on two important points to generate better accuracy:

1. *Choose of mother wavelet.* It is important to choose a wavelet function that has a frequency response near the ideal and has fast responding. Wavelet mother daubechies with 40 coefficients has good frequency response as shown in Fig.8 [8]. The algorithm uses the DB40 as the wavelet function.
2. *Combination of two adjacent frequency bands.* The method proposes to combine two adjacent frequency bands to reduce error caused by spectral leakage. The outputs of the filter bank are grouped to produce 15 output bands, with each harmonic frequency component (both odd and even harmonics) in the center of each band and with a uniform 50-Hz interval as depicted in Fig. 9.

VI. METHOD II

In the recently methods they place frequency of main harmonics on the edge of the bands [3-5]. It provides some errors because of nonideal characteristics of the filters. This makes measurement so inaccurate specially in frequencies near $f_{max}/2$. This method proposes to change the band width of output to 40 Hz. This causes that the main harmonics be in the band, not on the edge. This method has got the chance to measure flicker also. Then Sampling frequency selected is 2.56 kHz.

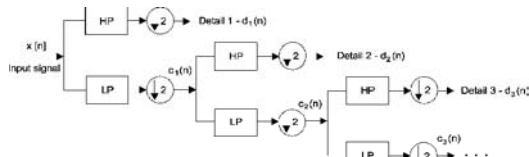


Figure 1. Multi Resolution Analysis (MRA)

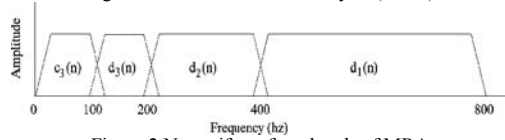
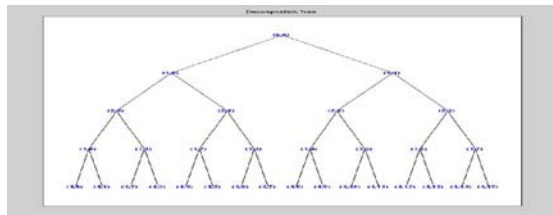
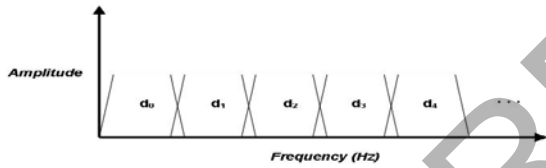


Figure 2. Nonuniform freq. bands of MRA



(a)



(b)

Figure 3. (a) Decomposition tree, (b) Uniform decomposition of WPT

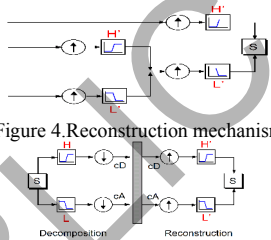


Figure 4. Reconstruction mechanism

Figure 5. quadrature mirror filters (QMF)

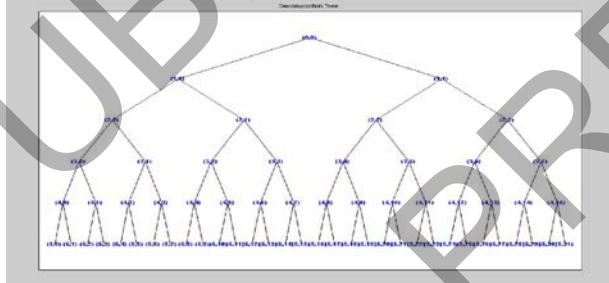


Figure 6. Decomposition tree in five levels

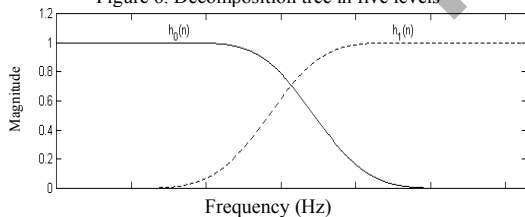


Figure 7. Nonideal characteristics of HP & LP filters

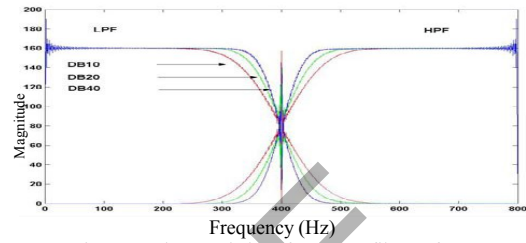


Figure 8. Characteristics of HP & LP filters of DB

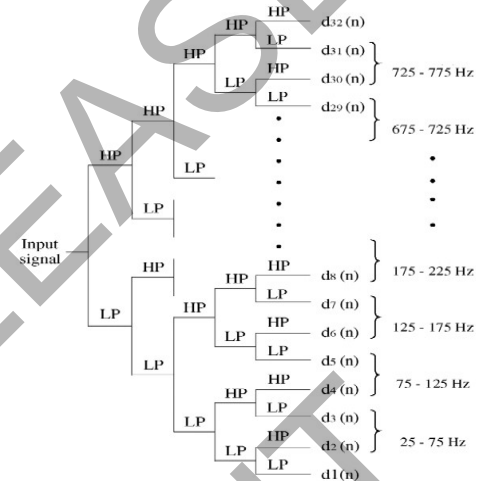


Figure 9. Combination of two adjacent frequency bands that each harmonic frequency component is in the center of each band and with a uniform 50-Hz interval.

VII. PRESENTATION

The derivation of the rms using discrete wavelet-based algorithm was proved in [2]. In practice, the analogue waveforms are digitized. In the WPT algorithm, only the wavelet coefficients at a certain level j are used for the rms and power calculations. More information can find in [2].

VIII. SIMULATION

Consider $V(t)$ as a periodic steady state signal. It has some harmonics that are mentioned in Table I. This signal is simulated and by MATLAB and WPT is applied to it. Table I and II represents the harmonics produced using method I and II respectively. Figs. 11-14 show the 4 first coefficients that are obtained. Results show that using RWPC has less error and better response. In practice signal is produced in 16 cycles and applied to WPT. The three cycle of beginning and three cycle of end of the obtained responses are deleted. This is for elimination edge effect of wavelet filter when applied to signal. (10 cycles is used).

IX. CONCLUSION

A wavelet packet transform (WPT) method is introduced as a powerful tool for detection, classification and quantification of power quality events. The paper proposed two methods can simultaneously measure the distribution of RMS quantities with respect to individual frequency bands directly from the wavelet transform coefficients. In first method paper proposes

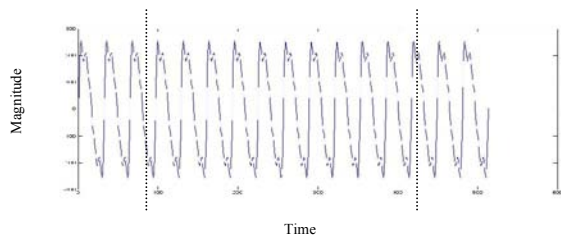


Figure 10. In practice signal is produced in 16 cycles the three cycle of beginning and end of the obtained responses are deleted for elimination edge effect of wavelet filter.

TABLE I
Simulation results of method I

Bands↓	True value	Method using WPC	Method using RWPC
1st	230	225.74	229.91
2nd	53	51.72	52.68
3rd	50	48.29	50.07
4 th	44	42.31	43.26
5 th	30	26.09	28.79
6 th	0	0.26	0.07
7 th	6	5.71	6.02
8 th	0	0.29	0.31
9 th	3	2.82	2.98
10 th	0	0.04	0.02
11 th	1	1.01	0.99
12 th	0	0.09	0
13 th	0	0.05	0
14 th	0	0.06	0.05
15 th	0	0.08	0.02

to combine two adjacent frequency bands to reduce error caused by spectral leakage. In second proposes to change the band width of output to 40 Hz. This causes that the main harmonics be in the band, not on the edge. This method has got the chance to measure flicker also. Use of a compensation method by use of Reconstructed WPC is effective in prevention in energy reduction. In addition, modification method to reduce edge effects and spectral leakage is applicable. Method is simulated and experimented. Parameters are compared with true values that it shows satisfactory results.

TABLE II
Simulation results of method II

Bands↓	Frequency (Hz)	True value	Method using WPC	Modified method using RWPC(40)
1st(flicker)	0-40	0	0	0.01
2nd	40-80	230	225.74	227.931
3rd	80-120	53	51.72	54.68
4 th	120-160	50	48.29	49.02
5 th	160-200	44	42.31	41.72
6 th	240-280	30	26.09	29.11
7 th	280-320	0	0.26	0.03
8 th	320-360	6	5.71	5.75
9 th	360-400	0	0.29	0.31
10 th	440-480	3	2.82	2.88
11 th	480-520	0	0.04	0.01
12 th	520-560	1	1.01	0.99
13 th	560-600	0	0.09	0
14 th	600-640	0	0.05	0
15 th	640-680	0	0.06	0.04
16	680-720	0	0.08	0.01

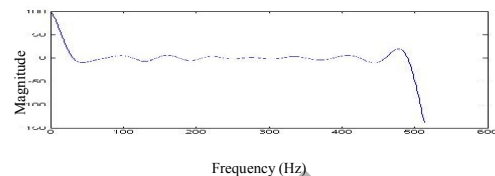


Figure 11. coefficient 1

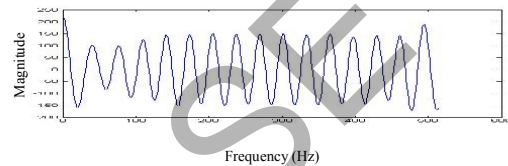


Figure 12. coefficient 2

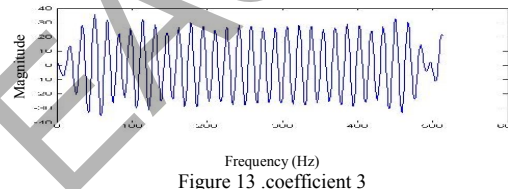


Figure 13. coefficient 3

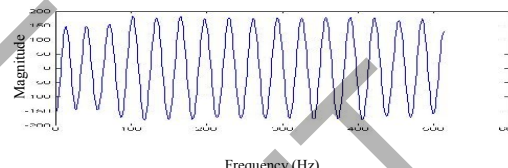


Figure 14. coefficient 4

REFERENCES

- [1] Sangeethapriya, M. Prabhakar, "Harmonic detection using Wavelet Transform", IEEE Proceedings of International joint conference on Neural Networks, Volume 4, 31 July-4 Aug. 2005 Page(s):2228-2231
- [2] V.L. Pham and K.P. Wong, "Wavelet-transform-based algorithm for harmonic analysis of power system waveforms," IEE Proc. On Generation, Transmission and Distribution, 146 (1999) 249-254.
- [3] J. Barros and R.I. Diego, "Application of the wavelet-packet transform to the estimation of harmonic groups in current and voltage waveforms," IEEE Trans. Power Delivery, Vol. 21, No.1, January 2006, pp. 533-535.
- [4] Julio Barros, Ramon I. Diego, "A new method for measurement of harmonic groups in power systems using wavelet analysis in the IEC standard framework" Elsevier power system research. Vol. 76 PP. 200-208, 2006
- [5] Julio Barros, Ramon I. Diego, "Analysis of Harmonics in Power Systems Using the Wavelet- Packet Transform" IEEE Trans. Instrumentation and Measurement, Vol. 57, No. 1, Jan 2008
- [6] E. Y. Hamid and Z. Kawasaki, "Wavelet packet transform for rms values and power measurements," IEEE Power Eng. Rev., vol. 21, no. 9, pp. 49-51, Sep. 2001.
- [7] C. Parameswariah and M. Cox, "Frequency characteristics of wavelets," IEEE Trans. Power Del., vol. 17, no. 3, pp. 800-804, Jul. 2002.
- [8] A. Mazloomzadeh, M. Mirsalim, H. Fathi and H. Sadeghi, "Optimized method measurement using discrete wavelet packet transform" 23th PSC, Iran, 1-3 December 2008
- [9] Stephane Mallat, "A Wavelet Tour of Signal Processing", Academic Press, London, 2nd Edition, 2001.
- [10] Francisco Jurado, Jose R. Saenz, "Comparison between discrete STFT and wavelets for the analysis of power quality events" electric power System Research
- [11] MATLAB help on Wavelet.

Combustion Characteristics of Palm Wastes in Fluidized Bed Combustion

Rosyida Permatasari, Kang Kin Hui, Mohammad Nazri Mohd. Ja'afar*
Faculty of Mechanical Engineering, Universiti Teknologi Malaysia, 81310 UTM
Skudai, Johor, Malaysia
prosyida@yahoo.com, nazri@fkm.utm.my

Abstract-Fluidized bed combustion (FBC) is one of the most promising energy conversion options available today. The emissions from FBC are very dependent on a number of operating conditions (temperature, staged air, excess air, fuel feed rate, etc.) and fuel properties. This paper described the experimental results taken in a staged air fluidized bed combustion scale laboratory, using palm shell and palm fiber as fuels and silica sand as the inert bed material. The silica sand was used for ensuring sustainable fuel ignition and combustion in FBC. The variation of excess air and fuel feeding rate were taken in these experiments. Gaseous emissions of CO concentrations, combustion efficiency and temperature along the combustor height as well as in flue gas were measured in the experimental tests. The experimental results showed that the axial temperature profiles decrease successively related along the FBC height. The CO emission obtained results lower for staged air condition than for un-staged air condition. And the combustion efficiencies give satisfied value. The palm wastes combustion give significant contribution for reduction of CO emission from combustion process.

I. INTRODUCTION

Fluidized Bed Combustion (FBC) is one of the most promising energy conversion options available today. FBC uses a continuous stream of air to create turbulence in a mixed bed of fuel, inert material and coarse fuel ash particles. It occurs at temperatures typically between 800 and 900°C. Constant mixing of particles encourages rapid heat transfer and complete combustion. Fluidization, combustion and emission formation constitute the fundamental issues of FBC.

In order to meet the increasing uses of energy with higher efficiency without significant environmental impact, the development and implementation of newer and cleaner energy conversion system are essential. The increased use of biomass in energy systems is an important strategy to reduce the emissions [1]-[3]. Biomass residues from palm oil are potential usage because of many palm oils planting area in Asian countries, like in Malaysia, Thailand, and Indonesia [4]-[5].

The method used in this work was air staging with controlling of operating conditions, i.e., temperature and excess air (EA). Air staging was achieved by dividing the air supply into in-bed fluidizing primary air and over bed secondary air (SA). Degree of air staging was expressed as the ratio of secondary to total air. Effects of air staging are characterized by the reduction of emissions.

II. EXPERIMENTAL SET-UP

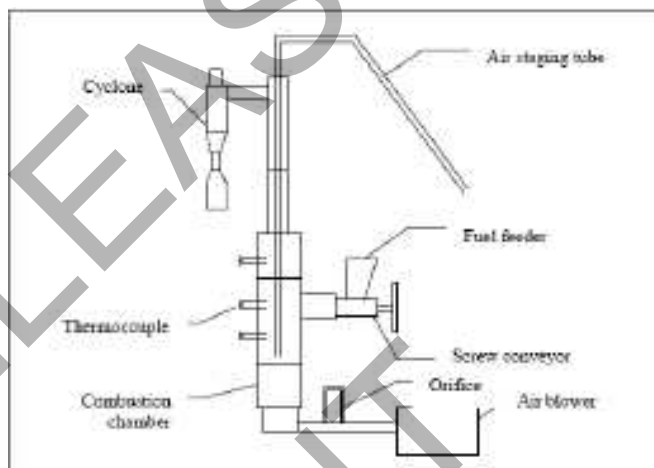


Figure 1. Schematic diagram of the experimental Combustor

Figure 1 shows a schematic diagram of the experimental combustor. The experimental combustor was fabricated from mild steel and is 0.5 m in height and 0.36 m squared in cross section. The insulated reactor is made from stainless steel cylindrical tube of 164 mm internal diameter and 2.0 m height and divided into five flanged sections. Silica sand of 300 μm mean particle diameter was used as the bed material. Air from a blower was introduced into the bed through a distributor with air outlets arrayed around a circular tube in six rows. There are a total of 36 air outlets with 6 outlets in each row of 5 mm diameter each. Reactor preheating was achieved by using auxiliary fuel. Flue gas exits the top of the freeboard and enters into a cyclone.

III. EXPERIMENTAL PROCEDURE

The task of heating the inert material is fulfilled by the pre-heating system. This was done by introducing the auxiliary flame directly into the combustion chamber. When the bed temperature reaches approximately 450°C, fuel was fed by a screw type feeder at the rate of 79 g/min. Emissions readings were then taken when the bed temperature stabilizes at approximately 950°C and above. Air staging is achieved by dividing the total combustion air supply for stoichiometric

operation into the primary air (in bed fluidizing air) and secondary air. Secondary air was introduced at 400 mm above the distributor plate with a 9.55 mm internal diameter stainless steel tube. The air staging experiments were performed with the secondary air to total air ratio varied from 0 to 0.2 at 0.1 increments.

TABLE I
FUEL COMPOSITIONS [8]

Type of fuel	Palm Shell	Palm Fiber
Proximate analysis (% by mass)		
Moisture content	12.15	13.98
Ash content	1.96	3.63
Volatile matter	79.22	84.78
Fixed carbon	18.82	11.59
Ultimate analysis (% by mass)		
Carbon, C	47.978	50.091
Oxygen, O	45.781	41.147
Hydrogen, H	5.487	6.247
Nitrogen, N	0.714	2.385
Sulphur, S	0.04	0.13
Other characteristics		
Net calorific value (MJ/kg)	18.84	17.64
Gross calorific value (MJ/kg)	21.44	19.6

IV. RESULT AND DISCUSSION

4.1. Temperature Distributions

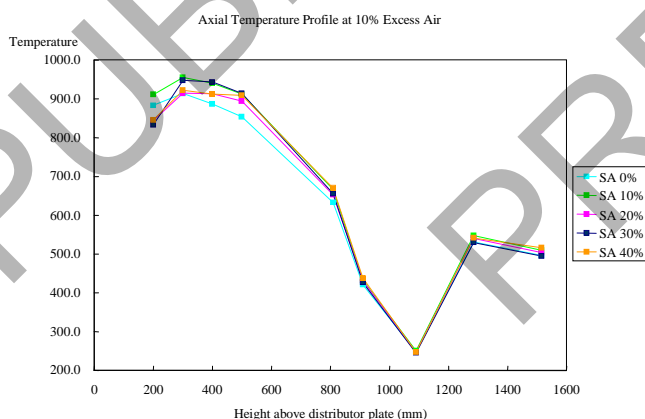


Figure 2. Temperature profile of Palm Shell for 10% Excess Air

Increasing the degree of secondary air tend to decrease temperature distributions along the FBC height, are showed in Fig. 2, 3, 4, 5. Increasing the proportion of secondary air in the combustor reduces flame temperatures and reduced the residence time due to the local air velocity increase which increases particles carry-over and volatiles speed.

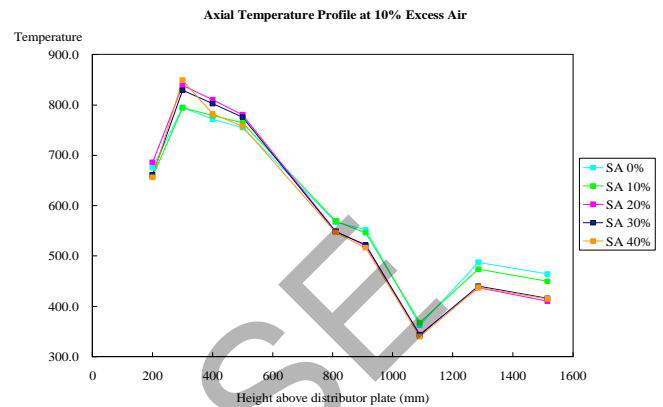


Figure 3. Temperature profile of Palm Fiber for 10% Excess Air

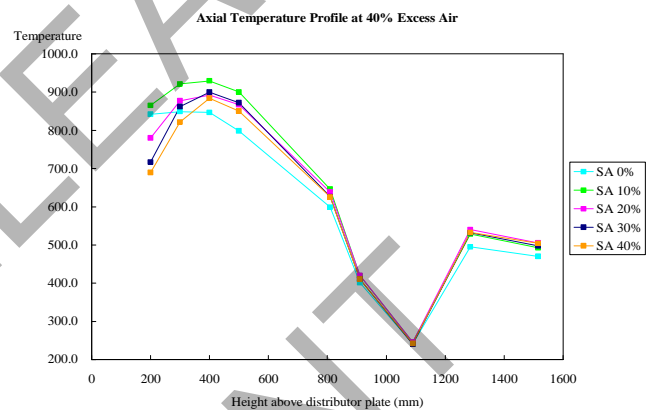


Figure 4. Temperature profile of Palm Shell for 40% Excess Air

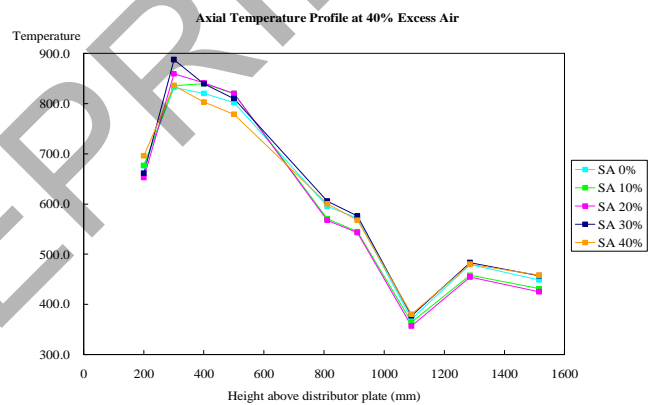


Figure 5. Temperature profile of Palm Fiber for 40% Excess Air

4.2. CO Emission

Figures 6, 7 show that the CO emission decreases with the increase of the secondary air to total air ratio. For palm shell the emission decreases at 30% secondary air (SA) and for palm fiber the emission decreases and at 20% SA.

Also (has been studied) the effect of excess air (EA) on formation and reduction of CO in a Fluidized-bed Combustor Fired with Thai Rice Husk, that CO emission decreases with increasing excess air.

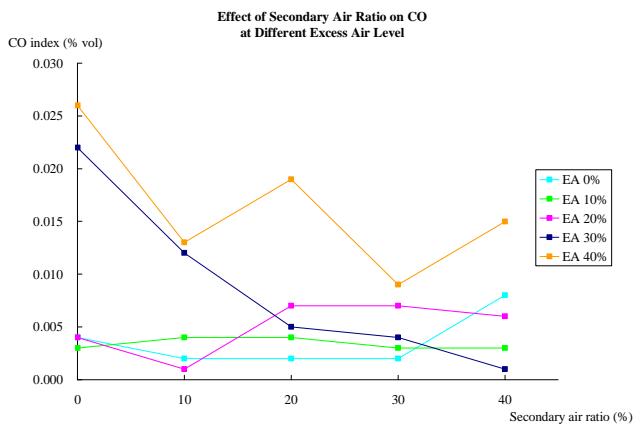


Fig.6. Effect Secondary Air Ratio on CO Emission of Palm Shell

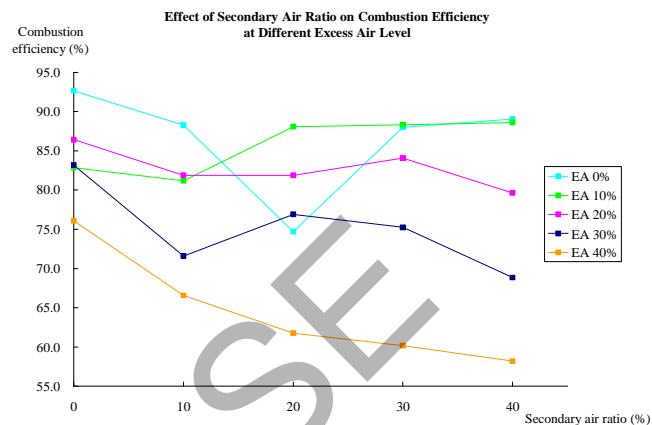


Fig.9. Effect Secondary Air Ratio on Combustion Efficiency of Palm Fiber

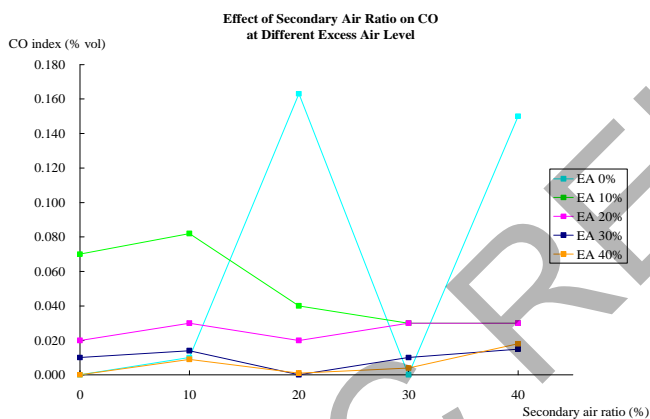


Fig.7. Effect Secondary Air Ratio on CO Emission of Palm Fiber

4.3. Combustion Efficiency

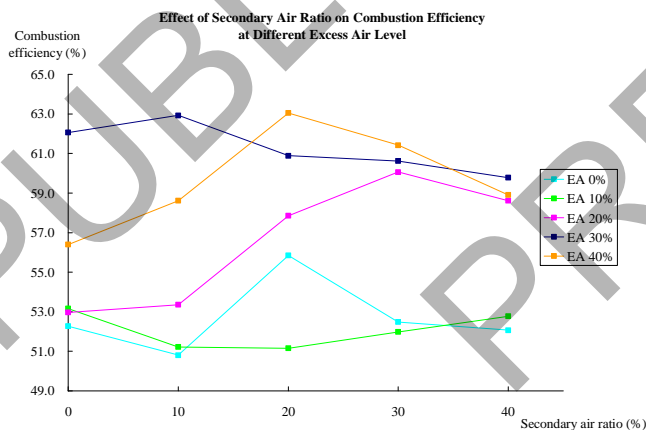


Fig.8. Effect Secondary Air Ratio on Combustion Efficiency of Palm Shell

From the results of our experiments, it was also observed that increasing the degree of air staging has the effect of increasing the combustion efficiency, especially for SA 20%, 30% and 40%, shown in Figure 8 and 9.

The combustion efficiency maximum for palm shell is 63% and for palm fiber is 89%.

V. CONCLUSIONS

Experiments on the combustion of palm shell and palm fiber have been successfully carried out in a laboratory scale fluidized bed combustor using the air staging technique. The following conclusions can be drawn.

- The axial temperature profiles decrease along the FBC height.
- The use of air staging is beneficial for the reduction of CO emission from a fluidized bed combustor.
- The combustion efficiency is also seen to increase with increased air staging.
- The palm wastes combustion give significant contribution for reduction of CO emission from combustion process.

ACKNOWLEDGMENT

We gratefully acknowledged the financial assistance from Institutional Grant Universiti Teknologi Malaysia.

REFERENCES

- [1] Wahlund, Bertil. "Rational Bioenergy Utilisation in Energy Systems and Impacts on CO₂ Emissions". *Doctoral Thesis. Department of Chemical Engineering and Technology Energy Processes*, Royal Institute of Technology, 2003.
- [2] Nussbaumer T. "Combustion and Co-combustion of Biomass". *12th European Conference and Technology Exhibition on Biomass for Energy, Industry and Climate Protection*. June 17-12, Amsterdam, 2002.
- [3] Slupek S., M. Poskart, L. Szcwoka. "Reduction of NO_x in Natural Gas Flame using Biomass as Reburning Fuel". *The seventh Asia-Pacific International Symposium and energy Utilization*, December 15-17, Hong Kong SAR, 2004.
- [4] Prasertsan, S. and Prasertsan, P. "Biomass Residues from Palm Oil Mills in Thailand: An Overview on Quantity and Potential Usage." *Biomass and Bioenergy*, 1996, 11(5), pp 387-395.

- [5] Barlow, C., Zen, Z., and Gondowarsito, R. "The Indonesian Oil Palm Industry". *International Oil Palm Study Group*, 2003.
- [6] Kaewklum, R, et al., "Influence of Fuel-moisture Content and Excess Air on Formation and Reduction of CO and NO in a Fluidized-bed Combustor Fired with Thai Rice Husk", *Proceeding of The 2nd Joint International Conference on "Sustainable Energy and Environment (SEE 2006)"*, 21-23 November, Bangkok, Thailand , 2006.
- [7] Gibbs, B.M., Pereira, F.J. and Beer, J.M., "The Influence of Air Staging On the 'NO' Emission from a Fluidised Bed Coal Combustor". *Chemical Engineering and Fuel Technology Department*, University of Sheffield, England, 1999
- [8] M.R. Taib, L.S. Yang, S.L. Yat Seong, "Palm Wastes Combustion in Bubbling Fluidized Bed". Article, Perpustakaan Sultanah Zanariah, UTM, Malaysia, 2002.

Dynamic Brake Regulator And Protection System in Locomotive

F.Takbiri

Dr.S.Frashad

Iran university of Science and technology

Email: fa_takbiri@rail.iust.ac.ir

Abstract

In this paper, dynamic braking system of locomotive is simulated by ORCAD software. Locomotive dynamic braking is a system which is used to retard locomotive speed through the conversion of kinetic energy to electrical energy. This energy conversion is accomplished by connecting the traction motors as separately excited generators with field current being provided by the main generator. This system consists of two modules DR and DP. Excitation current to the motor fields is controlled by the braking lever position and by the dynamic braking regulator module DR. The dynamic brake protection module DP provides backup protection for the traction motor fields and the dynamic braking resistor grids in case a fault develops in the dynamic braking regulator module DR.

Key words: Dynamic braking system, Regulator, Traction motor, Resistor grid.

1. Introduction

Locomotive dynamic braking is a system which is used to retard locomotive speed through the conversion of kinetic energy to electrical energy. This energy conversion is accomplished by connecting the traction motors as separately excited generators with

field current being provided by the main generator. The motor armatures are geared

to the axels and rotate whenever the locomotive is moving. Loading is provided by connecting the traction motor armature circuits to dynamic braking grids. Armature current is determined by the speed at which the armature rotate and by the amounts of excitation applied to the motor fields.

With maximum field excitation braking effort increases from minimum at zero miles per hour to maximum at approximately 24 miles per hour. Maximum braking effort for the lower braking lever position is progressively lower and is attained at progressively higher track speed as the braking lever position is decreased. After maximum braking effort is attained, an increase in track speed results in a decrease in braking effort.

The amount of kinetic energy that is converted into electrical energy is proportional to RI^2 Where I is braking grid current and R is the effective resistance of the braking grids. The increase in braking effort from zero to maximum results from increased motor armature grid current as track speed increases. This results in an

increase of RI^2 and consequently an increase in braking horsepower.

Excitation current to the motor fields is controlled by the braking lever position and by the dynamic braking regulator module DR. The DR module operates to limit the excitation current to a value that prevent armature or grid current from increasing above the maximum safe current carrying capacity of the braking grid. The dynamic brake protection module DP provides backup protection for the traction motor fields and the dynamic braking resistor grids in case a fault develops in the dynamic braking regulator module DR.

2. Dynamic brake protection

The motor field protection circuit, Fig 1, is connected across the main generator, in parallel with the traction motor field, during dynamic braking. Therefore the motor field protection circuit detects any changes in excitation voltage applied to the traction motor field.

During dynamic braking, zener diode Z8, in series with resistor R15 and R19, maintain 6.2 volts on the emitter of transistor Q5. Current flows from terminal 3 of DP module through the voltage divider consisting of resistor R19, R16, R17, R18

Q5 is reverse biased during normal operation. However, if a fault develops in the dynamic braking regulator module DR, the excitation voltage applied to the traction motor fields may tend to rise above a safe value. Transistor Q5 will become forward biased if the excitation voltage rises above a safe value. The collector of Q5 is connected, through R23, to the base of transistor Q6. Turn on of Q5 causes Q6 to be forward biased. Turn on of Q6 causes current to flow through the LED portion of opto-isolator

O11. This increases the collector current of photosensitive transistor portion of O11. This collector current is applied to the base of transistor Q7, causing Q7 to be forward biased. Turn on of Q7 energizes the motor

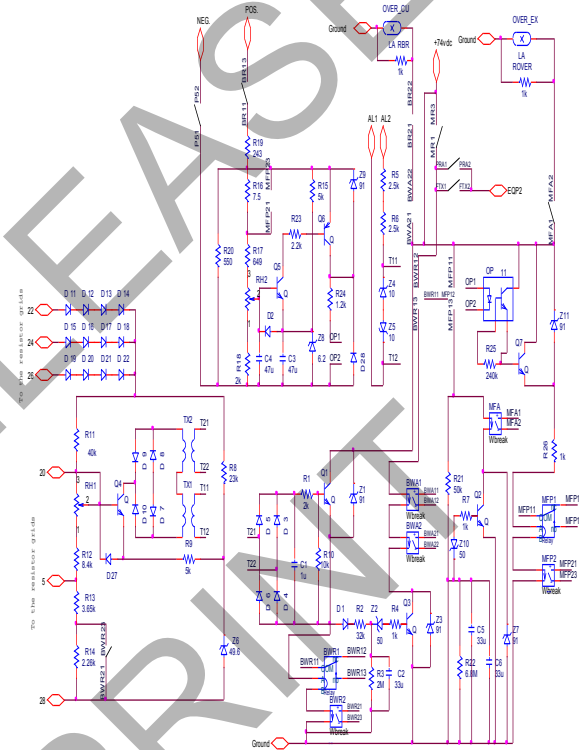


Fig1. DP module

field protection relay MFP. Pickup of MFP drops the feed to the equipment protection relay EQP and recalibrates the motor field protection circuit by shorting out resistor R16. Pickup of MFP also provides a positive feed to the motor field annunciator relay MFA and to the time delay circuit consisting of R21, R22, C5, and C6.

Drop out EQP drops the feed to the generator field contactor GFC which removes excitation voltage from the main generator field and this decreases the main generator output voltage. The inductance of the main generator field windings prevents an immediate collapse of current through the field. The decrease in main generator output Voltage results in a reduction in the voltage

applied to the base of Q5. This reduction in voltage causes Q5 to become reverse biased. Reverse bias on Q5 causes MFP to drop out. Dropout of MFP reestablishes the feed to EQP and results in reapplying excitation voltage to main generator field.

3. Dynamic brake regulator

Voltage signals proportional to current through grids with basic dynamic brakes, Fig 2, are applied to left port of circuit. The larger of these signals is applied between receptacles 1 and 13 of the DR module. The signal applied between terminal 13 and 1 is applied to a voltage divider consisting of rheostat RH1 and resistor R1, R2, R3, and R4. This same voltage is also applied to resistor R7 in series with zener diodes Z1 through Z9. The zener diodes provides a constant reference signal to the emitter of Q2.

A signal proportional to braking grid current is applied to the base of transistor Q1 by a voltage divider consisting of R5 and R6 connected between the wiper arm of RH1 and the emitter of Q2. When braking grid current rises above 600 amperes, the voltage at the wiper arm of RH1 is larger than the reference signal applied to the emitter of Q2. This causes current flow from the wiper arm of RH1 to the zener diodes. This current flow results in placing forward bias on Q1 and Q2. With forward bias on Q1 and Q2, current flows through the secondary winding of transformer T1-A and the primary winding of transformer T2-A, then from collector to emitter of Q1 and Q2. This current induces a voltage into the secondary T2-A. this voltage is rectified and applied to a voltage divider consisting of R8 and R9. Transistor Q3 is forward biased by the voltage developed across R9.

With forward bias on Q3, the braking lever signal is removed from the circuit of field. As a result, excitation to main generator

field decreases. When braking grid current decreases below 600 amperes, the signal at wiper arm of RH1 decreases and place a reverse bias on Q1 and Q2.

4. Basic dynamic brakes with trainlined grid current control

Output voltage of companion alternator is applied to the primary of transformer T4 in series with brake current transductor BCT. When braking current is low, the reactance of BCT is high and the voltage applied to primary of T4 is low. As braking grid current increases, the output voltage of T4 is applied between terminal 9 and 11. A voltage which is proportional to the braking lever signal, as determined by the braking lever position, is applied to terminal 7 of DR module.

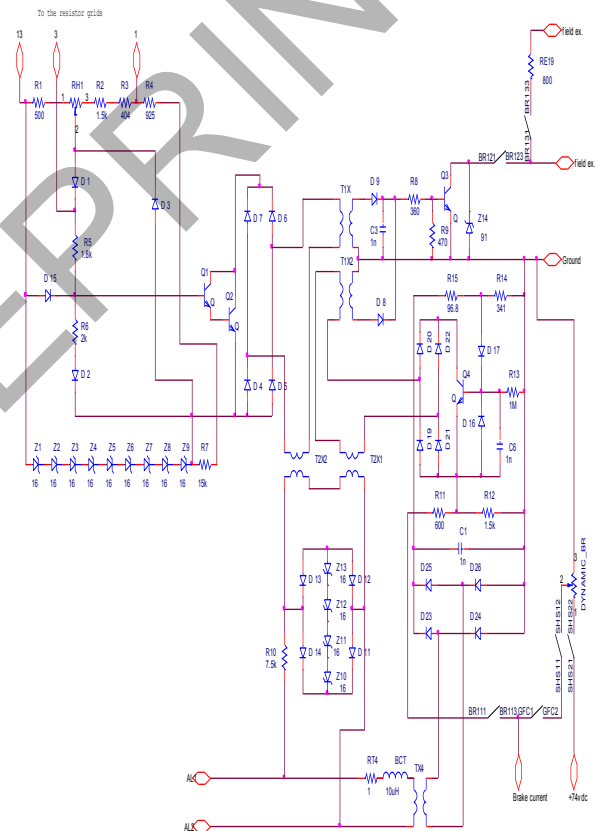


Fig2. DR module

Transistor Q4 compares the braking lever signal with the braking grid current signal. Q4 is forward biased if braking grid current increases above the braking lever signal. Turn on of Q4 provides a path for current flow through transformer T1-B secondary and T2-B primary. The output of T2-B is rectified and applied to a voltage divider consisting of R8 and R9. Forward bias on Q3 results in decreasing of excitation to the main generator field.

5. Simulation results

The simulation results applying voltage to the modules are shown in following figures:

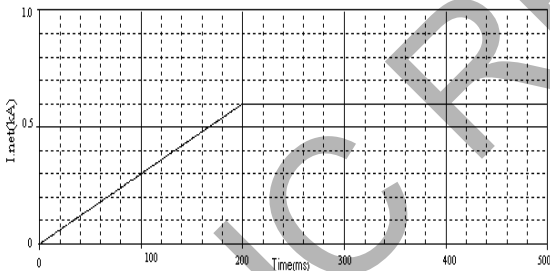


Fig3.resistor network current

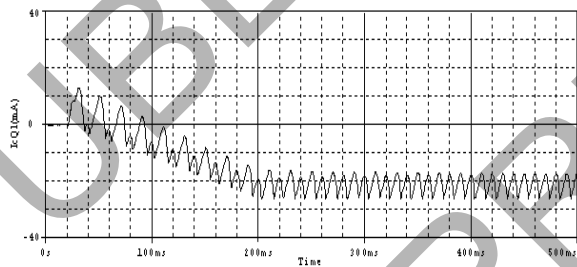


Fig4. Collector current of Q1

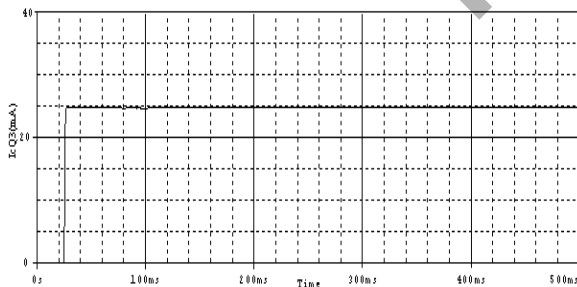


Fig5. Collector current of Q3

6. References

- [1] GT26CW-2 locomotive service manual.
- [2] Painter, T.D.; Barkan, C.P.L.; 'Prospects for dynamic brake energy recovery on North American freight locomotives'. 4-6 April 2006 Page(s):181 - 188 .IEEE CNF
- [3] Grobovoy, A.A.; Denisova, D.V.; Bondareva, N.V.; Kuznetsova, N.Y.; 'A fuzzy logic transmission system dynamic braking control'. 27-30 June 2005 Page(s):1 - 7. IEEE CNF
- [4] Cochran, Paul; 'Calculation of Dynamic Braking Characteristics of Wound Rotor Induction Motors'. Volume 72, Part III, Jan. 1953 Page(s):992 - 996. IEEE JNL
- [5] Al-Bahrani, A.H.; Malik, N.H.; ' Selection of the excitation capacitor for dynamic braking of induction machines'. Volume 140, Jan. 1993 Page(s):1 - 6. IET JNL
- [6] Joshi, Pradip Raghunath; Dubey, G. K.; 'Optimum DC Dynamic Braking Control of an Induction Motor Using Thyristor Chopper Controlled Resistance'. Volume IECI-21, May 1974 Page(s):60 - 65. IEEE JNL
- [7] Rahim, A.H.M.A.; Alamgir, D.A.H.; ' A closed-loop quasi-optical dynamic braking resistor and shunt reactor control strategy for transient stability [of synchronous generator]'. Volume 3, Aug. 1988 Page(s):879 - 886. IEEE JNL
- [8] Erdman, William L.; 'Dynamic Braking of DC Machines: A Mathematical Approach'. Volume IA-19, Part I, May 1983 Page(s):388 - 392. IEEE JNL
- [9] Hernandez, J.M.; Moreno, R.A.P.; 'Design of a variable speed drive with dynamic braking for induction motor for electric vehicles'. 15-19 Oct. 2000 Page(s):211 - 214. IEEE CNF
- [10] Croft, W. H.; Hartley, R. H.; ' Improving Transient Stability by Use of Dynamic Braking'. Volume 81, April 1962 Page(s):17 - 24. IEEE JNL

Lightning Phenomenon – Introduction and Basic Information to Understand the Power of Nature

Łukasz Staszewski
University of Technology
Wybrzeże Wyspińskiego 27
Wrocław, Poland

This paper introduces the history of lightning researches, some hypothesis of lightning forming process, types of lightning and triggering ways.

I. INTRODUCTION

Benjamin Franklin (1706-1790)[1] endeavored to test the theory that sparks shared some similarity with lightning using a spire which was being erected in Philadelphia. While waiting for completion of the spire, he got the idea of instead using a flying object, such as a kite. During the next thunderstorm, which was in June 1752, it was reported that he raised a kite, accompanied by his son as an assistant. On his end of the string he attached a key, and he tied it to a post with a silk thread. As time passed, Franklin noticed the loose fibers on the string stretching out; he then brought his hand close to the key and a spark jumped the gap. The rain which had fallen during the storm had soaked the line and made it conductive.

Although experiments from the past time of Benjamin Franklin showed that lightning was a discharge of static electricity, there was little improvement in theoretical understanding of lightning (in particular how it was generated) for more than 150 years. The impetus for new research came from the field of power engineering: as power transmission lines came into service, engineers needed to know much more about lightning in order to adequately protect lines and equipment.

Nowadays lightning is considered as an atmospheric discharge of electricity, which typically occurs during thunderstorms, and sometimes during volcanic eruptions or dust storms. In the atmospheric electrical discharge, a leader of a bolt of lightning can travel at speeds of 60,000 m/s (220,000 km/h), and can reach temperatures approaching 30,000 °C (54,000 °F), hot enough to fuse silica sand into petrified lightning, known scientifically as glass channels[2] or fulgurites which are normally hollow and can extend some distance into the ground. There are some 16 million lightning storms in the world every year.

How lightning initially forms is still a matter of debate. Scientists have studied root causes ranging from atmospheric perturbations (wind, humidity, friction, and atmospheric pressure) to the impact of solar wind and accumulation of charged solar particles. Ice inside a cloud is thought to be a key element in lightning development, and may cause

a forcible separation of positive and negative charges within the cloud, thus assisting in the formation of lightning.

II. FORMING PROCESS[3]

1) Charge separation – the first process in the generation of lightning. There are two hypothesis describing the process:

– POLARIZATION MECHANISM HYPOTHESIS

The mechanism by which charge separation happens is still the subject of research, but one hypothesis is the polarization mechanism, which has two components:

- a) Falling droplets of ice and rain become electrically polarized as they fall through the atmosphere's natural electric field;
- b) Colliding ice particles become charged by electrostatic induction.

Ice and super-cooled water are the keys to the process. Violent winds buffet tiny hailstones as they form, causing them to collide. When the hailstones hit ice crystals, some negative ions transfer from one particle to another. The smaller, lighter particles lose negative ions and become positive; the larger, more massive particles gain negative ions and become negative.



Figure 1. Lighting discharge.

– ELECTROSTATIC INDUCTION HYPOTHESIS

According to the electrostatic induction hypothesis charges are driven apart by as-yet uncertain processes. Charge separation appears to require strong updrafts which carry water droplets upward, super-cooling them to between -10 and -20 °C. These collide with ice crystals to form a soft ice-water mixture called graupel.^a The collisions result in a slight positive charge being transferred to ice crystals, and a slight negative charge to the graupel. Updrafts drive lighter ice crystals upwards, causing the cloud top to accumulate increasing positive charge. The heavier negatively charged graupel falls towards the middle and lower portions of the cloud, building up an increasing negative charge. Charge separation and accumulation continue until the electrical potential becomes sufficient to initiate lightning discharges, which occurs when the gathering of positive and negative charges forms a sufficiently strong electric field.

There are several additional hypotheses for the origin of charge separation.

According to one such hypothesis, charge separation is initiated by the ionization of an air molecule by an incoming cosmic ray.

^a snow pellets

2) Leader Formation

As a thundercloud moves over the Earth's surface, an equal but opposite charge is induced in the Earth below, and the induced ground charge follows the movement of the cloud.

An initial bipolar discharge, or path of ionized air, starts from a negatively charged mixed water and ice region in the thundercloud. The discharge ionized channels are called leaders. The negative charged leaders, called a "stepped leader", proceed generally downward in a number of quick jumps, each up to 50 meters long. Along the way, the stepped leader may branch into a number of paths as it continues to descend. The progression of stepped leaders takes a comparatively long time (hundreds of milliseconds) to approach the ground. This initial phase involves a relatively small electric current (tens or hundreds of amperes), and the leader is almost invisible compared to the subsequent lightning channel.

When a stepped leader approaches the ground, the presence of opposite charges on the ground enhances the electric field. The electric field is highest on trees and tall buildings. If the electric field is strong enough, a conductive discharge (called a positive streamer) can develop from these points. This was first theorized by Heinz Kasimir. As the field increases, the positive streamer may evolve into a hotter, higher current leader which eventually connects to the descending stepped leader from the cloud. It is also possible for many streamers to develop from many different objects simultaneously, with only one connecting with the leader and forming the main discharge path. Photographs have been taken on which non-connected streamers are clearly visible. When the two leaders meet, the electric current greatly increases. The region of high current propagates back up the positive stepped leader into the cloud

with a "return stroke" that is the most luminous part of the lightning discharge.

3) Discharge

When the electric field becomes strong enough, an electrical discharge (the bolt of lightning) occurs within clouds or between clouds and the ground. During the strike, successive portions of air become a conductive discharge channel as the electrons and positive ions of air molecules are pulled away from each other and forced to flow in opposite directions.

The electrical discharge rapidly superheats the discharge channel, causing the air to expand rapidly and produce a shock wave heard as thunder. The rolling and gradually dissipating rumble of thunder is caused by the time delay of sound coming from different portions of a long stroke.

a) Gurevich's runaway breakdown theory[4]

A theory of lightning initiation, known as the "runaway breakdown theory", proposed by Aleksandr Gurevich of the Lebedev Physical Institute in 1992 suggests that lightning strikes are triggered by cosmic rays which ionize atoms, releasing electrons that are accelerated by the electric fields, ionizing other air molecules and making the air conductive by a runaway breakdown, then "seeding" a lightning strike.

b) Gamma rays and the runaway breakdown theory

It has been discovered in the past 15 years that among the processes of lightning is some mechanism capable of generating gamma rays, which escape the atmosphere and are observed by orbiting spacecraft. Brought to light by NASA's Gerald Fishman in 1994 in an article in Science, these so-called Terrestrial Gamma-Ray Flashes (TGFs) were observed by accident, while he was documenting instances of extraterrestrial gamma ray bursts observed by the Compton Gamma Ray Observatory (CGRO). TGFs are much shorter in duration, however, lasting only about 1 ms.

Professor Umran Inan of Stanford University linked a TGF to an individual lightning stroke occurring within 1.5 ms of the TGF event, proving for the first time that the TGF was of atmospheric origin and associated with lightning strikes.

CGRO recorded only about 77 events in 10 years; however, more recently the RHESSI spacecraft, as reported by David Smith of UC Santa Cruz, has been observing TGFs at a much higher rate, indicating that these occur about 50 times per day globally (still a very small fraction of the total lightning on the planet). The voltage levels recorded exceed 20 MeV.

Scientists from Duke University have also been studying the link between certain lightning events and the mysterious gamma ray emissions that emanate from the Earth's own atmosphere, in light of newer observations of TGFs made by RHESSI. Their study suggests that this gamma radiation fountains upward from starting points at surprisingly low altitudes in thunderclouds.

Steven Cummer, from Duke University's Pratt School of Engineering, said, 'These are higher energy gamma rays than

come from the sun. And yet here they are coming from the kind of terrestrial thunderstorm that we see here all the time'.

Early hypotheses of this pointed to lightning generating high electric fields at altitudes well above the cloud, where the thin atmosphere allows gamma rays to easily escape into space, known as 'relativistic runaway breakdown', similar to the way sprites are generated. Subsequent evidence has cast doubt, though, and suggested instead that TGFs may be produced at the tops of high thunderclouds. Though hindered by atmospheric absorption of the escaping gamma rays, these theories do not require the exceptionally high electric fields that high altitude theories of TGF generation rely on.

The role of TGFs and their relationship to lightning remains a subject of ongoing scientific study.

4) Re-strike [5]

High speed videos (examined frame-by frame) show that most lightning strikes are made up of multiple individual strokes. A typical strike is made of 3 to 4 strokes. There may be more.

Each re-strike is separated by a relatively large amount of time, typically 40 to 50 milliseconds. Re-strikes can cause a noticeable "strobe light" effect.

Each successive stroke is preceded by intermediate dart leader strokes again to, but weaker than, the initial stepped leader. The stroke usually re-uses the discharge channel taken by the previous stroke.

The variations in successive discharges are the result of smaller regions of charge within the cloud being depleted by successive strokes.

The sound of thunder from a lightning strike is prolonged by successive strokes.

III. TYPES OF LIGHTNING

Some lightning strikes take on particular characteristics; scientists and the public have given names to these various types of lightning. Most lightning is streak lightning. This is nothing more than the return stroke, the visible part of the lightning stroke. Because most of these strokes occur inside a cloud, we do not see many of the individual return strokes in a thunderstorm.

The return stroke of a lightning bolt, which is the visible bolt itself, follows a charge channel only about a half-inch (1.3 cm) wide. Most lightning bolts are about a mile (1.6 km) long[6].

– CLOUD-TO-CLOUD LIGHTNING

Lightning discharges may occur between areas of cloud having different potentials without contacting the ground. These are most common between the anvil and lower reaches of a given thunderstorm. This lightning can sometimes be observed at great distances at night as so-called "heat lightning". In such instances, the observer may see only a flash of light without thunder. The "heat" portion of the term is



Figure 2. Cloud-to-cloud lightning.

a folk association between locally experienced warmth and the distant lightning flashes.

Another terminology used for cloud-cloud or cloud-cloud-ground lightning is "Anvil Crawler", due to the habit of the charge typically originating from beneath or within the anvil and scrambling through the upper cloud layers of a thunderstorm, normally generating multiple branch strokes which are dramatic to witness. These are usually seen as a thunderstorm passes over you or begins to decay. The most vivid crawler behavior occurs in well developed thunderstorms that feature extensive rear anvil shearing.

– DRY LIGHTNING[7]

Dry lightning is a term in the United States for lightning that occurs with no precipitation at the surface. This type of lightning is the most common natural cause of wildfires.

– ROCKET LIGHTNING

It is a form of cloud discharge, generally horizontal and at cloud base, with a luminous channel appearing to advance through the air with visually resolvable speed, often intermittently. It is also one of the rarest of cloud discharges.



Figure 3. Multiple paths cloud-to-cloud lightning.



Figure 4. Lightning triggered by a volcanic materials thrust high into atmosphere.

– CLOUD TO GROUND LIGHTNING

Cloud-to-ground lightning is a great lightning discharge between a cumulonimbus cloud and the ground initiated by the downward-moving leader stroke. This is the second most common type of lightning, and poses the greatest threat to life and property of all known types.

– BEAD LIGHTNING

Bead lightning is a type of cloud-to-ground lightning which appears to break up into a string of short, bright sections, which last longer than the usual discharge channel. It is fairly rare. One of theories is the observer sees portions of the lightning channel end on, and that these portions appear especially bright.

– RIBBON LIGHTNING

Ribbon lightning occurs in thunderstorms with high cross winds and multiple return strokes. The wind will blow each successive return stroke slightly to one side of the previous return stroke, causing a ribbon effect.

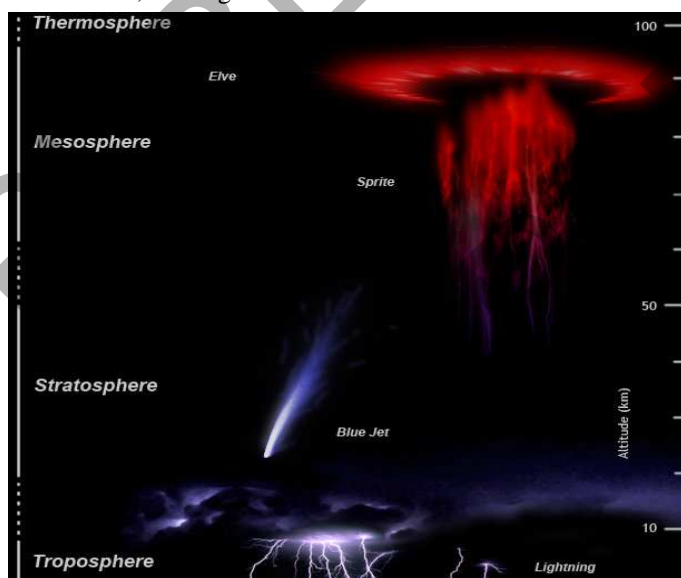


Figure 5. Representation of upper-atmospheric lightning and electrical-discharge phenomena.

– GROUND-TO-CLOUD LIGHTNING

Ground-to-cloud lightning is a lightning discharge between the ground and a cumulonimbus cloud from an upward-moving leader stroke.

– BALL LIGHTNING[8]

Ball lightning is described as a floating, illuminated ball that occurs during thunderstorms. They can be fast moving, slow moving or nearly stationary. Some make hissing or crackling noises or no noise at all. Some have been known to pass through windows and even dissipate with a bang. Ball lightning has been described by eyewitnesses but rarely recorded by meteorologists.

– UPPER-ATMOSPHERIC LIGHTNING[9]

Reports by scientists of strange lightning phenomena above storms date back to at least 1886. However, it is only in recent years that fuller investigations have been made. This has sometimes been called mega-lightning.

IV. TRIGGERING OF LIGHTNING

– ROCKET-TRIGGERED

Lightning has been triggered directly by human activity in several instances. Lightning struck Apollo 12 soon after takeoff. It has also been triggered by launching lightning rockets carrying spools of wire into thunderstorms. The wire unwinds as the rocket ascends, providing a path for lightning. These bolts are very straight due to the path created by the wire.

– VOLCANICALLY TRIGGERED[10]

Extremely large volcanic eruptions, which eject gases and material high into the atmosphere, can trigger lightning. This phenomenon was documented by Pliny The Elder during the AD79 eruption of Vesuvius, in which he perished.

– LASER TRIGGERED[11]

Since the 1970s, researchers have attempted to trigger lightning strikes on demand. Such triggered lightning is intended to protect rocket launching pads, electric power facilities, and other sensitive targets.

Researchers generated filaments^b that lived too short a period to trigger a real lightning strike. Nevertheless, a boost in electrical activity within the clouds was registered.

^b channel of ionized molecules

REFERENCES

- [1] <http://www.meteohistory.org/2004proceedings1.1/pdfs/01krider.pdf>
- [2] <http://plaza.ufl.edu/rakov/Gas.html>
- [3] http://science.nasa.gov/headlines/y2006/13sep_electricice.htm
- [4] http://en.wikipedia.org/wiki/Runaway_breakdown.
- [5] Martin A. Uman (1986). *All About Lightning*. Dover Publications, Inc.. pp. 103–110. ISBN 0-486-25237-X
- [6] <http://www.weatherquesting.com/skinny-lightning.htm>
- [7] http://en.wikipedia.org/wiki/Dry_lightning.
- [8] http://en.wikipedia.org/wiki/Ball_lightning.
- [9] http://en.wikipedia.org/wiki/Upper-atmospheric_lightning.
- [10] <http://www.ngdc.noaa.gov/hazard/stratoguide/galunfeat.html>
- [11] <http://newswise.com/articles/view/539709/>

Signal Processing Techniques used in Power Quality Monitoring

Umar Naseem Khan

Abstract— This paper gives a general review of different signal processing techniques which are widely used for the power quality monitoring. The majority of power quality problems can be characterized through measurements of voltage and current. To distinguish the type of disturbances, monitoring systems require the processing of signals, which concern the extraction of features and information from measured digital signals. In fact, the use of signal processing techniques can influence the way that voltage and current signals are measured and analyzed in power system field.

Index Terms—power quality, signal processing, power quality monitoring, disturbances, variations, events

I. INTRODUCTION

As it is well known, an ideal three-phase AC supply consists of three phase voltages that are 120 degrees out of phase and have identical magnitudes. Above all, these voltages should be sinusoidal and should be available continuously. Any diversion from these requirements is considered as poor quality of power. One of the major causes of disturbances in AC power system is the electronic switching circuits, which are widely used both in industry and in household systems. Most of the power electronic equipments are manufactured based on the available standards, but due to increase in the numbers of such equipments there are also an increase in disturbances in the power system. While the sources of disturbances in AC power systems increase continuously, the electric utilities and end users of electrical power have become more concerned about the quality issues of the AC power.

The research focuses on power quality monitoring systems are very much involved in the studies of signal-processing techniques applied to the monitored signals to extract valuable information for analyzing and diagnosing the cause of power quality problems. The analysis of this information then help the power quality experts to determine the sources and causes of such events and, thus, possible solutions for avoiding these disturbances can be identified.

The monitoring practice of power quality includes three steps, detecting and extracting the features of the power quality events, classifying these events into known waveform categories, and, if the size of the monitored data is very large, compression methods will be necessary for saving these data for further analysis.

A. Variations and Event

An important division of power quality disturbances is between variations and events. Variations are small deviations

from the normal or desired voltage or current sine wave that can be measured at predefined instances (or more precisely over predefined windows of time), whereas events are larger disturbances that trigger a recording or further processing [1].

The most common origin of variations are: voltage frequency variations, voltage magnitude variations; unbalance; voltage fluctuations or flicker and waveform distortion. While most common origins of events are interruptions, voltage dips, and transients.

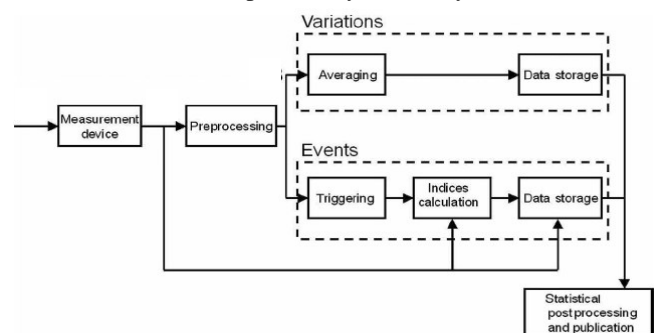
The issues to be discussed when measuring power quality variations include: (1) extracting the characteristics; (2) statistics to quantify the performance of the supply at one location; (3) statistics to quantify the performance of a whole system [1].

The issues to be discussed when measuring events include: (1) a method has to be defined to obtain the voltage magnitude from the sampled waveform; (2) threshold levels have to be set for the beginning threshold and for the ending threshold, these two thresholds could be the same or different. In addition, a value has to be chosen for the minimum duration of interruption; (3) characteristics have to be defined for the event, in this case the duration of the interruption [1].

A general scheme for carrying out power quality measurements is shown in Fig. 1. The first step in power quality monitoring is the transformation from analog voltages and currents in the power system to sampled digital values that can be processed automatically. The measurement device block in Fig 1 includes instrument transformers, analog anti-aliasing filters, sampling and digitizing, and digital anti-aliasing and down sampling. In this paper, our concentration will be focused on post processing and we will assume that the sampled and digitized voltage or current waveforms are available for processing.

II. DETECTION METHODS OF POWER QUALITY DISTURBANCES

The disturbance capturing techniques are usually based on detecting the power quality events when a certain threshold level is exceeded. The limits and threshold levels are primarily defined by the standards that provide the acceptable level of disturbance in AC power systems by the end users.



Umar Naseem Khan is with the Faculty of Electrical Engineering, Wrocław University of Technology, Wrocław 50-370, Poland (e-mail: umar.naseem@gmail.com).

Figure 1. General scheme for power quality measurements

These methods are divided in two main categories: Detection methods of variations and detection methods of events. Before, going further it is important to know about the stationary and non-stationary signals.

Stationary Signals: A signal is stationary when it is statistical time invariant (or the statistics of the signal are independent of time) [1]. All the variations in the voltage and current sine wave are among the stationary signals.

Non-stationary Signals: If a signal is statistical time varying, then it is a non-stationary signal.

A. Root Mean Square value (RMS)

The RMS of a signal is not an analysis technique in its own right, but it gives some basic information about an electrical system, and is used widely. The main disadvantage of this algorithm is its dependence on the size of the sample window. A small window makes the RMS parameter less relevant, as it follows the tendency of the temporal signal, and loses the meaning of mean value of power. A large window hides the events [3].

The deviation of the voltage or current signal from the ideal sine wave is characterized through a number of parameters (or features): magnitude, frequency, distortion, unbalance, Flicker Severity and very short variations. We will briefly discuss the different detection methods for these parameters.

1) Voltage Magnitude Variations

The vast majority of voltage (magnitude) variation studies use the rms value to quantify the voltage magnitude. In IEC 61000-4-30, a basic measurement window of 10 or 12 cycles (in 50- and 60-Hz systems, respectively) is prescribed: The measurement window shall be synchronized to the actual power system frequency. Non-synchronization leads to a small error in the estimated rms value, where the relative error in rms value is half the relative error in frequency. A number of alternative methods are introduced: among others, voltage amplitude, fundamental component, instantaneous three-phase rms, and positive-sequence voltage. The latter two values are suitable alternatives in a three-phase system.

For monitoring purpose, the point-by-point RMS values of PQ signals have to be calculated, which is defined as

$$V_{rms}(n_k + i) = \sqrt{\frac{1}{n_k} \sum_{k=i}^{n_k+i} v[k]^2} \quad (1)$$

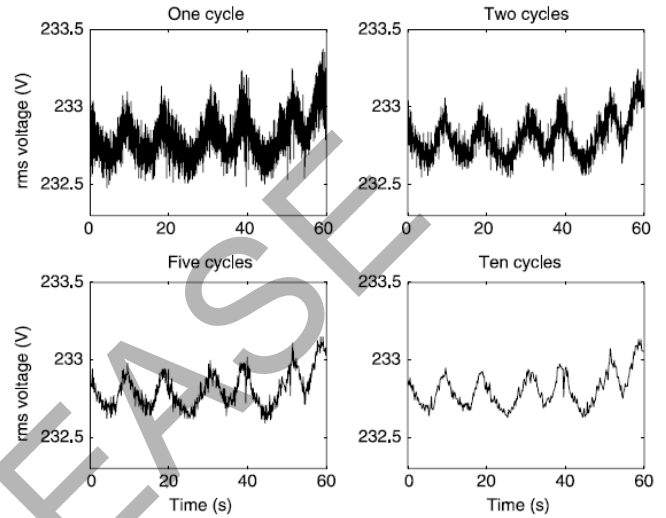
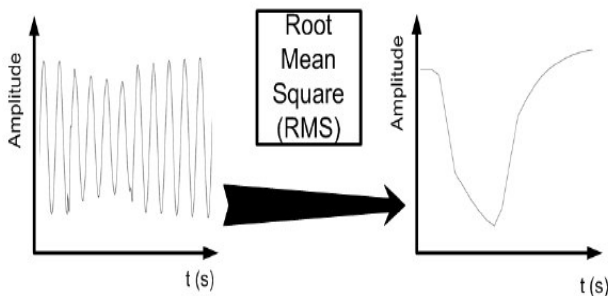


Figure 3. Effect of window size on the rms voltage-time waveform [1]

The effect of changing the length of the window is shown in Fig 3 for a 1-min window of the phase a voltage of the normal case. In all four cases, one value per window has been calculated. For a one- or two-cycle window, the rms voltage has a more noisy appearance. Applying a longer window gives a more smooth function of time.

For the three-phase measurement, three methods are mostly used:

Average of the magnitude values of the three phases:

$$V = \text{mean}(V_a, V_b, V_c) \quad (2)$$

The rms value of the amplitudes from three phases:

$$V = \sqrt{\frac{1}{3}(V_a^2 + V_b^2 + V_c^2)} \quad (3)$$

The absolute value of the positive-sequence voltage:

$$V = |V_p| \quad (4)$$

The instantaneous three-phase rms:

$$V = \sqrt{\frac{1}{3}(v_a^2(t) + v_b^2(t) + v_c^2(t))} \quad (5)$$

2) Voltage Frequency Variations

The standard method to characterize frequency variations consists of counting the voltage zero crossings during a time-period with an accurately known length (10 s according to IEC 61000-4-30). The high accuracy of this method is based on the very high accuracy for time measurements. The high accuracy that can be obtained by the standard method also limits the need for more advanced methods. Despite this, an alternative method is introduced, based on the dq-transform that is better suited to present short-time changes in frequency.

Use of dq-Transform in Three-Phase System

With most power quality measurements, the three phases or line voltages are available for processing. Despite this, the fre-

quency is typically only obtained from one channel, the so-called reference channel. It is however possible to consider all three phases in the calculation of the frequency by using the dq-transform, the dq-transform is defined as follows:

$$v_{dq}(t) = e^{-j2\pi f_0 t} \frac{1}{\sqrt{2}} (v_a(t)e_a + v_b(t)e_b + v_c(t)e_c) \quad (6)$$

Where,

$$e_a = 1$$

$$e_b = a = -\frac{1}{2} + \frac{j\sqrt{3}}{2}$$

$$e_c = a^2 = -\frac{1}{2} - \frac{j\sqrt{3}}{2}$$

3) Three-Phase Unbalance

The standard method for quantifying three-phase unbalance is as the ratio between negative- and positive-sequence voltage.

$$u_n = \frac{U^-}{U^+} \quad (7)$$

Alternative definitions for the three-phase unbalance are given in a number of IEEE standards. When the fundamental components of the phase-to-phase voltages U_{ab} , U_{bc} , and U_{ca} are known, the unbalance can be calculated from the expression

$$u_n = \sqrt{\frac{1 - \sqrt{3 - 6Q}}{1 + \sqrt{3 - 6Q}}} \quad (8)$$

where

$$Q = \frac{U_{ab}^4 + U_{bc}^4 + U_{ca}^4}{(U_{ab}^2 + U_{bc}^2 + U_{ca}^2)^2}$$

Under IEC 61000-4-30, the basic measurement window used to calculate the unbalance is the same as for voltage magnitude and harmonic distortion: 10 cycles in a 50-Hz system, 12 cycles in a 60-Hz system, about 200 ms in each case. Next to the negative-sequence unbalance, a "zero-sequence unbalance" may be calculated as the ratio between zero- and positive-sequence voltages.

B. Fourier Analysis

One of the most widely used tools in signal processing is Fourier analysis. This consists of the decomposition of the signal into a sum of sinusoidal signals of different frequencies. The signal in the frequency domain is characterized by the angle and the module of each sinusoidal wave. So this analysis can be viewed as a mathematical transformation from the time domain to the frequency domain, as shown in the Fig 4.

The Fourier transform in continuous time of an integrable function f can be expressed as follows:

$$f(\xi) = \frac{1}{\sqrt{2\pi}} \int_{-\infty}^{+\infty} f(x) e^{-j\xi x} dx \quad (9)$$

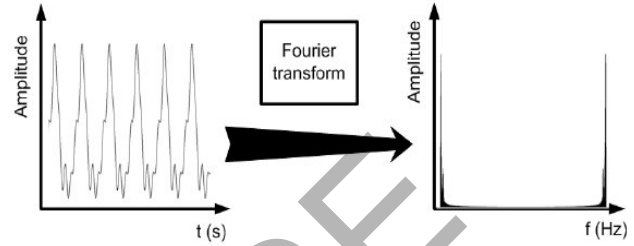


Figure 4. Transformation of time signal in its Fourier Transform

The discrete Fourier transform is thus:

$$f_k = \sum_{n=0}^{N-1} x_n e^{-\frac{2\pi j}{N} kn} \quad (10)$$

where

$$k = 0, \dots, N-1$$

The Fourier Transform is very useful in the analysis of harmonics, and is an essential tool for filter design. However, there are some disadvantages, such as losses of temporal information, so that it can only be used in the steady state, and cannot show the moment when the event is produced.

The DFT (Discrete Fourier Transform) has been applied with great success, thanks to its implementation through its calculus algorithm, FFT (Fast Fourier Transform), which provides very efficient and quick calculations.

C. Short Time Fourier Transform analysis

The short-time Fourier transform-m has been used in power quality analysis due to its applicability to non-stationary signals, as in the case of most power quality signals [3]. The advantage of the STFT technique is its ability to give the harmonic content of the signal at every time-period specified by a defined window. The STFT (V_{STFT}) of a sampled signal $v[k]$, is defined as [2]:

$$V_{STFT}(\omega, n) = \sum_k v[k] \cdot w[k-n] \cdot e^{-j\omega k} \quad (11)$$

Where $w = 2\pi n/N$, N is the length of $v[k]$; $n = 1, \dots, N$; and $w[k-n]$ is a selected window that slides over the analyzed signal. The main disadvantage of this technique is that the greater the temporal resolution required, the worse the frequency resolution will be, and vice versa. For a chosen a window size, this will be equal for all frequencies.

D. Wavelet Transform (WT)

The next logical step is to obtain a window that can vary in time, so as to be able to get better frequency or time resolution where necessary[3]. The wavelet transform is based on the decomposition of a signal in terms of small waves (daughter wavelets) derived from translation (shifting in time) and dilation (scaling) of a fixed wavelet function called the "mother wavelet". The

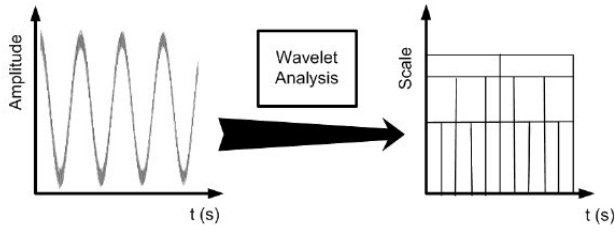


Figure 5. Analysis of signal with a possible scaled by means of wavelet.

main advantage of the wavelet transform is its varying-length window. The general formula of the continuous wavelet transform (V_{WT}) of a signal $v(k)$ is given by

$$V_{WT}(a,b) = \int_{-\infty}^{+\infty} v(t) \cdot \varphi_{a,b}^*(t) dt \quad (12)$$

Where $\varphi_{a,b}(t)$ is the mother wavelet (the window function, and the "*" denotes the complex conjugate), and a and b are the scaling and the translation, respectively [2]. The wavelet allows the use of long intervals of time where it is necessary a high resolution in low frequencies and a small intervals where is required a high frequency information, as it is shown in figure 5[3].

Wavelets have been very useful in electrical transients' analysis. According to the type of disturbance, a different type of wavelet is used. This renders its application less general.

E. S-Transform (ST)

The S-Transform technique is defined by convolving the analyzed signal, $v[k]$, with a window function. The window function is chosen to be a function of time and frequency, which gives this technique the advantage over the wavelet technique. The convolution is performed in the frequency domain by multiplying the Fourier transforms of the analyzed signal and the window function. Then taking the inverse Fourier transform to obtain the analyzed signal in the ST domain. For the discrete signal with a Gaussian window, the ST of a signal $v[k]$ is calculated as [2]:

$$V_{ST}[k, \frac{n}{N}] = \sum_{m=0}^{N-1} V[\frac{m+n}{N}] e^{-\frac{2\pi^2}{n^2}} \cdot e^{j\omega k} \quad (13)$$

Where k , m , and $n = 0, \dots, N-1$, and $V[\frac{m+n}{N}]$ is the Fourier transform of the analyzed signal $v[k]$.

F. Park's Vector Approach

The Park's vector approach is based on the locus of the instantaneous spatial vector sum of the three-phase vectors (v_1, v_2, v_3). The Park's vector component, (v_D, v_Q) are given by [2]:

$$V_D = \sqrt{\frac{2}{3}}v_1 - \sqrt{\frac{1}{6}}v_2 - \sqrt{\frac{1}{6}}v_3 \quad (14)$$

$$V_Q = \sqrt{\frac{1}{2}}v_2 - \sqrt{\frac{1}{6}}v_3 \quad (15)$$

G. Kalman filters

Kalman filters are special types of filters. Their solutions are based on a set of state-space equations. Kalman filters are useful tools for many power system applications, for example, real-time tracking harmonics, estimating voltage and current parameters in power system protection, and estimating the parameters of transients. Give the observation data $z(n)$, a Kalman filter is described by a set of state equations and a set of observation equations as follows[1]:

State equations:

$$x(n) = A(n-1)x(n-1) + w(n) \quad (16)$$

Observation equations:

$$z(n) = C(n)x(n) + v(n) \quad (17)$$

where $x(n)$ is a vector of state variables, $A(n-1)$ is the state transition matrix, $w(n)$ is a vector of model; $C(n)$ connects the measurement $z(n)$ with the state vector $x(n)$; $v(n)$ is a vector of observation. For stationary data, $A(n)$ and $C(n)$ are time independent, that is, $A(n) = A$ and $C(n) = C$.

III. CONCLUSION

Different signal processing techniques has been discussed in this paper. In terms of calculation RMS techniques is simple, fast, and much sensitive in sags, swells, and interruptions in the signals.


Comparison between signal processing techniques

	STFT	Wavelet	S Transform	Park's Vector
Speed	Moderate	Moderate	Low	High
Sensitivity	Low	Moderate	High	High
Implementation	Difficult	Difficult	Difficult	Easy

IV. REFERENCES

- [1] Math H.J Bollen, Irene Yu-Hua Gu, "Signal Processing of Power Quality Disturbances" Wiley & Sons Publication.
- [2] A. M. Gargoom, N. Ertugrul, and W. L. Soong, "A Comparative Study on Effective Signal Processing Tools For Power Quality Monitoring" The University of Adelaide.
- [3] T.Y. Vega, V.F. Riog, H.B.S Segundo, "Evolution of Signal Processing Techniques in Power Quality" 9th International Conference Electrical Power, Barcelona 9-11 October 2007
- [4] Jurado, F.; Acero, N.; Ogayar, B.; "Application of signal processing tools for power quality analysis"; Canadian Conference on Electrical and Computer Engineering, IEEE CCECE 2002. Vol. 1, 12 - 15 May 2002

V. BIOGRAPHY

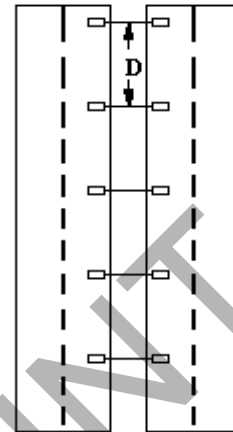
	<p>Umar Naseem Khan was born in 1983 in Pakistan. He received his B.Sc. degree in Electronic Engineering from Ghulam Ishaq Khan Institute, Pakistan, in 2005. After getting more than two years of experience in Electric Power Engineering, he enrolled in M.Sc. degree in 'Control in Electrical Power Engineering', Wroclaw University of Technology, Poland, in 2007. Currently with his studies, he is also attached with R&D Program in Electric Power Control and Protection with Wroclaw University of Technology and Areva T&D, Poland.</p>
---	---

Optimization of the costs of road lighting systems.

Andrzej Maćków
Wrocław University of Technology
Wybrzeże Wyspiańskiego 27 50-370
Wrocław, Poland

I. INTRODUCTION

Minimization of total costs of construction and exploitation of road lighting systems becomes a significant topic in Poland due to high development of road investment activity in Poland. Many new motor- and high- ways are built in all regions. They need to be in use before 2012, because in 2012 we are host of Euro. Thus high tempo and low costs are recommended. Optimization of road lighting should include economic aspects (expenses of lighting systems) carrying on many various constrains. Optimization of lighting include a lot of tasks. In paper only most important are consider. More difficult are neglected and analyses uses a large number of simplification.



where:
 H_1 -height of fitting suspension
 H_2 -height of lighting post
 W -bar length
 D -distance between the post

Fig.1 Geometry of fittings

A road consists of many various elements.: roadways, sidewalks, bicycle paths, green belts, crossings etc. Lighting systems is composed of lighting fittings. Kinds and configuraton of lighting fittings achieve lighting goal. Lighting fittings have different sources, rods, posts and equipment. In paper we consider straight- road case without crossings. There are many different road lighting configuration: one-sided, two-sided opposite, two-sided alternate, on separation belt. Cross symetry of the fittings is the same as road axis. Big variety of systems is connected with various road configuration and lighting requirements. It is main task in construction to choose right one, which ensures best lighting performance to considered road. Differentation of the lighting parameters is achieved by modifying the following features: fitting types,

way of their arrangement, height of fitting suspension, distance between the posts, projection of the fitting above the road components, number of fittings on single post.

II. OPTIMIZATION OF THE ROAD LIGHTING COSTS

The optimization process consists in searching an extreme value of $J(x)$ function, referred to as objective function, where x is for vector of decisive variables. Decisive variables of objective function are result from many factors as, available manufacturing technologies and standard requirements. They can be continuous or discrete character. Type and number of decisive variables influence on optimization method. We can distinguish two groups of decisive variables: equality and inequality character. In the lighting system optimization task only inequality constraints are dealt. Usually method of penalty function is used. It consists in replacing the task with constraints for a constraint-free task by formulation of the objective function $J(x)$ in modified form $J'(x)$:

$$J'(x) = J(x) + \sum F_p(x) \quad (1)$$

where $J'(x)$ -modified objective function, $\sum F_p(x)$ -penalty function.

Decisive variables are distance between the fittings, post height, bar length, fitting upward inclination angle, fitting type, source type, method of fitting arrangement.

Objective function for road lighting optimization has economic character. This function is a sum of investment $J_i(x)$ and operational $J_e(x)$ costs.

$$J_i(x) = K_o + K_z + K_s + K_{os} + K_t + K_p \quad (2)$$

$$J_e(x) = K_e + K_k + K_w + K_d \quad (3)$$

where: $J_i(x)$ -the investment part of objective function, $J_e(x)$ -operational part of the objective function, K_o - the costs of lighting fittings, K_z - the cost of lighting sources, K_s - the cost of the posts, K_{os} - the cost of additional fixtures, K_t - the installation cost, K_p - cost of design, K_e - the cost of electric power, K_k - maintenance costs, K_w - the costs of periodical exchange of the sources, K_d -additional expenses (transportation, utilization of the sources and fittings).

All solutions of the optimization task, considering all adopted constraints, is referred to as an admissible area. The form of objective function is definite beyond the admissible area. In case of the jobs of such a type the method of external penalty function may be used, in the minimization case, for the points located beyond the admissible area the value of the objective function is increased. Moreover, the penalty is different, in accordance with the amount of the transgression and number of current iteration.

The constraints of optimization process of road lighting system costs can be divided into three groups related to decisive variables, standard requirement, and the requirements imposed by investor related (esthetics, shape). The second group is related to controlling the lighting parameters (average roadway luminance, total uniformity of luminance etc.) In consideration third group is neglected.

Some local extremes may occur during searching optimal solution to the road lighting system. Vector of decisive variables x has its constant and discrete components. To solve the problem of costs optimization of the road lighting system a nondeterministic method of genetic algorithm is used. A genetic algorithm is a search technique used in computing to find exact or approximate solutions to optimization and search problems. This method has high effectiveness in dealing with jobs. Disadvantage of method is being frequent solutions that only approximate the global one. It is necessary to use some modifications to improve efficiency of method. There are scaling of the adaptation function, use of two-point crossing and use of tournament selection method with the elements of exclusivity strategy.

III. CONCLUSIONS

Optimization of a road lighting system consisting in minimization of total cost is feasible. Genetic algorithm method should be used for purpose of optimization of systems with such a objective function and different types of decisive variables and occurrence of local extreme points. Some modification are required to improve quickness of finding an optimal solution. Decreasing costs of road lighting can rise up to 20 % in comparison with several constructions.

REFERENCES

- [1] R.Nawrowski, A.Tomczewski, "Optimization of the costs of road lighting.", Oficyna Wydawnicza Politechniki Poznańskiej 2001
- [2] A.Stachurski, and A.P.Wierzbiński, *Podstawy optymalizacji*, 3rd ed., Oficyna Wydawnicza Politechniki Warszawskiej 1999.
- [3] PN-76/E-02032 *Oświetlenie dróg publicznych*, (in Polish)

Contemporary high voltage gapless surge arresters

Rafal Kurnatowski

Abstract- This paper presents general description of contemporary high voltage gapless surge arresters. Housing structure, additional equipment and ZnO element are presented here.

I. INTRODUCTION

Idea of using gapless arresters is quite old. First usage of gapless technology was in 1940. Resistors thyrite were used then. Their nonlinearity factor was about 3,5. Therefore they couldn't be used in surge arresters.

Only invention of varistor with nonlinearity factor about 50 in 1968 allowed to get rid of the spark gap. In 1976 first gapless surge arresters were manufactured.

First generation of varistors were very unstable. Their leakage current was increasing in time and caused increasing of temperature and decreasing of energy absorption ability. Nowadays we have inversed process. Leakage current of contemporary varistors is decreasing in time which is good.

Structure of varistors should be uniform and isolated from environment. This and many discovers have been noticed in nearly 70 years of varistors science

II. TYPES OF HOUSING

First generation of gapless surge arrester had porcelain housing [1]. Total length of contemporary transmission line gapless surge arrester 110kV is about 1,3m. To comparison the length of the same device but with spark gap is equal 2m.

Usually column of varistors is centered in housing but not always. Usually gas inside is SF₆ or nitrogen, sometimes sand.

General division of housing of surge arresters is:

- Polymer housing
- Porcelain housing

A. Polymer housing or porcelain housing

Basic advantage of polymer materials is hydrophobic property. The best hydrophobic properties has silicone rubber. Silicone as outer insulation has been used for over 30 years with good results. It is true that hydrophobic maintains even if there is a high pollution level. It is important because sometimes pollution flashover can occur. Structure of polymer housed arrester is shown in figure 1.

Guaranteed lifetime of porcelain housing is usually equal 50 years. Porcelain surface has hydrophilic properties. Contemporary scientific research show that breakdown voltage of porcelain & polymer housing in high humidity conditions don't differ too much. However in big pollution conditions polymer insulation electric strength is greater than in porcelain insulator.

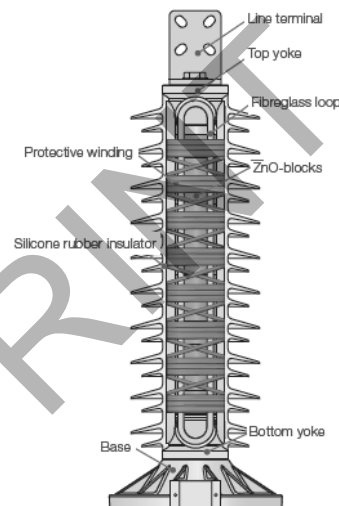


Figure 1. Structure of polymer housed arrester – here ABB design.

III. VARISTORS APPLICATION

A. Structure of ZnO varistor

Zinc oxide ZnO element has been used in gapless high voltage arresters up to now. Its nonlinearity factor is decreasing during big surge currents. Practically reduced voltage doesn't depend on temperature.

These varistors are polycrystalline semiconductors compound by ZnO grains and other metal oxides (e.g. CoO or MnO). 97% of all components is ZnO. However contents of the rest mentioned metal oxides is very important because it

has big influence to different features of all varistor. Even a small change in proportions or manufacturing process can affect the properties of this product. Therefore technological details of production are a secret of vendors.

TABLE I
MOST OFTEN USED ADDITIVES TO ZINC OXIDE CERAMICS

Chemical element	Impact
Co, Mn, Sb	Create potential barrier on grains border
Li	Reduce leakage current in working voltage conditions
Sb, Si	Reduce grain growth
Be, Ti, Sn	Increase grain growth
Al, Ga, F, Cr	Increase nonlinearity of U-I characteristic
Sb, Ag, V, Ni, Cr	Stabilization of potential barrier
Bi	Creates heterogenic path

Researches of oxide varistors structure were realized with electron microscopes. Result is visible below at figure 2. The structure consist grains of ZnO and dissolved cobalt Co and manganese Mn.

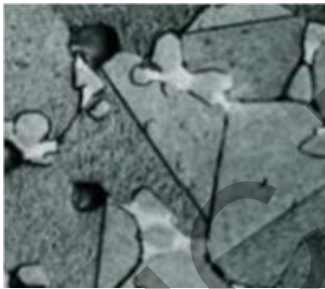


Figure 2. ZnO ceramic structure

ZnO grains touch each other without broking of another phase. Space between these grains is filled with Bi_2O_3 and spinels $\text{Zn}_7\text{Sb}_2\text{O}_{12}$.

B. Varistor conductance phenomena

In varistor's voltage-current characteristic (Figure 3) we can distinguish following zones: before breakdown, breakdown and saturation.

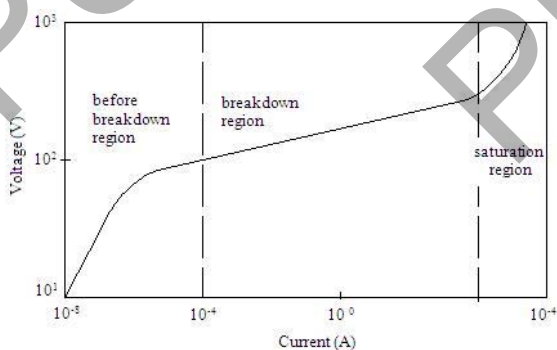


Figure 3. Voltage-current characteristic of varistor

In before breakdown zone resistance of varistor is of the order of $\text{G}\Omega$ and the current in working conditions is of the order of μA . Following equation (1) is empirical formulation of voltage-current characteristic in breakdown zone.

$$I = kU^\alpha \quad (1)$$

I – current, k – constant, U – voltage, α – nonlinearity factor.

Contemporary oxide varistors have nonlinearity factor equal even 80 which depends on manufacture process and on the current.

IV. ADDITIONAL EQUIPMENT

Additional equipment used with high voltage surge arrester is: insulated base, line terminals, grounding terminals, surge counters, function indicators, external grading rings [1].

Stationary 110kV surge arresters are mounted on 1,5m high reinforced concrete bracket. It protect surge arrester from intensive snowfall.

To install function indicators bottom of surge arrester can't be directly grounded. That's why insulated base is used.

Longer arresters often require external grading rings to maintain a uniform and acceptable voltage stress along their length. Operation of such arresters without the grading rings may lead to failure. We use them for voltages exceed 110kV. Usually two grading rings are used for 400kV. They are presented at Figure 4.

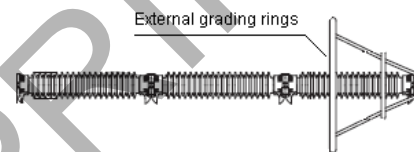


Figure 4. Additional grading rings in surge arrester

The most popular operation indicator is overpressure indicator. When there is operation the colorful cover is throw outside the jet.

Counting of operation number is made by special spark gaps. They also allow to estimate quantity of charge. When spark gap operate the electric arc leaves at electrodes after-arc track. Shape of these tracks depend on value and time of arc current.

REFERENCES

- [1] K.L.Chrzan, "Wysokonapieciowe ograniczniki przepieci," *Dolnośląskie Wydawnictwo Edukacyjne*, pp. 25-44, Wrocław 2003.
- [2] U. Braunsberger, "ZnO arresters in overvoltage protection in pulsed power circuits," *European Electromagnetic Launch Society 12th Topical Meeting. September 2001, Ayr.*
- [3] ABB Buyer's Guide, "High voltage surge arresters"

Evaluation of Chaotic Ferroresonance in power transformers including Nonlinear Core Losses

Ataolla Abbasi
Abbasi@shahed.ac.ir

Mehrdad Rostami
Rostami@shahed.ac.ir

Hamid Radmanesh
Hamid.nsa@gmail.com

Hamid Reza Abbasi
Abbasi1@shahed.ac.ir

Faculty of Engineering,
Shahed University,
Khalig-e-Fars free way,
1417953836 Tehran, Iran,
P.O. Box: 18151/159,
Tel: (+98-21)66639821, Fax: (+98-21)51212105, Tehran, Iran

Abstract

This paper investigates the effect of nonlinear core on the onset of chaotic ferroresonance and duration of transient chaos in a power transformer. The transformer chosen for investigation has a rating of 50 MVA, 635.1 kV, the data for which is given by Dommel et al. (Tutorial Course on Digital Simulation of Transients in Power Systems (Chapter 14), IISc, Bangalore, 1983, pp. 17_38). The magnetization characteristic of the transformer is modeled by a single-value two-term polynomial. The core loss is modeled by a third order power series in voltage. With nonlinearities in core loss included, two effects are clear: (i) onset of chaos at larger values of open phase voltage, (ii) shorter duration of transient chaos, It also shown that nonlinear core can cause ferroresonance drop out.

1. Introduction

Ferroresonance is initiated by improper switching operation, routine switching, or load shedding involving a high voltage transmission line. It can result in Unpredictable over voltages and high currents. The prerequisite for ferroresonance is a circuit containing iron core inductance and a capacitance. Such a circuit is characterized by simultaneous existence of several steady-state solutions for a given set of circuit parameters. The abrupt transition or jump from one steady state to another is triggered by a disturbance, switching action or a gradual change in values of a parameter. Typical cases of ferroresonance are reported in Refs. [1],[4]. Theory of nonlinear dynamics has been found to provide deeper insight into the phenomenon. Refs. [4],[7] are among the early investigations in applying theory of bifurcation and chaos to ferroresonance. The susceptibility of a ferroresonant circuit to a quasiperiodic and frequency locked oscillations are presented in Refs. [8],[9], the effect of initial conditions is investigated. Ref. [10] Isa milestone contribution highlighting the effect of transformer modeling on the predicted ferroresonance

oscillations. Using a linear model, authors of Ref. [11] have brought the effect of core loss in damping ferroresonance oscillations. The importance of treating core loss as a nonlinear function of voltage is highlighted in Ref. [12]. An algorithm for calculating core losses from no-load characteristics is given in Ref. [13]. The mitigating effect of transformer connected in parallel to a MOV arrester is illustrated in Ref. [14]. However, in all the references cited above, the effect of nonlinear core is either neglected. The present paper addresses the effect of nonlinear core on the global behavior of a ferroresonant circuit. The circuit under study represents a case of ferroresonance that occurred on 1100 kV system of Bonneville Power Administration as described in Ref.

2. Circuit Descriptions and Modeling

The three-phase diagram for the circuit is shown in Fig. 1.

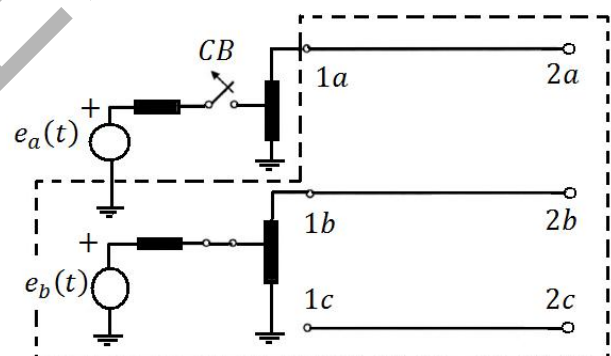


Fig.1. System Modeling

The 1100 kV transmission line was energized through a bank of three single-phase as reported in autotransformers. Ref. [1] ferroresonance occurred in phase A when this phase was switched off on the low-voltage side of the autotransformer; phase C was not yet connected to the

transformer at that time. The autotransformer is modeled by a T-equivalent circuit with all impedances referred to the high voltage side. The magnetization branch is modeled by a nonlinear inductance in parallel with a nonlinear resistance and these represent the nonlinear saturation characteristic ($\phi - i_{Lm}$) and nonlinear hysteresis and eddy current characteristics ($v_m - i_{Rm}$), respectively. The hysteresis and eddy current characteristics are calculated from the no-load characteristics by applying the algorithm given in Ref. [13]. The iron core saturation characteristic is given by:

$$i_{Lm} = s_1 \phi + s_2 \phi^q \quad (1)$$

The exponent q depends on the degree of saturation. It was found that for adequate representation of the saturation characteristics of a power transformer the exponent q may take the values 5, 7, and 11. In Ref. [15], the core loss is modeled by a switched resistor; which effectively reduced the core loss resistance by a factor of four at the time of onset of ferroresonance. In this paper, the core loss model adopted is described by a third order power series whose coefficients are fitted to match the hysteresis and eddy current nonlinear characteristics given in [1]:

$$i_{Rm} = h_0 + h_1 v_m + h_2 v_m^2 + h_3 v_m^3 \quad (2)$$

Per unit value of (i_{Rm}) given in (3)

$$i(R) = -.000001 + .0047V - .0073V^2 + .0039V^3$$

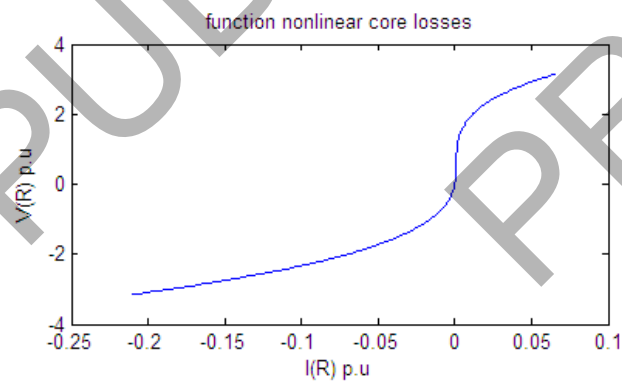


Fig 2.V-I characteristic of nonlinear core

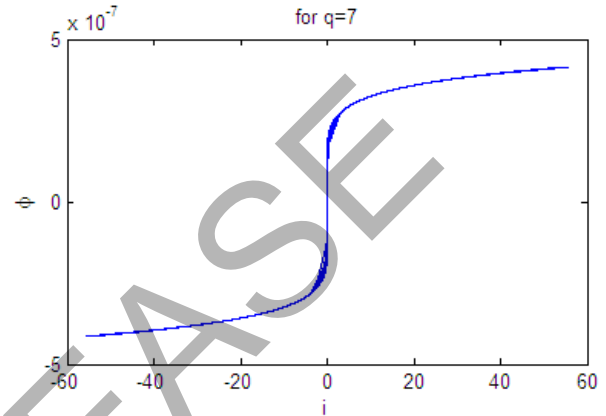


Fig 3.Hysteresis curve of nonlinear core

The circuit in Fig. 1 can be reduced to a simple form by replacing the dotted part with the Thevenin equivalent circuit as shown in Fig. 4. By using the steady-state solution of MATLAB Simulink [16] with the data of the 1100 kV transmission line [1], E_{th} and Z_{th} were found to be:

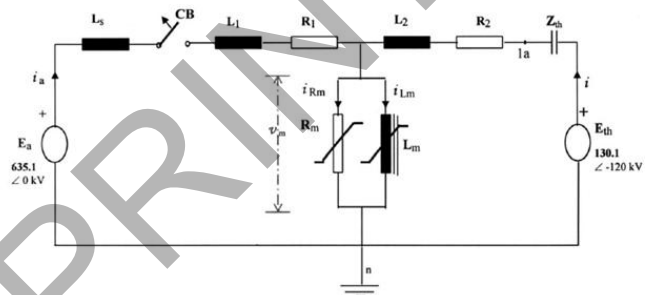


Fig 4.Thevenin circuit of figure 1

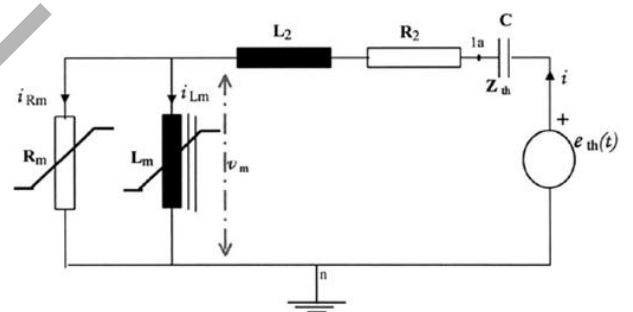


Fig. 5.Circuit of Ferro resonance investigations

$$E_{th} = 130.1kV ; z_{th} = -j1.01243E + 0.5\Omega$$

The resulting circuit to be investigated is shown in Fig. 5 where Z_{th} represents the Thevenin impedance. The behavior of this circuit can be described by the following system of nonlinear differential equations:

$$p2\phi = \frac{[e_{th}(t) - v_c - p\phi - R_2(s_1\phi + s_2\phi^q + h_0 + h_1p\phi + h_2p\phi^2 + h_3p\phi^3) - L_2(s_1p\phi + qs_2\phi^{(q-1)}p\phi)]}{[L_2(h_1 + 2h_2p\phi + 3h_3p\phi^2)]}$$

$$p_{v_c} = \frac{s_1\phi + s_2\phi^q + h_0 + h_1p\phi + h_2p\phi^2 + h_3p\phi^3}{C}$$

(5)

With these parameters:

$$V_{base} = 635.1Kv, I_{base} = 78.72A, R_{base} = 8067\Omega, L_{S_{p.u}} = .0188, C_{p.u} = .07955, R_{p.u} = .0014, R_{core} = 556.68 p.u$$

The formulation with ϕ , $p\phi$ and v_c taken as state variables are given by:

$$x_1 = \phi; x_2 = p\phi; x_3 = v_c \quad (6)$$

$$px_1 = x_2 \quad (7)$$

$$px_2 = \frac{[e_{th}(t) - x_3 - x_2 - R_2(s_1x_1 + s_2x_1^q + h_0 + h_1x_2 + h_2x_2^2 + h_3x_2^3) - L_2(s_1x_2 + qs_2x_1\phi^{(q-1)}x_2)]}{[L_2(h_1 + 2h_2x_2 + 3h_3x_2^2)]}$$

(8)

$$px_3 = \frac{s_1x_1 + s_2x_1^q + h_0 + h_1x_2 + h_2x_2^2 + h_3x_2^3}{C}$$

(9)

For these values of q, system simulated:

$$\text{for } q = 11 \quad s_1 = .0667, s_2 = .0001$$

$$\text{for } q = 7 \quad s_1 = .0067, s_2 = .001$$

$$\text{for } q = 5 \quad s_1 = .0071, s_2 = .0034$$

Equations of system with linear core are:

$$E - V_c - R_1\left(\frac{d\lambda}{dt} + a\lambda + b\lambda^q\right) - L_1\left(\frac{d^2\lambda}{dt^2} + a\frac{d\lambda}{dt} + bq\lambda^{q-1}d\lambda\right) - d\lambda = 0$$

$$\dot{V}_c = \frac{1}{C}\left(\frac{d\lambda}{dt} + a\lambda + b\lambda^q\right)$$

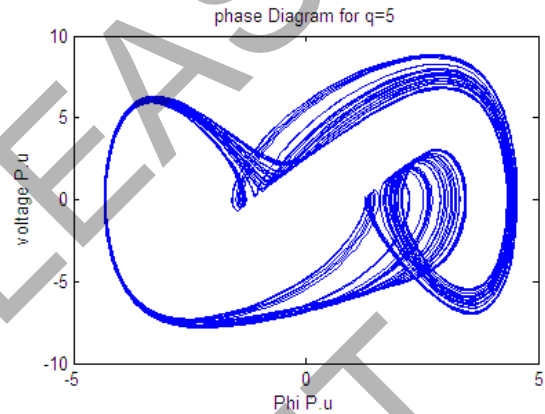


Fig 6. Phase plan diagram for q=5 with linear Core loss

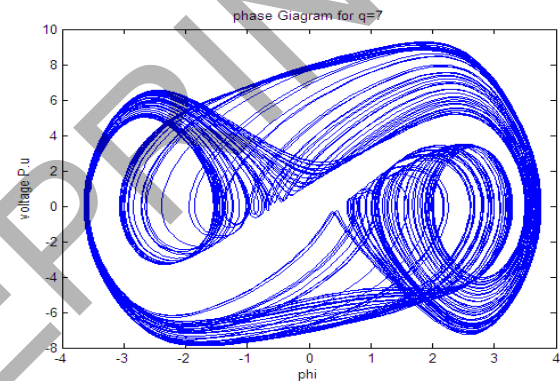


Fig 7. Phase plan diagram for q=7 with linear Core loss

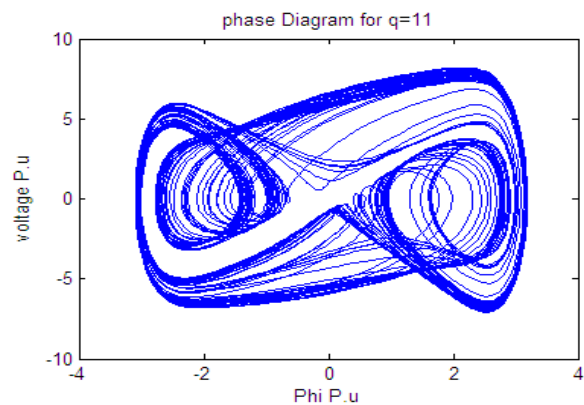


Fig 8. phase plane diagram for q=11 with linear Core loss

3. Simulation Results and Discussion

Time domain simulations were performed using fourth order Runge_Kutta method and validated against Matlab Simulink. The initial conditions as calculated from steady-state solution of Matlab are:

$$x_1 = 0,0 ; x_2 = 1.67 pu ; x_3 = 1.55 pu$$

The circuit in Fig.5 is analyzed by first modeling the core loss as a constant linear resistance. Figs. 6, 7 and Fig. 8 show the phase plan diagram for $q=5, 7$ and $q=11$ with nonlinear core. Bifurcation diagram for $q=5, 7$ and 11 generated by conventional time domain simulation show in Figs.12, 13 and 14. It was found that the chaotic behavior begins at a value of $(E_p = 0.8 pu)$ for $q=5$ and $(E_p = 1 pu)$ for $q=7,11$ where represents the amplitude of eth (t). Transient chaos settling down to the source frequency periodic solution was observed for some values of parameters as shown in Fig. 12 for a typical value of E_p in the chaotic Region. Conventional bifurcation diagrams with the nonlinear model of core loss are presented in Figs. 15, 16 and Fig. 17. Figs.9, 10 and 11 illustrates the corresponding phase plot from which a period 9 oscillation can be discerned for $q=11$.

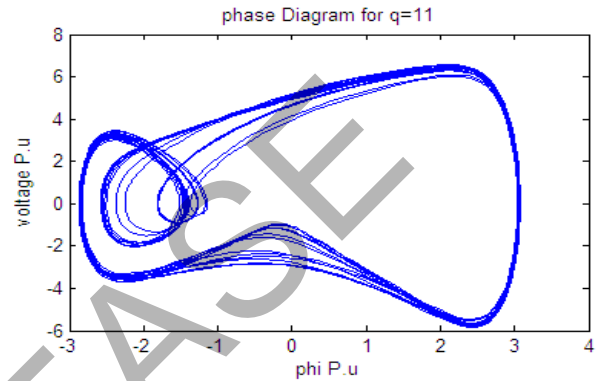


Fig.11. phase plan diagram for $q=11$ Nonlinear core loss

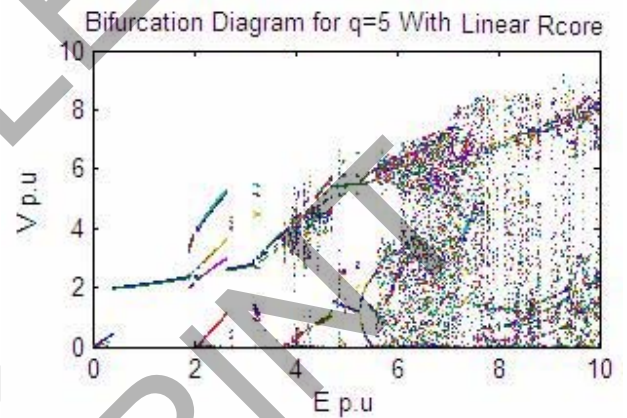


Fig. 12. Bifurcation diagram for $q=5$ with linear core loss

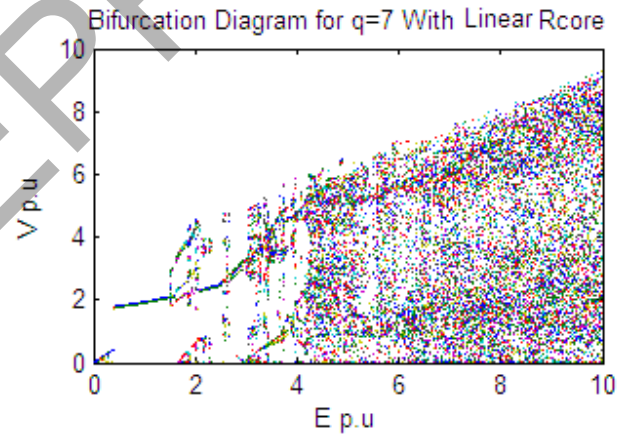


Fig. 13. Bifurcation diagram for $q=7$ with linear core loss

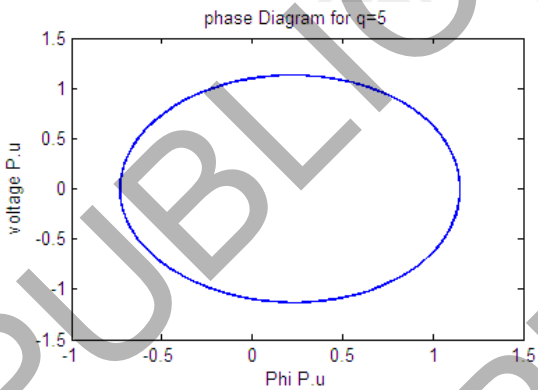


Fig 9. Phase plane diagram for $q=5$ Nonlinear core loss

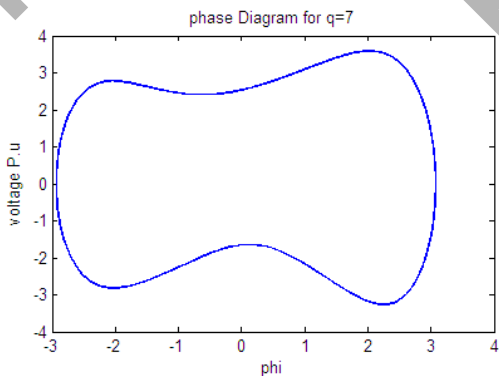


Fig10. Phase plane diagram for $q=7$ Nonlinear core loss

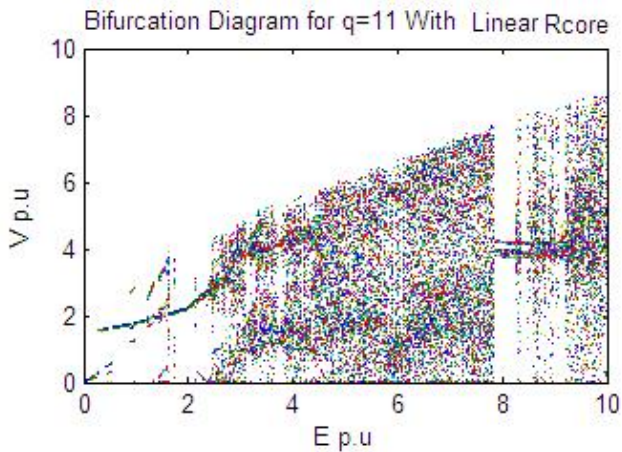


Fig. 14. Bifurcation diagram for $q=11$ with linear core loss

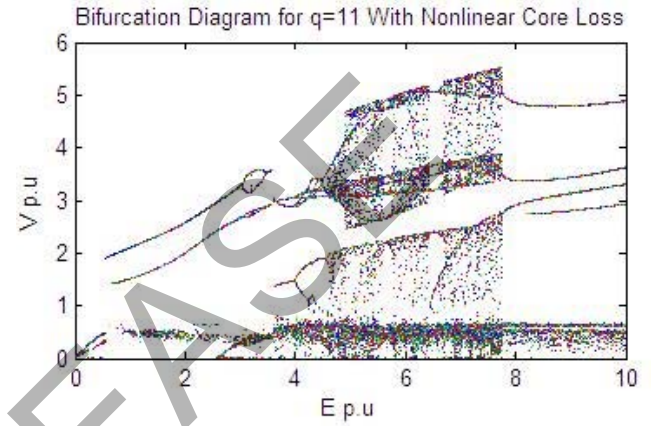


Fig.17. Bifurcation diagram for $q=11$ with nonlinear core loss

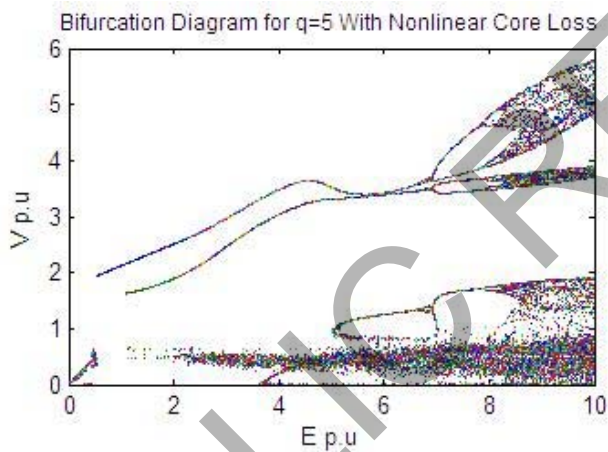


Fig.15. Bifurcation diagram for $q=5$ with nonlinear core loss

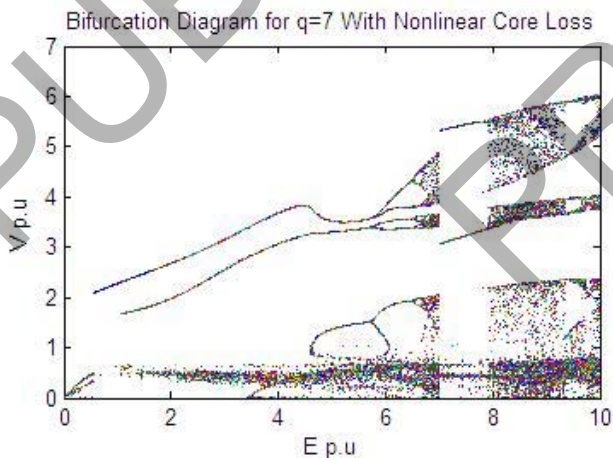


Fig.16. Bifurcation diagram for $q=7$ with nonlinear core loss

4. Conclusion

The dynamic behavior of a transformer is characterized by multiple solutions. Inclusion of nonlinearity in the core loss reveals that solutions are optimistic when compared with linear models. An operational guideline for the range of values of the core loss that avoids the jump between steady-state solutions and contains over voltages, is provided.

Appendix: Nomenclature

- a, b, c index of phase sequence
- $h0, h1, h2, h3, h4$ coefficient for core loss nonlinear function
- n index for the neutral connection
- $s1$ coefficient for linear part of magnetizing curve
- $s2$ coefficient for nonlinear part of magnetizing curve
- q Index of nonlinearity of the magnetizing curve
- Z_{th} Thevenin's equivalent impedance
- C linear capacitor
- R_m core loss resistance
- L nonlinear magnetizing inductance of the transformer
- i instantaneous value of branch current
- v instantaneous value of the voltage across a branch element
- $eth(t)$ instantaneous value of Thevenin voltage source
- e instantaneous value of driving source

p time derivative operator
 E_{th} R.M.S. value of the Thevenin voltage source
 E_p peak value of the Thevenin voltage source
 x state variable
 f flux linkage in the nonlinear inductance
 ω angular frequency of the driving force

References

- [1] H.W. Dommel, A. Yan, R.J.O. De Marcano, A.B. Miliani, in: H.P. Khincha (Ed.), Tutorial Course on Digital Simulation of Transients in Power Systems (Chapter 14), IISc, Bangalore, 1983, pp. 17_38.
- [2] E.J. Dolan, D.A. Gillies, E.W. Kimbark, Ferroresonance in a transformer switched with an EVH line, IEEE Transactions on Power Apparatus and Systems PAS-91 (1972) 1273_1280.
- [3] R.P. Aggarwal, M.S. Saxena, B.S. Sharma, S. Kumer, S. Krishan, Failure of electromagnetic voltage transformer due to sustained overvoltage on switching* an in-depth field investigation and analytical study, IEEE Transactions on Power Apparatus and Systems PAS-100 (1981) 4448_4455.
- [4] C. Kieny, Application of the bifurcation theory in studying and understanding the global behavior of a ferroresonant electric power circuit, IEEE Transactions on Power Delivery 6 (1991) 866_872.
- [5] A.E. Araujo, A.C. Soudack, J.R. Marti, Ferroresonance in power systems: chaotic behaviour, IEE Proceedings-C 140 (1993) 237_240.
- [6] S. Mozaffari, S. Henschel, A.C. Soudack, Chaotic ferroresonance in power transformers, IEE Proceedings* Generation Transmission and Distribution 142 (1995) 247_250.
- [7] B.A. Mork, D.L. Stuehm, Application of nonlinear dynamics and chaos to ferroresonance in distribution systems, IEEE Transactions on Power Delivery 9 (1994) 1009_1017.
- [8] S.K. Chkravarthy, C.V. Nayar, Frequency-locked and quasi periodic (QP) oscillations in power systems, IEEE Transactions on Power Delivery 13 (1997) 560_569.
- [9] S. Mozaffari, M. Sameti, A.C. Soudack, Effect of initial conditions on chaotic ferroresonance in power transformers, IEE Proceedings* Generation, Transmission and Distribution 144(1997) 456_460.
- [10] B.A. Mork, Five-legged wound* core transformer model: derivation, parameters, implementation, and evaluation, IEEE Transactions on Power Delivery 14 (1999) 1519_1526.
- [11] B.A.T. Al Zahawi, Z. Emin, Y.K. Tong, Chaos in ferroresonant wound voltage transformers: effect of core losses and universal circuit behavioral, IEE Proceedings* Sci. Meas. Technol. 145(1998) 39_43.
- [12] IEEE Working Group on Modeling and Analysis of Systems Transients, M.R. Irvani, Chair, Modeling and analysis guidelines for slow transients* part III: the study of ferroresonance, IEEE Transactions on Power Delivery, 15 (2000) 255_265.
- [13] W.L.A. Neves, H. Dommel, on modeling iron core nonlinearities, IEEE Transactions on Power Systems 8 (1993) 417_425.
- [14] K. Al-Anbari, R. Ramanujam, T. Keerthiga, K. Kuppusamy, Analysis of nonlinear phenomena in MOV connected Transformers, IEE Proceedings* Generation Transmission and Distribution 148 (2001) 562_566.
- [15] D.A.N. Jacobson, R.W. Menzies, Investigation of station service transformer ferroresonance in Manitoba hydro's 230-kV Dorsey converter station, IPST'2001* International Conference on Power Systems Transients, Rio de Janeiro (2001). Available from: <http://www.ipst.org/IPST01Papers.htm>.
- [16] H.W. Dommel, I.I. Dommel, Transients Program User's Manual, The University of British Columbia, Vancouver, 1978.
- [17] L.O. Chua, P.-M. Lin, Computer-Aided Analysis of Electronic Circuits (Chapter 17), Prentice-Hall Inc, New Jersey, 1975, p. 687.
- [18] W.C. Rheinboldt, J.V. Burkardt, A locally parameterized continuation process, ACM Transactions on Mathematical Software 9 (1983) 215_235.
- [19] A. Semlyen, A. Acha, J. Arrillaga, Harmonic Norton equivalent for the magnetizing branch of a transformer, IEE Proceedings-C134 (1987) 169.

Primary Energy Market and Electric Market interaction

Nuno Domingues

ISEL, Instituto Superior de Engenharia de Lisboa, Portugal

Rua Conselheiro Emídio Navarro, 1, 1959 – 007 Lisboa; ndomingues@deea.isel.ipl.pt

Abstract- A liberalised market is a market where customers can freely choose their supplier. This market model came with the introduction of competition into non-competitive regulated markets. In a non-competitive environment, supply and prices are regulated, while in a liberalized market regulation aims at avoiding the abuse of market power. In the case of electricity, the starting point was the rigorous analysis of the sectors of the industry which were natural monopolies and the identification of the activities where the barriers to entry were such that no competition will develop naturally. It had been assumed in former market organization that the whole of the electricity industry was a natural monopoly which led to the acceptance of vertically integrated monopoly supply utilities. On a closer inspection it was found that only certain activities were natural monopolies, in particular the transmission and distribution networks. This discovery led reformers to search for mechanisms of introducing competition wherever this seemed possible. Bearing in mind the upcoming Iberian Electricity Market – MIBEL, we studied the sensitivity of the Market Clearing Price to changes in the production inputs, such as coal, natural gas and fuel.

Index Terms— Electricity markets integration, Sensitivity analysis, Market Clearing Price

1. INTRODUCTION

Parallel to the privatization process of electricity utilities and the liberalization of the European electricity markets, the Portuguese and Spanish markets engaged in a process of integration which will lead to the upcoming Iberian Electricity Market (MIBEL). In both countries it has been introduced changes in the production, transmission and distribution of electricity sectors with the aim of achieving a legally, socially and economically unified market.

1) The liberalization process in Portugal

The market opening corresponds to the share of the national electric energy costumers potentially subjected to the competition and market mechanisms, integrating the global consumption of the eligible customers and the share of energy needs that the entailed deliverers can acquire in the scope of this free regime. At present, eligible customers are those at Medium Voltage (MV), High Voltage (HV) and Very High Voltage (VHV), with effective annual consumption. By the end of the 80's it started to be designed the current model of the Portuguese system (called SEN – *Sistema Eléctrico Nacional*), which promoted the privatization process through the publication of the Decree Law (DL) 449/88, of December 10th. The electricity sector passed through another key moment with the publication of DL 182 and the 187/95 that established the organization bases of the SEN and the principles of the activities of production, transmission, distribution, cogeneration and regulation of the Sector. In 19th of December of 1996 the European Union published the 96/92/CE that establishes common rules for the domestic market of electricity, which had started in 19th of February of 1997. This European Rule (CE), negotiated by the State Members of the European Union, obligated a review in the 1995 legislation, resulting then the DL 56/97. This also introduced the necessary changes to the process of privatization of the national electricity utility (EDP). The law suit was complemented with the approval of the Proceeding Manual (MP) by the Regulator (ERSE – *Entidade Reguladora dos Serviços Energéticos*), in 29th of February of 2000. So far, the legislative structure is completed by a set of seven regulations: four from the ERSE and three from the Economic Ministry (DGE - *Direcção Geral de Energia*). [1], [3], [4], [7], [9]

2) The liberalization process in Spain

In Spain, the government initiated the process in 1998, after the Ministry of the Industry and Energy signed a protocol with the utilities in December of 1996. Up to this date the system was regulated by the MLE (Marco Legal Estable), which compensated the sunk costs, aiming the return of investment, the increase of the operation efficiency and the increase of the competitiveness of the national production. After the 70's oil crisis, this body looked for stimulating the nuclear central offices (a process that was blocked in 1985 due to fear of terrorist attacks), the national coal and the lignite (both of weak quality and low energy rentability that by itself would not be competitive to the majority power plants) in order to decrease the existing dependence to the crude. Since the Spanish civil war (1936-1939) that the state-owned company (ENDESA), situated essentially the north and northeast, turned to these primary energy sources. Since 1985 the National Grid (REE - *Red Eléctrica de España*) operates the net, dispatch the system and owns the transmission grid. In 1991 the Iberduero and the Hidroeléctrica Española companies joined, creating the Iberdrola, and in October of 1996 ENDESA (already with the offices Viesgo and Enher) acquired 75% of the companies FECSA and Sevillana.

The regulating entity is now the CNE (*Comisión Nacional de Energía*) that replaced the CSEN (*Comisión del Sistema Eléctrico Nacional*). Since 1996 it strongly opposed to any company fusion. Due to its historic agreements, the liberalization process is difficult and slow. In this scenario, the entrance of new not competitive producers is possible which will increase the final tariffs, thus opposing the initial goals of the free market. In 24th of December of 1997 it was created the OMEL (*Compañía Operadora del Mercado Español de Electricidad, S.A.*), related in the article 33 of the Law 54/97 and the Real Proceeding R.D. 2019/97. [1], [3], [4], [6], [7]

2. DATA COLLECTION

For the purposes of our study I started by searching the market prices for different inputs: coal, fuel, natural gas and diesel. Based on different load factors of the different

technologies and different installed capacities, applying a conversion factor (from thermal to electrical energy) and the plant efficiency, it was possible to reach the marginal cost of production for each technology. Then, a quadratic cost function was estimated for the coal, fuel, natural gas and diesel power plants, applying a different approach to the hydro, nuclear and renewable production. Concerning the hydro power plants it was considered its installed capacity. It was considered, thus, an almost constant and coherent cost with the remaining costs. For the nuclear, constant cost for all was considered. For the renewals, as they are not dispatchable, as established in D.L. 339-C/2001, its production was accounted as a load decrease. In parallel, the characterization of the installed power and the produced energy of the Portuguese and Spanish grids were made. One can, then, shape the curves of cost of production curve of the Portuguese, Spanish and the aggregate System. [4], [5], [7], [8]

3. SIMULATION RESULTS

The simulation results for the winter scenario (PH) are:

- Market-clearing price (MCP): 32.4075 €/MWh
- Market-clearing quantity (MCQ): 46165.7028 MWh

And for the summer scenario (VS) are:

- Market-clearing price (MCP): 11.7925 €/MWh
- Market-clearing quantity (MCQ): 22420.0432 MWh

Changing the price of the fuel in percentage, I achieved the values for the MCP presented in Figure 1 in the appendix.

For each scenario I have represented the corresponding trend line, as shown in fig. 2 and in fig. 3 in the appendix.

In the winter scenario (PH) the water resources are not enough to satisfy the demand. The cheapest fuel is the coal, so will be the next technology to be used. The MCP is immune to coal price variations indicating that the marginal production came from another technology. Follows the electric production by oil resource. I can see that there are some competition between oil and the gas. So, if the price of any of these two change there is a reflection in the MCP. If the price of oil decreases there is no change in

MCP because the marginal production technology is gas. However, as the price of oil raises, less units will be produced by this technology and the MCP will also raise because there will be competition between gas and oil. In the Summer scenario (VS) the water and the coal fuels are enough to satisfy the demand. So, changes in gas and oil prices will not be reflected in MCP because neither are the marginal technology. However, raising the price of the coal too much or decreasing the price of oil too much will bring some competition between them and will be reflected in MCP.

Note that MCP goes from 32 €/MWh to 11 €/MWh as the MWh units produced goes from 46 165 to 22 420.

4. CONCLUSIONS

It is often being argued that a liberalised market will lead to real competition, with the consequence of welfare improvements, but that is not necessarily true. The basic assumption of a competitive market is, among others, the possibility to choose between different suppliers and that these suppliers are able to generate electricity at the lowest possible costs.

This paper focus on the sensitivity of the Market Clearing Price (MCP) to the change of the fuel price. Other sensitivities can be explored, such as demand curve, lost of an interconnection, lack of water resources, among others. One of the powerful tools of this simulator is analyse these kinds of sensitivities. Others are the impacts of

the aggregation for both Countries and for all players.

I stress that in a liberalized market volatility of MCP is a key issue. Demand forecast is quite difficult if compared to other commodities, giving a wider confidence range. Risk management joins this two properties and faces possible errors in the forecasting tools.

5. REFERENCES

- [1] Designing competitive electricity markets; 1997 Hung – po Chao, Hillard G.Huntington; Kluwer Academic Publisher
- [2] Electric power distribution reliability; 2002 Richard E. Brown; ABB inc. Raleigh North Carolina
- [3] Electricity Market Reform, 2002 IEA (International Energy Agency) HandBook
- [4] Restructured Electrical Power Systems Operation, Trading and Volatility; Mohammad Shahidehpour e Muwaffaq Alomoush; Marcel Dekker, Inc; 2002;
- [5] Market Operations in Electrical Power Systems Forecasting, Scheduling and Risk Management; Mohammad Shahidehpour, Hatim Yamim e Zuyi Li; A John Wiley & Sons inc; 2001;
- [6] Deregulation on Electric Markets, Comunicação «Introducing Competition to electricity industry in Spain», 2000
- [7] Electric Power Systems, B.M. Weedy, B.J. Cory, 4ª edição, 1998
- [8] Cogeneration, Operation and Control, Welley, 1996
- [9] www.ren.pt

6. APPENDIX

Technology	Scenarios	Fuel Price				
		80,00%	90,00%	100,00%	110,00%	120,00%
Coal	PH	32,41	32,41	32,41	32,41	32,41
	VS	9,43	10,61	11,79	12,97	14,15
Oil	PH	32,40	32,40	32,41	33,10	33,41
	VS	11,79	11,79	11,79	11,79	11,79
Gas	PH	26,73	29,87	32,41	35,64	38,88
	VS	11,79	11,79	11,79	11,79	11,79

Figure 1: MCP sensitive table for fuel price changes in €/MWh

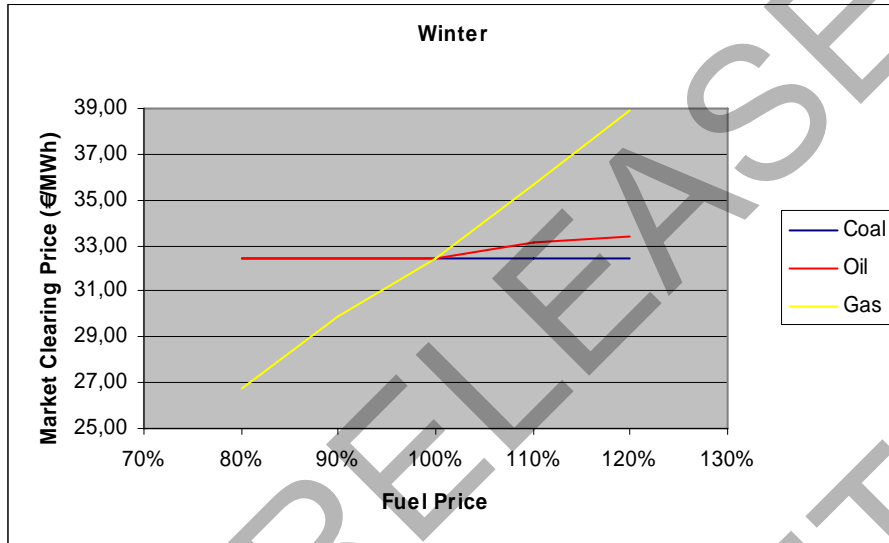


Figure 2: MCP sensitive table for fuel price changes in the Winter scenario

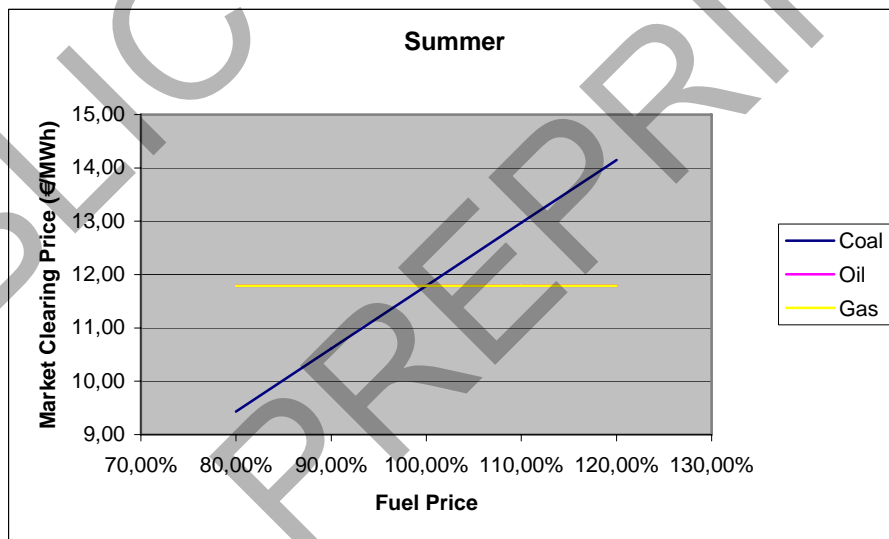


Figure 3: MCP sensitive table for fuel price changes in the Summer scenario

Measurements of electromagnetic compatibility using GTEM chambers

Marcin Dębowski
Wrocław University of Technology
Wrocław, Poland

Abstract – The paper will give basic knowledge about EMC from measurements point of view. Principals of tests done in GTEM chamber will be presented.

I. INTRODUCTION

Electromagnetic compatibility is relatively new concept. The producers of devices sold in the European Union common market are obligated to check EMC from year 1996. EMC is nothing else then ability of the device, installation or system to proper work in electromagnetic environment without adding additional distortions to this environment or other working devices. Because there are more then one possible scenario of interferences between two devices, the main problem is how to analysis those distortions. For this goal the GTEM chamber was design and build.

II. THEORY

From the entire EMC test, the measurements of radiation emission are the hardest, most time consuming and most expensive, because they need special, big enough field with low external radiation emission coming from other sources. Most of today's directives concerning EMC test, recommend performing the measurements in open area test site (OATS). Main elements of this environment are:

- low ambient and noise floor,
- oversized ground plane,
- host equipment area,
- Weather protection.

Building such location is very hard due to weather conditions and electromagnetic wave propagation. Taking into

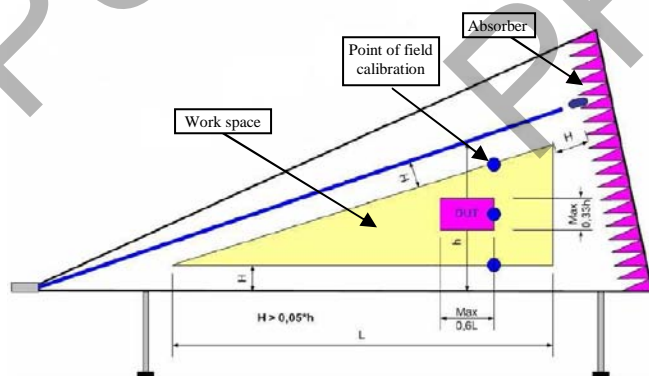


Figure 1. Schema of GTEM chamber

account many inconveniences of this method, other one is needed, which will allow carrying out test in more friendly conditions. One of the most common techniques is the anechoic and shielded chamber, which are independent from external weather and electromagnetic conditions.

III. CONSTRUCTION OF GTEM CHAMBER

The GTEM cell (Gigahertz Transverse Electromagnetic cell) is usually a construction in shape of the rectangular prism, equipped with screens limiting influence of external electromagnetic fields and special internal shields preventing leakage of electromagnetic wave generated in the chamber. With proper shielding level and wave absorption (absorbing function is carried out by special absorbers build in the chamber) it is possible to obtain restricted measurement area, which is usually few times smaller than dimensions of the chamber. In this area propagation of electromagnetic wave is known and can be controlled.

The GTEM chamber are developed version of TEM chamber, they are able to measure frequencies up to several GHz.

IV. MEASUREMENTS

The GTEM chamber is used to measure intensity of field distortions produced by examined devices. Basic equipment is the chamber and measurement device.

Emission of investigated device is obtained by measuring voltage at the output of the chamber for 3 planes of examined object. The emission distortion level is calculated basing on the dependence between obtained values and field intensity values



Figure 2. GTEM chamber in Laboratorium Urządzeń Elektronicznych Poznań

measured on OATS.

To fulfill standard EN 55022 the analyzer must be set to check the object in the range of frequencies from 30 MHz to 1 GHz with step of 120 Hz. The detector must be able to measure quasi peak value for which maximum emission levels are defined – table 1. Other values like peak, average, RMS are optional.

The main problem with performing the measurements is the time. It is easy to calculate that 8084 measures need to be taken. The quasi peak detector needs at least 1 second to register the value. For 1 plane it is more then 2 hours. This time needs to be multiply be 3, because the tests are performed in 3 planes.

To circumvent this barrier special procedure was created:

- pre-tests for whole frequencies range with peak value detector,
- choice of frequencies were the intensity exceeds or is close to threshold,
- precise tests for chosen frequencies with quasi-peak detector.

All three points are performed for each plane.

V. SUMMARY

Recently electronic and electric devices were checked only in a meaning of fundamental requirements. The EMC tests were not so important to producer. Now all producers must fulfill conditions given by EN 55022, because of that they are obligated to create the technical documentation of the product. The documentation will give overview if the object is safe in meaning of EMC. What is more the manufacturer need to guarantee the production procedure according to created documents.

It is estimated that 10% of nowadays devices are connected with usage of components that will not cause problem in point of electromagnetic compatibility.

Good strategy is to test main elements of designed device separately – it will give lower probability that they will cause problem working together.

REFERENCES

- [1] Ph. D. Maik Honscha Lecture material for Introduction to EMC – BTU Cottbus 2008.
- [2] Jarosław Łuszcz, Artur Knitter “Badanie emisyjności promieniowanej urządzeń energoelektronicznych w komorach GTEM”, XV Seminarium zastosowanie komputerów w nauce i technice 2005.
- [3] Clemens Icheln „The construction and application of a GTEM cell”, HUT Hmaburg 1995
- [4] Jan Bogucki, Andrzej Chudziński, Justyn Połujan “Emisja elektromagnetyczna urządzeń w praktyce” Telekomunikacja i techniki informacyjne 1-2/2007.
- [5] Krzysztof Sieczkarek „Badania Kompatybilności elektromagnetycznej” Instytut Logistyki i Magazynowania Poznań

Table 1

Permissible values of quasi-peak value for IT devices according to EN 55022

Frequencies range [MHz]	Permissible level [dBuV/m]	
	Class A devices Quasi-peak value	Class B devices Quasi-peak value
30 – 230	40	30
230 – 1000	47	37

Distributed Generation and Power Quality

Umar Naseem Khan

Abstract— The main purpose of this paper is to discuss the basic understanding of power quality in relation to the distributed generation. Due to considerable overlap between two technologies, disturbances affecting the power quality, which are mainly caused by the addition of Distributed Generation (DG) on the existing power system network. Injection of the DG into an electric power grid can affect the voltage quality. Distributed generation of different voltage levels when connected to the power system network could influence the voltage regulation, sustained interruptions, harmonics, sags, swells, etc. All the information given here is collected from different references by keeping in mind the students at the beginning level of the concerned topic.

Index Terms—power quality, distributed generation, distributed generators, distributed resources, disturbances.

I. INTRODUCTION

The demand of power is escalating in the world of electricity. This growth of demand triggers a need of more power generation. DG uses smaller-sized generators than does the typical central station plant. Distributed generators are small scale generators located close to consumers; normally Distributed Generators are of 1 kW to 100 MW [1].

Definition of DG [2]

Distributed generation in simple term can be defined as a small-scale generation. It is active power generating unit that is connected at distribution level.

- IEEE defines the generation of electricity by facilities sufficiently smaller than central plants, usually 10 MW or less, so as to allow interconnection at nearly any point in the power system, as Distributed Resources.
- Electric Power Research Institute (EPRI) defines distributed generation as generation from a few kilowatts up to 50 MW.
- International Energy Agency (IEA) defines DG as “Power generation equipment and system used generally at distribution levels and where the power is mainly used locally on site”.
- The International Council on Large Electricity Systems (CIGRE) defines DG as generation that is not centrally planned, centrally dispatched at present, usually connected to the distribution network, and smaller than 50-100 MW.

These generators are distributed throughout the power system closer to the loads. The DG penetration in the grid poses new challenges and problems to the network operators as these can have a significant impact on the system and equipment operations in terms of steady-state operation, dynamic operation, reliability, power quality, stability and safety for both customers and electricity suppliers. However as we are only concerned with power quality of the primary and secondary distribution system, we will only consider generator sizes less than 10MW

[2]. Generators larger than this are typically interconnected at transmission voltages where the system is designed to accommodate many generators. The normal distribution system delivers electric energy through wires from a single source of power to a multitude of loads. Thus, several power quality issues arise when there are multiple sources.

II. INTERFACE TO THE UTILITY

Here we are only concerned about the impact of distributed generation on power quality. While the energy conversion technology may play some role in the power quality, most power quality issues relate to the type of electrical system interface. Some notable exceptions include: (a) The power variation from renewable sources such as wind and solar can cause voltage fluctuations. (b) Some fuel cells and micro turbines do not follow step changes in load well and must be supplemented with battery or flywheel storage to achieve the improved reliability expected from standby power applications. (c) Misfiring of reciprocating engines can lead to a persistent and irritating type of flicker, particularly if it is magnified by the response of the power system.

The main types of electrical system interfaces are synchronous machines, asynchronous (induction) machines and electronic power inverters [2].

Synchronous Machines: Some actual examples of unexpected consequences are

1. The harmonic voltage distortion increases to intolerable levels when the generator is attempting to supply adjustable-speed-drive loads.
2. There is not enough fault current to trip breakers or blow fuses that were sized based on the power system contribution.
3. The voltage sag when elevator motors are being started causes fluorescent lamps to extinguish.

Generators must be sized considerably larger than the load to achieve satisfactory power quality in isolated operation.

Asynchronous (induction) machines: Induction generators are induction motors that are driven slightly faster than synchronous speed. They require another source to provide excitation. The requirements for operating an induction generator are essentially the same as for operating an induction motor of the same size. The chief issue is that a simple induction generator requires reactive power (vars) to excite the machine from the power system to which it is connected. To supply the reactive power locally, power factor correction capacitors are added. While this works well most of the time, it can bring about another set of power quality problems. One of the problems is that the capacitor bank will yield resonances that coincide with harmonics produced in the same facility. Another issue is self-excitation. An induction generator that is suddenly isolated on a capacitor bank can continue to generate for some period of time. This is an unregulated voltage and will likely deviate outside the normal range quickly and be detected.

Umar Naseem Khan is with the Faculty of Electrical Engineering, Wrocław University of Technology, Wrocław 50-370, Poland (e-mail: umar.naseem@gmail.com).

Electronic power inverters: All DG technologies that generate either dc or non-power frequency ac must use an electronic power inverter to interface with the electrical. The early thyristor-based, line-commutated inverters quickly developed a reputation for being undesirable on the power system. The line-commutated inverters produce harmonic currents in similar proportion to loads with traditional thyristor-based converters. Besides contributing to the distortion on the feeders, one fear was that this type of DG would produce a significant amount of power at the harmonic frequencies. Such power does little more than heat up wires. To achieve better control and to avoid harmonics problems, the inverter technology has changed to switched, pulse-width modulated technologies [2].

III. POWER QUALITY ISSUES

A major issue related to interconnection of distributed resources onto the power grid is the potential impacts on the quality of power provided to other customers connected to the grid.

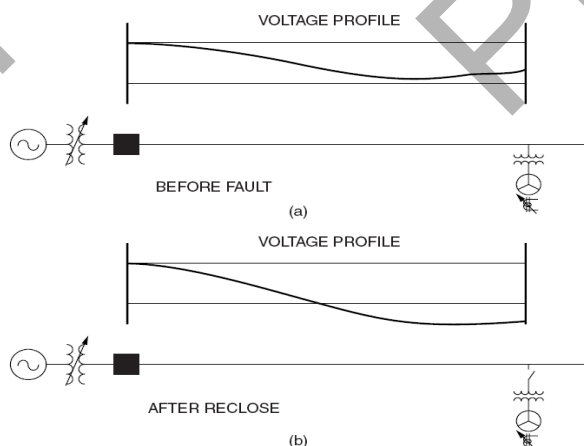
A. Voltage Regulation

Over-voltages due to reverse power flow: If the downstream DG output exceeds the downstream feeder load, there is an increase in feeder voltage with increasing distance. If the substation end voltage is held to near the maximum allowable value, voltages downstream on the feeder can exceed the acceptable range.

Interaction with load tap changers (LTC) and static voltage regulators (SVR) controls: The presence of DG can cause localized changes in flow patterns, which are not reflective of the general trend on the feeder. As a result, LTC or SVR can be set such that a good voltage profile may not be obtained.

Figure 1 illustrates one voltage regulation problem that can arise when the total DG capacity on a feeder becomes significant. This problem is a consequence of the requirement to disconnect all DG when a fault occurs.

Fig 1a shows the voltage profile along the feeder prior to the fault occurring. The intent of the voltage regulation scheme is to keep the voltage magnitude between the two limits shown. In this case, the DG helps keep the voltage above the minimum and, in fact, is large enough to give a slight voltage rise toward the end of the feeder.



When the fault occurs, the DG disconnects and may remain disconnected for up to 5 min. The breaker recloses within a few seconds, resulting in the condition shown in Fig. 1b. The load is now too great for the feeder and the present settings of the voltage regulation devices.

Therefore, the voltage at the end of the feeder sags below the minimum and will remain low until voltage regulation equipment can react. This can be the better part of a minute or longer, which increases the risk of damage to load equipment due to excessively low voltages.

Solutions include:

1. Requiring customer load to disconnect with the DG. This may not be practical for widespread residential and small commercial loads. Also, it is difficult to make this transition seamlessly and the load may suffer downtime anyway, negating positive reliability benefits of DG.

2. Installing more voltage regulators, each with the ability to bypass the normal time delay of 30 to 45 s and begin changing taps immediately. This will minimize the inconvenience to other customers.

3. Allow DG to reconnect more quickly than the standard 5-min disconnect time. This would be done more safely by using direct communications between the DG and utility system control.

4. Limit the amount of DG on the feeder.

B. DG Grounding Issue:

A grid-connected DG, whether directly or through a transformer, should provide an effective ground to prevent un-faulted phases from over-voltage during a single-phase to ground fault. Proper grounding analysis of DG will ensure compatibility with grounding for both the primary and secondary power systems. This analysis must consider (1) the generator-winding configuration (or inverter arrangement), (2) its grounding point, (3) the interface transformer configuration, and (4) grounding of both the primary and secondary power systems to which the DR is connected [4].

Solutions Include[1]:

Grounding recommendations for distributed resources:

Design of Primary Distributed System	Design of Secondary System	DR Grounding
Three-wire, ungrounded system or high-impedance, grounded system	4-wire, Grounded	DR should be ungrounded or high-impedance grounded with respect to primary and effectively grounded with respect to the secondary system
	3-wire, ungrounded	DR should be ungrounded or high-impedance grounded with respect to primary and secondary system
Four-wire, multi-grounded neutral system	4-wire, Grounded	DR should be effectively grounded with respect to the primary and secondary system.
	3-wire, ungrounded	DR should be effectively grounded with respect to the primary system and ungrounded or high-impedance grounded with respect to the secondary system

C. Harmonic Distortion

Voltage harmonics are virtually always present on the utility grid. Nonlinear loads, power electronic loads, and rectifiers and inverters in motor drives are some sources that produce harmonics. The effects of the harmonics include overheating and equipment failure, faulty operation of protective devices, nuisance tripping of a sensitive load and interference with communication circuits.

All power electronic equipments create current distortion that can impact neighboring equipment. DG like PV, fuel cells are likely to introduce harmonics problem in the system. Harmonics from DG come from inverters and some synchronous machines. The PWM (pulse width modulation) switching inverters produce a much lower harmonic current content than earlier line-commutated, thyristor-based inverters [1].

One new distortion problem that arises with the modern inverters is that the switching frequencies will occasionally excite resonances in the primary distribution system. This creates non-harmonic frequency signals typically at the 35th harmonic and higher riding on the voltage waveform. This has an impact on clocks and other circuitry that depend on a clean voltage zero crossing. A typical situation in which this might occur is an industrial park fed by its own substation and containing a few thousand feet of cable. A quick fix is to add more capacitance in the form of power factor correction capacitors, being careful not to cause additional harmful resonances [1].

Solutions include:

1. Newer PWM inverters have lower current distortion
2. Use non-resonant switching frequencies
3. Use reactors in the neutral, or generators with a 2/3 coil winding pitch

D. Flicker

Some energy source (e.g., wind turbine or fuel cell) has some mechanical (or chemical) fluctuations in power output and some electrical equipment (e.g., the dc bus and inverter) does not have sufficient energy storage to smooth out these fluctuations. This will result in fluctuations in the power delivered by a DG and can cause flicker in the power system in a fashion very similar to that caused by load fluctuations [3].

Solutions include [3]:

1. Utility companies try to limit flicker so that it is at a level that cannot be perceived by the human eye. This is accomplished by designing the power system to be sufficiently robust so that smaller load variations do not create noticeable voltage variations.
2. It is also controlled by imposing limits on the types of loads that are allowed to connect at various points on the system
3. When a larger DR unit is applied on a feeder, rapid response voltage regulators (static VAR compensators) or fast-response reactive compensation using inverter reactive-power capabilities can do mitigation of flicker.
4. Energy storage technologies can be applied to smooth the output fluctuations of solar and wind energy systems.

E. Islanding

Refers to a condition in which distributed generation is isolated on a portion of the load served by the utility power system. It is usually an undesirable situation, although there are situations where controlled islands can improve the system reliability. Islands may be intentional or unintentional [2].

If an island should occur, it should persist for only a very brief period, unless the aggregate real and reactive output of all the DG supporting the island is close to the load demand. Otherwise, island voltage and frequency will change rapidly and all the DG has to be shut down to prevent this.

In case the DG in the distribution system is capable to meet the load demand, DG can be operated in the island mode and continue to energize the distribution system. But the major issues with this type of inadvertent islanding are:

1. The voltage and frequency provided to other customers connected to the island are out of the utility's control, yet the utility remains responsible to those customers.
2. Protection systems on the island are likely to be uncoordinated, due to the drastic change in short-circuit current availability.

Out-of-step reclosing: Many utilities use an "instantaneous" reclosing practice, where breakers and circuit reclosers reenergize the protected circuit without any intentional delay and this could result in out of phase reclosing of the distribution system. As a result of out of phase reclosing:

1. Large mechanical torques and currents are created, which can damage the generator or the prime mover.
2. Transients are created which are potentially damaging to utility and other customer equipment.
3. Out-of-phase reclosing, if it occurs at a voltage peak, will generate a very severe capacitive switching transient. In a lightly damped system, the crest over-voltage can approach three times rated voltage.

Prevention [1]:

1. Inverter controls are designed to raise a rising frequency or lower a dropping frequency
2. The power system frequency acts to correct the inverter frequency
3. Without the power system to correct the frequency, the destabilizing signal in the inverter control quickly causes an over- or under-frequency condition, and frequency relays trip the inverter
4. Load/generation imbalance relies on an intentional and significant difference between the DG output and the local load. DG is operated at constant power factor or constant reactive power, and not permitted to regulate voltage. When an island forms, the mismatch between the DG and the load will quickly cause detectable voltage and/or frequency variations

F. Protection System [4]

Tradition distribution systems were not designed to have active power generating units in them. Power is supplied by the transmission system and power flow is mainly unidirectional. But with the DG in the system, power flow can be bi-directional.

Impact of DG on Protection System Coordination

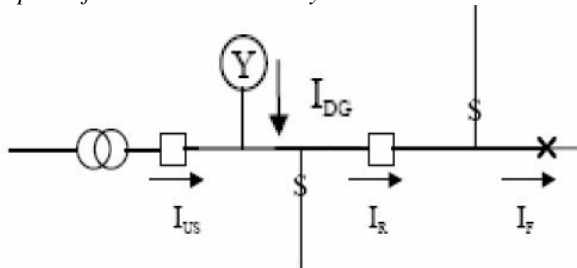


Figure 2. Typical feeder with recloser and fault

In fig 2, I_{US} is the current from the utility source. Fault current seen by the recloser is I_R . The fault current at the fault location is I_F .

Without DG,

$$I_{US} = I_R = I_F$$

With the DG connected

$$I_F = I_{US} + I_{DG} \text{ and } I_R = I_F$$

However,

$$I_R \neq I_{US}$$

The condition indicated is not seen in the typical radial distribution system. I_{US} without the DG does not equal I_{US} with the DG. With the DG connected, the fault current seen by the recloser (I_R) will be greater than without the DG connected.

This would normally not cause a problem with the recloser size as long as the new greater I_R does not exceed the recloser maximum interrupting rating. However, it is very likely that coordination between the recloser and any down-line fuses will be lost. Because both the recloser and fuses operate faster at higher fault currents, the required margins between the recloser fast curve and the fuse minimum melt curve could be reduced enough to lose coordination.

Depending on characteristics of the network and DG, various other protection problems can arise. They are namely:

1. False tripping of feeders (sympathetic tripping)
2. Fuse coordinate with recloser fast-trip varies with DG operation
3. Nuisance tripping of production units
4. Blinding of protection
5. Increased or decreased fault levels
6. Unwanted islanding
7. Prohibition of automatic reclosing

8. Unsynchronized reclosing

Solutions Include

1. Reduction of Reach: Adjust relay to increase reach. Add recloser to add another protection zone. Minimize DG contribution to ground faults
2. Sympathetic tripping: Directional relays, changes to circuit breaker settings
3. Defeat of fuse saving: Larger fuses, minimize DG contribution to ground faults


IV. CONCLUSION

Different issues related to power quality when DR is integrated with the existing power system has been discussed in the paper. It can be concluded from this discussion that when interconnecting DR to the power system, these issues must be considered which could affect power quality and safety. Penetration of DR can be successfully integrated with the power system as long as the interconnection designs meet the basic requirements that consider not only power quality but also system efficiency and power reliability and safety.

V. REFERENCES

- [1] EPRI White Paper, "Integrating Distributed Resources into Electric Utility Distribution System" Technology Review, December 2001
- [2] R.C. Dugan, M.F. McGranaghan, S. Santoso, H.W. Beaty, "Electrical Power System Quality", 2nd Edition, McGraw Hill.
- [3] C. Sankaran, "Power Quality", CRC Press
- [4] "Impact of Distributed Resources on Distribution Relay Protection", IEEE Power Engineering Society

VI. BIOGRAPHY

	<p>Umar Naseem Khan was born in 1983 in Pakistan. He received his B.Sc. degree in Electronic Engineering from Ghulam Ishaq Khan Institute, Pakistan, in 2005. After getting more than two years of experience in Electric Power Engineering, he enrolled in M.Sc. degree in 'Control in Electrical Power Engineering', Wroclaw University of Technology, Poland, in 2007. Currently with his studies, he is also attached with R&D Program in Electric Power Control and Protection with Wroclaw University of Technology and Areva T&D, Poland.</p>
---	---

Using ultracapacitors for saving energy in regenerative braking in hybrid vehicles

Amar Patil^a, Grzegorz Maliga^b

^a MSc's student of Department of Computer Science, Wrocław University of Technology
amar_ec006@yahoo.co.in

^b Phd's student of Department of Mechanical and Power Engineering, Wrocław University of Technology
grzegorz.maliga@pwr.wroc.pl

Abstract

An ultracapacitor bank control system for an Electric Vehicle has been simulated. The purpose of this device is to allow higher accelerations and decelerations of the vehicle with minimal loss of energy, and minimal degradation of the main battery pack. The control of the system measures the battery voltage, the battery state-of-charge, the car speed, the instantaneous currents in both the terminals (load and ultracapacitor), and the actual voltage of the ultracapacitor. This last indication allows knowing the amount of energy stored in the ultracapacitor. When the car runs at high speeds, the control keeps the capacitor discharged. If the car is not running, the capacitor bank remains charged at full voltage. Medium speeds keep the ultracapacitors at medium voltages, to allow future accelerations or decelerations. The battery voltage is an indication of the car instantaneous situation. When the vehicle is accelerating, the battery voltage goes down, which is an indication for the control to take energy from the ultracapacitor. In the opposite situation (regenerative braking), the battery voltage goes up, and then the control needs to store the kinetic energy of the vehicle inside the ultracapacitor. The measurement of the currents in both sides allows keeping the current levels inside maximum ratings. The battery state-of-charge is used to change the voltage level of the ultracapacitor at particular values. If the battery is fully charged, the voltage level of the capacitors is kept at lower levels than when the battery is partially discharged.

Keywords: Hybrid vehicles, Ultracapacitor, Regenerative braking, energy modeling, Battery pack.

I. INTRODUCTION

Ultracapacitors are a new technology that allows to store 20 times more energy than conventional electrolytic capacitors. Despite this important advance in energy storage, they are still far from being compared with electrochemical batteries. Even Lead-acid batteries can store at least ten times more energy than ultracapacitors. However, they present a lot better performance in specific power than any

battery, and can be charged and discharged thousand of times without performance deterioration. These very good characteristics can be used in combination with

normal electrochemical batteries, to improve the transient performance of an electric vehicle, and to increase the useful life of the batteries. Fast and sudden battery discharge during acceleration, or fast charge during regenerative braking can be avoided with the help of ultracapacitors. Besides, ultracapacitors allow regenerative braking even with the batteries fully charged. In this paper, an auxiliary ultracapacitor bank, using a Buck-Boost converter, has been simulated. The ultracapacitor has a capacity of 7 Farads, a nominal voltage of 300 Vdc, and a maximum voltage of 360Vdc. It comprises 144 units in series, each one with 1,000 Farads, and 2.5 volts dc nominal (2.7 volts maximum). The maximum current is 400 amps, and the weight of the capacitor bank is 45 kg. The total weight of the equipment is estimated in 70 kg.

II. THE SYSTEM PROPOSED

The Figure 1 shows a diagram of the ultracapacitor system proposed. The power circuit has two main components: the converter, and the ultracapacitor bank. The equipment is connected in parallel to the main battery, which has 26 batteries in series (312 Vdc nominal). The capacitor voltage is allowed to discharge until one third of its maximum voltage (around 120 Vdc), allowing to store an amount of 112 Wh of useful energy. This apparently poor amount of energy allows having more than 40 kW of power during 10 seconds, which is more than enough time for a good acceleration (or deceleration) without detriment in the battery life. The nominal power of the traction motor is 32 kW, and the peak power is 53 kW. During acceleration, transfer energy from the capacitor to the main battery. During regenerative braking, move

energy in the opposite direction. Because of the topology of converter, the ultracapacitor never reaches voltages higher than the battery pack (self-protection). To do all the duties during acceleration and deceleration correctly, a good control strategy is required. The control strategy strongly depends on the size of the ultracapacitor. With a large capacity, the vehicle can run taking an almost constant battery current (the average current). Under these conditions, the capacitor gives all the positive and negative variations around this average current and its voltage can indicate when is required to increase or decrease the average current given by the battery pack. However, this solution is costly because ultracapacitors are quite expensive right now. This reason forces to install an ultracapacitor as small as possible, but large enough to avoid battery voltages too low or too high, and battery currents (negative or positive) too high. Under these economical reasons, many variables need to be measured, each one with a different priority.

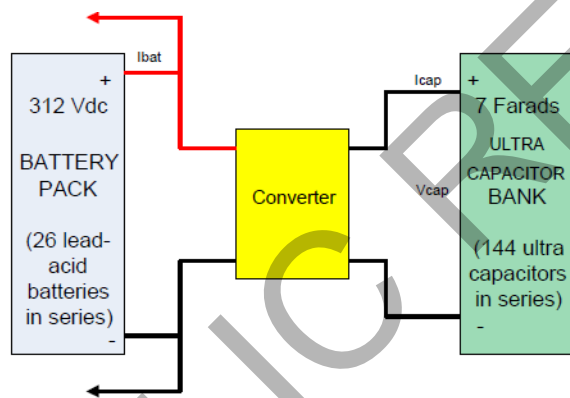


Figure1, Ultracapacitor system

III CONTROL STRATEGY

Considering the high cost of the ultracapacitors, the total capacity in Farads has to be minimized. Then, a more complicated control strategy is required, because the energy stored is in this case limited. Every variable, such as instantaneous battery voltage, battery state of charge, instantaneous battery current, ultracapacitor initial conditions, capacitor current, and so, need to be sensed. The speed of the vehicle also needs to be taken in account because when the vehicle is going to start, all the capacitor energy will be required. By contrast, when the vehicle run at high speeds (more than 80 km/h), the ultracapacitors need to be empty, to be able to receive the energy coming from a sudden emergency stop. At medium speeds, the ultracapacitor should have in-between charge inside. The state of charge has to be considered because full charged batteries do not accept any current, and hence, under this condition, the ultracapacitor has to be discharged (that means no

more than 15-20 % of its full capacity). Only if the car goes to a total detention, some amount of energy could be required. By contrast, if the battery state of charge is poor, the ultracapacitor should keep an amount of energy higher than under normal conditions. The state of charge is estimated by time integration of the battery current (positive or negative). The system also recognizes a fully charged battery when its voltage goes up rapidly under a regenerative braking condition. As the energy stored in the ultracapacitor is proportional to V_{CAP}^2 , this voltage gives a good indication of its remained charge. The capacitor voltage is being controlled, through the interaction of the other aforementioned variables, such as the vehicle speed, and the state of charge of the battery. The measurement of the instantaneous battery voltage, and the sign of the load current (positive or negative), If the battery voltage goes up rapidly, the controller activates, and a given amount of energy is transferred to the ultracapacitor. This situation happens when the vehicle is running and the brake is activated. Under this condition, the previous state of the overall system should have kept the ultracapacitor voltage at low levels. By contrast, in acceleration the control operation will be activated when the battery voltage goes down (acceleration), and when the vehicle is going to move, or accelerating from low speeds (positive current from the batteries). Under these conditions, and if the battery is not fully charged, the ultracapacitors should be at high levels of stored energy. All the operation described above, has to be controlled by a microprocessor, which discriminates and takes the appropriate decisions for each particular situation. The best way to give each variable a right significance, is by using a combined control. This combined control has two levels: a Primary Control, and a Secondary Control. The Primary Control establishes the current reference (IREF) to be given to the ultracapacitor for each operation condition, and the Secondary Control generates the PWM signals for Converter. The Figure 2 shows the Primary Control.

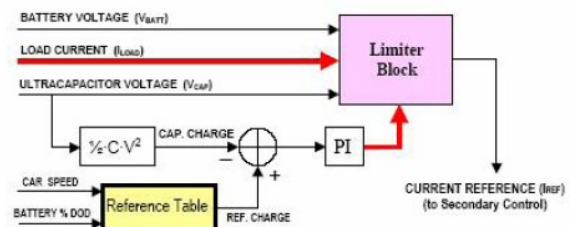


Figure 2, Primary Control

The first duty of the Primary Control is to keep an adequate level of energy into the ultracapacitor. This level of energy, or charge (REF. CHARGE in Figure 2), is calculated through the EV speed (CAR SPEED), and the battery state of charge (BATTERY % DOD). The block named Reference Table in Figure 2 makes this calculation, following a criterion

shown in Figure 3. The higher the speed, the lower the charge, and the higher the battery state-of-charge, the lower the charge too. The shape of these curves was estimated taking in account the time the control takes to reach the desired ultracapacitor charge.

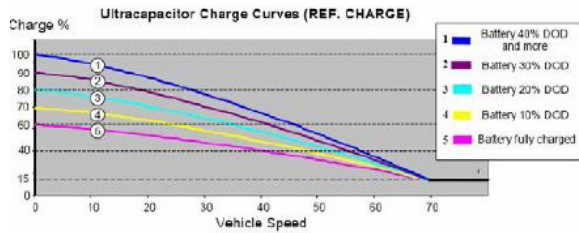


Figure 3, Family plots of the Reference Table, to evaluate the reference charge.

At the same time, the ultracapacitor voltage V_{CAP} is measured, and the actual charge is calculated. The error signal, between the reference charge and the actual charge is passed through a PI control, which evaluates the amount of current reference (I_{REF}), necessary to maintain the ultracapacitor bank with the desired amount of energy. All the process explained in the previous paragraph, to maintain an adequate charge into the ultracapacitor, is followed accordingly. However, if the battery voltage (V_{BATT}) exceeds their minimum and maximum settings, I_{REF} is modified. A similar action is performed when the ultracapacitor voltage V_{CAP} is too low or too high. The load current (I_{LOAD}) is also an important reference inside the Primary Control. When this current exceeds the maximum absolute values set on the battery pack (I_{BATT}), the current reference (I_{REF}) is also modified. Then, to take in account all these situations, some logical rules have been implemented. These rules are programmed inside the Limiter Block shown in Figure 2.

IV SIMULATION RESULTS

The next oscillograms show the results obtained with the simulation. Many different situations were simulated. To make the results more real, use the conclusions of some experiments with the electric vehicle were performed on the streets. These experiments allowed evaluating the time the vehicle needs, and the current and voltage variations during acceleration, and regenerative braking. These experiments showed that the vehicle can accelerate from 40 to 60 [km/h] in a little more than 4 seconds, and that the maximum current taken from the battery reaches 200 amps. When the vehicle reaches steady-state at 60 [km/h], the battery current goes down at a constant value of around 20 [A]. With these informations, the system proposed was simulated. The result of this simulation (from 40 to 60 [km/h]) is shown in Figure 4. This figure displays the battery

voltage V_{BATT} , the ultracapacitor voltage V_{CAP} , the load current to accelerate the car I_{LOAD} , the battery current I_{BATT} , and the compensation current I_{COMP} that comes from the energy stored in the ultracapacitor. The settings for the battery into the control were: $V_{min}=300$ V_{dc}, and $V_{max}=360$ V_{dc}; $I_{min}=-70$ A_{dc}, and $I_{max}=70$ A_{dc}.

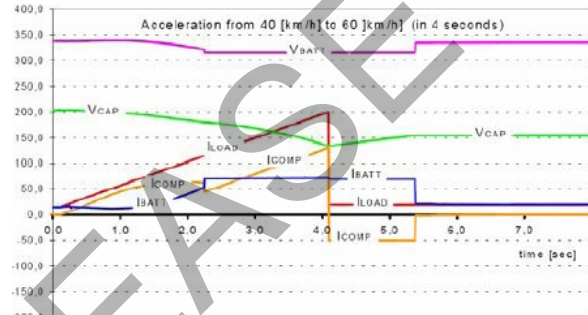


Figure 4, Acceleration from 40 to 60 [km/h]

When the load current begins to increase, most of the current is taken from I_{COMP} , which comes from energy stored into the ultracapacitor. As the capacitor voltage V_{CAP} decreases (energy is going down), more current begin to be taken from the battery, but when the battery reaches its limit (70 amps.), the capacitor is forced to give all the current in excess of 70 [A]. This action produces a faster decrease in the ultracapacitor voltage. If the capacitor voltage reaches its minimum setting (120 V_{dc} with a maximum of 360 V_{dc}), then the vehicle should not be able to continue accelerating, because at this point, 90% of the capacitor energy would have been used. If the capacitor is large enough (as in this case), this situation will not happens, and the capacitor will be able to end its duty. Later on, the capacitor will be able to recover energy, once the vehicle reaches constant speed. This case is also shown in the Figure 4. When the EV reaches constant speed (60 km/h), the compensating current I_{COMP} becomes negative, charging the capacitor. As the car is not braking, this energy is being taken from the battery, but at a maximum value given by the limit set by the controller (70 A_{dc}). Once the capacitor recovers its energy, the battery current goes down, as shown in the final seconds of simulations in Figure 4. Finally, when the ultracapacitor recovers the energy, which corresponds to the value given by the Reference Table of Figure 2, the load current takes power only from the battery pack. A second simulation, displayed in Figure 5, shows a deceleration from 40 [km/h] to stop. This regenerative action takes 2.1 seconds. The regenerative current goes from 200 A_{dc} to zero in the time indicated above. Both, the battery and the ultracapacitor, through I_{BATT} and I_{COMP} , receive this current respectively. The simulation shows that the battery receives a current smaller than the limit of 70 A_{dc}. This happens because the maximum voltage allowable by the battery (360 V_{dc}) is reached first. This means that the battery is almost fully charged, and then cannot receive more than 30 A_{dc}

approximately. For this reason, most of the current is taken by the ultracapacitor. Once the vehicle stops, the battery continues charging the capacitor until it reaches its final charge (the Reference Table of Figure 2 gives the required amount of charge). In this case the amount of energy stored in the ultracapacitor corresponds to a voltage of around 260 Vdc.

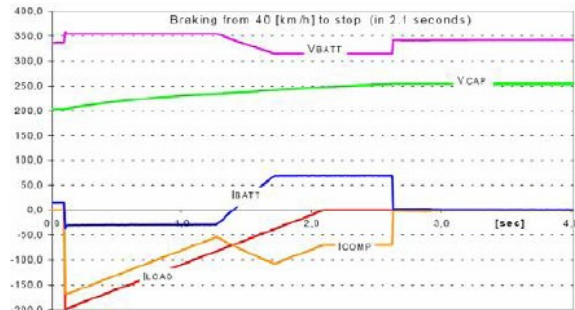


Figure 5, braking from 40 [km/h] to zero

It can be noted that the battery current begins to be positive before the vehicle reaches zero speed. This is because the capacitor needs to have more energy at that particular speed, and then the control begins to charge the capacitor in advance.

V. CONCLUSIONS

An ultracapacitor bank for an Electric Vehicle has been simulated. The purpose of this device is to allow higher accelerations and decelerations of the vehicle with minimal loss of energy, and minimal degradation of the main battery pack. The control of the system measures the battery voltage, the battery state-of-charge, the car speed, the instantaneous currents in both the terminals (load and ultracapacitor), and the actual voltage of the ultracapacitor. The simulations showed that the control system can work properly, taking in account all the aforementioned variables. It is interesting to mention that, if ultracapacitor reaches in the future, a specific energy of at least 20 Wh/kg (at this moment some laboratory samples reach 10 Wh/kg), it will be possible to implement EVs with ultracapacitors only. They could give a range of 100 kms with a 500 kgs capacitor bank, with very short charging time and excellent life expectancy. The EV will be able to be fully charged in few minutes. Besides, the ultracapacitor could last all the vehicle useful life.

REFERENCES

1. M.Ehsani, Modern Electric, Hybrid Electric and Fuel cells Vehicles, 2004
2. Maxwell. Ultracapacitors Data sheets and technical information for 1,000 and 2,500 Farads, [Maxwell publications]
3. L. A. Viterna, Ultra-Capacitor Energy Storage in a Large Hybrid Electric Bus, NASA Lewis Research Center, 21000 Brookpark Rd., Cleveland, Ohio 44135.

14th Electric Vehicle Symposium, 1996.

4. Robert G Wieggers, Donald M Blacketter, Herbert L Hess, Modeling performance of ultracapacitor arrays in hybrid electric vehicles, Int. J. Alternative Propulsion, Vol. 1, No. 1, 2006

Solar energy in Spain

Dariusz Szymański
Wrocław University of Technology
Janiszewskiego 8 str
Wrocław, Poland

Abstract- The article shows what kind of solar power plants is used in Spain. It describes what technologies are used to build this objects and how do they work.

I. INTRODUCTION

Every country spends large amount of money for renewable energy sources. What type of “green energy” a country can use, depends on what climatic conditions does it have. For example in places with strong winds we can develop wind energy. Another countries, especially those lying on the south of Europe, have great conditions for using sun in their energetic economy.

Spain is one of the most attractive countries for the development of solar energy (fig. 1). The Spanish government said that they will achieve a target of 12 percent of primary energy income from renewable energy by 2010. This includes solar power system, which will be generating a capacity of 3000 megawatts (MW). Spain is the fourth largest manufacturer in the world of solar power technology and exports 80 percent of this output to Germany.

Through a ministerial ruling in March 2004, the Spanish government removed economic barriers to the connection of renewable energy technologies to the electricity grid. The widely applauded Royal Decree 436/2004 equalises conditions for large-scale solar thermal and photovoltaic plants and guarantees feed-in tariffs.

In Spain are three interesting power station using solar radiation to generate electricity. There are PS 10, Andasol and photovoltaic power stations.



Figure 1. Yearly total of global horizontal irradiation [kWh/m²/year] in Spain and Portugal

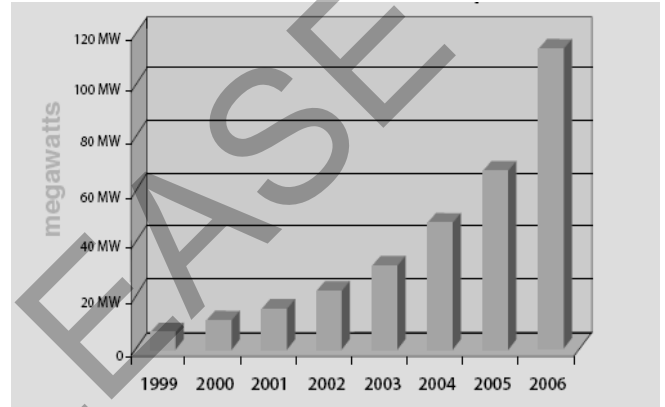


Figure 2. Growth of Solar power in Spain

II. PS 10

Construction of the PS10 project, an 11 MW Solar Thermal Power Plant in Southern Spain has been completed in 2008. This object is located in Sanlúcar la Mayor, 15 km west of the city of Seville. This type of electric power station is called Central Receiver System (CRS). The fig. 4 shows how does it work. This power plant is the first solution of this type in Europe. All technologies used in this project, like glass-metal heliostats, a pressurized water thermal storage system and a saturated steam receiver and turbine, have been developed by European companies.

The heliostat field is composed of 624 heliostats each of 120 m², with a mobile curved reflective surface which concentrates solar radiation on a receiver at the top of a 100 m tower. In the receiver, the steam is heated up to 40 bar (250°C) by thermal energy supplied by the concentrated solar radiation flux.

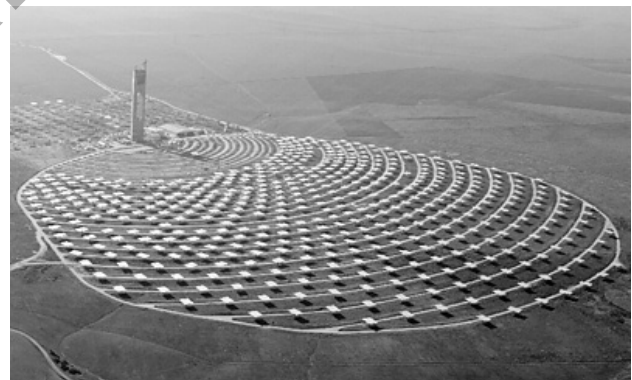


Figure 3. PS 10 power plant (bird's-eye view)

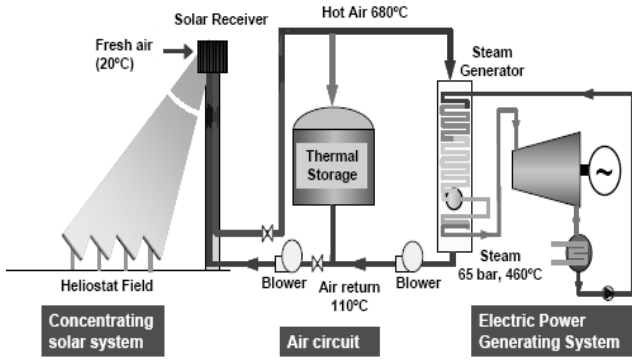


Figure 4. Main schema of working PS 10

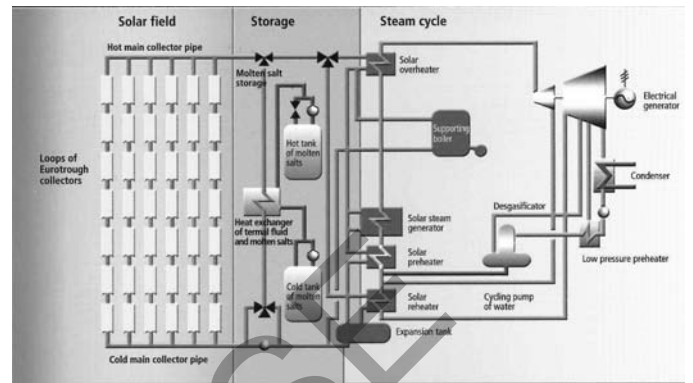


Figure 5. Main schema of working Andasol

Next, the steam is sent to the turbine, where it produces mechanical work, which is in the next step changed into electricity by synchronic generator. The turbogenerator output goes to a water-cooled 0.06 bar pressurized condenser. The condenser output is preheated by 0.8 bar and 16 bar turbine extractions. The output of first preheater is sent to a deaerator fed with steam from another turbine extraction. A second preheater is fed with steam coming from the receiver. This preheater increases the water temperature to 245°C. This solution has a task to increase the water returning from the drum to temperature to 247°C, which is flowing out from the condenser.

Sometimes clouds curtain the sun. In that case, the plant has a 20-MWh thermal capacity saturated water thermal storage system (equivalent to 50 minutes of 50% load operation). The system is made up of 4 tanks that are sequentially operated in order of their charge status. On the figure 4 is shown, that part of the 250°C/40 bar steam produced by the receiver is going to the thermal storage system. When energy is needed to cover a transient period, the energy is recovered from the saturated water at 20 bar to run the turbine at 50% load.

This is a big structure, so to reduce the visual impact of this building the body of the tower is rather thin when we look at from the side. The tower has 115m total height, 18m wide and is just 8m width. The front has to have that length because it has to allocate the 14 m wide receiver. A large space has been left open on the bottom of the tower to give the impression of a lightweight structure. For the visitors there is a special platform, which is 30 m height. From that places there is a good view of the heliostat field lying north of the tower, and the Sevilla photovoltaic plant (PV) south of the PS10 power plant.

III. ANDASOL SOLAR POWER STATION

This kind of solar power plant was for first time used in commercial operation in California in 1985. Parabolic trough power plants have already generated over twelve billion kilowatt hours of solar electricity, which equates to providing 12 million people with electricity for one year. In parabolic trough power plants electricity is generated using a steam turbine which is connected with the generator. This is the same solution like the one which is used in conventionally fuelled

power plants, including nuclear power plant. However, in Andasol power station steam is not produced by burning fossil fuels but by usage of solar energy. The solar radiation is captured and concentrated by long rows of parabolic mirrors. The radiation from the sun is reflected from the mirrors and concentrates on long pipes filled with water or another liquid, which has big heat capacity and small viscosity. The heat generated in this way is enough to produce the steam required.

Solar Millennium developed parabolic trough power plants in Europe. The Andasol 1 plant works since autumn 2008, Andasol 2 and 3 are currently under construction in southern Spain. The amount of electricity this power station produces is about 180 GWh per year. The collector surface area can be compared to 70 football fields. This is over 510,000 m².

When the Andasol 2 and 3 will be finished they will supply over 200,000 people with solar electricity. The construction will probably last about two more years. They will also contribute to Spain's supply reliability and in particular, cover the demand peaks in the Spanish electricity grid during the summer months. Each power plant has an electricity output of 50 megawatts and operates with a thermal storage. The task of this storage is the same like in the PS 10. There are two tanks which have 36m in diameter and 14m in height. Each of them can be filled with 28,500 tons of the storage medium. A full thermal reservoir can continue to run the turbines for about 7.5 hours at full-load, even if it rains or long after the sun has set.



Figure 6. Andasol solar power station (bird's-eye view)

IV. PHOTOVOLTAIC POWER STATIONS

Photovoltaics is a method for transform a solar radiation into electrical power. Photons from sunlight knock electrons into a higher state of energy, creating electricity. It can be achieved by using solar cells packaged in photovoltaic modules, often electrically connected in multiples, as solar photovoltaic arrays, to convert energy from the sun into electricity. The term photovoltaic denotes the unbiased operating mode of a photodiode in which current through the device is entirely due to the transduced light energy.

Solar cell is a device that converts sunlight directly into electricity, which can be used to power equipment or to recharge a battery. The first practical application of photovoltaics was to power orbiting satellites and other spacecrafts, but today they are used usually as photovoltaic modules, used for grid connected power generation. There is a smaller market for off grid power for remote dwellings, roadside emergency telephones, remote sensing and cathodes protection of pipelines.

Cells are sensitive for the environment so they are packaged usually behind a glass sheet. To achieve more power from the photovoltaic modules we can connect them together to form solar panels. Cells can be connected in series creating an additive voltage. Connecting cells in parallel will yield a higher current Although the price of modules is still too high to compete with grid electricity in most places, significant financial incentives in Japan and then Germany triggered a huge growth in demand, followed quickly by production.

In last years many solar photovoltaic power stations have been built in Spain. As of January 2009, the largest photovoltaic power plants in Spain are the Parque Fotovoltaico Olmedilla de Alarcon (60 MW), Planta Solar Arnedo (30 MW), Parque Solar Merida/Don Alvaro (30 MW), Planta solar Fuente Álamo (26 MW), Planta fotovoltaica de Lucainena de las Torres (23.2 MW), Parque Fotovoltaico Abertura Solar (23.1 MW), Parque Solar Hoya de Los Vincentes (23 MW), Huerta Solar Almaraz (22.1 MW), Solarpark Calveron (21 MW), and the Planta Solar La Magascona (20 MW).



Figure 7. Solar Panels – Spain

V. CONCLUSION

The Spanish government continues to promote the investment and expansion of both photovoltaic and solar thermal power in the country, with a goal of 400 MW installed power for PV and 500 MW for solar by 2010. This is still only a small piece of the country's total power use and total renewable energy production.

The government, however, is committed to advance this sector. The new requirements of 2006 requires increased energy efficiency and an obligation to meet a significant part of the hot water demand with passive solar heating. The Plan of Renewable Energies sets lofty goals of 5 million square feet of solar collectors by 2010. They new Royal Decree approved in May 2007 improves the feed-in tariffs for both solar thermal and photovoltaic facilities. Spanish companies and research institutions plan to continue to be at the forefront of the growing global field.

The president of the Spanish Photovoltaic Industry Association, Javier Anta said that the solar industry will be a major part of the government's goal of 20 percent renewable energy by 2020. This is still a small percentage of renewable power. However, it's grown more than 100 percent a year in the past few years. Anta wants to continue developing new technology which improve using solar energy.

REFERENCES

- [1] <http://www.solarpaces.org/>, 29.02.2009
- [2] http://en.wikipedia.org/wiki/Solar_power_in_Spain, 29.02.2009
- [3] http://en.wikipedia.org/wiki/Andasol_solar_power_station, 29.02.2009
- [4] <http://www.technologyreview.com/spain/solar>, 29.02.2009
- [5] http://www.solarmillennium.de/Technologie/Referenzprojekte/Andasol/Die_Andasol_Kraftwerke_entstehen_lang2,109,155.html, 29.02.2009
- [6] http://www.nrel.gov/csp/troughnet/pdfs/2007/martin_andasol_pictures_storage.pdf, 29.02.2009

SINGLE PHASE STATCOM –ITS CONTROL ALGORTHIM

Linju Jose

Department of Electrical & Electronics Engineering
Rajiv Gandhi Institute of technology, Kottayam

Kerala, India

E-mail:linju_j@yahoo.co.in

Abstract- In this paper, a new type of single phase static compensator (STATCOM) for low rating used in customer side is proposed. This new STATCOM is constructed by cascading a full-bridge (H Bridge) voltage-source inverter (VSI's) to the point of common coupling (PCC.) A so-called sinusoidal pulse width modulation (SPWM) unipolar voltage switching scheme is applied to control the switching devices of each VSI. A new control strategy is adopted for compensating the harmonics and reactive current required by the load. The proposed STATCOM has the advantage of a fewer number of VSI's, the VSI's being identical and extremely fast in response to reactive power change and the control strategy adopted shows a good response.

Index Terms—Static compensator, voltage-source inverter, PCC, reactive power, harmonic current.

1. Introduction

The proliferation of power electronics systems in a wide range of equipments, from home VCRs and digital clocks to automated industrial assembly lines and hospital diagnostics systems has increased the vulnerability of such equipment to power quality problems. These problems include a variety of electrical disturbances, which may originate in several ways and have different effects on various kinds of sensitive loads. As a result of this vulnerability, increasing numbers of industrial and commercial facilities are trying to protect themselves by investing in more sophisticated equipment to improve power quality. Moreover, the proliferation of nonlinear loads with large rated power has increased the contamination level in voltages and currents waveforms, forcing to improve the compensation characteristics required to satisfy more stringent harmonics standards.

Now a days the requirement for power quality becomes more and more important to keep safety of the electrical devices and consumer satisfaction. The growth of the non-linear loads like the devices with switching power supplies have increased current harmonics, EMI problems, unnecessary reactive power and power losses. Fast switching devices like CMOS or IGBT transistors provide implementation of full bridge inverters to serve as a real time parallel compensators by bidirectional energy flow to control and compensate reactive power and current harmonics. Static Var Compensator can be

utilized to regulate voltage, control power factor, and stabilize power flow [1].

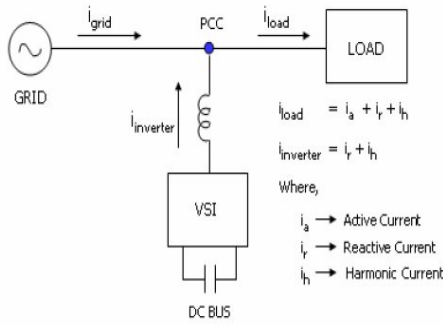
Most of Var compensators employ a combination of fixed or switched capacitance and thyristor controlled reactance. Several Var compensator based on a voltage sourced inverter, known as STATCOM, have been proposed and demonstrated [2-4].

In this paper the main goal is proposing a low cost single phase commercial STATCOM control topology to act as an active filter for single phase nonlinear load by using controller using PIC microcontroller. The control technique is useful to modify harmonics current required by the load and compensate reactive power due to relatively asymmetrical unbalanced non-linear loads. The required data's are achieved from dc bus voltage, grid voltage, load current and inverter current. Main tuning parameters are obtained from conventional PI controller.

2. CIRCUIT CONFIGURATION

2.1) Statcom a simplified picture

STATCOM is a Voltage Source Inverter (VSI) connected in shunt to the system at the point of common coupling (PCC) as shown in Fig.1. The load current can be thought of as having three components – active, reactive and harmonic. The idea is to control the voltage source inverter in such a way as to make it deliver the reactive and harmonic currents demanded by the load so that the grid has to supply only the active current. This means that the grid current will be purely sinusoidal and will be in-phase with the grid voltage on connecting the STATCOM. Ideally, it is possible to supply the reactive and harmonic current requirement of the load with a VSI having a DC bus capacitor and no external power source as the net power supplied by the STATCOM during any given fundamental period is zero. However, a small amount of real power will be absorbed from the grid practically – to compensate for the energy losses in the system.



A1 Fig.1 Voltage source inverter as a grid connected STATCOM

to the power system. In these types of applications PWM-VSI operates as current controlled VSI. In Statcom the aim is to make VSI continuously track and deliver the reactive and harmonic currents demanded by load. This calls the use for current controller. The VSI act as a bidirectional converter operates as an inverter to supply the compensating voltage to load and as a converter when charging the capacitor. The topology adopted for the bidirectional converter is full bridge topology [6] and a capacitor of medium rating.

2.2) Circuit explanation

The Statcom should essentially consist of a single phase inverter, Dc side capacitor meant for dc voltage for inverters, filter components to filter out high frequency components of inverter output voltage, link inductor that links the inverter output to the ac supply side and interface magnets(if required)and related control blocks.

Figure2 shows the circuit diagram consisting of 4 self commutated semiconductor switches (IGBT, MOSFET) with anti-parallel diodes which, act as a full bridge converter. In this converter configuration, IGBT constitute the switching devices. With a dc voltage source (i.e. charged capacitor), the converter can produce balanced voltage waveforms of given frequency.

The reference signals are generated by sensing the grid voltage, dc voltage, converter current and load current. The sensed values are given as the input to the controller so as to generate the reference values for compensation.

The inverter generates a three phase voltage which is synchronized with the ac supply, from the dc side capacitor and links this voltage to ac source. The current drawn by the inverter from ac mains is controlled to be reactive with little active component which is needed to supply the losses. Main condition for operation of the circuit is the amount of charged voltage on the dc link capacitors, so as to have bidirectional current flow of current, the following condition should be satisfied

$$V_c \geq \sqrt{2}V_l \quad \text{-----(1.1)}$$

Term V_c is capacitor voltage and V_l is effective grid voltage. For this the converter acts like a Boost converter to transfer the stored energy to the load.

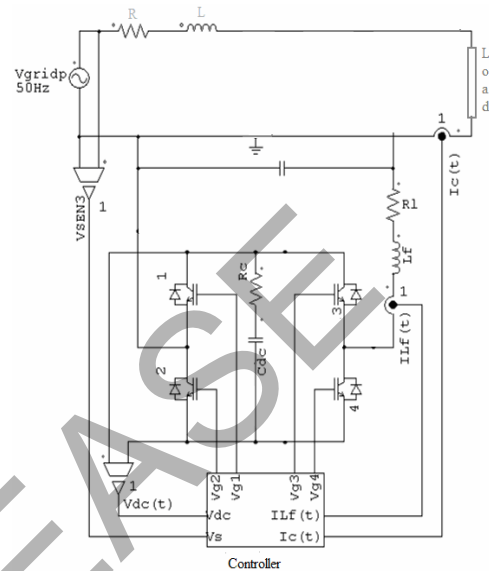


Fig.2. Proposed circuit configuration

3. CONTROL STRATEGY FOR THE SYSTEM

The control strategy has mainly three sections, as follows

1. Extraction of harmonic or reactive current from load current
2. Generation of Unit Vectors from Grid Voltage
3. Reference voltage for PWM generation

3.1)Control block of STATCOM

The main control block diagram is shown in the figure 3. The required data's are sensed d from dc bus voltage V_{dc} , grid voltage V_g , load current $i_c(t)$ and inverter current $i_l(t)$, and corresponding unit vectors is generated which is in phase and 90° phase shift sine and cosine waves respectively. With respect to these voltage vectors the pulse is generated.

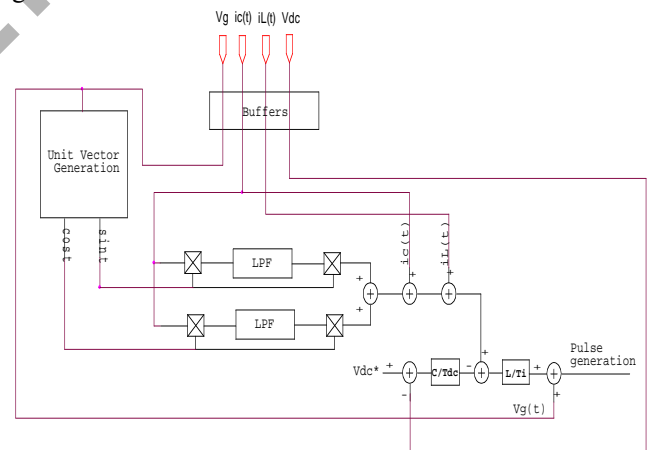


Fig.3. Control block of the Statcom controller

3.2) Unit Vector Generation

There is no backup or battery for the system. Taking voltage from the grid and using it for compensation but grid voltage cannot be pure sinusoid, it consist of harmonics and therefore corresponding to grid voltage the current cannot be generated. One method

for PWM generation is creating truth table for grid voltage and then triangular comparison can be done, but the change in grid voltage affect the truth table. More the values in truth table more accurate will be the signals but then memory required increases therefore a strategy known as Unit vector generation is adopted.

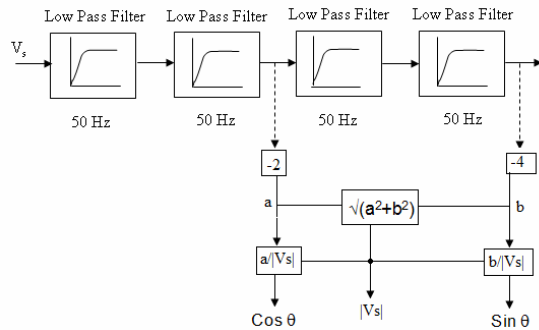


Fig.4 Block diagram for unit vector generation

In this method corresponding voltage is generated whose magnitude is always unity. Fig.4 shows the block diagram for unit vector generation in which the peak value of the grid voltage is sensed by sensing the zero crossing of the cosine wave (i.e. 90° phase lag with the grid voltage.). Each low pass filter has 45° phase difference which create cosine and in phase component.

3.3) Harmonic current generation:

Let us assume that unit vectors are known and the direction of current from inverter to grid is taken as positive.

Let the grid voltage be

$$V_{grid} = V_g * \sin \omega t \dots\dots\dots (3.1)$$

Generalised Load current be

$$I_{load} = I_o + I_p \sin \omega t + I_q \cos \omega t + I_{harmonic} \dots(3.2)$$

$$I_{harmonic} = I_{load} - (I_o + I_p \sin \omega t + I_q \cos \omega t) \dots(3.3)$$

Where I_o =dc component, I_p =peak of active current, I_q =peak of reactive current.

Figure 6 shows the diagram for generating the harmonic current that's required by load for compensation. The dc component can be neglected as it the low value and then the harmonic current is obtained by

$$I_{harmonic} = I_{load} - (I_p \sin \omega t + I_q \cos \omega t) \dots(3.4)$$

The active part is obtained by multiplying by in phase component and the reactive part by phase lag component.

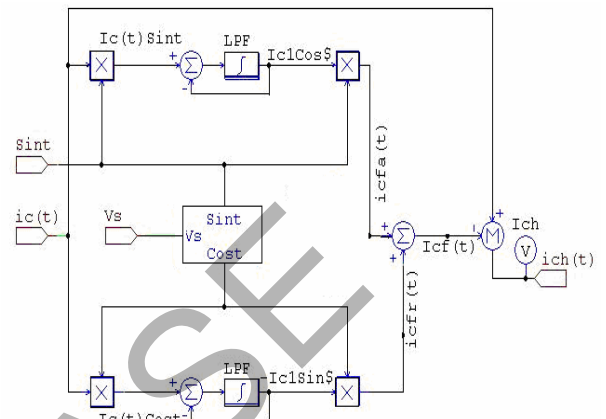


Fig 5 Block Diagram for Harmonic current extraction

Sint and Cost are generated unit vectors, icfa(t) and icfr(t) are active and reactive components respectively.

4. CONTROL ALGORITHM FOR SINGLE PHASE STATCOM

This section describes about the control of the proposed circuit. The flow diagram given explains the control of Statcom for compensating the harmonic current. The controller used is PIC microcontroller aiming for low cost system. The controller used here is PIC18FXXXX series.

The main concept is

1. First sense the DC bus voltage and make sure it's greater than grid voltage
2. Check if grid voltage within range, if it's within range then starts charging the capacitor and enter the Statcom Controller loop.

At the time of start, the condition of the controller is unknown there may be chance of starting the system with the previous conditions therefore the controller has to be reset first then the initialisation process takes place. After that the controller has to be started for that first the timers are started and then unit vector generation takes place according to the fig.4, in user interface the protection algorithm is given such that over current, overvoltage, initial start-up conditions are all satisfied according to the conditions and then if flag is set then Statcom controller is called after the conditions the ADC process takes place and the parameters are displayed through DAC and the process continues.

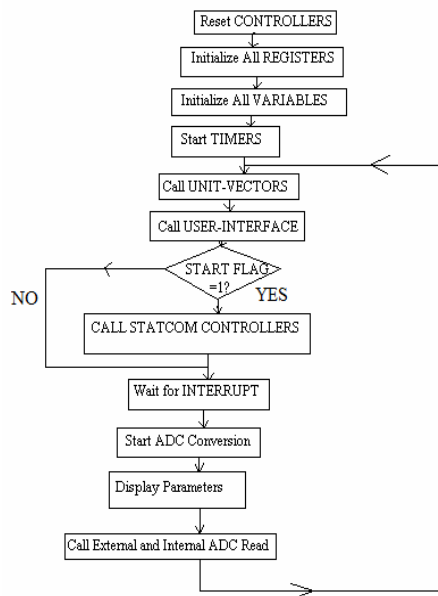


Fig.6. Flow diagram of proposed circuit

The PWM generation takes place according to the sensed value. The switching frequency given is 10 kHz and therefore controller has to complete one full cycle within 100 μ sec.

5. CONCLUSION

The basic principle and controller design of a STATCOM was studied in detail in the present work. The methods so far used were depending upon the synchronous reference frame, hysteresis band control and many more. In this paper a new control strategy was developed and the harmonic current compensation was made. On focusing the low cost factor the controller used is PIC microcontroller. The control strategy shows good results.

7. References:

- [1]. Don A.G. Peedder , A.D.Brown, "A parallel-connected active filter for reduction of supply current distortion", *IEE Trans. Ind.Elect.* , Vol.47, No.5, pp 1108-1117.Oct 2000
- [2]C.W.Edwards, K.E.Mattern, E.J.Stacey, P.R.Nannery, J.Gubernick, "Advanced Static VAR generator employing GTO thyristors," *IEE Trans.on Power Delivery*, vol.3,no.4,pp 1622-1627, Oct.1998.
- [3]. S.Mori, K.Mansuno, M.Takeda and M.Seto, "Development of a large static var generator using self-commutated inverter for improving power system stability", *IEEE Trans.Power Systems* , vol.8,no.1,pp 371-377 Feb.1993
- [4].C.Schauder, M.Gernhardt, E. Stacey , T.Lemak, L.Gyungi, T.W.Cease, and A.Edris,"Development of a +/-100MVAR Static condenser for voltage

control of transmission system,"*IEEE Power Engineering Society, Summer Meeting 1994.* pp.479-6.1-8.

[5] Y.Sumii, Y.Harumoto, T.Hasegawa, M.yano, K.Ikeda, and T.Matsuura, "New static VAR control using force-commutated inverters," *IEEE Trans. Power Apparent.Syst.*, vol.PAS-100.pp.4216-4224, Sept.1981.

[6] C.K.Lee, S.K. Leung, S.Y.Ron Hui, Henry Shu-Hung Chung," Circuit-level comparison of STATCOM Technologies,"*IEEE Trans. Power Electronics*, vol.18.no.4 pp.1084-1092,July, 2003.

[7]Simone Buso, Luigi Malesani, Paolo Mattavelli, "Comparison of current control techniques for active filter applications", *IEEE Trans. Ind.Elect*,vol.45.,No.5,pp. 722-729 Oct.1998

[8]Bhim Singh, Kamal Al-Haddad, Ambrish Chandra," A review of active filters for power quality improvement",*IEEE Trans. Ind.Elect.* ,vol.46,No.5,pp.960-971Oct.1999

Transients phenomena in capacitive voltage transformers – distance protection point of view.

Rafal Kurnatowski

Abstract – This paper presents problems of distance protection due to transients in capacitive voltage transformers (CVT's). CVT is a basic equipment which sends information to relay about voltages in protected system. During transmission lines faults severe transients can occur. As a result we can obtain mal-operation of distance protection.

I. INTRODUCTION

Operation of distance relays with capacitive voltage transformers meets problems. They are directly connected to transients states of capacitive voltage transformers which appear during transmission lines faults. In this case mal-operation can occur. Relay may not recognize fault place. Moreover it's difficult for distance relay to distinguish quickly between fault within protection zone and fault at the reach point. Another problem is a low speed and worse accuracy of distance protection. Therefore these problems have to be taken into consideration.

II. CVT TRANSIENTS

A. Equivalent circuit of CVT

Main components of a generic CVT are: tuning reactor, step-down transformer, ferroresonance suppression circuit and a capacitive voltage divider. It consists also many additional devices which are not important in point of view transients phenomena. There are two important diagrams below. Figure 2 is a simplification of equivalent circuit of CVT from figure 1.

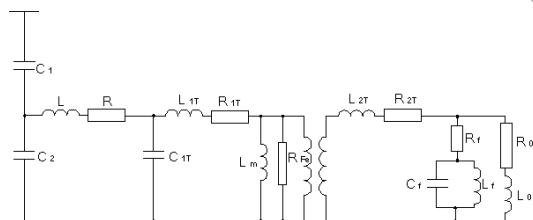


Figure1. Equivalent circuit diagram of a CVT

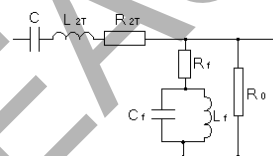


Figure 2. Simplified model of a CVT from Figure 1

Diagram from figure 2 consists following parameters:

- C – sum of the stack capacitances
- L,R – equivalent inductance and resistance of the tuning reactor and the step down transformer
- R₀ – burden resistance
- R_f, C_f, L_f - parameters of anti-resonance circuit

B. Nature of transients

During line faults primary voltage of CVT collapses. Energy stored in stack capacitances and tuning reactor need to be dissipated. This produce a severe transients for distance relays. These transients can have different nature. It can be forecasted by analysis of CVT transfer function (1), where factors A and B in nominator and denominator are functions of parameters marked on simplified CVT diagram in figure 2.

$$G_{CVT}(s) = \frac{A_3 s^3 + A_2 s^2 + A_1 s}{B_4 s^4 + B_3 s^3 + B_2 s^2 + B_1 s + B_0} \quad (1)$$

Eigenvalues of (1) determine nature of transient. Analysis of CVT transient nature [1], shows that induced transient can be:

- Combination of four aperiodically decaying dc components
- Combination of two oscillator decaying components
- Combination of one oscillatory decaying component and two aperiodically decaying dc components (general case)

C. High SIR problem

Drastic problems can be created by CVT transients during high System Impedance Ratios. It is proved (ref. [1]) that for higher SIR the fault voltage at the reach point drops to very small values. Also another problem appears. It is extremely unfavorable signal to noise ratio. It's illustrated at figure 3.

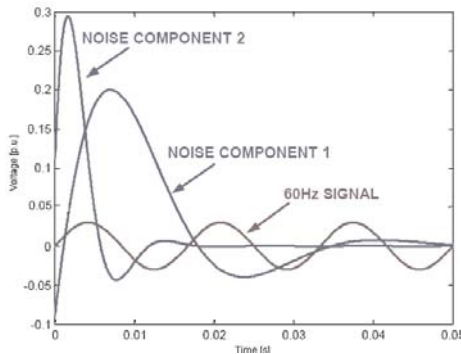


Figure 3. Signal-to-noise ratio for the CVT transients and high System Impedance Ratio

As illustrated in Figure 3, the magnitude of the noise components may be 10 times larger than the magnitude of the 60Hz operating signal. Noise dominates for 1.5 to 2 cycles.

Noise component frequency can be close to 60Hz in some part of time axis. Moreover noise vector can be in opposition to operating signal. In this case both signals cancel mutually to certain extent. Thus the phasor estimator tends to underestimate the magnitude.

III. CONTROL OF TRANSIENTS

Transients are basically controlled by the following factors (reference [1]):

- Sum of stack capacitances
- Shape and parameters of the ferroresonance suppression circuits
- CVT burden
- Point on wave when a fault occurs

A. Sum of stack capacitances

Magnitude of the transients is lower when the sum of stack capacitances is higher. It is true that behavior of a distance relay doesn't depend only on magnitude of fault signal. Price of stack capacitance is quite high. Therefore transient's magnitude takes secondary importance for transient overreach and speed of operation.

B. Ferroresonance suppression circuit

A ferroresonance suppression circuit is designed to prevent subsynchronous oscillations. They appear when there is saturation of the core of a step-down transformer during overvoltage conditions. This circuit has significant impact on the characteristic of the CVT transients because it creates an extra path (apart from the burden) for dissipating energy.

C. CVT load

Better CVT performance is obtained when it is fully loaded. Contemporary digital relays introduce a very low burden for CVT (100-400VA). As a solution we use often artificial load.

D. Point on wave when a fault occurs

The most severe transients appear at the zero crossing of the primary voltage. In this case transients can reach 40% of the nominal voltage magnitude.

IV. DISTANCE PROTECTION PROBLEM

Distance relays measure impedance to determine location of a fault. Due to transients in CVT's, voltage signal can be underestimated. Moreover current can be overestimated. These problems often lead to error in impedance measurement. It results in mal-operation of distance protection.

Nowadays there are known methods of control a current overestimation. As a solution we use mimic filter or band-pass differentiating filter. Unfortunately problems connected to voltage underestimation due to CVT transients are still significant. Series of simulation show that voltage estimation error can be equal even 90%. If we assume that current was estimated correctly, still we have 90% of impedance measure error.

There are a lot of methods to improve distance protection during CVT transients. One idea is pre-filtering voltage with non-symmetrical FIR filter. Another ideas are e.g. to use artificial intelligence techniques or testing new algorithms.

REFERENCES

- [1] B. Kasztenny, D. Sharples, V. Asaro, M. Pozzuoli, "Distance relays and capacitive voltage transformers – balancing speed and transient overreach," *55th Annual Georgia Tech Protective Relaying Conference Atlanta*, May 2001.
- [2] J. Izykowski, B. Kasztenny, E. Rosolowski, M.M. Saha, B. Hillstrom "Dynamic compensation of capacitive voltage transformers," *IEEE Transactions on Power Delivery*, Vol. 13, No. 1, January 1998

Power quality in automatic restoration systems using stand alone generators

Piotr Danielski, Marcin Dębowski
Wrocław University of Technology
Wrocław, Poland

Abstract – The aim of this paper is to give an introduction to automatic restoration of voltage techniques and technology. There is also basic generator power quality test presented, with specification of typical small power stand-by usage. All the tests were taken with Fluke 345 PQ meter. Introduction concerns also basic European Directives for power quality measurements and requirements.

I. INTRODUCTION

Lately automatic restoration subject become very important. Reasons for this to happen are economic, political and technical. For economic we could find: to big power demand factor for production of energy ratio, negligence in maintenance cost predictions and demanded high interest rate on each level of energy market. For political reasons we can try to find more restrictive energy quality directives, too big pressure on low energy price (depending on the market energy price is national or free). And at the end we can describe technical reasons which in many cases are partly technical because of their origin in one of the above groups. For instance low maintenance expenditure effects with many failures in the network, though insulators and lines have defined lifetime often this period, due to other important works, is being exceeded. Another technical problem comes with load factor in the grid. Many faults are due to reactive power unbalance, involving generator under-excitation, sustained overvoltage, and switched capacitors/reactors. Other which are partly connected with those were problems due to load and generation unbalance, including responses to sudden increases in load and under-frequency load shedding including lack of black-start capability, problems with switching operation, line overloads and control center coordination. [2]

To prevent consequences of failures many systems are equipped in fast disconnectors and automatic restoration system with auto reclosing procedures (for over-head lines) or which is also common (mostly for private usage) with standby source able to work instead of mains supply. Typical AR system is presented on fig. 1.

[1] We can distinguish two groups of AR systems. One will be created by systems using evident stand-by source, which are often working with some flat period (with break after failure). These systems are using some stand alone generators (e.g. petrol [III.] or diesel generators, batteries and other energy storage devices). The other group will be systems using hidden stand-by source, so called reserve power source which is

designed to fulfill requirements of full load even if one of the supplying lines is cut off. In this system there are no breaks in supply and during normal stable work lines are only loaded with 60-70% of theoretical capacity, but during failures there is possibility to overload system even with more than 30 % over the maximum nominative power capacity.

What is important when talking about Automatic Restoration are operation times (also as a factor of division). Main times of interest are:

- operation time, the time between the detection of failure and restoration of voltage (full or partial depending on characteristic of the system),
- cut-off time, the time when there is no power supply in secured circuits.

There is also difference on the cycle depending on the failure character. If AR is being activated because of CB operation on main supply we are talking about *shorter cycle*, else if AR is activated by the detection of voltage collapse (e.g. swell or sag) we are talking about *full cycle*, which is bigger than cut off time.

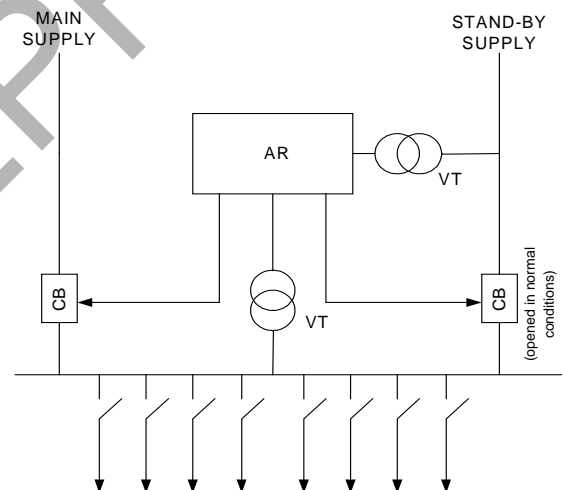


Figure 1. Typical evident stand-by AR system [1]

Of course both mentioned times must be coordinated with other system operation times like protection operation times of

both plant and distribution/transmission networks as well. During automatic restoration also number of electric motors needed to be taken into account, when time of operation is being chosen.

Often after voltage restoration we can observe in the system with connected electric drives voltage drop due to associated inrush current, then torque drop because of voltage drop, motors stall and as a consequence either tripping of motors protection, bus bar CB or another operation of AR. To eliminate these faults two restrictions were introduced. First is the level of AR power, which should be sufficient, second is that motors are allowed to restart only with respect to their inrush current (can't make voltage drop $0,7 U_{AR}$). [2]

II. DIRECTIVES

Most important documents that influence automatic restoration parameters as well as detection parameters are standards and normalizations. For Poland these papers are, (taken from European Council Directives)[3] PN-EN 50160 "Parameters of supplying voltage in communal distribution networks", PN – IEC 60038 "Normalized voltages IEC". For other countries respectively are being used 96/92/EC "Concerning common rules for the internal market in electricity", and the 89/336/EEC with add-ons 92/31/EEC and 93/68/EEC "Electromagnetic Compatibility Directive". Regulations concern general requirement factors as frequency, voltage deviation, shaping of voltage and content of unwanted harmonics related to base harmonic and overall time of failures in circuit.

So base values are:

- For frequency grid values for synchronized connected circuit requirement is:
 - o 50 Hz $\pm 1\%$ for 95% time during usage period
 - o 50 Hz $\pm 4\text{-}6\%$ for the remaining period

For other circuits 95% period can use threshold $\pm 2\%$, and for 100% period $\pm 15\%$
- For voltage, average value with sampling time 10 min. should be:
 - o 95% of these values should be 230/400 V $\pm 10\%$
 - o 100% of these values should be in range of 230/400 V $+10\%/-15\%$.

For harmonics normalization is shown in table 1:

TABLE 1
Admissible values of harmonics in LV/MV networks

odd harmonics				even harmonics	
multip. of 3.		not multip. of 3		Harm. order	Rated volt. [%]
Harm. order	Rated volt. [%]	Harm. order	Rated volt. [%]		
5	6	3	5	2	2
7	5	9	1,5	4	1
11	3,5	15	0,5	6..24	0,5
13	3	21	0,5		
17	2				
19	1,5				
23	1,5				
25	1,5				

European Directives are also using THD factor (total harmonics distortion) which cannot exceed 8% for networks with nominal voltage level beneath 110kV and 3% for networks with nominal voltage level above 110kV.

III. LABORATORY TESTS

The goal of laboratory test was to examine the behavior of simple power generation unit as a stand-by power source. Device chosen for testing was 1-phase generator powered by no-PB petrol engine produced by NUAIR POLSKA Sp. z o.o. The nominal power is 0,65 kW and the maximum power is 0,78 kW. More specific data are listed in table 2.

Not like other big machines, this one is provided with manual starter, which is useless with auto power restoration control system, but will give overview of advantages and disadvantages of stand-by power source commonly used for fulfilling needs of simple small countryside household – typically most unsecured in power supply.

Before the tests started there was found a problem with the load. The idea of the tests was to create environment which will be similar to real conditions. On the other hand, reduction of the influence of inductances and capacitances was necessary. Decision was made to take 0,5 kW halogen lamp as a load, which is almost 100% resistance and will not cause big inrush currents during start procedure. Additional researches were performed with 2 computer (laptop) power supply adaptors, to verify compatibility with energoelectronic devices.

The measurements and transients where recorded using FLUKE 345. All the data was transferred directly do the computer using software provided by the producer. The lamp was connected through special socket with splited input wires to ensure reliable usage of current clamps. For the purposes of the test 5 connection's of FLUKE inputs were used – 2 current clamps, 2 voltage probes and 1 PE wire.

The measurements were divided into three parts. All began with cold startup. Cold startup can be understood as starting the generator from temperature below 0°C. Such strict parameters were taken to simulate hard winter conditions – the result from pre-test is the smooth behavior during start from temperature above 15°C.

In first part after starting the generator, there was up to 10 seconds of idle work and then the load was connected. Difference between first and second part is joined with duration of idle work – in second section it was increased to 2-3 minutes, this time was sufficient for engine to get to the nominal work temperature. The last part was very similar to second, but the load was changed to two computer power supply adaptors connected in parallel.

From all attempts listed below values and transients were taken:

- Current RMS,
- Voltage RMS,
- Total power,
- $\cos\phi$,

- Total harmonic distortion (THD) parameter.

TABLE 2
NPEGG780 STAND-BY POWER SOURCE DATA

Rated power	650 W
Maximum power	780 W
Nominal voltage	230 V
Output	1-phase socket
Protection	Over current (5 A)
Engine rotation speed	3000 rpm
Engine power	2 HP at 3000 rpm
Capacity of fuel tank	4,2 l
Maximum continuous work length	6 h
Level of noise	57 db (7 m away)
Weight	17,5 kg
Dimensions	328x325x337 (mm)
Engine type	Two stroke

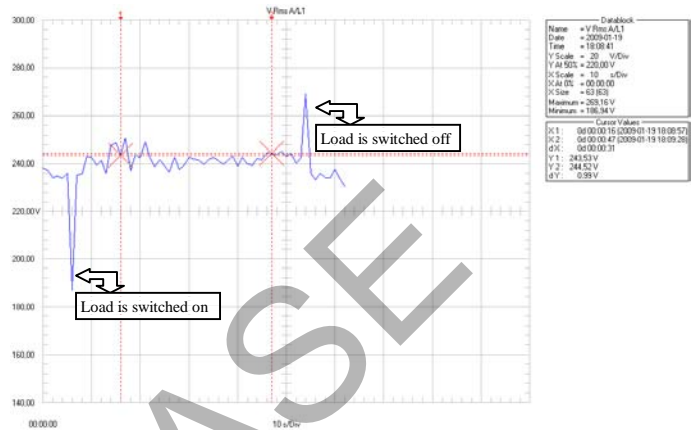


Figure 3. Voltage RMS transient for warm engine [B]

A. Cold startup, 10 seconds of idle work

This attempt will show if generators powered with petrol engines are able to withstand load demand during power system voltage collapse. Performances of generator after cold start were poor. Just after the startup value of RMS voltage is going up to almost 300V – this transient lasts maximum 3 seconds, but usually ends after 1 second. Then the voltage level is stabilizing, till the moment of connecting the load. After connecting the load, the RMS value goes up to 250V. Almost all of the attempts finished after 15-20 seconds, because the generators could not withstand the load demand and stopped working. Figure 2 shows voltage RMS value transient.

Value of $\cos\phi$ was constant – 1 for non-load period and 0.98 for load period. Just before the generator stopped it started to decrease.

Current level was stable (2,1 Amps), only during switching period reached 2,2 Amps but this limitation was only due to small power of cold generator, normal conditions were presented in [B].

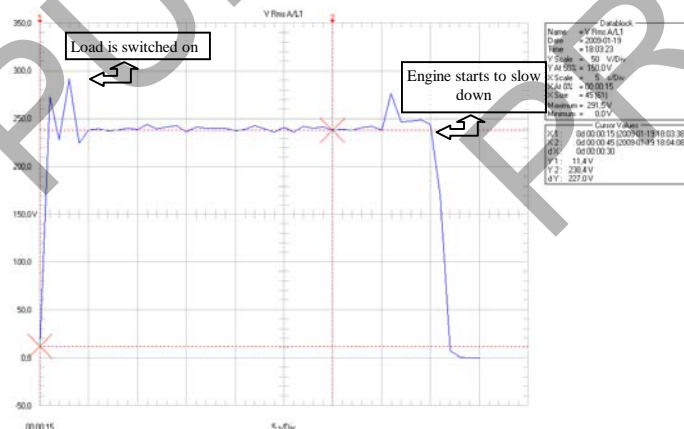


Figure 2. Voltage RMS transient for cold engine [A]

B. Cold startup, 2-3 minutes of idle work

The pre-test trials showed that the engine needs time to stabilize its work. Basing on this knowledge next part tests were performed after reaching the work temperature. After this time the voltage level of idle work was about 230V, so it was similar to parameters decelerated by the producer. After switching on the load, there was a big voltage decrease, down to 186V. The drop duration was short – less than 1 second. During work voltage average value was 240V. The transient is not stable – it is oscillating around average value. Transient of the voltage RMS value is shown on figure 3.

The current level, like while first part, was stable (2,1 Amps). The peak during load switching operation reached 3,3 Amps, which is significant for other connected devices.

Value of $\cos\phi$ were constant – 1 for non-load period and 0.98 for load period. Only changes were registered when the load was connected – 0,58 for switching on and 0,91 for switching off operation.

During this part the THD parameter was measured. It is giving overview of harmonic content in signal. The parameter is defined as the ratio of the sum of the powers of all harmonic components related to the power of the fundamental frequency, as in

$$THD = \frac{\sum \text{harm. powers}}{\text{fund. freq. power}} = \frac{P_2 + P_3 + P_4 + \dots + P_{40}}{P_1} [\%]$$

The acceptable level of this coefficient is 20% (for separated LV networks, including up to 40th harmonic). Obtained value from measurements is in range – around 17% for non load period and slightly above - 21% for load period. The producer of the generator does not give the THD value for the unit.

C. Computer power supply adaptors

The aim of last part was only to check if power source is able to work efficiently with normal household devices. The most interesting values, from investigation point of view, were THD and reactive power.

Unexpectedly THD value for 2 devices connected, was very low – 2.5%.

As expected reactive power was twice bigger then active power – 90 Var. This is the result of AC-DC converter.

All other measured parameters were on expected level:

- voltage 235 V,
- current 0,42 A,
- active power 43 W.

IV. SUMMARY

The tests were performed to prove abilities of stand-by power sources. Second topic, which should be taken under consideration, is the control of reserve power source – it should be 100% automatic. The basic requirement for generator is the electric starter. From the second view not all the devices and machines connected can be connected to second power source, the best example are the engines due to inrush currents.

Designer of control systems should pay attention to the temperature of the engine. As it was shown during laboratory tests it is strongly connected with efficiency and work stability. It can be noticed that during switching load procedure on cold

engine, the peak voltage is lower, it is probably connected with dose of fuel and poor performance of cold engine – larger dose allows engine to work against provided load.

During cold start, control system could take as a control variable the value of $\cos\varphi$ – it was observed that it is decreasing while the generator is not able to withstand the load demand. This theory needs further investigation.

The main problem of small generation units is the power quality, which is decreasing in proportion to load. If the receivers are sensitive to harmonic content, then they can not be used.

The tests showed that even small generator unit can be used as stand-by power source. What is more, if there is no need of continuity of supply, the control system can be replaced by manual control – the blackout (operation) time will be extended to few minutes.

REFERENCES

- [1] prof. B. Miedziński “ Lecture materials for System Opaeration and Security”. Wrocław 2008 (not published).
- [2] D.Glover, M. Sarma, T. Overbye Power System: Analysis and Design. Fourth edition (International Student Edition), USA 2008 by Thomson Corp.
- [3] Edward Siwy, „Dostosowywanie przepisów polskich w zakresie jakości energii elektrycznej do wymogów Unii Europejskiej” Instytut Elektroenergetyki i Sterownia Układów, Politechnika Śląska, Gliwice

Ocean Power: tidal and wave energy

Dennis Grzelak, Nico Brose, Lennardt Schünemann

The growing necessity of a sustainable energy supply requires a great expansion of renewable energy production. While developing and realizing different concepts of energy usage like photovoltaic, wind, geothermal or biomass energy, another big potential energy source has got very low attention – energy from tidal power. Tidal power allows many ways of electricity production and can be classified into two different main types:

- Tidal stream systems make use of the kinetic energy of moving water to power turbines, in a similar way to windmills that use moving air. This method is gaining in popularity because of the lower cost and lower ecological impact compared to barrages.
- Barrages make use of the potential energy in the difference in height (or head) between high and low tides. Barrages suffer from very high civil infrastructure costs, a worldwide shortage of viable sites, and environmental issues.

Since the economical potential of hydroelectric power plants in Europe is nearly exhausted, this work will be focused on different concepts of tidal barrages, tidal stream and wave generators.

Tidal power stations are a variation of the classical hydroelectric power plants using the level difference of the water between low tide and flood, also called tidal range, for the production of electricity. For this purpose, dams can be established in estuaries or sea bays as a separation from the high seas. Such embankments get notches so that water will stream in when the tide is high and drain off when the tide is out, a process under the driving mechanism of the turbines. In both operation phases electric current is therefore produced. The big advantage of this technology is that low tide and flood continuously alternate and, hence, the tidal force displays a computable and dependable energy source. The potential energy

from the resultant tidal range can be calculated as follows:

$$W_{pot} = \frac{1}{2} * \rho * A * g * h^2$$

- ρ is the density of seawater (approximately 1025 kg/m³)
- A is the swept area by the rotors (m²)
- g is the gravitational acceleration (9,80665 m/s²)
- h is the difference between ebb and flut(m)

The best known representative of this technology is the tidal power station in the mouth of the river La Rance near Saint-Malo at the French Atlantic coast. It was established already in 1966 and has a tidal range of 12 - 16 m with which a maximum power of 240 MW is reached. The concrete embankment has a length of 750 m and the storage reservoir basin's magnitudes add up to 22 km in length and, on average, about 1 km in width.

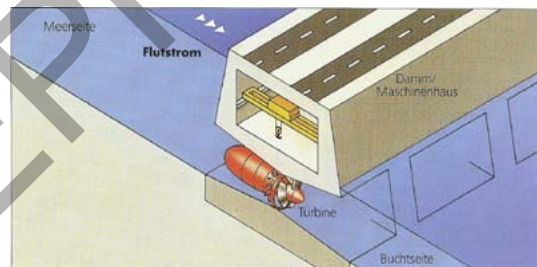


figure 1: water inflow (flood)

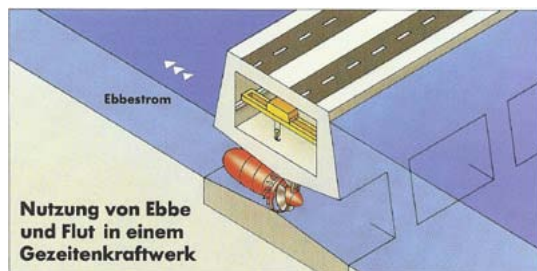


figure 2: water outflow (ebb)

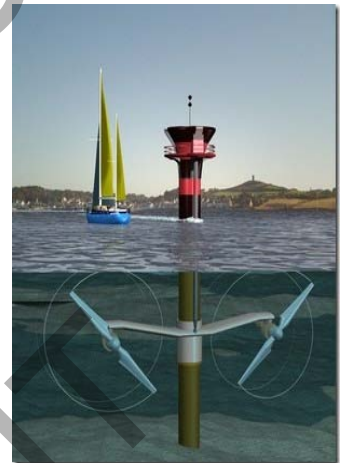
Tidal power stations can only produce electricity at the precise moment of the occurrence of either flood or low tide. When the flood comes, the water streams through the notches in the embankment into the reservoir with the lower water level, making the turbines turn. Being coupled to the turbines, generators are then driven just as well, producing electric current. As soon as the maximum water level is reached, the streaming comes to a standstill and no more electricity is produced before the low tide arrives. During low tide the water from the reservoir runs off again into the ocean, driving the generators once more. The turbines are generally pipe turbines, equipped with adjustable and reversible shovels. This makes it possible that the turbines can work in both streaming phases. Between the flood and the low tide streamings the equipment comes to a brief shutdown in each case. Consequently, a periodically variable amount of power is produced, each streaming period lasts about 12.5 hours. In addition the power, albeit to a minor degree, is influenced by weather conditions like wind or precipitation.

If suitable turbines are installed and the storage basin is big enough, a tidal power station can also be used as a pumping accumulator power station. In this special case the turbines still pump water into the storage basin beyond the reached water level, even if the flood stream has already come to the shutdown. Then, with low tide, more water is blown off and therefore more electricity is produced.

The difficulty of this energy change process lies mainly in the fact that, as a rule, an economic application is only possible from a tidal range of 5 m on. That is why only few locations can be considered. Possible application places for tidal power stations are, for example, in the mouth of the river Severn between Britain and Wales, in Alaska near Anchorage, at the Cambridge Gulf in Western Australia and in the Fundy Bay in Canada. Worldwide there are approximately at least 100 possible locations for those facilities. In Germany the potential is estimated to be very little on account of the relatively low tidal range of about 2 - 3.5 m. Furthermore the tidal power stations are also facing the danger of corrosion, which is clearly higher than in soft water areas. Additionally impurities caused by salt and sediments are problematic because they require a large complexity in the operation management. Finally it

must be mentioned that, above all, the establishment of big dams always makes such equipments affect or damage nature, and therefore interferences of the flora and fauna can be the results. Since tidal power stations also have effects on the rhythm of low tide and flood, an adaptation to the changed living conditions becomes necessary for the creatures in that sphere.

Alternatively to those tidal power stations which used the tidal range to produce electricity, the first projects are being realised whose technology intends the winning of electricity from sea flows. They are sea flow power stations, resembling the wind power equipments with the difference that the rotor turns underwater



and that it is driven by the constant tidal change. A suitable pilot plant was successfully installed already in summer, 2003 near the coast of North Devon in England under the project name "Seaflo". In another step, a new equipment with a power of 1.2 MW originated in April, 2008 near Strangford Lough under the project name "Seagen". The principle of turbines around which the waters are freely circulating has the big advantage that it can be employed in numerous locations and means only low disturbance of the environment. Optimum locations have a water deepness of 15 - 20 m and streaming speeds of at least 2 - 3 m/s in the streaming maximum with the steadiest course possible.

The power that can be extracted from marine currents (by turbine generators) is dependent on the speed of the water flow, and the area and efficiency of the turbine, as follows:

$$\text{Power} = 0.5 * \rho * A * v^3 * C_p$$

- ρ is the density of seawater (approximately 1025 kg/m³)
- A is the area swept by the rotors (m²)
- v is the current speed (m/s)
- C_p is the efficiency factor of the turbine.

The density of seawater means that marine turbines are significantly smaller than wind turbines of similar generation capacity, and rotate at approximately 20 to 30 rates per minute.

The essential components like rotor, hub, gear, generator and tower come from the wind power technology. But, in contrast to the power production from wind force, water has a much higher density than air. The result is thousandfold as much as the power of airflow when there is a steady water flow, which is why the flow speeds (relatively slow in the water), as they originate possibly from the tides, are sufficient for the production of electricity.

The 2-blade rotor has a solid orientation along the direction of the flow and a pitch settlement which allows a blade adjustment of about 180°. Therefore the operation is possible equally with low tide as well as with flood. Besides, the pitch settlement is used for the line limitation and retardation of the equipment. Rotor, gear and generator are fastened together in a framework and can be lifted out of the water with the help of a lift device to carry out the maintenance.

Another concept for the use of sea flows is the Stingray Tidal Stream generator. The Stingray uses, in contrast to tidal turbines, no air-screw but a compensator arm for the power production from the sea flow. To guarantee the stability at the bottom of the sea, a star base with four beams is applied, which are anchored in the ground. The compensator arm is fastened to a column on the star base. The construction weighs approx. 180 t and it is its simple dead weight which gives it a good anchorage at the bottom of the sea. By the undulation of the water the fin of the compensator arm oscillates up and down. That is how the pressure is generated inside a hydraulic cylinder which is used to power a generator.

In the years 2002 and 2003 the equipment was tested with an installed rating of 150 kW as a pilot scheme. After building a demonstration equipment in 2005, the enterprise Engineering Business Ltd had arrived at the conclusion that the equipment construction would possibly not be practicable in consideration of profitability.

All in all, sea flow power stations could become reliable energy suppliers in the future above all due to the computability of the tides. They work silently and hardly disturb the landscape. Besides, a combination with offshore wind parks could create considerable synergy potentials, for example, by using a common grid connection. Only in Europe more than 100 suitable locations for such equipments would be possible at a guess. Nevertheless, it is problematic that suitable and unsuitable locations are often established close to each other. When a good location is being searched for, it is also important to consider the possible potential for conflicts with other ocean users sufficiently, apart from disputable environmental conditions. Before a commercial production of electricity can become reality, a huge number of detailed questions is still to be solved with regard to the equipment technology to guarantee a safe and frictionless operation under rough conditions, like the sea water.



figure 4: Stingray Tidal Stream Generator

Another alternative of producing electricity is using wave energy. At this, 3 possible technologies are available after all:

- *Oscillating Water Column:* the periodical, vertical movement of the water compresses

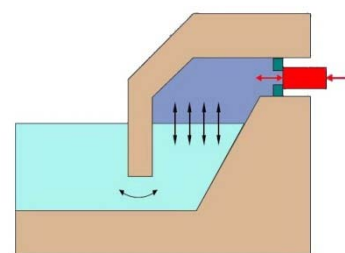


figure 5: Wavegen
and relaxes air with an airborne turbine.

- *Wave-induced Drop Height:* shafts lift the water on a higher energy level. The potential energy is taken up by a "low head" turbine.

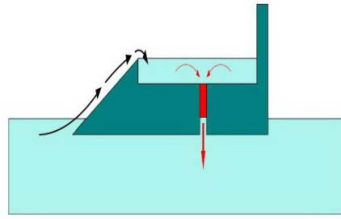


figure 6: Wavedragon

- *Hydrodynamic Movement:* buoyancy bodies follow the undulation. Out of this, the most different possibilities of direct energy conversion arise.

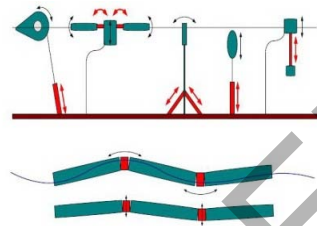


figure 7: Pelamis



figure 8: Pelamis- Wave-Generator

The Pelamis-wave power station is a 750-t-steel construction which generates electric current by moving the single limbs in opposite directions. This 150-m-long and 3.5-m-wide steel tube is divided into four cylinders which are connected by power modules. In the modules there are piston pumps which take up the kinetic energy and deliver it to a hydraulic generator by means of the hydraulic liquid. The capacity of the equipment constitutes 750 kW. An anchor holds the construction in the intended position and is flexibly applicable with it, in contrast to other sea power stations, and has a lower impact on the ecological balance. The first commercial employment occurs in 2008 in Portugal, being part of the pilot project of 2006. In this connection it concerns three equipments. For the future it is planned to start another 25

equipments running which will have a total capacity of 18.75 MW.

The Wavegen project is one of the most reliable sea power stations. The energy of the water is not used directly, but the working medium

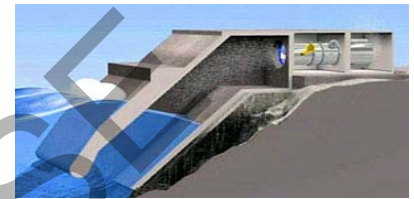


figure 9: Wavegen

air is. The structure is partly on shore and in the water. It contains a hollow cavity which is flooded by the sea. With waves streaming in, the water level changes inside the structure. An alternately high and low air pressure inside arises from it. The pressure is compensated with the aid of an open end towards the environment. Close to the open end, there is a Wells turbine which dissipates the kinetic energy of the flowing air into electric energy. The Wells turbine distinguishes itself by the fact that it maintains its running direction while the air flow is varying, so that it supplies permanent electricity. Before a Wavegen project can be realised, comprehensive investigations about the characteristics of the waves have to be carried out.

An implementation of the equipment construction has been on the Scottish island of Islay since the year 2000.

References:

- **Voith (2006):** Meeresenergien – eine Innovative Ergänzung der klassischen Wasserkraft; Berlin, 18. Januar 2006
- **Boyle, G. (2004):** Renewable energy, Oxford University Press
- **Lübbert, D. (2005):** Das Meer als Energiequelle: Wellenkraftwerke, Osmose-Kraftwerke und weitere Perspektiven der Energiegewinnung aus dem Meer, Wissenschaftliche Dienste des Deutschen Bundestages, Berlin, 10.11.2005
- **Bard, J. (2004):** Energienutzung im Offshore-Bereich, Informationen zur Raumverteilung, Heft 7/8. 2004
- http://www.poweron.ch/de/stromprod/beispiele_content---1--1034.html, 04.03.2009

OVERVOLTAGE PROTECTION DEVICES

C. Szafron

Wroclaw University of Technology
Janiszewskiego 8 Str.
50-370 Wroclaw, Poland

Abstract – This article states about overvoltage protection methods, especially lightning overvoltages. Different types of lightning protection devices are presented and described, according to their construction and application methods. The pressure was put on protection in accordance with European standards.

I. INTRODUCTION

Nowadays business, industry and all public institutions depend on electronic data engineering. Electronic data processing, measuring and control systems, instrumentation and control as well are all part of a modern industrial plant. All data recording devices at the production plants are connected to terminals and computers at offices by information networks distributed between buildings - together making the computer integrated manufacturing. Often, the basis of computer integrated manufacturing are open networks, where different types of computers and different operating systems communicate. This business process is rapidly expanding and is now approaching the computer integrated enterprise or computer integrated business. Differently speaking all ranges of administration are completely integrating into a electronic data processing system. It can be clearly seen that the future lies in the computer-integrated factory or in computer-integrated business and administration. This networked system, with its growing flow of information, is severely hindered by damage to the essential transmission systems in the telephone and data networks, as well as at terminals or by interference. Strong dependence on electronic data processing can quickly lead to catastrophe if the system will fail. An American investigation in 1987 highlighted the seriousness of the situation. According to it, banks will be able to manage without electronic data processing for only 2 days, enterprises that are sales-oriented will be able to manage for 3.3 days, manufacturers for 4.9 days and insurance companies for about 5.6 days. Enterprises without functioning EDP, according to an investigation by IBM Germany, will collapse after about 4.8 days. It has to be taken into account that in the past 15 years the growth of computer appliances in business, industry and everyday life has increased rapidly, so former mentioned times have probably decreased. Computer safety experts have pointed out that ninety percent of enterprises would close if their computer fails for two weeks. Disturbance of the data flow and destruction of

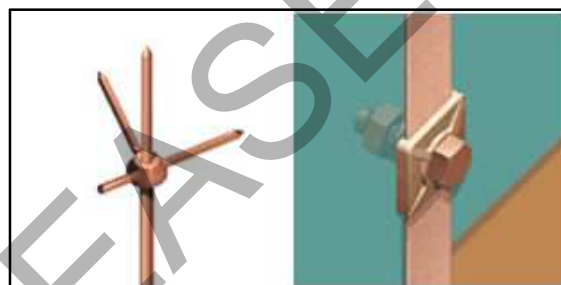


Fig.1. Air terminator and equipotential bonding

electronic equipment is the most frequent reason for the failure of such electronic systems. Mostly it is made by transient electromagnetic interferences. This risk can be controlled by electromagnetic compatibility measures, what specifies conditions under which any kinds of electric equipment disturbs or not each other. Also where electromagnetic phenomena, like lightning discharges, will not disturb their function. In 1989 the European Community has declared electromagnetic compatibility as a protection goal by issuing the "Council Directive of 3 May 1989 to Harmonise Laws of the Member Nations concerning Electromagnetic Compatibility". According to it all apparatus, facilities and systems that include electric or electronic components must demonstrate sufficient withstand levels against electromagnetic disturbances, to guarantee stable and proper operation of all equipment. The directive of the Council especially mentions the industrial equipment, telecommunication networks and equipment facilities. Violation of the electromagnetic compatibility general instructions, is deemed with a summary offence. A great extent the protective measures that must be undertaken in the framework of electromagnetic compatibility. Among the threats from the electromagnetic environment, lightning discharge is the most dangerous and therefore it determines the protective measures. Modern lightning protection does not only mean protection of buildings, but especially the protection of devices stored in it, meaning that a lightning protection system also must be achieved, even if it is not necessary for the building itself, but for the equipment it contains.

II. AIR TERMINATIONS

To protect the volume from direct lightning strikes and to avoid uncontrolled strikes air termination are used [Fig.1], which are fixed points for likely

lightning strikes. Air termination is comprised by air-termination rods and air-termination wires. The location of air terminations is usually defined by the 'rolling sphere' method. It bases on use of an imaginary sphere of radius S over the surface of a protected object. The sphere rolls up and over and is supported by lightning masts, shield wires, substation fences, and other grounded metallic objects that can provide lightning shielding. A piece of equipment is said to be protected from a direct stroke if it remains below the curved surface of the sphere [Fig.2]. This means that a certain radius of rolling sphere will be assigned to every protection level. Finally, air terminations form a system of protection for structures on the roof, such as ventilators and air-conditioning systems.

Partially isolated lightning protection systems are usually installed on flat roofs. This protection can be achieved by individual or a combination of several air termination rods for smaller roof structures. For larger roof structures protection by means of air termination rods is not often possible as the rods would be too high and thus there is danger of their leaning. An isolated air termination is a second solution as an alternative. The calculated safety distance must be smaller than distance between air terminations and structures on the roof. Air-termination networks must form a protective volume that is including all structures on the roof.

III. BUILDING AND ROOM SHIELDS

Extended metal components, like for example: metal roofs and facades, steel reinforcements in concrete, expanded metals in walls, lattices, metal supporting constructions and piping, which form an effective electromagnetic shield by their meshed interconnection are especially important for shielding magnetic fields. They are also important for creation of lightning protection zones.

In principle, a steel reinforcement and the metal window and door frames can form an electromagnetic cage. In practice, however, it is not possible to weld or clamp every nodal point for large structures. For bridging expansion joints or bonding the reinforcement of prefabricated concrete parts, fixed earthing terminals are provided. To such earthing terminals or projecting bonding conductors the "earth bus" or "earth ring bus" (ring equipotential bonding bars) are connected. Metal facades are also used for shielding purposes. The facade steel sheets, being interconnected, are to be bonded to the metal construction and to the reinforcement.

Some of the above mentioned shielding measures can also be applied to the establishment of room shields (lightning protection). In particular this concerns the use of steel reinforcements (in floors, walls and ceilings), expanded metal (in walls and ceilings) and lattices.

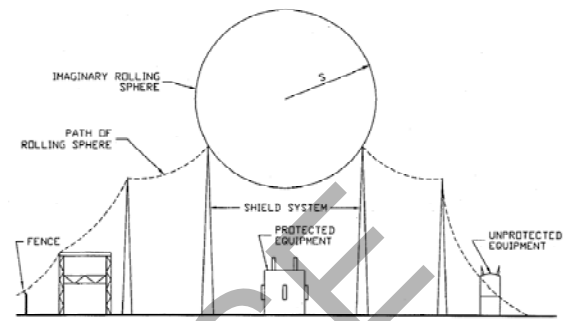


Fig.2. "Rolling sphere" method

Smaller shields for lightning protection zones and higher, or shields of local lightning protection zones are usually formed by the enclosures (sheet steel cabinets, sheet steel covered racks, sheet steel enclosures) of telecommunication systems and devices.

IV. SHIELDS FOR CABLES IN BUILDINGS

Cables shall be run near the equipotential bonding lines. These are parts of the steel construction, reinforced walls, cable supporting structures, cable trays or other electrically conductive parts which are connected to the equipotential bonding system at least at both ends. In principle, shielded cables should be used. This applies for electronic or data cables as well as for higher voltage levels. Pair-twisted signal cables are to be preferred. For related lines of one signaling circuit a twisted pair each is to be used, so that the incoupled transverse voltage on cable runs must be neglected. The limitation of the incoupled series voltage determines the protection measures.

To lessen surges by overcoupling, power and signaling cables must be consequently separated, if possible by using cable supporting structures which are included in the equipotential bonding. Different separations are needed depending on the cable parallel running length.

Also in existing systems it may become necessary to shield the cable routes (subsequently). For this purpose a retrofit set consisting of shielded sleeves provided with a closing system in the longitudinal direction.

V. EQUIPOTENTIAL BONDING

Lightning protection equipotential bonding of a protected volume includes all incoming metal installations. In the case of extended telecommunication systems, a duly shaped lightning protection equipotential bonding bar installed at ground level inside the building also functions as an earth bus and is usually installed as an earth ring bus inside the building. The earth ring bus, a ring equipotential bonding bar, is a copper bar having a minimum cross section of 50mm^2 for surface mounting at a distance of some centimeters

from the wall. At distances about 5m it should be bonded to the foundation earth electrode. This bonding can also be realized over the reinforcement. An equipotential bonding bar can be sufficient for small local systems. If the discharge system consists of plain metal components which constitute an effective electromagnetic shield, the equipotential bonding bars can be directly bonded with the shield. Equipotential bonding is, therefore, often carried out using a bonding plate with multiple radial or even coaxial connections of the conduits or line shields.

Equipotential bonding is not only for the protection of electronic systems, but it must also fulfill special functions. A low-impedance equipotential bonding system, which is an entity formed of interconnected equipotential bonding lines including the metal parts of the electric systems (such as enclosures, racks, cable trays etc.) and the building (e.g. reinforcement in floors, walls [Fig.1.] and ceilings, supporting structures between floors) is possible using a meshed, plane-covering or space-covering formation. Such a meshed overall building equipotential bonding system is the best way to reduce overvoltages in telecommunication systems and is the basis for the coordinated use of arresters (surge protection devices, filters, etc.).

Different types of functional equipotential bonding systems are needed for telecommunication facilities and systems. Metal supports, cabinets, enclosures, cable racks etc. in rooms with telecommunication facilities and systems must be included in the meshed functional equipotential bonding. Another possibility for achieving functional equipotential bonding is to create an equipotential bonding network by means of the metal supporting structures between floors. It is useful to install a local ring equipotential bonding bar which then is connected to the earth ring bus several times.

Above all, equipotential bonding should include:

- metal enclosures and racks of the telecommunication systems
- conductors of electrical systems which do not carry operational voltages and/or currents.

In the latter case, these include: protective conductors of the power system, earth electrode conductors of the telecommunication system, outer shields of the telecommunication cables and if necessary, the chassis terminals of the electronic devices and systems.

TABLE 1
Comparison of arresters classes according to standards

DIN VDE 0675 Part 6/A1	IEC 37A/447/CDV
Arresters class B, for lightning protection equipotential bonding purposes according to DIN VDE 0185 Part 1	Arrester 'Class I'
Arresters class C, for surge protection purposes in the permanent installation, especially for use in surge withstand category III	Arrester 'Class II'
Arresters class D, for surge protection purposes in the mobile/permanent installation, especially for use in surge withstand category II	Arrester 'Class III'

VI. ARRESTERS

According to their range of application, surge protective devices (SPDs) for power engineering and for information technology can be subdivided into two kinds: lightning current arresters and surge arresters. SPDs are internationally standardized in IEC 61643-1:1998-02 "Surge protective devices connected to low-voltage power distribution systems" part 1: "Performance requirements and testing methods". In this standard the SPDs are distinguished according to test classes. It is difficult for the user to understand this classification because it is primarily meant for the producers of the SPDs. A rather user-convenient SPD standardization is included in the German DIN VDE 0675 Part 6/6A1 and 6A2. As requirements and tests of the German standard are more severe than the international standards, the German standard is taken as a basis for arrester classification (Table 1).

We distinguish many kinds of arresters, generally basing on their application:

- Lightning current arresters must be able to discharge lightning currents or considerable parts of them non-destructively. They are dimensioned and tested in accordance with IEC 61643-1/E DIN VDE D675 Part 6 and Part 6/A1.
- Surge arresters only serve limiting overvoltages at relatively low-energy surge currents.

VII. SUMMARY

Application of devices mentioned in this article can significantly increase the reliability of protected networks and safety of people and equipment inside protected structures .

REFERENCES

- [1] P. Hasse, "Overvoltage protection of low voltage systems", 2nd edition, The Institution of Electrical Engineers, London, United Kingdom, 2000
- [2] <http://www.furse.com>, 09.01.2009
- [3] <http://www.moeller.pl>, 09.01.2009
- [4] <http://www.dehn.pl>, 09.01.2009

High-voltage direct current transmission lines

Tomasz Drobik
Wroclaw University of Technology
Wyb. Wyspianskiego 27
50-370 Wroclaw, Poland

Abstract – this article treat about HVDC (high-voltage direct current) technology. In history of energy transmission, crucial moment was “War of Currents” in XIX century . From conflict between supporters of AC and DC was winning Nikola Tesla. In effect, the most popular way to transmission energy are AC transmission lines. Despite many advantages of AC transmission, in some conditions better is DC transmission, which demand presence of high-voltage. The serious acceleration in development of this technology was 1954 when was built the first such system. Since those time, HVDC has developed very intensive, and will be very important technology in problem of transmission energy.

I. INTRODUCTION

Power does not rely only from voltage, but is equal of voltage times current.

$$P=UI \quad (1)$$

For a given power a low voltage require a higher current and a higher voltage requires a lower current. However, since metal conducting wires have a certain resistance, some power is wasted, and transfer as heat. The power losses in a conductor are proportional to the square of current and resistance of conductor.

$$P=RI^2 \quad (2)$$

Power is also proportional to voltage, so for given power level, higher voltage let decrease a current level. Higher level of voltage, give us also lower power loss. Power loss can be also reduced by decreasing resistance e.g. by increasing diameter of conductor, but it’s demand higher economical costs.

High voltage transmission is used to reduce lost of power, but it cannot be used for lightning system and supplying motors. High voltage level has to be adjust to receivers. In AC are using transformers which decreasing or increasing voltage to required level. In DC does not exist such possibility. In those technology manipulation is possible for more complicated way. To changing a level of voltage are used electronic devices as mercury arc valves, semiconductors devices, thyristors, insulated-gate bipolar transistors (IGBTs), high power capable MOSFETs (power metal–oxide–semiconductor field-effect transistors) and gate turn-off thyristors (GTOs).

In AC voltage conversion is simple, and demand little maintenance. Further three-phase generator is superior to DC

generator in many aspects. Those reasons causes that AC technology is today common in production, transmission and distribution of electrical energy. However alternative current transmission has also drawback which can be compensate in DC links. It’s the main reason why DC technology is chosen instead AC:

- inductive and capacitive elements of lines put limits to the transmission capacity and transmission distance
- is not possible transmission between two points of different current frequency

Therefore electrical engineers research and applied DC technology which doesn’t have such limitation.

II. HISTORY

The first transmission of direct current was in 1882, distance was 50 km long (distance between Miesbach-Munichbut) and voltage level was only 2 kV. DC transmission was developed by Rene Thury. This scientist created own method, which based on series-connected generator and was used in practice by 1889 in Italy. System based on Thury’s idea transmitted 630 kW at 14 kV over distance 120 km. The next important

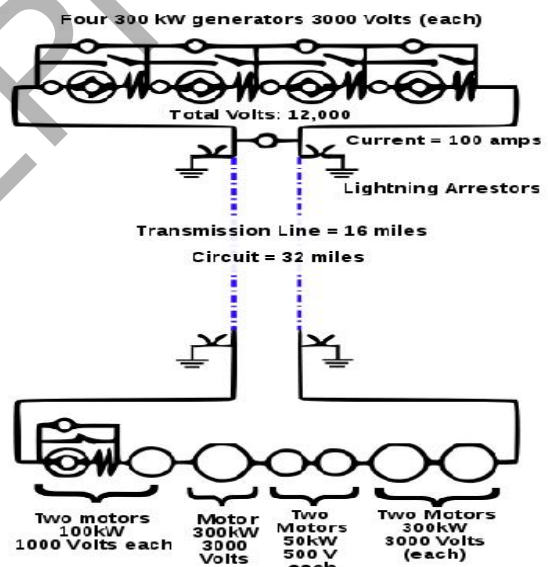


Figure 1. Scheme of Thury’s installation from 1889.

project was line Mountiers-Lyon in France which was working between 1906 until 1936. Mountiers power plant had eight generators which was connected in series. Line of Mountiers-Lyon connected hydroelectric power plant, transmitted 8600 kW, had 200 long kilometers and voltage between two poles was 150 kV. In sum was built fifteen similar systems. Other systems worked at up to 100 kV DC,

and was using to 30s'. Economical and technical low efficiency caused that Thury's systems was withdrawal, but despite those reasons – it was little commercial success.

The next era, was attempts with mercury arc valve. The first such technology was put in 1932 by General Electric, which tested mercury-vapor valves in 12 kV DC line. System could convert current from 40 Hz to 60 Hz frequency. This installation worked in Mechanicville, New York. In 1941 existed underground DC (with mercury arc valves) connection in Berlin, but due to war project was never completed.

Crucial moment in development of HVDC was in 1954. This moment began era of static mercury arc valve. This system was created by ASEA and connected Sweden with island Gotland. Up to 1975 had used technology based on solid-state devices. From this time to 2000 had been lasting era of thyristor valves. Future probably will belong to commutated converters.

III. COMPOTENTS AND RECTIFYING/INVERTING SYSTEMS

HVDC using mercury arc rectifiers but the most modern way are thyristors. Thyristor is a solid- state semiconductor, similar to the diode, but has particular property in control of AC cycle. The insulated-gate bipolar transistor (IGBT) is simpler and cheaper way of control.



Fig 2. Simplification scheme of HVDC transmission

Rectifying and inverting systems usually use the same devices. At the AC end a set of transformers, often three physically separate single-phase transformers, isolate the station from the AC supply, to provide a local earth, and to ensure the correct eventual DC voltage. The output of these transformers is then connected to a bridge rectifier formed by a number of valves. The basic configuration uses six valves, connecting each of the three phases to each of the two DC rails. However, with a phase change only every sixty degrees, considerable harmonics remain on the DC rails. An enhancement of this configuration uses 12 valves (often known as a twelve-pulse system). The AC is split into two separate three phase supplies before transformation. One of the sets of supplies is then configured to have a star (wye) secondary, the other a delta secondary, establishing a thirty degree phase difference between the two sets of three phases. With twelve valves connecting each of the two sets of three phases to the two DC rails, there is a phase change every 30 degrees, and harmonics are considerably reduced.[1]. In elements which take share in conversion, are applied filters which limit harmonic in DC cycle.

IV. CONFIGURATIONS

In the most popular configuration - monopolar, one terminal of rectifier is connected with the ground. Second terminal with potential another than ground, is connected with transmission line.

Current flows in the earth between electrodes two stations when not metallic conductor is installed. It's a single wire earth return type of configuration. If not exist return conductor, configuration may gives such problems:

- corrosion because long underground objects (e.g. pipelines),
- submerged return electrodes may participate in chemistry reaction
- unbalanced current may disturbed magnetic field and influent on navigations ships equipment.

Presence of return wire can eliminate such effects. Those line has to be connected between two ends of monopolar transmission line. Second conductor is applied in depending on economical, technical and environmental factors. In the future will spread bipolar systems. *Modern monopolar systems for pure overhead lines carry typically 1500 MW. If underground or underwater cables are used the typical value is 600 MW.[2]*

The next system is bipolar transmission. In this configurations, is used two wires with the same potential as ground, and opposite polarity. Costs of this line is higher than monopole, but despite economical aspect bipolar system has advantages:

- return losses and environmental effect are reduced
- in case of fault in one line, current can flow by return path in monopolar mode
- in very uncomfortable surrounding, second conductor can be track in transmission towers, it gives possible flow power even at the completely breaking second line.

Bipolar systems may carry as much as 3000 MW at voltages of +/-533 kV. Submarine cable installations initially commissioned as a monopole may be upgraded with additional cables and operated as a bipole.[1]

Back to back is configuration with both inverters and rectifiers are in the same area. This system is used as follows areas:

- in Japan, where occur necessity of changing current frequency
- in lines with different phase relationship
- in lines with different frequency and phase number

System with transmission line is the most common configuration. In this structure two inverter or rectifier stations are connected by powerline. This system is applied in long lines, unsynchronized grids and underwater connections.

Tripole: current modulating control. It's new idea of transmission DC (since 2004). This structure based on two circuit which work as bipole and third wire which operate as parallel monopole. Parallel monopole relive current in periods from other pole. Bipole wires are loaded for few minutes. In tripole system can be carry higher current. Tripole system let pick up about 80% transferred power than AC lines.

V. ADVANTAGES AND DISADVANTAGES

The advantage of HVDC than AC is ability to transmission big amount of power on long distances with lower wastes. DC technology is better in such situations:

- undersea connections
- power transmission and stabilization between unsynchronized AC distribution system
- connection generating plants remote from power grid
- stabilizing AC grid
- connection between countries with different current frequency/voltage
- synchronize AC produced by renewable energy sources

Long underwater lines have a high capacitance. In AC transmission is required process of charging and discharging, what is causes of power losses. HVDC has minimize this effect. In AC lines occurs also dielectric losses.

To disadvantages of HVDC we can include conversion, switching and control. Static converters are expensive. In short distances losses in static inverter may be even bigger than in AC transmission. In the future static converters will be replaced by thyristors.

In DC system controlling of multiterminal configuration is quite hard, because required good communication between terminals. Also circuit-breakers are difficult than AC.

VI. ECONOMICAL ASPECTS

Is not simple estimate a cost of buildings HVDC transmission line and operations unit. Cost are very different and depends on power of line, length connection, environment of track wires (air or water) and so on. Usually the biggest producers of high-voltage direct current transmission as Areva, Siemens or ABB don't reveal financial information about investments. Despite narrow basement of information, we can estimate some costs of built DC line, which is show on Fig.3

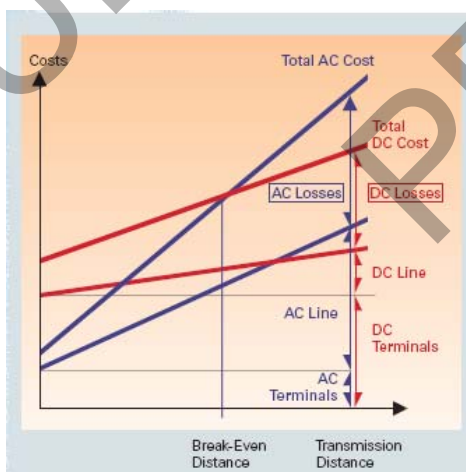


Fig.3 Relation between length of line and costs in AC and DC line

About 50% cost of DC structure are converter transformers, valves and infrastructure as buildings.

VII. APPLICATIONS

8. IEEE International Conference on Environment and Electrical Engineering, Karpacz, Poland, May 10-13, 2009

HVDC system can connected unsynchronized grids, therefore such lines very often are natural boundaries between countries. DC line is also meeting in places where is require undersea transmission (e.g. wind farm) and between two long distant points. From such reasons was built grids e.g. in Siberia, Canada, Australia or Scandinavia. Problem of synchronized AC because of different frequency system occur e.g. in Japan, North America, South American (enormous hydroelectric power plant) – between Brazil and Paraguay In Europe the most lines are between UK, Scandinavia and continental Europe.



Fig 4. Nicolet convert station in transmission line Québec - New England

VIII. CONCLUSIONS

Today HVDC is very important issue in transmission energy. In near future this technology probably will be develop very intensive. Influence on future may have intensive spread of renewable energy source, also wind farm which need undersea connections. Also problem of cascade blackout, can be reduced by application of HVDC. Intensive, very large investments in e.g in China and India shows that high-voltage direct current will very important in the future, especially in big, new-industries countries.

VIII. REFERENCES

- [1] <http://en.wikipedia.org/wiki/HVDC>
- [2] G. Czisch, A "Low Cost but Totally Renewable Electricity Supply for a Huge Supply Area – a European/Trans-European Example
- [3] www.siemens.com
- [4] www.areva.com
- [5] Roberto Rudervall J.P. Charpentier Raghuvveer Sharma, *High Voltage Direct Current (HVDC) Transmission Systems Technology Review Paper*

Transient response of doubly fed induction generator under voltage sag using an accurate model

Alireza abbaszadeh*, Saeed lesan*, Vahid mortezapour**
a.abbaszadeh@stu.nit.ac.ir

* Electrical Engineering Department-Iran Babol (Noshirvani) University of Technology

** School of ECE University of Tehran
 Babol*, Tehran**, Iran

Abstract- In order to investigate the transient response of doubly fed induction generator (DFIG) under grid disturbances, an accurate model is required. In this paper transient response of DFIG during voltage sag considering saturation effect of leakage flux for different order models is simulated. Then, rotor over-current due to voltage sag and factors that affect it, is investigated.

NOMONCLATURE

Symbols

I	Effective phase current
i	Current
u	Voltage
R	Resistance
X	Reactance
ψ	Flux
ω	Angular velocity
H	Combined inertia of wind turbine and DFIG rotor
γ	Current ratio
K	Saturation factor
Subscript	
m	Mutual
d	d axis component
q	q axis component
r	Rotor
s	Stator
M	Mechanical
cb	Crowbar
max	Maximum
sat	Saturation
b	Base
l	Leakage

I. Introduction

Due to the increasing concern about CO_2 emissions, renewable energy systems and specially wind energy generation have attracted great interest in recent years. Large wind farm have been installed or planed around the world and the power rating of the wind turbine is

increasing. Nowadays, the most widely used wind turbine in wind farm is based on doubly fed induction generator (DFIG) due to noticeable advantages: the various speed generation, the decoupled control of active and reactive power and the improvement of the power quality. However, wind turbines based on the DFIG are very sensitive to grid disturbance, especially to voltage dips [1]. in recent years, many papers investigated it from various aspect. For studying a DFIG, at first an accurate model is needed. In some papers different order model was proposed [2-5]. The computational time can be ameliorated by reducing the order of the generator. The reduce order is obtained by neglecting differential term in the voltage equation of the machine [5].in these papers the effect of leakage flux saturation is usually neglected. In other kind of papers saturation effect was considered, but investigation doesn't perform for different orders. X_s , and X_r aren't constant in these papers, but vary depend on current pass through them [6,7]. According to mentioned above, the voltage dip could cause over-voltage and over-current in rotor winding and consequently damaged the rotor side converter. So studying the transient behavior of DFIG during the three phase voltage dip is very important.

The aim of this work is to present a comparative study among different orders of the DFIG model accompany with saturation effect during three phase voltage sag and at next step the most accurate model was used to show rotor over-current. Finally various factors reducing the maximum value of over-current is investigated.

II. unsaturated induction generator model

in this section the unsaturated model for DFIG is given.

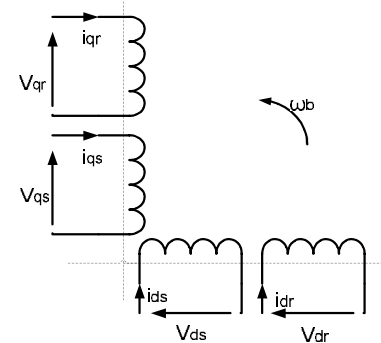


Figure 1. direct (d) and quadrature (q) representation of induction machine.

The voltage equations for the induction generator are given below, where all quantities except the angular frequency, ω_b , are in pu.

$$u_{ds} = -R_s i_{ds} + \psi_{qs} - \frac{1}{\omega_b} \frac{d\psi_{ds}}{dt} \quad (1)$$

$$u_{qs} = -R_s i_{qs} - \psi_{ds} - \frac{1}{\omega_b} \frac{d\psi_{qs}}{dt} \quad (2)$$

$$u_{dr} = -R_r i_{dr} + (1 - \omega_m) \psi_{qr} - \frac{1}{\omega_0} \frac{d\psi_{dr}}{dt} \quad (3)$$

$$u_{qr} = -R_r i_{qr} - (1 - \omega_m) \psi_{dr} - \frac{1}{\omega_0} \frac{d\psi_{qr}}{dt} \quad (4)$$

Using these equations, a model for both the squirrel cage and wound rotor generators can be developed. The difference between these two generators lies in the rotor: the first one has short circuited winding, so rotor voltage is zero, and the second one has these winding fed by a converter, responsible of controlling the generator[5]. Flux linkage used in previous equation, is obtained from (5) and (6):

$$\begin{cases} \psi_{qs} = X_s i_{qs} + X_m i_{qr} \\ \psi_{ds} = X_s i_{ds} + X_m i_{dr} \end{cases} \quad (5)$$

$$\begin{cases} \psi_{qr} = X_m i_{qs} + X_r i_{qr} \\ \psi_{dr} = X_m i_{ds} + X_r i_{dr} \end{cases} \quad (6)$$

The electromagnetic torque is calculated by

$$T_e = \psi_{ds} i_{qs} - \psi_{qs} i_{ds} \quad (7)$$

Finally if T_M is the mechanical torque dependent upon the local wind speed:

$$T_M - T_e = 2H \frac{d\omega_m}{dt} \quad (8)$$

The model of an induction generator can have various orders, such as 1, 3 or 5. The fifth-order model is considered to be a full order model for an induction generator. The third-order model ignores the stator dynamics and is widely used in power system transient stability analysis. The first order model ignores both the stator and rotor dynamics. The only differential equation left is the swing equation. This model is suitable for long term power system dynamic study including the induction motor load characteristics [4]. Table 1 briefly describe above sentences [5].

Table 1. simplifications used in different order models

Fifth order	Third order	First order
$d\psi_{sq(d)}/dt \neq 0$	$d\psi_{sq(d)}/dt = 0$	$d\psi_{sq(d)}/dt = 0$
$d\psi_{rq(d)}/dt \neq 0$	$d\psi_{rq(d)}/dt \neq 0$	$d\psi_{rq(d)}/dt = 0$
$d\omega_m/dt \neq 0$	$d\omega_m/dt \neq 0$	$d\omega_m/dt \neq 0$

III. saturated induction generator model

for better representation of the induction machine under transient condition, saturation effect should also include the variation in the stator and rotor leakage inductances due to saturation in the leakage flux path. The effect of saturation in leakage flux path is considered by modifying the unsaturated stator and rotor leakage reactances with saturation factor K_{sat} [7]. K_{sat} is introduced as follow [6]:

$$K_{sat} = \begin{cases} 1 & I \leq I_{sat} \\ \frac{2}{\pi} \left(\tan^{-1} \left(\frac{\gamma}{\sqrt{1-\gamma}} \right) + \gamma \sqrt{1-\gamma} \right) & I > I_{sat} \end{cases} \quad (9)$$

Where γ is equal to the ratio between current at which the saturation begins, I_{sat} , to the current through the leakage reactance. The saturation factor characteristic is shown in fig.2.

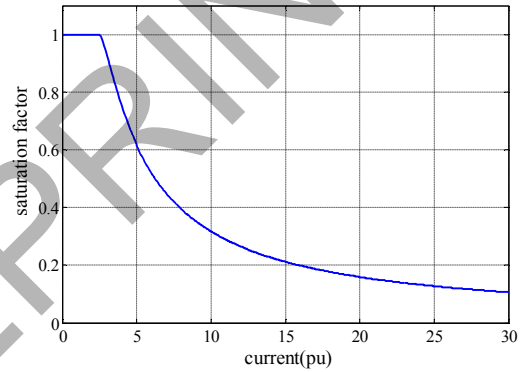


Figure 2. saturation factor characteristic

IV. transient response of DFIG during voltage sag

short duration under voltages are called "voltage sags" or "voltage dips". The latter term is preferred by the IEC. Within the IEEE, the term voltage sag is used. According to the IEC, a supply voltage dip is a sudden reduction in the supply voltage to a value between 90% and 1% of the declared voltage, followed by a recovery between 10 ms and 1 minute later. For the IEEE a voltage drop is only a sag if the during sag voltage is between 10% and 90% of the nominal voltage [8]. In this paper a 50% voltage sag is considered for simulation. At $t = 5s$, a voltage sag happens. Then at $t = 7s$ the voltage is restored to its presage value, i.e. 1pu.

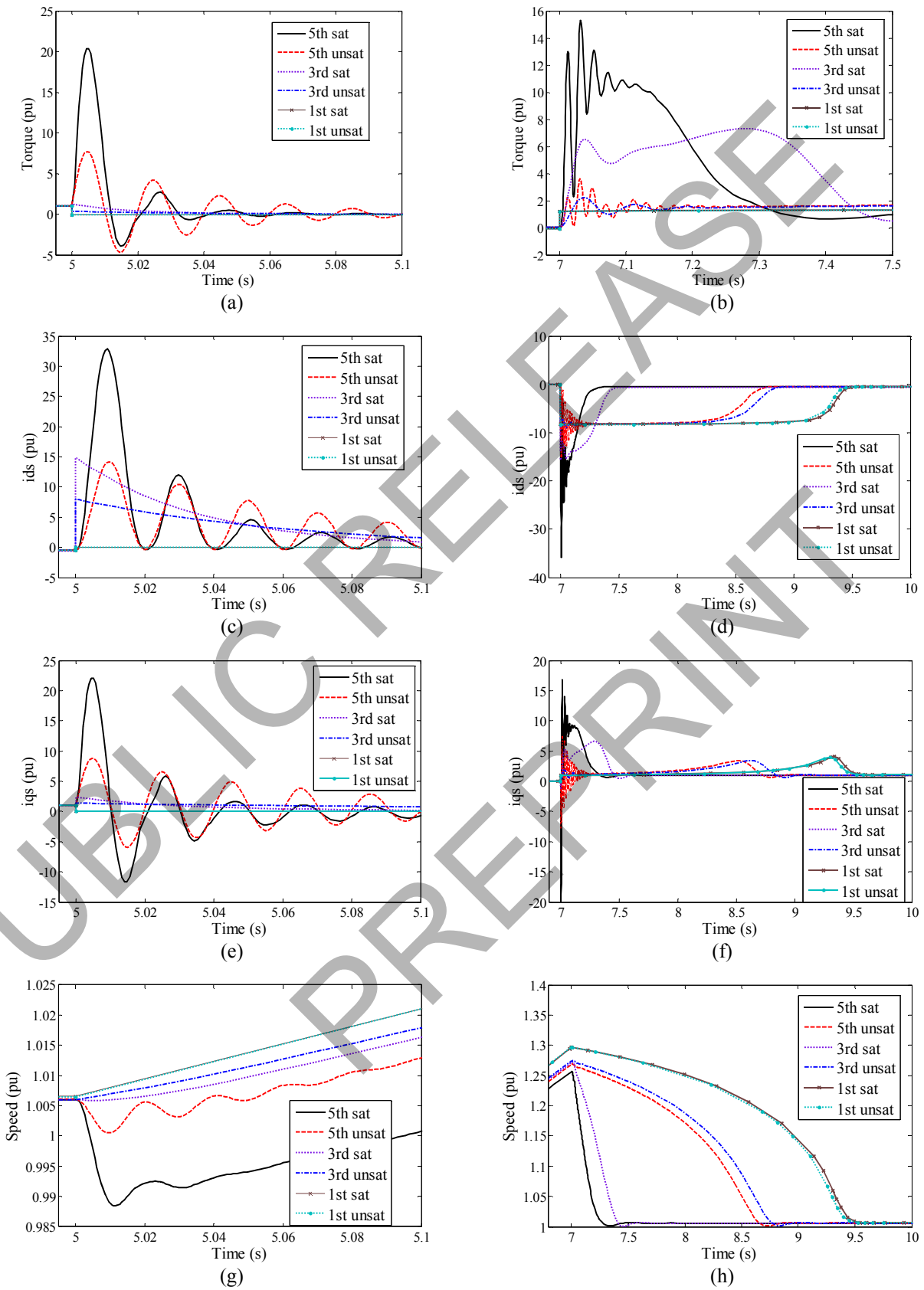


Figure 3. DFIG transient response due to 50% voltage sag. (a) torque at voltage sag occurrence, (b) torque at voltage recovery, (c) ids at voltage sag occurrence, (d) ids at voltage recovery, (e) iqs at voltage sag occurrence, (f) iqs at voltage recovery, (g) speed at voltage sag occurrence, and (h) speed at voltage recovery

The effect of saturation using different orders on the transient performances of the generator associated with such events is shown in fig.3. the machine used for simulation was a 2 MW, 690 V wind turbine and machine parameters are given in appendix.

The following results can be seen from above simulation:

1. after the fault occurred:
 - the effect of leakage flux saturation is to increase the current and torque.
 - In spite of fifth order model there isn't any oscillation in third and first order model.
 - Difference between saturated and unsaturated of first order model is negligible, but for higher order model this is significant.
 - The rotor speed decreases for saturated and unsaturated of fifth order model, but for other models there isn't any decrease in speed.
2. after the fault cleared:
 - fifth order saturated model reach its steady state faster than the other models.
 - Saturation doesn't affect the steady state value of torque, current and speed but it affects transient response of these variables.

V. rotor over-current due to voltage sag

The abrupt drop of the grid voltage causes over-voltages and over currents in the rotor windings that could even destroy the converter if no protection element is included. In [9] the factors that affect over-current was investigated mathematically. In this paper the effect of these factors is simulated considering an accurate model. For all simulation in this section fifth-order model considering saturation effect is used.

A. crowbar resistance

The first factor is rotor resistance. If we neglect the stator resistance, the amplitude of over-current is proportional to $1/R_r$. So the solution to protect converter is to short circuit the rotor windings with the so-called crowbar resistance. There are two main requirements that give an upper and a lower limit to the resistance [7]:

- 1) the resistance should be high to limit the short circuit current .
- 2) on the other hand, it should be low to avoid a too high voltage in the rotor circuit.

A too high voltage can result in break down of the isolation material of the rotor and the converter. Fig.4 shows a simulation that uses crowbar resistance in series with rotor resistance as a solution to reduce rotor over-current. Simulation was done for different value of crowbar. When the voltage sag occurs the crowbar resistance is added to rotor resistance.

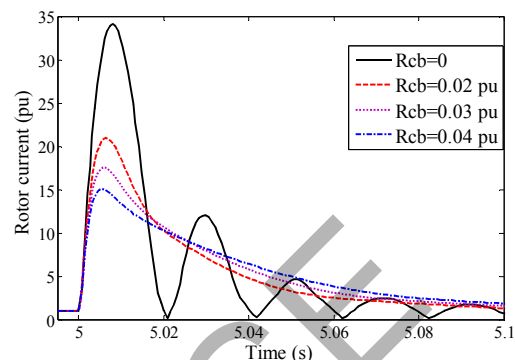


Figure 4. rotor over-current due to voltage sag for different crowbar resistance value

As shown in fig.4, the more the value of crowbar resistance, the less the maximum of rotor current. Table 2 shows the maximum of rotor current while the crowbar resistance changes.

Table 2
maximum of rotor current while the crowbar changes

$R_{cb} (\Omega)$	0	0.02	0.03	0.04
$I_{r,max} (A)$	34.12	20.96	17.51	15.02

B. depth of voltage dip

The second factor is depth of voltage dip. In fact, the more severe of voltage drop, the bigger of the rotor current amplitude was. To quantify sag magnitude in radial systems, the voltage divider model, shown in fig.5, can be used. The voltage at the DFIG terminals can be found from (10).

$$V_{sag} = \frac{Z_F}{Z_S + Z_F} E \quad (10)$$

Any fault impedance should be included in the feeder impedance Z_F .

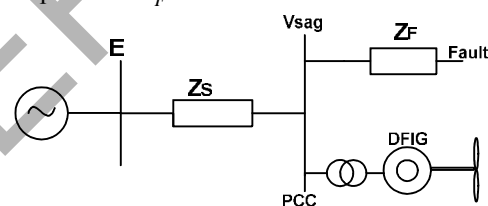


figure 5. voltage divider model for a voltage sag

It's seen from (10) that the sag becomes deeper for faults electrically closer to the DFIG (when Z_F becomes smaller), and for systems with a smaller fault level (when Z_S becomes larger). In (10) $E=1$ pu and $Z_F = z \times l$, with z the impedance of the feeder per unit length and l the distance between the fault and the pcc, leading to (11).

$$V_{sag} = \frac{zl}{Z_S + zl} \quad (11)$$

The sag magnitude as a function of the distance to the fault has been calculated for a typical 11 kV overhead line, resulting in fig.6.

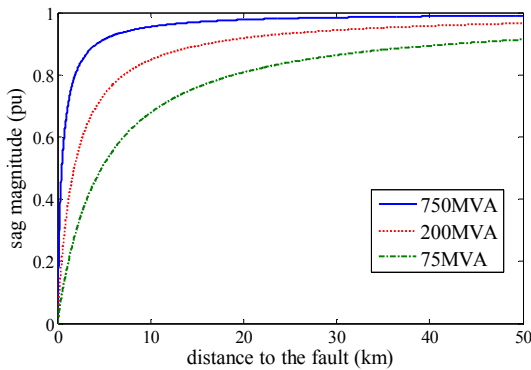


Figure 6. sag magnitude as a function of the distance to the fault, for faults on an 11 kV, overhead line.

The fault level is used to calculate the source impedance at the pcc. In this paper, 11 kV overhead line, and 200MVA fault level is considered. The impedance of overhead line is $0.117 + j0.315\Omega$ per km[8]. Simulations are done for different distance between fault and pcc.

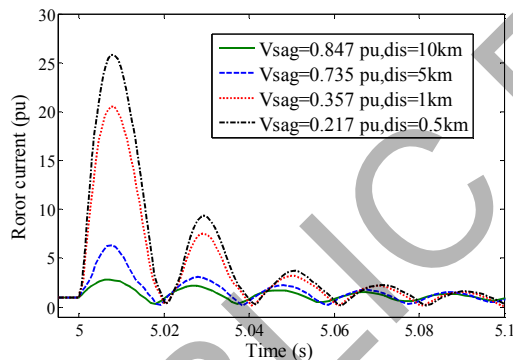


Figure 7. rotor over-current due to voltage sag for different distance between fault and pcc.

Fig.7 shows that the distance between fault and terminal of DFIG is an important factor for maximum amplitude of rotor current. For example when it is 500m, rotor maximum current is 25.8A, while it is 10km, rotor maximum current is 2.85A.

VI. Conclusion

In this paper transient performance of different order model of DFIG considering or ignoring saturation effect was compared. Then some parameters that affect rotor over-current due to voltage sag was simulated. The main findings can be summarized in the following points:

1. the stator and rotor current of DFIG calculated by considering the saturation effect are significantly higher than the ones that ignores it.
2. the rotor speed of saturated model reaches the steady state value faster than unsaturated model,

and fifth order model reaches faster than the reduced orders.

3. it's crucial to incorporate the saturation effect to study the transient performance of DFIG, but it's not important for steady state study.
4. in the case of strong voltage sags, the induced voltage on rotor can even be higher than the stator voltage. In this situation, there appear over-current whose amplitude depends on the depth of the dip, the machine parameters, and the protection element.

Appendix

Rated power (W)	2000
Rated voltage (V)	690
Rated frequency (Hz)	50
X_m (pu)	3.188
R_s (pu)	0.00562
R_r (pu)	0.00575
X_{ls} (pu)	0.0708
X_{lr} (pu)	0.0486

$$X_s = X_m + X_{ls}$$

$$X_r = X_m + X_{lr}$$

REFERENCE

- [1] Jesus Lopez, Pablo Sanchis, Xavier Roboam and Luis Marroyo, "Dynamic behavior of the doubly fed induction generator during three-phase voltage dip", IEEE Transactions on energy conversion, vol.22, no.3, September 2007.
- [2] J.B.Ekanayake, L.Holdsworth, and N.Jenkins, "Comparison of 5th and 3rd order machine models for doubly fed induction generator (DFIG) wind turbines", Electric Power Systems Research 67 (2003), pp.207-215
- [3] Andres Feijoo, Jose Cidras, and Camilo Carrillo, "A third order model for the doubly-fed induction machine", Electric Power Systems 56 (2000), pp.121-127
- [4] Zhixin Miao, and Lingling Fan, "The art of modeling and simulation of induction generator in wind generation applications using high order model", Simulation Modeling Practice and Theory, 2008
- [5] Miguel Garcia-Gracia, M.Pez Conech, Jesus Sallan, and Andres Lombart, "Modeling wind farms for grids disturbance studies", Renewable Energy 33(2008), pp.2109-2121
- [6] Hony M.Jabr, and Narayan C.Kar, "Effect of main and leakage flux saturation on the transient performances of doubly-fed wind driven induction generator", Electric Power Systems Research 77 (2007), pp.1019-1027
- [7] Hony M.Jabr, and Narayan C.Kar, "Leakage flux saturation effects on the transient performance of wound rotor induction motors", Electric Power Systems Research 78(2008) 1280-1289
- [8] Math H.J.Bollen, Understanding power quality problems, Chalmers University of Technology Gothenburg, Sweden, 2000.
- [9] Aoyang Han, Zhe Zhang, and Xianggen Yin, "Study of factors affected the rotor over-current of DFIG during the three phase voltage dip", DRPT 2008, 6-9 April 2008.

Reverse electrodialysis for Power Generation

Sameer Deshmukh
Wroclaw University of Technology
Wroclaw, Poland

Abstract- The use of reverse electrodialysis, to derive energy from the difference between the chemical potentials of concentrated and dilute salt solutions is reviewed. The process employ the flows of brine and dilute solutions through alternating cells bounded by cation- and anion-exchange membranes in a stack placed between two electrodes to generate a voltage by the passage of salt through the membranes. Potential sources of brine include the salt domes of oil and gas wells, salt water lakes, and geothermal brines. This paper also reviews a range of membrane properties of the commercially available membranes.

Keywords: Power generation, Reverse electrodialysis, membranes for RED.

1. INTRODUCTION

Renewable and sustainable energy sources are playing an important role in the 21st century and are becoming increasingly important due to environmental problems, such as global pollution phenomena and global warming. Membrane technology provides an opportunity to gain renewable and sustainable energy from salinity gradients via, e.g. pressure retarded osmosis and reverse electrodialysis. The latter method seems more attractive for power generation using sea and river water. Reverse electrodialysis (RED) is a non-polluting, sustainable method for energy generation by mixing fresh and salt water. RED converts the free energy generated by mixing the two aqueous solutions into electrical power and the system can be applied wherever two solutions of different salinity are mixed, e.g. where river water flows into the sea. The principle of RED was first proven by Pattle, who with his pioneering work in this field was the first one that generated power using RED. In the 70s, Weinstein and Leitz investigated the effect of solution composition on power output and the main conclusion of this work was that large-scale energy conversion by RED may become practical, but only with major advances in the manufacturing of ion exchange membranes and with careful optimization of the operating conditions. In the early 1980s, Lacey conducted a comprehensive investigation on RED. Conclusion of his work was that to make RED commercially available it is necessary to minimize the internal stack resistance of the RED cells and to maximize the net power output from the cell. Lacey concluded that membranes for RED should have a low electrical resistance and a high selectivity combined with a long service life time, acceptable strength, dimensional stability and low-cost. In the mid 1980s, Jagur-Grodzinski investigated membrane spacer modifications and different salt solution streams in order to generate more energy. In 2007, Turek and Bandura studied the effect of solution velocity on cell power output and process

economy. Turek, mentioned that the main bottleneck for a successful RED system seems to be the membrane price. Despite that remark, the focus of most of the earlier work on RED was on stack design, solution flow and solution composition, but not on membrane characterization and membrane performance. Most scientists used electrodialysis membranes to study the RED process. The ion exchange membranes are the key elements in the RED system. The most important membrane properties for RED are ion exchange capacity, swelling degree, and of course the membrane resistance and its selectivity (the ability of the membrane to distinguish between cations and anions), because of their direct effect on the overall RED performance. Up to now, it is still not known which membrane parameter is the dominant factor with respect to power generation in RED. It is essential to identify the key membrane parameters for RED in order to further improve the power output of RED. The data available in the existing literature do not offer sufficient information on membrane properties relevant to RED to enable proper mutual comparison of the different commercially available membranes. Currently, no complete overview is available with respect to the application of ion exchange membranes in RED which covers the full range of membrane types.

This review presents an overview of reverse electrodialysis. It investigates a range of membrane properties of commercially available membranes that are important with respect to application in RED. The objective of this study is to analyze the membrane properties under equivalent conditions to enable a fair comparison of the results and a proper evaluation for application in RED.

2. Theoretical background

2.1. Principle of reverse electrodialysis

In RED, a concentrated salt solution and a less concentrated salt solution are brought into contact through an alternating series of anion exchange membranes (AEM) and cation exchange membranes (CEM) (Fig. 1,1.1).

The membranes separate the concentrated solution from the diluted solution and only ions can pass through the ion selective membranes. Anion exchange membranes contain fixed positive charges which allow anions to permeate through the AEM towards the anode and cation exchange membranes contain fixed negative charges which allow cations to be transported through the CEM towards the cathode. The difference in chemical potential between both solutions is the driving force for this process. At the electrodes a redox couple is used to mitigate the transfer of electrons. The chemical potential difference generates a voltage difference over each membrane.

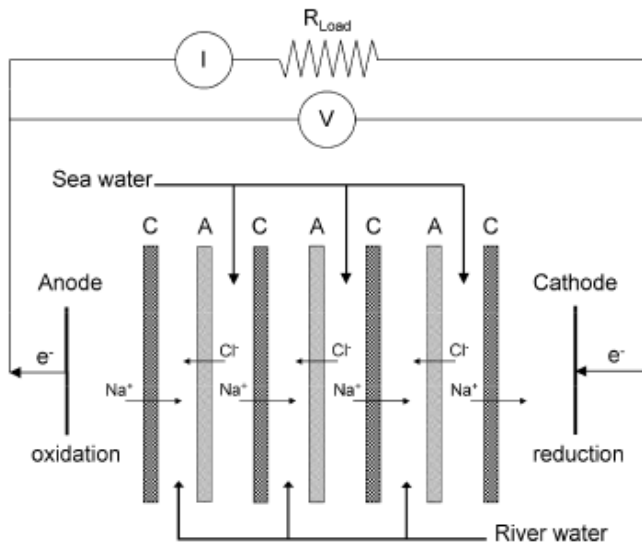


Fig. 1. Schematic representation of reverse electrodialysis: A is an anion exchange membrane, C a cation exchange membrane, V is the potential difference over the applied external load (V), I is the electrical current (A) and R_{Load} is the resistance of the external load (Ω). A redox couple is used at the electrodes to mitigate the transfer of electrons.

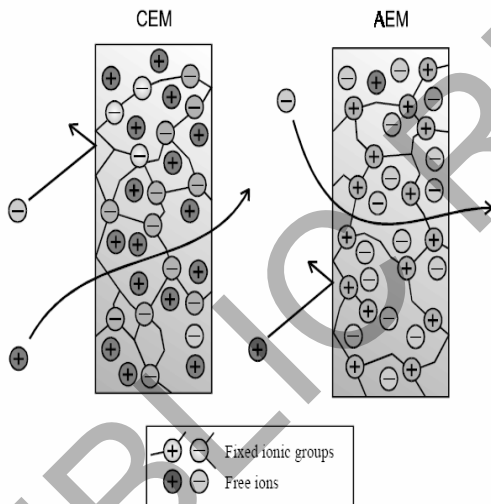


Figure 1.1: The two types of (mono polar) electrodialysis membranes. On the left: cation-exchange membrane, on the right anion-exchange membrane.

The theoretical value of the potential over the membrane for an aqueous monovalent electrolyte (e.g. NaCl) can be calculated using the Nernst equation (Eq.(1)):

$$\Delta V_{theo} = \frac{RT}{zF} \ln \frac{a_c}{a_d} \quad (1)$$

where ΔV_{theo} is the theoretical membrane potential for a 100% selective membrane (V), R is the gas constant (8.314J/(mol K)), T is the absolute temperature (K), z is the electrochemical valence, F is the Faraday constant (96,485 C/mol), a_c is the activity of the concentrated solution (mol/l) and a_d is the activity of the diluted solution (mol/l). For fresh water (0.017 M NaCl, $y_{\pm} = 0.878$) and sea water (0.5 M NaCl, $y_{\pm} = 0.686$), the theoretical voltage difference per membrane is 80.3 mV. The overall potential of the system is the sum of the potential differences over each pair of membranes.

2.2. Ion exchange membrane properties

Ion exchange membranes are membranes with fixed anionic or cationic exchange groups that are able to transport cations or anions. The specific properties of ion exchange membranes are all related to the presence of these charged groups. Amount, type and distribution of ion exchange groups determine the most important membrane properties. Based on the type of fixed charge group, ion exchange membranes can be classified as strong acid and strong base, or weak acid and weak base membranes. Strong acid cation exchange membranes contain sulfon groups as charged group. In weak acid membranes, carboxylic acid is the fixed charged group. Quaternary and tertiary amines are the fixed positive-charged groups in strong and weak base anion exchange membranes, respectively.

2.2.1. Ion exchange capacity

The ion exchange capacity (IEC) is the number of fixed charges inside the ion exchange membrane per unit weight of dry polymer. The ion exchange capacity is a crucial parameter which affects almost all other membrane properties. The IEC is expressed in milli equivalent of fixed groups per gram of dry membrane (mequiv./g membrane).

2.2.2. Fixed charge density

Ion exchange membranes contain fixed-charged groups attached to the polymer backbone. In cation exchange membranes, the fixed negative charges are in electrical equilibrium with the mobile cations (counter-ions). The opposite relation exists in anion exchange membranes. The fixed charge density, expressed in milli equivalent of fixed groups per volume of water in the membrane (mequiv./l) strongly depends on the IEC and the swelling degree of the membrane: in the swollen state, the distance between the ion exchange groups increases thus reducing the fixed charge density. The transport of counter ions through the membrane is determined by the fixed charge density in the membrane and the difference between the concentrations of the electrolyte solution in contact with that membrane. The concentration and type of the fixed ionic charges determine the permselectivity and the electrical resistance of the membrane.

2.2.3. Permselectivity

When an ion exchange membrane is in a contact with an electrolyte (salt solution), ions with the same charge (co-ions) as the fixed ions are excluded and cannot pass through the membrane, while the oppositely charged ions (counter ions) can pass freely through the membrane. This effect is known as Donnan exclusion [14]. The permselectivity of a membrane describes the charge selectivity of the ion exchange membrane. It reflects the ability of the membrane to discriminate between ions of opposite charge.

2.2.4. Electrical resistance

The electrical resistance of the membrane is an important property of ion exchange membranes, because it is directly related to the maximum power output in reverse electrodialysis and the energy consumption in electrodialysis processes. The membrane resistance is determined by the ion exchange capacity and the mobility of the ions within the membrane matrix. The electrical

resistance is dependent on temperature and decreases with increasing temperature. The specific membrane resistance is in principle reported in 2 cm. However, more useful and most often reported in literature is the membrane resistance in 2 cm².

2.2.5. Heterogeneous and homogenous ion exchange membranes

Ion exchange membranes can be divided with respect to their structure and preparation procedure into two categories: homogenous and heterogeneous membranes. In homogenous ion exchange membranes the fixed charge groups are evenly distributed over the entire membrane matrix. Homogenous membranes can be manufactured via polymerization and polycondensation of functional monomers (e.g. fenylosulfonic acid with formaldehyde) or via functionalization of a polymer by for example dissolving the polymer in a suitable solvent and subsequent functionalization by, e.g. post-sulfonation. Heterogeneous membranes have distinct macroscopic uncharged polymer domains of ion exchange resins in the membrane matrix. This type of membranes can be produced by melting and pressing of a dry ion exchange resin with a granulated polymer (e.g. polyvinylchloride). Another method to prepare heterogeneous membranes is dispersion of the ion exchange resin in a polymer solution. The distinct difference between homogenous and heterogeneous ion exchange membranes also influences the properties of the specific membrane.

2.3. RED membrane model

To predict the relative contribution of the different components in a RED stack, a theoretical model was used. The relationship between the salt concentration (activity) in the two compartments (diluted and concentrated), the process temperature and the selectivity of the membrane is shown in the following equation:

$$V^o = N \frac{2\alpha_{av}RT}{zF} \ln \frac{a_c}{a_d}$$

where V^o is the open circuit potential of the membrane stack (V), α_{av} is the average membrane permselectivity of an anion and a cation exchange membrane pair, N is the number of membrane pairs, R is the gas constant (8.314J/(mol K)), T is the absolute temperature (K), z is the electrochemical valence, F is the Faraday constant (96,485 C/mol), a_c is the activity of the concentrated salt solution (mol/l) and a_d is the activity of the diluted salt solution (mol/l).

The stack resistance can be defined as the sum of the resistances of the individual stack components as shown in the following equation:

$$R_{stack} = \frac{N}{A} \left(R_{aem} + R_{cem} + \frac{d_c}{\kappa_c} + \frac{d_d}{\kappa_d} \right) + R_{el} \quad (3)$$

where N is the number of membrane pairs, A is the effective membrane area (m²), R_{aem} is the anion exchange membrane resistance (2 m²), R_{cem} is the cation exchange membrane resistance (2 m²), d_c is the thickness of the concentrated compartment (m), d_d is the thickness of the diluted compartment (m), κ_c is the concentrated compartment conductivity (S/m), κ_d is the diluted compartment conductivity (S/m) and R_{el} is the electrode resistance (2).

The final stack power output of the RED stack can be found from Kirchhoff's law and is defined as

$$W = I^2 R_{load} = \frac{(V^o)^2 R_{load}}{(R_{stack} + R_{load})^2} \quad (4)$$

Here I is the current (A), R_{load} is the load resistance (2), R_{stack} is the stack resistance (2) and V^o is the stack open circuit potential (V).

To generate a maximum power output (W_{max}), R_{load} needs to be equal to R_{stack} .

In that case, Eq. (4) changes into Eq. (5) which shows the relationship between the open circuit potential, the maximum power output and the stack resistance.

$$W_{max} = \frac{(V^o)^2}{4R_{stack}} \quad (5)$$

Combination of Eq. (5) with Eqs. (2) and (3) finally yields Eq. (6) which relates the maximum power output of the RED stack to the individual contributions of each component. More specifically, it relates the maximum power output of the system (W_{max}) to the average membrane selectivity (α_{av}) and the membrane resistance (R_{aem} and R_{cem}).

$$W_{max} = NA \frac{[\alpha_{av}RT/F \ln(a_c/a_d)]^2}{R_{aem} + R_{cem} + (d_c/\kappa_c) + (d_d/\kappa_d)} \quad (6)$$

where N is the number of membrane pairs, α_{av} is the average membrane pair permselectivity, R is the gas constant (8.314J/(mol K)), T is the absolute temperature (K), F is the Faraday constant (96,485 C/mol), a_c is the concentrated solution activity (mol/l), a_d is the diluted solution activity (mol/l), R_{aem} is the anion exchange membrane resistance (2 m²), R_{cem} is the cation exchange membrane resistance (2 m²), A is the effective membrane area (m²), d_c is the thickness of the concentrated compartment (m), d_d is the thickness of the diluted compartment (m), κ_c is the concentrated (0.5 M NaCl) compartment conductivity (4.648 S/m) and κ_d is the diluted (0.05 M NaCl) compartment conductivity (0.551 S/m).

Eq. (6) predicts the theoretical membrane stack power output and relates the maximum power output of the system to the individual membrane characteristics, it can be used as a tool to compare different anion and cation exchange membranes with respect to their performance in a RED stack. If Eq. (6) is used to predict the power output obtainable with only a cation exchange membrane, then the average membrane pair permselectivity (α_{av}) is replaced by the individual membrane selectivity (α). The resistance of the anion exchange membrane term will be removed in that case and the concentrated and diluted compartment thickness (d) will be divided by two. The same procedure is applicable for anion exchange membranes. This calculated power output for only one type of the membrane is used to compare the different anion or cation exchange membranes with each other.

In the model a few assumptions were made: (i) concentration polarization phenomena near the membrane surface are negligible due to the small current densities obtained through the membranes. This phenomenon can be minimized with well designed fluid dynamics between the membranes, (ii) the resistance of the electrodes is assumed to be negligible compared to the membrane resistance. This assumption is allowed when a large number of membrane cell pairs is used, (iii) the feed solution does not change in concentration along the channels. This assumption has a strong relationship with the feed channel design and in a well-designed system this effect can be neglected.

In order to compare commercially available membranes with each other it is more desirable to convert the power output into power density by normalizing it for the membrane area (W/m²). Power density per square meter of membrane can be easily calculated from the maximum power output:

$$w_{\max} = \frac{W_{\max}}{AN_m} \quad (7)$$

where w_{\max} is the maximum power density (W/m^2), W_{\max} is maximum power output (W), A is the effective membrane area (m^2) and N_m is the number of membranes.

Obtained power output per type the membrane (anion or cation exchange membrane) is used only to benchmark membranes with each other.

5. Conclusion

This paper evaluates the potential of commercially available anion and cation exchange membranes for application in RED. Different membrane properties and characterization methods are discussed and a theoretical membrane model for RED was used to allow fair comparison of the characterization results for application in RED. Literature shows that the charge density has a strong influence on the permselectivity and the membrane resistance, but that there does not exist a straight forward relationship between these properties. In general cation exchange membranes have a higher charge density and a corresponding higher permselectivity than anion exchange membranes. Heterogeneous ion exchange membranes have a relatively low charge density compared to homogeneous membranes and a much higher resistance due to the membrane structure and the separation of charged domains in an uncharged polymer matrix. This makes RED a potentially attractive alternative for energy production.

Nomenclature

a_c	concentrated solution activity (mol/l)
a_d	diluted solution activity (mol/l)
A	membrane area (m^2)
c_{fix}	fixed charge (mol/l)
F	Faraday constant (96,485 C/mol)
i	current density (A/m^2)
I	current (A)
N	number of cell pairs
N_m	number of membranes
R	gas constant (8.314 J/(mol K))
R_{aem}	anion exchange membrane resistance (Ωm^2)
R_{cem}	cation exchange membrane resistance (Ωm^2)
R_c	concentrated solution resistance (Ω)
R_d	diluted solution resistance (Ω)
R_{el}	electrode resistance (Ω)
R_{load}	load resistance (Ω)
R_{stack}	resistance of the stack (Ω)
T	absolute temperature (K)
V^o	stack open circuit potential (V)
w	power density (W/m^2)
W_{\max}	maximum power output (W)
<i>Greek symbols</i>	
α	permselectivity of the membrane
α_{av}	average permselectivity of an anion and a cation membrane pair
γ_{\pm}	mean activity coefficient
ΔV_{meas}	measured membrane potential (V)
ΔV_{theo}	theoretical membrane potential (V)

REFERENCES

- [1]. R.E. Lacey, Energy by reverse electrodialysis, Ocean Eng., 7 (1980) 1–47
- [2]. J. Weinstein and B. Leitz, Electric power from differences in salinity: the dialytic battery, Science, 191 (1976) 557–559.
- [3]. <http://www.wetsus.nl/eng/Themes5b.htm>
- [4]. M. Turek, Cost-effective electrodialytic seawater desalination, Desalination, 153 (2002) 371–376.
- [5]. Piotr Długołęcki, Kitty Nymeyer, Sybrand Metz and Matthias Wessling, Current status of ion exchange membranes for power generation from salinity gradients, Journal of Membrane science, 319, July 2008, Pages 214–222.

Microbial fuel cells to produce electricity

Sameer Deshmukh, Yogesh Khambhia
Wroclaw University of Technology
Wroclaw, Poland

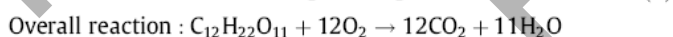
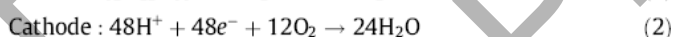
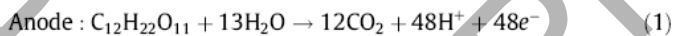
Abstract- Microbial fuel cell (MFC) provides a new opportunity for the sustainable production of energy in the form of direct electricity from biodegradable compounds present in the wastewater achieving the simultaneous water treatment. MFC is a device that converts chemical energy to electrical energy with the aid of the catalytic reaction of microorganism. This article provides a brief introduction to MFC along with its envisaged applications as one of the class of biological fuel cell.

Keywords: Microbial Fuel cell, Electricity

I. INTRODUCTION

The high energy intensive conventional wastewater treatment systems invites for the development of alternative treatment technology. There is a tremendous need to develop suitable and reliable technology for the treatment of wastewater. Such treatment technology should be cost effective, requiring less energy for its efficient operation and should generate less sludge. In addition, the treatment system should recover energy to make overall operation of wastewater treatment self sustainable.

Microbial fuel cell (MFC) provides new opportunity for the sustainable production of energy, in the form of direct electricity from biodegradable compounds present in the wastewater, achieving simultaneous wastewater treatment. MFC is a device that converts chemical energy to electrical energy with the aid of the catalytic reaction of microorganisms¹. In a MFC, substrate (organic matter or biomass) is oxidized in the anode chamber producing carbon dioxide, protons and electrons². Microorganisms here fulfill the role of catalysts in analogs to chemical fuel cells. The electrons and the protons produced in the anode chamber ends up at the cathode, via the external electrical circuit and through the proton exchange membrane (PEM), respectively. In the cathode, an oxidant (normally oxygen) is being reduced. Eqs. (1)–(3) illustrates the basic reactions occurring in MFCs, in the case of a sucrose fed wastewater in anode and oxygen as electron acceptor in cathode.



$$\Delta_r G^\circ = -5792.2 \text{ kJ/mol} \quad (3)$$

Performance of a MFC is affected by the substrate conversion rate, over-potentials at the anode and at the cathode, the PEM performance, and internal resistance of the cell². The optimization of MFCs requires extensive exploration of the operating parameters that affect the power output.

All the literature review supports performance of MFC under controlled conditions using different cultures. Enough attention has not been paid so far on evaluating performance of MFC

exposed to changes in operating temperature and pH, which are among the important aspects for field application of the MFCs.

After a brief outline of the long and winding history of biological fuel cells, this article deals with the operating principles of Microbial fuel cells and their technological applications.

II. HISTORY OF BIOLOGICAL FUEL CELLS

For centuries, microorganisms, which transform food into an electron flow, were only a biological curiosity; but now scientists have made it possible to use them in watches and cameras as power sources³. Luigi Galvani, who noticed twitching of isolated frog leg when a brief electrical discharge was passed through it⁴, was the first to observe the bioelectric phenomenon as early as in 1790 and the term bioelectricity was coined after that observation. In 1910, Michael Cresse Potter, a professor of botany at the University of Durham, UK,

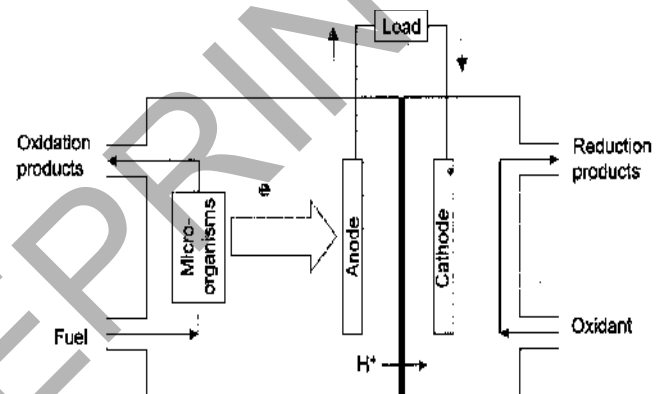


Figure 1. A typical biological fuel cell representing current generation with the help of microorganisms. The fuel generated by microbial metabolism gets oxidized at the anode and usually oxygen is reduced at the cathode.

demonstrated that organisms could generate a voltage and deliver current. Cohen at Cambridge revived Potter's idea in 1931. He described how a batch of biological fuel cells produced more than 35 V. But biological fuel cells became popular in the 1960s, when the National Aeronautics and Space Administration evinced interest in turning organic waste into electricity on its long-haul space flights. Algae and bacteria were among the first organisms used in biological fuel cells. During the mid 19th century, for the first time, Rohrbach *et al*⁵ designed a biological fuel cell in which *Clostridium butyricum* was used as a biological material to generate hydrogen by

glucose fermentation. In 1963, biological fuel cells were already commercially available for use as a power source in radios, signal lights and other appliances at sea. However, these fuel cells were not a commercial success and soon disappeared from the market. With the successful development of technical alternatives, e.g. solar photovoltaics for the energy supply on space flights, biological fuel cells suffered a short setback. Later, during the oil crisis of the 70s and 80s, the interest in the development of biological fuel cells was revived. In 1966, Williams⁶ showed that biological fuel cells powered by rice husk produced 40 mA at 6 V. Rice husk is a potential source of lignocellulose, which on fermentation yields many useful enzymes and biofuels like ethanol that could be used in biological fuel cells. In 1969, Yao *et al.*⁷ showed that glucose could be used as a fuel in the presence of platinum-black. Later, Karube *et al.*⁸ reported the generation of about 300 mA electric current from an *Anabaena* spp.-based biological fuel cell, in which phosphoric acid was used as the electrolyte. Bennetto and co-workers have made noteworthy contributions to biological fuel cells. They have developed and demonstrated improved biological fuel cells using various microorganisms and mediator systems. They showed that the mediators could enhance both the efficiency of electron-transfer and the reaction rate. Recently, Chaudhuri and Lovely⁹ have reported that a microorganism *R. ferrireducens* can recover an electron from glucose oxidation in the presence of Fe³⁺ up to 83% without a mediator. Presently, efforts are being expended to improve the performance of mediator-less biological fuel cells as well as on finding an effective route to wire the microorganism to the electrode so as to promote the efficiency of electron-transfer.

III. Microbial fuel cells

The use of microorganisms in biological fuel cells eliminates the isolation of individual enzymes, thereby providing cheaper substrates for biological fuel cells. Microorganisms can be used in four ways for producing electrical energy:

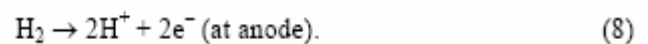
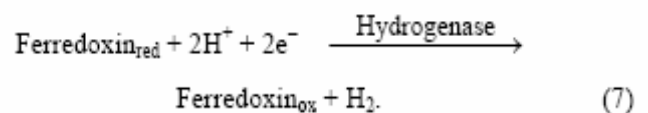
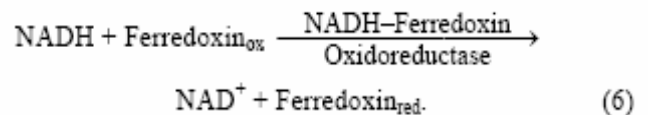
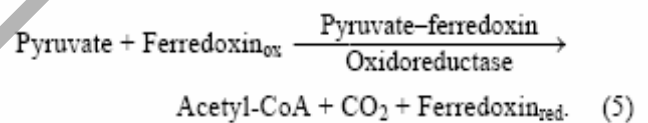
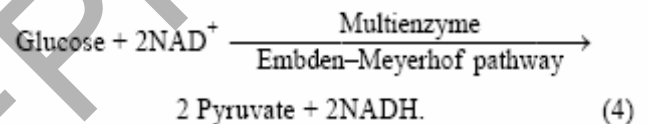
- (i) Microorganisms can produce electrochemically active substances through fermentation or metabolism. For the purpose of energy generation, fuels are produced in separate reactors and transported to the anode of a conventional fuel cell. Accordingly, in this configuration, the microbial bioreactor is kept separated from the fuel cell.
- (ii) In the second configuration, the microbiological fermentation process proceeds directly in the anodic compartment of the fuel cell.
- (iii) In the third configuration, electron-transfer mediators shuttle electrons between the microbial biocatalytic system and the electrode. The mediator molecules accept electrons from the biological electron transport chain of the microorganisms and transport them to the anode of the biological fuel cell.

- (iv) In the fourth configuration, the metal-reducing bacterium having cytochromes in its outer membrane and the ability to communicate electrically with the electrode surface directly result in a mediator-less biological fuel cell.

A brief description of the aforesaid configurations is given below:

Microbial-systems producing hydrogen as fuel for conventional fuel cells: Various bacteria and algae, e.g. *Escherichia coli*, *Enterobacter* aero-genes, *C. butyricum*, *Clostridium acetobutylicum* and *Clostridium perfringens*, are known to be active for hydrogen production under anaerobic condition^{10,11}. The most effective hydrogen-producing microorganism is *C. butyricum*¹². *E. coli* and *Enterobacter* aero-genes are facultative anaerobes and ferment both glucose and lactose as a carbon source to produce hydrogen.

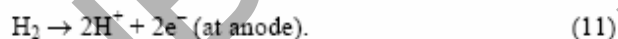
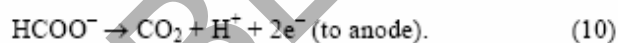
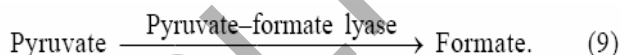
The conversion of carbohydrate to hydrogen is achieved by a multienzyme system. In bacteria, it involves the conversion of glucose to 2 mol of NADH, a reduced form of coenzyme 1, namely -nicotinamide adenine dinucleotide of the vitamin niacin, and 2 mol of pyruvate formed by Embden–Meyerhof pathway. Pyruvate is then oxidized through a pyruvate–ferredoxin oxidoreductase producing acetyl-CoA, CO₂ and reduced ferredoxin. NADH–ferredoxin oxidoreductase oxidizes NADH and reduces ferredoxin. The reduced ferredoxin is reoxidized to form hydrogen by hydrogenase. As a result, 4 mol of H₂ are produced from 1 mol of glucose under ideal conditions as shown below. In practice, however, H₂ yield is only about 25% of the theoretical value¹³. Improvement in H₂ production is possible by genetic engineering techniques and screening of new hydrogen-producing bacteria.



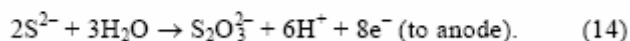
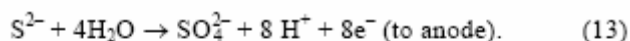
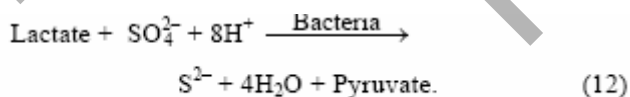
A H₂/O₂ fuel cell comprising a platinum-black–nickel mesh anode and a palladium-black–nickel mesh cathode, and separated by a nylon filter operating at room temperature was connected to a bioreactor producing hydrogen^{14,15}. The current and voltage output were dependent on the rate of hydrogen production in the fermenter. For example, an open-circuit voltage (*v*_{oc}) of 0.95 V and a short-circuit current density (*i*_{sc}) of 40 mA/cm² were obtained at a H₂ flow of 40 ml/min. The biological fuel cell operating under steady-state conditions for a week produced a continuous current between 500 and 550 mA.

The immobilization of the biocatalyst is primarily important in a bioreactor. In the biological fuel cell configuration described above, the immobilization of hydrogen-producing bacteria, *C. butyricum* is of great value as this stabilizes the relatively unstable hydrogenase system. The immobilization steps could be the trapping of microorganisms into polymeric matrices of polyacrylamide, agar gel or filter paper. The immobilized microbial cells continuously produced H₂ under anaerobic conditions for several weeks, whereas non-immobilized bacterial cells were fully deactivated in less than two days.

Microbial systems producing electrochemically active metabolites in the anodic compartment of biological fuel cells: In this configuration, the fermentation process is conducted directly at the electrode surface supplying the anode with H₂ fuel. Additional by-products of the fermentation process, namely formic acid, acetic acid and lactic acid are also utilized as fuels¹⁶. Besides, the base substrate glucose used for the fermentation process, byproducts could as well contribute to the anodic current. Hence, H₂ provided by the microorganisms can be a source of anodic current as indicated by the side reactions below.



In addition to fuels like H₂, formic acid, lactic acid and sulphur-containing electrochemically active metabolites like S²⁻ species, can be produced during the fermentation of lactate by *Desulfovibrio desulfuricans*, which are known to be sulphate-reducing bacteria, shown as follows.



The presence of sulphides in the medium results in the inhibition of the metabolic bacterial processes because of their interaction

with iron-containing proteins, e.g. cytochromes, causing the electron transport systems to be blocked. S₂²⁻ species poison many metallic electrodes because of their strong and irreversible adsorption. In a typical experiment, porous graphite electrode impregnated with cobalt hydroxide as catalyst was used as the anode. Cobalt hydroxide undergoes transition into a highly catalytically active cobalt oxide/cobalt sulphide mixture. A biological fuel cell has been constructed with the above biocatalytic anode along with a graphite cathode activated with iron(II) phthalocyanins and vanadium(V) compounds. The anode and cathode are separated to maintain anaerobic conditions at the anode compartment. The poor performance of fuel cells arising due to the adsorption of by-products on the electrode surface is improved by an electrode modification process. The microorganisms processing glucose in a tank of the fermentation fluid are continuously pumped through a separate anode space. This is separated from the cathode space by a semi-permeable membrane. These bio-fuel cells have a new type of anode where a platinum electrode or a platinized graphite electrode is coated with a layer of the electrically conducting polyaniline, which is both biocompatible and electro-catalytically active. It absorbs electrons from the metabolism of the bacteria and transfers them to the anode. In this way, it plays a decisive role in current flow. During operation, the bacterial metabolic products along with the by-products of the electro-catalytic oxidation process settle on an uncoated anode and rapidly deactivate it. The polymer slows down this process considerably. Additional regular voltage pulses chemically convert the deposit and release them from the anode surface. This fuel cell continuously provides up to 1.5 mA/cm² of current¹⁷

Mediator-coupled microbial fuel cells: Reductive species generated by metabolic processes inside microbial cells are isolated by a microbial membrane. Thus, the contact of the microbial cells with an electrode usually results in only a diminutive electron-transfer across the membrane of the microbes¹⁸, except in some special cases as described later. The electro-active groups responsible for the redox activity of enzymes present in the microbial cells are deeply buried inside their prosthetic groups, which leads to poor electrical communication between the cells and the electrode surface. The cells can, however, be wired to the electrode surface with the help of mediators. Low molecular weight redox species may assist the shuttling of electrons between the intracellular bacterial space and an electrode, and are referred to as mediators. The working principle of these mediators is shown schematically in Figure 2.

The mediator molecules should meet the following requirements¹⁹:

- (i) The oxidized mediator should easily penetrate through the bacterial membrane to reach the reductive species inside the bacteria.
- (ii) The redox potential of the mediator should match the

potential of the reductive metabolite.

- (iii) None of the oxidation states of the mediator should interfere with other metabolic processes.
- (iv) The reduced mediator should easily escape from the cell through the bacterial membrane.
- (v) Both the oxidized and reduced states of the mediator should be chemically stable in the electrolyte solution, should be easily soluble, and should not adsorb on the bacterial cells or electrode surface.
- (vi) The electrochemical kinetics of the oxidation process for the mediator-reduced state at the electrode should be fast.

A variety of organic compounds have been studied in combination with bacteria to test the electron-transfer efficiency of the mediator between the microorganism and anode surface.

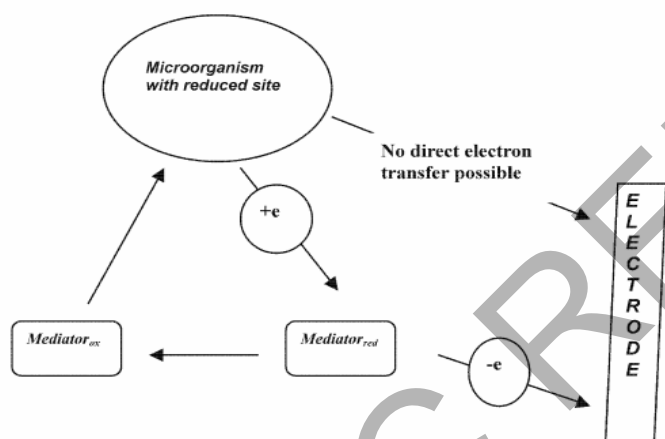


Figure 2. Working principle of redox mediators.

Thionine and organic dyes²⁰ have been frequently used as mediators in biological fuel cells. Redox potentials and structures of some of the electron relays (mediators) are summarized in Table 1. The overall efficiency of the electron-transfer mediators depends on many parameters, particularly on the electrochemical rate-constant of mediator re-oxidation, which depends on the electrode materials²¹. It is difficult to realize the perfect conditions for electron transport from a bacterial cell to an electrode. A mixture of two mediators can be useful in optimizing the efficiency. Two mediators, namely thionine and Fe(III) EDTA, are employed with the biocatalyst *E. coli* for the oxidation of glucose²². It was found that thionine is reduced over 100 times faster than Fe(III) EDTA. But the electrochemical oxidation of thionine is much slower than the oxidation of Fe(II) EDTA. Therefore, electrons obtained from the biocatalysed oxidation of glucose are transferred mainly to thionine. The reduced thionine is rapidly reoxidized by Fe(III) EDTA. The reduced Fe(II) EDTA transfers the electrons to the anode, and is kinetically fast.

Another example of a mixture of mediators promoting electron-transfer across the anode is demonstrated with the help of methyl viologen and 2-hydroxy-1,4-napthoquinone in the case of bioelectrocatalysed oxidation of glucose in the

presence of *E. coli* immobilized on graphite particles. Table 2 summarizes the characteristics of biological fuel cells containing mediators.²³

The electrodes should be designed so as to facilitate electrical contact between a biocatalytic system and an anode, and to improve the cell output. The mediators can be coupled to the microorganisms in three ways¹ (Figure 3): (i) as diffusional mediator shuttling between the microbial suspension and the anode surface, (ii) a diffusional mediator shuttling between the anode and microbial cells covalently linked to the electrode. The microbial cells can be covalently linked to the electrode surface having -COOH groups through amino groups of the microbial membrane resulting in the formation of amide bond. Standard organic reagents like carbodiimide and acetyl chloride are used to link the microbial cells to the surface, and (iii) mediator adsorbed on the microbial cells providing electron transport from the cells to the anode.

*Mediator-less microbial fuel cells*²³: Fe(III)-reducing microorganisms are found to be electrochemically active as they have cytochromes in their outer membranes. It was first demonstrated with the Fe(III) reducers, *Shewanella putrefaciens*, that these can be used as a catalyst in a mediator-less microbial fuel cell. Recent studies have demonstrated that Fe(III) reducing microorganisms of the family Geobacteraceae can directly transfer electrons on to electrodes. However, the range of electron donors that these organisms can use is limited to simple organic acids such as acetate.

Table 1. Redox potential with structural formula of mediators used

Redox relay	Structural formula	Redox potential V (vs NHE)	Rate of reduction $\mu\text{mol (g dry wt)}^{-1}\text{s}^{-1}$ *
Resorufin		-0.051	0.61
New methylene blue		0.021	0.20
Phenothiazinone		1.43	0.130
Thionine		0.064	7.10

*The dye reduction by *Proteus vulgaris* at 30°C, with 50 mM dye and 0.10–0.15 mg (dry wt) ml⁻¹ microbial cells.

Table 2. Examples of microbial-based biological fuel cells utilizing electron relays for coupling of intracellular electron-transfer processes with electrochemical reactions at the anode^{76,a}

Microorganism	Nutritional substrate	Mediator	Cell voltage	Current or current density	Anode ^c
<i>Pseudomonas methanica</i>	CH ₄	1-Naphthol-2-sulphonate indo-2,6-dichloro-phenol	05–06 V (oc) ^d	2.8 μA cm ⁻² (at 0.35 V)	Pt-black 12.6 cm ²
<i>Escherichia coli</i>	Glucose	Methylene blue	0.625 V (oc)	–	Pt, 390 cm ²
<i>Proteus vulgaris</i> <i>Bacillus subtilis</i> <i>E. coli</i>	Glucose	Thionine	0.64 V (oc)	0.8 mA (at 560 Ω)	Reticulated vitreous carbon 800 cm ²
<i>P. vulgaris</i>	Glucose	Thionine	350 mV (at 100 Ω) ^b	3.5 mA (at 100 Ω)	Reticulated vitreous carbon 800 cm ²
<i>P. vulgaris</i>	Sucrose	Thionine	350 mV (at 100 Ω) ^b	350 mA (at 100 Ω)	Carbon
<i>E. coli</i>	Glucose	Thionine	390 mV (at 560 Ω) ^b	0.7 mA (at 560 Ω)	–
<i>Lactobacillus plantarum</i> <i>Streptococcus lactis</i>	Glucose	Fe(III) EDTA	0.2 V (oc)	90 μA (at 560 Ω) ^b	–
<i>Erwinia dissolvens</i>	Glucose	Fe(III) EDTA	0.5 V (oc)	0.7 mA (at 560 Ω) ^b	–
<i>P. vulgaris</i>	Glucose	2-Hydroxy-1,4- naphthoquinone	0.75 V (oc)	0.45 mA (at 1 kΩ)	Graphite felt 1 g (0.47 m ² g ⁻¹)
<i>E. coli</i>	Acetate	Neutral red	0.25 V (oc)	1.4 μA cm ⁻² (sc) ^e	Graphite 100 cm ²
<i>E. coli</i>	Glucose	Neutral red	0.85 V (oc)	17.7 mA (sc)	Graphite felt 12 g (0.47 m ² g ⁻¹)
<i>E. coli</i>	Glucose	2-Hydroxy-1,4- naphthoquinone	0.53 V (at 10 kΩ)	0.18 mA cm ⁻² (sc)	Glassy carbon 12.5 cm ²

^aIn most of the studies, the biological anode was conjugated with an O₂-cathode; ^bValue calculated from other data using Ohm's law; ^cAnode surface is given as a geometrical surface; ^dOpen-circuit measurement; ^eShort-circuit measurement

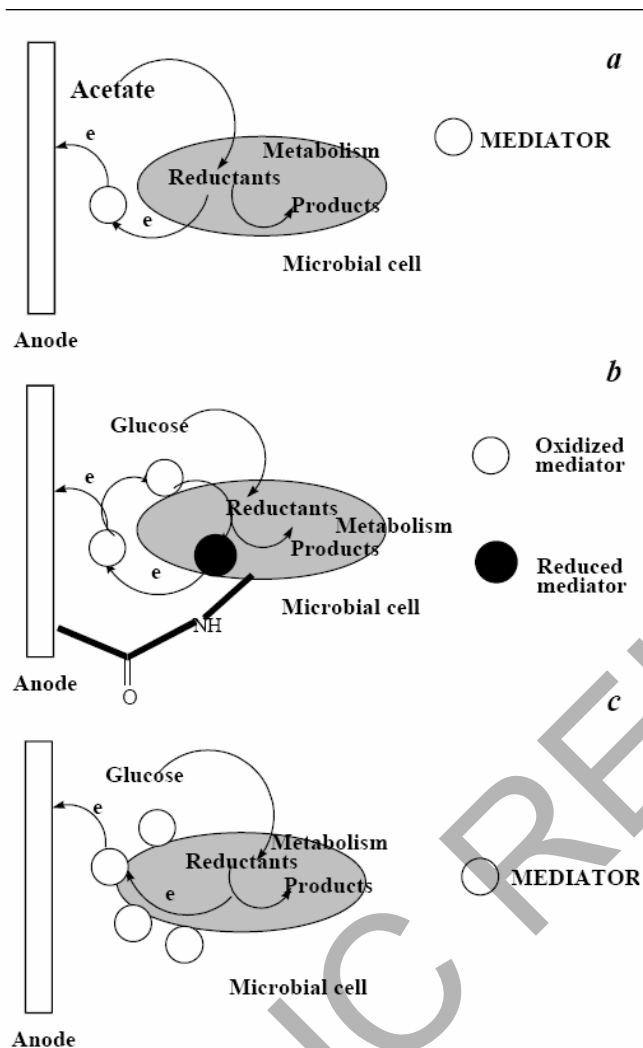
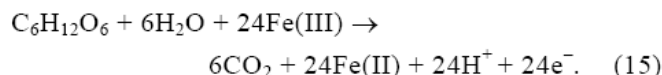


Figure 3. Various modes of attachment of mediators: *a*, Mediator and microorganisms are present in the solution phase; *b*, Microorganisms are covalently attached to the electrode surface; *c*, mediators are covalently linked to the outer membrane of microorganisms.

Metal-reducing bacteria are the most used species in this type of fuel cells. Studies have been conducted to understand the mechanism of Fe(III) reduction by bacteria such as *Shewanella putrefaciens* and *Geobacter metallireducens*. Development of mediator-less microbial fuel cells using *Shewanella putrefaciens* IR-1 has been reported by Kim *et al.*⁴⁸. In these fuel cells, the electrochemical activity of the microorganism has been confirmed by cyclic voltammetry when grown under anaerobic conditions, although no activity was found when they were grown under aerobic conditions. A gradual decrease in both coulombic yield and maximum current values was observed during the sequential batch operation of microbial fuel cells. Recently, there is a report on the bacteria, *Rhodospirillum rubrum* that can be used in microbial fuel cells effectively without a mediator²². *R. ferrireducens* was isolated from anoxic sub-surface sediments of Oyster Bay, Virginia, USA as a dissimilatory Fe(III) reducing microorganism. *R. ferrireducens* grows on glucose in

the presence of Fe(III). The stoichiometry of glucose utilization and Fe(III) reduction can be explained as below.



The performance was tested in a system that comprised a reactor containing an anaerobically growing suspension of *E. coli* K12 in a standard glucose medium (55 mM glucose) and the fuel cell consisting of an anode compartment through which the bacterial medium was pumped. The cathode was woven graphite and the catholyte was a 50 mM ferricyanide solution in a phosphate buffer, akin to the buffer in a bacterial medium.

The recovery of electrons from glucose oxidation is 83% of the theoretical value available from glucose oxidation. Microbial growth is supported by energy derived from the electron-transfer process itself and results in a stable, long-term power production. This type of microbial fuel cell exhibits many of the desirable features of secondary batteries, including the ability to be recharged to the nearly original charged state subsequent to the discharge, the ability to accept fast recharge, reasonable cycle-life and low capacity-loss under open-circuit conditions as well as on prolonged storage under idle conditions. Thus, mediator-less fuel cells have an advantage over those with mediators in terms of cost as well as non-desirability of toxic mediators. In mediator-less fuel cells, there is also ample room to increase the efficiency of electron-transfer.

Comparison Between Chemical fuel cell and biological fuel cell.

	Chemical fuel cell	Biological fuel cell
Catalyst	Noble metals	Microorganism/enzyme
pH	Acidic solution (pH < 1)	Neutral solution (pH 7.0–9.0)
Temperature (°C)	Over 80	Room temperature, 22–25
Electrolyte	Phosphoric acid, sulphuric acid, etc.	Phosphate solution
Efficiency (%)	40–60	Around 40
Voltage (V)	≈ 1	≈ 1
Fuel type	Methanol, H ₂ , etc.	Any carbohydrate or hydrocarbon

III. Applications of biological fuel cells^[23]

In about 200 years from now, vehicles will not have petrol tanks because our petroleum reserves will be depleted. An alternative, which is less wasteful and cleaner, is to power

vehicles directly with carbohydrates using biological fuel cells. The energy liberated during the complete oxidation of a monosaccharide like glucose or a disaccharide such as sucrose to carbon dioxide and water is about 16×10^6 J/kg, which is about 5 kWh of electrical energy and is just less than half the energy that can be obtained from equivalent amounts of fuels such as octane. But the efficiency of burning carbohydrate in biological fuel cells is potentially greater than burning gasoline. For example, a medium-sized car that needs about 200 Wh/km, could travel 25–30 km on one kilogram of a concentrated solution of a carbohydrate. Accordingly, 50 l of a strong sugar solution would give the car a range of more than 1000 km.

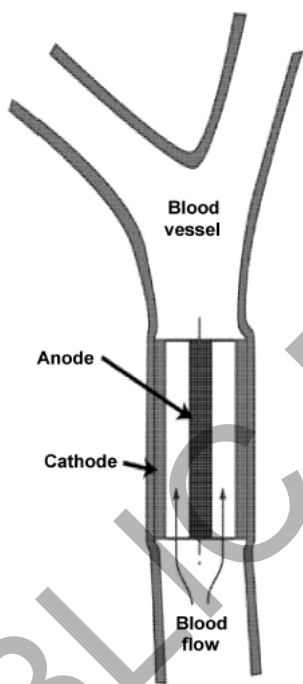


Figure 9. A biological fuel cell directly attached to the blood vessel (from Haselkorn⁷²).

A biological fuel cell that is just 0.07 cm^2 in area, has been designed to generate as much as 300 μV for 2 h, an amount sufficient to operate tiny devices, including microscopic drug-delivery systems. Such a microbial fuel cell could power implantable medical devices as shown in Figure 9 and could help individuals who require regular doses of drugs, for example, AIDS patients. Apart from its small size, the system is unique because it utilizes glucose, a sugar present in the blood stream, as fuel. Such miniaturization has become possible due to the advent of BIOMEMS (Bio-micro electromechanical systems). Since biological fuel cells are known to supply low but stable power density, they are suitable for running devices constructed using MEMS technology. It has been shown by researchers at the University

of California that a miniaturized microbial fuel cell could be integrated with MEMS based implantable medical devices. In comparison to lithium batteries as power sources for implantable devices, microbial fuel cells are smaller, less expensive and have a longer shelf-life.

A mobile robot platform has been built that derives its propulsive power from the digestion of real food in a bioreactor. This robot called ‘Gastrobot’ used harmless yeast and adopted a gas propulsion system without an electrical generation. When a carbohydrate-rich aqueous solution is mixed with yeast in a reaction chamber, fermentation takes place with liberation of carbon dioxide and it leads to substantial pressure build-up when constrained. Energy available in this pressurized CO_2 gas is used to propel the Gastrobot, which is achieved purely by mechanical means.



A Slugbot (from www.robotics.usc.edu).

‘Slugbot’ is a robot that utilizes the electrical power produced from biomass (Figure 10). Slugs are common pests found on agricultural land in the UK, where farmers spend about £20 million per annum on buying and spreading molluscicides. Slugbot ferments slug mass and converts it into electrical energy, which it uses to catch the slugs in the field. Stuart Wilkinson at the University of South Florida, who is currently interested in the development of hybrid biological fuel cells, has developed a meat-eating robot ‘Chew Chew’, which is powered by a microbial fuel cell and uses meat as a fuel. This has three wagons, each about a metre long. These robots could even kill human beings accidentally. One could construct molecular biological cells, which could deliver electrical energy to remove tumours and cancerous cells, and could act as drug-delivery systems.

Another important application of microbial fuel cells is in the field of waste water engineering. Microorganisms can discharge the dual duty of degrading effluent and generating power. When microorganisms oxidize organic compounds present in waste water, electrons are released yielding a steady source of electrical current. If power generation in these systems can be increased, microbial fuel cells may provide a new method to offset operating costs of waste water treatment plant, making advanced waste water treatment more affordable in both developing and industrialized nations. Different designs of fuel cell reactors based on chemical engineering principles like fluidized bed reactors, packed bed reactors, etc. are under trial. Tests have been conducted using single chamber microbial fuel cell (SCMFC) containing eight graphite electrodes as anodes and a single air cathode. The system was operated under

continuous-flow conditions with waste water. The prototype SCMFC reactor generated an electric power of 26 mW/m², while removing up to 80% of chemical oxygen demand of the waste water.²³

Conclusions

The main challenge is in the electrical coupling of the biological component of the system with the electrodes of the fuel cells. By tapping the complete multi-enzyme metabolic pathways inside living cells, microbial fuel cells could last long and could utilize complex biofuels. A detailed characterization of the interfacial electron-transfer rates, biocatalytic rate constants and cell resistance is essential for the construction of microbial fuel cells. Although microbial fuel cells are in their infancy, the prospects of their applications look attractive.

REFERENCES

- [1]. Allen, R.M., Bennetto, H.P., 1993. Microbial fuel cells: electricity production from carbohydrates. *Appl. Biochem. Biotechnol.*, 27–40
- [2]. Rabaey, K., Verstraete, W., 2005. Microbial fuel cells: Novel biotechnology for energy generation. *TRENDS in Biotechnol.* 23 (6), 291–298.
- [3]. Bennetto, H. P., Mason, J. R., Stirling, J. L. and Thurston, C. F., Research and development in non-mechanical electrical power sources. In *Power Sources 11* (ed. Pearce, L. J.), 1987, p. 373.
- [4]. Cole, K. S., In *Membranes, Ions and Impulses*, University of California Press, 1972.
- [5]. Rohrbach, G. H., Scott, W. R. and Canfield, J. H., Biochemical fuel cells. In *Proceedings of the 16th Annual Power Sources Conference*, 1962, p. 18.
- [6]. Williams K. R., In *An Introduction to Fuel Cells*, Elsevier, Amsterdam, 1966, p. 248.
- [7]. Yao, S. J., Appleby, A. J., Geise, A., Cash, H. R. and Wolfson, S. K., Anodic oxidation of carbohydrates and their derivatives in neutral saline solution. *Nature*, 1969, 224, 921–922.
- [8]. Karube, I., Ikemoto, H., Kajiwar, K., Tamiya, E. and Matsuok, H., Photochemical energy conversion using immobilized blue-green algae. *J. Biotechnol.*, 1986, 4, 73–80.
- [9]. Chaudhuri, S. K. and Lovely, D. R., Electricity generation by direct oxidation of glucose in mediator-less microbial fuel cells. *Nature Biotechnol.*, 2003, 21, 1229–1232.
- [10]. Gottschalk, G., In *Bacterial Metabolism*, Springer Verlag, New York, 1979, 2nd edn.
- [11]. Heyndrickx, M., Devos, P. and De Ley, J. U., Hydrogen production from chemostat fermentation of glucose by *Clostridium butyricum* and *Clostridium pasteurianum* in ammonium and phosphate limitation. *Biotechnol. Lett.*, 1990, 12, 731–736.
- [12]. Suzuki, S. and Karube, I., Energy production with immobilized cells. *Appl. Biochem. Bioeng.*, 1983, 4, 281–310.
- [13]. Suzuki, S., Karube, I., Matsuoka, H., Ueyama, S., Kawakubo, H., Isoda, S. and Murahashi, T., Biochemical energy conversion by immobilized whole cells. *Ann. N.Y. Acad. Sci.*, 1983, 413, 133–143.
- [14]. Karube, I., Suzuki, S., Matsunaga, T. and Kuriyama, S., Biochemical energy conversion by immobilized whole cells. *Ann. N.Y. Acad. Sci.*, 1981, 369, 91–98.
- [15]. Suzuki, S., Karube, I., Matsunaga, T., Kuriyama, S., Suzuki, N., Shirogomi, T. and Takamura, T., Biochemical energy conversion using immobilized whole cells of *Clostridium butyricum*. *Biochimie*, 1980, 62, 353–358.
- [16]. Karube, I., Matsunaga, T., Tsuru, T. and Suzuki, S., Biochemical fuel cell utilizing immobilized cells of *Clostridium butyricum*. *Biotechnol. Bioeng.*, 1977, 19, 1727–1733.
- [17]. Schroder, U., Nieâ er, J. and Scholz, F., A generation of microbial fuel cells with current output boosted by more than one order of magnitude. *Angew. Chem.*, 2003, 115, 2986–2989.
- [18]. Allen, M. J., Biofuel cells. In *Methods in Microbiology* (eds Norris, J. R. and Ribbon, D. W.), Academic Press, New York, 1972, pp. 247–283
- [19]. Wilkinson, S., Gastrobots – benefits and challenges of microbial fuel cells in food powered robot applications. *Autonomous Robots*, 2000, 9, 99–111.
- [20]. Ikeda, T., Kato, K., Tatsumi, H. and Kano, K., Mediated catalytic current for the oxidation of ethanol produced by *Acetobacter acetii* cells suspended in solution. *J. Electroanal. Chem.*, 1997, 440, 265–269.
- [21]. Ikeda, T., Kato, K., Tatsumi, H. and Kano, K., Mediated catalytic current for the oxidation of ethanol produced by *Acetobacter acetii* cells suspended in solution. *J. Electroanal. Chem.*, 1997, 440, 265–269.
- [22]. Tanaka, K., Vega, C. A. and Tamamushi, R., Thionine and ferric chelate compounds as coupled mediators in microbial fuel cells. *Bioelectrochem. Bioeng.* 1983, 11, 289–297.
- [23]. Shukla A. K. ; Suresh P.; Berchmans S. ; Rajendran A, Biological fuel cells and their applications, *Current science*, 2004, vol. 87, pp. 455-468.

Cable Shielding to Minimize Electromagnetic Interference

Anke Fröbel

Cottbus University of Technology, Germany
Wrocław University of Technology, Poland

Abstract - A cable shield is necessary to prevent emission of electromagnetic waves from the cable respectively to protect data and signal conductors from external electromagnetic interference (EMI). The effectiveness of a cable shield installation depends on the kind of EMI to be shielded and the type of termination at both ends. This paper depicts the different types of cable shielding. Moreover shielding effectiveness is analyzed.

I. INTRODUCTION

Electromagnetic shielding reduces, or rather prevents coupling of undesired radiated electromagnetic energy in electrical equipment. It is established over a large part of the electromagnetic spectrum from DC to microwave frequencies.

In general, shielding is produced by insertion of a metallic barrier in the path of electromagnetic waves between the source of the radiation and the device which is supposed to be protected. The shielding may be applied at the source (if the source is known) or at the susceptible equipment. Fig.1. illustrates the two modes of shielding.

Cable shielding is commonly used for data and signal cables. The design of cable shielding and grounding is important for the reduction of electromagnetic interference. Each application requires individual considerations given that parameters such as cable lengths, noise frequency, signal frequency and cable termination methodology impact the final result. Improperly cable shielding can actually increase noise coupling and thus make the problem worse.

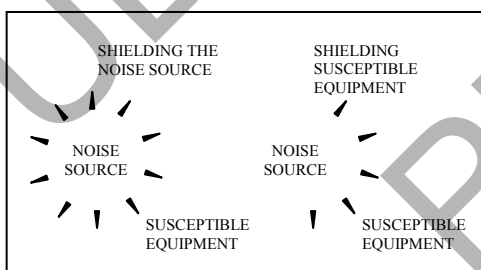


Figure 1. Modes of shielding: Shielding the source of noise or shielding the susceptible equipment.

II. TYPES OF SHIELDED CABLES

Since data or signal cables carry broadband signals, up to high frequency ranges, they need to be shielded to minimize

radiated coupling. In addition, the impedance has to be controlled. The selection of a certain type of cable as well as the arrangement of signals and grounds rather shields in the cable determine the characteristic impedance of the transmission path.

In the following paragraphs the various versions of shielded cables are introduced.

A. Coaxial cables

A coaxial cable consists of an inner conductor, surrounded by an insulating layer which is then surrounded by another conductive layer, typically a fine woven braid for flexibility or a thin metallic foil, and then covered again with a thin insulating layer on the outside, shown in Fig. 2. The shield is grounded at multiple points at high frequencies and a single point at low frequencies. Coaxial cables are used in a frequency range of 20 kHz up to 50 GHz.

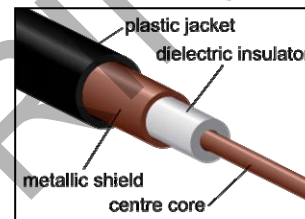


Figure 2. Coaxial cable cutaway

B. Triaxial cables

A triaxial cable is similar to coaxial cables but with another shield isolated from the signal return shield. The second shield is grounded, as shown in Fig. 3. Thus, triaxial cables provide a greater rejection of interference than coax.

C. Twinaxial cables

A twinaxial cable is a two-wire twisted balance line in a ground shielding braid, as shown in Fig. 4. The twisting provides cancellation of any induced noise voltage pickup caused by a leakage of the low-frequency magnetic field through the copper braid. Twinax are used up to 10 MHz.

D. Quadraaxial cables

A quadraaxial cable is a double-shielded twinax, as shown in Fig. 5. The outer shielding is grounded to the earth while the inner shielding is connected to the system ground. If there is no system ground available, both shields are earth grounded.

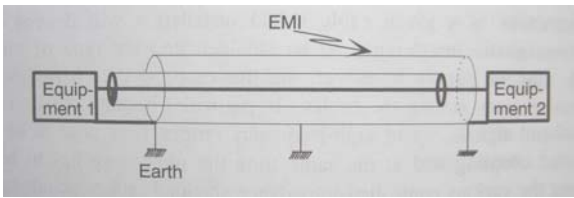


Figure 3. Shielded triaxial cable

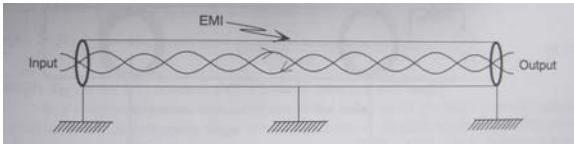


Figure 4. Shielded twinaxial cable

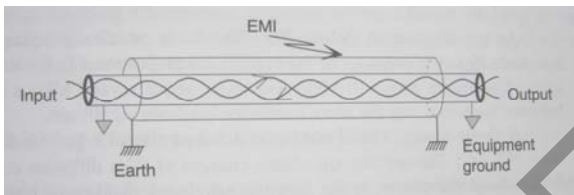


Figure 5. Shielded quadaxial cable

III. CABLE SHIELD GROUNDING

If a shielded cable is used to connect two systems, the shield has to be connected to a single ground reference. In order to prevent that electromagnetic energy penetrates through the shield, the outer surface of the shield has to be grounded, as shown in Fig. 6.

It is possible to ground the shield at one end (asymmetric), at both ends (symmetric) or in intervals along the length of the cable. The effectiveness of these different methods depends on the electromagnetic coupling mode and the length (l/λ) of the cable used for the interconnection.

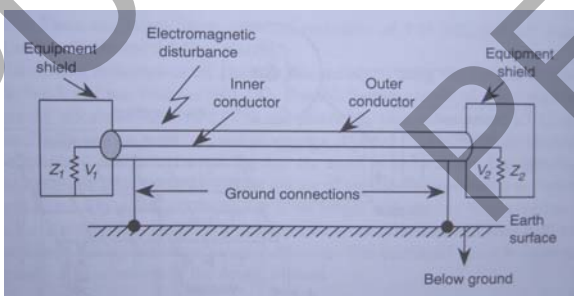


Figure 6. Cable grounding

There are two kinds of electromagnetic coupling in a cable:

1. Electric field coupling, the incident wave is polarized parallel to the conductor length, and

2. Magnetic field coupling, the incident wave is polarized normal to the loop formed by the cable and the ground plane.

The EMI voltage pickup in a cable increases with frequency. At high frequencies resonance phenomena produce maximum induced voltages for a certain cable length l such that

- both ends grounded + H-field excitation → no resonance
- both ends grounded + E-field excitation → resonance for $l = k\lambda / 2$
- one end grounded + H-field excitation → resonance for $l = (2k + 1)\lambda / 4$
- one end grounded + E-field excitation → resonance for $l = (2k + 1)\lambda / 4$

At low frequencies for E-field excitation it is more efficient to ground both ends, whereas for H-field excitation one end grounding has to be favored, since this eliminates the formation of a current loop by the cable and the ground plane.

At high frequencies both ends grounded configurations avoids resonances for E-field and H-field excitations.

In practice one ground connection is often preferred, since this avoids ground loops. However, for short cables, at low frequencies, the voltages induced by EMI at both ends of a coaxial cable become nearly equal and one end grounding is needed for E-field as well as for H-field excitations.

IV. TRANSFER IMPEDANCE OF CABLE SHIELD

The finite conductivity of shielding material as well as its small thickness and small openings in the braid allow electromagnetic fields to penetrate through the shield and induce currents in the line. Therefore it is necessary to evaluate the ultimately shielding effectiveness.

It is difficult to measure the field inside of a cable shield accurately. Moreover, the voltage measured at the end of the line depends on the type of termination. Therefore a definition of shielding effectiveness using the ratio of fields before and after the shield, or the ratio of voltage induced with and without a shield, is not adequate. An evaluation of the shielding effectiveness regarding the transfer impedance is more common.

The transfer impedance of a cable shield relates the current I_S flowing on the shield surface to the longitudinal induced voltage V_i per unit length on the outer side of this surface (see Fig. 7).

The sheath current I_S may result from an externally incident field or ground potential difference between the two ends of the cable.

Hence

$$V_i = I_S \times Z_t \quad (1)$$

where Z_t is the transfer impedance of the shielded cable.

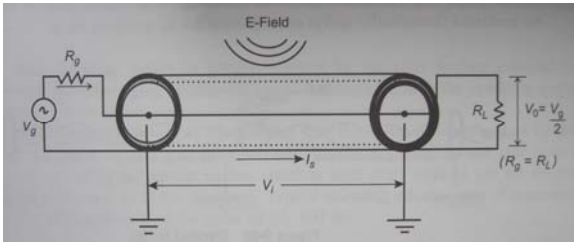


Figure 7. Model of transfer impedance coupling in coaxial cable

Z_t is expressed in ohms normalized to a one-meter shield length. The better the shielding the lower are the values of Z_t .

At frequencies below 100 kHz, Z_t is practically equal to the DC shield resistance R_{DC} . Above several MHz a capacitive coupling between the shield and the inner conductor has to be considered. At frequencies above 10 MHz, Z_t is proportional to the leakage inductance.

A single braided shield is a solid tube with rhombic or elliptical holes. The transfer impedance consists of three components. One of them is the diffusion impedance Z_r , which expresses the relation between the shield current and the longitudinal electric field caused by the finite conductivity of the equivalent shield tube. The second component is the coupling inductance L_t term. It considers the magnetic field coupling through the openings in braided wire shields and the inductance between two interwoven parts of the braid. The third component is the so called skin inductance L_s , which results from magnetic fields penetrating the shield.

$$Z_t = Z_r + j\omega L_t + (1 + j)\omega L_s \quad (2)$$

The transfer impedance of a single braided cable can be reduced by wrapping a metallic band (e.g. aluminum), or rather a conductive envelope (e.g. polycarbonate) over the braid. This way the coupling inductance L_t is reduced.

For thin-walled tubular shields the transfer impedance can be expressed as follows:

$$Z_t = \frac{1}{2\pi a \sigma} \frac{(1 + j)t / \delta}{\sinh[(1 + j)t / \delta]} \quad (3)$$

where a is the inner radius of the shield, t is its wall thickness, σ is the conductivity of the shield and δ is the skin depth of the shield.

At low frequencies and $t / \delta \ll 1$ the transfer impedance is

$$Z_t = \frac{1}{2\pi a \sigma} = R_{DC} \quad (4)$$

as mentioned above.

The transfer impedance and in order to that the shielding effectiveness differs significantly for the different types of shielded cables. Most common in use are solid semi-rigid coaxial, braided triaxial, braided coaxial, shielded quadraxial and shielded twinaxial cables (with descending order of effectiveness).

V. CONCLUSIONS

This paper presented analytical and practical aspects of cable shielding to mitigate electromagnetic interference. It was shown that the best shielding for any application depends on the application itself. The best solution for one situation may be bad for another set of conditions.

REFERENCES

- [1] V.Prasad Kodali, *Engineering electromagnetic compatibility: principles, measurements, and technologies*, vol. I. New York: Institute of Electrical and Electronics Engineers, 1996, pp. 199-227.
- [2] C.Sankran, *Power Quality*, vol. I Florida: CRC Press LLC, 2002, pp. 154-164.
- [3] G. Vijayaraghavan, Mark Brown, and Malcom Barnes, *Practical Grounding, Bonding, Shielding and Surge Protection*, vol. I Oxford: Newnes, 2004
- [4] <http://en.wikipedia.org/wiki/Coax>, February 7, 2009

Fault Location System for Transmission Lines in One-terminal By using Impedance-Traveling Wave Assembled Algorithm

Sachin R. Yerekar

Department of Electrical Engineering
Veer mata Jijabai Technological Institute,
Matunga, Mumbai-400019
sachin_yerekar@yahoo.co.in

Abstract: - Considering roundly reliability and accuracy of one terminal fault location system for transmission lines, an impedance-traveling wave assembled algorithm, which combines measurement impedance method with traveling wave method, is presented. At first, it uses measurement impedance method to calculate roughly fault distance. Then regions of reflected waves from fault point and opposite bus to detective bus are confirmed respectively through the distance. At last, exact time of reflected wave from fault point to detective bus and that of reflected wave from opposite bus to detective bus are identified respectively in corresponding regions, and fault location is implemented according to the result detected. It has complementarities of both methods, because measurement impedance method guarantees reliability and traveling wave method improves accuracy. Results of simulation are that located errors are within 100m if fault location based on traveling wave algorithm is available. It is improved that assembled algorithm proposed is correct.

Keywords:- Accuracy; Assembled algorithm; Fault currents; Fault location; Fault resistance; Measurement impedance; One-terminal; Reliability; Transmission lines; Traveling wave.

I. INTRODUCTION:

Transmission lines are vital in electric power systems, because they shoulder missions of transmitting power energy. However, they are also the parts which are bounded to have faults, and it is very difficult to find the faults. Thus, fast and accurate fault location for transmission lines, which is an imperative problem to be solved, plays an increasingly important role in electric power systems. It not only saves a large amount of manpower and material resource, but also makes it easy to find some covert faults, such as the insulator puncture. Various fault location methods have been developed and fault location techniques have been a subject for many researchers [1].

One-terminal fault location system just installs fault location device on one terminal of transmission lines, and doesn't have to use communication device, so it is more economical than two-terminal fault location system [2], [3]. In one-terminal fault location system, there are two categories, one is based on power frequency quantities, and the other is based on traveling wave. The former is economical and easy to implement, especially, measurement impedance algorithm is the most robust algorithm of one-terminal fault location based on power frequency quantities [4], [5], but has no high accuracy. The latter has high accuracy except of reliability [6]. However, both reliability and accuracy are vital in fault location technology. Thus, considering roundly reliability and accuracy of one-terminal fault location system, an impedance-traveling wave assembled algorithm, which combines measurement impedance method with traveling wave method,

is presented. The assemble algorithm have complementarities, because measurement impedance method guarantees reliability and traveling wave method improves accuracy [7], [8].

II. IMPEDANCE - TRAVELING WAVE ASSEMBLED ALGORITHM:

The algorithm proposed includes two parts, one is measurement impedance method, and the other is traveling wave method.

A. Measurement impedance method:

An algorithm named measurement impedance method is proposed in document [9]. It eliminates fault resistance for calculating fault distance according to measurement impedance, transmission line positive-sequence impedance angle and detective currents.

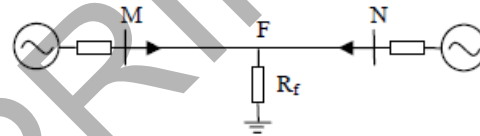


Fig.1 Fault diagram of three-phase power system

According to fault location algorithm based on measurement impedance method, fault distance can be calculated by Equation (1).

$$xx_1 = X_M - \frac{R_M \operatorname{tg} \varphi_L - X_M b}{a \operatorname{tg} \varphi_L - b} \quad (1)$$

Where $a = \operatorname{Re}[I_{Mf} / I_M]$, $b = \operatorname{Im}[I_{Mf} / I_M]$, x is fault distance from bus M to fault point F, x_1 is positive-sequence reactance per kilometer of transmission lines, φ_L is transmissions' line positive-sequence impedance angle, I_{Mf} is fault component current, U_M and I_M are respectively detective voltage and current with the definition of distance protective measurement impedance, that's $R_M + jX_M = U_M / I_M$.

In the algorithm named measurement impedance method, it's assumed that the phase angle between fault current I_f and fault component current I_{Mf} is zero, so the fault error will be inevitably led.

Simplicity and reliability are the main characteristic of algorithm based on measurement impedance. It's basic principle is the same as the one of distance protection. With measurement impedance, distance relay determines the fault section and trip fault line selectively. So the algorithm based on measurement impedance can be taken to boundary the fault section of transmission lines [8].

B. Traveling wave method:

When a fault occurs in transmission lines, fault traveling wave will transmit from fault point to detective bus and opposite bus along the transmission lines. Because of discontinuous impedance, fault traveling wave to detective bus will be reflected at detective bus and transmit to fault point, then will be reflected at fault point and transmit to detective bus for the second time. For the same reason, fault traveling wave to opposite bus will be reflected at opposite bus and transmit to fault point, and may be refracted at fault point and transmit to detective bus.

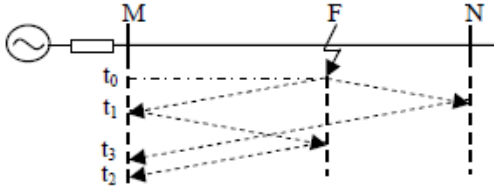


Fig.2 Diagram of fault traveling wave propagation

As shown in Fig.2, L is the length of the fault lines, x is the fault distance from detective bus M , t_0 is the time when fault occurs, t_1 is the time when initial traveling wave arrives at detective bus, t_2 is the time when traveling wave reflected at fault point arrives at detective bus, t_3 is the time when traveling wave reflected at opposite bus and refracted at fault point arrives at detective bus.

A great deal of computer simulation showed that the largest error of algorithm based on measurement impedance is within the limit of 10% under different fault case [8]. So the actual distance to fault point is sure in the region of $(x-10\%L, x+10\%L)$. t_M , t_N and δ_i are defined as the needed time that fault traveling wave transmits from fault point to detective bus M , the needed time that fault traveling wave transmits from fault point to opposite bus N , and the corresponding time error of the distance error of 10% L . They are expressed as in (2).

$$\begin{cases} t_M = \frac{x}{v} \\ t_N = \frac{L-x}{v} \\ \delta_i = \frac{10\%}{v} L \end{cases} \quad (2)$$

Where v is defined as velocity of traveling wave which can be calculated according to lines' parameters or be obtained from former velocity of traveling wave modified by (4).

Using t_1 as time reference, t_2 is in the region of $(t_1+2t_M-2\delta_i, t_1+2t_M+2\delta_i)$ and t_3 is in the region of $(t_1+2t_N-2\delta_i, t_1+2t_N+2\delta_i)$.

In case of that both 2 t and 3 t can be detected, simultaneous equation will be expressed as in (3).

$$\begin{cases} v'(t_1 - t_0) = x' \\ v'(t_2 - t_0) = 3x' \\ v'(t_3 - t_0) = 2L - x' \end{cases} \quad (3)$$

Where v' , t_0 and x' are unknown, denoting respectively as the true velocity of traveling wave, the time when fault occurs and fault distance.

The equation as in (4) can be obtained from equation as in (3).

$$\begin{cases} t_0 = \frac{3t_1 - t_2}{2} \\ x' = \frac{t_2 - t_1}{t_2 + t_3 - 2t_1} L \\ v' = \frac{2L}{t_2 + t_3 - 2t_1} \end{cases} \quad (4)$$

In case of that t_2 can be detected, but t_3 cannot be, simultaneous equation will be expressed as in (5).

$$\begin{cases} v(t_1 - t_0) = x' \\ v(t_2 - t_0) = 3x' \end{cases} \quad (5)$$

The equation as in (6) can be obtained from equation as in (5).

$$\begin{cases} t_0 = \frac{3t_1 - t_2}{2} \\ x' = \frac{1}{2}(t_2 - t_1)v \end{cases} \quad (6)$$

In case of that t_3 can be detected, but t_2 cannot be, simultaneous equation will be expressed as in (7).

$$\begin{cases} v(t_1 - t_0) = x' \\ v(t_3 - t_1) = 2(L - x') \end{cases} \quad (7)$$

The equation as in (8) can be obtained from equation as in (7).

$$\begin{cases} t_0 = \frac{t_1 + t_3}{2} - \frac{L}{v} \\ x' = L - \frac{1}{2}(t_3 - t_1)v \end{cases} \quad (8)$$

In worst case of that both t_2 and t_3 cannot be detected, t_0 and x' will be expressed as in (9).

$$\begin{cases} t_0 = t_1 - \frac{x}{v} \\ x' = x \end{cases} \quad (9)$$

C. Analysis in theory:

Simplicity and reliability are the main characteristic of algorithm based on measurement impedance. Its basic principle is the same as the one of distance protection. With measurement impedance, distance relay determines the fault section and trip fault line selectively. So algorithm based on measurement impedance can be taken to boundary the fault section of transmission lines.

In the algorithm, exact time of reflected wave from fault point to detective bus and that of reflected wave from opposite bus to detective bus are identified respectively in the regions of $(t_1+2t_M-2\delta_i, t_1+2t_M+2\delta_i)$ and $(t_1+2t_N-2\delta_i, t_1+2t_N+2\delta_i)$. So it's unnecessary to detect t_2 and t_3 in full region of $[t_1, t_1+2L/v]$, but in its sub-regions of $(t_1+2t_M-2\delta_i,$

$t_1+2t_M+2\delta_t$) and $(t_1+2t_N-2\delta_t, t_1+2t_N+2\delta_t)$. As a result, total length of its sub-regions is $v L t 8^M = 0.8$, only 40% of the length of full region. Moreover, the algorithm can also decrease the disturbance of traveling wave reflected from neighbor buses.

In case of that both t_2 and t_3 can be detected, the precision of fault location can avoid the effect of traveling wave velocity, what's more, the velocity of traveling wave can be modified online [11]. Because of the velocity of traveling wave modified endlessly, it will approach the true velocity. In case of that just t_2 or t_3 can be detected, the precision of fault location calculated by Equation (6) or (8) is hardly affected by the effect of traveling wave velocity. In worst case of that both t_2 and t_3 cannot be detected, fault location based on traveling wave algorithm isn't available, but fault location algorithm based on measurement impedance method can guarantees reliability.

III. SIMULATION TEST:

In order to demonstrate the correctness of the assembled algorithm proposed, a model with length of 300km, voltage grade of 500kV and frequency of 50Hz is built for simulation. As shown in Fig.3, single transmission lines between bus M and bus N connect Equivalent system M and Equivalent system N. Fault distance can be set by the means of changing the lengths of line part1 and line part2. Fault type and fault resistance can be set through the module of Fault Setting. Ports for measurement are set at bus M. Waveforms of currents and voltages at bus M can be detected by the way of oscillograph module, and data of voltages and currents will be put out through the outputs of Out1 and Out2.

Transmission lines' distributed parameters are given as following:

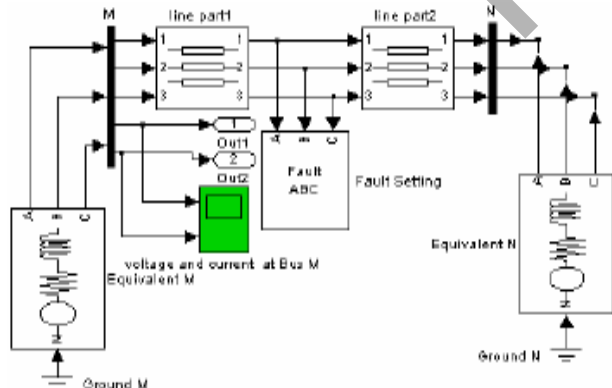
$$\begin{aligned} r_1 &= 0.0270 \Omega / km, & x_1 &= 0.2783 \Omega / km, \\ c_1 &= 0.0127 \mu F / km, & r_0 &= 0.1948 \Omega / km, \\ x_0 &= 0.6494 \Omega / km, & c_0 &= 0.0090 \mu F / km. \end{aligned}$$

Parameters Equivalent system M and Equivalent system N are given as following:

$$\begin{aligned} Z_{M1} &= Z_{N1} = 2.534 + j 120.46 (\Omega), \\ Z_{M0} &= Z_{N0} = 1.121 + j 40.23 (\Omega). \end{aligned}$$

The velocity of traveling wave can be obtained from the transmission lines' distributed parameters [11]:

$$v = \sqrt{1/l_1 c_1} = 2.98137 \times 10^5 \text{ km} / \text{s}.$$



8. IEEE International Conference on Environment and Electrical Engineering, Karpacz, Poland, May 10-13, 2009
Fig.3 Model for simulation

Single phase-to-grounded fault with distance of 100km from bus M is taken as an example. Setting sample frequency at 2 kHz and sampling ten power frequency cycles, fault distance of $x=102.4\text{km}$ is calculated via Equation (1) with Fourier transform, and results of $t_M=343.5\mu\text{s}$, $t_N=662.8 \mu\text{s}$ and $\delta_t = 100.6 \mu\text{s}$ are also calculated. Then just keeping the current output of Out1 and setting sample frequency at 2MHz and sampling half power frequency cycles, data are treated with using digital filter, modal transform and wavelet analysis [12],[13]. According to maximum likelihood estimation, time reference of $t_1=2817 \mu\text{s}$ is obtained, and times of $t_2=3488 \mu\text{s}$ and $t_3= 4158 \mu\text{s}$ are identified respectively in corresponding regions of (3302.8,3705.2) and (3941.4, 4343.8) as shown in Fig.4. The results of $t_0 = 2481.5 \mu\text{s}$, $v'=2.98211 \cdot 10^5 \text{ km} / \text{s}$ and $x'=100.05 \text{ km}$ are calculated finally.

Changing respectively fault resistance, fault distance, fault type and so on, a number of results of fault location are gained using assembled algorithm proposed. Results of simulation are that located errors are within 100m if fault location based on traveling wave algorithm is available. So it is improved that assembled algorithm proposed is correct.

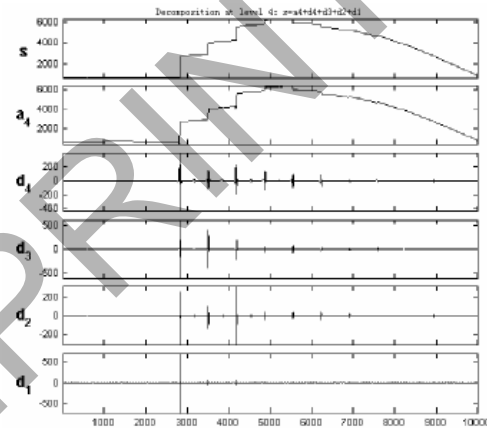


Fig.4 Wavelet analysis

IV. CONCLUSION:

Considering roundly reliability and accuracy of oneterminal fault location system for transmission lines, an impedance-traveling wave assembled algorithm, which combines measurement impedance method with traveling wave method, is presented. The assemble algorithm have complementarities, because measurement impedance method guarantees reliability, especially when fault point is very near to the detective bus, and traveling wave method improves accuracy, especially when fault point is far from the detective bus. Results of simulation test have improved that assembled algorithm proposed is correct. In the case of that exact time of reflected wave from fault point to detective bus and that of reflected wave from opposite bus to detective bus can both be detected, traveling wave velocity has no relation with fault accuracy, and can be corrected to its actual velocity online. In the worst situation, measurement impedance method can still guarantees reliability in despite of that traveling wave method is no available. So it is prospected that the assemble algorithm will have a positive effect on fault location technology for

transmission lines of electric power systems and be applied practically.

V. REFERENCES:

- [1] A. Elhaffar and M. Lehtonen: An improved GPS current traveling-wave fault locator in EHV transmission networks using few recordings. Presented at Future Power Systems, 2005 International Conference
- [2] M. Aurangzeb, P.A. Crossley, P. Gale, "Fault location using the high frequency traveling waves measured at a single location on a transmission line," in *Proc. 2001 IEE Developments in Power System Protection, Seventh International Conf.*, pp: 403-406.
- [3] Darren Spoor and J. G. Zhu, "Improved Single-Ended Traveling-Wave Fault Location Algorithm Based on Experience with Conventional Substation Transducers," *IEEE Trans. Power Delivery*, vol. 21, pp. 1714-1720, Jul. 2006,
- [4] Z. Chen, X. Z. Dong and C. M. Lou, "Robustness of one-terminal fault location algorithm based on power frequency quantities," in *Proc. 2002IEEE, Power Engineering Society Summer Meeting*, vol.3 pp. 1118-1122.
- [5] K. Zimmerman, D. Costello, "Impedance-based fault location experience," in *Proc. 2006 IEEE, Rural Electric Power Conf.*, pp.1-16
- [6] D.W.P. Thomas, C. Christopoulos, Y. Tang, P. Gale and J. Stokoe, "Single ended travelling wave fault location scheme based on wavelet analysis," in *Proc. 2004 IEE, Developments in Power System Protection, Eighth IEE International Conf.*, pp. 196 –199.
- [7] X. Z. Dong, Z. Chen, X. He, K. Wang, and C. Luo, "Optimizing solution of fault location," in *Proc.2002 IEEE Power Eng. Soc. Summer Meeting*, pp. 1113–1117.
- [8] V. Pathirana, P. McLaren, and E. Dirks, "Investigation of a hybrid travelling wave/impedance relay principle," in *Proc. IEEE Power Eng. Society Transmission and Distribution Conf.*, pp. 48-53.
- [9] Sant and Y. Paithankar, "Online digital fault locator for overhead transmission line," in *Proc. 1979 IEE*, vol. 126, pp.1181-1185, Nov. 1979.
- [10] T. Jiang, Y. P. Lu. "Study of fault locating based on single traveling waves avoiding wave speed influence," *Electric Power Automation Equipment*, vol. 24, pp. 29-32, Dec. 2004.
- [11] A. Gopalakrishnan, M. Kezunovic, S.M. McKenna and D.M. Hamai, "Fault location using the distributed parameter transmission line model," *IEEE Trans. Power Del.*, vol. 15, pp. 1169-1174, Oct. 2000.
- [12] A. Abur and F. Magnago, "Fault location using wavelets," *IEEE Trans. Power Del.*, vol. 13, pp. 1475--1480, Oct. 1988.
- [13] G. Kim, H. Kim, and J. Choi, "Wavelet transform based power transmission line fault location using GPS for accurate time synchronization," in *Proc. IEEE Power Eng. Soc. Transm. And Distribution Conf.*, vol. 1, 2001, pp. 495-499.

Market behaviour to promote renewable energy

Nuno Domingues

ISEL, Instituto Superior de Engenharia de Lisboa, Portugal

Rua Conselheiro Emídio Navarro, 1, 1959 – 007 Lisboa; ndomingues@deca.isel.ipl.pt

Abstract- This paper presents results of a study concerning the generation strategic bids for a single hour.

In this study I incorporated the price and quantity bids.

I considered an elastic demand curve, approximated by an affine function, assuming that there is consumer's reaction and that the market price and the demand are related. Also, I consider the competitors reaction using a parameter that represents the conjectural variation.

I studied the market behaviour assuming that the market price is represented by a normal probability function.

I studied and compared the market behaviour for two price markets types, the MCP (Market Clearing Pay) and PAB (Pay As Bid), in two situations: without incorporating the externalities and taking account with the emissions.

Index Terms— Strategic Bidding, Generation Surplus, Conjectural Variation, Elastic Demand, Normal Price Distribution, Emissions.

I. NOMENCLATURE

- block i surplus: $m_i(\cdot) = m_i(a_i, a_i^*, \lambda, \lambda_i^{sell}, P_{gi}^*)$
- block i production cost: a_i
- price strategic bid: a_i^*
- quantity strategic bid: P_{gi}^*
- block i selling price, λ_i^{sell}
- expected price assuming a rigid demand: λ
- maximum expected price assuming a rigid demand: λ_{max}
- minimum expected price assuming a rigid demand: λ_{min}
- expected price assuming an elastic demand: λ^θ
- maximum expected price assuming an elastic demand: λ_{max}^θ
- minimum expected price assuming an elastic demand: λ_{min}^θ

II. INTRODUCTION

It's desirable that the electricity market work in a perfect competition. However, due to the limited number of generation companies (lack of competitors), due to the high investment (one of the biggest barriers to new players), due to the long period of time taking from the planning to the exploration of a plant, the grid capacity and the transmission losses, the markets tend to work as an Oligopoly. Thereby, some companies can have a significant market share and make strategic bids to improve their profit.

The study of the market behaviour with the conjectural parameter, developed in 1924 by Bowley and in 1933 by Frisch, was used by several authors [3], [4], [5] but only to simulate oligopoly markets with linear bids and determining just one strategic bid.

The experience shows us that the normal distribution is the one that best represents the market prices [6]. When we consider a normal price distribution, the block surplus function is more complicated than when we consider an uniform price distribution. [1].

III. METHODOLOGY

I consider a market with several companies that bid by blocks, each block is identified by i. The block i surplus depends on both strategic bids: price and quantity. For each strategic bid it is assumed that all the companies want to maximize the surplus of each block separately.

I assume that the demand is elastic, allowing the price to change with the demand. Also, it is assumed that the market price depends on the demand, as illustrated in Fig. 1:

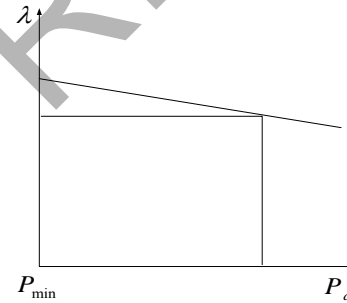


Fig. 1: Demand curve.

Thereby, the market price can be ruled by the equation:

$$\lambda = e - s(P_d - P_{min}) \quad (1)$$

The value e is the maximum price when the demand is equal to the minimum quantity, P_{min} , and isn't equal to λ_{max} .

The demand is:

$$P_d(P_{gi}, P_{-gi}) = P_{gi} + P_{-gi}(P_{gi}) \quad (2)$$

Where P_{-gi} is the aggregated opponents quantity strategic bid.

The value 's' is the slope of the demand curve and is associated with the consumer's reaction.

According to equation (1) and (2):

$$\lambda = e - s(P_{gi} + P_{-gi} - P_{min})$$

thereby,

$$\frac{d\lambda}{dP_{gi}} = -s(1 + \theta) \quad \text{with} \quad \theta = \frac{dP_{-gi}}{dP_{gi}} \quad (3)$$

θ is a parameter which represents the conjectural variation. This parameter introduces the competitors reaction to the block i quantity strategic bid. When the block i changes its quantity bid the competitors change their quantity bid by dP_{-gi} .

It's assumed that θ is constant for each case study. Thereby,

$$\theta = \frac{dP_{-gi}}{dP_{gi}} = \frac{\Delta P_{-gi}}{\Delta P_{gi}} \quad (4)$$

then

$$\frac{\Delta\lambda}{\Delta P_{gi}} = -s(1 + \theta) \Leftrightarrow \lambda = K - s(1 + \theta)P_{gi} \quad (5)$$

K is the expected market price for the minimum value of P_{gi} .

For different values of the parameter θ I have:

$$\lambda_n = K_n - s(1 + \theta_n)P_{gi} \quad (6)$$

which, assuming s constant, can be illustrated by Fig. 2:

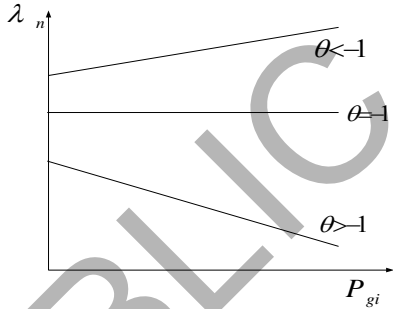
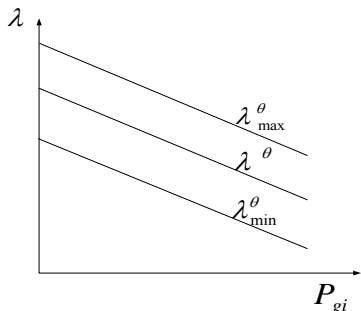


Fig. 2: Market price variation according to P_{gi} and θ

$d\lambda/dP_{gi}$ represents the influence of the quantity bid in the market price, according with θ . It's assumed that it is valid for all prices. Thereby,

$$\frac{d\lambda_{\min}}{dP_{gi}} = \frac{d\lambda_{\max}}{dP_{gi}} = -s(1 + \theta) \quad (7)$$

For θ , $\lambda^\theta \in [\lambda_{\min}^\theta, \lambda_{\max}^\theta]$ and can be illustrated by Fig. 3.



The market price with the conjectural variation approach is $\lambda^\theta = \lambda + \Delta\lambda$, where $\Delta\lambda = f(P_{gi}, \theta)$ is the market price difference to the market assuming a rigid demand.

$$\lambda^\theta = \lambda + s(1 + \theta)\Delta P_{gi} \quad (8)$$

It's defined ΔP_{gi}^* as

$$\Delta P_{gi}^* = P_{gi}^{\max} - P_{gi}^* \quad (9)$$

Thereby

$$\begin{cases} \lambda_{\max}^\theta = \lambda_{\max} + s(1 + \theta)\Delta P_{gi}^* \\ \lambda_{\min}^\theta = \lambda_{\min} + s(1 + \theta)\Delta P_{gi}^* \end{cases} \quad (10)$$

The quantity strategic bid is $P_{gi}^* \in [0, P_{gi}^{\max}]$. Otherwise, I consider that the quantity strategic bid is the respective active restriction.

The selling price, λ_i^{sell} , depends on the quantities. In the MCP market, the active participant's payment is equal to the marginal price. In the PAB market, the active participant's payment is equal to their bid.

For $\theta > -1$, when the block reduces its quantity to P_{gi}^* the market reacts rising the marginal price to $\lambda^\theta = \lambda + \Delta\lambda$. In the MCP market, the block i will sell less quantity at a higher price. In the PAB market, the probability of dispatch of the block i is higher for the blocks that $a_i > \lambda_{\min}^{MCP}$. For both markets, there are a dispatch probability for the block i that $a_i > \lambda_{\max}^{MCP}$.

Thereby, the determination of the strategic generation quantity and price bids leads to interesting dynamic market behaviour. Also, since $\theta \neq -1$, the demand will change and $P_d = f(\theta, P_{gi})$.

I studied the market behaviour assuming that the market price is represented by a normal probability function. With the normal probability function I assumed that the market price has higher probability to be in the middle of the reliable range $[\lambda_{\min}, \lambda_{\max}]$, as shown by Fig. 4

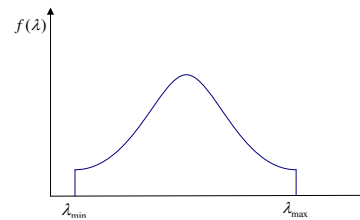


Fig. 4: Truncated normal probability price function

The normal function has an error when it's limited by the range $[\lambda_{\min}, \lambda_{\max}]$ since it's defined for all domain. However, I

assume that $8\sigma = \lambda_{\max} - \lambda_{\min}$, thereby the maximum error will be 0,006% [6].

The price probability distribution is then

$$f(\lambda) = \frac{1}{\sigma\sqrt{2\pi}} e^{-\frac{1}{2}\left(\frac{\lambda-\mu}{\sigma}\right)^2}; f(\lambda) \sim N\left(\frac{\lambda_{\max} + 3\lambda_{\min}}{2}, \frac{\lambda_{\max} - \lambda_{\min}}{8}\right)$$

Thereby we have

$$f(\lambda) = 4 \frac{\sqrt{2}e^{J_x}}{\sqrt{\pi}(\lambda_{\max} - \lambda_{\min})}$$

where

$$J_x = -\frac{8(-2\lambda + \lambda_{\max} + \lambda_{\min})^2}{(\lambda_{\max} - \lambda_{\min})^2}$$

It's also defined an auxiliary variable

$$J = -\frac{8(-2a_i^* + \lambda_{\max} + \lambda_{\min})^2}{(\lambda_{\max} - \lambda_{\min})^2}$$

According to the production cost, the block surplus function is:

$$m_i(.) = \int_0^{+\infty} f(\lambda^\theta)(u(\lambda^\theta - \lambda_{\min}^\theta) - u(\lambda^\theta - \lambda_{\max}^\theta))(\lambda_i^{sell} - a_i)(P_{gi}^{\max} - dP_{gi})d\lambda^\theta$$

where $u(.)$ is the step function.

For the block i , the strategic bids are determined by the resolution of the following maximization problem:

$$\begin{aligned} \max_{a_i^*, P_{gi}^*} \quad & m_i(a_i^*, a_i, \lambda, \lambda_i^{sell}, P_{gi}^*) \\ \text{s.t.} \quad & P_{gi}^* - P_{gi}^{\max} \leq 0 \\ & P_{gi}^{\min} - P_{gi}^* \leq 0 \\ & a_i - a_i^* \leq 0 \end{aligned}$$

I assume only the production limits restriction for the quantity strategic bid.

To avoid negative surplus for the block i , I assume that the price strategic bid is always $a_i^* \geq a_i$.

If the surplus function is concave and the restrictions are not active, the strategic bids can be determined by:

$$\begin{cases} \frac{\partial}{\partial a_i^*} m_i(.) = 0 \\ \frac{\partial}{\partial P_{gi}^*} m_i(.) = 0 \end{cases}$$

I consider that the strategic price bid of the block i doesn't influence the market price, thereby $\frac{\partial \lambda^\theta}{\partial a_i^*} = 0$.

IV. CASE STUDY

1) For the MCP market

In the MCP market, the selling price, λ_i^{sell} , is the marginal price, $\lambda^{\theta MCP}$. The price strategic bid a_i^* that maximize the expected block i surplus is a_i^{MCP} . The quantity strategic bid that maximizes the expected block i surplus is P_{gi}^{MCP} . Based on the production cost, the strategic bids are

$$\begin{aligned} 1^a) \text{ if } a_i > \lambda_{\max}^{\theta MCP} & \begin{cases} a_i^{MCP} = a_i \\ P_{gi}^{MCP} \in [0, P_{gi}^{\max}] \end{cases} \\ 2^a) \text{ if } \lambda_{\min}^{\theta MCP} < a_i \leq \lambda_{\max}^{\theta MCP} & \end{aligned}$$

First option

$$\begin{cases} a_i^{MCP} = \frac{\lambda_{\max}^{MCP} + \lambda_{\min}^{MCP} + 3a_i + 2s(1+\theta)P_{gi}^{\max}}{5} \\ P_{gi}^{MCP} = \frac{2}{5}P_{gi}^{\max} + \frac{\lambda_{\max}^{MCP} + \lambda_{\min}^{MCP}}{5s(1+\theta)}2a_i \end{cases}$$

Or second option

$$\begin{cases} a_i^{MCP} = a_i \\ P_{gi}^{MCP} = P_{gi}^{\max} + \frac{\lambda_{\max}^{MCP}}{s(1+\theta)}a_i \end{cases}$$

According to the option that leads to higher expected surplus for block i .

3^a) if $a_i \leq \lambda_{\min}^{MCP}$

$$\begin{cases} a_i \leq a_i^{MCP} \leq \lambda_{\min}^{\theta MCP} \\ P_{gi}^{MCP} = \frac{P_{gi}^{\max}}{2} + \frac{\lambda_{\min}^{MCP} + \lambda_{\max}^{MCP} - 2a_i^{MCP}}{4s(1+\theta)} \end{cases}$$

According to the strategic bids, the maximum expected surplus for block i is

a) if $a_i^{MCP} > \lambda_{\max}^{MCP}$

$$m_i^{MCP \max}(\cdot) = 0$$

b) if $\lambda_{\min}^{MCP} < a_i^{MCP} \leq \lambda_{\max}^{MCP}$

$$m_i^{MCP \max}(\cdot) = \frac{1}{8\sqrt{2\pi}} ((e^8 - e^{8(Jaux)^2}) (\lambda_{\max}^{MCP} - \lambda_{\min}^{MCP}) +$$

$$+ (e^{8+8(Jaux)^2}) (\frac{\lambda_{\max}^{MCP}}{s(1+\theta)} a_i + \frac{2}{5} P_{gi}^{\max}) +$$

$$+ 2e^{8+8(Jaux)^2} \sqrt{2\pi} (\lambda_{\max}^{MCP} +$$

$$+ \lambda_{\min}^{MCP} - 2a_i) (ERF(2\sqrt{2}) + ERF\left(\frac{16\sqrt{2}Jaux}{\lambda_{\max}^{MCP} - \lambda_{\min}^{MCP}}\right)))$$

where for the first condition

$$Jaux = \frac{3(\lambda_{\max}^{MCP} + \lambda_{\min}^{MCP}) - 6a_i + 4s(1+\theta)P_{gi}^{\max}}{5(\lambda_{\max}^{MCP} - \lambda_{\min}^{MCP})}$$

and for the second condition

$$Jaux = \frac{\lambda_{\max}^{MCP} + \lambda_{\min}^{MCP} - 2a_i}{\lambda_{\max}^{MCP} - \lambda_{\min}^{MCP}}$$

$ERF(X)$ is the integral of the Gaussian distribution, given by

$$ERF(X) = \frac{2}{\sqrt{\pi}} \int_0^X e^{-t^2} dt = \frac{2}{\sqrt{\pi}} \sum_{n=0}^{+\infty} \frac{(-1)^n X^{2n+1}}{(2n+1)n!}$$

c) $a_i^{MCP} \leq \lambda_{\min}^{MCP}$

$$m_i^{MCP \max}(\cdot) = P_{gi}^{\max} \left(\frac{\lambda_{\max}^{MCP} + \lambda_{\min}^{MCP}}{2} a_i \right) (ERF(2\sqrt{2}))$$

2) For the PAB market

In the MCP market, the selling price, λ_i^{sell} , is the price strategic bid, $a_i^* = a_i^{PAB}$. The quantity strategic bid that maximizes the expected block i surplus is P_{gi}^{PAB} .

According to the production cost, the strategic bids are

1^a) if $a_i > \lambda_{\max}^{OPAB}$

$$\begin{cases} a_i^{PAB} \geq a_i \\ P_{gi}^{PAB} \in [0, P_{gi}^{\max}] \end{cases}$$

2^a) if $\lambda_{\min}^{OPAB} < a_i \leq \lambda_{\max}^{OPAB}$

First option

$$\begin{cases} a_i^{PAB} = \frac{3\lambda_{\max}^{PAB} + 3\lambda_{\min}^{PAB} + 2a_i + 2s(1+\theta)\Delta P_{gi}^{PAB}}{8} \\ P_{gi}^{PAB} = 3 \frac{\lambda_{\max}^{PAB} + \lambda_{\min}^{PAB} + 2s(1+\theta)P_{gi}^{\max} - 2a_i^{PAB}}{8s(1+\theta)} \end{cases}$$

Or second option

$$\begin{cases} a_i^{PAB} = \frac{\lambda_{\max}^{PAB} + \lambda_{\min}^{PAB} + 3a_i + 2s(1+\theta)P_{gi}^{\max}}{5} \\ P_{gi}^{PAB} = \frac{2}{5} P_{gi}^{\max} + \frac{\lambda_{\max}^{PAB} + \lambda_{\min}^{PAB} - 2a_i}{5s(1+\theta)} \end{cases}$$

According to the option that leads to higher expected surplus for block i.

3^a) if $a_i \leq \lambda_{\min}^{OPAB}$

$$P_{gi}^{PAB} = P_{gi}^{\max}$$

If $a_i < \lambda_y^{OPAB}$ then $a_i^{PAB} = \lambda_{\min}^{OPAB}$.

If $\lambda_y^{OPAB} < a_i \leq \lambda_{\max}^{PAB}$ then $a_i^{PAB} = \frac{3\lambda_{\max}^{OPAB} + 3\lambda_{\min}^{OPAB} + 2a_i}{8}$

I define $\lambda_y^\theta = \frac{5,5\lambda_{\min}^\theta - 3\lambda_{\max}^\theta}{2}$ as an auxiliary variable.

According to the strategic bids, the maximum expected surplus for block i is

a) if $a_i^{PAB} > \lambda_{\max}^{OPAB}$

$$m^{PAB \max}(\cdot) = 0$$

$$b) \lambda_{\min}^{\theta PAB} < a_i^{PAB} \leq \lambda_{\max}^{\theta PAB}$$

$$m_i^{PAB \max}(\cdot) = \frac{1}{250s(1+\theta)} (\lambda_{\max}^{PAB} + \lambda_{\min}^{PAB} + 2s(1+\theta)P_{gi}^{\max} - 2a_i)(3(\lambda_{\max}^{PAB} + \lambda_{\min}^{PAB}) + 16s(1+\theta)P_{gi}^{\max})(ERF(2\sqrt{2}) - ERF(\frac{2\sqrt{2}(9(\lambda_{\max}^{PAB} - \lambda_{\min}^{PAB}) - 18a_i - 2s(1+\theta)P_{gi}^{\max})}{25(\lambda_{\max}^{PAB} - \lambda_{\min}^{PAB})}))$$

$$c) \lambda_Y^{\theta PAB} < a_i^{PAB} \leq \lambda_{\min}^{\theta PAB}$$

$$m_i^{PAB \max}(\cdot) = \frac{P_{gi}^{\max}}{8} (\lambda_{\max}^{PAB} + 3\lambda_{\min}^{PAB} - 6a_i)(ERF(2\sqrt{2}))$$

$$d) a_i^{PAB} \leq \lambda_Y^{\theta PAB}$$

$$m_i^{PAB \max}(\cdot) = P_{gi}^{\max} (\lambda_{\min}^{PAB} - a_i)(ERF(2\sqrt{2}))$$

V. RESULTS

The results are for the following cases:

Case	s	θ
1	0.0001	-0.9900
2	1.0000	0.0000
3	1.0000	0.5000
4	1.0000	1.0000
5	1.0000	1.5000
6	1.0000	2.0000

Fig. 5: Case Study.

The emissions of a coal power plant are 1000kg/MWh [7], thereby the cost of introducing the emission externality is 20 €/MWh.

The results were obtained for the following values:

- for $a_i = 15$, coal technology without taking account with the externalities;
- for $a_i = 35$, coal technology taking account with the externalities;
- $\lambda_{\min} = 22$; $\lambda_{\max} = 38$.

The results are in the Appendix.

VI. CONCLUSIONS

I assume that the companies have price and quantity strategic bids to maximize their surplus. According to the tables in appendix, we can see that the influence of all technologies is bigger in the MCP market than in the PAB market, when I assume a normal price distribution. The demand satisfied is lower and the market price is higher in the MCP market than in the PAB market.

Also, when the emission externality is introduced as a production cost, the surplus is lower. Therefore, the market can work as an incentive for sustainability.

REFERENCES

- [1] Domingues, N., Mendes, V., Correia, P., «Oferta Estratégica da Geração em Mercados de Energia», ISEL, 18 e 19 de Outubro de 2005, 1st Workshop in ISEL;
- [2] Ren, Y., Galiana, F., «Pay-as-bid versus Marginal Pricing- Part I: Strategic Generator Bid», IEEE Transactions On Power Systems, Vol. 19, No. 4, November 2004;
- [3] Song, Y., Hou, Z., Wen, F., Yixin, N., Félix, F., Conjectural Variation Based Learning of Generator's Behaviour in Electricity Market», IEEE Transactions On Power Systems, Vol., No. , 2003;
- [4] Day, C., Hobbs, B., Pang, J., «Oligopolistic Competition in Power Networks: a Conjectural Supply Function Approach», IEEE Transactions on Power Systems, Vol. 17, n°3, Ago 2002;
- [5] Song, Y., Ni, Y., Wen, F., Wu, F., «Analysis of strategic Interactions Among Generation Companies Using Conjectured Supply Function Equilibrium Model», IEEE, 2003;
- [6] Montgomery, D., Runger, G., «Applied Statistics and Probability for Engineers», Wiley, 2007.
- [7] www.edp.pt

VII. BIOGRAPHY

Nuno A. S. Domingues (b. 1972) received the Licenciante (5-year) degree in Electrical Engineering from ISEL (2005) and Master degrees in Electrical Engineering and Computer Science from IST (2008). Presently he is a PhD candidate at FCT with his thesis on energy, sustainability and efficiency.

Presently he works as a Labour Engineer at ISEL (2001-2008) in Engineering Systems.

His topics of research include electricity markets modelling and simulation, energy systems, sustainability, efficiency.

I. APPENDIX

$a_i = 15$	MCP Market						PAB Market					
	Bid		Surplus		Market Price		Bid		Surplus		Market Price	
	Price	Quantity	Per unit	Total	Minimum	Maximum	Price	Quantity	Per unit	Total	Minimum	Maximum
1	15,00	10,00	15,00	149,99	22,00	38,00	28,13	10,00	10,84	108,38	22,00	38,00
2	15,00	8,75	16,25	142,18	23,25	39,25	28,13	10,00	10,84	108,38	22,00	38,00
3	15,00	7,50	18,75	140,62	25,75	41,75	28,13	10,00	10,84	108,38	22,00	38,00
4	15,00	6,88	21,25	146,08	28,25	44,25	28,13	10,00	10,84	108,38	22,00	38,00
5	15,00	6,50	23,75	154,37	30,75	46,75	28,13	10,00	10,84	108,38	22,00	38,00
6	15,00	6,25	26,25	164,05	33,25	49,25	28,13	10,00	10,84	108,38	22,00	38,00
	15,00	5,63	41,25	232,02	48,25	64,25	28,13	10,00	10,84	108,38	22,00	38,00

Table. 1: Market behaviour without externalities

$a_i = 35$	MCP Market						PAB Market					
	Bid		Surplus		Market Price		Bid		Surplus		Market Price	
	Price	Quantity	Per unit	Total	Minimum	Maximum	Price	Quantity	Per unit	Total	Minimum	Maximum
1	35,00	10,00	0,004	0,04	22,00	38,00	35,25	10,00	0,002	0,02	22,00	38,00
2	37,00	2,00	2,78	5,56	30,00	46,00	35,50	4,69	0,04	0,19	27,31	43,31
3	37,00	2,67	6,00	16,00	33,00	49,00	35,50	5,00	0,11	0,55	29,50	45,50
4	35,00	2,25	10,50	23,62	37,50	53,50	36,25	5,16	1,20	6,17	31,69	47,69
5	35,00	2,40	14,00	33,60	41,00	57,00	37,50	5,25	2,46	12,94	33,88	49,88
6	35,00	2,50	17,50	43,75	44,50	60,50	38,50	5,31	3,74	19,84	36,06	52,06

Table. 2: Market behaviour with emission externalities

The future goes offshore...

Robert Hoyer, Henry Römer, and Jonathan Saudhof

Abstract—Within the renewable energies wind parks are playing an important role. Since onshore wind energy market is already high developed and concerns are more about repowering, offshore wind plants have gained enormous popularity. In consideration of the high potential German government set the target to accommodate 15 percent of the energy demand with the help of offshore wind plants in 2030. Despite the high potential there are still risks and problems hindering the installation of huge offshore plants. In fact there is still no such wind park completely installed in Germany.

Index Terms—Economic potential, offshore, Renewable energy, wind energy

I. INTRODUCTION

Germany is one of the leading countries in using renewable energy. The German government and others try to reduce their CO₂ emissions rapidly. Besides expanding solar- and photovoltaic techniques the main energy source is wind power. 2005 4.3 % of the produced energy were generated by onshore windmills [3]. In the future the expansion and new installation of those wind farms is limited due to the present legal conditions for ecological safety. In this context new ways are going to be approached. Offshore Wind parks are actually the best choice to extend the use of wind power simultaneously with an increase of efficiency.

The advantages of these offshore solutions in contrast to wind parks are the stable and higher level of wind speed. Currently the using of wind power is connected with occurring gaps between generated power and the actual system load due to the onshore wind speed fluctuation.

Actually in Germany no offshore projects have been realized yet. 2008, the installation of the first test park “alpha ventus” has been started. Twelve wind turbines with 5-6 MW turbines are going to be built in 30m depth [1]. In the international comparison of realized offshore projects Germany shows that

Manuscript received March 20, 2009.

Robert Hoyer is a student of industrial engineering at the Brandenburgische Technische Universität Cottbus, Germany (e-mail: robert.hoyer@jata.de).

Henry Römer is a student of industrial engineering at the Brandenburgische Technische Universität Cottbus, Germany (e-mail: henry.roemer@jata.de).

Jonathan Saudhof is a student of industrial engineering at the Brandenburgische Technische Universität Cottbus, Germany (e-mail: jonathan.saudhof@jata.de).

the installed number of turbines in Germany is irrelevant to the United Kingdom with 591 MW, Denmark 426,35, Netherlands with 246,8 MW and Sweden with 132,5 MW [2]. The prognosis says that a possible capacity of 20000 up to 30000 MW can be realized. In long terms offshore wind power will affect the market of renewable energy sources [4].

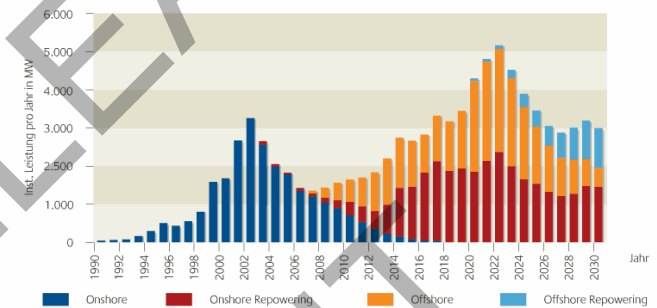


Fig. 1 Development of renewable energy

Chances:

Wind speed and development:

As mentioned before the less fluctuation and higher wind speed is a major advantage of offshore wind parks. This means a push of generating efficiency and the possibility that wind turbines can supply with base load current.

Figure 2 shows the differences in wind speed per minute depending on the geographical location and gives an inside of benefits from those installations.

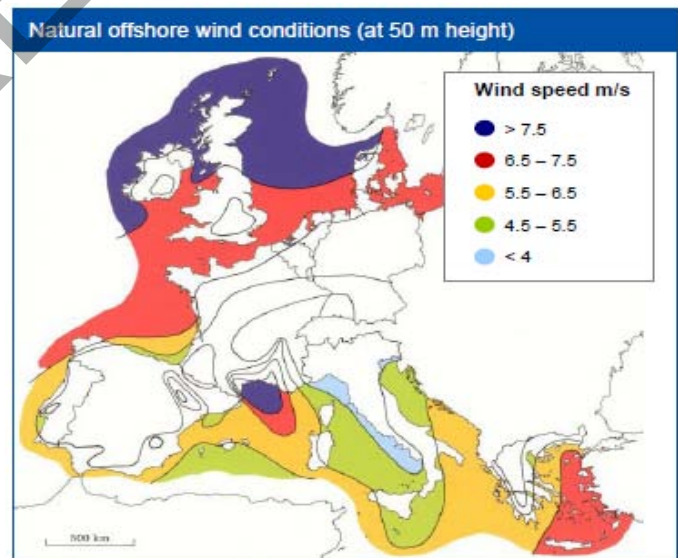


Fig. 2 Offshore wind conditions in Europe

The future of windmills in Germany is in offshore farms. New installations of onshore turbines will be stopped due to the present legal conditions for ecological safety. This means a limited size for turbines because of their air noise emission and the casting of shadow. The target for Germany is to explore and lead the market after the United Kingdom within the next years. Figure shows the size of installed turbines planned till 2015.

Parallel to reducing new installations repowering is going to be the key for increasing the efficiency of existing windmills. Learning effects in various technical sciences will determine the development of future turbines. Material science, Aerospace and experiences in the installation of offshore platforms will highly influence the future offshore wind parks. A project actually presented in the press called ‘FloDesign Wind Turbine’ is a new way for designing windmills to maximize the used wind power.



Fig. 3 Operating offshore wind farms

II. ECONOMY

The initial costs of wind energy onshore have drastically decreased because of the gradual technical advancement of the arrangements. In Germany the costs of wind energy arrangements per kilowatt of achievement were lower according to the federal association Windenergie inc. in 2000 almost around half than still in 1990. According to the European wind energy association EWEA the actual costs of modern wind strength arrangements in good wind locations are at the moment to 5.1€ cent / kWh. Up to 2013 3.2€ of cent / kWh are accessible according to this association in such locations [5].

a) Actual cost of power generation

In 2001 the external research project of the European commission came to the result that the average stream actual costs amount to 4€ of cent / kWh in the European Union. The Institute of energy industry and rational energy use (IER) of the University of Stuttgart estimates the stream actual costs

for gas and steam power stations established in 2005 at 3.6€ cent per kWh. For brown coal-fired power stations the IER comes on approximately 3.1 and for coal-fired power stations on approximately 2.8€ cent per kWh. According to the external investigation done by the IER in Germany, the external costs of the stream production of coal or brown coal amount from 3 to 6€ cent per kWh. Wind energy – onshore or offshore - has extremely low external production costs in comparison.

Average stream actual costs in the EU	4 € of cent/kWh
In 2005 established gas and steam power stations	3,6 € of cent/kWh
Brown coal-fired power stations	3,1 € of cent/kWh
Coal-fired power stations	2,8 € of cent/kWh
Additional external costs for coal-fired power stations and brown coal-fired power stations in Germany	3 – 6 of cent/kWh

b) Present Offshore experiences

For the first smaller Offshore-wind parks close to coast stream actual costs have been determined abroad in the area from 6 to 8€ cent. Besides, the later projects show a sinking trend. The DEWI (German Wind Energy Institute) has published estimates, for which the planned wind parks in Germany, standing 40 kilometers far from the coast remotely will reach stream actual costs of from 7.4 to 8.1€ cent per kWh. At the moment installed power is 2 MW [5]. However, the applications planned from 4 to 5 MW arrangements what will lead probably to a lowering of the costs in the future.

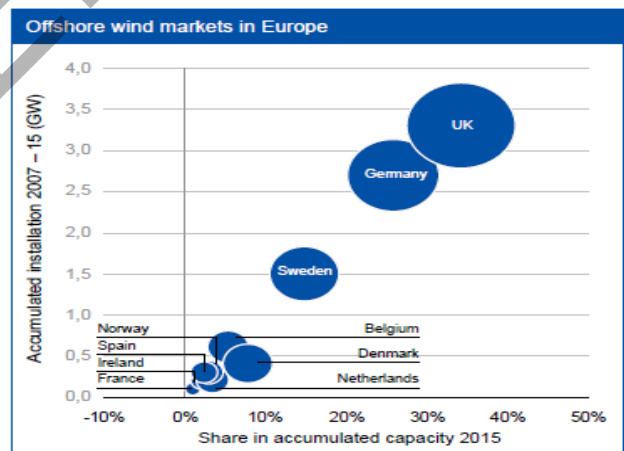


Fig. 4 Offshore wind markets in Europe

III. RISKS

Despite the fact offshore wind energy to be a solution with high potential within the renewable energies it is still facing a variety of problems to solve. On the one hand there several

concerns about how offshore wind parks may influence the maritime environment negatively. Among conservationists the threat of collision of birds with rotor blades are mentioned as well as their displacement from their native environment. In fact there is still no scientific evidence of a high rate of collisions. Indeed Danish researchers with the help of their Thermal Animal Detection System (TADS) could show that the number of incidents is quite small. Nevertheless this problem is considered to be locally different. But not only birds seem to be threatened. Sea fish and marine mammals may suffer the artificially created magnetic and electric fields by the cables connecting the plants offshore with the electrical network. For this reason these animals such as whales might lose orientation. Additionally benthos are losing their habitats because of the building of the fundament at the ground of the sea [6]. Nevertheless research in this field is ongoing, e.g. considering the research station Fino I near the Island of Borkum, Germany and there is still no conclusion [8]. But there are not only environmental concerns to deal with. The installation of wind parks is still not only a technical challenge but a financial risk as well [7]. A wind park planned consisting of 150 to 180 plants by the German Enterprise RWE near the island of Juist will take an investment of ca. 2.8 Billion Euro. Aware of that fact high investments are needed only the huge energy provider will be able to build the first commercially used offshore wind parks. The installation of wind parks is much more complicated and referring to that expensive. Installing a 1 Megawatt plant offshore takes about 2.5 Million Euro, two times the price for a plant to build onshore [9]. According to a study by Price Waterhouse Coopers (PWC) financing offshore projects suffer two significant problems. First there has been a high increase of investing costs due to higher price for natural resources, especially steel and copper. Furthermore the increasing demand for onshore plants has raised the price for offshore plants too since these are technically based on onshore technologies although there have been built prototypes specially designed for offshore operation. Additionally the uncertainty of investment and maintenance cost at the beginning of a project is still an obstacle for potential investors considering that the experiences regarding wind parks far from the shore in thirty meter depth are low. The second issue concerns the so called interface problem. An offshore project joins a number of enterprises for building the wind park whereas onshore plants are built by one corporation normally. Next to the plant the building of the electrical and structural connection has to be done too. But these different works refer to different amount of risk. The organization of the project must guarantee a fair distribution of risk for any enterprise within it in order to make enterprises invest and reduce risk surcharge. A very important point determining the economic success of offshore projects refers to maintenance. Because plants are located at difficult accessible locations availability is threatened in the case of technical breakdown. So, in fact there might be the problem of delayed repairs when weather conditions are bad [7]. Another risk is the potential impact on the environment and

the peril of collisions with oil tanker leading to environmental catastrophes.

IV. CONCLUSION

Although Germany is supposed to be the vanguard considering renewable energies, especially in wind energy it has lost this role in the field of offshore wind parks just by taking a look at the number of installed plants. First commercially used plants are already running near the costs of its European neighbors Great Britain and Denmark [10]. At least there is no doubt offshore wind energy will face a high growth during the next years in all countries verging on to the sea. Nevertheless with the construction of the Alpha Ventus wind park by the German RWE a large step for the future of offshore wind energy has been done.

ACKNOWLEDGMENT

Robert Hoyer would like to thank his parents, grandparents and God. He specially thanks Rommy for the loving support all the time. Henry Römer thanks his family especially his brother Stephan for reading proof of this paper. Jonathan Sauthof would to thank all of his friends and his family.

REFERENCES

- [1] Dena (2009, February). Internationale Windprojekte: <http://www.offshore-wind.de/page/index.php?id=4765&L=0&fs=1>
- [2] Deutsche Windindustrie in Deutschland (2009, February). Onshore-Windenergie und Repowering: <http://www.deutsche-windindustrie.de/fakten/onshore/index.html>
- [3] Dena (2009, Februar). Offshore-Testfeld alpha ventus: Deutschlands erster Windpark auf dem Meer: <http://www.offshore-wind.de/page/index.php?id=9352&L=1&fs=1&L=0>
- [4] Köller, Julia. Offshore wind energy. Berlin: Springer, 2006
- [5] Dena. (2009, February). Fakten Wirtschaftlichkeit. Available: <http://www.offshore-wind.de/page/index.php?id=2601>
- [6] T. Merck, H. v. Nordheim (1999) Probleme bei der Nutzung von Offshore-Windenergie aus Sicht des Naturschutzes. German Journal of Hydrography Supplement 10
- [7] J. Ondraczek, H. Stohlmeyer, S. Küver (2006). Finanzierung der Offshore-Windenergie in Deutschland: Probleme und Lösungsansätze. Available: <http://www.PWCglobal.com>
- [8] D. Asendorpf. (2008, June). Viel Energie auf hoher See. Available: <http://www.zeit.de/2008/27/windpark>
- [9] M. Uken (2006, November). Riskante Wellenbrecher. Available: <http://www.zeit.de/online/2006/46/Offshore-Windkraft>
- [10] RWE (June, 2008). Fact Book Renewable Energy Available: <http://www.rwe.com/web/cms/de/184208/rwe/innovationen/services/inforthek-forschung-entwicklung/>

Strong Electromagnetic Impulse Generation

Daniel Pyda
Wroclaw University of Technology
27 Wybrzeze Wyspianskiego
Wroclaw, Poland

Abstract - Electromagnetic fields can have not only disturbing but also damaging influence on equipment. There are many ways to generate such electromagnetic field. In this paper some of electromagnetic field generators will be introduced and how dangerous such field is for today electric and electronic equipment.

I. INTRODUCTION

The fact that an electromagnetic pulse is produced by a nuclear explosion was known since the earliest days of nuclear weapons testing, but the magnitude of the EMP and the significance of its effects were realized very slowly.

In July, 1962, a 1.44 megaton united states nuclear test in space, 400 km. Above the mid-pacific ocean, called the starfish prime test demonstrated to nuclear scientists that the magnitude and effects of a high altitude nuclear explosion were much larger than had been previously calculated. Starfish prime also made those effects known to the public by causing electrical damage in Hawaii, more than 800 miles away from the detonation point, knocking out about 300 streetlights, setting off numerous burglar alarms and damaging a telephone company microwave link.

The EMP damage of the starfish prime test was quickly repaired because of the ruggedness (compared to today) of the electrical and electronic infrastructure of Hawaii in 1962. Realization of the potential impacts of EMP became more apparent to some scientists and engineers during the 1970s as more sensitive solid-state electronics began to come into widespread use.

The larger scientific community became aware of the significance of the EMP problem after a series of three articles was published about nuclear electromagnetic pulse in 1981 by William broad in the weekly publication *science*.

The relatively small magnitude of the starfish prime EMP in Hawaii (about 5,700 volts/meter) and the relatively small amount of damage done (for example, only 1 to 3 percent of streetlights extinguished) led some scientists to believe, in the early days of EMP research, that the problem might not be as significant as was later realized. Newer calculations showed that if the starfish prime warhead had been detonated over the northern continental united states, the magnitude of the EMP would have been much larger (22,000 to 30,000 volts/meter) because of the greater strength of the earth's magnetic field over the united states, as well as the different orientation of the

Earth's magnetic field at high latitudes. These new calculations, combined with the accelerating reliance on EMP-sensitive microelectronics, heightened awareness that the EMP threat could be a very significant problem.

In 1962, the Soviet Union also performed a series of three EMP-producing nuclear tests in space over Kazakhstan called "the k project". Although these weapons were much smaller (300 kilotons) than the starfish prime test, since those tests were done over a populated large land mass (and also at a location where the earth's magnetic field was greater), the damage caused by the resulting EMP was reportedly much greater than in the starfish prime nuclear test. The geomagnetic storm-like E3 pulse even induced an electrical current surge in a long underground power line that caused a fire in the power plant in the city of Karagandy. After the collapse of the soviet union, the level of this damage was communicated informally to scientists in the united states. Formal documentation of some of the EMP damage in Kazakhstan exists but is still sparse in the open scientific literature.

II. CHARACTERISTIC

The case of a nuclear electromagnetic pulse differs from other kinds of electromagnetic pulse (EMP) in being a complex electromagnetic multi-pulse. The complex multi-pulse is usually described in terms of 3 components, and these 3 components have been defined as such by the international standards commission called the International Electrotechnical Commission (IEC).

The 3 components of nuclear EMP, as defined by the IEC, are called E1, E2 and E3.

The **E1** pulse is a very fast pulse that generates very high voltages. E1 is the component that can destroy computers and communications equipment and is too fast for ordinary lightning protectors.

The **E2** component of the pulse many similarities to the electromagnetic pulses produced by lightning. Because of the similarities to lightning-caused pulses and the widespread use of lightning protection technology, the E2 pulse is generally considered to be the easiest to protect against.

The **E3** component of the pulse is a very slow pulse, lasting tens to hundreds of seconds, that is caused by the nuclear detonation heaving the earth's magnetic field out of the way, followed by the restoration of the magnetic field to its

natural place. The E3 component has similarities to a geomagnetic storm caused by a very severe solar flare.

III. EXPLOSION ON EARTH SURFACE

During the case of a nuclear explosion on Earth surface (Fig.1) the symmetry conditions aren't preserved. We can treat earth as a perfect absorber for γ radiation and current conductor. Because of that un symmetry a current vertical component is forming which generates an electromagnetic field like vertical monopole. Electromagnetic energy is been radiated beyond deposition region.

The conditions of electromagnetic impulse propagation are in accordance with theory of wave propagation near Earth. Some of electrons that propagates radial from place of explosion returns to this place through ionized magnetic paths in air and Earth. Therefore current circles are forming and produce strong azimuth magnetic field. The electric field made during the explosion is very high but it decreasing quite fast, at first inversely proportional to power third of distance. In bigger distances from influence area we engage to so called far zone and field decrease inversely proportional to distance from explosion place. The range of influence for electromagnetic field generated in such conditions is relatively small reaching several kilometers. Typical on Earth nuclear explosion electromagnetic impulse shape is shown on (Fig.2).

Main parameters of electromagnetic impulse can be shown as below:

- impulse increasing time $< 5\text{ms}$
- impulse lasting time $< 200\text{ns}$
- $E < 40\text{kV/m}$
- $H < 200\text{A/m}$

IV. EXPLOSION IN ATMOSPHERE

During the case of a nuclear explosion in atmosphere (Fig.3) equivalent electric dipole is been formulating, what is caused by atmosphere inhomogeneity, which is a radiation producer. Some of this radiation is been reflected from Earth surface and interfere with direct radiation explosion electric field has lower intensity than the on Earth explosion field.

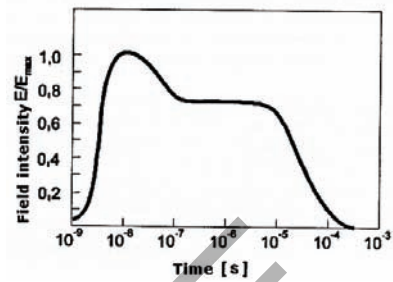


Figure 2. Earth nuclear explosion electromagnetic impulse shape

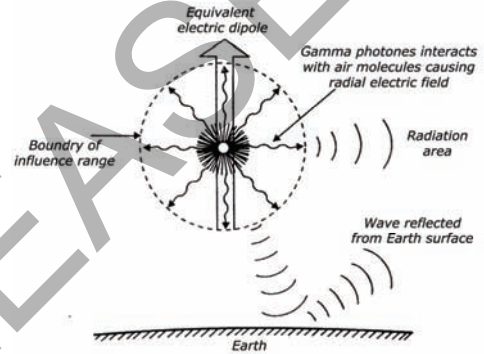


Figure 3. The in atmosphere explosion

Main parameters of electromagnetic impulse can be shown as below:

- impulse increasing time $< 50\mu\text{s}$
- impulse lasting time $< 100\mu\text{s}$
- $E < 10\text{kV/m}$
- $H < 50\text{A/m}$

V. EXPLOSION IN GREAT ALTITUDE

During the case of a nuclear explosion in great altitude (Fig.4), recoil electrons are produced only when photons γ reaches the thicker parts of atmosphere. These electrons are deflect by Earth magnetic field producing crosswise directed electric current, which is the source of electromagnetic radiation propagating radial from hot spot. Such rising electromagnetic impulse (HEMP – High Altitude EMP) has great range (Fig.5).

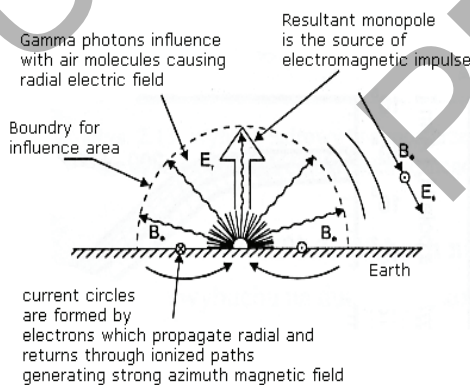


Figure 1. Nuclear explosion on Earth surface

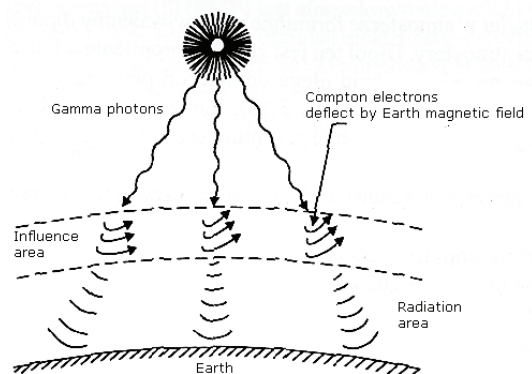


Figure 4. Nuclear explosion in great altitude

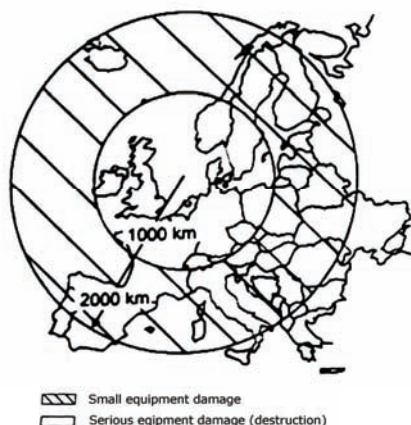


Figure 5. Nuclear explosion in great altitude damage range

Main parameters of electromagnetic impulse can be shown as below:

- impulse increasing time < 10ms
- impulse lasting time < 100ns
- $E < 100kV/m$
- $H < 300A/m$

Parameters and maintenance of electromagnetic produced during nuclear explosion in great altitude are base for determine parameters and time run for conventional disturbance (test signal), recommended by many standards to perform tests for equipment sensitivity for electromagnetic field.

VI. NON-NUCLEAR ELECTROMAGNETIC IMPULSE

Non-nuclear electromagnetic pulse (NNEMP) (Fig.6-7) is an electromagnetic pulse generated without use of nuclear weapons. There are a number of devices that can achieve this objective, ranging from a large low-inductance capacitor bank discharged into a single-loop antenna or a microwave generator to an explosively pumped flux compression generator. To achieve the frequency characteristics of the pulse needed for optimal coupling into the target, wave-shaping circuits and/or microwave generators are added between the pulse source and the antenna. A vacuum tube particularly suitable for microwave conversion of high energy pulses is the vircator.



Figure 6. A right front view of a Boeing E-4 advanced airborne command post (AABNCP) on the electromagnetic pulse (EMP) simulator for testing.



Figure 7. USS Estocin (FFG-15) moored near the Electro Magnetic Pulse Radiation Environmental Simulator for Ships I (EMPRESS I) facility. (Antennae at top of image)

NNEMP generators can be carried as a payload of bombs and cruise missiles, allowing construction of electromagnetic bombs with diminished mechanical, thermal and ionizing radiation effects and without the political consequences of deploying nuclear weapons.

NNEMP generators also include large structures built to generate EMP for testing of electronics to determine how well it survives EMP. In addition, the use of ultra-wideband radars can generate EMP in areas immediately adjacent to the radar; this phenomenon is only partly understood.

Information about the EMP simulators used by the United States during the later part of the Cold War is now in papers under the care of the SUMMA Foundation, which is now hosted at the University of New Mexico.

The SUMMA Foundation web site includes documentation about the huge wooden Trestle simulator in New Mexico, which was the world's largest EMP simulator which used a specialized version of a Marx generator.

VII. EXAMPLE OF VIRCATOR GENERATOR

(Fig.8) A vircator (VIRtual CATHode OscillatOR) is a microwave generator that is capable of generating brief pulses of tunable, narrow band microwaves at very high power levels. A typical vircator is built inside an evacuated resonant cavity or waveguide. An electrode at one end injects an intense electron beam, such as from a Marx generator or a flux compression generator. The electrons are attracted to a thin anode, such as an aluminized PET film, that is connected to the grounded waveguide body.

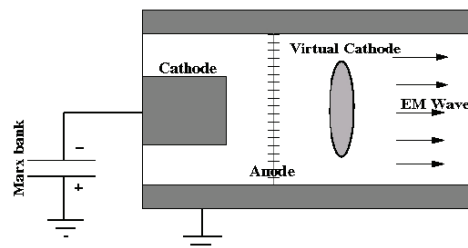


Figure 6. A right front view of a Boeing E-4 advanced airborne command post (AABNCP) on the electromagnetic pulse (EMP) simulator for testing.

The unit is surrounded by a magnet. Due to the intensity of the electron beam, many electrons pass through the anode into the region beyond it, forming a virtual cathode. The electron beam must be intense enough to exceed the space charge limiting current in that region, causing oscillations that generate microwaves. The frequency, efficiency and other characteristics of the emitted beam depend on the precise physical configuration and operating parameters.

Vircators have been used as electromagnetic pulse generators and for generating X-rays. Power levels on the order of 10^{10} to 10^{12} watts are possible.

REFERENCES

- [1] Donald J. Sullivan, "High Power Microwave Generation From a Virtual Cathode scillator (Vircator)," IEEE Trans. Nucl. Sci., vol. NS-30, No. 4, 3426-3428 (Aug. 1983)
- [2] www.wikipedia.org
- [3] Tadeusz W. Wieckowski, "Electromagnetic Compatibility Examination For Electric and Electronic Equipment"

Detection of Fault Position with Respect to the Compensating Bank in Series Compensated Line by Measurement of Phase Shift for Distance Relay Input Currents

Piotr Maźniewski, Jan Iżykowski

Wroclaw University of Technology (I-8), Wyb. Wyspianskiego 27, 50-370 Wroclaw, Poland
(email: piotr.mazniewski@pwr.wroc.pl, jan.izykowski@pwr.wroc.pl)

Abstract--This paper presents an analysis of possibility of detection of a fault position with respect to the compensating bank in a series compensating transmission line. The algorithm designed for this purpose is based on determining the change of phase shift for the distance relay input currents. Fuzzy logic technique is applied for making the decision whether a fault is in front of the compensating bank or behind it. The algorithm has been tested and evaluated with use of the fault data obtained from versatile ATP-EMTP simulations of faults in the test network containing the 400 kV, 300 km transmission line, compensated with the aid of the compensating bank installed at mid-line. The sample results of the evaluation are reported and discussed.

I. INTRODUCTION

Increased transmittable power, improved power system stability, reduced transmission losses; enhanced voltage control and flexible power flow control are the reasons behind installing Series Capacitors (SCs) on long transmission lines [2]. The environmental concerns stand for that too.

Both, capacitors of fixed value (FSC – Fixed Series Capacitors) and of controlled value (TCSC – Thyristor Controlled Series Capacitors) are installed in series compensated lines. This paper deals with distance protection issues for a line compensated with a three-phase bank of fixed series capacitors (SCs) installed at mid-line (Fig. 1). SCs are equipped with their overvoltage protection devices: typically Metal Oxide Varistors (MOVs). Each MOV is in turn protected from overheating with the aid of the thermal protection (TP), which eventually sparks the respective Air-Gap, in order to by-pass its MOV.

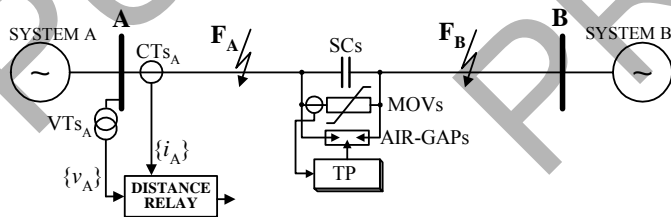


Figure 1. Schematic diagram of series compensated line for protection study:
 F_A – fault in front of SCs/MOVs, F_B – fault behind SCs/MOVs.

The compensating bank when installed in a line creates, however, certain problems for its protective relays and fault locators. If a series compensated line suffers a fault behind the SCs, as seen from the relaying point (fault F_B in

Fig. 1), a fault loop measured by a distance relay contains, depending on a type of fault, one (for single phase faults) or even two (for inter-phase faults) systems of SCs and MOVs. As a consequence, the operating conditions for protective relays become unfavourable and include such phenomena as voltage and/or current inversion, subharmonic oscillations, high frequency oscillations due to MOVs [2]. The most important peculiarity of a series compensated line as the object to be protected, lays, however, in the fact that the positive sequence impedance measured by a traditional distance relay is no longer an indicator of the distance to a fault. The SC and its MOV affect both, the steady state and transient conditions of the distance relay measurements.

Protection of networks with series compensated lines is considered as one of the most difficult tasks. There is still much room for developing efficient protective relaying for such networks. The approach presented in this paper is one of the attempts for realizing that [1], [3], [11].

In this paper a new criterion of qualification of a fault place with respect to the compensating bank is introduced. It is based on measuring the change of a phase shift of input currents of a distance relay.

II. FUZZY LOGIC BASED ALGORITHM FOR DETECTING FAULT POSITION WITH RESPECT TO COMPENSATING BANK

The concept of fuzzy logic was conceived by Lotfi Zadeh as a way of processing data by allowing a partial set membership rather than a crisp set membership or non-membership. It offers several unique features that make it a particularly good choice for many problems [6], [9].

A classic logic is based on two values, the most often represented by 0 and 1, or truth and falsehood. A border between them is definite unambiguously and invariable. Fuzzy logic introduces values between the standard 0 and 1 and fuzzification of the borders between them, giving the possibility of appearing the values between these values.

Schematic diagram of the proposed fuzzy logic algorithm is presented in Fig. 2.

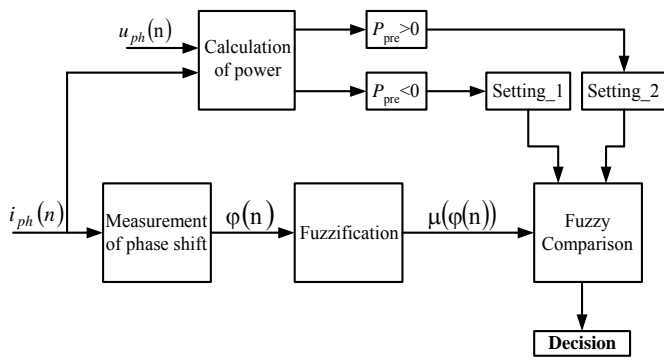


Figure 2. Schematic diagram of fuzzy logic based detection of fault position.

First, digital measurement of phase shift for phase currents is performed [8]:

$$\varphi(n) = \text{atan} \left[\frac{\text{imag}(i_{ph}(n))}{\text{real}(i_{ph}(n))} \right] \quad (1)$$

where:

n – index denoting the current sample of the processed phase current.

From pre-fault voltages and currents, an active power is calculated [8]:

$$P_{pre}(n) = 0.5[u_{1C}(n) \cdot i_{1C}(n) + u_{1S}(n) \cdot i_{1S}(n)] \quad (2)$$

where:

$u_{1C}(n)$, $i_{1C}(n)$, $u_{1S}(n)$, $i_{1S}(n)$ – voltages and currents after full-cycle Furrier filtering (a pair of sine and cosine filters).

The calculated pre-fault power is used for detecting a power flow direction. Appropriate setting is applied according to the detected direction.

The calculated samples of the phase shift undergo fuzzification. For this purpose the set of five consecutive samples are taken for determining the membership function in the shape of the triangle. The points of this triangle are determined with the minimum, average and maximum values of the phase shift.

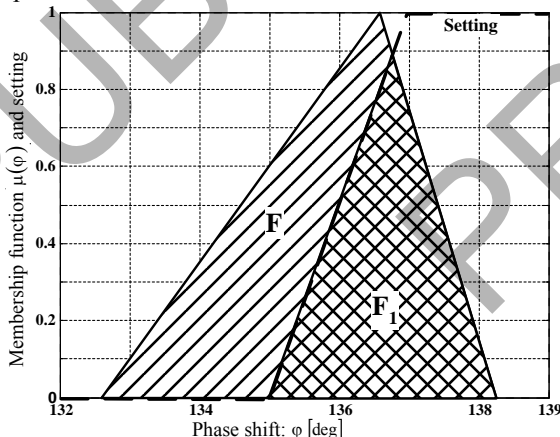


Figure 3. Illustration of fuzzy comparison.

The setting applied in the fuzzy comparison (Fig. 3) was determined arbitrary, for each fault type separately. In further investigations, the self-adjusting fuzzy settings will be applied

Making the decision on the fault position is a result of the fuzzy comparison determined with the following relationship:

$$W = \frac{F_1}{F} \quad (3)$$

where:

F – area below the membership function $\mu(\varphi)$,

F_1 – area obtained from F by limiting it with the applied setting (Fig. 3).

If the ratio (3) exceeds the specified threshold, the decision is taken that a fault is in front of the compensating bank; otherwise a fault is classified as behind the bank.

III. SIMULATIONS AND TESTING CONDUCTED WITH USE OF MATLAB AND ATP-EMTP

The presented algorithm for detecting the position of the fault with respect to the compensating bank, in terms whether a fault occurred in front or behind the bank, has been tested and evaluated with the fault data obtained from versatile ATP-EMTP [4] simulations of faults in the test network (Table I).

The test power network contains the 400 kV, 300 km transmission line, compensated with a three-phase bank of series capacitors installed at mid-line. The compensation rate of 70% was assumed. MOVs installed in parallel to series capacitors were modelled as nonlinear resistors defined with the analytical characteristic and its parameters as given in Table I. The thermal protection (TP in Fig. 1) preventing the MOV from overheating was modelled as the component integrating the accumulated energy. After exceeding the set threshold for energy, the sparking of the associated air-gap undergoes, and the MOV becomes shunted. It has been checked that for the air-gap sparking does not take place prior to detecting a fault position. Thus, the thermal protection does not influence the algorithm.

The model includes the Capacitive Voltage Transformers (CVTs) and the Current Transformers (CTs). The analogue filters with 350 Hz cut-off frequency were also included. The sampling frequency of 1000 Hz was applied.

Faults, occurring in front and behind the compensating bank, of different specifications have been modelled:

- distance to fault – 17 values: 30, 40, 45, 50, 60, 90, 120, 149, 151, 180, 210, 240, 250, 255, 260, 270, 290 [km],
- fault resistance:
for faults L-E and L-L-E – 5 values: 0.1, 5, 10, 25, 50 [Ω],
for faults L-L, L-L-L (L-L-L-E) – 5 values: 0.1, 0.5, 1, 2, 5 [Ω],
- point on the wave at which the fault is applied – 10 cases: by changing the angle from 0° (at zero crossing) up to 90° (at maximum),
- angle of EMFs at the end A was set as $\varphi=0^\circ$ (the cosine wave with zero phase shift in the phase a), while for the end B – 4 cases: -20° , -15° , 15° , 20° .

TABLE I
BASIC PARAMETERS OF THE TEST TRANSMISSION NETWORK

Equivalent system at terminal A ($\varphi=0^\circ$)	Z_{ISA}	$(0.656+j7.5) \Omega$
	Z_{OSA}	$(1.167+j11.25) \Omega$
Equivalent system at terminal B ($\varphi=-15^\circ$)	Z_{ISB}	$(1.31+j15) \Omega$
	Z_{OSB}	$(2.33+j26.6) \Omega$
Line AB	Z'_{IL}	$(0.028+j0.315) \Omega/\text{km}$
	Z'_{OL}	$(0.275+j1.027) \Omega/\text{km}$
	C'_{IL}	13.0 nF/km
	C'_{OL}	8.5 nF/km
Series compensation	Series capacitors	0.70 X_{IL}
	Position of the compensating bank	0.5 p.u.
MOV characteristic:	P	1 kA
	V_{REF}	150 kV
	q	23
$i_{MOV} = P \left(\frac{V_V}{V_{REF}} \right)^q$		
Line length		300 km
System voltage		400 kV

The presented algorithm for detecting the fault position (as in Fig. 2) has been reflected in MATLAB [5] environment. The sample obtained results are shown in Fig. 4–Fig. 5.

The example 1, for which the relay input currents are presented in Fig. 6, is for the fault F_A (occurring in front of the compensating bank) with the following specifications – fault distance: $d=0.2$ p.u., fault resistance: $R_F=5 \Omega$.

The example 2, for which the relay input currents are presented in Fig. 7, is for the fault F_B (occurring behind the compensating bank) with the following specifications – fault distance: $d=0.8$ p.u., fault resistance: $R_F=5 \Omega$.

The presented sample results illustrate effectiveness of the proposed detection algorithm. The results of the overall evaluation are gathered in Table II.

TABLE II
EFFICIENCY OF DETECTION OF FAULTS F_A, F_B

Fault type	Number of fault cases	Detection of faults F_A [%]	Detection of faults F_B [%]	Average time of detection [ms]
Phase-to-phase	10200	100	100	16
Double phase-to-earth	10200	100	100	17
Three phase	10200	100	100	15

F_A – fault in front of SCs/MOVs
 F_B – fault behind SCs/MOVs

In Fig. 6 (Example 1) the phase currents under a–b fault occurring in front of the compensating bank are shown. DC components are present in the currents from the faulted phases.

The phase shift is as the one presented by the curve F_A in Fig. 4.

In contrast, for the example 2 (fault occurring behind the compensating bank) the currents from the faulted phases are contaminated with the subharmonic oscillations (Fig. 7). The phase shift is as the one presented by the curve F_B in Fig. 4.

In Fig. 5 the decision signal for the example 1 is shown. The decision that this is a fault in front of the compensating bank (fault F_A) is reached after 16 ms from the fault inception.

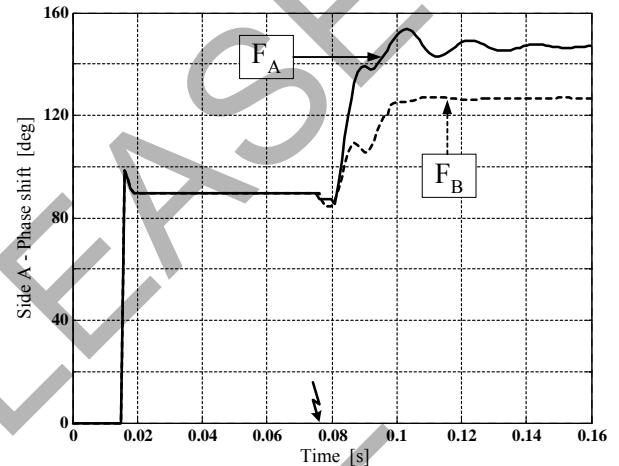


Figure 4. Typical shapes of phase shift: a) fault position in front of compensating bank (F_A), b) fault position behind compensating bank (F_B).

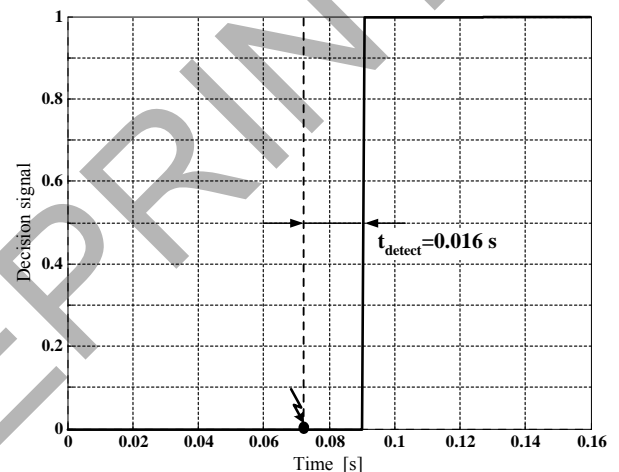


Figure 5. Example 1 – making a decision with utilizing the relationship (3).

For each fault type (phase-to-phase, double phase-to-earth and three phase faults) 30 600 cases were applied in evaluation of the fault position detecting algorithm.

All faults occurring in front of the compensating bank (fault F_A) and occurring behind the compensating bank (fault F_B) were successfully detected (100% efficiency). This concerns only inter-phase faults since in the case of single phase faults the recognition of fault position appeared as unreliable and thus these results are not shown here.

Average time of the fault position detection is around 16 ms. In order to get higher speed of detection, the other filtering

digital algorithm, as for example applying the half-cycle dc rejection [8] can be applied.

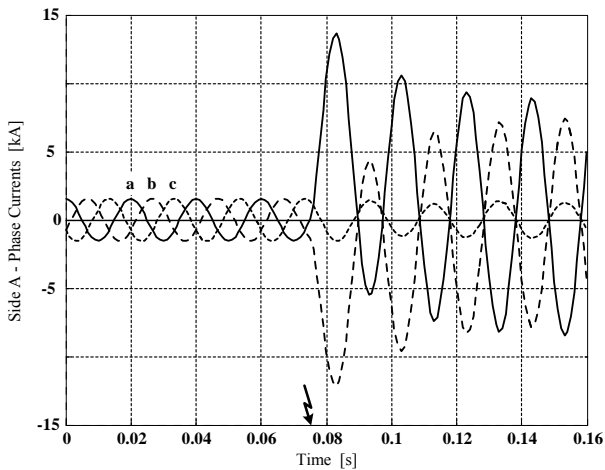


Figure 6. Example 1 – currents for fault in front of SCs&MOVs (fault F_A).

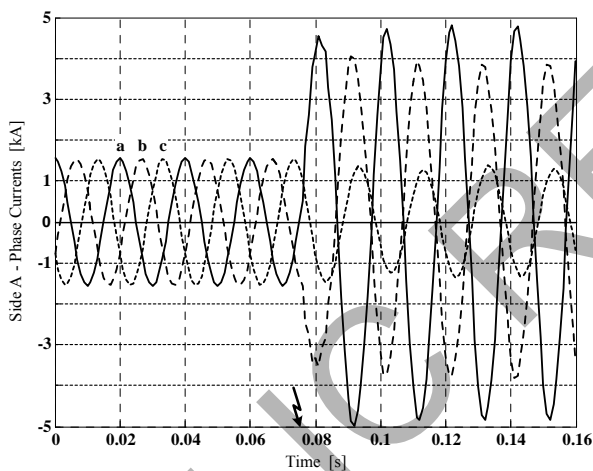


Figure 7. Example 2 – currents for fault behind SCs&MOVs (fault F_B).

IV. CONCLUSION

This paper presents the algorithm aimed at recognising the fault position with respect to the compensating device. The decision with respect to the fault position, i.e. whether a fault occurred in front of the bank or behind it is highly required for design of the adaptive distance relay. Knowledge of the fault position allows making the distance relay adaptable to presence of the compensating bank in the fault loop. There is a need for reflecting the presence of SC&MOV (or SCs&MOVs in the case of inter-phase faults) in the fault loop, considered by the distance relay under faults occurring behind the compensating bank. For this purpose, the differential equation or fundamental frequency equivalent approaches, known from the numerous references, can be applied. By reflecting the presence of SCs&MOVs in the fault loop (for faults occurring behind them) the quality of distance protection can be substantially improved. In particular, one can avoid shortening of the reach for the high-speed first zone.

Autorzy pragną podziękować Ministerstwu Nauki i Szkolnictwa Wyższego za finansowanie prac badawczych z zakresu adaptacyjnych zabezpieczeń prowadzonych w ramach projektu badawczego N511 008 32/1688

The presented algorithm for detecting the position of the fault with respect to the compensating device is based on exploring the change of the phase shift for the protective relay input currents. The decision with respect to the fault position is made using fuzzy logic reasoning.

The delivered algorithm has been tested and evaluated with the fault data obtained from versatile ATP-EMTP simulations of faults in the test power network with the 400 kV, 300 km transmission line. Different specifications of faults and pre-fault power flows (in total, above 30 thousand cases) have been considered in the evaluation study.

Application of fuzzy logic appeared as the tool which allowed obtaining efficient detection of the fault place. Inter-phase faults occurring behind and in front of SCs&MOVs have been detected perfectly correct (100%).

It is expected that in future research on the issue of detecting the faulted section of the series compensated line, a multi-criteria algorithm will be developed. It seems that only multi-criteria approach can assure completely correct recognition of the fault position, for very wide range of specifications of faults and the transmission network parameters. This is so also since the position of single phase-to earth faults is not well recognised with the presented algorithm.

V. REFERENCES

- [1] B. Bachmann, D. Novosel, D. Hart, Y. Hu and M. M. Saha, "Application of artificial neural networks for series compensated line protection," in *Proc. of the International Conference on Intelligent Systems Applications to Power Systems*, Orlando, FL, pp. 68–73, Jan. 28–Feb. 02, 1996.
- [2] CIGRE SC-34 WG-04, *Application guide on protection of complex transmission network configurations*, CIGRE materials, August 1990.
- [3] P. K. Dash, S. R. Samantaray and G. Panda, "Fault classification and section identification of an advanced series-compensated transmission line using support vector machine," *IEEE Trans. on Power Del.*, vol. 22, no. 1, pp. 67–73, Jan. 2007.
- [4] H. W. Dommel, *Electro-Magnetic Transients Program*, BPA, Portland, Oregon, 1986.
- [5] MATLAB, High-performance numeric computation and visualization software. External interface guide, The Mathworks, Inc., January 1993.
- [6] W. Rebizant, A. Wiszniewski and L. Schiel, "Acceleration of transformer differential protection with instantaneous criteria," in *Proc. Advanced Power System Automation and Protection*, Jeju, Korea, April 24–27, 2007.
- [7] E. Rosolowski, J. Izykowski and B. Kasztenny, "A new half – cycle adaptive phasor estimator immune to the decaying dc component for digital protective relaying," in *Proc. of North America Power Systems (NAPS) Conference*, University of Waterloo, Canada, October 23–24, 2000.
- [8] E. Rosolowski, J. Izykowski, B. Kasztenny and M. M. Saha, "A new accurate fault algorithm for series compensated lines," *IEEE Trans. on Power Del.*, vol. 14, no. 3, pp. 789–795, Jan. 1999.
- [9] A. Wiszniewski, B. Kasztenny, "A multi-criteria differential transformer relay based on fuzzy logic," *IEEE Trans. on Power Del.*, vol. 10, no. 4, pp. 1786–1793, Oct. 1995.
- [10] A. Wiszniewski, J. Szafran, "Algorytmy pomiarowe i decyzyjne cyfrowej automatyki elektroenergetycznej." ("Measuring algorithms and decisions digital power system automation") WNT Warszawa 2001 – book in polish.
- [11] Q. Y. Xuan, Y. H. Song, A. T. Johns, R. Morgan and D. Williams, "Performance of an adaptive protection scheme for series compensated EHV transmission systems using neural networks," *Electric Power System Research*, vol. 36, no. 1, pp. 57–66, Jan. 1996.

Lightning Protection of Aircraft

Lukasz Mackowiak
Wroclaw University of Technology
Wybrzeze Wyspianskiego 27
Wroclaw, Poland

Abstract - this paper concerns lightning phenomenon and methods of aircraft protection against the lightning effects .

I. INTRODUCTION

It is estimated that on average, each airplane in the U.S. commercial fleet is struck lightly by lightning more than once each year. In fact, aircraft often trigger lightning when flying through a heavily charged region of a cloud. In these instances, the lightning flash originates at the airplane and extends away in opposite directions. Although record keeping is poor, smaller business and private airplanes are thought to be struck less frequently because of their small size and because they often can avoid weather that is conducive to lightning strikes. The last confirmed commercial plane crash in the U.S. directly attributed to lightning occurred in 1967, when lightning caused a catastrophic fuel tank explosion. Since then, much has been learned about how lightning can affect airplanes. As a result, protection techniques have improved. Today, airplanes receive a rigorous set of lightning certification tests to verify the safety of their designs. Although passengers and crew may see a flash and hear a loud noise if lightning strikes their plane, nothing serious should happen because of the careful lightning protection engineered into the aircraft and its sensitive components.[6]

II. LIGHTNING PROTECTION REQUIREMENTS

For modern transport aircraft, the ANAC (Civil Aviation National Agency), FAA (Federal Aviation Administration) and EASA (European Aviation Safety Agency) include the Requirements:

- 25.581 for structural parts lightning protection,
- 25.901 and 25.903 for engines,
- 25.954 for fuel system lightning protection,

Also SAE's (Society of Automotive Engineers) Aerospace Recommended Practices 5412, 5413 and 5414 are extensively used as the basis for the current aircraft lightning environment definition and for compliance demonstration. SAE has emitted ARP 5412 regarding lightning environment and waveforms, and ARP 5413 that provides guidance for compliance with indirect effects of lightning regulations. In addition to the 25.1301 and 25.1309 current airworthiness requirements, the ANAC, FAA and EASA have emitted 25.1316 requirement, which define operation condition for electrical-electronic system level A (critical system) and level B /C (essential system).

The requirements of EMI (Electromagnetic Interference) and lightning direct and indirect effects are complied by

incorporating, since the early design phases, special electrical bonding and EMI shielding protection devices and techniques:

- Metal parts electrical bonding is extensively used;
- Composite materials parts include embedded expanded copper foil and specially developed electrical bonding interfaces to metal structure;
- Wiring harnesses are segregated by separately routing the different EMI categories of signal and power leads and shield termination make extensive use of 360 degrees termination and bonding to connector backshells.

The use of the composite material in fuel tanks and fuel system are in development, where special attention will be given to protection against lightning direct effects.[1,3]

III. LIGHTNING PHENOMENON

Lightning is an atmospheric discharge of electricity, which typically occurs during thunderstorms, and sometimes during volcanic eruptions or dust storms. In the atmospheric electrical discharge, a leader of a bolt of lightning can travel at speeds of 60,000 m/s (220,000 km/h), and can reach temperatures approaching 30000 °C. There are some 16 million lightning storms in the world every year. An average bolt of lightning carries an electric current of 40 kA, and transfers a charge of five coulombs and 500 MJ. Large bolts of lightning can carry up to 120 kA and 350 coulombs. The voltage depends on the length of the bolt, with the dielectric breakdown of air being three million volts per metre; this works out to approximately 1GV for a 300 m lightning bolt. With an electric current of 100 kA, this gives a power of 100 terawatts.[7]

The lightning current consists of 4 components (Fig. 1):

- Component A appears during initial stroke. The peak amplitude of this component is equal 200kA \pm 10% with time duration \leq 500 μ s.
- Component B is an intermediate current with average amplitude about 2kA. The maximum charge transfer for this component is 10 coulombs.
- Component C is a continuing current with amplitude in the range 200-800A. Charge transfer is equal 200 coulombs \pm 20%.
- Component D appears during restrike. The peak amplitude of this component is equal 100kA \pm 10% with time duration \leq 500 μ s.

Those current components described above may be utilized for analyses or test purposes, or for combinations thereof to assess the potential lightning effects on the aircraft structure or system, and verify adequacy of protection designs.

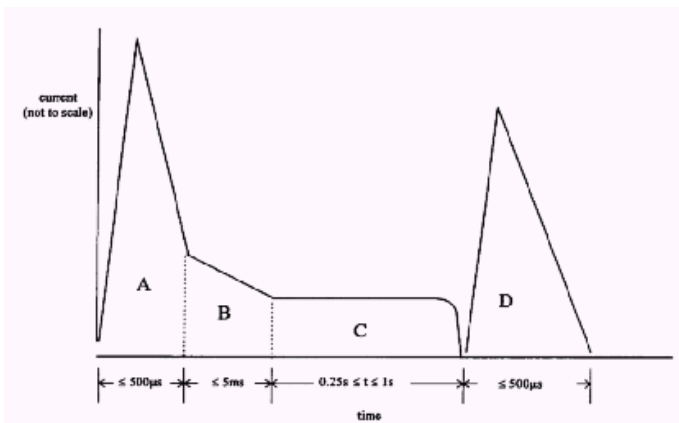


Figure 1. Lightning current components [1].

The lightning effects to which aircraft are exposed are divided into direct effects and indirect effects. Direct effects are physical effects to the aircraft and/or equipment due to the direct attachment of the lightning channel and/or conduction of lightning current and its high power and short time transient. This includes dielectric puncture, blasting, bending, melting, burning and vaporization of surfaces and structures. It also includes directly injected voltages and currents in associated wiring, plumbing, and other conductive components. The thermal effects at the arc attachment and the high current flowing in adjacent structures can produce direct damage. For example, the heating and mechanical effects of the strike could result in the puncture of thin fuel tank skins or damage to control wires. Shock waves may shatter thin panels and the huge magnetic forces derived from the lightning currents may buckle metalwork and snap bonding braids. In addition, the radome, which is a non-conducting aerodynamic fairing over the weather radar, might be punctured and shattered by a lightning strike. A further effect resulting from a strike is the occurrence of sparks which might be generated on the inside of a fuel tank by the passage of the current. These sparks could ignite the fuel/air vapour present resulting in fires and explosions. Indirect effects are resulting predominantly from the interaction of the electromagnetic fields accompanying lightning with electrical apparatus in the aircraft. When the aircraft is struck by lightning, it becomes part of the lightning channel. Lightning could flow into an attachment point such as a wing tip and out from another such as a tail fin. A large current pulse is thus driven through the aircraft enveloping it in a large and changing magnetic field which can induce voltages in the long wire and cable runs which are routed throughout the aircraft. The field penetrates the aircraft by "electromagnetic windows" such as the cockpit windshield. Unless protective measures are taken, induced voltages and currents can easily be large enough to destroy electrical components or disrupt electronic and computer systems. It is the same changing fields which generate the clicks heard on the radio even hundreds of miles from the lightning source. [1][2]

To analyze of the lightning effect is necessary to determine the aircraft surfaces, or zones, where lightning strike attachment to the aircraft is more or less probable.

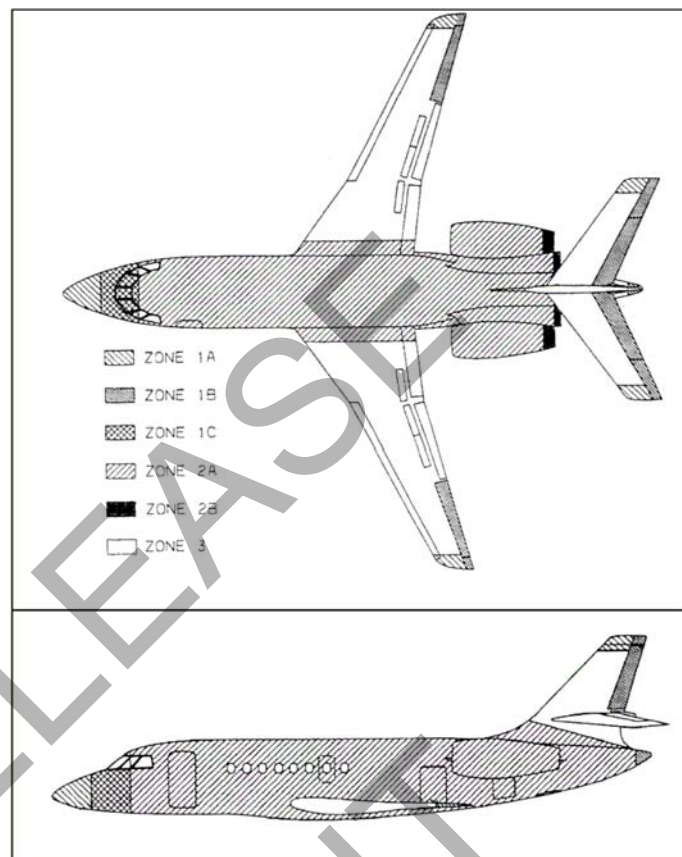


Figure 2. Example of lightning strike zone details for Transport Aircraft [3]

The Federal Aviation Administration has defined the following zones in its Advisory Circular AC 20-53A and in a proposed draft AC 20-53B associated with specific external lightning waveforms.

The specific zones definitions are as follows [3]:

- Zone 1A: Initial attachment point with low possibility of lightning channel hang-on.
- Zone 1B: Initial attachment point with high possibility of lightning channel hang-on.
- Zone 2A: A swept-stroke zone with low possibility of lightning channel hang-on.
- Zone 2B: A swept-stroke zone with high possibility of lightning channel hang-on.
- Zone 3: Portions of the airframe that lie within or between the other zones, which may carry substantial amounts of electrical current by conduction between areas of direct or swept stroke attachment points.

The advisory circulars do not prescribe the actual locations of these zones on a particular aircraft since they depend critically upon the geometry of the aircraft, materials and operational factors. However, they give generic examples for different classes of aircraft (large jets, small single and twin-engine propeller aircraft, helicopters).

IV. LIGHTNING PROTECTION

It is true that some aircraft are less prone to lightning strikes. Size, shape, and speed are all aircraft-specific variables which determine an aircraft's susceptibility to a lightning strike. However, it is also true that all aircraft damage varies with aircraft type. Careful aircraft design can minimize lightning damage. [4]

Some pilots are better at avoiding lightning strikes than others, but all of them have to remember some basic rules about flying. Those rules can help to avoid the lightning strikes.

- The most important thing is to stay clear of thunderstorms. Do not attempt to "pick your way through".
- The higher the aircraft altitude, the farther away from a thunderstorm you should fly. Lightning strikes have been known to occur in the clear air up to 80km downwind from the nearest thunderstorm.
- At low levels, avoid flying close to high surface features (ridge tops, towers, etc.), or between such features and an overhead thunderstorm.
- If you fly above the freezing level in or near thunderstorms, you can trigger an in-cloud or cloud-to-cloud discharge. If you fly below the freezing level, you could be involved with a cloud-to-ground lightning strike. Overall, if you must penetrate or fly close to a thunderstorm system, you can expect more strikes penetrating a thunderstorm area well above the freezing level.
- Lightning damage is usually worse for large total current transfers. At altitudes above the freezing level, you are more likely to experience longer-lasting lightning attachments made up of numerous small pulses and large total current transfer. Below the freezing level, you are more likely to experience shorter lightning attachments with a few strong current pulses; however the total current transfer is usually less than that above the freezing level.
- Electrical activity generated by a thunderstorm may exist even after the thunderstorm cell has destroyed. Therefore, avoid penetrating the cirrus decks that were recently associated with thunderstorms.[4]

The complying of above rules can be treated as a first level of aircraft lightning protection. If the pilots remember above rules the probability of lightning strike to the aircraft will be lower. Unfortunately, this probability will never be equal zero, therefore we have to apply some protection system or devices against direct and indirect effects of lightning strikes. The most popular protection system against lightning strikes is Lightning Diversion Strips LDS. Lightning Diversion System has developed a new and improved lightning protection device that diverts lightning strokes from aircraft nose radomes and other sensitive areas. The protection system consists of a segmented diverter strip which provides maximum multiple-strike protection.

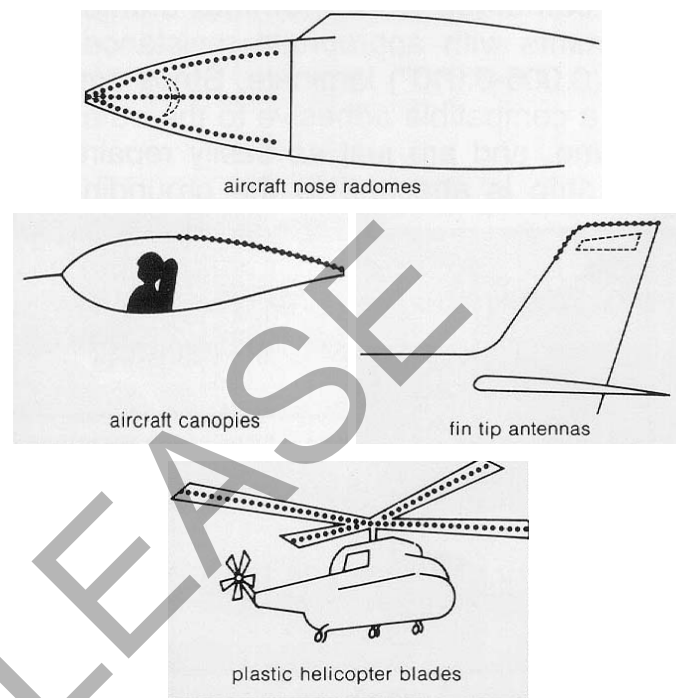


Figure 3. Application of LDS [8]

Attached to an aircraft's radome, the system allows a lightning stroke to travel safely and directly to ground in an ionized channel created in the air above the diverter strip. It combines permanent protection with a low drag aerodynamics and has insignificant effect on radar antenna radiation patterns. The electrostatic shield created by the system provides a new source of streamers outside the radome wall to the fuselage. The small diameter of the disc segments makes the strip compatible with radar system operation. If necessary, disc size can be reduced for optimum antenna patterns at higher frequencies.[8]

To protect an electrical devices we can apply surge suppressors. For example the 115 VAC high energy surge suppressor combines in one unit the low clamping voltage and high surge current capabilities needed to protect solid state power and electronic systems from severe lightning-induced and other over-voltage surges. This suppressor meets the need for low clamping voltage and exceptionally high surge current capability packaged in a single, small size unit. The suppressor is packaged to withstand rugged airborne and ground-based environments and will clamp repetitive high energy transients. The 115 VAC high energy surge suppressor is especially suitable for clamping lightning-induced surges appearing on aircraft 115 volt AC power distribution busses feeding solid-state avionics. The suppressor clamps the high energy surges to levels easily tolerated by most solid state power supply inputs without interruption of power or tripping of circuit breakers. Its surge current capability exceeds that of many spark-gap devices, and its response ("turn on") time is virtually

instantaneous. The suppressor meets applicable requirements of most aircraft power quality specifications. [8]

Applications of surge suppressors in aircrafts:

- Primary power distribution busses.
- Secondary power distribution circuits, at utilization equipment.
- Externally mounted electrical apparatus (windshield and air data probe heater circuits, navigation lights, and electrical de-icing systems.)
- AC power and control circuits within advanced composite airframes

V. CONCLUSIONS

According to [5], lightning aircraft incidents most often occur when the air temperature is in the range of -5 to 0°C. Lightning incidents frequency depend on altitude and season, thus in winter more incidents happen at about 1km above sea level and in summer more incidents occur at about 5km above sea level. Taking into account that pilots know this information and rules from chapter IV, flying by plane should be very safe. And it is. But sometimes thunderstorm can surprise even the best of pilot. Therefore all kinds of airships have to fulfill a lot of lightning protection requirements. But we have to remember, that even the best lightning protection system does not replace the human being. Thus, in my opinion if the pilot sees a thunderstorm he should change flight direction to bypass this hazard.

REFERENCES

- [1] S. A. Baldacim, N. Cristofani, J.L.F. Junior, J.R. Lautenschlager, "Lightning effects in aircraft of the composite material," 17^o CBECIMat - Congresso Brasileiro de Engenharia e Ciência dos Materiais, 15 a 19 de Novembro de 2006, Foz do Iguaçu, PR, Brasil
- [2] John Hardwick "Protect and survive", Aircraft Engineering and Aerospace Technology, Volume 69 · Number 5 · 1997 · 428-431
- [3] Alain Broc, Philippe Lalande, Emmanuel Montreuil, Jean-Patrick Moreau, "A lightning swept stroke model: A valuable tool to investigate the lightning strike to aircraft", Aerospace Science and Technology 10 (2006) 700–708
- [4] Anonymous, "New research produces new information about aircraft and lightning strikes", Flying Safety; Aug 1997; 53, 8; Career and Technical Education, pg. 29.
- [5] Rakov, V. A., Uman, M. A., "Lightning: Physics and Effects", Cambridge University Press, UK 2003.
- [6] <http://www.sciam.com>
- [7] <http://en.wikipedia.org>
- [8] <http://www.lightningdiversion.com>

Elimination of Chaotic Ferroresonance in power transformers including Nonlinear Core Losses applying of Neutral Resistance

A.Abbasi **M.Rostami** **H.Radmanesh** **H.Abbasi**
abbasi@shahed.ac.ir Rostami@shahed.ac.ir hamid.nsa@gmail.com H.abbasi@gmail.com

Faculty of Engineering,
Shahed University,
Khalig-e-Fars free way,
1417953836 Tehran, Iran,
P.O. Box: 18151/159,

Tel: (+98-21)66639821, Fax: (+98-21)51212105, Tehran, Iran

Abstract

This paper studies the effect of neutral resistance on the onset of chaotic ferroresonance and chaotic transient in a power transformer including nonlinear core losses. It is expected that this resistance cause ferroresonance 'dropout'. Time-domain study has been carried out to study this effect. Simulation has been done on a three phase power transformer rated 50 MVA, 635.1 kV with one open phase. The magnetization characteristic of the transformer is modeled by a single-value two-terms polynomial. The core loss is modeled by third order power series in terms of voltage includes nonlinearities in core model. The simulation results reveal that connecting the neutral resistance to the transformer, exhibits a great mitigating effect on voltage ferroresonance. Phase plane along with bifurcation diagrams are also derived. Having Significant effect on the onset of chaos, the range of parameter values that may lead to chaos along with ferroresonance voltages has been obtained and presented.

Key word: Chaos, Bifurcation diagram, Ferroresonance, Power transformer, Neutral Resistance

1. Introduction

Ferroresonance may be initiated by switching actions, or load shedding in power system. It can produce unpredictable over voltages and high currents. The prerequisite for ferroresonance is a circuit containing nonlinear iron core inductance and a capacitance. Such a circuit is characterized by simultaneous existence of several steady-state solutions for a given set of circuit parameters. The abrupt

transition or jump from one state to another is triggered by a disturbance, switching action or a gradual change in system parameters.

Typical cases of ferroresonance are reported in [1], [4]. Theory of nonlinear dynamics has been found to provide deeper insight into the phenomenon [5].

Fundamental theory of nonlinear dynamics and chaos can be found in [4], [7]. The susceptibility of a ferroresonance circuit to a quasiperiodic and frequency locked oscillations are presented in [8], [9]. The effect of initial conditions which is investigated. [10] is a milestone contribution

highlighted the effect of transformer modeling on the predicted ferroresonance oscillations. Using a linear model, [11] has shown the effect of core loss in damping ferroresonance oscillations. Reference [12] emphasizes treating core loss as a nonlinear function of voltage. An algorithm for calculating core losses based on no-load characteristics of transformer is given in [13]. The mitigating effect of transformer connected in parallel to a MOV arrester is illustrated in [14]. Effect of circuit breaker grading capacitance on ferroresonance in VT is investigated in [15]. In all previous studies, the effects of neutral resistance including nonlinear core losses are neglected. In these works, it has been shown that nonlinear core loss can decrease ferroresonance phenomena in power transformer. Later, the effect of neutral resistance on power transformer including linear core loss has been investigated [16]. Current paper studies the effect of neutral

resistance on the global behavior of a ferroresonance circuit with nonlinear core loss.

1. System Modeling (Base System)

System Modelling Without Neutral Resistance in Transformer is assumed to be connected to the power system while one of the three circuit breaker poles is open and only two phases of it are energized, which produces induced voltage in the open phase. This voltage, back feeds the line, and consequently ferroresonance will occur if the distribution line is enough capacitive. System involves the nonlinear magnetizing reactance of the transformer's open phase and resulted shunt and series capacitance of the distribution line.

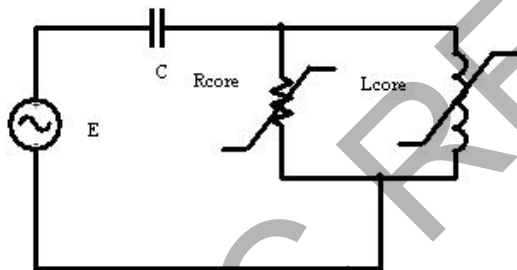


Fig 1. Equivalent circuit of system

Fig.1. shows the equivalent circuit of system described above. The magnetization branch is modelled by a nonlinear inductance in parallel with a nonlinear resistance accordingly represent the nonlinear saturation characteristic $\lambda - i_{Lm}$ and nonlinear hysteresis and eddy current characteristics ($v_m - i_{Rm}$), respectively. The hysteresis and eddy current characteristics of core can be obtained from no-load states of transformer by applying the algorithm given in [13]. The iron core saturation cure characteristic is given by:

$$i_{Lm} = s_1 \lambda + s_2 \lambda^q \quad (1)$$

Exponent q depends on the degree of saturation. It has been found that for adequate representation of the saturation characteristics of a power transformer the exponent q may acquire values 5, 7, and 11. Fig.2 shows iron core characteristic for $q=5, 7, 11$.

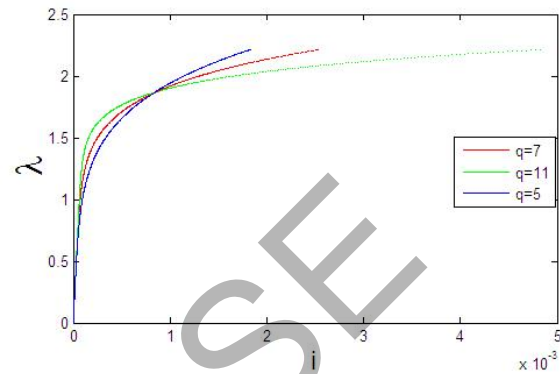


Fig. 2. Nonlinear characteristics of transformer core with different values of q

Beside, to study the case, the core loss model is formulated by a third order power series with coefficients, fitted to match the hysteresis and eddy current nonlinear characteristics given in [1]:

$$i_{Rm} = h_0 + h_1 v_m + h_2 v_m^2 + h_3 v_m^3 \quad (2)$$

Per unit value of i_{Rm} is given in (3)

$$i_{Rm} = -.000001 + .0047V_m - .0073V_m^2 + .0039V_m^3 \quad (3)$$

The differential equation for the circuit in fig. 1 neglecting neutral resistance can be presented as follows:

$$V = \frac{d\lambda}{dt} \quad (4)$$

$$\dot{V}_c = \frac{1}{C} (h_0 + h_1 V + h_2 V^2 + h_3 V^3 + a\lambda + b\lambda^q) \quad (5)$$

$$dE - \dot{V}_c - \dot{V}_L = 0 \quad (6)$$

$$dE - \frac{1}{C} (h_0 + h_1 V + h_2 V^2 + h_3 V^3 + a\lambda + b\lambda^q) = \frac{d^2 \lambda}{dt^2} \quad (7)$$

Where E is the peak value of the voltage source, shown in fig.1.

Typical values for system parameters without neutral resistance are as follows:

$$\text{for } q = 11 \quad s_1 = .0067, s_2 = .0001$$

$$\text{for } q = 7 \quad s_1 = .0067, s_2 = .001$$

$$\text{for } q = 5 \quad s_1 = .0071, s_2 = .0034$$

$$\omega = 377 \text{ rad/sec}$$

$$R = 8067\Omega$$

$$C_{pu} = 0.7955$$

$$V_{base} = 635.1 \text{ kV}, I_{base} = 78.72 \text{ A}$$

And initial conditions are:

$$\lambda(0) = 0.0; \quad p\lambda(0) = \sqrt{2}$$

1.1. Simulation Results

Table 1 shows different values of E, considered for analyzing the circuit in absence of neutral resistance.

Table 1: Simulation results (Without Neutral Resistance)

q/ E	1	3	5	7	9	10
5	P 2	P2	P3	P6	Chaot ic	P9
7	P 2	P2	P3	chaotic	Chaot ic	Chaot ic
11	P 2	P3	chaoti c	chaotic	P4	P4

*Pi: Period i

Fig.3, 4, and 5 show the phase plane plot of system states without neutral resistance For E=3 p.u. Figs.6, 7 and 8 show the corresponding bifurcation diagrams of system states without neutral resistance and including nonlinear core losses for q=5, 7, 11 which depicts chaotic behaviour.

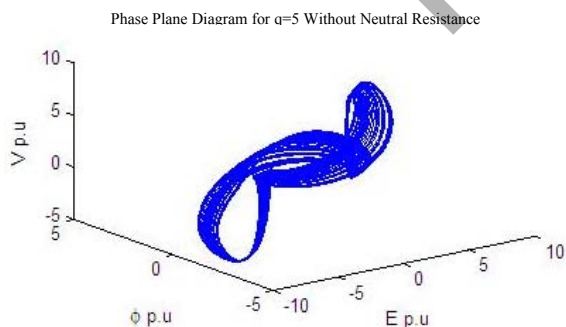


Fig. 3. Phase Plane diagram of system with q=5, without neutral resistance

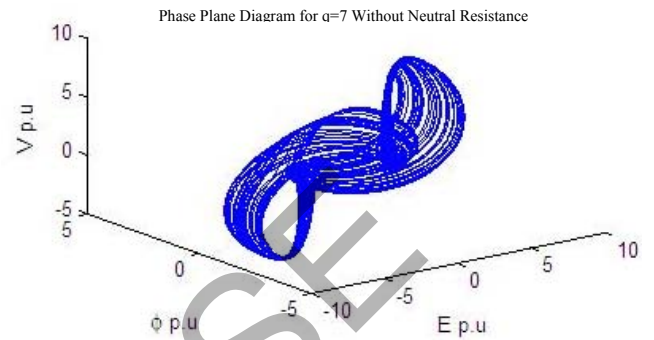


Fig 4. Phase Plane diagram of system with q=7, without neutral resistance

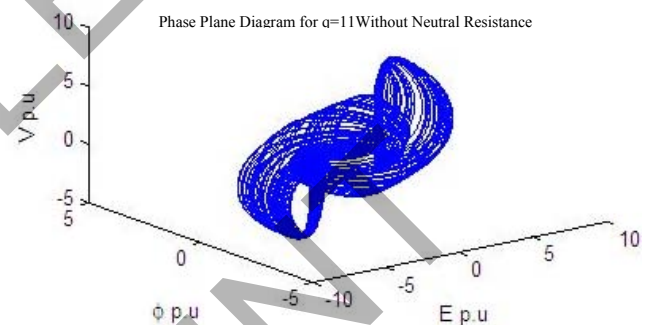


Fig 5. Phase Plane diagram of system with q=11, without neutral resistance

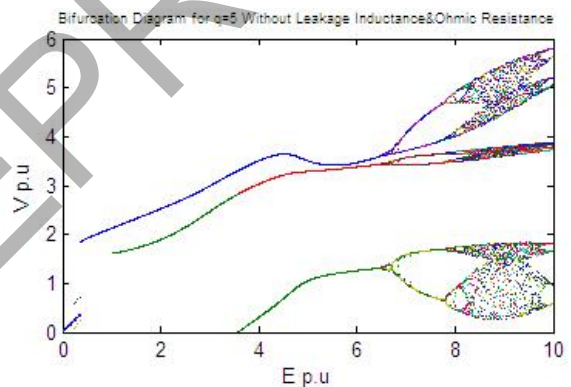


Fig 6. Bifurcation diagram with q=5, without neutral resistance

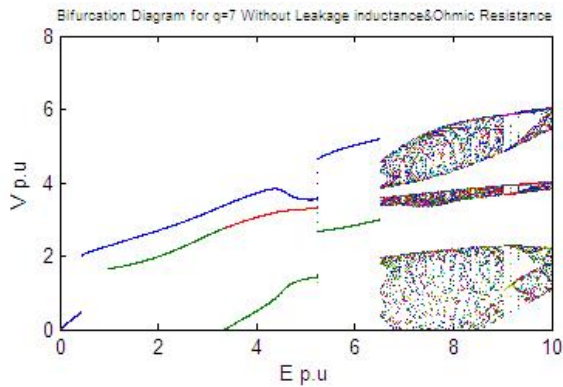


Fig 7. Bifurcation diagram with q=7, without neutral resistance

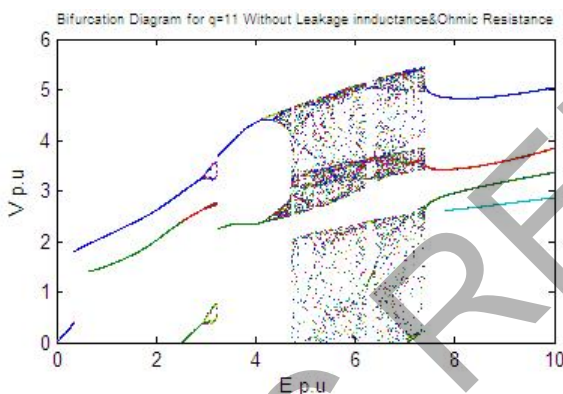


Fig 8. Bifurcation diagram with q=11, without neutral resistance

2. System modeling with neutral resistance

Including Neutral resistance, system of fig 1, can be Modified as shown in fig 9.

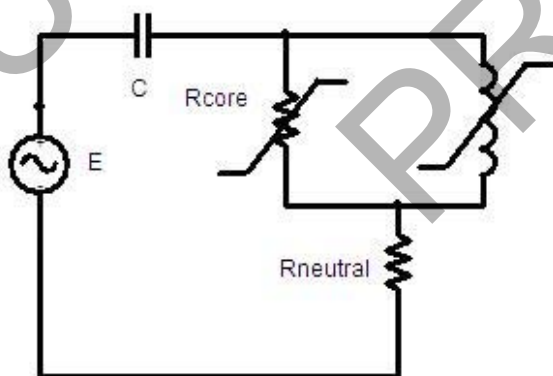


Fig. 9. Equivalent circuit of system with neutral resistance

Typical values for various system parameters has been considered for simulation kept the same by case 1, while neutral resistance has

been added to the system and its value is given below:

$$R_{neutral} = 40k\Omega$$

The differential equation for the circuit in fig.9 can be presented as follows:

$$dE - \dot{V}_c - \dot{V}_{R_{neutral}} - \dot{V}_L = 0$$

$$dE - \frac{1}{C}(h_0 + h_1V + h_2V^2 + h_3V^3 + a\lambda + b\lambda^q) -$$

$$R_{Neutral} \left(+h_1 \frac{d^2\lambda}{dt^2} + 2h_2 \frac{d^2\lambda}{dt^2} \frac{d\lambda}{dt} + 3h_3 \frac{d^2\lambda}{dt^2} \left(\frac{d\lambda}{dt} \right) + \right.$$

$$\left. a \frac{d\lambda}{dt} + qb \frac{d\lambda}{dt} \lambda^{q-1} \right) = \frac{d^2\lambda}{dt^2}$$

Where λ is the flux linkage and V, is the voltage of transformer

Initial conditions:

$$\lambda(0) = 0 \quad p\lambda(0) = \sqrt{2}$$

2.1. Simulation results

Fig.10 shows the corresponding phase plane diagram and Fig. 11 shows voltage wave form for system in fig.9 in case of q=11. Consequently figs.12, 13 and 14 shows bifurcation diagrams for corresponding system including neutral resistance. It can be seen that chaotic region mitigates by applying neutral resistance and there is no chaotic region. which means, tendency to chaotic behaviour reduces dramatically if neutral resistance effect been included.

Comparing to table 1 table 2 includes the results considering circuit with neutral resistance. Again, its clear that ferroresonance drop will be occurred.

Table 2: Simulation results (with neutral resistance)

q/E	1	2	3	4	5	6
5	P1	P1	P1	P1	P2	P2
7	P1	P1	P2	P3	P3	P3
11	P1	P1	P3	P3	P3	P3

*Pi: Period i

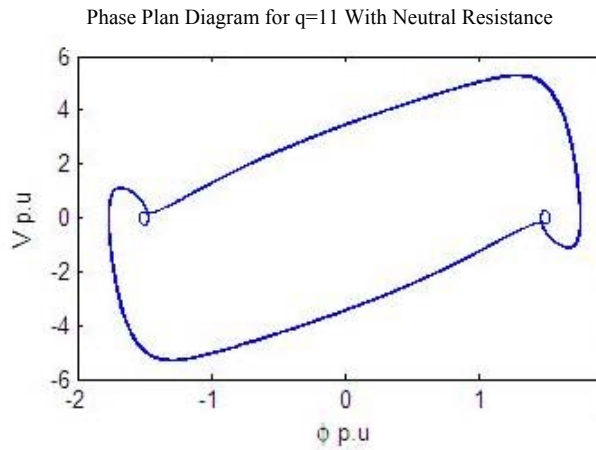


Fig 10. Phase Plan diagram of system with $q=11$, including neutral resistance

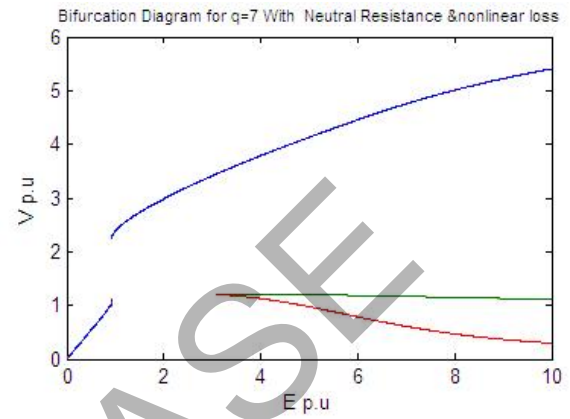


Fig 13. Bifurcation diagram with $q=7$, with neutral resistance

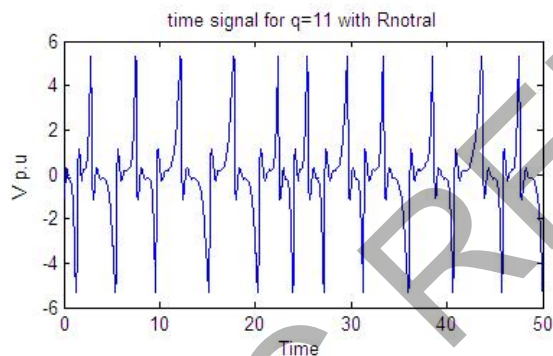


Fig 11. Time domain simulation with $q=11$, including neutral resistance

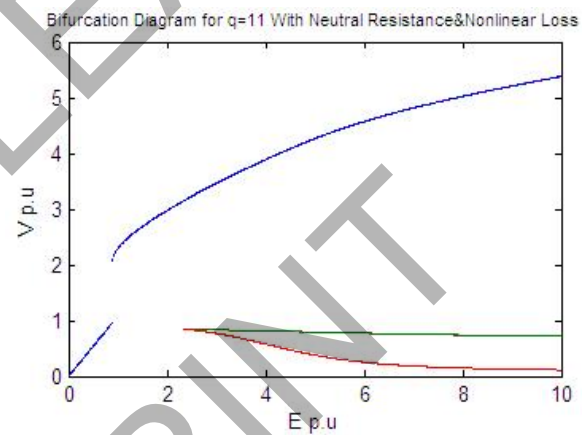


Fig 14. Bifurcation diagram with $q=11$, with neutral resistance

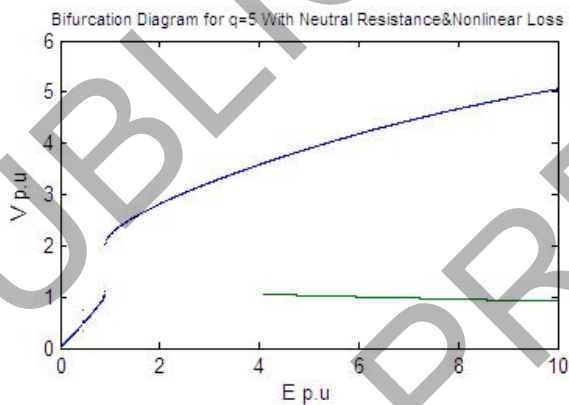


Fig 12. Bifurcation diagram with $q=5$, with neutral resistance

3. Conclusions

The dynamic behaviour of a transformer can be characterized by different presentation. Inclusion of nonlinearity in the core loss reveals that bifurcation diagrams will be smoother but more complicated when compared with linear models.

Adding Neutral resistance, It has been shown that system has been greatly affected by it. The presence of the neutral resistance results clamping the Ferroresonance over voltages in studied system. The neutral resistance successfully, suppresses the chaotic behavior of proposed model. Consequently, the system shows less sensitivity to initial conditions in the presence of the neutral resistance.

4. References

- [1] H.W. Dommel, A. Yan, R.J.O. De Marcano, A.B. Miliani, in:H.P. Khincha(Ed.), Tutorial Course on Digital Simulation of Transients in Power Systems (Chapter 14), IISc, Bangalore, 1983,pp. 17_ 38.
- [2] E.J. Dolan, D.A. Gillies, E.W. Kimbark, Ferroresonance in a transformer switched with an EVH line, IEEE Transactions on Power Apparatus and Systems PAS-91 (1972) 1273_ 1280.
- [3] R.P. Aggarwal, M.S. Saxena, B.S. Sharma, S. Kumer, S. Krishan, Failure of electromagnetic voltage transformer due to sustained overvoltage on switching* an in-depth field investigation and analytical study, IEEE Transactions on Power Apparatus and Systems PAS-100 (1981) 4448_ 4455.
- [4] C. Kieny, Application of the bifurcation theory in studying and understanding the global behavior of a ferroresonant electric power circuit, IEEE Transactions on Power Delivery 6 (1991)866_ 872.
- [5] A.E. Araujo, A.C. Soudack, J.R. Marti, Ferroresonance in power systems: chaotic behaviour, IEE Proceedings-C 140 (1993) 237_ 240.
- [6] S. Mozaffari, S. Henschel, A.C. Soudack, Chaotic ferroresonance in power transformers, IEE Proceedings* Generation Transmission and Distribution 142 (1995) 247_ 250.
- [7] B.A. Mork, D.L. Stuehm, Application of nonlinear dynamics and chaos to ferroresonance in distribution systems, IEEE Transactions on Power Delivery 9 (1994) 1009_ 1017.
- [8] S.K. Chkravarthy, C.V. Nayar, Frequency-locked and quasi periodic (QP) oscillations in power systems, IEEE Transactions on Power Delivery 13 (1997) 560_ 569.
- [9] S. Mozaffari, M. Sameti, A.C. Soudack, Effect of initial conditions on chaotic ferroresonance in power transformers, IEE Proceedings* Generation, Transmission and Distribution 144(1997) 456_ 460.
- [10] B.A. Mork, Five-legged wound* core transformer model: derivation, parameters, implementation, and evaluation, IEEE Transactions on Power Delivery 14 (1999) 1519_ 1526.
- [11] B.A.T. Al Zahawi, Z. Emin, Y.K. Tong, Chaos in ferroresonant wound voltage transformers: effect of core losses and universal circuit behavioral, IEE Proceedings* Sci. Meas.Technol. 145(1998) 39_ 43.
- [12] IEEE Working Group on Modeling and Analysis of Systems Transients, M.R. Iravani, Chair, Modeling and analysis guidelines for slow transients* part III: the study of ferroresonance, IEEE Transactions on Power Delivery, 15 (2000) 255_ 265.
- [13] W.L.A. Neves, H. Dommel, on modeling iron core nonlinearities, IEEE Transactions on Power Systems 8 (1993) 417_ 425.
- [14] K. Al-Anbari, R. Ramanujam, T. Keerthiga, K. Kuppusamy, Analysis of nonlinear phenomena in MOV connected Transformers, IEE Proceedings* Generation Transmission and Distribution 148 (2001) 562_ 566.
- [15]: H.Radmanesh, M.Rostami,A.Abbasi; Effect of Circuit Breaker Shunt Resistance on Ferroresonance phenomena in Voltage Transformer, IEEE 2009 conference, Georgia,USA
- [16] H.Radmanesh,A.Abbasi M.Rostami. Analysis of Ferroresonance Phenomena in Power Transformers Including Neutral Resistance Effect, IEEE 2009 conference, Georgia,USA

Geothermal energy as renewable energy source

S. Kitscha, J. Schmeckeber, M. Steckel
BTU Cottbus
Cottbus, Germany

I. INTRODUCTION

The earth is a dynamic planet and can be described as a gigantic thermal engine. The available heat is called geothermal energy.¹ Geothermal energy is a renewable energy source just like wind, hydro or solar power. By using geothermal energy, greenhouse gas emissions can be reduced significantly. However, other than solar or wind power, geothermal energy is neither dependent on climatic influences, nor daytime or season and is available at almost any place and time. Although as a renewable energy source geothermal energy offers many advantages and is available at many potential sites, it has so only a comparatively low proportion of the total energy supply so far. As experts assume, geothermal energy consists of approximately 30% residual heat caused by the earth's formation process about 5 billion years ago, when gases, rocks and dust were condensed. In this process a huge amount of energy was released. Temperatures of about 6000 °C are reached in the earth's core.²

II. APPLICATION

Geothermal energy is generally subdivided into depth and near-surface geothermal energy. The near-surface geothermal energy is mainly used to heat or cooling buildings. However, the depth-geothermal energy primary generates electricity and heat in (for) power plants, since this method is too complex to be used for cooling or heating individual buildings. Depth-geothermal energy, based on its technical application, is further subdivided into hydrothermal geothermal energy, HDR systems and deep geothermal heat probes. Geothermal energy enables a supply of individual homes, mostly detached houses, independently from the main power supply network.³ In order to realize this, there are many different techniques available today, from which private households can to select the most effective according to their specific situation and region.

The heat pump is the heart of each individual plant. This heat pump receives the heat transfer medium that was headed by the ground. Then, the heat pump absorbs the heat and feeds the

storage tank from which the house's entire heating and hot water system is supplied. For security reasons, an additional boiler can be installed in the system. This is necessary because it might happen that the geothermal heat collectors are influenced by the seasons, so that during winters the energy from the ground is not sufficient in order to heat the building. The geothermal heat collectors are placed horizontally at 80 - 160 cm under the surface to be subject to weather conditions.⁴ The most widespread plant is the geothermal heat probe. When installing the geothermal heat probe, first a plastic tube bundle is inserted in a prepared hole. Then the ring area is sealed with a bentonite / cement / water mixture. The Plastic tube bundle contains a heat carrying liquid, usually water with an antifreeze. They are inserted 25 to 200 meters vertically into the floor and deliver a constant temperature level. Because a legal procedure is necessary for drilling holes into the soil deeper than 100m, most of these facilities do not exceed this limit. The heat transfer medium circulates inside the heat probes, continuously receiving heat from the ground and transporting it up to the heat pump. This method does not only provide heat (and energy) for individual houses but also supplies offices and commercial buildings, even apartment complexes or whole neighborhoods.⁵ Energy earthbound piles and static parts are needed for new buildings anyway. These parts can be equipped with heat exchanger tubes, so that combined with a heat pump buildings can be economically heated and cooled.

III. INVESTMENTS

Regarding the investments for a geothermal plant there are five points to consider. In the calculation the costs for official approvals, drilling (only for geothermal heat probes), the heat pump, a separate electric meter and several accessories need to be taken into account. The investments for these facilities are about € 15600-25150. Thus the costs for geothermal power plants are about € 3000-5000 higher than for gas- or oil-heaters. Since the investments for geothermal power plants are comparatively (quite) high, the government offers financial help to

Activity	Costs
Official approval	€ 500 – 1,500
Drilling	€ 60 - 90 per meter
Heat pump (to 17 kW)	€ 9,000 – 13,000
Accessories	€ 500 – 1,500
Electric meter	€ 500 – 1,500

Table 1: Overview about acquisition costs (2007)
(http://www.junkers.com/de/de/beratung/technik/wp/ewp/kosten/Standardpage_7.html)

support the installations of environmentally friendly equipment.⁶ Since 1.1.2008 the installation of heat pumps in the residential and commercial sector has been supported by the federal government.

IV. POTENTIAL

The geothermal energy offers a big potential as an alternative energy source for the future. To reach an exact appraisal of this form of power generation it is necessary to look at the energy-political aims. These aims concern the economic efficiency, environmental compatibility and last but not least the security of the energy supply. Concerning the environmental compatibility, the emission of greenhouse gases of alternative energy sources should be as low as possible which helps to protect the climate and environment with a friendly energy supply. The security of energy supply should be improved by the high-priority use of locally available resources. The steadily rising energy prices are in the focus of the economic efficiency and the alternative energy source should allow an increasingly economic use and offer independence from high energy expenses.⁷

In the following it is demonstrated to what extent the geothermal energy, as an alternative energy source, fulfill the energy-political objectives. A cost saving potential of approximately 80% was identified in comparison to fossil energy sources by the use of the geothermal energy. Furthermore the geothermal heating installation needs only small quantities in electric energy in comparison to gas heating installations or oil heating installations. It has to be mentioned here, that the effectiveness of this technology is a multiple higher than with fossil heating systems. A further advantage of these systems is that the whole installation could not only be used for heating in winter, but also for cooling in summer. Because of this advantage the user does not have to pay for an additional cooling system. Moreover the costs of maintenance are less expensive than for traditional heating systems. After some time it is only necessary to substitute filters of the heat pump and gaskets of the whole cycle system. Geothermal installations can be also installed in any building to any time

and they have a life span of approximately 50 years. However, negative points are the high costs and requirements for the building insulation. The requirements for the building's insulation are so high because geothermal systems heat a building substantially slower than customary systems and take a lot of time when the building has an insufficient insulation. Finally it is to be ascertained that this form of power production is absolutely economic.⁸

When you take a look to the environmental compatibility, a representation of the environmental consequences of the geothermal energy must follow. First, there should not be released any CO₂-emissions by the use of geothermal energy. The only component which needs electric energy is the heat pump. Because of this, the usage of this energy form is directly connected to the CO₂-intensive generation of electricity. Moreover share-fluoridated hydro-fluorocarbons (HFC) are used in heat pumps. These media do not attack the ozonosphere; nevertheless, they forward the greenhouse effect. If these HFCs reach the atmosphere the influence to the greenhouse effect is approximately 1500-3000 stronger than CO₂-emissions.⁹ Another disadvantageous is that with very low outside temperatures an additional heating system like gas- or oil heating is needed because the energy from the earth is not sufficient. There are often problems with the geothermal energy collectors, because these lie close under the earth's surface and can only record a relatively little warming up. At last it is ascertained that the geothermal systems are absolutely environment-friendly as an alternative energy source, but there is still a big need for action concerning the used cooling medium.

The security of the energy supply is for all systems guaranteed, when the geothermal energy is only used privately. Then there are no regional restrictions. Indeed, it is to be noticed, that at some places the geothermal energy cannot be used, even if the geologic conditions would be given. This is justified upon to the fact that geothermal energy probes and geothermal energy collectors needs a lot of space. A surface which is one and a half times larger as the surface to be heated is an approximate value. This is especially problematic for households which are based on a relatively small property. These households could install only smaller variations of this technology in the earth and use them merely for heating or cooling support which is economically questionable. So they have to abdicate of this alternative energy source. The application ranges of depth-geothermal energy are more limited than near-surface geothermal energy. This energy system type can be used for electricity and heat generation in power plants. But the

geothermal requirements must be given. This is only possible at places where the points of the tectonic disks are. Otherwise the bores are too deep in the earth and a cost-covering production is impossible. In summary geothermal energy is theoretically available everywhere, but in many areas there are restrictions for the use in private households.¹⁰

IV. SUMMARY

About 0.4% of the worldwide power generation is geothermal energy. The annual growth rate was stable in the last decade and is still at about 5.0% (about 200-250 MW capacity increase p.a.). Illustration 1 shows the previous development and the future trend in comparison to other energy forms. The geothermal capacity installed worldwide will exceed 10 GW (year 2008) soon, for 2010 the forecast is about 11 GW. Within the next 30 years an increase to about 85 GW is regarded as possible. The most important markets for this energy form are the USA, Philippines, Mexico, Indonesia, Japan, New Zealand, Italy and Iceland. Iceland is advancing the development of the geothermal capacity and the research very actively at present.

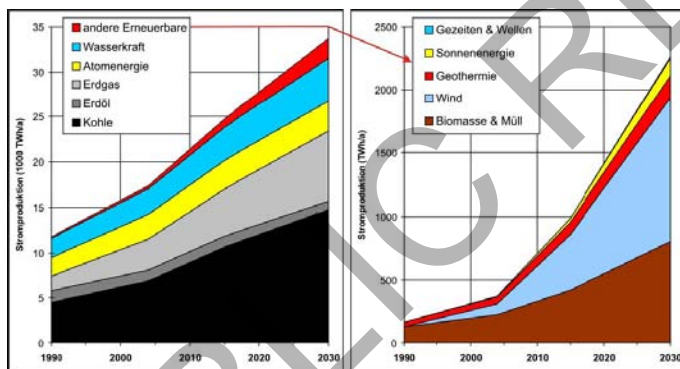


Illustration 1: Electricity generation (in TWh/a)-temporal development of the different energy sectors to 2005 and forecast to 2030 (http://www.eeg.tuwien.ac.at/events/iewt/iewt2009/papers/3D_4_PONWEISER_K_P.pdf)

The biomass still dominates globally the field of the warmth generation. By the increase in the world population the need for heated rooms and energy supply for the eating preparation also rises further strongly. For this 58% of renewable energies are used. The renewable energies which fundamentally contribute to the supply of useful heat are solar energy and geothermal energy. The capacity of the geothermal energy installed at present is only a third in comparison to the solar heat because of the higher degree of utilization the energy output is comparable. An increase for these energy forms around 10-fold at solar energy utilization and 6-fold at geothermal energy is forecast for the year 2030, how

illustration 2 shows. World market leaders in the area of direct use will be China, Sweden, the USA, Turkey, Iceland and Japan. Leading and at the same time the largest growth market is the People's Republic of China at this energy form. But Iceland is worldwide at first place with 25% of the electricity and 85% of the required space heating made out of geothermal energy.¹¹

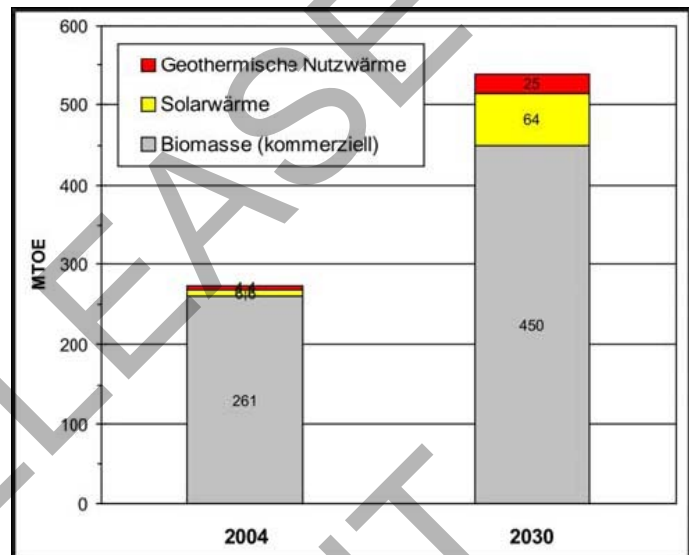


Illustration 2: Quota of the relevant energy sectors of the worldwide provision to geothermal using warmth (in MTOE) for 2004 and forecast for 2030 to IEA 2007 (http://www.eeg.tuwien.ac.at/events/iewt/iewt2009/papers/3D_4_PONWEISER_K_P.pdf)

The geothermal energy offers an enormous rate of potential for the generation of electricity and heat. The two and a half-fold amount of energy which the mankind needs rises from the inside of the earth daily. The geothermal energy is available every day and season and is independent of weather influences or climate conditions. The huge potential of this alternative energy source was recognized meanwhile and utilization was started. Nowadays geothermal energy gets more and more frequently in the focus of political discussions about the future energy supply. This has been the case since the costs for fossil fuels increase rapidly. Due to the long-term safeguarding of the geothermal energy as an alternative energy source in combination with the flexible use possibilities in the areas of heating, cooling and electricity generation the number of plants which are planned and installed worldwide, increase steady.

REFERENCES

- [1] Innovationsbeirat der Landesregierung (2003): Zukunft der Energieversorgung, Springer Verlag, Heidelberg

- [2] Geitmann, S. (2005): Erneuerbare Energien und alternative Kraftstoffe - Mit neuer Energie in die Zukunft, 2. Auf., Hydrogeit Verlag, Kremen
- [3] Greenpeace (2000): 2000MW - sauber!
http://www.greenpeace.de/fileadmin/gpd/user_upload/themen/energie/Studie_2000MWsauber.pdf
- [4] Umweltministerium Baden Württemberg (2008): Leitfaden zur Nutzung von Erdwärme mit Erdwärmekollektoren, 1. Aufl.,
http://www.um..de/servlet/is/46216/Leitfaden_Erdwaermekollektoren.pdf?command=downloadContent&filename=Leitfaden_Erdwaermekollektoren.pdf
- [5] The same as in [5]
- [6] Wärmepumpen-welt.de (2008): Jetzt in Zukunftswärme investieren und der Staat zahlt mir,
<http://www.waermepumpenwelt.de/imperia/md/content/STIEBELELTRON/themenwelt/informieren/inhalt/marktanreizprogramm.pdf>
- [7] Institut für Energetik und Umwelt gGmbH: Geothermische Strom- und Wärmeerzeugung in Deutschland und Europa – Stand und Perspektiven,
<http://www.ie-leipzig.de/Veranstaltungen/Geothermie/Kaltschmitt-Bohnschaefer.pdf>
- [8] Erneuerbareenergiequellen.com (2008): Geothermische Heizung – Vorteile und Nachteile,
http://www.erneuerbareenergiequellen.com/geothermische_heizung_vorteile_und_nachteile.html
- [9] WDR (2008): Nicht alle Wärmepumpen retten das Klima
http://www.wdr.de/themen/wirtschaft/wirtschaftsbranche/energie/regenerative_energien/interview_waerpumpen.jhtml
- [10] Strom-infos.net : Vor- und Nachteile der Geothermie,
<http://www.strom-infos.net/vor-und-nachteile-der-geothermie.html>
- [11] 6. Internationale Energiewirtschaftstagung an der TU Wien - G02 IEWT 2009: Der Beitrag der Geothermie
http://www.eeg.tuwien.ac.at/events/iewt/iewt2009/papers/3D_4_PONWEISER_K_P.pdf

Slot harmonics in stator current as symptoms of reparation of induction motors

Jan Pytlarz, Paweł Ewert
Wrocław University of Technology
Janiszewskiego 8
Wrocław, Poland

Abstract—Nowadays in many industry branches all over the world more than 90% of all installed motors are of induction motor type. During induction motor operation in electrical parts of stator and rotor circuits (windings) and in mechanical part of the motor and cooperating machine together with coupling elements there occur numerous failures. Every failure brings disturbances in technological process and in worst case leads to whole plant stoppage, what in consequence leads to rise of production costs. In this connection early failure detection on the electrical drives monitoring basis has a great weight. In the paper the attention will be focused on one of the mechanical failures – eccentricity, that is non-axial rotor to stator orientation. There will be presented theoretical considerations and examination results connected with this problem. On the basis of carried out theoretical and experimental considerations there will be made an assessment of stator current signal usability in induction motor operation diagnostics.

I. INTRODUCTION

The history of failure diagnostics is old as the motor itself. Initially the electrical motors producers and users, to assure safe and reliable operation, have turned to simple protection connected with overcurrents, overvoltages, earth faults, etc.

Nowadays in many industry branches all over the world more than 90% of all installed motors are of induction motor type. During induction motor operation in electrical parts of stator and rotor circuits (windings) and in mechanical part of the motor and cooperating machine together with coupling elements there occur numerous failures. Every failure brings disturbances in technological process, and in worst case leads to whole plant stoppage, what in consequence leads to rise of production costs. In this connection early failure detection on the electrical drives monitoring basis has a great weight.

Therefore to avoid production stoppages, lower the repair costs and lower the operation costs there should be assured ways of their detection and information about their occurrence.

Ideal motor monitoring system should recognize all possible failures kinds which can occur in tested drive. It should be noticed that simultaneous occurrence of several failures gives similar, and even the same, quality effects. Occurrence of such case complicates the estimation of their quantity influence on the machine condition. Without independent standard creation for every failure we cannot

estimate the degree in which the particular disturbance affects the total condition of examined circuit.

II. INDUCTION MOTOR FAILURE REVIEW

To assure safe and reliable operation of electrical motors initially the electrical motors producers and users have turned to simple protection connected with overcurrents, overvoltages, earth faults, etc. However electrical motors development, functions performed by them in technological process have feed to diagnostics development. At present non-planned motor standstills can lead to large financial losses.

Main failures of electrical motors can be classified [2]:

- 1) Stator failures, which lead to break or short-circuit of one or several stator phases,
- 2) Improper stator winding connection,
- 3) Rotor rods break or short-circuit ring cracking,
- 4) Static or/and dynamical irregularities of air gap,
- 5) Shaft bend (connected with dynamical eccentricity), which can lead to friction between stator and rotor causing serious damage of stator core and windings,
- 6) Shorted rotor exciting windings,
- 7) Transmission and bearing failures.

This failures cause among other things changeable size of the air gap, current asymmetry, pulsating increase of torque, lowering of mean torque, loss increase, efficiency lowering and heat excess.

To detect failures there have been elaborated many diagnostics method. These methods take advantage of achievements form different science [2]:

- 1) Methods based on stator current spectrum analysis (MCSA – motor current signature analysis),
- 2) Methods based on measurements of engine noise and vibration,
- 3) Methods based on flux analysis (additional coils on stator shaft winding),
- 4) Methods based on artificial intelligence models and neural networks,
- 5) Methods based on temperature measurement,
- 6) Methods based on chemical analysis,
- 7) Radio frequency emissions monitoring,

8) Methods based on infrared radiation recognition.

III. ECCENTRICITY AS FAILURE SOURCE

According to Nandi's [2] motor eccentricity is a state of unequal air-gap which exists between the stator and rotor. Eccentricity detection and diagnosis is a very important element of induction motor condition monitoring. It is caused by very small air-gap toleration between stator and rotor. Small tolerance limit exceed can lead to serious machine failure (stator friction against rotor which in consequence leads to stator or rotor failure), but also deepen the emergency state, caused by other adverse phenomena, such as: asymmetrical feeding, stator or rotor circuit damage, work with excessive load, etc.

Air-gap eccentricity can be a primary or secondary failure. We are speaking about primary failure when the motor has the asymmetry from the operation beginning. It is caused most often by oval stator hole or when the rotor cross-section is not a circle. While when as consequence of sustained non-axial operation the asymmetry of air-gap will exist, then we speak about secondary failure.

We distinguish three types of eccentricity:

- static eccentricity,
- dynamical eccentricity,
- mixed eccentricity (simultaneous occurrence of static and dynamical eccentricity).

In new motors the allowable air-gap eccentricity is up to 10% [2]. Although, the producers try to assure as small as possible total eccentricity level to reduce the vibrations and noise, and to lower the asymmetric radial force.

Most often in motors the mixed eccentricity occurs. In this case the rotation axle can be found between C1 and C2 as shown on figure 1.

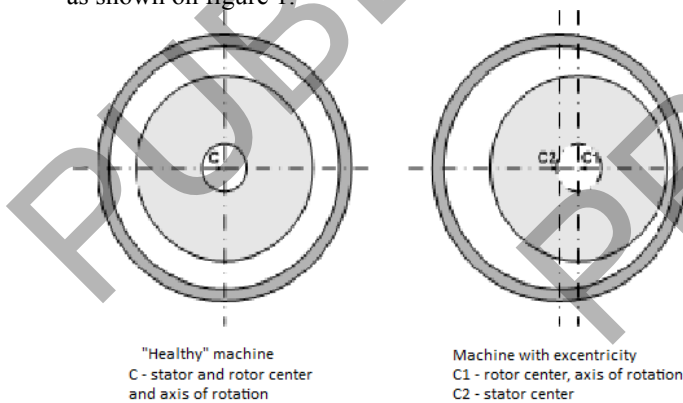


Figure 1. Coaxial and eccentric location of rotor in stator hole

Eccentricity occurrence often does not exclude the motor from further operation. In this case the eccentricity should be

detected and controlled because of it's deepen tendency, what in consequence can lead to motor permanent failure.

Eccentricity monitoring and diagnostics causes a lot of trouble because it must be realized during motor normal operating conditions, non-invasive not to change the motor forces. For this reason, except monitoring using X-rays which is very costly, most often applied method is the spectral analysis of stator current.

IV. SLOT HARMONICS IN STATOR CURRENT SPECTRUM

Induction motor rotor out-of-line location in respect to stator brings air-gap asymmetry. Because of characteristic changes of this asymmetry in mutual magnetic couplings between motor windings influences on stator current spectrum form. That is the reason for which the method of stator current spectral analysis (MCSA) is the most often used in eccentricity detection [1].

In case of induction motors characteristic frequencies describing every kind of eccentricity can be written by equation:

$$f_e = f_s \left[\left(k N_r \pm n_d \right) \frac{1-s}{p_b} \pm n_w \right] \quad (4.1)$$

where:

f_s – net frequency, $k = 1, 2, 3, \dots$, every integer, N_r – quantity of rotor slots, $n_d = 0$ in case of static eccentricity, $n_d = 1, 2, 3, \dots$

in case of dynamical eccentricity (n_d – dynamical eccentricity grade), s – slip, p_b – number of pole pairs, $n_w = \pm 1, \pm 3, \pm 5, \pm 7, \dots$ – grade of stator temporal harmonics.

On the ground of dependence (4.1) in stator current there can be determined the frequencies connected with static and dynamical eccentricity and so called principal slot harmonics (PSH). In a healthy motor those harmonics can be used to estimate the angular speed.

Characteristic frequencies connected with static eccentricity are described by the equation:

$$f_{es} = f_s \left[k \frac{N_r}{p_b} (1-s) \pm 1 \right] \quad (4.2)$$

where $k = 0, \pm 1, \pm 2, \dots$

In case of simultaneous occurrence of static and dynamical eccentricity harmonics with frequencies positioned near net frequency occurs:

$$f_{ed} = |f_s \pm kf_r| \quad (4.3)$$

6. FINAL THOUGHTS

Basing on above mentioned considerations and mentioned examples we can formulate the following conclusions:

- Stator current spectral analysis – a great method to monitor, diagnose and valuate of basic failures occurring in inductive motor;
- Detailed analysis is possible with assurance of high resolution of measuring apparatus and wide frequency band in measured signal;
- Spectrum complexity and disturbance presence cause, that diagnosis accuracy largely depends on expert knowledge and experience;
- Diagnosis on the basis of current spectrum depends on harmonics amplitude valuation with characteristic frequencies for given failure;

REFERENCES

- [1] Cz. Kowalski “Monitorowanie i diagnostyka uszkodzeń silników indukcyjnych z wykorzystaniem sieci neuronowych” *Oficyna Wydawnicza Politechniki Wrocławskiej, Wrocław*
- [2] S. NANDI, “Condition monitoring and fault diagnosis of electrical motors”, *IEEE Transactions on Energy Conversion*, Vol. 20, No. 4, December 2005, str. 719-729S

5. LABORATORY TESTS

The tests were made using Brüel&Kjaer PULSE 3560 analyzer. For INDUKTA SSh 90L-4 engine with parameters: $N_r=26$, $p_b=2$, and work with nominal load ($s=0,0366$) we get, basing on equation (4.1), the following harmonics distribution:

Table 1. Theoretical harmonics distribution in stator current spectrum for SSh 90L-4 engine

$f_s=50\text{Hz}$, $p_b=2$, $s=0,0366$, $n_w=1$, $k=1$, $N_r=26$			
Component	de, $n_d = -1$	PSH, $n_d = 0$	de, $n_d = 1$
Frequency	652	676	700
de- dynamical eccentricity, PSH- principal slot harmonic			

On figure 2 there are presented chosen examples of stator current spectra for SSh 90L-4 inductive motor.

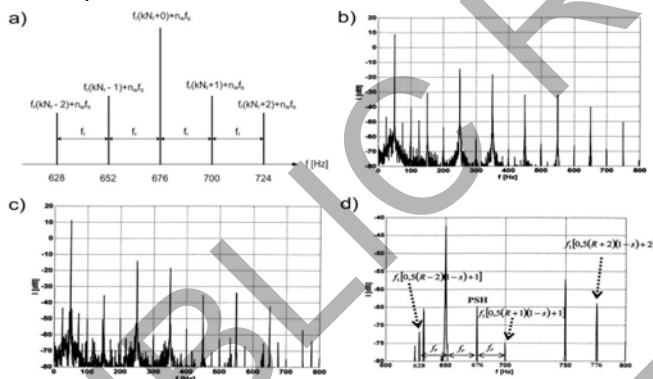


Figure 2. SSh 90L-4 motor stator current spectrum: a) theoretical harmonics distribution in spectrum, b) motor without load, c) motor with nominal load and out-of-line settlement with machine, d) motor harmonics distribution with nominal load and out-of-line settlement with machine

In table 1 there have been presented calculated frequencies, according (4.1) equation, which may be expected in SSh 90L-4 motor stator current spectrum. The measurements were made on the test stand equipped with Brüel&Kjaer analyzer. The results were presented on 2b-d figures. From comparison of theoretical (2a) and actual (2b, c, d) results we can conclude, that the frequencies characterizing the eccentricity are visible even for an engine with unknown eccentricity (non-damaged motor), what confirms the usability of current spectral analysis in eccentricity diagnostics.

Model of a Wind Turbine with PMSG and Wind Park Configuration

Michal Piotr Jankow
Ryerson University, Toronto, Canada
Wroclaw University of Technology,
Wroclaw, Poland, 2009

Abstract—Nowadays the number of dispersed generators (DG) is growing rapidly. This change will greatly influence the power system dynamics. A distribution network, where DG are connected to the grid, cannot be considered as passive anymore. So in future it will not be possible to use simple equivalents of distribution networks for power system dynamic modeling as it was before. In dynamic studies the whole power system cannot be represented in a detailed manner because of huge system dimensions. Therefore special techniques have to be applied for aggregation and order-reduction of distribution networks with DG. Future of power generation which is cleaner and more efficient to meet the targets of the Kyoto protocol is a head of us. Distributed energy resources systems are small-scale power generation technologies used to provide an alternative to or an enhancement of the traditional electric power system. Therefore, distributed generation will play a vital part in the future of electricity generation. However the connection of distributed generation may pose several problems to local distribution networks, therefore, analysis and tackling these problem areas will be needed to address new challenges for a network design, operation and modeling of a power system is required of utmost importance. In this paper brief review of load and generation models have been given.

I. INTRODUCTION

As we strive to create a future of power generation which is cleaner and more efficient to meet the targets of the Kyoto protocol and reduce the dependency of our now limited resources of fossil fuel, distributed generation will play a vital part in the future of electricity generation.

Currently, industrial countries generate most of their electricity in large centralized facilities, such as coal, nuclear, hydropower or gas powered plants. These plants have excellent economies of scale, but usually transmit electricity long distance. Most plants are built this way due to a number of economic, health and safety, logistical, environmental, geographical and geological factors.

Distributed generation (DG) is another approach. It reduces the amount of energy lost in transmitting electricity because the electricity is generated very near where it is used, perhaps even in the same place. This also reduces the size and number of power lines that must be constructed. Therefore, distributed energy resources systems are small-scale power generation technologies used to provide an alternative to or an enhancement of the traditional electric power system. It is the expectation that electricity customers will wish to invest in

their own local generation system which will make use of these DG technologies [1], [2].

However the connection of distributed generation plants may pose several problems to local distribution networks. Analysis and tackling these problem areas will be needed to address new challenges for network design and operation as well as looking for new methods of modeling of power system network is required of utmost importance. Therefore, power control performance of the DG unit determines its impact on the utility grid it connects to.

The process for analysis have been automated, with the addition of adapted existing load and generation profiles being put in place to provide realistic load and power flows within the network. This analysis will be used to provide an insight to the anticipated behavior of distribution network allowing for the suitability of alternative novel network technologies to be assessed to wider development [2].

II. DESCRIPTION OF GENERATION MODELS

In recent years, the problem of energy crunch has become more and more aggravating, resulting in increased exploitation and research for new power energy resources around the world. Natural resources in the world have depleted rapidly as mankind venture into the new millennium. The energy consumption is steadily increasing and the deregulation of electricity has caused that the amount of installed production capacity of classical high power stations cannot follow the demand [1]. A method to fill out the gap is to make incentives to invest in alternative energy sources such as photovoltaic systems, biomass and hydropower resources.

III. MODEL OF WIND TURBINE WITH PMSG

As numerous WTG systems have been developed and connected to power systems worldwide, many different wind turbine models have been developed. Three of the most popular wind turbine generator topologies are outlined in Fig. 1 namely, the fixed-speed design employing a squirrel-cage induction-machine and variable-speed designs using the doubly-fed induction generator (DFIG) and the multi-pole synchronous machine.

Each of the wind turbines in Fig. 1 comprises a prime mover and an electrical generator/power system interface. The prime mover consists of the wind-turbine blades, which may include a pitch controller, the wind turbine shaft, and possibly a gearbox. The electrical generators typically comprise squirrel-cage induction machines, wound rotor induction machines, or synchronous machines.

Traditionally, a wind turbine with PMSG is connected to the AC grid through back-to-back full converters. Nowadays, with the evolution of power electronics, voltage source converter based HVDC (VSC-HVDC) has been considered as a feasible solution to integrating wind farms to grids due to its favorable features. The analysis in the paper is under the background of VSC-HVDC.

A. Generator Model

The dynamic model of PMSG is derived from the two-phase synchronous reference frame in which the q axis is 90° ahead of the d -axis with respect to the direction of rotation. The synchronization between the dq -rotating reference frame and the abc -three phase frame is maintained by a phase locked loop (PLL).

The electrical model of PMSG in the synchronous reference frame is given in (1),(2).

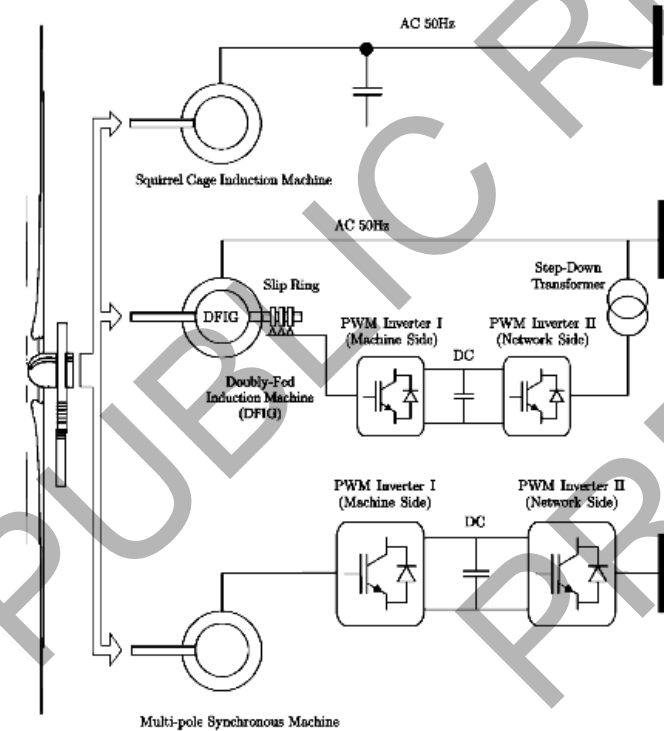


Fig. 1. Fixed-speed, DFIG, and multi-pole synchronous WTG topologies.

$$di_d/dt = (-R_a/L_d)i_d + \omega_e(L_q/L_d) i_d + (1/L_d) u_d \quad (1)$$

$$di_q/dt = (-R_a/L_q)i_q - \omega_e[(L_q/L_d)i_d + (1/L_q) \lambda_0] + (1/L_q) u_q \quad (2)$$

where subscripts 'd' and 'q' refer to the physical quantities that have been transformed into the dq -synchronous rotating reference frame; R_a is the armature resistance; ω_e is the electrical rotating speed which is related to the mechanical rotating speed of the generator as $\omega_e = n_p \omega_g$ where n_p is the number of pole pairs; λ_0 is the permanent magnetic flux. The electric frequency is determined by $f_e = \omega_e/2\pi$. The frequency is obtained by PLL. The inductances, L_d and L_q are the summation of the inductances of the generator on the d- and q-axis and the inductance of the transformer L1, respectively. u_d and u_q are, respectively, the d- and q-axis components of u_g in Fig.7. The q-axis counter electric potential $e_q = \omega_e \lambda_0$ and the d-axis counter electric potential $e_d = 0$. In the paper, we assume $L_d = L_q = L$ and (3), (4) can be rewritten as

$$di_d/dt = (-R_a/L)i_d + \omega_e i_q + (1/L) u_d \quad (3)$$

$$di_q/dt = (-R_a/L)i_d - \omega_e [i_d + (1/L_q) \lambda_0] + (1/L) u_d \quad (4)$$

For the complete representations of the wind turbine with PMSG the following models are required: Aerodynamic, Pitch Angle Control, Speed Control and Phase Locked Loop. In the [3] all of them have been described clearly.

PMSG model could also be modeled by linearization technique. This proposed method [4],[5], removes the dominant quadratic nonlinearity of the model as well as higher order terms involving the input in the system. PM synchronous motor can be linearized using the following transformations [5],[6]

$$y = x + \phi(x) \quad (5)$$

$$u = (I + \beta(x))v + a(x) \quad (6)$$

$$x = Ax + Bu + f^2(x) \quad (7)$$

$$x = [x_1 \ x_2 \ x_3]^T, u = [u_1 \ u_2]^T \quad (8)$$

$$f^2(x) = [k_1 \ x_2 \ x_3; k_2 \ x_3 \ x_1; k_3 \ x_2 \ x_1] \quad (9)$$

where k_1, k_2, k_3 are as defined as:

$$k_1 = (L_{ds} - L_{qs})/a_{31}, \quad (10)$$

$$k_2 = (-L_{ds}a_{31})/L_{qs}, \quad (11)$$

$$k_3 = (L_{qs}C_1^2 a_{31})/L_{ds} \quad (12)$$

where a_{31} and C_1 is :

$$a_{31} = (3P^2 L_{dm} I_f' / 8J), C_1 = 1/L_{qs} \quad (13)$$

I_f' is the field current equivalent to the permanent magnet. L_{ds} , L_{qs} and L_{dm} are the direct, quadrature and magnetizing inductances respectively. R_s is the stator resistance. P is the

number of poles and J is the system moment of inertia. A and B are in Brunovsky form as in:

$$A = \begin{bmatrix} 0 & 1 & 0 \\ 0 & 0 & 1 \\ 0 & 0 & 0 \end{bmatrix} \quad (14)$$

$$B = \begin{bmatrix} 0 & 0 \\ 0 & 1 \\ 1 & 0 \end{bmatrix} \quad (15)$$

Equation (7) can be linearised using the transformations (5) and (6) (with (6) modified for the case of two inputs) where

$$\phi(x) = \dot{\phi}^2(x) = [0; k_1 x_2 x_3; k_1 x_3^2], \alpha(x) = [-k_3 x_2 x_1; -k_2 x_3 x_1] \quad (16)$$

$$\beta^{(m-1)}(x) = (-1)^{m-1} [B^T \{\delta\phi^2(x)/\delta x\} B]^{m-1}, m \geq 2 \quad (17)$$

The system then reduces to $y = Ay + Bv$. Proof: See [5],[6].

IV. WIND FARM MODEL

The mathematical model used for the wind farm behavior in power systems is presented in this section. Typically, the number of wind turbines in a wind farm is high. The example of wind farm is shown in Fig. 2. In fact, a large wind farm can feature hundreds of wind turbines. Therefore, only for wind farm projects it is necessary to analyze in detail the entire generating facility, with each wind turbine represented individually.

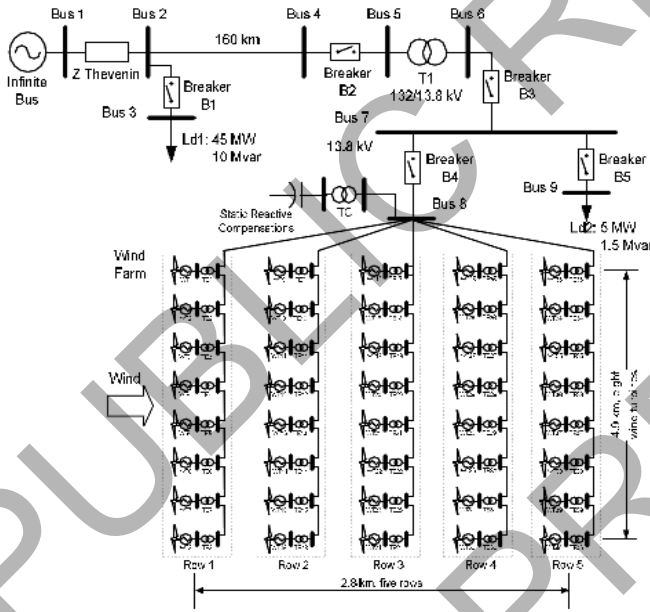


Fig. 2. Example of wind farm model.

In studies where the objective is to verify the influence of the wind farm on the electrical system, the model of every individual turbine of the wind farm would need excessively long processing times and a very robust computational infrastructure. In such studies, the wind farm is represented by an equivalent model from the viewpoint of the electrical system [7].

The simplest way to represent the wind farm is to model the entire farm as an equivalent single wind turbine. This approach assumes that the power fluctuations from each wind turbine are all equal throughout the farm. This assumption, however, does not reflect reality, because the power fluctuations of a wind farm are relatively smaller than those of a wind turbine. Another way to model the wind farm is through a detailed modeling of the farm and considering factors such as the coherence and the correlation of wind turbulence as the presented in. These models imply a heavy load of mathematical modeling and sizable hardware to process them. The model presented in this work takes into account the aggregation effect of the wind farm using an equivalent for the wind added to groups of wind turbines in the farm. The model thus conformed renders a good approximation of the behavior of the wind farm, from the electric system viewpoint. As an advantage, the need for computational resources is reduced [7]

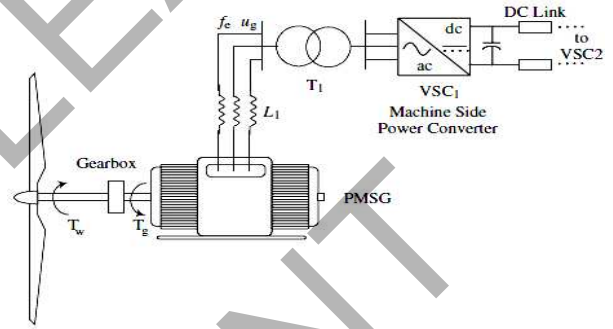


Fig. 3. Dynamic model of an asynchronous generator.

A. Proposed Linear Dynamic Model Applied to a Wind Park

In [8] induction generator dynamic model was presented as a Thevenin equivalent voltage source E' behind the impedance $R_s + jX_s$ as can be seen in Fig. 3. The proposed linear dynamic model can be applied to a wind park consisting of several asynchronous generators. In this case the variation of stator current, for machine number "i," is expressed as:

$$\Delta I_{s,i} = (\Delta U_i - \Delta E'_i) / (R_{s,i} + jX'_i) \quad (18)$$

where ΔU_i is the nodal voltage defined by nodal analysis of the circuit.

$$\Delta U = K \Delta E' \quad (19)$$

Applying equations which are derived in detail in [20], the result is a matrix expression such as

$$\frac{d}{dt} \begin{bmatrix} x_1 \\ \vdots \\ x_i \\ \vdots \\ x_n \end{bmatrix} = \begin{bmatrix} A_{1,1} & \dots & A_{1,2} & \dots & A_{1,n} \\ \vdots & \dots & \vdots & \dots & \vdots \\ A_{i,1} & \dots & A_{i,i} & \dots & A_{i,n} \\ \vdots & \dots & \vdots & \dots & \vdots \\ A_{n,1} & \dots & A_{n,i} & \dots & A_{n,n} \end{bmatrix} \begin{bmatrix} x_1 \\ \vdots \\ x_i \\ \vdots \\ x_n \end{bmatrix} + \begin{bmatrix} b_1 \\ \vdots \\ b_i \\ \vdots \\ b_n \end{bmatrix} \quad (20)$$

where x_i 3 x 1 vector, $A_{i,i}$ 3 x 3 matrix with parameters of machine i , $A_{i,k}$ 3 x 3 matrix that represents the relationship between variables of machine i and k , b_i 3 x 1 vector.

In [8], more general expressions for this induction generator model are presented. Therefore steady-state situation of (20), for sinusoidal fluctuations of $\Delta P'_m$ can be obtained by superposition. Therefore, for $\Delta E'_r$, $\Delta E'_m$ and Δs , the following general expression can be written

$$x(t) = \sum_{i=1}^n X_{r,i} \sin(\Omega_{0,i}t) + X_{m,i} \cos(\Omega_{0,i}t) \quad (21)$$

V. CONCLUSIONS

In this paper brief review of load and generation models have been given. The whole next part of this paper was dedicated to wind energy. The paper presents a model of the variable speed wind turbine with PMSG that is scheduled to connect an AC grid through VSC-HVDC. The complete model consists of a PMSG model, a pitch-angled controlled wind turbine model and a drive train model. The generator rotational speed control scheme features the concept of vector control in the dq-synchronous rotating reference frame. MATLAB/Simulink was implemented to build the dynamic model of the wind turbine with PMSG [3]. PMSM model could also be modeled by linearization technique. This proposed method [4],[5], removes the dominant quadratic nonlinearity of the model as well as higher order terms involving the input in the system. Next, a linear dynamic model for an asynchronous wind turbine and for the wind farm with mechanical sinusoidal fluctuation was developed. This proposed linear model presents good accuracy compared to the dynamic model. The proposed model has the following advantages: 1) it has low complexity; 2) it permits modal analysis, direct solution of differential equations, and easy implementation in several conventional tools for power system analysis (load flow analysis and power system stability) [8].

Future of power generation which is cleaner and more efficient to meet the targets of the Kyoto protocol is a head of us. Therefore, it is needed to address new challenges for a network design, operation and modeling of a power system is required of utmost importance.

ACKNOWLEDGMENT

I would like to thank all the authors, and those advancing in power energy systems and distribution technology worldwide. This special issue would not be possible without your achievements also I wish to thank the IEEE and to all authors for their content-related support and materials who provided all the research in load and generators modeling so this paper could be done in pulling all the papers together which you can find in references.

REFERENCES

- [1] M. Dai, M. N. Marwali, J. W. Jung, and A. Keyhani, "Power flow control of a single distributed generation unit with nonlinear local load," in Proc. IEEE PES Power Syst. Conf. Expo (PSCE'04), New York, NY, Oct. 2004, vol. 1, pp. 398-403.
- [2] S. J. Haig, R. M. Tummit, G. M. Burt, J. R. MacDonald, "Analysing the technology needs of future distribution networks", UPEC '06, 41st International Proceeding, Vol.1 6-8Sept. 2006, pp. 217-221
- [3] Y.Ming, L. Gengyin, Z. Ming, Z. Chengyong "Modeling of the Wind Turbine with a Permanent Magnet Synchronous Generator for Integration," IEEE PES General Meeting ,24-28 June 2007.
- [4] A.K.Parvathy, V.Kamaraj, R. Devanathan,"A New Linearisation Technique for Permanent Magnet Synchronous Motor Model", Pwer System Technology, IEEE Power India Conference 2008, POWERCON 2008, 12-15 Oct. 2008.
- [5] A.K.Parvathy, Aruna Rajan, R. Devanathan,"Complete Quadratic Linearisation of PM Synchronous Motor Model ", NPEC 2005, pp 49-52.
- [6] A.K.Parvathy, Aruna Rajan, R.Devanathan," Linearisation of PM Synchronous Motor Model", Technical Report, Department of EEE, Hindustan College of Engineering, Tamil Nadu 2005.
- [7] Y. Coughlan, P. Smith, A. Mullane, M. O'Malley, "Wind Turbine Modelling for Power System Stability Analysis – A System Operator Perspective", vol. 22, pp.929-936, Aug. 2007.
- [8] J. Cidras, A. Feijoo, "A linear dynamic model for asynchronous wind turbine with mechanical fluctuations", IEEE Transactions on Power Systems, vol. 17, pp.681-687, Aug. 2002.

BIOGRAPHY



Michal Piotr Jankow was born in Wroclaw, Poland, in 1985. He is currently studying for a M.Sc. degree in Control in Electrical Power Engineering at Wroclaw University of Technology, Wroclaw, Poland and for a MEng. degree at Ryerson University, Toronto, Canada. His present interests are wind energy, wind turbines, offshore and onshore wind parks. His also the finalist of the national competition by LOREAL in the topic: "Applying renewable energy sources in industry".

Load Modeling For Power System Analysis

1

Jakub Kepka
Wroclaw University of Technology

Abstract—This paper covers overview of the load models for distribution systems. The basic concepts for static, dynamic and combined models are introduced. The following discussion shows importance of accurate system parameters modeling for analysing power system stability. The accurate load representation is not easy issue regarding to its changeable nature and variety. Basic load classification is described.

I. INTRODUCTION

Power system stability and reliability have been very important issues over the years. It is hard to predict the system behaviour in case of outage, voltage or frequency variation or other factors that can affect system stability without proper information, or system behaviour data. The powers system are mostly nonlinear and operates in constantly changing conditions, so it is hard to obtain precise information and data about i.e. generators or loads during disturbance[2]. This required to either assume or measure certain quantities like real and reactive power, to predict system response to abnormal conditions. Very important factor is to not interrupt power flow to the residential, industrial or any other end users. That is why certain measurements need to be made with specialized, expensive equipment to allow get the data under operating system. This type of data collecting involves a continuous monitoring process and requires data to be processed after the measurements are done.[3]. A lot of studies have been carried out so far to provide as accurate model of load as possible, and still new techniques are being developed through big electric concerns. There is a lot of computer software existing that allows for load modeling and system behaviour simulation, however, as mentioned above, the more accurate data typed in to the program, the more accurate model and the simulation results."It has become clear that assumptions regarding the load model can impact predicted system performance as significantly as the models chosen for excitation systems and synchronous machines, which have received greater industry attention"[5]. "Analysis of power system dynamic performance requires the use of computational models representing the nonlinear differential-algebraic equations of the various system components. While scale models or analog models are sometimes used for this purpose, most power system dynamic analysis is performed"[2].

II. LOAD TYPES AND CLASSIFICATION

Before load modeling process will get started, it is required to understand its applications that are divided into two categories: static, called "snap-shot" – with respect to time as well as dynamic – time varying. Since the "static model based

represents variation of the load with the frequency. The fundamental starting point for the load modeling is at the distribution level, thus, the applications outside of power system can be as follows:[1]

Static applications – this model considers only voltage – depended characteristic[1]:

- Power Flow (PF)
 - Harmonic Power Flow (HPF)
 - Transmission System (TPF)
 - Transmission Power Flow
- Voltage Stability

Dynamic applications –considers both voltage-dependent and frequency dependent characteristics[1]:

- Transient Stability (TS)
- Dynamic Stability (DS)
- Operator training simulators (OTS)

As one already mentioned, the loads are quite difficult to be modeled in terms of their variety and change in load depending on the time of the day or season. It is necessary to classified them according to particular area, composition of each one as well as regarding to load characteristic. The loads can be also combined in groups and exhibited as: industrial, residential, commercial and agricultural[3]. The industrial loads includes mainly induction motors, up to 95%, the residential loads includes most of domestic appliances, i.e. refrigerators, washing machines etc. as well as heating and air conditioning units. The commercial load is refers to air condition units and discharge lighting in particular, whereas agricultural loads corresponds to induction motors, i.e. as a prime movers for pumps.[3]. Having presented load classification and general load requirements, it is possible now, to carry out the theoretical analysis to express the system load as a mathematical models. In order to do this, one needs to use some mathematical expressions to describe the load as accurate as possible, what is described in the next section of this paper.

III. LOAD MODELING CONCEPTS

Generally, one can distinguish tow basic load modeling concepts: component based and measurement based models. Component – based model is built on the base of the information on each elements that consist of the load being simulated. "Each load component type is tested and to determine the relationship between real and reactive power requirements versus applied voltage and frequency."[1], then the load model is developed mainly in either exponential or polynomial form basing on obtained data."The range of validity of each model is directly related to the range over which the component was tested"[1]. Usually, the load model is expressed on the p.u values for convenience. By combining appropriate load model types one can approximate the composite load. Mentioned load

on the steady state method of the network representation in the power flow networks"[1], these models express loads as a voltage magnitude function. The dynamic model in turn,

model types are obtained basing on the load survey information.[1] The composition of the load depends upon the time of the day, month, or season as well as atmospheric conditions. One can notice, that the country with fine weather reveal higher demand for air conditioning, while in the cold climate countries it is just opposite, there is a big demand for electricity heating. One can point out, that these demand can also vary seasonally, in the summer/winter periods, demand for heating/cooling can either increase or decrease.[3] Having introduced the model types and its variation depending on certain factors, one can propose some mathematical load model representation as a set of equations in order to give details of the relationship between the input and output system parameters. Considering load modeling, mathematical representations is related to voltage and/or frequency measured at the buses as well as real and reactive power consumed by the loads.[3]

IV. LOAD MODELING

“For dynamic performance analysis, the transient and steady-state variation of the load P and Q with changes in bus voltage and frequency must be modeled” [5]. For power system analysis load can be thought as real and reactive power launched to lower voltage distribution system at buses represented as network model. Among lots of devices and appliances being connected to the system and considered as a load, one should include intervening distribution systems feeders, shunt capacitors, transformers etc. as well as voltage controlling devices or voltage regulators. The simplest load model is *static model*. Next chapter introduces static models as well as dynamic ones that are being used for i.e. system stability studies.

V. DELTA AND WYE CONNECTED LOADS

First load models to be described are Wye and Delta connected loads. Each of these loads can be represented as being connected phase-to-neutral or phase-to-phase in a four wire Wye system or phase-to-phase in a three wire delta system[4]. All of model above can be three, two, or single phase and modeled as: constant real and reactive power, constant current, constant impedance as well as any random combination of the above. This model is one of the basic static load models.

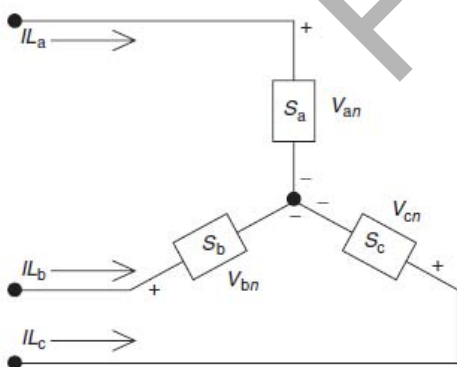


Fig.1 Wye connected load[1]

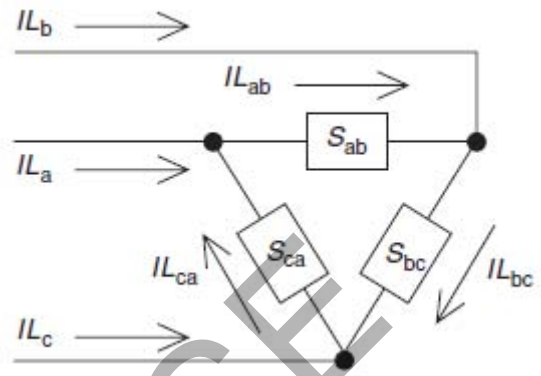


Fig.2 Delta connected load[1]

Both load models depicted in the figures above require the load component current coming into the load to be determined.[r4]. Assumption is made, that the loads have an initial complex power

$$|S|_{a,b,c} \angle \theta = P_{a,b,c} + jQ_{a,b,c} \quad (1)$$

, where indices a,b,c denotes that formula is expressed in the same way for each single phase of Wye connected load, this notation will be kept in further formulas describing model above

A. Constant Real and Reactive power loads for Y connection

“In this model the line to neutral voltage will change during each iteration until convergence is achieved”[4]

$$IL_{a,b,c} = \left(\frac{S_{a,b,c}}{V_{(a,b,c)n}} \right)^* = \frac{|S|_{a,b,c}}{V_{(a,b,c)n}} \angle \delta_{a,b,c} - \theta_{a,b,c} = \angle \alpha \quad (2)$$

B. Constant Impedance Load for Y connected loads

Constant impedance is first determined from the specified complex power and line-to-neutral voltage for each phase.

$$Z_{a,b,c} = \frac{|V_{(a,b,c)n}|^2}{S_{a,b,c}^*} = \frac{|V_{(a,b,c)n}|^2}{|S_{a,b,c}|} \angle \theta_{a,b,c} = |Z_{a,b,c}| \angle \theta_{a,b,c} \quad (3)$$

Having “constant load impedance”, it is possible to express load currents as the function of those impedance. This current for each phase is given by equation (4):

$$IL_{a,b,c} = \frac{V_{(a,b,c)n}}{Z_{a,b,c}} = \frac{|V_{(a,b,c)n}|}{|Z_{a,b,c}|} \angle \delta_{a,b,c} - \theta_{a,b,c} = |IL|_{a,b,c} \angle \alpha_{a,b,c} \quad (4)$$

“In this model the line to neutral voltage will change during each iteration until convergence is achieved”[4]

C. Constant Real and Reactive power loads for Y connection

$$IL_{a,b,c} = |IL|_{a,b,c} \angle \delta_{a,b,c} - \theta_{a,b,c}$$

For this model, current magnitudes are obtained according to the equation (2). These magnitudes do not change until the voltage angle δ changes during each iteration[4],

D. Delta connected load model

Similarly to the Y connected load, the delta connected load model can be made. The equations describing this model are the same, except that voltages and currents in this models are taken as phase-to-phase instead of phase-to-neutral, so delta load model is described by following equations:

Constant real and reactive power:

$$IL_x = \left(\frac{S_x}{V_x}\right)^* = \frac{|S_x|}{V_x} \angle \delta_x - \theta_x = |IL_x| \angle \delta_x \quad (6)$$

Constant Impedance Load

$$Z_x = \frac{|V_x|^2}{S_x^*} = \frac{|V_x|^2}{|S_x|} \angle \theta_x = |Z_x| \angle \theta_x \quad (7)$$

Constant Current Load

$$IL_{a,b,c} = \frac{V_x}{Z_x} = \frac{|V_x|}{|Z_x|} \angle \delta_x - \theta_x = |IL_x| \angle \alpha_x \quad (8)$$

, where index x denotes line-to-line values ab, bc, and ca respectively.

Models presented above can be modeled as combination of above constant Z, I, and P and can be assigned as a percentage of total load shown above. For the Wye connection, it is simply the sum of the three components Ia, Ib and Ic, while for all delta connected loads the line current is determined by:

$$\begin{bmatrix} IL_a \\ IL_b \\ IL_c \end{bmatrix} = \begin{bmatrix} 1 & 0 & -1 \\ -1 & 1 & 0 \\ 0 & -1 & 1 \end{bmatrix} \begin{bmatrix} IL_{ab} \\ IL_{bc} \\ IL_{ca} \end{bmatrix}$$

Considering Wye and Delta connected loads one can mention of the Shunt Capacitor models that are very often used for voltage regulation in a distribution system as well as in order to provide reactive power support.

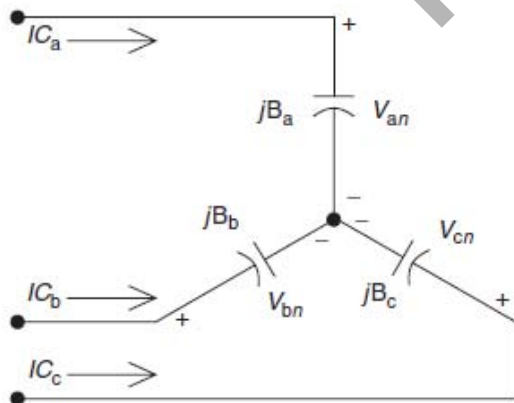


Fig. 3 Wye connected capacitor bank[1]

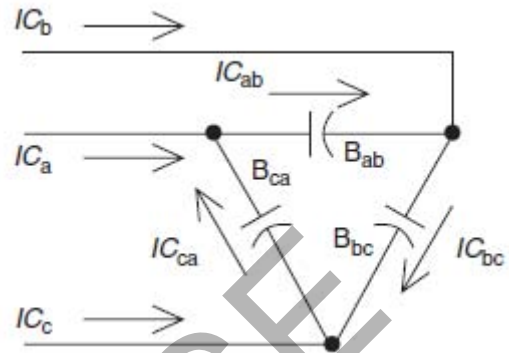


Fig. 4 Delta connected capacitor bank[1]

The capacitor banks are modeled as constant susceptances connected as above. The susceptance can be found as:

$$B_{actual} = \frac{kVAr}{kV^2 1000} [Siemens] \quad (10)$$

$$B_{p.u} = \frac{kVAr_{p.u}}{V^2} [per\ unit] \quad (11)$$

$$where \frac{kVAr_{p.u}}{kVA_{signature\ phase\ base}} \quad (12)$$

$$V_{p.u} = \frac{kV_{actual}}{kV_{line\ to\ neutral\ base}} \quad (13)$$

Having computed susceptance one can find out the line currents given by:

$$IC_a = jB_a V_{an} \quad (14)$$

$$IC_b = jB_b V_{bn} \quad (15)$$

$$IC_c = jB_c V_{cn} \quad (16)$$

For delta connection currents flowing in capacitors are given as below:

$$IC_{ab} = jB_{ab} V_{ab} \quad (17)$$

$$IC_{bc} = jB_{bc} V_{bc} \quad (18)$$

$$IC_{ca} = jB_{ca} V_{ca} \quad (19)$$

The line currents feeding the delta connected capacitor bank are as follows:

$$\begin{bmatrix} IC_a \\ IC_b \\ IC_c \end{bmatrix} = \begin{bmatrix} 1 & 0 & -1 \\ -1 & 1 & 0 \\ 0 & -1 & 1 \end{bmatrix} \begin{bmatrix} IC_{ab} \\ IC_{bc} \\ IC_{ca} \end{bmatrix} \quad (20)$$

VI. POLYNOMIAL AND EXPONENTIAL LOAD MODELS

There are two mathematical forms that are commonly used in modeling studies: polynomial and exponential load models. Polynomial model is a static model describing relationship of the power and voltage magnitudes as a polynomial equation and can be expressed as[6]:

$$P = P_0 \left(a_1 \left(\frac{V}{V_0}\right)^2 + a_2 \left(\frac{V}{V_0}\right) + a_3 \right) \quad (21)$$

$$Q_L = Q_0 \left(a_4 \left(\frac{V}{V_0}\right)^2 + a_5 \left(\frac{V}{V_0}\right) + a_6 \right) \quad (22)$$

$$P = P_0 \left(\frac{V}{V_0} \right)^{np} \quad (23)$$

$$Q = Q_0 \left(\frac{V}{V_0} \right)^{nq} \quad (24)$$

“The parameters of this model are exponents, and the power factor of the load”[6]. Setting these parameters to 0,1, or two the load model becomes constant current, power, or impedance, like in case of the Wye and Delta connected loads shown in previous section.[6]

A. PSS/E Static Model[12]

This static model introduces the active and reactive power that are both frequency and voltage dependent and given by the following formulas:

$$P_L = P_0 \left(a_1 \left(\frac{V}{V_0} \right)^{n1} + a_2 \left(\frac{V}{V_0} \right)^{n2} + a_3 \left(\frac{V}{V_0} \right)^{n3} \right) (1 + a_7 \Delta f) \quad (25)$$

$$Q_L = Q_0 \left(a_4 \left(\frac{V}{V_0} \right)^{n4} + a_5 \left(\frac{V}{V_0} \right)^{n5} + a_6 \left(\frac{V}{V_0} \right)^{n6} \right) (+a_8 \Delta f) \quad (26)$$

,”where a_1 - a_8 and n_1 - n_8 – parameters to be estimated when $V=V_0$

VII. CONCLUSIONS

The both static, and dynamic model of loads were described in this work as well as combined ones. Load modeling is a challenge for today`s engineers. It`s variety and not constant nature makes them hard to simulate. There have been a lot of studies on load modeling in order to represent it with maximum accuracy. There are many simulation software that allows to simulate power system loads basing. i.e. on polynomial and exponential load model representation.

VIII. REFERENCES

- [1] Prabha Kundur, “Power System Stability and Control”, 2007
- [2] Prabha Kundur, “Electric Power Generation, Transmission, and Distribution
- [3] Inés Romero Navarro, “Dynamic Load Models for Power Systems, Estimation of Time-Varying Parameters During Normal Operation
- [4] William H. Kersting, “Electric Power Generation, Transmission, and Distribution”
- [5] M. Sedighzadeh, and A. Rezaadeh, “Load Modeling for Power Flow and Transient Stability Computer Studies at BAKHTAR Network”
- [6] IEEE Task Force on Load Representation for Dynamic Performance, “Load representation for dynamic performance analysis”, IEEE Transactions on Power Systems, Vol. 8, No. 2, May 1993
- [7] Byoung-Kon Choi, *Member, IEEE*, Hsiao-Dong Chiang, *Fellow, IEEE*, YinHong Li, Yung-Tien Chen, Der-Hua Huang, and Mark G. Lauby, “Development of Composite Load Models of Power Systems using On-line Measurement Data”
- [8] Jingchao Zhang Anhe Yan Zhuoya Chen and Kun Gao “Dynamic Synthesis Load Modeling Approach Based on Load Survey and Load Curves Analysis”
- [9] Pablo Ledesma, Member, IEEE, and Julio Usaola, Member, IEEE, “Doubly Fed Induction Generator Model for Transient Stability Analysis”, IEEE TRANSACTIONS ON ENERGY CONVERSION, VOL. 20, NO. 2, JUNE 2005
- [10] Zhijun Li and Lijuan Cui Department of Electrical Engineering and Automation, Hebei University of Technology, China. “The Building and Analyzing of the Fifth-Order Model of the Synchronous Generator in Stand-Alone Infinite System”
- [11] Prabha Kundur, Neal J. Balu, Mark G. Lauby. “Power System Stability and Control”, McGraw-Hill Professional, 1994
- [12] Y. Li, H.-D. Chiang, B.-K. Choi, Y.-T. Chen, D.-H. Huang and M.G. Lauby. “Representative static load models for transient stability analysis: development and examination”, McGraw-Hill Professional, 1994

Loads and Synchronous Generator Modeling

Robert Pliszcak
Wroclaw University of Technology

Abstract-- This paper survey of different accurate models of load and synchronous generator model. I would like to described one out of two basic types of load modeling. One is component-based load modeling which contain 'ZIP' (polynomial) model, exponential model, combination of this two called exponential-'ZIP' model and ETMSP & EPRI model as an example of combination of fundamental models. Second one is measurement-based load modeling, however, this is not on my consideration. The second part survey consists synchronous generator modeling by electrical circuits. Moreover, there are dc generators, but this model is not covered in this paper.

I. INTRODUCTION

There are two general issues to consider modeling of power systems. One of them is loads modeling as well as generators modeling. Loads and generators modeling are very important in determining the stability of power systems. Moreover there are valuable tools in the stability studies.

Load modeling application can be distinguished into static and dynamic models. First of all I would like to shortly describe static load model. The static models were discovered to investigate steady-state power systems. In this models occurs constant voltage magnitude, but on the other hand there is variation of load frequency. Lastly the static load models feature is voltage-dependent characteristic. Second of all it is mentioned in the technical literature about dynamic load modeling. This load model is in time-domain and contains loads electromechanical behavior. Phasors method is the load steady-state representation. The dynamic load model is based on time variation frequency. Moreover, the dynamic load model is describe by dynamic voltage and frequency characteristics.[1]

The second part of this paper is to survey generators modeling. The Generators can be classified as a electrical motors. There are dc generators, synchronous generators and inductor generators. The dc generators are rarely used in power systems. The most popular and common use in the industrial applications is synchronous generator. There have been developed big number of synchronous generators. The generators are the heart of power systems. " With the increasing cost of detailed prototyping of electrical machine, it is becoming necessary to replace or supplement it with mathematical methods and computer simulation." [2] However, the inductor generators are used in power systems, but mostly in wind turbines. The number of wind turbines connected to the grid increase every year. Papers [8], [9], [10] are contained more information's about double fed induction generators modeling.

II. LOAD MODELING

Load modeling is a very important issue in power system analysis and control. Accurate load models have significant impact on the operations flexibility and exploitation costs in power systems. Exploitation costs can be reduced because of there is possible to test new solution and change power system configuration without any disturbances of normal power system work. The operations flexibility is also very important regarding to beater fit power system modeling into real power system. That is why both power industry and academia are looking for now, and more accurate loads representation. We can distinguish two approaches for load models developing: component-based and measurement-based. "The component-based approach builds a load model using detailed information about all the individual components at each load bus. The measurement-based approach involves placing measurement systems at the load buses for which load models are to be developed." [3] The measurement-based approach gives us actual load behaviors at any given moment. In the power industry is also used on-line data recording system. This tool gives important information about actual load behaviors during system disturbances. Dynamic load models regarding to possible disturbances response are highly recommended for a lot of power system models representations, moreover this models are commonly used in power industry for transient stability analysis. On the other hand, it increases of system representation for simulation. [3]

Loads modeling has always been a difficult issue because:

- many different types of load are connected to the power system at any period of time,
- level of complication and quantity of data is very high at any given moment,
- it is hard to predict loads response (behavior), [4]

We can distinguish three main load models:

- ✓ 'ZIP' (polynomial) model,
- ✓ exponential model and
- ✓ exponential – 'ZIP' model - combination of this two above [1]

A. Polynomial-'ZIP' Model

One of the oldest load representation is polynomial model. It is essentially combination of constant impedance (Z), constant current (I) and constant power (P), that is why it is commonly called 'ZIP' model. This model is not accurate representation of the system, because of high number of inductor motor loads in the system. Nowadays there are more complex and accurate load models which capture both the static and dynamic load, such as induction motors.[4]

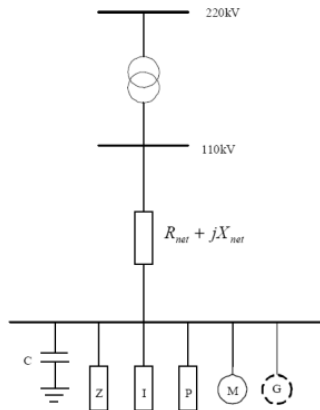


Fig.1. The structure of 'ZIP' load model. [5]

$$P_L = P_0 \left[p_1 \left(\frac{V}{V_0} \right)^2 + p_2 \left(\frac{V}{V_0} \right)^1 + p_3 \right] (1 + K_{pf} \Delta f)$$

$$Q_L = Q_0 \left[q_1 \left(\frac{V}{V_0} \right)^2 + q_2 \left(\frac{V}{V_0} \right)^1 + q_3 \right] (1 + K_{qf} \Delta f)$$

p_1 and q_1 are the constant impedance load parameters, p_2 and q_2 are the constant current load parameters, p_3 and q_3 are the constant power load parameters, K_{pf} and K_{qf} are the frequency sensitivity parameters, and $p_1 + p_2 + p_3 = 1$, $q_1 + q_2 + q_3 = 1$ when $V = V_0$. [2]

B. Exponential Model

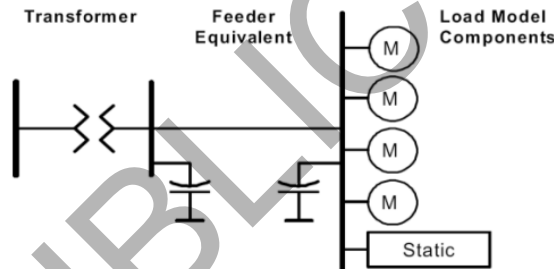


Fig.2. The structure of any static load models.[6]

This scheme can be used for any static load modeling. So, it fit for every presented in this paper load model.

$$P_L = P_0 \left(\frac{V}{V_0} \right)^{K_{pV}} (1 + K_{pf} \Delta f)$$

$$Q_L = Q_0 \left(\frac{V}{V_0} \right)^{K_{qV}} (1 + K_{qf} \Delta f)$$

K_{pV} -voltage-dependent parameter of real power, K_{qV} -voltage-dependent parameter of reactive power, K_{pf} and K_{qf} are the frequency sensitivity parameters.[3] Comparing of 'ZIP' and exponential load modeling the second one is more accurate.

C. Exponential-'ZIP' Model

This is the combination of both exponential and 'ZIP' models which are shown above. Diagram can be the same as in previous model.

$$\begin{aligned} \frac{P}{P_0} &= \left(1 + (K_{pi} + K_{pc} + K_{p1} + K_{p2}) \right) \left(\frac{V}{V_0} \right)^2 + \\ &+ K_{pi} \left(\frac{V}{V_0} \right) + K_{pc} + K_{p1} \left(\frac{V}{V_0} \right)^{npv1} \times (1 + K_{pf1} \Delta f) \\ &+ K_{p2} \left(\frac{V}{V_0} \right)^{npv2} (1 + K_{pf2} \Delta f) \\ \frac{Q}{Q_0} &= \left(1 + (K_{qi} + K_{qc} + K_{q1} + K_{q2}) \right) \left(\frac{V}{V_0} \right)^2 + \\ &+ K_{qi} \left(\frac{V}{V_0} \right) + K_{qc} + K_{q1} \left(\frac{V}{V_0} \right)^{nqv1} \times (1 + K_{qf1} \Delta f) \\ &+ K_{q2} \left(\frac{V}{V_0} \right)^{nqv2} (1 + K_{qf2} \Delta f) \end{aligned}$$

K_{pi} and K_{qi} are the constant current parts of the total load, K_{pc} and K_{qc} are the constant power parts of the total load, K_{p1} , K_{pf1} , $npv1$, K_{p2} , K_{pf2} , $npv2$, K_{q1} , K_{qf1} , $nqv1$, K_{q2} , K_{qf2} , $nqv2$ are the parameters of exponential part of the total load.[3]

D. ETMSP & EPRI Model

Scheme is shown in Fig.2. However, there are some more models discovered by the companies. The companies which have made distribution system computers programs (software). They have used this three types of load modeling and modify them. EPRI's LOADSYN and ETMSP packages are one of the most commonly used software for dynamic studies. This two packages based on load models presented above with little changes. Below the result of this changes is shown:

$$\begin{aligned} P_L &= P_0 \left\{ P_{a1} \left(\frac{V}{V_0} \right)^{K_{pv1}} (1 + K_{pf1} \Delta f) + (1 - P_{a1}) \left(\frac{V}{V_0} \right)^{K_{pv2}} \right\} \\ Q_L &= P_0 \left\{ Q_{a1} \left(\frac{V}{V_0} \right)^{K_{qv1}} (1 + K_{qf1} \Delta f) \right. \\ &\left. + \left(\frac{Q_0}{P_0} - Q_{a1} \right) \left(\frac{V}{V_0} \right)^{K_{qv2}} (1 + K_{qf2} \Delta f) \right\} \end{aligned}$$

where,

P_{a1} is the frequency dependent fraction of real load, Q_{a1} is the reactive load coefficient of uncompensated reactive load to real power load, K_{pv1} and K_{pv2} are the voltage exponents for frequency-dependent and frequency-independent real power load, K_{qv1} and K_{qv2} the voltage exponents for the uncompensated and compensated reactive power load, K_{pf1} and K_{pf2} are the frequency sensitivity coefficients for real and uncompensated reactive power load K_{qf2} is the frequency sensitivity coefficient for reactive compensation [3].

We have showed this load model as a example of one combination of this fundamental models.

III. GENERATORS MODELING

Generators convert mechanical energy to electrical energy. There are three possible types of generators: dc generators, induction generators and synchronous generators. The first one are useless because all the power systems around the world are AC. So there are two main types of generators: one of them is synchronous generator and second is induction generator. The inductor generators mostly occur in the wind mills. The synchronous generators are common use in most types of power plants.

First of all the synchronous machines work with constant speed what means constant frequency. The speed of the synchronous generator linearly depends on the frequency and numbers of poles. The constant frequency is very good feature because one of the power systems requirements is to keep frequency in one specified level. Another advantage comes from reactive power compensation in the grid. The synchronous generators produce active power and reactive power. The last important feature is high efficiency of synchronous generators.

The inductor generators are less popular then the synchronous generators. However, they have some advantages. One of them is that inductor generators are simplified in construction. Furthermore, they are lighter and cheaper than any others. However the frequency cannot be adjusted as simple as in the synchronous generator and the reactive power cannot be compensated. When one would like to use inductor generator it should also have special control system. The speed controllers are going to be cheaper and cheaper and inductor generators are commonly used in the wind mills.

I would like to present synchronous generator modeling by electrical circuits. There are more synchronous generators models in papers [7],[11], [12], [13].

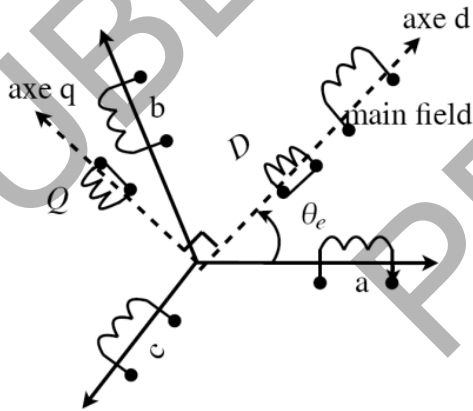


Fig.3. Synchronous generator winding with dampers.

D and Q represent d-axis and q-axis dampers. The three synchronous generator modeling methods presented below are based on this scheme.[2]

A. Synchronous Generators Modeling by Electrical Circuit

From figure above the machine equations in three axis framework is shown below:

$$\begin{aligned} v_{abc} &= -r_s i_{abc} + \frac{d}{dt} \Psi_{abc} \\ v_f &= r_f i_f + \frac{d}{dt} \Psi_f \\ 0 &= r_D i_D + \frac{d}{dt} \Psi_D \\ 0 &= r_Q i_Q + \frac{d}{dt} \Psi_Q \end{aligned}$$

i_D and i_Q are the direct and transverse dampers` currents, i_f is the exciter current, Ψ_D and Ψ_Q are the direct and transverse dampers` total flux, Ψ_{abc} is the stator total flux, Ψ_f is the main field total flux, The Park`s matrix can be written as:

$$P(\theta_e) = \frac{1}{\sqrt{3}} \begin{bmatrix} \cos(\theta_e) & \cos(\theta_e - \frac{2\pi}{3}) & \cos(\theta_e + \frac{2\pi}{3}) \\ -\sin(\theta_e) & -\sin(\theta_e - \frac{2\pi}{3}) & -\sin(\theta_e + \frac{2\pi}{3}) \end{bmatrix}$$

$$P(\theta_e) \cdot v_{abc} = P(\theta_e) \begin{bmatrix} v_a \\ v_b \\ v_c \end{bmatrix} = \begin{bmatrix} v_d \\ v_q \end{bmatrix}$$

We can rewrite first equations as:

$$\begin{aligned} v_d &= -r_s i_d + \frac{d}{dt} \Psi_d - \omega_e \Psi_q \\ v_q &= -r_s i_q + \frac{d}{dt} \Psi_q - \omega_e \Psi_d \\ v_f &= r_f i_f + \frac{d}{dt} \Psi_f \\ 0 &= r_D i_D + \frac{d}{dt} \Psi_D \\ 0 &= r_Q i_Q + \frac{d}{dt} \Psi_Q \end{aligned}$$

Then the following relationships can be written considering the generator convention for stator

$$\left\{ \begin{aligned} \Psi_d &= \Psi_{ad} + \Psi_{\sigma sd} + \Psi_{\sigma fd} = \\ &= l_{ad}(-i_d + i_D + i_f) - l_{\sigma sd} i_d + l_{\sigma fd}(i_f - i_d) \\ \Psi_q &= \Psi_{aq} + \Psi_{\sigma sq} = \\ &= l_{aq}(-i_q + i_Q) - l_{\sigma sq} i_q \\ \Psi_f &= \Psi_{fd} + \Psi_{\sigma fd} + \Psi_{\sigma fd} = \\ &= l_{ad}(-i_d + i_D + i_f) + l_{\sigma fd} i_f + l_{\sigma fd}(i_f - i_d) \\ \Psi_D &= \Psi_{ad} + \Psi_{\sigma D} = \\ &= l_{ad}(-i_d + i_D + i_f) + l_{\sigma D} i_D \\ \Psi_Q &= \Psi_{aq} + \Psi_{\sigma Q} = \\ &= l_{aq}(-i_q + i_Q) - l_{\sigma Q} i_Q \end{aligned} \right.$$

From all this equations we can draw the synchronous machine electrical scheme as follows:

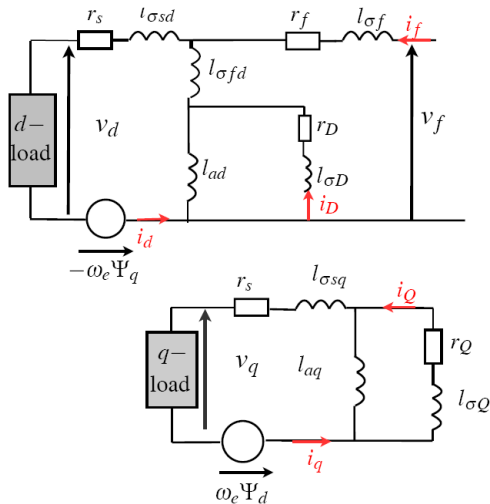


Fig.4. d-axis and q-axis electrical equivalent circuits. [2]

$\Psi_{\sigma f}$ is the rotor leakage flux,
 $\Psi_{\sigma D}$ and $\Psi_{\sigma Q}$ are direct and transverse dampers leakage flux,
 $\Psi_{\sigma sd}$ and $\Psi_{\sigma sq}$ are direct and transverse stator dampers leakage flux,
 $\Psi_{\sigma fd}$ is the linkage flux between main field and stator d-axis,
 Ψ_{ad} and Ψ_{aq} are direct and transverse main flux,
 $l_{\sigma sd}$ and $l_{\sigma sq}$ are direct and transverse stator leakage inductances,
 $l_{\sigma f}$ is the rotor main field leakage inductance,
 l_{ad} and l_{aq} are the direct and transverse stator main inductances,
 $l_{\sigma D}$ and $l_{\sigma Q}$ are dampers leakage inductances,
 $l_{\sigma fd}$ is the linkage inductance between the rotor main field and the stator d-axis,

In these scheme the linkage inductance between d-axis stator and direct damper is neglected. "In the Fig.4. the blocks "d-load" and "q-load" represent the equivalent loads in Park's framework of the real power factor load. This last is star-connected and an inverse Park's transformation is needed to elaborate "d-load" and "q-load". This is useful because all equations involved in the simulation are given in Park's framework" [2]

IV. CONCLUSIONS

In this paper, different accurate models of load and generation were examined. As a load models component-based load modeling were shown which contain 'ZIP' (polynomial) model, exponential model, exponential-'ZIP' model and ETMSP & EPRI model as a example of combination of fundamental models. All models examined in this paper are static load models. The static load models can be used for approximation of the dynamic behavior of the power system. Moreover static nonlinear load models can be used for transient stability analysis. However this model is not appropriate for capturing true load response and for industrial applications

measurement-based models are required. 'ZIP' model gives only approximate results of real power behavior. Exponential model is more accurate and has only two parameters to be estimated. Exponential-'ZIP' model is also very promising but it is a little bit more complex what can give unwanted confusion [3]. "With continued expansion of power grid, it becomes more and more important that the model used in simulation programs consist with the actual characteristics of electric apparatus. Up to now, the model of generators, transformers and power lines have been established perfectly, as for the model of load, due to its randomness, time-varying and distribution property, it could barely describe the whole characteristics exactly by one or more groups of equations. Accurate load modeling has become one of the most difficult problems in power system research fields." [5]

Second part of the survey consists synchronous generator model by electrical circuit. This model consists the global electrical scheme of the generator by flux equations. Paper [2] contains tests of the three synchronous generator models which can be distinguished into: synchronous generator modeling by electrical circuits, by state equations using an inside load and by state equations using an outside load.

V. REFERENCES

- [1] Prabha Kundur, "Power System Stability and Control", 2007
- [2] Emile MOUNI, Slim TNANI and Gérard CHAMPENOIS, "Comparative study of three modeling methods of synchronous generator.", IEEE, 2006
- [3] Y. Li, H.-D. Chiang, B.-K. Choi, Y.-T. Chen, D.-H. Huang and M.G. Lauby, "Representative static load models for transient stability analysis: development and examination", IET Gener. Transm. Distrib., 2007, 1, (3), pp. 422–431
- [4] A. Maitra, A. Gaikwad, P. Pourbeik, D. Brooks, "Load Model Parameter Derivation Using an Automated Algorithm and Measured Data", IEEE, 2008
- [5] Jingchao Zhang Anhe Yan Zhuoya Chen and Kun Gao, "Dynamic Synthesis Load Modeling Approach Based on Load Survey and Load Curves Analysis", IEEE, DRPT2008 6-9 April 2008 Nanjing China
- [6] Dmitry Kosterev, Anatoliy Meklin, "Load Modeling in WECC", IEEE, 2006
- [7] Emile Mouni, Slim Tnani and Gérard Champenois, "Synchronous generator output voltage control via a generalized predictive R S T controller.", IEEE, 2008
- [8] E. Spahic, J. Morren, G. Balzer and G. Michalke, "Mathematical Model of the Double Fed Induction Generator for Wind Turbines and its Control Quality", IEEE, POWERENG 2007, April 12-14, 2007, Setubal, Portugal
- [9] Srinivas R. Chellapilla, Badml H. Chowdhury, "A Dynamic model of Induction Generators for Wind Power Studies", IEEE, 2003
- [10] José Cidrás and Andrés Elías Feijóo, "A Linear Dynamic Model for Asynchronous Wind Turbines With Mechanical Fluctuations", IEEE TRANSACTIONS ON POWER SYSTEMS, VOL. 17, NO. 3, AUGUST 2002
- [11] J. R. Marti and K. W. Louie, "A Phase-Domain Synchronous Generator Model Including Saturation Effects, IEEE Transactions on Power Systems, Vol. 12, No. 1, February 1997
- [12] E. Lu, G. Bronner, A. Ilk, C. Neumeyer, S. Ramakrishnan, "MODEL for TFTR Motor-Generator (MG)", IEEE, Princeton, New Jersey, 1995
- [13] Zhijun Li and Lijuan Cui, "The Building and Analyzing of the Fifth-Order Model of the Synchronous Generator in Stand-Alone Infinite System", IEEE, 2005

Renewable energy from the oceans – Wave power, tidal power and ocean streams

Lars Bork, Bastian Garnitz, Thomas Krisch, Carsten Schwartze
BTU Cottbus

I. INTRODUCTION

When thinking about renewable energies, wind, solar and hydro energy typically come to mind.

To tackle climate change and all the challenges imposed by the need to find alternative and reliable energy sources, there is one major resource that has remained untapped until now: marine energy.

The potential of wave energy has been recognized for long, and mostly associated with a destructive nature. The following paper will give the reader a short overview about using wave and tidal energy as a renewable energy source.

Wave energy is a concentrated form of solar energy: the sun produces temperature differences across the globe, causing winds that blow over the ocean surface. These cause ripples, which grow into swells. Such waves can then travel thousands of miles with virtually no loss of energy.

The total wave energy resource is as large as world electricity consumption, approximately 2 TW. About 10-25 % of this resource is economically usable. [1]

Tidal power occurs because gravities of the moon and sun combined with the rotation of the earth cause periodic changes of the oceans. These changes are called tidal range. The considerable level difference between high tide and ebb at many coasts of the earth generates an enormous energetic potential, which can be opened and used by the mankind.

Furthermore, it is possible to use the energy of ocean streams which are caused by the complex interactions between warm and cold layers of water.

The global theoretic potential of tidal energy is approximated at 3000 GW, but about 100 GW are realistically recoverable. [2], [3]

II. UTILIZATION OF THE TIDAL RANGE - TIDAL POWER PLANTS

Tidal power is the result of the gravitational interaction between the moon and the earth. This gravitational force, combined with the rotation of the earth, produces a twice-daily rise and fall of the sea level, called ebb and flood.

The period of one tide is for example 12.4 hours at the France coast. The difference in water levels is used to convert the potential energy into kinetic energy, by passing through the turbines. [4], [5]

Tidal power is predictable and reliable, but it can be used economically first at a tidal range of 3-5 meters.

At a tidal power plant the water fills during the high tide a basin that is separated from the sea by a barrage.

During the following low tide the accumulated water is used to drive the turbines of the power station. The turbines can work also in the time of the filling process. Tidal barrages are built across a suitable estuary or bay. [6]

There are several operational modes: ebb and flood generation and a two-way-generation.

At the flood generation (see at Fig. 1) the sea level is higher than the basin level, so the water passes the barrage and fills the basin. The barrage then is closed to dam and to create a hydrostatic head. At the ebb generation (see at Fig. 2) the water will pass the barrage from the basin to the sea when the sea level has fallen under the basin level.

A single basin system can deliver electrical energy only half a day. An option is the double-basin system. One basin will operate in flood generation and the other in ebb generation. Both basins are connected and it is possible to use this construction as pump storage power plant. The main basin will be filled at the high tide and pumped the water to the second basin. During the ebb, the second basin will generate the electricity. [4], [5], [7]

There are different types of turbines that are available for use in a tidal barrage: bulb, rim and tubular turbines.

A bulb turbine is one in which water flows around the turbine. If maintenance is required then the water must be stopped which causes a problem and is time consuming with possible loss of generation.

When rim turbines are used, the generator is mounted radially around the rim and only the runner is in the flow. This turbine is more efficient because the water flow is not so constricted.

The tubular configuration sets the runner at an angle so that a long tubular shaft can take rotational power out to an external generator. [6]

The idea of tidal power plants is known since the end of the 19th century. In 1913 the first tidal power plant was built in Husum / Germany. At present there are only a few tidal power plants in operation. The largest power plant is situated at the river Rance / France near St. Malo with a maximum power of 240 MW. [5], [7]

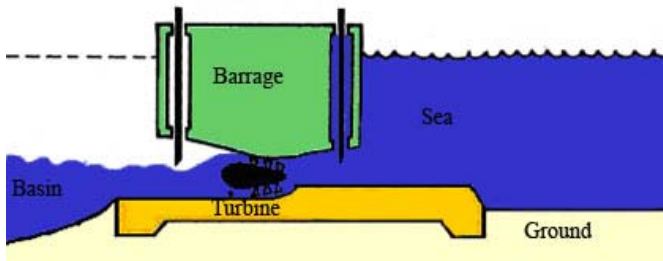


Figure 1: flood generation with a bulb turbine
Source: www.seas.upenn.edu; date: 25 February 2009

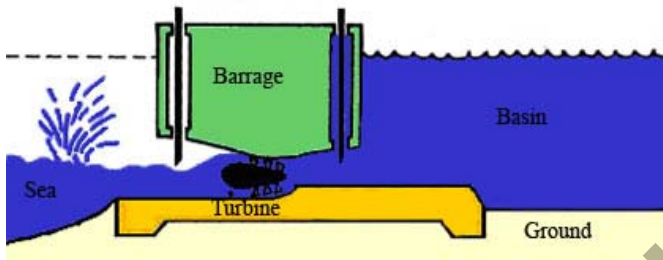


Figure 2: Ebb generating system with a bulb turbine
Source: www.seas.upenn.edu; date: 25 February 2009

III. UTILIZATION OF NATURAL ENERGY FLOWS – OCEAN CURRENT POWER PLANTS

An Ocean Current Power Plant (OCPP) works similar to the functionality of wind turbines. Both types of power plants make use of the kinetic energy of the streaming medium, which they are surrounded by.

Advantageously for sea turbines a lower flow speed is needed [8]. Compared to the air current it is much easier to predict marine current due to less important random effects. The streaming is whether driven by the tides or by oceanic circulations. Therefore prognoses for generated electricity are more reliable as well [9].

The submarine turbines are anchored at the bottom of the ocean and the outlet of electricity happens via undersea cable. To achieve an ideal economic usage, the water depth must be 20 – 35 meters and the flow velocity must reach 1.5 – 2.5 meters per second [10]. Due to the water density, which is a thousand times higher than air, ocean current has a much higher power density. Compared to the face of wind turbine, submarine rotors realize a performance that is eight times higher. The prototype of „Seaflow“, an OCPP, reaches a performance of 350 kW at 20 cycles per minute. Prototypes using a twin rotor already reach a performance of 2.1 MW (see Figure 3, right) [10].

The impact of saline environment is problematical due to the process of decomposition that affects on the construction materials of the machines. The construction of OCPPs has effects on the speed of the ocean current and with this on maritime ecological system as well. The locations of OCPPs influence the barge traffic by getting into the ships routes [8].

In Europe approximately 100 locations exist, where OCPPs are going to be built. The whole potential is estimated on 70 TWh per year. Thereby 2-3% of the European current drain could be satisfied [10].



Figure 3
left: prototype „Seaflow“ at the west coast of Britain (photo: ISET)
right: planned OCPP (graphic: *Marine Current Turbines*)
Source: Quaschnig, V. (2007): *Regenerative Energiesysteme – Technologie, Berechnung, Simulation*, 5. Auflage, München: Hanser-Verlag 2007

IV. UTILIZATION OF THE CONTINUOUS UNDULATION - WAVE POWER PLANTS

A wave carries both kinetic and potential energy. The total energy of a wave depends roughly on two factors: its height (H) and its period (T). The power carried by the wave is proportional to H^2 and to T, and is usually given in Watt per meter of incident wave front. The energy content of a wave is determinable by application of the linear wave theory. [11] The total area of the seas amounts to 360.8 million km². If half of the body of water is raised only around 0.5 m, then 0.6 EJ are stored in the form of potential energy. [12] To use the wave energy however only areas of offshore regions with low water depths are possible. Thus less than 1% of the demand of electricity could be covered by German waters. [12] The energy of the sea waves can be used differently for power production. Attention should be paid to the capacities of a wave which are not always constant. That means an energy converter is needed that works with a high efficiency at all ranges of performance. In addition with to the construction of the plant you have to consider the largest wave which can be expected to accident avoidance. Furthermore the used material must be adapted on the rough maritime climate and the aggressiveness of sea water. [11]

At this point of time three considerable operational principles for wave power stations are developed:

- OWC system (oscillating water column)
- Floating system (Pelamis technology)
- TapChan

A. Oscillating water column

With OWC systems a chamber with air inclusion is created. A wave enters from the bottom in the closed chamber. The air of the chamber is compressed and drives a turbine and a generator. With the reverse flow of the wave, air flows again through the turbine back into the chamber. [11], [12] For OWC a Wells turbine is used which rotates in the same direction regardless of the air flow, thus generating irrespective of upward or downward movement of the water column. [3] The capacity range of these plants extends over 500 kW up to several MW capacities. [11]

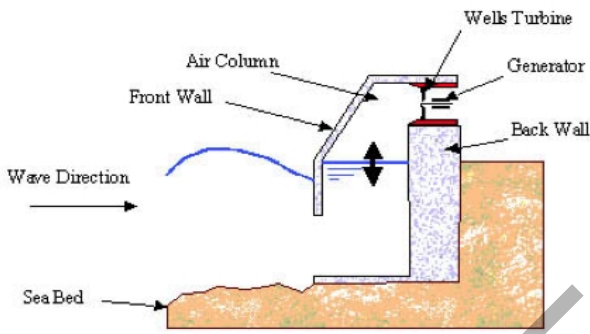


Figure 4: Schematic of an Oscillating water column,
Source: www.montaraventures.com/pix/oscillating-water-column.jpg
date: 25 February 2009

B. Floating System

Floating systems use the potential energy of a wave. These systems consist of a tubular with an air filled lifting body. At the hinged joints from the lifting body, hydraulic pistons are fixed. Due to the undulation the hydraulic pistons are pressing an operating liquid under high pressure into a compensating reservoir. Thus a hydraulic generator is powered [11], [12]. The stationary part of the plant is deep-seated at the sea bed [13]. The capacity of a generator amounts to approx. 750 KW. By linkage of several generators a total output about 30 MW could be obtained [12].

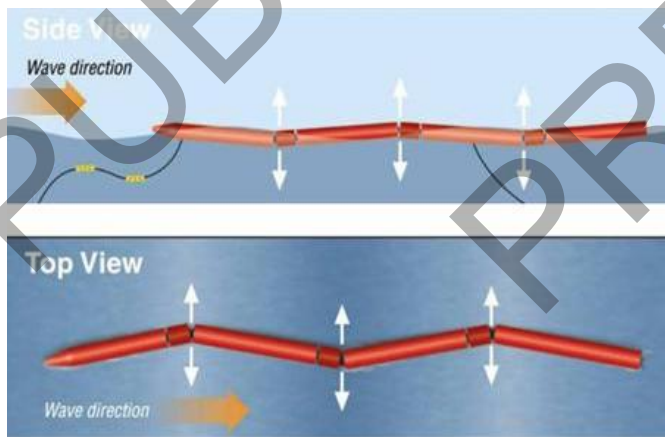


Figure 5: Floating system
Source: www.enel.it/azienda_en/ricerca_sviluppo/dossier_rs/img/Pelamis.JPG
date: 23 March 2009

C. Tap Chan

Tap Chan is an abbreviation for “Tapered Channel”. The waves in coastal area taper to an artificial ramp. The water which has a higher potential energy is collected in an upper reservoir. The artificial head is used to operate turbines, for example Kaplan turbines. [11] A huge disadvantage of this installation type is the high place requirement in the coastal area [12]. If “Sea-parks” were build with a lot of such plants then approx. 30% of European power requirement could be covered with wave energy [11].

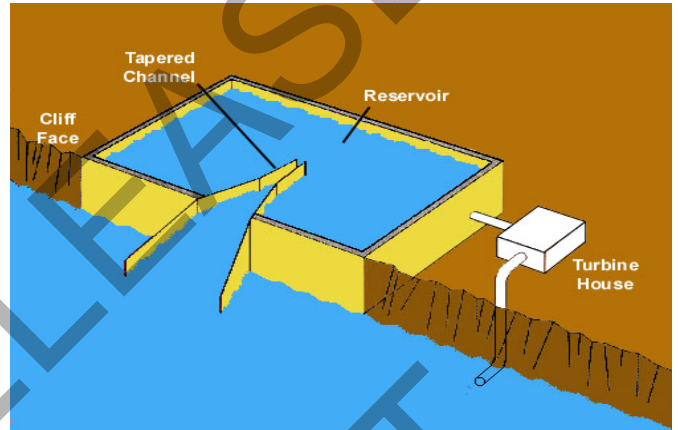


Figure 6: Schematic of a Tapered Channel
Source: <http://www.rise.org.au/info/Tech/wave/image007.jpg>
date: 25 February 2009

V. OUTLOOK

Presently there are only a few power plants that are operated commercial, the others are for research. Therefore it is difficult to say how much it will cost, for example the investment for each kW.

There is still a lot to be done. As already mentioned the potential for renewable energy from the oceans is still there. Altogether, although tidal energy is a reliable source, however the technically usable potential of the tidal energy appears globally seen too low, that it could make a substantial contribution for power supply of the future. For Germany it is not possible to use tidal energy because of technical reasons. At German coastlines the tidal ranges amount to just under 3 meters.

The basic problems in using wave power are trivial and generally known: Wave power is unstably and could not affect in its size. Large waves have also a destructive nature. The problem solutions, in order to arrange an economical usage of wave energy with justifiable impact on the environment, are however not trivial. It is very complex and expensive to build a power plant which resists the large waves. Researchers believe that only large power plants with a high efficiency are competitive.

As well as the potential of wave power is relative low in Germany because the waves and streams at the coastlines and estuaries are too small for an economical usage.

Finally, against the background of more scarcely becoming resources of fossil fuels much efforts will be made to use the actual potentials in order that energy from the oceans make a contribution, whatever to which amount, to the world's energy mix. [14], [15]

REFERENCES

- [1] Cruz, J. (2008): Ocean Wave Energy – Current Status and Future Perspectives, Berlin, Heidelberg: Springer-Verlag 2008, pp. 1-2, 93-94
- [2] www.neurohr-info.de/html/gezeitenenergie.html, date: 25 February 2009
- [3] www.tud.uni-duisburg-essen.de/exarb/imig/sonnewindwasser/reg-energie.html#343, date: 25 February 2009
- [4] Kaltschmitt, M., Streicher, W., Wiese, A. (Hrsg.) (2006): Erneuerbare Energien Systemtechnik, Wirtschaftlichkeit, Umweltaspekt, 4. Auflage, Berlin, Heidelberg: Springer-Verlag 2006, pp. 598-600
- [5] Giesecke, J., Mosonyi, E. (2005): Wasserkraftanlagen - Planung, Bau und Betrieb, 4. Auflage Berlin, Heidelberg: Springer-Verlag 2005, pp. 107-115
- [6] www.esru.strath.ac.uk/EandE/Web_sites/01-02/RE_info/Tidal%20Power.html, date: 26 February 2009
- [7] www.worldenergy.org/publications/survey_of_energy_resources_2007/tidal_energy/755.asp date: 25 February 2009
- [8] Quaschnig, V. (2007): Regenerative Energiesysteme – Technologie, Berechnung, Simulation, 5. Auflage, München: Hanser-Verlag 2007, pp. 285-286
- [9] www.marineturbines.com/23/advantages_of_marine_currents, date: 28 February 2009
- [10] Giesecke, J., Mosonyi, E. (2005): Wasserkraftanlagen - Planung, Bau und Betrieb, 4. Auflage Berlin, Heidelberg: Springer-Verlag 2005, p. 116
- [11] Giesecke, J., Mosonyi, E. (2005): Wasserkraftanlagen - Planung, Bau und Betrieb, 4. Auflage Berlin, Heidelberg: Springer-Verlag 2005, pp. 117-121
- [12] Quaschnig, V. (2007): Regenerative Energiesysteme – Technologie, Berechnung, Simulation, 5. Auflage, München: Hanser-Verlag 2007, pp. 286-287
- [13] Cruz, J. (2008): Ocean Wave Energy – Current Status and Future Perspectives, Berlin, Heidelberg: Springer-Verlag 2008, pp. 287-290
- [14] www.tud.uni-duisburg-essen.de/exarb/imig/sonnewindwasser/regenergie.html#343, date: 29 February 2009
- [15] www.unendlich-viel-energie.de/de/wasser/detailansicht/article/160/potenziale-der-meeresenergie.html, date: 29 February 2009

Carbon Capture and Storage – Part of the solution to the climate change problem?

Robin Kuscheck, Sören Schlüter, Martin Noack
Brandenburgische Technische Universität Cottbus

I. INTRODUCTION

Focusing the state-of-the-art of renewable energy science and technology, you are forced to advance the established energy sources. Today, it's not possible to substitute coal-burning power plants, nuclear power plants or gas-fired power plants for solar power stations or wind power stations.

The task is also to explore environmentally compatible technologies for reduce the carbon dioxide emission and uncouple it of the economic growth. The energy demand grows because of the emerging markets like China or India and their coal deposits. The Kyoto Protocol or the objectives of the European Union are confronted the countries with the problem of global warming resulting from the greenhouse gases.

II. CARBON CAPTURE AND STORAGE

For example, the Carbon Capture and Storage (CCS) technology allows an environmentally compatible consumption of fossil fuels. Before, during or after the power plants process the carbon dioxide should be absorbed followed by underground storage at the point sources. According to experts and scientists the CCS technology will be fully developed around 2020 and will be a part of the future energy mix.

The CCS is a process consisting of three elements: capture, transportation and storage of carbon dioxide.

There are several ways for capturing: the pre-combustion, the oxyfuel, the post-combustion.

During the *pre-combustion* a fuel (e.g. coal) will be extricated before the combustion at power plant. At a high temperature, the fuel is separated into synthesis gas of carbon monoxide and hydrogen. In the next step, the carbon monoxide converts with a help of steam into carbon dioxide, which can be sectioned out of this gas mixture and be compacted into liquidity. This procedure is also known as Integrated Gasification Combined Cycle.

→ Air
Separation of air
→ Coal / O ₂
Gasification
Gas purification
Deposition of CO ₂ →
Power generation

At the *oxyfuel*, the proportion of oxygen in air is boosted to reduce the fumes. Instead of nitrogen and sulfur compounds, only hydrogen and carbon dioxide are the residues of the combustion in oxygen followed by the cooling down and

condensation of water. The advantage of the oxyfuel is the clean carbon dioxide after the burning in clear oxygen (see below "Schwarze Pumpe").

→ Air
Separation of air
→ Coal / O ₂
Boiler
Fume Cleaning
Deposition of CO ₂ →

Another possibility is the *post-combustion* with the expansion of the conventional flue gas cleaning. After the denitrification and desulfurization, the flue gas flows through a fluid of amine which reacts with the carbon dioxide. After heating, the carbon dioxide is available in a clear state that can be compacted.

→ Air / Coal
Conventional Steam Power Plant
Fume Cleaning
Deposition of CO ₂
→ CO ₂

In the majority of cases, the carbon dioxide cannot be stored close to the power plant. It is necessary to transport the liquid carbon dioxide in pipelines or by motor trucks or ships. The storage locations which can be in run are utilized natural gas or oil fields (Enhanced Oil Recovery), deep coal steams (Enhanced Coal Bed Methane) or saline aquifers.

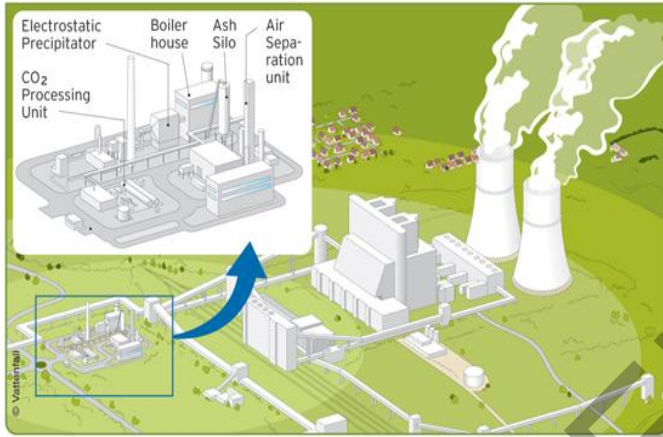
III. SCHWARZE PUMPE/GERMANY

In 2005 Vattenfall decided on building a 30 MW oxyfuel pilot plant, with an investment of 50 Mil. €, which is the first visual sign of Vattenfall's project on CCS. This installation is located near the existing lignite fired 1600 MW power plant in Schwarze Pumpe, Germany.

On May 29th 2006 was the groundbreaking ceremony of the Vattenfall pilot plant, which has been in operation from the middle of 2008. The initial testing programme will run for three years. Thereafter, the pilot plant will be available for other tests. The plant is planned to be in operation for at least 10 years. The pilot plant is an important milestone to reach the goal of commercial concepts for carbon capture and storage at coal fired power plants by 2015 until 2020. It will be the first pilot plant in the world to use the oxyfuel capture method. The construction of the 30 MW thermal pilot plant at "Schwarze

Pumpe” is an important thing for the Vattenfall project. It is the necessary link between initial engineering and successful operation of the future 250—350 MW electricity demonstration plant. Vattenfall’s goal is to develop a concept at a total cost of approximately €20/tonne of avoided CO₂. But it is to mention, that not only the plant in Schwarze Pumpe is inaugurated to CSS.

Figure 1. Carbon Capture Unit



Further, nearby the plant in Jämschalde, which uses no CO₂ reducing system, Vattenfall currently investigates the possibilities of implementing both oxyfuel and post-combustion technology at these plants. The complete implementing could be realized in the year 2015.

IV. WORLDWIDE DEVELOPMENTS AND PROJECTS

The mentioned desire to use fossil fuels without polluting the atmosphere implicates other projects in research and development on CCS technology. The center of that can be sight in Europe and the United States. Furthermore, developing and emerging markets even show the readiness for cooperation. For example, the public Algerian energy association and a joint venture of international associations prove the separation of CO₂ in the Sahara Desert. In addition, India and China cooperate with the Great Britain or rather with the United States. First of all, these cooperations conduce to find storage locations. The important role of China in CCS technology because of the determining importance of climate protection depends of the rapid economic growth, the growth of the energy demand or the coal deposits.

Beside German companies, Great Britain and the United States regard the CCS technology as a central topic of their energy policy. For example, the US-“Clean Coal Power Initiative” receives a two billion Dollar budget annually till 2011.

In Germany, the public research spending for the projects “Geotechnologien” or “Cooretect” aggregate around 1.5 Billion Euro for the whole energy und climate section from 2008 till 2011.

The priorities and research objectives of the CCS projects reached a big variety. Engineers and academics are engaged in

sub-process or whole the process chain of deposition of CO₂ and in questions of transport and storage.

The Australian Otway Basin Pilot Project wants to press big quantities in empty natural gas fields as soon as to study the other CCS technologies.

The US-CO₂ Capture Project focuses the competitive deposition of CO₂ and the safety aspect of the three methods.

The European CO₂ ReMoVe (research, monitoring, verification) explores the criteria of the storage and technologies of feeding storage locations.

The international Carbon Sequestration Leadership Forum consists of 21 countries and supports the exchange of information and multilateral collaboration.

V. CONCLUSION

The Carbon Capture and Storage technology seems to be a trendsetting way in future energy mix, next to the renewable energy. It is an advancement of conventional power plants, which ensure the power supply. It is necessary to broaden the existing international cooperation to reach the goal as soon as possible.

But we are also forced to ask, if the carbon capture in natural gas or oil fields, deep coal steams or saline aquifers is the right solution. At the moment, we don’t see possible risks in the far-away future. In order to guarantee the success of the project, it is necessary that all countries which use coal plants introduce the CSS technology. If this takes part of the energy production, the benefits for the environment will be increased.

REFERENCES

- Vattenfall AB:
http://www.vattenfall.com/www/co2_en/co2_en/399559ourxr/index.jsp
- CCS: IZ Klima – Informationszentrum klimafreundliches Kohlekraftwerk e.V.
http://www.iz-klima.de/fileadmin/website/downloads/CCS-Broschuere_RZ_Web.pdf

FFT algorithm optimization using Stream SIMD Extension instruction set

Pawel Dawidowski
Wroclaw University of technology

This paper explain how to perform Cooley and Tukey fast Fourier transform for sequence length being power of 2 using modern Stream SIMD¹ Extension known as SSE. Basis of FFT algorithm will be shown pointing on which parts can be significantly speed up using SSE focusing on programming side rather than FFT algorithm itself. Also basic SSE instruction will be introduced.

I. FFT

The idea of calculating digital convolution is to approximate integral in (1) to (2) on finite sum over N samples of signal:

$$\int_{-\infty}^{\infty} f(t) \cdot e^{-j\omega t} dt \quad (1)$$

$$X_k = \sum_{n=0}^{N-1} x_n \cdot e^{-\frac{2\pi j kn}{N}} \quad k = 0, 1, \dots, N-1 \quad (2)$$

Point is this raw calculation need to perform N multiplication over k which takes also N values so overall complexity of algorithm is N^2 . Even for relatively small numbers of samples the amount of calculation can be pretty high. Assuming N is power of 2 Cooley and Tukey has split odd and even elements of sum (2):

$$W^{kn} = e^{-\frac{2\pi j kn}{N}} \quad (3)$$

$$X_k = \sum_{n \text{ even}}^{N-1} x_n \cdot W^{kn} + \sum_{n \text{ odd}}^{N-1} x_n \cdot W^{kn} \quad (4)$$

Each of those summations is recognized as being an N/2 point DFT of the respective sequence because:

$$W^2 = e^{-\frac{2\pi j 2}{N}} = e^{-\frac{2\pi j}{\frac{N}{2}}} \quad (5)$$

So if we calculate DFT for odd and even indexed k in (2) we can calculate overall DFT combining (4) together:

$$\bar{X}(k) = \bar{X}_{\text{even}}(k) + W^k \bar{X}_{\text{odd}}(k) \quad (6)$$

Using this approach we will need only $N \cdot \log_2 N$ complex multiplication to perform, because we need exactly $\log_2 N$ of 2 times smaller DFT to calculate.

For example if $N = 1024$:

$$DFT : \text{multiplication need} = N^2 = 1048576 \quad (7)$$

$$FFT : \text{multiplication need} = N \log_2 N = 10240$$

Because of this great time reduction FFT algorithm is widely used in many application which need Fourier transform.

¹ SIMD is abbreviation from Single Instruction Multiple Data. In the term of SSE instruction 4 single precision floating point or 2 double precision floating point operation are performed in parallel on one processor core.

II. STREAM SIMD EXTENSION

SSE is a mathematical coprocessor which operates on floating point numbers. It has 8 additional and independent 128-bit registers for calculation which are 4x32-bit single precision floating point value or 2x64 double precision one. The main advantage of using it is performing 4 or 2 operation in parallel, so depending on precision we need it can cut the algorithm execution time 4 or 2 times.

Basic SSE instruction set is shown in table 1, while full instruction set with descriptions and timing is available at Intel web site (Ref. [2]). All instruction which end -PS is doing 4 parallel operations at simultaneously while -SS mean only one operation.

TABLE 1
SSE BASIC INSTRUCTION SET

Instruction	Operation
MOVSS, MOVAPS, MOVUPS	Copy operation: from memory. to register
MOVSD, MOVAPD, MOVUPD	from register to memory from register to register
ADDPS, ADDSS, ADDPD, ADDSD	Addition
SUBPS, SUBSS, SUBPD, SUBSD	Subtraction
MULPS, MULSS, MULPD, MULSD	Multiplication
DIVPS, DIVSS, DIVPD, DIVSD	Division
SHUFPS	In register data shuffle

There are few things which can be optimized using those instructions. First thing is to rewrite complex multiplication to take advantage of parallel operation. Second is to notice, that in first step $W^{kn} = -1$ so no complex operation is actually necessary. In second step we have at most 4 W^{kn} values 1, j, -1, -j which can threaten as a special case. Since W^{kn} are k^{th} root of one we can calculate it inside of SSE register for next steps. Only value need to load is to load complex number for $k = 1$ in (3). Next values for next k can be calculated by recursion (8):

$$W^{kn+1} = W^{kn} \cdot W^1 \quad (8)$$

III. COMPLEX MULTIPLICATION ON SSE

To calculate complex multiplication using SSE we can assume at the beginning that we want to perform 2 multiplications at once. With 4 floating point register each pair of 2 values can be complex real and imaginary part. For start assume we want to calculate:

$$\begin{aligned}\bar{Z}_A &= a_A + jb_A \\ \bar{Z}_B &= a_B + jb_B \\ \bar{Z}_C &= \bar{Z}_A \cdot \bar{Z}_B\end{aligned}\quad (9)$$

From algebra we know:

$$\bar{Z}_C = a_A \cdot a_B - b_A \cdot b_B + j(a_A \cdot b_B + b_A \cdot a_B) \quad (10)$$

We need 4 multiplications and 2 algebraic additions to calculate complex multiplication.

Now let's try to do this using SSE. Since we have 4 floating value in one register we can perform 2 multiplications in parallel. Let's assume we have loaded our complex numbers into XMM0 and XMM1 registers and XMM3 and XMM4 has values to change signs. Each of them contains 2 complex numbers as in the Table 2:

TABLE 2
INITIAL VALUES IN REGISTER

Register name	reg[0]	reg[1]	reg[2]	reg[3]
XMM0	a _{A1}	b _{A1}	a _{A2}	b _{A2}
XMM1	a _{B1}	b _{B1}	a _{B2}	b _{B2}
XMM3	1.0	-1.0	1.0	-1.0
XMM4	-1.0	1.0	-1.0	1.0

The program which realizes complex multiplication is:

```

1.  MOVAPS          %%XMM0, %%XMM2
2.  SHUFPS         $0xA0, %%XMM2, %%XMM2
3.  MULPS          %%XMM1, %%XMM2
4.  SHUFPS         $0xF5, %%XMM0, %%XMM0
5.  MULPS          %%XMM3, %%XMM0
6.  MULPS          %%XMM1, %%XMM0
7.  SHUFPS         $0xB1, %%XMM0, %%XMM0
8.  ADDPS          %%XMM2, %%XMM0

```

Table 3. shows how register has changed as a result of operation:

TABLE 3
REGISTER VALUES AFTER OPERATION

Line	register	reg[0]	reg[1]	reg[2]	reg[3]
1.	XMM2	a _{A1}	b _{A1}	a _{A2}	b _{A2}
2.	XMM2	a _{A1}	a _{A1}	a _{A2}	a _{A2}
3.	XMM2	a _{A1} a _{B1}	a _{A1} b _{B1}	a _{A2} a _{B2}	a _{A2} b _{B2}
4.	XMM0	b _{A1}	b _{A1}	b _{A2}	b _{A2}
5.	XMM0	b _{A1}	-b _{A1}	b _{A2}	-b _{A2}
6.	XMM0	b _{A1} a _{B1}	-b _{A1} b _{B1}	b _{A2} a _{B2}	-b _{A2} b _{B2}
7.	XMM0	-b _{A1} b _{B1}	b _{A1} a _{B1}	-b _{A2} b _{B2}	b _{A2} a _{B2}
8.	XMM0	a _{A1} a _{B1} - b _{A1} b _{B1}	a _{A1} b _{B1} + b _{A1} a _{B1}	a _{A2} a _{B2} - b _{A2} b _{B2}	a _{A2} b _{B2} + b _{A2} a _{B2}

As we can see we need only 3 parallel multiplications and one parallel addition to calculate 2 complex multiplications at once. It means we need only 1.5 multiplications not 4 and only 0.5 additions not 2 per one complex multiplication. So optimization has reduced floating point operation from 6 to 2. That's 3 times faster than without use SSE. All copy and shuffle operation are only on internal registers which is done much faster than copying values from/to memory.

IV. MEMORY OPERATION FROM AND TO SSE REGISTERS

There are two main instructions to load from memory into XMM register and to store XMM register into memory: MOVUPS and MOVAPS. First one work as a normal MOV operation but it will copy 4x32bit floating point number into XMM register. MOVAPS is faster but with one constraint: all memory addresses has to be 16 bytes aligned, it means four least significant bits in address has to be equal zero. The speed difference in practical application is about 20-30% with MOVAPS in comparison to MOVUPS. Luckily for FFT calculation every step will be 16 bytes aligned since overall data length is power of 2 so only thing to do is enable 16 bytes align in compilation options.

V. OPTIMIZING 1ST AND 2ND FFT STEP

For 1st step $W = -1$ so there is no need to perform any complex calculation. For second step $W = 1, j, -1, -j$. For those special cases we can write even shorter program. Only 3th and next steps will need full complex multiplication.

Multiplication by j is only shuffling real and imaginary part and change the sign properly as shown in (11) so it can be realized on 2 SSE instructions for 2 complex numbers in parallel.

$$\bar{Z} \cdot j = (a + jb)j = -b + ja \quad (11)$$

The program which realize complex multiplication by j using initial values as in Table 2 except XMM1 and XMM4 are skipped:

```

1.  SHUFPS         $0xB1, %%XMM0, %%XMM0
2.  MULPS          %%XMM4, %%XMM0

```

The point is that even if we want to swap real and imaginary part it could result in multiple memory read/write operation. Here 2 complex numbers are read from and write to memory exactly once so overall floating point operation number is 0.5 multiplications per one complex number.

VI. SUMMARY

Well optimized FFT algorithm can calculate Fourier transform online, even for quite large samples number, while it would be impossible to use raw DFT algorithm to calculate it even on modern processors. Using SSE cuts computation time even more by taking advantage of parallel calculation and coprocessor designed especially for floating point operation. All instructions presented in this paper are available in C++ either by inline assembly code or by intrinsic functions fully described on Microsoft web page (Ref. [3]).

VII. REFERENCES

- [1] Leland B. Jackson "Digital Filters and Signal Processing", 3th ed. University of Rhode Island. Kluwer Academic Publishers Boston Dordrecht London
- [2] <http://www.intel80386.com/simd/mmx2-doc.html>
- [3] [http://msdn.microsoft.com/en-us/library/t467de55\(VS.71\).aspx](http://msdn.microsoft.com/en-us/library/t467de55(VS.71).aspx)

Abuse of transmission congestion existing naturally or created by bidding strategies in order to exert market power

Abouzar Estebsari, Seyyed Mohammad Sadeghzadeh, Mehrdad Rostami

Faculty of Engineering,
Shahed University,
Khalig-e-Fars free way,
1417953836 Tehran, Iran,
P.O. Box: 18151/159,

Tel: (+98-21)55277560, Fax: (+98-21)55277561, Tehran, Iran

Abstract- Market power refers to conditions where the providers of a service can consistently charge prices above those that would be established by a competitive market. Market power assessment within electric power markets requires the consideration of the ever-changing network conditions that result from congestion. This paper explores the effect of changes in network congestion conditions on competitive market. Bidding strategies, such as withholding capacity and bidding at higher price, influence the network and cause transmission congestion. These strategic biddings are analyzed and the impacts of the congestion on the location marginal price (LMP) are demonstrated in detail. Congestion will cause relative scarcity of generating capacities in the congested areas, so generation companies in these areas have location market power. A 9-bus system is used to evaluate the impacts of congestion caused either by low transmission capacity or suppliers' strategic biddings. Focuses are on a transmission network with six sellers in which network constraints give rise to market power opportunities. Finally we compare two bidding strategies which exert market power by abuse of transmission limits and show enhance of location market power in congested area.

Keywords: Transmission congestion, market power, nodal marginal price, bidding strategy, electricity markets

I. INTRODUCTION

A certain electricity market has one fixed network, a certain set of geographical locations, called nodes or buses, where energy may be injected or withdrawn. The buses are interconnected in a certain way, with transmission lines that each has a certain fixed thermal limit. The thermal limit is the capacity limit to which extent power may flow over the line, without damaging it or burning it off [1]. Furthermore, expansion of the transmission network might be of interest in some cases but it is very expensive and not always of interest to the bigger market participants [2].

Transmission can play a significant role in influencing the incentives of firms to exercise market power with their generation resources, as is demonstrated in a more general model by Joskow and Tirole (1998 and 1999).

Congestions in the transmission network may split a market into regions unable to compete properly with each other. This

may cause lack of cheap energy in some areas and surplus in others. It segregates electricity market and limits competition mechanism. Segregation of markets increases location market power and weakens market efficiency in power systems [3].

Since generators' market power has direct impact on normal operation of electricity market, many literatures have discussed the market power in electricity market [4]-[10]. In economics, market power is defined as the ability to alter profitably price away from competitive levels [11]. Market power is a symptom of an uncompetitive industry and exercising market power can raise price and lower market efficiency [12].

If transmission constraints makes it impossible to bring in more power from other regions, buyers who are willing to pay prices that exceed the highest competitive will offer to do so. This leads to a price rise that will keep on going until the supply meets the demand [13].

In this paper the definitions of market power are presented from the views of economics and regulation. Bidding strategies, such as withholding capacity and bidding at high price, are analyzed and the impacts of network congestion on location market power are considered by simulating on a 9-bus system.

In the next part the OPF AC model will be explained briefly, then discuss about simulation in our case study. Congestion will cause relative scarcity of generating capacities in congested areas, so the generation companies in these areas have location market power. We segregate our system by putting transmission limits and investigate the impacts of congestion on generators' profits.

II. MARKET POWER

There are two main reasons why the potential of market power is brought to the electricity market. First there is market dominance and then there are transmission constraints [14]. Market power due to market dominance is a scenario that applies for every imperfect market and not only for the electricity market. On the electricity market, a supplier that is

large enough to affect price can exploit market power by either economical withholding or physical withholding. When dealing with economical withholding a seller keeps bidding above the marginal cost of production and thereby driving up the price. Physical withholding simply means that a seller withholds some of its available capacity.

Market power due to transmission constraints makes it necessary to get a full understanding of the topology of the transmission system before starting any plan of detecting the potential for market power [15].

A load pocket is an area where transmission constraints make it impossible to transfer electricity from elsewhere than from the local supplier. If a supplier is placed within a so called load pocket, this participant will have a local market power. A supplier in this case can find himself in a position of monopoly by intentionally create congestion and limit access of competitors. This means that, by getting dispatched at strategic points in the network, a supplier in a load pocket can gain profit even by increasing its generation rather than withholding it [16]. Conclusively, transmission constraints in the electricity market make it possible even for a small supplier to exploit market power.

In a Network loads can't be accurately forecasted and energy can't be stored economically. Demand and supply must be balance all the time in order to maintain the system frequency, voltage, stabilization standards; Kirchhoff's laws and impedance of the whole network determine the power flows in the system [17]. When there is congestion, generating capacity in congested area will be relative scarcity, so congestion results in locational market power and causes invalidation of the optimization of generating resources in the whole network.

The LMP represents the willingness to supply an additional MW of load at a particular location. It is useful to break the LMP into parts to distinguish between costs resulting from network losses and those resulting from network congestion. The LMP includes a reference cost of generation and relative costs of congestion and losses in the system:

LMP = (generation marginal costs) + (congestion cost) + (cost of marginal losses).

The generator marginal cost is taken from a specified reference generator in the system. The congestion cost represents the effect of congestion on the LMP relative to the reference generator marginal cost.

III. AC OPF FORMULATION

The AC optimal power flow problem solved by MATPOWER is a "smooth" OPF with no discrete variables or controls. The objective function is the total cost of real and/or reactive generation [18]. These costs may be defined as polynomials or as piecewise-linear functions of generator output. The problem is formulated as follows:

$$\min_{\theta, V, P_{gi}, Q_{gi}} \sum_i f_{1i}(P_{gi}) + f_{2i}(Q_{gi}) \quad (1)$$

subject to:

$$\begin{aligned} P_i(\theta, V) - P_{gi} + P_{di} &= 0 && \text{(active power balance equations)} \\ Q_i(\theta, V) - Q_{gi} + Q_{di} &= 0 && \text{(reactive power balance equations)} \\ |S_{ij}^f(\theta, V)| &\leq S_{ij}^{\max} && \text{(apparent power flow limit of lines, from end)} \\ |S_{ij}^t(\theta, V)| &\leq S_{ij}^{\max} && \text{(apparent power flow limit of lines, to end)} \\ V_i^{\min} &\leq V_i \leq V_i^{\max} && \text{(bus voltage limits)} \\ P_{gi}^{\min} &\leq P_{gi} \leq P_{gi}^{\max} && \text{(active power generation limits)} \\ Q_{gi}^{\min} &\leq Q_{gi} \leq Q_{gi}^{\max} && \text{(reactive power generation limits)} \end{aligned} \quad (2)$$

Here f_{1i} and f_{2i} are the costs of active and reactive power generation, respectively, for generator i at a given dispatch point. Both f_{1i} and f_{2i} are assumed to be polynomial or piecewise-linear functions. By defining the variable x as:

$$x = \begin{bmatrix} \theta \\ V \\ P_{gi} \\ Q_{gi} \end{bmatrix}$$

The problem can be expressed compactly as follows:

$$\begin{aligned} \text{Min } f(x) \\ \text{subject to} \end{aligned} \quad (4)$$

$$\begin{aligned} g_1(x) &= 0 && \text{(power balance equations)} \\ g_2(x) &\leq 0 && \text{(branch flow limits)} \\ x_{\min} &\leq x \leq x_{\max} && \text{(variable limits)} \end{aligned}$$

IV. SIMULATION

Matlab version 7.1 is used as simulation environment. For this simulation MATPOWER version 3.2 was used as OPF solver. The simulation study has been done on a 9-bus system with 6 loads and 6 generators. This System is shown in figure 1:

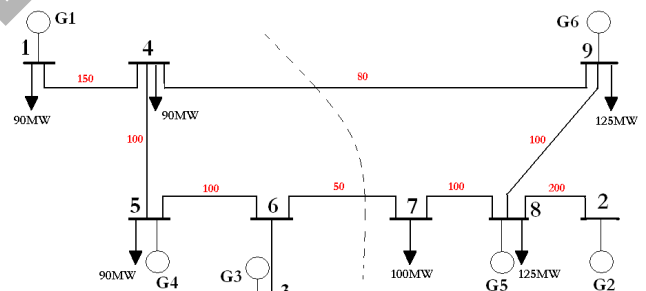


Figure 1. 9-bus system

The following capacities are offered by these generators:

Table 1. The system generators production capacities

Generator	Bus	Pmin(MW)	Pmax(MW)
1	1	10	250
2	2	10	300
3	3	10	270
4	5	10	250
5	8	10	300
6	9	10	300

The cost functions of all these generators are in appendix.

table 2. OPF results in order to Evaluate the congestion impact of the line between buses 4 and 9 on LMPs and producers' profits

Case		G1	G2	G3	G4	G5	G6	Total
Uncong.	ρ /(\$/MWh)	22.347	21.387	21.478	22.173	21.387	22.023	
	Output/MW	70.00	126.35	75.00	70.00	126.35	155.00	622.70
	Cost / (\$/h)	1039.00	2108.54	1099.06	1039.00	2108.56	2828.12	10222.29
	Profit / (\$/h)	525.26	593.72	511.79	513.10	593.72	585.51	3323.11
Cong.	ρ /(\$/MWh)	27.000	21.387	23.225	25.810	21.387	20.744	
	Output/MW	105.23	145.58	75.00	70.00	145.58	82.50	623.90
	Cost / (\$/h)	1894.34	2576.18	1099.06	1039.00	2576.24	1277.53	10462.35
	Profit / (\$/h)	946.99	537.44	642.84	767.72	537.43	433.86	3866.28
Profit Differences/ (\$/h)		421.73	-56.28	131.05	254.62	-56.29	-151.65	543.1700

As it is shown, there is congestion in network in normally competitive conditions while limiting the transmission capacities and the generators number 1, 3 and 4 which are located in congested area, have the suitable conditions to gain much more profit. The outputs of generators, LMPs, generating costs, profits, and profit differences, with or without congestion, are listed in Table 2.

If power losses are neglected and there is no congestion, the LMPs are equal in all the buses, but in this simulation we consider transmission losses. So in both cases there are locational marginal prices. The point is the differences between these two cases in LMPs and the generators profits. When there is congestion in the system, the market is divided into two parts: the congested area and the uncongested area. In the congested area, all LMPs are higher than those without congestion.

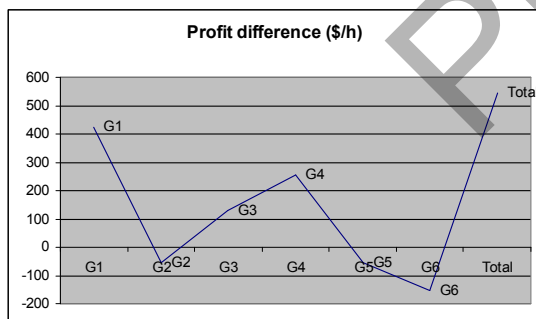


Figure 2. profit difference in simulation part A

A. Evaluation of congestion impact of the line between buses 4 and 9 on LMPs and producers' profits:

In Fig.1, the generation companies bid at their actual costs, without considering the constraints of line transmission capacity, the active power flow in Line 4-9 is 79.8MW. Then reduce the capacity of the line 4-9 to 40MW in order to evaluate the congestion impact of this line on locational marginal prices and producers' profits. See table 2:

When there is congestion, in the congested area the more generating capacities are called upon in order to meet the load requirement. In this example, the incremental generating capacity in congested area is implementing by increasing G1 capacity from 70.00MW to 105.23MW. And you see in figure 2, its profit difference is the most of all.

Because of congestion, the market total generating costs are increased by 240.06\$/h and the generators' profits are increased by 543.17\$/h. In the same time, the customers have to pay more for energy. Generally congestion has segregated the market.

B. Generators exert strategy bidding to create congestion:

B – 1) The Strategy of bidding at high prices:

As we discuss before, one of producers' bidding strategies is bidding at high prices to create congestion in some transmission lines. In our system, the generator number 1 which had gained the most profit due to congestion has the potential of exerting market power by this bidding strategy. G1 has a linear piecewise cost function and the factor K is added to its initial value to increase its bidding price. The simulation results of this bidding strategy are shown in table 3:

Table 3. G1 bidding strategy at high prices:

K	0	10	10.5	11	11.5	12
/(\$/MWh) ρ	22.347	27.162	28.470	28.501	28.593	28.703
Output / MW	70.00	46.85	48.25	35.21	27.86	17.884
) \$/h / (Cost	1039.00	701.254	585.812	473.261	346.885	188.953
) \$/h / (Profit	525.26	571.28	787.86	503.26	449.71	324.37
L9-4	U ¹	C	C	C	C	C

The results in Table 3 show that when the bidding prices of G1 are increased step by step, the LMPs in relevant bus (Bus 1) are decreased gradually. When K is zero, the LMP is 22.347 \$/MWh and G1's output is 70MW; when k is 12, the LMP is 28.703 \$/MWh and G1's output is 17.884MW. Because the profits of G1 depend on LMP, its output and corresponding generating costs, the G1's profits are increased from 525.26\$/h to 787.86\$/h (maximum, when k is 10.5), and then reduced gradually. When k is larger than 12, the relevant LMP increase, but G1's outputs decrease, so G1's profits are less than 525.26\$/h, which is the profits that G1 gains in normally competitive conditions. When k is 10, Line 4-9 is congested.



Figure 3. Generators' profits and output power

B – 2) Withholding some capacity to exert congestion and gain more profit

Similarly, G1 bids its actual costs but withhold some capacity, and other generators' bidding curves are the same as those in normal competitive conditions, G1's outputs, profits, LMPs and congestion conditions of Line 4-9 are all listed in Table 4. As you see in part (B – 1) there is no limitation in G1 production capacity and this generator is not constrained by its maximum capacity, because its output share is 70 MW and its maximum capacity is 250 MW. In order to see the effect of this strategy – withholding capacity – we will reduce this maximum capacity which is bided by this company from 70 MW to 20 MW and then run market simulation program.

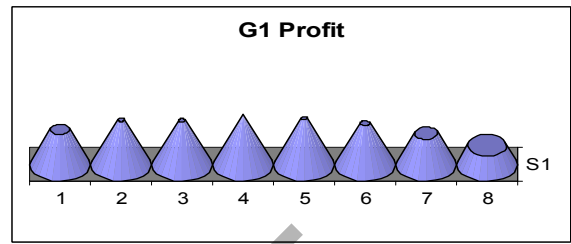


Figure 4. G1 profit by strategy of withholding capacity

From Table 4 we conclude that because the costs of G1 are lower, all of its bidding capacities are dispatched namely, G1's outputs are its bidding capacities. When the bidding capacities of G1 are decreased step by step, the LMPs in relevant bus are increased gradually. G1's profits are increased from 524.04 \$/h to 744.45\$/h (maximum, when G1's output is 50MW), and then decreased gradually. When the bidding capacity (output) is 60MW Line 4-9 is congested.

From Table 3 and Table 4, we conclude that bidding at high price and withholding capacity both can artificially create transmission congestion. When k is 10 or G1's bidding capacity (output) is 46.85 MW, Line 4-9 begins to congest. When there is congestion, and the generators in congested area bidding at higher price (by increasing k) or withholding capacity (by decreasing G1' bidding capacities), they can gain additional profits.

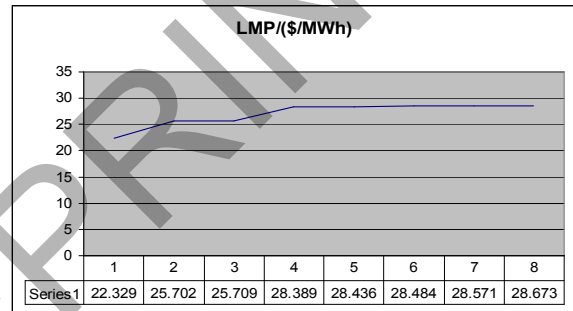


Figure 5. Location marginal prices after exerting bidding strategy of withholding capacity by G1

¹ U means unconstrained and C means constrained.

Table 4. G1'S DATA WITH WITHHOLDING CAPACITY

Bidding/MW	70	60	55	50	45	40	30	20
Output/MW	70	60	55	50	45	40	30	20
/(\$/MWh) ρ	22.329	25.702	25.709	28.389	28.436	28.484	28.571	28.673
Cost /(\$/h)	1039.01	846.01	757.76	675.01	597.76	526.01	399.01	294.00
)\$/h / (Profit	524.04	660.13	656.23	744.45	681.89	613.37	458.13	279.47
L9-4	U	C	C	C	C	C	C	C

From the above tables, we conclude that the impacts of two bidding strategies (withholding capacity and bidding at higher price) are equivalent. When G1 bids at higher price, G1 gains maximal profit 787.86\$/h (when k is 10.5 and G1's output is 48.25MW). When G1 bids by withholding capacity, it also gains maximal profit 744.45\$/h (when G1's bidding capacity is 50 MW). So both bidding strategies at the same values result the same profits.

V. CONCLUSION

The grid structure in which the power transactions need to be accommodated in modern electricity markets may impact greatly the market efficiency and, more generally, the market outcomes. Network and commodity of energy have some particular characteristics, in the congested area, all LMPs are higher than those without congestion. If generators bid in strategies to exercise the market power, they can gain high additional profits.

VI. APPENDIX

Table 5. Generators' piecewise linear cost functions

Generators	X0	Y0	X1	Y1	X2	Y2
G1	1500	0	3	0.11	5	150
G2	2000	0	3	0.085	1.2	600
G3	3000	0	3	0.1225	1	335
G4	1500	0	3	0.11	5	150
G5	2000	0	3	0.085	1.2	600
G6	2000	0	3	0.085	1.2	600

For piecewise linear cost:

$x_0, y_0, x_1, y_1, x_2, y_2, \dots$

Where $x_0 < x_1 < x_2 < \dots$ and the points $(x_0, y_0), (x_1, y_1),$

$(x_2, y_2), \dots$ are the end- and break-points of the cost function.

REFERENCES

- [1] Ettore Bompard, Yuchao Ma, Roberto Napoli, and Graziano Abrate, "The Demand Elasticity Impacts on the Strategic Bidding Behavior of the Electricity Producers", IEEE TRANSACTIONS ON POWER SYSTEMS, VOL. 22, NO. 1, FEBRUARY 2007
- [2] James Bushnell, "Transmission Rights and Market Power", University of California Energy Institute, April 1999 This paper is part of the working papers series of the Program on Workable Energy Regulation (POWER)
- [3] Galloway, S (2006), "Introduction to Market Power" [lecture notes]. University of Strathclyde, Glasgow
- [4] Yang Jian and G. Jordan, "System dynamic index for market power mitigation in the restructuring electricity industry, "in *Proc. 2000IEEE Power Engineering Society Summer Meeting*, pp.2217-2222.
- [5] Fernando L. Alvarado, "Market power: a dynamic definition, " in *Proc. 1998 Bulk Power System Dynamic and Control- Restructuring Conf.*
- [6] D.Gan and D. V.Bourcier, " Locational market power screening and congestion management: experience and suggestions, " *IEEE Trans. On Power Systems*, vol. 17 pp 180 -185, Feb. 2002.
- [7] Gerald B.Sheble, " Computational auction mechanisms for restructured power industry operation," Kluwer Academic Publishers, 1999.
- [8] Marija Ilic , Francisco Galiana, and Lester Fink, power system restructuring: engineering and economics," Kluwer Academic Publishers, 1999.
- [9] D. Gan and D. V.Bourcier, " A simple method for locational market power screening, " in *Proc. 2002IEEE Power Engineering Society Winter Meeting*, pp 434-439.
- [10] R.Moreira e Silva and L.D.B. Terra, "Market power under transmission congestion constraints, " in *Proc. 1999International Conference on Electric Power Engineering*, pp.82.
- [11] A. Mas-Collel, A. Whinston, and J. Green, *Microeconomic Theory*. New York: Oxford Univ Press, 1995.
- [12] S. Stoff, *Power Systems Economics: Designing Markets for Power*. New York: IEEE/Wiley, 2002.
- [13] Claudia P. Rodriguez, and George J. Anders, "Bidding Strategy Design for Different Types of Electric Power Market Participants", IEEE TRANSACTIONS ON POWER SYSTEMS, VOL. 19 NO. 2, MAY 2004
- [14] David A. Kumar. "Market Power in Electricity Supply", IEEE Transactions on energy conversion, Vol.16, No. 4, Pages: 352-353, December 2001.
- [15] Mary B. Cain and Fernando L. Alvarado. "Metrics for Application of Revenue Sensitivity Analysis to Predict Market Power Coalitions in Electricity Markets", IEEE Proceedings of the 36th Annual North American Power Symposium, August 9-10 2004 University of Idaho, Moscow, Idaho.
- [16] Robert J Thomas Bernard C. Lesieutre and Timothy D. Mount. "Identification of load pockets and market power in electrical power systems, Decision Support Systems," Vol. 40 Issue 3-4 , October 2005, Pages: 517 - 528, ISSN:0167-9236.
- [17] Daniel Kirschen and Goran Strbac, "Fundamentals of Power System Economics", 2004 John Wiley and Sons Ltd.
- [18] Ray D. Zimmerman and Deqiang Gan. Matpower, user's manual, 24 december 1997.

“Banning of Incandescent Bulbs” and Its Influence to Electromagnetic Compatibility

LU Yan

Abstract—This paper presents worldwide “Banning of incandescent bulbs” campaign, which aims to replace traditional incandescent bulbs that have long been known as inefficient sources of electrical lighting, with compact fluorescent lamps (CFLs). Controversy, operations and comparisons between these two alternatives are introduced in succession. Electromagnetic compatibility (EMC) issues, such as light flicker, which emerge more apparently because of the coming popularization of CFLs, will be discussed. Additionally, precautionary senses and steps to limit adverse interferences are mentioned when installing lighting systems.

Index Terms—incandescent light bulbs, compact fluorescent lamps, flicker, electromagnetic compatibility

I. BACKGROUND

The worldwide “Banning of incandescent bulbs” campaign has been supported by most governments, according to pass measures to phase out incandescent light bulbs. In some jurisdictions this has been done through legislation (Cuba, Brazil and Venezuela phased out incandescent light bulbs in 2005); while others, like United Kingdom, through voluntary measures. The aim is to encourage use of more energy efficient lighting alternatives, such as compact fluorescent lamp (CFLs) and LED lamps.

For European Union, the Irish government was the first member state to ban the sale of incandescent light bulbs. It was later announced that the member states of the EU agreed to a phasing out of incandescent light bulbs by 2012, which will save the European economy up to 10 billion euros. Nevertheless, it is up to the government of each member state on how to accomplish the eventual phase out. For example Italy will accomplish this through a ban on their sale, while the UK has enlisted the help of retailers with a voluntary, staged phase out.[1][2][6]

II. CONTROVERSY OF THE CAMPAIGN

A. Environmental concerns

As the recommended alternative, CFLs, like all fluorescent lamps, contain small amounts of mercury as vapour inside the

glass tubing, averaging 4.0 mg per bulb. A broken compact fluorescent lamp will release its mercury content. Safe cleanup of broken compact fluorescent lamps differs from cleanup of conventional broken glass or incandescent bulbs. Because household users in most regions have the option of disposing of these products in the same way they dispose of other solid waste, most CFLs are going to municipal solid waste instead of being properly recycled.

B. Cost and existing fixtures

The cost of CFLs is higher than incandescent light bulbs. Typically this extra cost may be repaid in the long-term as CFLs use less energy and have longer operating lives than incandescent bulbs. However, there are some areas where the extra cost of a CFL may never be repaid, typically where bulbs are used relatively infrequently such as in little-used closets and attics. Use in situations such as stairways where the lamp is turned on for less than five minutes at a time will cause a significantly shorter lifespan for a CFL. In the case of a 5-minute on/off cycle the lifespan of a CFL can be up to 85% shorter, reducing its lifespan to the level of an incandescent lamp.

Typical CFLs may have issues when being used in older dimmer light fixtures and with some electric timers, meaning many people would need to replace fixtures to retain that functionality. However some specialized CFLs can be purchased which may fit into the fixture without the need for replacement.[6]

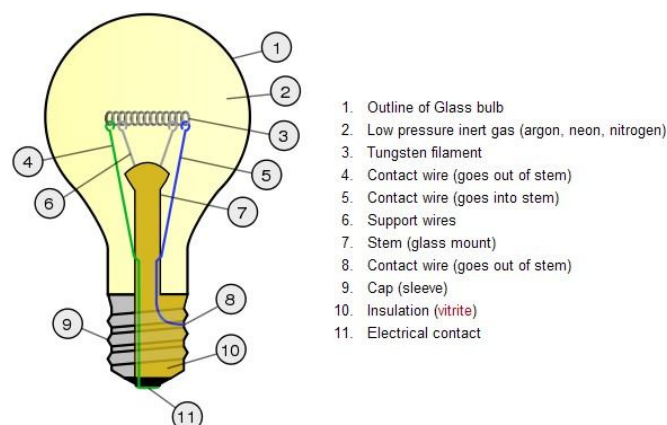


Figure 1. Interior configuration of an incandescent bulb

LU Yan is with the Faculty of Electrical Engineering, Wroclaw University of Technology, Wroclaw 50-370, Poland (e-mail: yanr61@gmail.com).

III. OPERATIONS AND COMPARISONS OF INCANDESCENT BULBS AND CFLs

Incandescent lamps, with the interior configuration shown in Fig. 1, consist of a tightly coiled tungsten filament supported in an inert gas typically argon encapsulated in a glass bulb.[6] Electrical current passes through the filament heating it to 2000-3000°K where it emits photons in the visible range as well as considerable amount in the Infra-Red range.

Fluorescent lighting excites gaseous mercury atoms in a plasma arc. These atoms release photons in the UV range which then excite a phosphor coating to produce visible light. The plasma arc exhibits negative resistance and therefore requires an electrical ballast to limit the current.

Traditional incandescent lamps have remained relatively unchanged since the invention in the 19th century and have long been known as inefficient sources of electrical lighting. With current global pressures towards energy efficiency, CFLs offer 4-5 times the efficiency using fluorescent technology. From the statistical result of Fig. 2, we can get the straightforward understanding of efficiency discrepancies.[6] By compacting the discharge tube and developing low cost electronic ballasts, domestic use is increasing.

However, a number of concerns have been raised when replacing incandescent lamps with CFLs. Some lamps: 1) produce a 'cool white' colour not matching the 'warm white' colour of incandescent bulbs, 2) have delayed start-up and/or take considerable time reach full brightness, 3) fail to produce the equivalent rated light output, 4) produce audible sound, and 5) are usually non-dimmable. Aside from these consumer aspects, CFLs like incandescent lamps are susceptible to power system disturbances resulting in light flicker.[3]

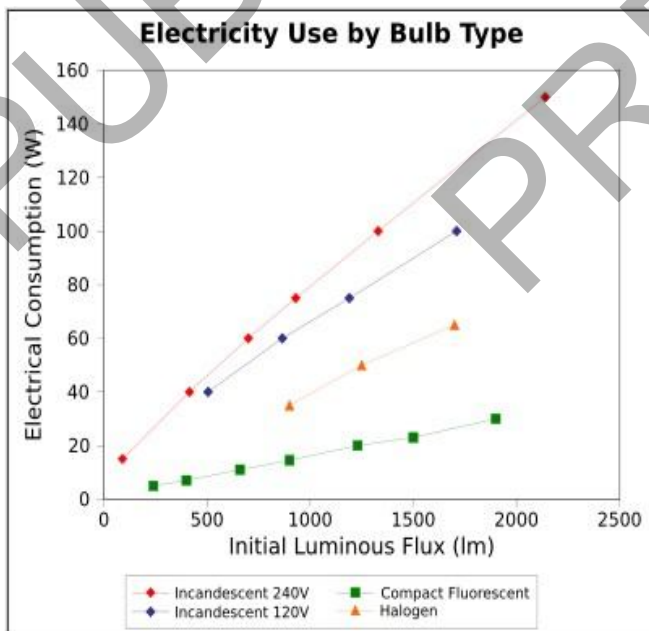


Figure 2. Energy usage for different types of light bulbs

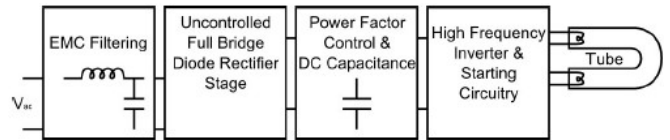


Figure 3. Typical CFL ballast design

IV. INFLUENCE TO THE ELECTROMAGNETIC COMPATIBILITY

Light flicker (Flicker) is the variation of luminous flux (or visible light) within the frequencies perceptible by people. It generally has an adverse physiological effect on persons causing eye strain and/or even annoying emotion. In rare cases it can have serious health risks such as being stranded in distraught situation, loss of concentration, headaches or the triggering of epileptic seizures.[3][6]

However, because CFLs use electronic ballasts, their subsequent non-linear behaviour has made modelling of their operation difficult. Equally their susceptibility to voltage disturbances resulting in visible light flicker is widely unknown and difficult to predict. This has given rise to discrepancies between the measured flicker levels by relevant international flicker standards and the actual flicker produced.

A typical CFL ballast[5], as shown in Fig. 3, consists of a single phase rectifier stage creating a DC bus from which a high frequency inverter resonates to control the fluorescent tube current. Due to the diode rectifier, some require EMC filtering to comply with national harmonic standards, some however omit this. During starting two filaments at either ends of the tube are heated to create enough free ions for the plasma to be formed. Depending on the designed heating time, a delayed start-up can occur, on the other hand, insufficient heating reduces the lamps life.

For an uncontrolled full bridge rectifier the AC side voltage relates to the DC bus voltage through the switching function (modulation) by the diodes. Fig. 4, shows a generalised case of a rectifier switching function on a voltage waveform with a small distortion. Given that an AC side disturbance results in a modulated DC disturbance, the light output is likely to experience a similar fluctuation and result in visible flicker.[3]

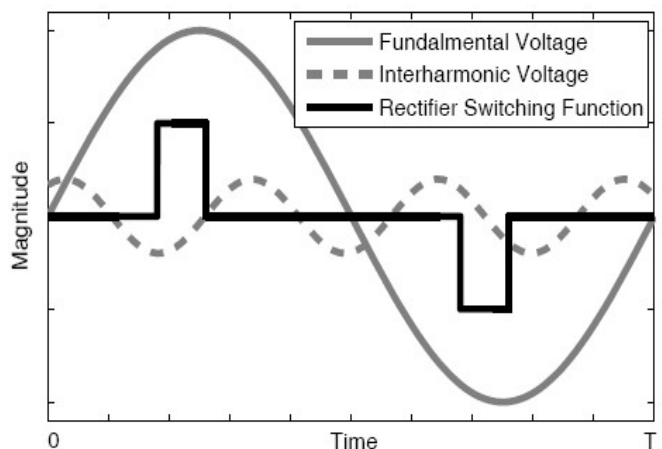


Figure 4. Switching operation of uncontrolled single phase rectifier

V. INSTALLING PRECAUTIONS RELATED TO EMC ISSUES

The lighting system is one of the most pervasive of the electrical loads. Lighting can create localized electrical field problems and affect susceptible electronic equipment.[4]

Especially for the coming popularization of CFLs, problems related to electromagnetic compatibility emerge apparently. Electric fields develop around fluorescent lighting fixtures, and today's electronic ballasts create high-frequency fields. The impact of these fields depends upon the sensitivity of equipment within those fields and the distance from the fixtures to the equipment.

Obviously, installation engineers should consider adverse interference effects when making selection of lighting fixtures. Our advice is to control the end results in the beginning rather than spend countless dollars and hours combating problems after the fact.

To minimize interference effects, take the following steps:

1. Install all wiring for lighting in separate conduits and power lighting circuits from dedicated-use isolation transformers.
2. Never combine lighting circuit wiring with computer system or other susceptible electronic system wiring in the same raceway.
3. In areas with susceptible equipment, use lighting systems without high-frequency electric fields (e.g., DC) or lighting fixtures with electromagnetic interference screens to control the electric fields.

Also, there are a few simple precautions should be taken for installing lighting systems near computers and data cables. They aren't new, and can be found in numerous site preparation manuals. Nevertheless, they warrant repeating here:[4][6]

1. Keep lighting circuits out of computer power panels.
2. Do not install data cables so that they run on top of fluorescent lighting fixtures because the magnetic fields from electronic ballasts may inductively couple

into the data cable.

3. Make sure that you do not install poorly shielded data cables in the electric fields below lighting fixtures.

VI. CONCLUSION

“Banning of incandescent bulbs” is the governmental campaign to phase out the inefficient incandescent bulbs with compact fluorescent lamps (or LED lamps), which are not only taken into account of improving efficiency, but also should be considered of its following influence to electromagnetic compatibility issue, such as light flicker.

Because of CFL ballast, the induced flicker is much more complex, which may cause serious healthy problems to customers and subsequential detriment to the whole system's power quality. To minimize those potential interferences, installing precautions should be noticed and checked as the indispensable condition.

VII. REFERENCES

- [1] Georges Zissis: CFL Quality and Strategies to Phase-out Incandescent Lamps. International Energy Agency, Paris (France), February 16th, 2007
- [2] Beletich Associates: Phase-out of Inefficient Incandescent Lamps and Standards for Compact Fluorescent Lamps. Prepared for Australian Greenhouse Office, December 2007
- [3] L. P. Frater, N. R. Watson: Light Flicker Sensitivity of High Efficiency Compact Fluorescent Lamps. Proceeding of Universities Power Engineering Conference, Australia, December 2007, page 1-6
- [4] Tom Shaughnessy: Lighting System and Electromagnetic Compatibility. PowerCET Corporation, Calif., USA, May 2007
- [5] Eur Ing Ir David Cogan: Technical Specifications for Compact Fluorescent Lamps with Integral Ballast. APEC Energy Efficiency Standards
- [6] Wikipedia website: www.wikipedia.org

VIII. BIOGRAPHIES

LU Yan was born in 1984 in China. He received his B.Sc. degree in University of Electronics Science and Technology of China, Chengdu, in July 2007. From October 2007, he started his master study of Control in Electric Power Engineering in Wroclaw University of Technology, Poland. Currently, he is taking one-year BOND project with AREVA T&D Ltd in UK. His interests are power quality and artificial intelligence.

Reactive power in one-phase circuits with periodical voltages – reactive power compensation

Sebastian Slabosz

Wroclaw University of Technology, Institute of Electrical Engineering Fundamentals
Janiszewskiego 8 Str., 50-370 Wroclaw, E-mail: s.slabosz@gmail.com

Abstract - The article states about reactive power compensation methods for circuits with non-sinusoidal voltages, there have been presented selected theories application in order to compensate the reactive power in one-phase circuits. Also measurement results after compensation of an actual object supplied from an non-sinusoidal voltage source were presented. Also algorithms of optimal capacity selection were given, which connected in parallel to the circuit with inductive character will cause current root-mean-square value minimization.

I. INTRODUCTION

Significant part of electrical energy receivers draw active energy and convert it for work and heat, as well as reactive energy. Reactive power describes the process of electrical and magnetic field energy exchange. The process of energy exchange can proceed independently from work and heat exchange process. The utilization measure of energy supplied to receiver is the power factor:

$$PF = \frac{P}{S} \quad (1)$$

where: PF – power factor, P – active power, S – complex power.

As complex power we name the biggest active power value, which can occur for given root-mean-square value of voltage and current:

$$S = UI \quad (2)$$

where: U_{RMS} – voltage root-mean-square value, I_{RMS} – current root-mean-square value.

If the receiver works with small power factor, it means that it draws bigger current than it is necessary. If the reactive power is drawn from distant sources it causes a rise of supply currents and in consequence rises the transmission losses. As a result it is needed to increase the transmission line conductor cross section and lowering the ability to load the generators and transformers with active power. All this aspects are causing increase of operation costs incurred by the electrical energy recipients.

II. REACTIVE POWER IN CIRCUITS WITH PERIODIC VOLTAGES

Reactive power is correctly defined for linear circuits with sinusoidal voltages (3):

$$Q = UI \sin \varphi \quad (3)$$

Basing on above mentioned dependence (3) it is possible to select the optimal capacity with which we will achieve power factor correction:

$$C = \frac{Q \cdot T}{U^2 \cdot 2 \cdot \pi} \quad (4)$$

Whereas for non-linear circuits or circuits supplied with distorted voltages many power theories exist. In this article selected reactive power theories will be demonstrated and used to compensate an actual object (choke with ferromagnetic core) supplied from public network.

III. REACTIVE POWER IN CIRCUITS WITH NON-SINUSOIDAL VOLTAGES

Most disseminated reactive power theory for non-sinusoidal voltages and currents is the one defined in 1927 by C.I. Budeanu [1]:

$$Q = \sum_{n=1}^{\infty} U_n I_n \sin \varphi_n \quad (5)$$

where: n – harmonic number, φ_n - phase displacement between voltage and current of the n-th harmonic.

From the beginning the reactive power theory proposed by Budeanu, besides many adherents, had many opponents. The main charges for this theory are lack of physical deformation power interpretation and unauthorized oscillatory components summation of particular harmonics. In 1987 L.S. Czarnecki has published a scientific work in which he criticized the Budeanu power theory [2]. He advanced a hypothesis about its worthlessness for the sake of lack of possibilities to:

- minimize the reactive power and therefore no possibility to correct the power factor,
- reactive power Q_B is no measure of energy oscillation,
- it doesn't enable the calculation of capacitor capacity, by which the power factor is the biggest,
- it suggests incorrect energetic phenomena interpretation with distorted voltages.

One of the advantages arguing for this theory usage is its conservatism and relatively simple measuring devices construction. However this argument, in actual signal

processing theory state, is insufficient according to the article Author.

In the twenties of 20th century M. Iliovici has presented a reactive power interpretation as loop area which is made by current and voltage coordinates [5].

$$Q = -\frac{1}{2\pi} \oint idu \quad (6)$$

Characteristics in I, U coordinates of non-linear objects are usually complex and create multiple loops and furthermore their shape changes strongly under the influence of voltage change. Areas inside loops are circulated clockwise or counterclockwise. Therefore the energy of electric or magnetic field is sometimes drawn and sometimes returned. We select the capacitor capacitance connected to the object to achieve a state in which the resultant loop area will be equal zero, and so the reactive power will be equal zero. But it doesn't mean that magnetic and electric field energy won't be mentioned. If energy is not mentioned the object characteristic in I, U coordinates is reduced to a line segment. The reactive power compensation basing on above mentioned theories is made using the formula (7), for given supplying voltage we can determine an optimal capacity, which connected to circuit (Figure 1) will cause rms value decrease.

$$C_{opt} = \frac{2 \cdot \pi \cdot Q}{\dot{u}^2 \cdot T} \quad (7)$$

where: Q – reactive power, \dot{u} - voltage derivative rms value, T – time period.

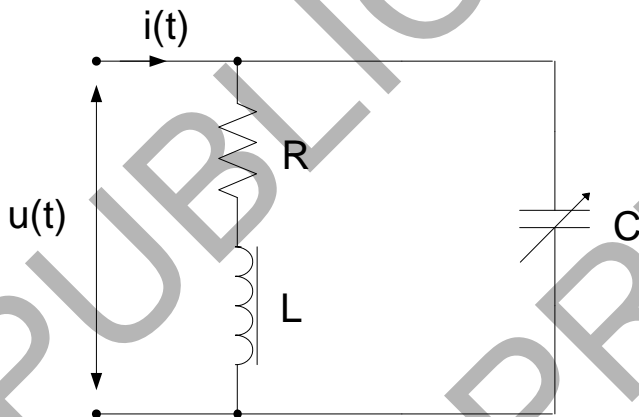


Figure 1. Parallel compensation.

In 1931 S. Fryze proposed reactive power determination for distorted voltages in such a way that the power equation is fulfilled (8) [4], [5]:

$$S = \sqrt{P^2 + Q^2} \quad (8)$$

Fryze thought that power is a too elementary concept to define it with assistance of such complicated instrument like Fourier series, which was introduced by Budeanu. In his theory Fryze distributed current to sum of two, mutually orthogonal, currents:

$$i(t) = i_a(t) + i_b(t) \quad (9)$$

where: $i_a(t)$ – active current component, $i_b(t)$ – reactive current component.

And so the reactive power was equal (10):

$$Q_F = |U||I_b| \quad (10)$$

where:

$$i_a(t) = G_e u(t) \quad (11)$$

Where G_e can be determined from (12):

$$G_e = \frac{P}{\|u\|_{L^2}^2} = \frac{\frac{1}{T} \int_0^T u(t)i(t)dt}{\frac{1}{T} \int_0^T u^2(t)dt} \quad (12)$$

An unquestionable advantage of Fryze's theory is elimination, from initial Budeanu theory, of Fourier series and third power component (deformation power).

For many years there hasn't existed a generally accepted theory describing energetic properties of circuits with non-sinusoidal voltages. The problem gathered meaning with power electronics development. In seventies of twentieth century Shepherd and Zakikhani have presented their reactive power idea [7]. This theory is limited only to one-phase circuits. The authors have distributed current sources into two components:

$$i(t) = i_R(t) + i_r(t) \quad (13)$$

where:

$$i_R(t) = \sqrt{2} \sum_{n=1}^{\infty} |I_n| \cos \varphi_n \cos(n\omega t + a_n) \quad (14)$$

Resistive current component,

$$i_r(t) = \sqrt{2} \sum_{n=1}^{\infty} |I_n| \sin \varphi_n \sin(n\omega t + a_n) \quad (15)$$

Reactive current component, where:

$$a_n - \arg U_n,$$

φ_n - angle (U_n, I_n)

Whereby these currents are mutually orthogonal:

$$\int_0^T i_R(t) i_r(t) dt = 0 \quad (16)$$

The current defined by dependence (17) is called the passive reactance current and can be interpreted as current which is connected with reflexive source-receiver energy flow, and his measure is the reactive power Q.

$$i_r(t) = \sqrt{2} \operatorname{Re} \sum_{n=1}^{\infty} j_0 B_n U_n \exp(jn\omega t) \quad (17)$$

This current can be compensated for finite harmonics number with a reactive two-terminal network connected parallel to receiver (Figure 1) with susceptance for every examined harmonic.

This property was noticed for the first time by E. Emmanuel [3]. On the basis of Shepherd and Zakikhani's theory it was possible to determine compensatory capacitor capacitance - "optimal capacitance", for which the source coefficient is the biggest:

$$C_{opt} = \frac{\sum_{n=1}^{\infty} n |U_n| |I_n| \sin \varphi_n}{\omega \sum_{n=1}^{\infty} n^2 |U_n|^2} = \frac{\sum_{n=1}^{\infty} n Q_n}{\omega \sum_{n=1}^{\infty} n^2 |U_n|^2} \quad (18)$$

The advantages of this method are:

- $i_r(t)$ current determination, which can be compensated for finite harmonics number using reactive two-terminal network,
- optimal capacitance value determination.

Kusters and Moore have created a theory which enables to calculate the optimal compensating capacity [6], which significantly simplifies the compensation in comparison with Shepherd and Zakikhani's theory, because of its harmonics manipulation, which requires the knowledge on phase displacement of particular harmonics.

According to this theory the current can be resolved into three orthogonal components: active current i_a (identical with active current from Fryze's definition), reactive capacity current i_{rC} and complementary reactive current i_{rCs} .

$$i = i_a + i_{rC} + i_{rCs} \quad (19)$$

Optimal compensation capacitance is then defined in the time domain as:

$$C_{opt} = - \frac{\dot{u} \circ i}{\|\dot{u}\|^2} = \frac{Q}{\left\| \frac{du}{dt} \right\| \|u\|} \quad (20)$$

Compensation made with this method is a lot easier than according to Shepherd and Zakikhani's theory. Also the capacitance values calculated according to formula (20) are identical like for dependence (18).

IV. REACTIVE POWER COMPENSATION

In order to present the compensation effect with the help of proposed by author theories, a choke with unknown parameters was supplied with net voltage as shown on (Figure 2):

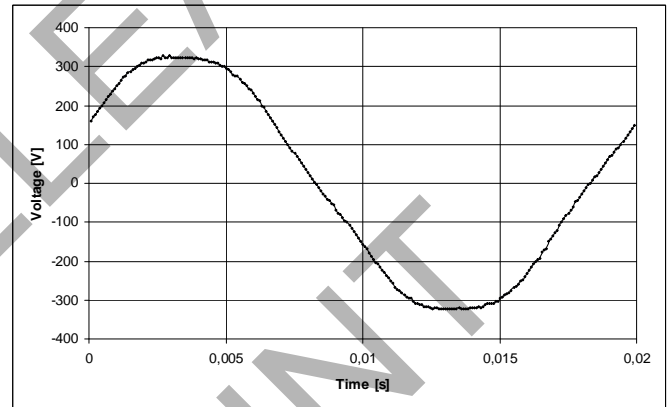


Figure 2. Voltage versus time graph

For voltage rms value $U_{rms}=235.65$ V the system response was current shown on (Figure 3) with current rms value $I_{rms}=2.7511$ A. The power factor value was $PF=0.127$.

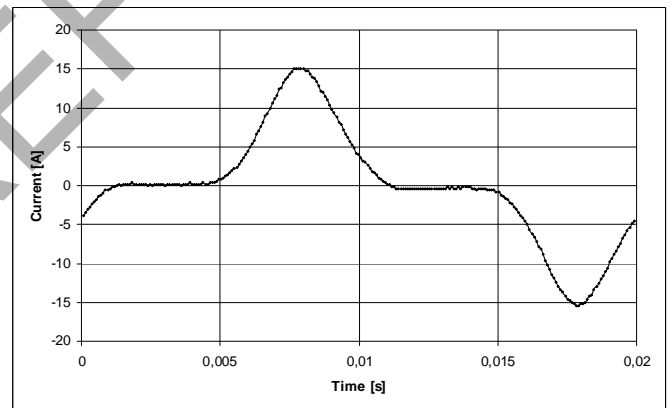


Figure 3. Current versus time graph

After making the observation of current it can be seen that the element is a strongly nonlinear object. Reactive power according to C.I. Budeanu, evaluated from (5) equation, equals $Q=550.59$ var. Optimal capacitance, which has to be connected to the circuit to achieve the compensation, was evaluated

according to (4) equation, equals $C_{opt}=2.40$ mF. Within making the measurements this capacity was corrected depending on the value of reactive power; more and more the reactive power was closer to zero, the capacitor capacitance was determined more precisely. The current rms value was $I_{rms}=1.3680$ A and the power factor was $PF=0.177$.

Performing the reactive power compensation supported by the M. Iliovici [5] theory, for the same measurement conditions, the reactive power calculated from the loop area which is made by drawing the $u=f(i)$ function (Figure 4) equals $Q=546.48$ var; and the optimal capacitance equals $C_{opt}=2.34$ mF. Within making the circuit compensation the capacitance value was corrected. After the circuit compensation the current rms value was $I_{rms}=1.3601$ A and the power factor was $PF=0.189$.

For comparison the reactive power value according to C.I. Budeanu was $Q=15.422$ var. This means that making the compensation according to (5) the circuit is overcompensated.

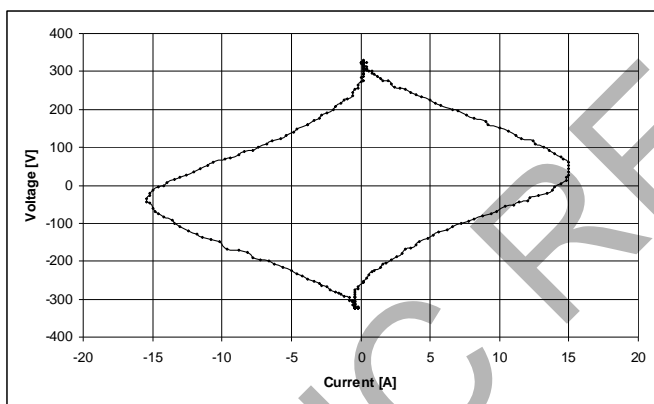


Figure 4. Reactive power loop before the compensation.

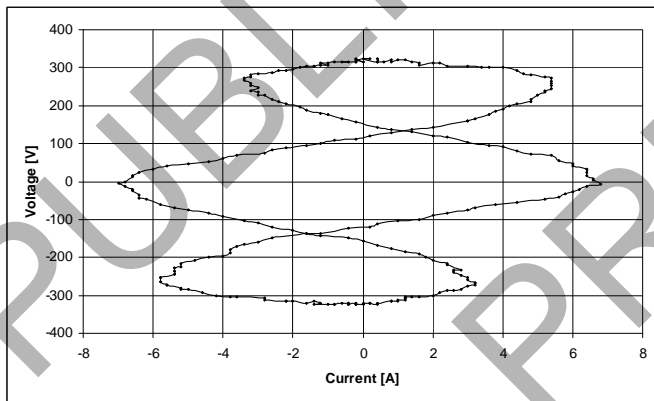


Figure 5. Reactive power loop after the compensation – loop area equals zero.

Performing the reactive power compensation supported by the Kusters and Moore theory for the same measurement conditions, the optimal capacity $C_{opt}=36.04$ uF was determined according to (20) dependence. After making the compensation the current rms value was equal $I_{rms}=2.5925$ A and the power factor was equal $PF=0.128$. It means that the compensation made using the dependence (20), proposed by Kusters and Moore, the circuit will be undercompensated.

V. CONCLUSIONS

Taking advantage of mathematical dependences and modern measurement techniques we can match the compensator capacitances, without knowledge on receiver parameters. It is a very important practical feature because the compensation can be made in real-time. Thanks to this it is possible to make quick changes in capacity value and its adjustment to receiver work conditions and supplying voltage variations. The best compensation of reactive power, this means the biggest power factor is obtained taking advantage of M. Iliovici power theory. While making the compensation using the C.I. Budeanu and Kusters and Moore theory the circuit is overcompensated or undercompensated and therefore current rms value increases and the receiver operates with small power factor. Making use of power theory utilizing the loop area calculation it is possible, as shown in the article, to compensate strongly nonlinear receivers supplied with distorted signals. It is a very important practical feature.

REFERENCES

- [1] C.I. Budeanu: Puissance reactiva et fictives. RGE, T.XXIII, 1928, 762-773.
- [2] L.S. Czarnecki: What is wrong with the Budeanu concept of reactive and distortion powers and why it should be abandoned. IEEE Trans. Instrum. Meas. IM-Vol.36, No.1, March 1988, 834-837.
- [3] S. Fryze: Moc czynna, bierna i pozorna w obwodach o przebiegach odkształconych prądu i napięcia. Przegląd Elektrotechniczny, nr 7, 1931, 193-203, nr 8, 225-234 oraz nr 22, 1932, 673-676.
- [4] S. Fryze: Wybrane zagadnienia teoretycznych podstaw elektrotechniki. PWN, Warszawa – Wrocław 1966.
- [5] M. Iliovici: Definition et Mesure de la Puissance et de l'Energie Reactives, Bull. Soc. Franc. Electryciens, LIV, (1925), n. 5, 931-956.
- [6] N.L. Kusters, W.J.M. Moore: On the definition of reactive power under nonsinusoidal conditions. IEEE trans. Pow. Appl. Systems. Vol.99, 1980, 1845-1854.
- [7] W. Shepherd, P. Zakikhani: Suggested definition of reactive power for nonsinusoidal systems. Proc. IEEE Vol.119, No.6, 1973, 704-706.
- [8] S. Slabosz: Moc bierna w obwodach jednofazowych z okresowymi przebiegami, V Konferencja Naukowa Studentów Politechniki Wrocławskiej, Wrocław, 2007.

Grid integration of renewable energy sources

P. Kammer, A. Kober
BTU Cottbus
Cottbus, Germany

I. INTRODUCTION

The growing lack of fossil fuels, the increasing demand for electricity and the harmful effect of carbon dioxide output on the climate force nations - especially industrialized countries and their governments - to find new ways of producing the amount of energy in demand. The integration of alternative energies to reduce emissions and to conserve available fossil sources is a known political aim. EU directive 2001/77/EC requires feeding in renewable energies into electricity grids. Although the potential of renewables is very high and the technical conditions to produce electricity are achieved, the current generated rates are clearly lower. A key problem is the integration of renewable energies into the existing grid. This paper analyzes the reasons for this deficit and assesses possible solutions.

II. RENEWABLE ENERGY SOURCES

There are different options for producing electricity from renewable energy sources. Consequently, there are several ways of connecting the gained electricity with the existing grid.

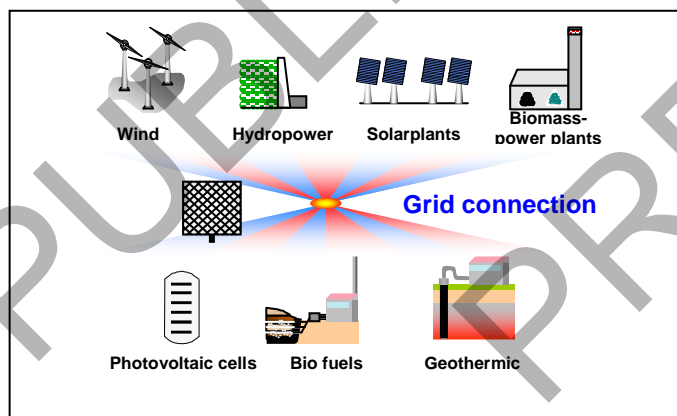


Illustration 1: in dependence on BITSCH, R.; GJARDY, G.; WOLDT, T.: Aspects of large scale RES/DG integration in existing energy supply systems -considering as example the situation in Germany, in: *International Journal of Distributed Energy Resources*, Volume 2, Number 1, 2006, S. 59-81)

Preferred sources are wind, hydro, solar, biomass, photovoltaic cells, bio fuels and geothermic (*illustration 1*). The electricity is induced by asynchronous or synchronous generators except for photovoltaic cells. This operation creates co-current flows and gets through an inverted rectifier into the power grid.

III. INTEGRATION IN EXISTING GRID / BARRIERS

To understand the problem of why the potential of renewable energy sources is not exhausted, you have to consider the actual grid conditions and the resulting barriers. The public electricity supply in most European countries presents an extensive central configuration. Grids are designed to transmit electricity generated by large conventional power plants. An aggregation occurs by using transformers between the transmission and the distribution grid. At the end is the consumer. *Illustration 2* demonstrates that the load flow mainly takes place in one direction from the highest voltage of the transmission grid with less bulk consumer to the lower ones in the distribution grid with many small consumers.¹

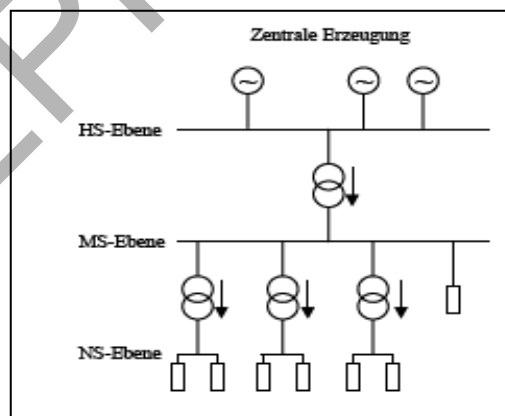


Illustration 2: B. HASCHE; R BARTH; D. J. SWIDER (*Verteilte Erzeugung im deutschen Energiesystem*) centralized energy supply and the electricity direction (source: Barth 2006)

The interconnection directly or indirectly allocates the electricity to connected users in a central way. In the distribution grid the voltage falls in the direction of the current flow. The decline depends on resistance and inductance in the cable. These two factors grow with rising cable length. To provide all consumers with enough voltage, a transformer slightly increases the voltage at the beginning of a cable. Energy generation from renewable sources requires an installation of the plant in locations with a high energy supply, for example, in areas with a grand wind velocity. Therefore, the installations are connected at different local points to the grid. In contrast to large power plants, renewable plants have less capacity and are integrated in lower grid levels. When decentralized generators integrate electricity in low-voltage lines, conditions can change and the power flows in the direction of the transformer. In this case voltage levels increase at the end of a line shown in *illustration 3*. Voltage rise aggravates in practice if more and more distributed generators, especially in pastoral areas with mostly weak grids, are integrated. This barrier of insufficient grid capacity available for renewable energy is the main problem.²

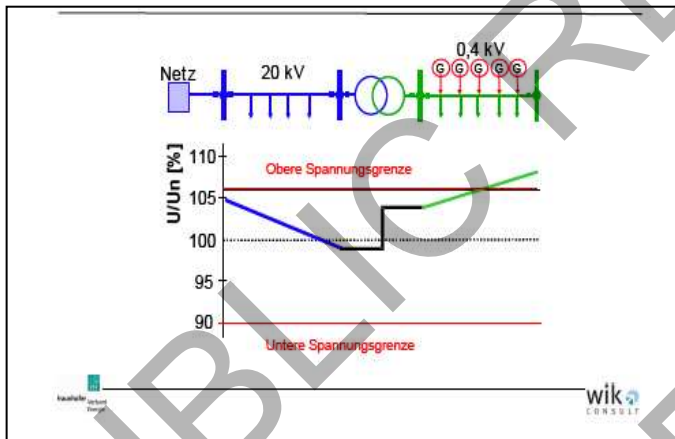


Illustration 3: voltage curve by integration of renewable energy in low voltage level
 (source: Fraunhofer ISE; wik consu
 Studie für das Bundesministerium für Wirtschaft und
 Technologie (BMWi))

The integration of distributed energy producers seriously influences the operation of the whole grid and calls for new requirements of the mains operation. For example, in Germany the “Erneuerbaren-Energien-Gesetz” (EEG) requires the permanent input of available energy from distributed renewables plants. Thus central large power plants are forced to work in part load and have additional starts. These actions have negative effects on materials, efficiency, costs of generation and lead to additional input of fossil fuels and

output of carbon dioxide.³ To avoid voltage rises, the grid has to be partly extended. The costs of grid reinforcement are often very high. The benefits of producing energy from renewable sources are often considered less important than the costs. Moreover, alternative power developers have highlighted that it is impossible to determine the available grid capacity so that they are unable to verify the technical and cost data of the grid connection presented to them by the grid operator. Furthermore, Distribution System Operators (DSO) are often linked to electricity generation companies. It is disputable whether such a DSO is fully objective towards independent renewable energy producers when the electricity generation company is involved in developing alternative energy programs. The insufficient transparency of grid connection causes long lead times to obtain grid connection authorization. Polls show that stakeholders’ perceptions of grid barriers per renewable energy source are very high.⁴

IV. DECENTRALIZED GENERATION / FUTURE INTEGRATION

The trend for additional energy supply systems (especially by using renewable sources) in the medium and low voltage level is highly visible. But to solve all mentioned barriers and to afford integration of renewable energy sources, many changes are necessary, including the configuration of an intelligent distributed electricity system as the most important alteration. However, there is no clear definition of this concept. In Europe it is called “decentralized generation”. Decentralized energy supply aims at generating the energy where it is required, or respectively consuming the energy where it is generated.

It is necessary to supply the available energy – in particular supply-dependent renewable energy – to that load which at the moment of occurrence has the most urgent demand or is being used for the optimum purpose. Additionally, supply of an area has to be economically and ecologically optimized according to criteria which yet have to be specified.⁵ The character of a distribution grid will move from the pure allocation of electricity to the consumer to an orientation of the generation measured on the demand of the complete system due to the accession of distributed generation. *Illustration 4* shows the modification of the whole grid. The main difference is the generation and integration of distributed producers in the medium and low voltage level and possible input of electricity in higher sections if the demand falls below the supply.⁶

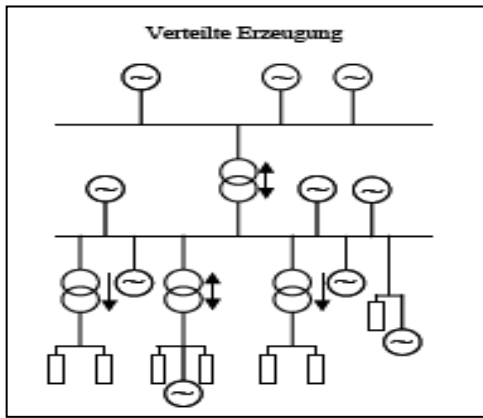


Illustration 4: B. HASCHÉ; R BARTH; D. J. SWIDER
 (Verteilte Erzeugung im deutschen Energiesystem)
 decentralized energy supply and the electricity direction

To avoid interferences and overcharge in circuits, storage facilities such as accumulator systems, capacitors or compressed-air stores have to be developed and used. This operation requires that network operators actively incorporate distributed generators in the grid management. Energy management can facilitate such interactions between different electricity levels. Functions like communication, information, control, metering, services, planning, optimization and forecast will be of high importance to manage the grid system error-free.⁷

The integration of many decentralized generators can be concentrated in a “virtual plant” to increase the efficiency. Such projects contain the optimization of the energy mix of different renewable energy source characteristics in one area. This concentration of many small generators allows the supply of huge quantities of electricity by considering them as one large power plant. Such an integration of renewable energy sources not only supplies additional energy but is a part of the grid’s capacity. Virtual plants can also act as “microgrids” and work independently from the main grid. Such network expansions which are not grid-controlled do not aggravate mains power failure but help to hold the grid steady. Projects in this vein help to increase the total benefits from renewable generation and integration by smoothing and fulfillment of planning.⁸

IV. SUMMARY

Energy supply will pass through a technological change from a so far generation-dominated, security- and reserve-thinking centralized grid to a demand-oriented, economically-/

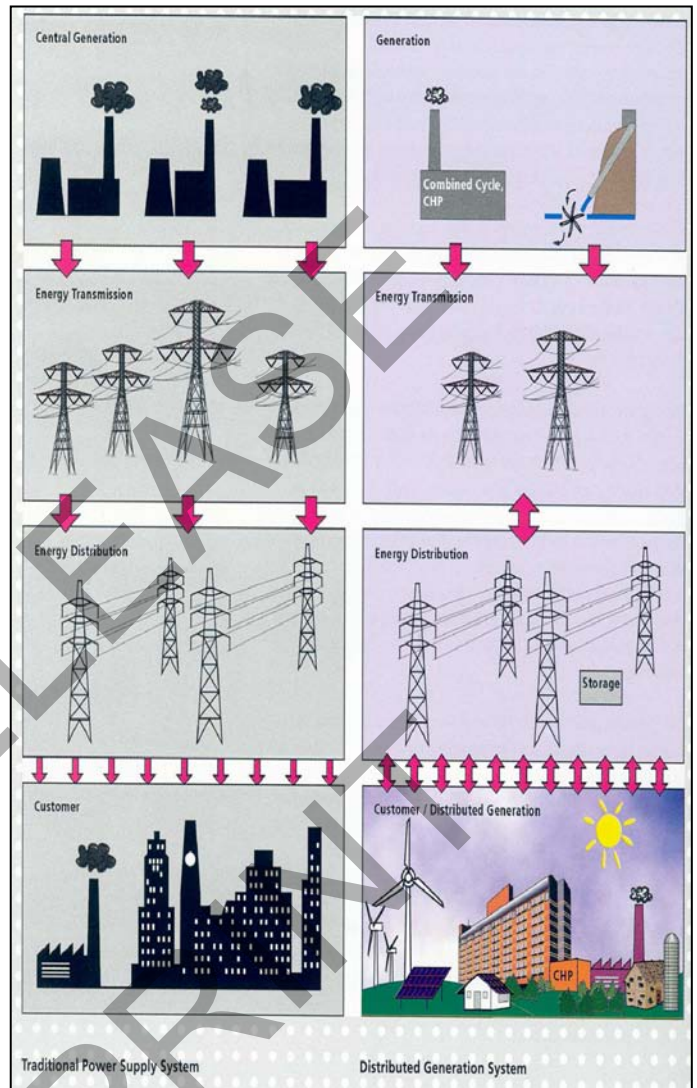


Illustration 5: EU Research 2002
 comparison of available grid systems

ecologically-optimized decentralized grid with many distributed generators, especially using renewable energy sources. The plants have to be part of the grid system so that renewable sources do not only produce energy but are actively incorporated into grid management and capacity. The allocation of technologies to store the excess electricity and control the different processes in the grid with adequate communication ports is one of the basic requirements for a better integration of alternative energy sources. A future task will be to find solutions for a better operation mode of large power plants, especially in part load so that the benefits of using renewable energy will not be lost because of low efficiency. If these conditions are achieved, the integration of alternative energy sources can help to stabilize the current grid in perturbations and do not aggravate the situation.

REFERENCES

- [1] EnergieUniversität Stuttgart Institut für Energiewirtschaft (IER) und Rationelle Energieanwendung; Verteilte Erzeugung im deutschen Energiesystem
Bernhard Hasche; Rüdiger Barth; Derk Jan Swider
- [2] wik-Consult – FhG Verbund Energie
Potenziale der Informations- und Kommunikations-Technologien zur Optimierung der Energieversorgung und des Energieverbrauchs (eEnergy); Bad Honnef, 21. Dezember 2006
- [3] Same as in [1]
- [4] OPTRES: Assesment and optimisation of renewable energy support schemes in the European electricy market (february2007); Intelligent Energy Europe
- [5] Lehrstuhl Dezentrale Energiesysteme und Speichertechnik Prof.Dr.Ing. Rainer Bitsch BTU Cottbus
Aspects of grid integration of decentralized generation (energy management and LSVPP)
- [6] Fraunhofer ISE
Electrical Energy Distribution Networks: Actual Situation and Perspectives for Distributed Generation (<http://www.ise.fraunhofer.de/veroeffentlichungen/nachjahrgaengen/2003/electrical-energy-distribution-networks-actual-situation-and-perspectives-for-distributed-generation>)
- [7] Lehrstuhl Dezentrale Energiesysteme und Speichertechnik Prof.Dr.Ing. Rainer Bitsch BTU Cottbus
Integration Erneuerbarer Energien in die Stromversorgung/ Technische Anforderungen an dezentrale Versorgungsstrukturen in Europa
- [8] Dr.-Ing.Christine Schwaegerl, Dipl.-Ing. Anton Heher
OGE-Fachtagung „Realität und Vision der ökologischen Stromversorgung“

Solar potential of the Sahara Desert with an introduction to solar updraft power plants

Stefanie Fiedermann, Jadranka Halilovic and Torsten Bogacz

Abstract— Considering the rising energy demand, it is necessary to support new sources and possibilities for energy extraction. Renewable energies play a determining role. Amongst others, it is inescapable to regard geographic regions with extreme climatic circumstances. The desert Sahara has a huge potential of solar energy. Its dimension and climatic circumstances give cause to inspect those factors, which would permit solar power generation. An excellent way to use the premises is e.g. solar updraft power plants.

Index Terms— Sahara, updraft, Renewable energy, solar potential, wind

I. INTRODUCTION

As a consequence of the rising worlds demand for electric energy it is necessary to use alternative possibilities to the conventional generation of electricity.

The focal point is on the renewable energies. The sun plays a major role if its potential is used properly. It produces huge amounts of energy. In one hour it radiates enough energy to earth to cover the yearly energy demand of the whole world. If just 0.1 % of the solar energy would be used, the problems of energy supply could be solved (Figure 1).

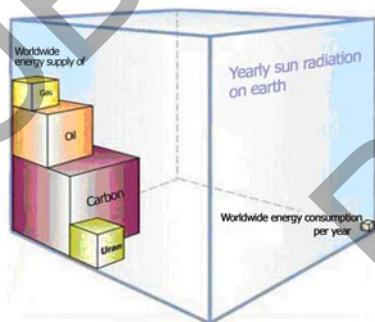


Fig. 1: yearly solar radiation on earth

Manuscript received March 20, 2009.

Stefanie Fiedermann is a student of industrial engineering and electrical engineering at the Brandenburgische Technische Universität Cottbus, Germany

(e-mail: stefanie.fiedermann@tu-cottbus.de).

Jadranka Halilovic is a student of industrial engineering at the Brandenburgische Technische Universität Cottbus, Germany

(e-mail: jadranka.halilovic@tu-cottbus.de).

Torsten Bogacz is a student of industrial engineering at the Brandenburgische Technische Universität Cottbus, Germany

(e-mail: torsten.bogacz@tu-cottbus.de).

The desert Sahara extends over nine million square kilometer and thus gets the most solar radiation in the world. [4] Due to the geographical position and the resulting low clouding the sunshine duration is very high. This leads to a long-time average of 4000 hours, or eleven hours of sunshine a day in the deserts heart. This number is shortened to 3285 hours per year (9 hours/day) on the outside margins.

The sunshine hours of selected sunny meteorological stations in Germany are well below 2000 hours. [3]

This huge potential of available solar power combined with the very low population density predestines the Sahara as a central location for the generation of electricity. The condition for this is the realization of the transfer of electric energy over long distances with a minimization of losses. One option for using the solar power is the solar updraft power plant. The typical build-up will be described below.

In this power plant the sun heats up the air mass which is situated below the solar collector. Due to a central chimney occur differences of pressure. The following equalization of pressure generates up winds. One or more turbines produce electric energy as a result of the airflow. [1]

This method of generating electricity was described by Isidoro Cabanyes for the first time in 1903. The pilot scheme in the 1980's should prove the technical feasibility as well as the efficiency for a period of years.

II. GLOBAL AND LOCAL FACTORS

Capabilities for the use of solar power are especially sunny regions. The generated electric energy, which gets along with almost no consumption, could be used primary for the own requirements of this region and later for the external trade by exporting this electricity. There is no necessity for fossil burning (coal, oil, gas) moreover the investment grows and a lot of jobs can be created.

Especially developing countries would profit from work and energy. Furthermore the generation of updraft energy is environment-friendly and inexhaustible.

III. MODE OF OPERATION

The mode of operation of updraft power plants is based on the three physical doctrines: greenhouse effect, chimney draft and transformation of kinetic energy.

The build-up of such energy-producing facilities consists basically of three essential components. These are the solar collectors, the chimney and the turbines with generator and gear (Figure 2).

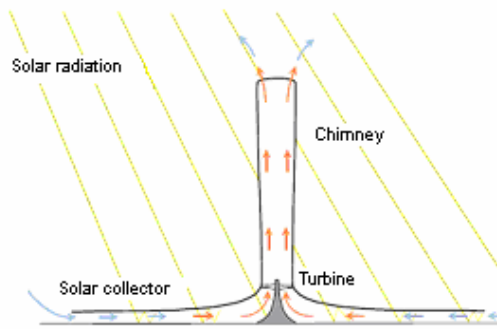


Fig. 2: typical construction of a solar updraft power plant

The solar radiation impacts on the solar collectors and on the water reservoir which heats up the air mass and the ground below. The consequence of this is a pressure difference between the chimney and the heat store.

Through the lesser density of the warm air mass under the glass roof it rises up in the chimney. The Stack Effect intensifies the pull of more air mass.

Due to these effects a continuous upwind is ensured for driving one or more turbines. The gear transmits the mechanic energy to the generator, which finally transforms it to electric energy.

One big advantage of solar updraft power plants is the possibility of a 24/7 operation. This is possible because of the constant heat emission of the heat stores. These are realized by water tanks under the glass roof as well as heated ground. Therefore the heat, saved during the day, can be released in the night. This opportunity makes the operation possible during darkness and without fossil burning. [2]

IV. COMPONENTS OF SOLAR UPDRAFT POWER PLANT

a) Solar collectors

This basic component of the solar updraft power plant consists of glass- and foil-cover and uses the greenhouse effect. For instance, a 200-megawatt disposition would need eight kilometers diameter of solar collector area and a 1000 metres tower. The warm air mass, which is the result of the heating under the glass-roof, flows radial through the collector towards the base of the chimney where it rises up. [1]

b) Chimney

The main task of the chimney is the conversion of the heat energy into kinetic energy. Furthermore, the chimney is an important constituent because the performance of solar updraft power plant depends largely on two factors: on the one hand the surface of collectors and on the other hand the height of the chimney.

There are different solutions for the chimney construction (Figure 3), e.g. out of Ferro concrete or as a steel construction, which should be taken under consideration of the location.

This is a crucial point, whether it is about the investment-calculation or construction. The primary factors, which should take attention, are the wind- and climate-terms, but mainly the strength and commonness of earthquakes. [1]

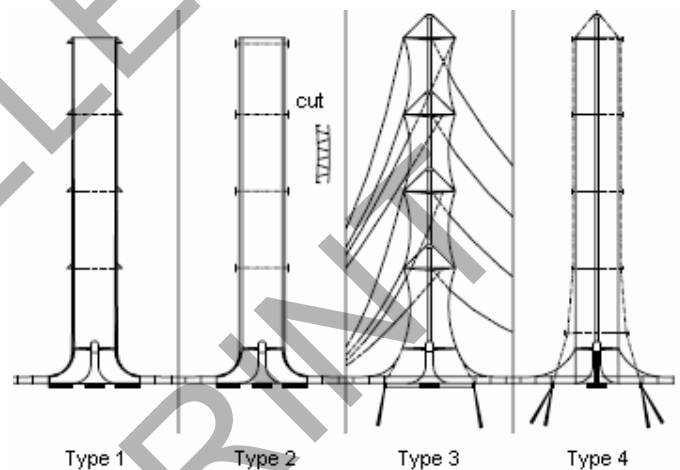


Fig. 3: different kinds of chimney construction

c) Turbine and generator

By dint of turbines it is possible to detract the mechanical energy of the airflow.

Several turbines fill the diameter of the chimney and are driven by the constant airflow in the chimney (updraft).

Through the kinetic energy of the turbines a generator is provided which then converts the accrued energy into electricity. [1]



Fig. 4: solar updraft power plant

V. CONCLUSION

The solar updraft power plant distinguishes through a simple concept in connection with a simple construction. The basic components consisting of collectors, turbines and chimney do not have to be newly developed, solely an adaptation and possibly advancement is necessary.

Important assumptions for the operation of such power plant are a capacious surface for the collectors and long solar radiation. This can be warranted in areas like the Sahara desert e.g. another advantage of the Sahara location is the closeness to Europe. Considering the fact of the high energy demand in Europe, the EU states could be potential electricity importer. Therefore, it is certainly fundamental that low-loss energy transfer is assured.

By achieving the mentioned requirements, the solar updraft power plant could develop into an environmentally friendly power generation alternative and become an important economic factor in an economically underdeveloped region.

REFERENCES

- [1] dos Santos Bernardes, Marco Aurélio (2002): Technische, ökonomische und ökologische Analyse von Aufwindkraftwerken
- [2] Egger, Daniel (2002): Moderne Solartechnologien und ihre zukünftigen Perspektiven. ETH Zürich.
- [3] Kulzer, Wolfgang (2003): Extremklimate: Zentrale Sahara
- [4] Seefeldt, Katja (2002): Strom aus der Wüste: <http://www.heise.de/tp/r4/artikel/11/11777/1.html>

FIGURE REFERENCES

- [1] Brütting, Benedikt (2005): Regenerative Energien: <http://www.rze.uni-erlangen.de/ausbildung/berufsausbildung/pdf/regenerativeenergien.pdf>
- [2] dos Santos Bernardes, Marco Aurélio (2002): Technische, ökonomische und ökologische Analyse von Aufwindkraftwerken
- [3] Schlaich, Jörg (2002): Aufwindkraftwerke: http://www.fvee.de/fileadmin/publikationen/Themenhefte/th2002/th2002_05_03.pdf
- [4] Die Zeit (2008): Das Aufwindkraftwerk, <http://images.zeit.de/bilder/2008/25/bildergalerien/galerien/bg-kraftwerke/04.jpg>

Power Quality in distribution power networks with photovoltaic energy sources

Ricardo Albarracín, Hortensia Amarís
Universidad Carlos III de Madrid.
Madrid, Spain
ricardo.albarracin@uc3m.es, hamaris@ing.uc3m.es

Abstract- Solar radiation is characterized by short fluctuations introduced by passing clouds. These solar fluctuations will produce Voltage and power fluctuations at the PCC (Point of common coupling). Flicker level should be evaluated by using a flickermeter according to the standard IEC 61000-4-15. Models of the solar fluctuation, photovoltaic modules and power converter are shown in this paper and the flickermeter model is tested according to the IEC requirements and the CIGRE/CIREU/UIE test protocol.

Index Terms – Power quality, Flicker, PV.

I. INTRODUCTION

Due to the increasing penetration of distributed generation in electric power systems, power quality is becoming of crucial importance for the further deployment of renewable generation.

The irregular solar radiation is considered to be one of the main drawbacks of the large-scale application of photovoltaic (PV) in distribution networks. Moving clouds can produce fast and short irradiance fluctuations, which can produce voltage fluctuations in power networks. This effect is more important in weak residential and rural grids with high series resistance.

Flicker is defined as the impression of fluctuating brightness or color, occurring when the frequency of observed variation lies between a few hertz and the fusion frequency of images according to the IEEE standard dictionary of electrical and electronic terms (IEEE standard 100-1977). The flicker level is dependent on the amplitude of the voltage fluctuation, their frequency, and the shape of the waveform. All types of voltage fluctuations may be assessed by direct measurement using a Flickermeter, which complies with the specification given in IEC-61000-4-15 [1].

A test protocol is proposed by the CIGRE/CIREU/UIE voltage quality working group [2] to characterize the performance of existing flicker meters in the field.

In this paper, voltage fluctuation in power networks with photovoltaic energy sources will be analyzed and a flickermeter model will be used for the evaluation of the flicker assessment under sunny and cloudy situations.

II. DESCRIPTION OF THE MODEL

The scheme used for the implementation of the model is shown in Fig. 1.

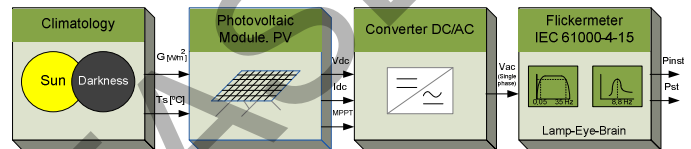


Figure. 1. Block diagram of the whole system.

A. Climatology

This block represents the effect that weather has on the PV generation. The outputs of this block are solar radiation G (W/m^2) and temperature T ($^{\circ}\text{C}$). Previous studies modeled this effect on photovoltaic panels [3], [4]. The effect of sunlight on a PV and its connection to the network through a converter is simulated in [5]. The purpose of all these studies is to calculate the Maximum Power Point Tracking (MPPT) to get the most use of the solar resource for getting maximum power production.

In this study, different weather scenarios will be taken into account. Such as the presence of solar radiation to a greater or lesser intensity depending on time, day and season or the presence of darkness caused by obstacles, clouds or other elements.

B. Photovoltaic module, PV

This block defines the characteristics of solar cells and their interconnection to the power network.

Some authors have used a model of solar cell consisting of five parameters [3], [5] that allow obtaining the inherent non-linear current voltage (I-V) relationship of a typical PV cell. To obtain the curves we use the features provided by the modules manufacturers. In this study the model of the solar cell shown in Fig.2 will be used.

In the presence of solar radiation, the diode (D) produces a current called I_{sc} (Short-circuit current). This current is directly proportional to the solar radiation on the cell. Cell works as a diode. During darkness the solar cell is not an active device.

A control method for calculating the MPPT point will be applied. This model will allow obtaining the current I_{dc} and the voltage V_{dc} , of the PV in these conditions.

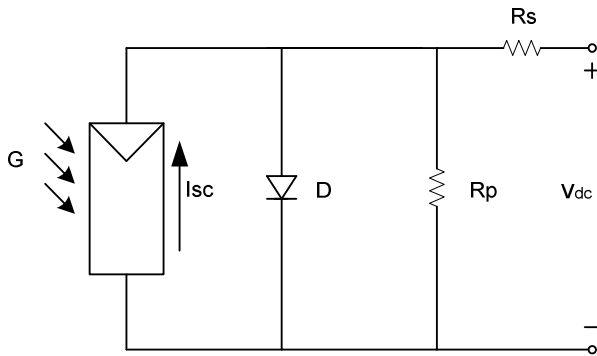


Figure. 2. Equivalent circuit model of a solar cell.

C. Converter DC/AC

This block contains a voltage converter from the PV voltage V_{dc} to the V_{ac} that is injected to the power network. For the connection to the network it is necessary to use a power transformer at the PCC (Point of Common Coupling). Both are included in this block.

D. Flickermeter model

The flickermeter model [1] is composed by the following 5 blocks:

- Block 1: Input voltage adaptor
This block includes a voltage adapting circuit that scales the RMS value of the input voltage down to an internal reference level.
- Block 2: Squaring
This block simulates the squaring part of the lamp model. The lamp model consists of a squaring function and a low pass filter function.
- Block 3: Filtering
 - a) Demodulator filter
The demodulator filter consist of a first order high pass filter for suppressing the direct current component and a low pass filter for suppressing all components equal to or greater than the fundamental frequency of the carrier voltage.
 - b) Weighting filter
The weighting filter simulates the frequency response of a coiled coil filament gas filled lamp and the human visual system. The transfer function is of the following type:

$$\underline{F}_w(s) = \frac{k\omega_s}{s^2 + 2\lambda s + \omega_1^2} \frac{(1+s/\omega_2)}{(1+s/\omega_3)(1+s/\omega_4)}$$

Where s is the Laplace complex variable and the constant values are given in [1].

- Block 4: Variance estimator
This block, called non-linear variance estimator, is composed by a squaring multiplier and a first order low pass filter with a time constant of $\tau = 300\text{ms}$. The purpose of this block is to simulate the storage effect of the human brain. The time signal at the output of block 4 represents the instantaneous flicker sensation, $P_{inst,max}$.
- Block 5: Statistical analysis
Block 5 basically represents a statistical method that classifies and computes the short term Flicker level P_{st} .

In this study, the flickermeter model will be used to obtain flicker level (P_{st}) at the PCC where both the photovoltaic plant and the residential area are connected.

III. EXPERIMENTAL RESULTS

The current version of IEC61000-4-15 [1] specifies a performance test limited to a set of rectangular voltage fluctuations. The CIGRE/CIRED/UIE Joint Working Group on Voltage Quality has defined several different test voltage patterns [2], (see Table I).

The additional tests with specific voltage fluctuation patterns are introduced with the goal to standardize the technical implementation of Flickermeters. In comparison tests it was shown that commercial Flickermeters connected in parallel to the same voltage source with arbitrarily selected voltage fluctuation patterns, yielded substantially different P_{st} values, even though all Flickermeter manufacturers claimed that their products meet the voltage fluctuation tests specified in IEC 61000-4-15 [1].

A. Test #1: Rectangular Voltage Modulation Performance.

For all voltage fluctuations tabulated in Table II the flicker severity indicator P_{st} must be within the range of $P_{st} = 1.000 \cdot (1.00 \pm 5\%)$. Test that did not pass the Test Protocol are green marked.

TABLE I
Summary of Test Protocol

Category	Test	Excitation Signal	Output
IEC 61000-4-15	1	Rectangular fluctuation	P_{st}
	2	Rectangular fluctuation	$P_{inst,max}$
	3	Sinusoidal fluctuation	$P_{inst,max}$
No Influence test	4	Frequency variation	P_{st}
	5	High Frequency	$P_{inst,max}$
	6	Linearity	P_{st}
	7	Single Interharmonic	$P_{inst,max}$
Influence test	8	Harmonic-Interharmonic Pairs	$P_{inst,max}$
	9	Phase Jump	P_{st}
	10	Interruptions	P_{st}
Complex Systematic	11	Wood Chipper pattern	P_{st}
		Rolling Mill pattern	
		Arc Furnace pattern	

TABLE II

Results for Test #1

Rectangular changes per minute	Pst results		Pst results	
	120-V lamp 60 Hz system	230-V lamp 50 Hz system	120-V lamp 50 Hz system	230-V lamp 60 Hz system
1	0.9999	0.9830	1.0015	0.9827
2	1.0135	1.0170	1.0137	1.0155
7	0.9758	0.9804	0.9864	0.9795
39	0.9911	0.9933	0.9917	0.9947
110	0.9952	0.9923	1.0010	0.9927
1620	0.9957	0.9972	0.9964	0.9968
4000	Test not required	1.2385	1.2383	Test not required
4800	1.0573	Test not required	Test not required	1.0575

Note: 1620 rectangular changes per minute corresponds to a rectangular square wave modulation frequency of 13.5 Hz.

TABLE III

Results for Test #2

Hz	Pst results		Pst results	
	120-V lamp 60 Hz system	230-V lamp 50 Hz system	120-V lamp 50 Hz system	230-V lamp 60 Hz system
0.5	0.9960	0.9902	0.9958	0.9905
3.5	0.9985	0.9919	0.9962	0.9902
8.8	1.0031	0.9933	1.0006	0.9948
18	0.9993	0.9872	0.9894	0.9937
21.5		0.9876		
22	0.9950			0.9874
25		0.9993	1.005	
25.5	0.9939			0.9877
28		1.0325	1.0391	
30.5		1.0548	1.0530	
33+1/3	1.0440	0.7194	1.5428	1.0246
37	0.9956			0.9990
40	1.1231			1.1186

TABLE IV

Results for Test #3

Hz	Pst results		Pst results	
	120-V lamp 60 Hz system	230-V lamp 50 Hz system	120-V lamp 50 Hz system	230-V lamp 60 Hz system
0.5	0.9996	0.9939	0.9996	0.5304
1.5	0.9999	0.9934	0.9999	0.9934
8.8	0.9999	0.9937	1.0000	0.9937
20			1.0012	0.9920
25	0.9926	1.0040		
33+1/3	1.0518	1.5310	1.5427	1.0450
40	1.1311			1.1244

TABLE V

Results for Test #4

Power frequency (Hz)	Pst
49	0.9925
49.5	0.9926
50.5	0.9956
51	0.9948

TABLE VI

Results for Test #6

Pst results		
120-V lamp 60 Hz system	230-V lamp 50 Hz system	Pst = $(1.00 \pm 0.05)^*(x) \pm 0.1$
0.1917	0.1905	0.2 ± 0.1
1.9912	1.9852	2 ± 0.1
4.9547	4.9587	5 ± 0.1
9.9363	9.9324	10 ± 0.1
19.773	19.74	20 ± 0.1

B. Test #2: Normalized Response for Rectangular Voltage Fluctuations.

This test is to verify that the voltage modulation levels, for a maximum instantaneous value $P_{inst,max}$ of 1.00 are within a tolerance of ± 0.05 of the voltage modulation percentages given in IEC 61000-4-15. Table III shows the results for Test #2.

C. Test #3: Normalized Response for Sinusoidal Voltage Fluctuations.

To perform a further evaluation of flickermeter implementations, sinusoidal modulation tests points have been defined in IEC 61000-4-15, Amendment 1 Table 1. Test #3 is to verify that the voltage modulation levels for a maximum instantaneous value $P_{inst,max}$ of 1.00 are within a tolerance of $\pm 5\%$ of the voltage modulation percentages given in IEC 61000-4-15, Amendment 1 Table 1. Table IV shows the results for Test #3.

D. Test #4: Power Frequency Variation.

The purpose of this test is to verify that a steady state frequency, within a specified tolerance of the nominal frequency, does not result in light flicker. A test point passes if the result is Pst of 1.00 ± 0.05 . Table V shows the results for Test #4.

E. Test #6: Linearity.

This test will show whether the measured Pst has a linear relationship to the amplitude of the voltage fluctuations in the range 0.2 to 20. Table VI shows the results for Test #6.

IV. CONCLUSIONS.

In this paper, a detailed model of the flickermeter according to the IEC 61000-4-15 has been shown. The flickermeter model fulfils the requirements defined in the IEC 61000-4-15 standard. Additionally, it has been tested under additional tests defined in the CIGRE/CIREU/UIE test protocol.

Once the flickermeter model has been validated, it will be used for evaluating the flicker severity and the voltage fluctuations produced by photovoltaic energy sources.

Research studies have proved that irregular solar irradiation caused by cloud movement can produce voltage and power fluctuation from PV sources. For voltage fluctuation and flicker assessment is necessary to use a flickermeter such as the one shown in this paper.

ACKNOWLEDGMENT

This research has been partially supported by the Spanish Ministry of Education and Science under contracts ENE2006-28503 and ENE2008-06504-C02-01.

REFERENCES

- [1] IEC std., 61000-4-15, *Electromagnetic Compatibility (EMC) Part 4: Testing and Measurement Techniques – Section 15: Flickermeter Functional and Design Specifications*, 2008.
- [2] Joint Working Group on Power Quality Cigré C4.1.01/CIRE2 2 CCO2/UIE WG2, *Test Protocol for IEC Flickermeter used in Power System Voltage Monitoring*, Draft 11. July, 2004.
- [3] F. González-Longatt, *Model of photovoltaic module in Matlab™*, II CIBELEC, 2005.
- [4] Nabil A. Ahmed, Masafumi Miyatake, *A novel maximum power point tracking for photovoltaic applications under partially shaded insolation conditions*, ELSEVIER, 78 (2008) 777-784.
- [5] T. DenHerder., *Design and simulation of photovoltaic super system using Simulink*, Electrical Engineering Department, California Polytechnic State University, San Luis Obispo, 2006.
- [6] W. Mombauer, *Additional requirements to the IEC flickermeter. Cigré/Cired/UIE. 2009.*

Author Index

A

Abbasi, Ataollah 220, 308
Abbasi, Hamid Reza 220, 308
Abbaszadeh, Alireza 263
Adamowicz, Marek 57
Ajayi, Adekunle Babatope 151
Al-Awaad, Ahmad-Rami 175
Al-Hasawi, Wael 155, 185
Alvarez, Carlos 1
Amaris, Hortensia 1, 360
Anczykowska, Agata 83
Anil, Aditya 19

B

B, Chitti Babu 107
Bartkiewicz, Stanislaw 83
Belmadani, B. 141
Benghanem, M. 141
Benzaoui, Mohamed Lassaad 124
Berkani, Aberrahmane 118
Bogacz, Torsten 357
Bork, Lars 333
Borowski, Gabriel 110
Brose, Nico 253

C

C, Poongothai 107
Cerny, Vaclav 23
Chlodnicki, Zdzislaw 65
Conlon, Michael 91

D

Dębowski, Marcin 230, 249
Danielski, Piotr 249
Daoud, Ahmed A. 127
Dawidowski, Pawel 339
Deshmukh, Sameer 263, 268
Djilali, Kairous Djilali 141
Dolega, Waldemar 133
Domingues, Nuno Soares 226, 287
Doskocz, J. 179
Drobik, Tomasz 260

E

Egorov, Mikhail 57
Esteban, Abouzar 341
Ewert, Pawel 318

F

Fantik, Josef 95
Farshad, Siamak 204
Fialova, Andrea 23
Fiedermann, Stefanie 357
Fröbel, Anke 280

G

Garnitz, Bastian 333
Gaworska-Koniarek, Dominika 54
Ghiasi Varzeghan, Mahdi 114
Gilany, Mahmoud 155, 185
Golkhah, Mohammad 145
Gono, Radomir 45
Grzelak, Dennis 253

H

Halilovic, Jadranka 357
Havel, Petr 49

Heideck, Guenter 103
Heuer, Maik 103
Horacek, Petr 49, 95
Hoseini, Sied Hadi 114
Houdova, Lenka 32
Houdova, Lucie 23
Hoyer, Robert 293
Hrabcik, Miroslav 45
Hui, Kang Kin 200

I

Iwan, A. 179
Iwanski, Grzegorz 65
Izykowski, Jan 300

J

Janecek, Eduard 23, 32
Janecek, Petr 23
Janik, Przemyslaw 1
Jankow, Michal Piotr 321
Jelinek, Libor 32
Jhapté, Rajkumar 164
Jose, Linju 243

K

K B, Mohanty 107
Kaebisch, Mathias 103
Kammer, P. 353
Kepka, Jakub 325
Khambia, Yogesh 272
Khan, Umar Naseem 212, 232
Kitscha, Stefanie 314
Kober, Andreas 353
Koczara, Włodzimierz 65
Krisch, Thomas 333
Kulinski, R. 190
Kurnatowski, Rafal 218, 247
Kuscheck, Robin 337

L

Labaf Khaneiki, Majid 27
Leccese, Fabio 8
Leonowicz, Zbigniew 1, 193
Lesan, Saeed 263
Linh, Nguyen Tung 36
Lu, Yan 346

M

Maćków, Andrzej 216
Mackowiak, Lukasz 304
Maliga, Grzegorz Pawel 99, 137, 236
Mazniewski, Piotr 300
Mohanta, Dusmanta Kumar 19
Mohd. Ja'afar, Mohammad Nazri 200
Mortazavi, Seyed Saeidollah 196
Mortezapour, Vahid 263
Mysliwiec, Jaroslaw 83

N

Napierala, Artur 73, 77
Nekoui, Mohammad Ali 145
Noack, Martin 337
Novak, Ondrej 95

O

Ozimek, Mariusz 54

P

Palewicz, Marcin 179
Panda, Ajit Kumar 19
Patil, Amar Mohan 99 , 137 , 236
Patil, Pankaj M. 170
Pawlowski, Maciej Stanislaw 160
Permatasari, Rosyida 200
Pliszczyk, Robert 329
Podzemsky, Jiri 41
Pyda, Daniel 296
Pytlarz, Jan Stanislaw 318

R

Radmanesh, Hamid 220 , 308
Rahmati, Hojat 145
Rashtchi, Vahid 114
Rezine, Hacene 118
Rezmer, Jacek 1
Rostami, Mehrdad 220 , 308 , 341
Roy, Diptendu Sinha 19
Ruczewski, Piotr 1 , 79
Rusek, Stanislav 45
Römer, Henry 293

S

Słabosz, Sebastian 349
Saadati, Marjan 196
Sadeghzadeh, Seyyed Mohammad 341
Saffar Shamsirgar, Sahar 145
Sanchez, Ricardo Albarracin 360
Saudhof, Jonathan 293
Sayed, Ahmad Galal 13
Schade, Wolfgang 41
Schlüter, Sören 337
Schmeckebier, Jürgen 314
Schwartz, Carsten 333
Schünemann, Lennardt 253
Sek, D. 179
Sikorski, Tomasz 79
Singh, Mahesh 164
Sonawane, Naresh D. 170
Sonawane, Sayali Y. 170
Sonawane, Yogesh Devidas 170
Staszewski, Luke 208
Steckel, Marcel 314
Strek, W. 179
Strnad, Tomas 95
Strzelecki, Ryszard 57
Stuermer, Henryk 61
Styczynski, Zbigniew 103
Sunderland, Keith 91
Swistacz, Bronislaw 183
Szafron, Cezary Pawel 257
Sznitko, Lech 83
Szubzda, B. 190
Szymanski, Dariusz 240

T

Takbiri, Farzad 204
Tivari, Vaibhav 164

V

Verstege, J. F. 87
Vinnikov, Dmitri 57
Völler, Steve 87

W

Waclawek, Zbigniew 1
Wilczynski, Wieslaw 54

Y

Yazdi, Ali Asghar Semsar 27
Yerekar, Sachin Ramrao 283

Z

Ziaja, Jan 73
Zylka, Pawel 69

PRZEDSIĘBIORSTWO ENERGETYKI CIEPLNEJ SP. Z O.O. W JELENIEJ GÓRZE

Municipal Heat Supply Company (PEC) Ltd. in Jelenia Góra is a local leader and a main supplier of the system heat in the city. The company is also providing services associated with the sales and consulting in the field of electric energy and specialist repair and maintenance services. PEC offer is based on the long-term practice and the specialist know-how of employees and experience acquired in cooperation with customers, allows achieving goals using the most economic solutions.

Experience and knowledge:



- qualified professionals
- the production, distribution and sale of the thermal energy, electric and of technological steam
- providing special services

Technology:

- preinsulated piping
- weather automation
- radio meter reading



Ecology:

- cogeneration
- limiting of greenhouse gas emission
- reducing network losses



Local activities:

- Sponsor of the education and culture in the region
- Fair Play Company



PRZEDSIĘBIORSTWO
FAIR PLAY

Future:

- growth in production of the electric energy
- investments in infrastructure
- development of the renewable sources of energy



PEC Jelenia Góra – safe and trusted partner in the field of heating technologies.

More informations on our webpage: www.pecjg.pl. Welcome.

Instytut Automatyki Systemów Energetycznych Sp. z o.o.

www.iase.wroc.p



Founded in 1949, the Institute of Power Systems Automation Ltd. is an independent research and development organisation specialising in automated control and monitoring systems for the electricity industry.

We supply prove, reliable systems for a whole range of applications, from single operations to providing total integrated solutions. Our service is comprehensive and covers:

- process control systems,
- monitoring systems,
- power plants and combined heat + power plants,
- generation, transmission and distribution,
- specialist advice/consultancy,
- hardware and software,
- design, production and installation,
- staff training.

We provide flexible solution to meet individual requirements.

References:

- Polish Power Grid Company - National Dispatching Centre;
- Ukrainian Dispatching Centre - Lvov;
- polish power plants: Kozienice, Połaniec, Dolna Odra, Bełchatów, Opole, Jaworzno, Turów, Łagisza, Łaziska, Siersza, Miechowice and foreign power plants: Chine, Turkey, Finland, former Yugoslavia, Bułgaria, Spain;
- heat and power plants: Wrocław, Gdynia, Gdańsk, Bytom, Łódź, Siekierki, Kraków, Szczecin, Lublin, Stalowa Wola, Bydgoszcz, Toruń and hydro-electric plants: Dychów, Solina, Włocławek, Rożnów.

We have extensive laboratory testing facilities and production unit to help ensure the quality of our products and services.

IASE has established and applies a quality system EN ISO 9001:2000 for consulting, research, engineering design, putting power system installations into operation as well as production of the control system for turbine generating set and automatic control equipment.

INSTITUTE OF POWER SYSTEMS AUTOMATION Wrocław - Poland

51-618 Wrocław; ul.Wystawowa1;
POLAND

Tel. +48-071-348 42 21

Fax +48-071-348 21 83



www.zpue.pl



ZPUE S.A. in the electric power system

Full scope of our plants allows us to implement any order from the range of electrical energy transmission and distribution

ZPUE S.A.
29-100 Włoszczowa
ul. Jędrzejowska 79c

ZPUE®